INFORMATION TO USERS

This manuscript has been reproduced from the microfilm master. UMI films the text directly from the original or copy submitted. Thus, some thesis and dissertation copies are in typewriter face, while others may be from any type of computer printer.

The quality of this reproduction is dependent upon the quality of the copy submitted. Broken or indistinct print, colored or poor quality illustrations and photographs, print bleedthrough, substandard margins, and improper alignment can adversely affect reproduction.

In the unlikely event that the author did not send UMI a complete manuscript and there are missing pages, these will be noted. Also, if unauthorized copyright material had to be removed, a note will indicate the deletion.

Oversize materials (e.g., maps, drawings, charts) are reproduced by sectioning the original, beginning at the upper left-hand corner and continuing from left to right in equal sections with small overlaps.

ProQuest Information and Learning
300 North Zeeb Road, Ann Arbor, MI 48106-1346 USA
800-521-0600

University of Alberta

Transmission of Column Loads through Lower Strength Concrete Floors: Experimental and Analytical Study

by

Ehab Abdel Wahab Abdel Mohsen Abdel Wahab

A thesis submitted to the Faculty of Graduate Studies and Research in partial fulfillment of the requirements for the degree of

Doctor of Philosophy

in

Structural Engineering

Department of Civil and Environmental Engineering

Edmonton, Alberta

Fall 2005

0-494-08603-3

To my family, I dedicate this work.

Abstract

This research covers both experimental and analytical investigation of the effective compressive strength (f'_{ce}) and behaviour of the joints between high-strength concrete columns and normal strength concrete floors under a combination of axial compressive loads from the columns and gravity loads from the floors. f'_{ce} is notionally the cylinder strength of some virtual concrete that combines the effect of the joint concrete(s) and the effect of the confinement provided to the joint.

The experimental stage included fabrication, instrumentation, and testing of seven 2/3 scale specimens. The main variables in this research program are adding high-strength-concrete inside the joint, debonding of the floor main reinforcement through the joint, and the loading regime. The analytical stage covers the previously mentioned factors and other factors related to properties and arrangement of the materials composing the joint.

The main findings of the experimental stage are: (1) casting the joint with the top column can restore the full strength of the column, (2) partial debonding of the floor main reinforcement can improve the joint effective strength, (3) the vertical and lateral strains at maximum concrete stress are sufficient to develop high strength steel reinforcement to increase capacity of the joint if the joint is made of normal strength concrete, (4) the combination of ultimate load on the floor and service load on the column causes a reduction in the cross-sectional area of the joint without failing the joint.

The main contribution of analyzing the test results of this research is to crystallize the awareness of the joint behaviour under different loading regimes. That was achieved through deriving concrete confinement model to predict the strength and behaviour of any column-floor joint under any condition. The models were validated by comparison to the experimental results found in the literature.

A parametric study was conducted to investigate the sensitivity of the effective strength and behaviour of the joint to any change in the different variables.

Acknowledgement

First and before all, the author of this dissertation thanks "*The Almighty ALLAH*" (GOD) for the countless bestowed bounties.

Special thanks are due to the Portland Cement Association Education Foundation for sponsoring the experimental work of this research (PCA Project Index No. F13-02).

The author would like to express his gratitude to the staff of the civil and environmental engineering department of the University of Alberta for the help, and the friendly environment they provided. Sincere gratitude and appreciation are due to Dr. Scott Alexander for all the guidance, supervision and constructive criticism he provided throughout this study. Special thanks are due to Larry Burden and Richard Helfrich for their valuable technical assistance at I.F. Morrison Structural Engineering Laboratory.

Finally yet importantly, I, the author, offer special thanks to my big family to whom I am greatly indebted: my mother, my wife, my daughters and my sisters. I owe you all more than I can ever express and I pray to *ALLAH* to pay you some of what you deserve. I dedicate this work to all of you and to the soul of my father- may *ALLAH* be merciful to him- who passed away six months after I started this study.

Table of Contents

8 SENSITIVITY STUDY

List of Tables

List of Figures

List of Notations

θ : angle of the curve separating confined and unconfined areas between tie levels

η: the reserve strength or the reserve strain of the floor

A_c: the effectively confined concrete area

A_{ce} : the effectively confined core area at the critical section between ties

A_{cg} : the gross confined area at level of ties

A_{co} : the area at the least confined section midway between ties

A_g: column gross area

A_s : area of the beam flexural reinforcement

A_{st}: total area of vertical rebars

B and H : center to center dimensions of the perimeter tie or the total column dimension confined by the floor

b_w : the beam width

c: column small dimension

C_i : center to center distance between longitudinal bars

d : nominal diameter of vertical rebars, and depth to tension reinforcement

d'' : nominal diameter of ties

d-d_2 : the center to center distance between top and bottom reinforcement of the beam

E_c: static Young's modulus of unconfined concrete

E_{cr} : Young's modulus of a cracked-section

E_s , E_{sec}: secant value of Young's modulus for the concrete section (column or joint)

f'_c : the specified compressive strength of the concrete

f'_{cc} : the cylinder strength of the column concrete

f'_{co} : the cylinder strength of the concrete under consideration

f'_{cs} : the cylinder strength of the floor concrete section

f''_s : stress in ties at maximum compressive stress

f''_y : yield strength of ties

f_c : the average compressive stress applied on the concrete

f_{ce} : the effective compressive strength of the joint concrete

f_{cl} , f_l: the confining stress due to ties

F_r : effective lateral confining pressure

f_{sl} : maximum stress in the vertical rebars at failure of the specimen

f_y : yield strength of vertical rebars or of the beam flexural reinforcement

h'' : length of one side of the rectangular ties

h: vertical thickness of the joint

h_b : vertical distance from the lower end of the middle LVDT to the beam-bottom level

h_t: vertical distance from the upper end of the middle LVDT to the slab-top level

$k_{Conf;Test}$: actual total strength enhancement

$k_{End;Conf}$: strength enhancement due to end confinement

$k_{Floor.Conf}$: strength enhancement provided by the floor

$k_{Floor;Deb}$: strength enhancement due to debonding of the floor negative reinforcement.

$k_{Floor;Res}$: strength enhancement due to the floor reserve strength

$k_{HSC;Core}$: strength enhancement due to high-strength-concrete inside the joint

$k_{RFT;.Conf}$: strength enhancement provided by the column reinforcement

k_s : the confinement effectiveness coefficient

$k_{STR;Conf}$: strength enhancement due to interaction between column reinforcement and floor.

l_b : original height of LVDT aluminium-frame fixed on the bottom column

l_t : original height of LVDT aluminium-frame fixed on the top column

m: number of arcs between longitudinal bars along the unconfined sides

n : the number of arcs between longitudinal rebars *or* number of longitudinal steel bars

P_c, P_o, P_u: the column axial capacity

P_r: factored axial resistance of the column as defined in A23.3-94

S: the smaller of the tie spacing or the vertical rebar spacing

s : the tie spacing

t_j : the joint thickness

v^a : secant value of Poisson's ratio for the ascending branch of the stress-strain curve

v^a_d : secant value of Poisson's ratio for the descending branch of the stress-strain curve

w : maximum expected floor load

w_u : the floor load capacity

x_f and x_n : the distance from centre of the joint in the transverse direction to the far and near horizontal LVDTs respectively.

z : slope of the descending branch

Δ_b : the total deformation recorded by the bottom vertical LVDT

$\Delta f'_{ce}$: the enhancement in the effective strength of the joint

Δ_j : the total deformation recorded by the middle vertical LVDT

Δ_t : the total deformation recorded by the top vertical LVDT

α_1 : factor defined in a23.3-94 as ratio of average stress in rectangular compression block to the specified concrete strength.

β : nonlinearity index

ε_1, ε_2 : axial and lateral strain in the joint respectively

ε_{20c} : the concrete strain at $0.2 f_{co}$ on falling branch for confined concrete

ε_{2i} : strain at an arbitrarily selected point on the descending branch

ε_{50c} : the concrete strain at $0.5 f_{co}$ on falling branch for confined concrete

ε_{50h} : the increase in concrete strain at $0.5 f_{co}$ on falling branch due to ties

ε_{50u} : the strain at $0.5 f_{co}$ on falling branch for unconfined concrete

$\varepsilon_{b;ave}$: average strain values of the bottom beam reinforcement at face of the column

ε_c: the concrete strain at stress f_c

ε_{co}: the concrete strain at unconfined strength f_{co}

ε_f: lateral strain value calculated from the far horizontal LVDT

ε_i : strain at the inflection stress f_i on the descending branch

$\varepsilon_{j;t}$: lateral strain of the joint through the beam thickness

ε_n : lateral strain value calculated from the near horizontal LVDT

ε_{s1} and ε_{s2}: the concrete strain values at the effective strength f_{ce}

ε_{s30} : the strain corresponding to $0.30 f_{ce}$ on the descending part

ε_{s85} : the strain corresponding to $0.85 f_{ce}$ on the descending part

$\varepsilon_{t;ave}$: average strain values of the top beam reinforcement at face of the column

ϕ_c, ϕ_s: resistance factors for the concrete and steel as defined in A23.3-94

ϕ: curvature of the beam at the column face

γ: ratio between the high-strength-concrete area and the cross-sectional area of the joint;

ψ: percentage of the debonded floor reinforcement

λ : ratio of A_c to A_{co}

ρ: the reinforcement ratio of vertical rebars. It is defined as area of the reinforcing bars to the gross area of the concrete section.

ρ'': the tie-volumetric ratio. It is defined in the literature as ratio of volume of ties to volume of the confined concrete core measured from center to center of the outer ties. In the model of this research, it is defined as ratio of volume of ties to the gross concrete volume.

ζ: ratio of the effectively confined concrete area to the core area

1 INTRODUCTION

1.1 Introduction

One of the main challenges to exploiting fully the advantages of high-strength concrete in the construction of multi-storey reinforced concrete buildings is the usual practice of casting the floor concrete continuous through the columns, which leads to the joint region being cast using the same concrete as the floor. While using high-strength concrete in the columns reduces the capital cost of the structure and improves utility by increasing usable space, there are limited advantages to using high-strength concrete in the floor system. As a result, the floors may be made with concrete of much lower design strength than the supporting columns. The effect of this is to place a layer of lower strength concrete in the column. The magnitude of the strength loss depends on the ratio of the column strength (f'_{cc}) to the floor concrete strength (f'_{cs}), the level of floor loading, and the geometry of the joint.

1.2 Problem Statement

A design question arises about the compressive strength of floor-column joints to be used in designing the column and how that strength can be maximized without reducing the competitive advantage of high-strength concrete. In extreme cases, the column concrete may be as much as six times stronger than the floor concrete. As a result, the crushing capacity of the joint concrete will be much less than the service dead load on such a column.

Design provisions in ACI 318-95 (Section 10.15) and in CSA A23.3-M84 (Section 10.13) are based on the experimental work carried out by Bianchini, Woods and Kesler in 1960. These test results correspond to slab-column specimens subjected to column load only. Bianchini et al. (1960) addresses strength loss but not how to avoid this loss. Design

guidelines in ACI 318M-02 (Section 10.15) and in CSA A23.3-94 (Section 10.12) were based on an expanded database that included a set of test results of interior joint specimens with loaded slabs.

Following current standards, designers may add reinforcement in the joint, puddle higher strength concrete around the floor-column joint, or cast the entire floor system with a higher strength concrete. All these solutions add cost.

There is a need to explore some methods to strengthen the column-floor joint and to come up with a general model for the concrete confinement.

1.3 Goals and Objectives of the Research

The goal of this study is to build on the available literature to understand the behaviour of column-floor joints in order to develop a good tool for estimating the effective strength and modeling the performance of any column-floor joint. There are four main objectives:

- To expand the understanding of the behaviour of joints between high-strength-concrete columns and normal-strength-concrete floors under axial loading.
- To model the general behaviour of columns or column-floor joints of any type under axial loading.
- To develop a general design equation or equations to determine the concrete effective strength.
- To come up with effective techniques to utilize the capacity of high strength concrete columns by maximizing the effective strength of the joints.

The specific steps followed to achieve the above-mentioned goal and objectives are enumerated as follows:

1. Review the literature covering experimental and analytical research work on the strength and behaviour of high strength concrete columns intervening with normal strength concrete floors.
2. Review current design provisions, pertaining to the research topic, in the Canadian and American standards.

3. Conduct an experimental program and analyze its results.
4. Quantify contribution of the various elements to the strength of the different floor joints through rational and simplified approaches.
5. Develop a confinement-based strength model and examine the ability of the model to predict the actual strength values reported in the literature.
6. Develop a stress-strain model and examine the ability of the model to replicate the actual behaviour reported in the available test data.
7. Develop design provisions that account for the characteristics of the different materials in the joint, and compare these provisions to the current standards and to those previously proposed in the literature.

1.4 Organization of the Research

Chapter 2 presents a literature survey. It briefly outlines the experimental and analytical work reported by previous researchers, and it reviews their recommendations. It addresses also the current design standards.

Chapter 3 presents a detailed description of the materials and specimens tested throughout the experimental phase of this research. It also contains a description of the fabrication, and instrumentation that were followed.

Test protocol, test results, observations of behaviour of the specimens throughout the tests are presented in chapter 4.

In chapter 5, analysis of the test results is presented.

Chapter 6 presents a detailed method for estimating the concrete effective compressive strength (strength model). The method accounts for mechanical properties, geometrical characteristics and construction details of the joint, and finally loading and deformation capabilities of both the floor and the column. The chapter covers the procedures necessary to predict the behaviour of the column-floor joint up to failure. The model considers the non-linear behaviour of the materials: the plastic stage for steel reinforcement and strain softening for the concrete material.

Chapter 7 introduces a simplified method to determine the joint effective strength and examines it together with the detailed method from chapter 6 by comparing them to the current design code provisions and to other empirical design equations found in literature.

The crucial parameters for the strength and ductility of the joint are investigated in chapter 8, which covers a comprehensive example on the design of such joints.

The work is summarized in chapter 9, where all pertinent conclusions are listed with recommendations made for design, construction, and research work in this area. Complementary materials to document all the experimental work and analytical results are added in appendices.

2 LITERATURE REVIEW

2.1 Published Test Results

This section summarizes the past studies on the joints between high-strength-concrete (HSC) columns intervening with normal-strength-concrete (NSC) floors. Focus is on the main parameters that were investigated and the main conclusions that were validated or refuted in this research. Table 2.1 summarizes the main variables of each study.

2.1.1 Bianchini, Woods and Kesler (1960)

Bianchini, Woods and Kesler (1960) tested 45 specimens: 14 interior, 18 edge, 9 corner sandwich plate specimens, and 4 sandwich columns. The major variables accounted for in this study were the ratio of the column concrete compressive strength to the slab concrete compressive strength, f'_{cc}/f'_{cs}, and the joint type. Column concrete strengths ranged between 15.8 and 56 MPa. Slab concrete strengths varied from 8.8 to 24.8 MPa. Specimens were tested when the floor concrete was 28 day old. The load was applied only to the columns. Duration of the tests ranged between 1.5 to 2 hours. There was no instrumentation to measure actual strain values in rebars or concrete during the test. Failure of the different test specimens was found to be dependent on the ratio f'_{cc}/f'_{cs}.

For the slab-series specimens, failure of the interior specimen occurred in the top or bottom column; failure of the edge and corner specimens occurred either in the visible face (or faces) of the joint or in the top or bottom columns.

For beam series specimens, failure of interior specimens occurred either in top or bottom columns; failure of edge specimens occurred either in bottom columns or in bottom of the beams next to the columns, except one specimen that failed in top column; failure of the sandwich columns occurred in the joints by yielding of the vertical reinforcement and crushing of the concrete.

2.1.2 *Gamble and Klinar (1991)*

Gamble and Klinar tested 6 edge and 6 interior sandwich-plate specimens, and one specimen without slab. Major parameters involved were type of the specimen and the ratio of the column compressive strength to the slab compressive strength, f'_{cc}/f'_{cs}. Column concrete strengths ranged between 72.4 and 104.8 MPa. Slab concrete strengths varied from 15.9 to 45.5 MPa. The amount of column vertical and lateral reinforcement was held constant (1.8% and 0.13% respectively). Vertical strain was measured via electrical resistance foil strain gauges attached to two of the vertical rebars at two locations: at the joint mid-height and at the bottom column. Specimens were tested at ages between 61 and 157 days. Load was applied only to the columns.

The first crack occurred at a concrete stress higher than the concrete specified strength and equal to 66% of the maximum concrete stress. For interior specimens, the slab curled upwards because there was more slab top reinforcement than there was bottom reinforcement. At failure, the cracks extended into the bottom column and the specimens failed explosively. Edge specimens failed explosively in joint regions, with spalling off the cover concrete and buckling of the vertical rebars.

The study concludes that the ratio of column concrete strength, f'_{cc}, to slab concrete strength, f'_{cs}, is applicable across the range of concrete strengths that were used. Similar test results for a joint-specimen with f'_{cc}/f'_{cs} of 4.0 are reached with either an 80 MPa column concrete and a 20 MPa slab concrete, or with a 120 MPa column concrete and a 30 MPa slab concrete. The study also suggests that the column width-to-slab thickness ratio, c/h, affects the effective strength of the joint concrete, f_{ce}. However, no tests were carried out to demonstrate this hypothesis.

2.1.3 *Shu and Hawkins (1992)*

Shu and Hawkins reported test results of 54 sandwich column specimens to study the behaviour of joints restrained solely by two column ends. Major variables examined were the aspect ratio (h/c), where h is the slab thickness and c is the column width, and the ratio f'_{cc}/f'_{cs}. The amount of column reinforcement was systematically varied to study the effect of this variable on the interaction of column and slab concrete. The specimens were tested at age of seven days. Concrete strength for the columns ranged from 38.5 to

48.5 MPa. The slab concrete strength varied from 6.9 to 39.2 MPa. Axial compressive load was applied to the sandwich column specimens. The duration of each test was reported to be about an hour.

For specimens with small *h/c* values (0.5 or less) and f'_{cs} close to f'_{cc}, vertical cracks appeared in the columns. Such cracks widened enough so that the vertical rebars buckled and then the concrete crushed. For specimens with intermediate *h/c* values (1.0), cracks formed first in the joints and then extended into the upper columns. For specimens with large *h/c* values (2 and bigger), failure was limited to the joint region.

The study concludes that *h/c* is a significant variable affecting f_{ce}; as *h/c* increases, the column effective compressive strength decreases. According to the study, the vertical reinforcement reduces f_{ce} and so it is safer to base the design equation on the tested reinforced concrete columns rather than the tested plain concrete columns.

2.1.3.1 Comments

Shu and Hawkins reported using 19 mm size aggregate in their specimens. For *h/c* equal to 0.17, the joint thickness was approximately 25mm thick; so, the coarse aggregate effectively bridged the joint region. This resulted in an undue increase of f_{ce}. Moreover, the use of 19 mm aggregate in 25 mm or 46 mm thick concrete joints is questionable given the observations of Avram et al. (1981) that the effect of *h/c* cannot be separated from that of the maximum aggregate size. Avram et al. suggest a maximum ratio of aggregate size to cube specimen side between 1/3 and 1/4.

The surprising conclusion that the column reinforcement reduces the joint effective strength contradicts other experimental results on columns, such as Razvi et al. (1992 and 1999), Attard et al. (1996), and Liu et al. (2000), that suggest the concrete effective strength is enhanced by the confinement provided by the reinforcement.

2.1.4 Kayani (1992)

Kayani tested 2 edge sandwich plates and 4 sandwich columns: two with ties and two without ties in the joint. The two edge specimens had twice as much vertical and lateral reinforcement as in the specimens of Gamble and Klinar (3.6% and 0.25% respectively). Kayani investigated the type of the specimen and the ratio of f'_{cc}/f'_{cs}.

Specimens were tested at ages between 42 and 99 days. Concrete strength for the columns ranged from 92.2 to 104.6 MPa. The slab concrete strength varied from 25.3 to 39.6 MPa. Only column load was applied to the specimens. Duration of tests ranged from 40 to 60 minutes.

All the specimens failed in the joint with crushing of the concrete and buckling of the vertical rebars. The outer rebars buckled in the edge specimens. The sandwich columns without ties in the joints failed suddenly in the joint with crushing of the concrete and buckling of the vertical rebars. The joint was completely destroyed once the peak load was reached; there was no ductile softening. For the sandwich columns with ties in the joints, spalling of the joint concrete was followed by a drop in the applied loads rather than sudden failure.

2.1.5 Ospina and Alexander (1997)

Results from testing 26 slab-column specimens and 4 sandwich columns were presented. The slab-column specimens were subjected either to column load or to column plus slab loads. Specimens were tested at ages between 17 and 54 days. Concrete strength for the columns ranged from 89 to 120 MPa. Strengths of the slab and unconfined concrete varied from 15 to 46 MPa. Duration of each test ranged from one to three and half hours.

The experimental program was divided into four series. Series A (12 interior specimens) examined the effect of slab loading. The levels of slab loading were based on strain criteria. Series B (8 interior specimens) examined the effect of changing *h/c*, column rectangularity, concrete strength, and slab loading that was based on finite element analysis. Specimen B3 had HSC core embedded in the joint region. Series C (6 edge specimens) examined the level of the slab load. Slab loads were applied and increased until readings from strain gauges averaged 1000 or 2000 με. Two sets of three specimens were built and tested. Each set had similar f'_{cc}/f'_{cs} and *h/c* values. Series D (4 specimens) modeled unconfined slab-column joints to examine the effect of *h/c* on f_{ce}.

The study concludes that f_{ce} decreases by increasing the floor load; heavily loaded slabs do not provide as much confinement as lightly loaded slabs; and that f_{ce} decreases by increasing *h/c*. The decrease in f_{ce} under the floor load increases by increasing the

ratio f'_{cc}/f'_{cs} or h/c. Floor loading appears to be less important at edge and corner column locations. Finally, high strength concrete in the joint increases f_{ce}.

This study highlights the need for reproduction and confirmation of the test data because of the dramatic scarcity of such results. The study recommends further testing of slab-column joints under realistic slab loading and under incremental slab loading. The study emphasizes the need of testing joints between slab-beam floors and columns with realistic load and boundary conditions. Finally, the study suggests an effort to be made to evaluate the effect of h/c and placement of HSC inside the joint.

2.2 Methods of Estimating the Joint Effective Strength

2.2.1 Bianchini, Woods and Kesler (1960)

In this study, the test results are presented graphically by plotting f_{ce}/f'_{cs}, against f'_{cc}/f'_{cs} where f'_{cc} represents the top or bottom column stub cylinder strength, whichever is lower. The effective strength is calculated from the ACI 318-56 design equation for short tied columns, as in equation 2.1, where $P_o = P_{col}$, the maximum column load applied in a test. Re-arranging terms and replacing the f'_{co} term by f_{ce} yields equation 2.2.

$$P_o = 0.85 f'_{co}\left(A_g - A_{st}\right) + f_y A_{st} \qquad [2.1]$$

$$f_{ce} = \frac{P_o - f_y A_{st}}{0.85\left(A_g - A_{st}\right)} \qquad [2.2]$$

The study concludes that under certain f'_{cc}/f'_{cs} values, the presence of the weaker slab concrete may reduce the axial compressive strength of the column. For interior columns, this critical value is equal to 1.5. When exceeding this ratio, only 75 % of the column concrete strength above 1.5 times the floor concrete strength may be effective in sustaining the column load. For edge and corner specimens, the critical ratio is 1.4 and no significant benefits may be obtained by increasing the column concrete strength beyond 1.4 times the floor concrete strength.

2.2.2 Gamble and Klinar (1991)

For f'_{cc}/f'_{cs} values less than 1.4, this study concludes that f_{ce} is equal to f'_{cc}. For higher ratios, f_{ce} is evaluated as follows:

$$f_{ce} = 0.67 f'_{cs} + 0.47 f'_{cc} \qquad \text{for interior columns} \qquad [2.3]$$

$$f_{ce} = 0.85f'_{cs} + 0.32f'_{cc} \quad \text{for edge columns} \quad [2.4]$$

Gamble and Klinar found that design provisions in ACI 318-89 overestimate the strength of joints in which the ratio f'_{cc}/f'_{cs} is large.

2.2.3 Shu and Hawkins (1992)

Equations 2.5 and 2.6 are proposed in the study by Shu and Hawkins to evaluate f_{ce} for edge and corner joints. The study concludes that the ACI 318-83 provisions are unconservative for edge and corner columns for values of f'_{cc}/f'_{cs} equal to or less than 1.4, and the ACI 318-83 provisions are unduly conservative for f'_{cc}/f'_{cs} values greater than 1.4. For interior columns, the study suggests that ACI design provisions may be unsafe for certain h/c and f'_{cc}/f'_{cs} values.

$$f_{ce} = f'_{cs} + A(f'_{cc} - f'_{cs}) \quad [2.5]$$

$$A = \frac{1}{(0.4 + 2.66h/c)} \quad [2.6]$$

2.2.4 Kayani (1992)

In addition to his test results, Kayani reprocessed the test results of Bianchini et al. and of Gamble and Klinar. His research suggests that sandwich column specimens adequately model corner slab-column joints. The study concludes that placing hoops in the joint increases its ductility rather than its axial load capacity. The study confirms the conclusion by Gamble and Klinar that the ACI 318-89 provisions overestimate f_{ce} for interior and edge columns intersected by floors made of weaker concrete, particularly when high values of f'_{cc}/f'_{cs} are considered.

The design equation suggested for estimating f_{ce} is of a different form than that adopted by Bianchini et al. or by Gamble and Klinar. The effective strength, f_{ce}, is suggested to be proportional to the ratio of the product of f'_{cc} and f'_{cs} to the sum of them, as indicated in equation 2.7.

$$f_{ce} = 2.0\lambda_G \frac{f'_{cc} f'_{cs}}{f'_{cc} + f'_{cs}} \quad [2.7]$$

where λ_G is a constant that depends on the joint type and is taken equal to 1.25, 1.0, and 0.9 for interior, edge, and corner joints respectively.

2.2.5 *Canadian Standard Association (CSA A23.3-94)*

Section 10.12 of the 1994 Canadian standard addresses the transmission of column loads through concrete floors as follows:

When f'_{cc} is greater than f'_{cs}, transmission of the load through the floor system shall be done in one of two ways. The first is concrete puddling, where concrete of the column is placed in the joint and the top surface of that concrete is extended at least 500 mm into the floor from the face of column. The second is adding vertical dowels, spirals, or hoops to increase f_{ce}. The value of f_{ce} is taken equal to f'_{cc} if the ratio f'_{cc}/f'_{cs} is less than or equal to 1.4, 1.4 and 1.0 for interior, edge and corner columns respectively. Above the limiting values of f'_{cc}/f'_{cs}, f_{ce} is calculated using equations 2.8 to 2.10 and in no case is taken bigger than f'_{cc}.

$$f_{ce} = 1.05f'_{cs} + 0.25f'_{cc} \quad \text{for interior columns} \quad [2.8]$$

$$f_{ce} = 1.4f'_{cs} \quad \text{for edge columns} \quad [2.9]$$

$$f_{ce} = f'_{cs} \quad \text{for corner columns} \quad [2.10]$$

2.2.6 *Ospina and Alexander (1997)*

The study supports the design equation for edge columns given by CSA A23.3-94 and by ACI 318-95 and proposes a design limit of a f'_{cc}/f'_{cs} value of 1.2 for the case of corner columns. For interior joints, the study proposes equation 2.11 to estimate f_{ce}.

$$f_{ce} = \left(1.4 - \frac{0.35}{h/c}\right) f'_{cs} + \frac{0.25}{h/c} f'_{cc} \quad [2.11]$$

Equation 2.11 matches the expression given in CSA A23.3-94 for $h/c = 1$, while it matches the expression given in ACI 318-95 for h/c=1/3, the minimum allowable value. To account for column rectangularity, c is defined as the shorter column dimension. Test-to-predicted f_{ce} using the proposed equation are substantially less scattered and on average closer to unity than when using the existing design-standards at that time.

2.2.7 *Committee 318, ACI (ACI 318M-02)*

The design provisions given in ACI 318M-02 regarding transmission of column loads through concrete floors are, in essence, the same as those originally adopted since

the ACI 318-63 code; they are based on the results of Bianchini et al. (1960) on unloaded slabs. The design provisions read as follows:

> *When the specified compressive strength of concrete in a column is greater than 1.4 times that specified for a floor system, transmission of load through the floor system shall be provided by one of three solutions:*
>
> *10.15.1 Concrete of strength specified for the column shall be placed in the floor at the column location. Top surface of the column concrete shall extend 600 mm into the slab from face of column. Column concrete shall be well integrated with floor concrete, and shall be placed in accordance with 6.4.5 and 6.4.6.*
>
> *10.15.2 Strength of a column through a floor system shall be based on the lower value of concrete strength with vertical dowels and spirals as required.*
>
> *10.15.3 For columns laterally supported on four sides by beams of approximately equal depth or by slabs, it shall be permitted to base strength of the column on an assumed concrete strength in the column joint equal to 75 percent of column concrete strength plus 35 percent of floor concrete strength. In the application of 10.15.3, the ratio of column concrete strength to slab concrete strength shall not be taken greater than 2.5 for design.*

The limit of 2.5 in item 10.15.3 is based on the work done by Ospina and Alexander (1998). Because loaded slabs do not provide as much confinement as unloaded slabs, item 10.15.3, without the 2.5 limit, tends to overestimate the joint strength. The overestimate becomes significant for large values of f'_{cc}/f'_{cs}.

2.3 Modeling the Behaviour of Concrete

Many models have been proposed in literature including Kent and Park (1971), Sheikh and Uzumeri (1982), Mander et al. (1988), Yong et al. (1988), Cusson et al. (1995), Attard et al. (1996), Bing et al. (2001), Cheong et al. (2002), and Harries et al. (2002). Only the first four mentioned models were used in this study for their common use as references in the later studies and for their simplicity.

2.3.1 Kent and Park (1971)

This paper presents figure 2.1 as a good representation of the stress-strain relation for unconfined or confined concrete based on the existing experimental evidence of that time. Part AB is a parabola determined by equation 2.12, in which f_c is the stress at any strain value ε_c. The falling branch of the curve is assumed to be linear and shown in the figure as part BC. The concrete stress at any point on the line BC is estimated by equation 2.13 in which the slope z is obtained from equation 2.14 by defining the strain values ε_{50h} and ε_{50u} when the concrete stress falls to 50% of its maximum value. The strain ε_{50h} can be defined as in equation 2.15 and can be obtained using equation 2.16. The strain ε_{50u} can be obtained as in equation 2.17, which is given in U.S. customary units, stresses are in lb/in^2. Region CD in the figure is horizontal assuming that the concrete can sustain a stress equal to 20% of its maximum stress.

$$f_c = f'_{co}\left[\frac{2\varepsilon_c}{\varepsilon_{co}} - \left(\frac{\varepsilon_c}{\varepsilon_{co}}\right)^2\right] \qquad [2.12]$$

$$f_c = f'_{co}\left[1 - z(\varepsilon_c - \varepsilon_{co})\right] \qquad [2.13]$$

$$z = \frac{0.5}{\varepsilon_{50h} + \varepsilon_{50u} - \varepsilon_{co}} \qquad [2.14]$$

$$\varepsilon_{50h} = \varepsilon_{50c} - \varepsilon_{50u} \qquad [2.15]$$

$$\varepsilon_{50h} = \frac{3}{4}\rho''\sqrt{\frac{B + d''}{s}} \qquad [2.16]$$

$$\varepsilon_{50u} = \frac{3 + 0.002 f'_{co}}{f'_{co} - 1{,}000} \qquad [2.17]$$

where f'_{co} is the cylinder strength. ε_{50c} and ε_{50u} are the strains at $0.5 f'_{co}$ on falling branch for confined and unconfined concretes respectively. ε_{50h} is the increase in concrete strain at $0.5 f'_{co}$ on falling branch due to ties. ρ'' is the volumetric ratio of ties. B and H are the center to center distances of the perimeter ties. d'' is tie-diameter. s is the tie spacing.

The paper assumes that the confining steel has no effect on the shape of part AB. This is based on previous studies showing that lateral strain that will cause the hoops to be significantly stressed occurs only when the maximum concrete stress is almost

reached. It is also assumed that the maximum stress reached by both unconfined and confined concrete is the same equal to f'_{co}. The strain at f'_{co} is assumed as ε_{co}=0.002, a commonly accepted assumption for unconfined concrete.

2.3.2 Sheikh and Uzumeri (1982)

Sheikh and Uzumeri propose a model based on tests of 24 concrete columns as well as test results from literature. The strength of the confined concrete is calculated using the concept of an effectively confined concrete area, within the nominal concrete core, as follows:

$$A_{co} = B \times H \qquad [2.18]$$

$$A_c = \zeta \times A_{co} \qquad \text{at tie level} \qquad [2.19]$$

$$\zeta = 1 - \frac{\sum_{1}^{n} C_i^2}{\alpha A_{co}} \qquad [2.20]$$

$$A_{ce} = \zeta (B\text{-}0.5\ s \tan\theta)\ (H\text{-}0.5\ s \tan\theta) \qquad [2.21]$$

where A_{co} and A_c are the core area and effective area at tie level. B and H are the center to center distance of perimeter tie of rectangular core. A_{ce} is the effectively confined core area at the critical section between ties. ζ is ratio of the effectively confined concrete area to the core area at tie level. C_i is the center to center distance between longitudinal bars. (n) is the number of arcs between longitudinal rebars. α is constant depending on the exact shape of the arc. $\sum Ci^2/\alpha$ is the unconfined area between longitudinal bars. (s) is the tie spacing. θ is angle of the curve separating the tension and compression zones (confined and unconfined areas between tie levels). The factors α and θ are constants; θ is observed to be 45° and α is taken as 5.5 based on a regression analysis over the tested 24 columns.

The stress-strain model, shown in figure 2.2, consists of three parts: part OA is a 2nd degree parabola with point A (f_{ce}, ε_{s1}); part AB is a horizontal line with B (f_{ce}, ε_{s2}); and part BCD is the descending part that can be identified by either determining point C ($0.85f_{ce}$, ε_{s85}) or the descending slope, z, in addition to point B. The value f_{ce} represents the compressive strength of the confined concrete in the specimen and is given by equations 2.22 and 2.23.

$$f_{ce} = k_s f'_{co} \quad [2.22]$$

$$k_s = 1 + \frac{A_{ce}}{P_{occ}} \beta (\rho'' f''_y)^{\gamma} \quad [2.23]$$

Where: k_s is the strength coefficient including enhancement because of lateral confinement. f_{co} is the compressive strength of the concrete in plain specimen. P_{occ} is the nominal capacity of the concrete section in kN.

The factors γ, and β are constants determined from the regression analysis over the 24 columns and are found to be γ=0.5, and β=0.0071 for metric units. So, equation 2.23 is rewritten as 2.24 and 2.25.

$$k_s = 1 + \frac{A_{ce}}{140 P_{occ}} (\rho'' f''_y)^{0.5} \quad [2.24]$$

$$k_s = 1 + \frac{B^2}{140 P_{occ}} [(1 - \frac{nC^2}{5.5B^2})(1 - \frac{s}{2B})^2](\rho'' f''_y)^{0.5} \quad [2.25]$$

$$\varepsilon_{s1} = 80 k_s f_{co} * 10^{-6} \quad [2.26]$$

$$\frac{\varepsilon_{s2}}{\varepsilon_{co}} = 1 + \frac{248}{C}[1 - 5(\frac{s}{B})^2] \frac{\rho'' f''_y}{\sqrt{f'_{co}}} \quad [2.27]$$

Equation 2.28 is suggested for the slope (z) of the unloading part BCD. The slope can be replaced by the strain value corresponding to 0.85 (ε_{s85}) times the maximum concrete stress, which is calculated as in equation 2.29.b.

$$z = \frac{0.5}{\frac{3}{4}\rho'' \sqrt{\frac{B}{s}}} \quad [2.28]$$

$$\varepsilon_{s85} = \frac{0.15}{z} + \varepsilon_{s2} \text{ or} \quad [2.29.a]$$

$$\varepsilon_{s85} = 0.225 \rho'' \sqrt{\frac{B}{s}} + \varepsilon_{s2} \quad [2.29.b]$$

2.3.3 Mander, Priestly and Park (1988)

Mander et al. (1988) propose a unified stress-strain approach for confined concrete. The model is applicable to both circular and rectangular NSC columns and provided with lateral reinforcement. The model, originally proposed by Popovics (1973),

was compared with results of forty concentric axial compression tests on columns. The variables studied were the column shape, arrangements of longitudinal and transverse reinforcement, and yield strength of the reinforcement. For a nearly-static strain rate and monotonic loading, the effective concrete strength f_{ce} is determined in Mander et al. as:

$$f_{ce} = f'_{co}\left(-1.254 + 2.254\sqrt{1 + \frac{7.94 f_l}{f'_{co}}} - 2\frac{f_l}{f'_{co}}\right) \quad [2.30]$$

$$f_l = \frac{1}{2} k_s \rho'' f''_y \quad [2.31]$$

$$k_s = \frac{(1 - \frac{\sum_{1}^{n} C_i^2}{6BH})(1 - \frac{s}{2B})(1 - \frac{s}{2H})}{(1 - \rho)} \quad [2.32]$$

where f'_{co} is the cylinder concrete strength; f_l is the lateral confining stress because of the lateral reinforcement that has a yield strength of f''_y; ρ'' is the ratio of transverse reinforcement volume to volume of confined core; ρ is the ratio of vertical reinforcement area to area of core; k_s is the confinement effectiveness coefficient; C_i is the clear spacing between longitudinal bars; s is the clear spacing between hoop bars; and B and H are core dimensions to centerline of perimeter hoop. Stresses are in MPa.

As seen from the strength model given by equations 2.30 to 2.32, the effect of the various types of confinement is considered and is dependent on the configuration of longitudinal and lateral reinforcement. The stress-strain curve shown in figure 2.3 is modeled by the following equations:

$$f_c = \frac{f_{ce} x r}{r - 1 + x^r} \quad [2.33]$$

$$x = \frac{\varepsilon_c}{\varepsilon_{sl}} \quad [2.34]$$

$$r = \frac{E_c}{E_c - E_{sec}} \quad [2.35]$$

$$E_c = 5000\sqrt{f'_{co}} \quad [2.36]$$

$$E_{sec} = f'_{ce} / \varepsilon_{sl} \quad [2.37]$$

$$\varepsilon_{sl} = \varepsilon_{co}\left[1 + 5\left(\frac{f_{ce}}{f'_{co}} - 1\right)\right] \quad [2.38]$$

Where: f_c is the concrete stress at any strain value ε_c; ε_{sl} is the concrete strain corresponding to the effective concrete strength; and ε_{co} is the strain corresponding to the cylinder strength f'_{co}. A similar model was proposed by Carreira and Chu (1985) except that r was defined as:

$$r = \frac{1}{1 - f_{ce}/(\varepsilon_{sl}.E_c)} \qquad [2.39]$$

According to Mander et al., numerous tests carried out by different investigators on nearly full size specimens conclude the confinement is improved if: the transverse reinforcement is placed at relatively close spacing; additional supplementary ties are included; the longitudinal rebars are well distributed around the perimeter; and tie volumetric ratio or tie yield strength is increased.

2.3.4 Yong, Nour and Nawy (1988)

The model by Yong et al. (1988) is based on results of 18 tests of reinforced concrete columns and 6 plain concrete columns of dimensions 152x152 mm loaded concentrically until failure. The compressive strength of the concrete ranged from 83.6 to 93.5 MPa. An empirical strength model is proposed as f_{ce} is equal to $k_s * f'_{co}$, where k_s and f'_{co} are the effective confinement and the concrete cylinder strength respectively. The expression for k_s, originally suggested by Sargin (1971) and modified by Vallenas et al. (1977), is shown in equation 2.40. Stress unit is (psi).

$$k_s = 1 + 0.0091(1 - \frac{0.245s}{h''})(\rho'' + \frac{nd''}{8sd}\rho)\frac{f''_y}{\sqrt{f'_{co}}} \qquad [2.40]$$

where s is the center to center spacing between ties in inches, h'' is length of one side of the rectangular ties in inches, n is number of longitudinal steel bars, d'' is nominal diameter of ties in inches, d is nominal diameter of longitudinal rebars in inches, ρ'' is volumetric ratio of lateral reinforcement, ρ is reinforcement ratio of the longitudinal reinforcement and f''_y is yielding stress of the lateral steel in psi.

An empirical model for the stress-strain curve of the confined concrete is proposed in figure 2.4. Parameters of the curve are: the peak stress and strain (f_{ce}, ε_{sl}); the inflection stress and strain on the descending branch (f_i, ε_i); and the stress and strain (f_{2i},

ε_{2i}) at an arbitrarily selected point on the descending branch. An expression was developed to predict the strain at maximum stress.

$$\varepsilon_{s1} = 0.00265 + 0.0035[1 - 0.734s/h"](\rho" f"_y)^{2/3} / \sqrt{f'_{co}} \quad [2.41]$$

$$f_i = f_{ce}[0.25(\frac{f'_{co}}{f_{ce}} + 0.4)] \quad [2.42]$$

$$\varepsilon_i = k_s[1.4(\frac{\varepsilon_{ce}}{k_s}) + 0.0003] \quad [2.43]$$

$$f_{2i} = f_{ce}[0.25(\frac{f_{ce}}{1000}) - 0.065] \geq 0.3 f_{ce} \quad [2.44]$$

The empirical model consists of two polynomial equations: equation 2.45 is used for the ascending branch up to the peak stress value, and equation 2.46 is used for the descending branch.

$$Y = \frac{AX + BX^2}{1 + (A-2)X + (B+1)X^2} \qquad \varepsilon_c \leq \varepsilon_{s1} \quad [2.45]$$

$$Y = \frac{CX + DX^2}{1 + (C-2)X + (D+1)X^2} \qquad \varepsilon_c \geq \varepsilon_{s1} \quad [2.46]$$

where: $Y = f_c/f_{ce}$, $X = \varepsilon_c/\varepsilon_{s1}$, $A = E_c\,\varepsilon_{s1}/f_{ce}$, $B = [(A-1)^2/0.55] - 1$, $E_c = 27.55 w^{1.5} f'^{0.5}_{co}$, $C = [(\varepsilon_{2i} - \varepsilon_i)/\varepsilon_{s1}]\{[\varepsilon_{2i} E_i/(f_{ce} - f_i)] - [4\varepsilon_i E_{2i}/(f_{ce} - f_{2i})]\}$, $E_i = f_i/\varepsilon_i$, $E_{2i} = f_{2i}/\varepsilon_{2i}$, $D = (\varepsilon_i - \varepsilon_{2i})\{[E_i/(f_{ce} - f_i)] - [4E_{2i}/(f_{ce} - f_{2i})]\}$, and f_c and ε_c are the concrete stress and strain respectively.

The predicted stress-strain behaviour matches the observed in the tests. The maximum stress, its corresponding strain and strain values of the descending branch of the stress-strain curve of the concrete core increases with increasing the amount of lateral confinement. Increasing the number of longitudinal bars and distributing them around the core perimeter increases the effectiveness of the confinement of the concrete core. Spalling of the concrete cover does not seem to affect the percentage increase in the strength of the concrete core, but it does reduce the ductility of the core. Tie strain may or may not reach its yield point at the maximum core stress in some specimens. Lateral confinement of high-strength-concrete by ties does improve the general behaviour of concrete such that failure of the confined concrete specimens is ductile. The study did not recommend the use of lateral steel with yield stress higher than 500 MPa.

2.3.5 *Lokuge, Setunge, Mendis and Sanjayan (2002)*

Lokuge at al. (2002) use a triaxial constitutive model to model the behaviour of a joint between NSC slab and an interior HSC column using an iterative procedure. The model can be used to predict both axial and lateral stress-strain behaviour under triaxial conditions. The failure stress can be obtained for the loaded slab by considering the stress-gradient applied on the column in calculating the confining pressure.

$$\varepsilon_1 = \frac{f_c - v^a(F_r + F_r)}{Es}, \text{ perhaps there is a typo in the reference} \quad [2.47]$$

$$\varepsilon_2 = \frac{F_r - v^a(F_r + f_c)}{E_s} \quad [2.48]$$

$$v^a = v_i^a \quad \text{if } \beta \le \beta, \text{ perhaps another typo} \quad [2.49.a]$$

$$v^a = (v_f^a - v_i^a)\sqrt{1-(\frac{\beta-\beta_l}{1-\beta_l})^2} \quad \text{if } \beta > \beta_l \quad [2.49.b]$$

$$\beta = \frac{f_c}{f_{ce}} \quad [2.50]$$

$$\beta_l = 0.7 \quad \text{if } f'_{cs} \le 40 \text{ MPa} \quad [2.51.a]$$

$$\beta_l = 0.7 + 0.005(f'_{cs} - 40) \quad \text{if } 40 < f'_{cs} \le 60 \text{ MPa} \quad [2.51.b]$$

$$\beta_l = 0.8 \quad \text{if } f'_{cs} > 60 \text{ MPa} \quad [2.51.c]$$

$$v^a{}_i = 8*10^{-6}(f'_{cs})^2 + 0.0002f'_{cs} + 0.138 \quad \text{Active confinement} \quad [2.52.a]$$

$$v^a{}_i = 0.15 \quad \text{Passive confinement} \quad [2.52.b]$$

$$v^a{}_f = 0.5 \quad [2.53]$$

$$v^a{}_d = 0.5 + 1.29\sqrt{1-\beta} \quad \text{Active confinement} \quad [2.54.a]$$

$$v^a{}_d = 0.5 + 2.43\sqrt{1-\beta} \quad \text{Passive confinement} \quad [2.54.b]$$

$$E_s = \frac{1}{2}E_i - \beta(\frac{1}{2}E_i - E_f) \pm \sqrt{[\frac{1}{2}E_i - \beta(\frac{1}{2}Ei - E_f)]^2 + E_f^2\beta[D(1-\beta)-1]} \quad [2.55]$$

$$E_f = \frac{E_c}{1 + 2.5\frac{Eo}{Ec}\left(\frac{(\sqrt{J_2})_f}{f'_c} - \frac{1}{\sqrt{3}}\right)} \quad [2.56]$$

$$D = -31(\frac{F_r}{f'_{cs}})^2 + 19.3(\frac{F_r}{f'_{cs}}) - 0.1 \quad [2.57]$$

Where: f'_{cs}= strength of unconfined concrete, f_c= axial stress, F_r= effective lateral confining pressure, v^a= secant value of Poisson's ratio for the ascending branch, v^a_d= secant value of Poisson's ratio for the ascending branch, E_s= secant value of Young's modulus, $\varepsilon_1$and ε_2 =axial and lateral strain respectively, β = nonlinearity index, E_i = initial Young's modulus, E_f= secant value of Young's modulus at peak stress, E_o, E_c= initial and peak uniaxial secant value of Young's modulus respectively, J_{2f}= invariant at failure, and D = a parameter added to fit the post peak shape of the curve.

The model is validated against behaviour of some of the A-series interior-specimens tested by Ospina and Alexander (1997). Experimental and theoretical curves are in good match in terms of general shape and peak load. The ascending branches of the theoretical curves are steeper than those from experiments.

The model by Lokuge at al. (2002) distinguishes between cases of active and passive confinement without giving instructions of how to define them to be used in the model.

2.3.6 Discussion of the Available Analytical Models

There is no analytical model for predicting the strength or stress-strain behaviour of an edge-joint or a corner joint. All available models were developed for columns, except the model by Lokuge et al., which is designed to model the behaviour of interior joints.

The stress-strain model by Kent and Park (1971) neglects the increase in concrete strength but accounts for the increase in post-peak ductility due to ties.

According to the models by Sheikh and Uzumeri (1982) and by Yong et al. (1988), more uniform distribution of the vertical rebars and smaller tie spacing result in higher strength and ductility. The advantage of the model by Yong et al. over that by Sheikh and Uzumeri is in accounting for not only the volumetric ratio of the column reinforcement but also for arrangement of the reinforcement inside the column. This is shown by using the form ($\rho''+\rho nd''/8sd$) instead of using ρ''. Equation 2.21 by Sheikh and Uzumeri for calculating the effectively confined area may lead to underestimation of the effective strength of the concrete for sections without ties by overlooking other confining factors such as the vertical rebars.

The advantage of the model by Sheikh and Uzumeri (1982) over that by Yong et al. (1988) is in accounting for the distribution of vertical rebars on the effectively confined area. Both models can be criticized for failing to account for yield strength of the vertical rebars and for presuming the ties will yield. In addition, the model by Yong et al. implies that the longer the tie, the better its confining effect. This might be true for small column sections. For large column dimensions, ties bulge out under the lateral pressure.

The unloading part as proposed by Mander et al. (1988) is based on first hoop rupture and does not describe the behaviour for other modes of failure. The equation proposed by Sheikh and Uzumeri to determine the slope of the descending branch leads to a vertical line with no ties provided. That would mean a complete sudden collapse not verified by experimental results. Even for unconfined/lightly confined HSC sections, the descending stress-strain relation is steep but not vertical, indicating low toughness, low ductility, and rapid loss of resistance after reaching the maximum strength. James et al. (2001) show that an increase in the confinement ratio decreases the slope of the descending branch regardless of the concrete compressive strength.

2.4 Lateral expansion of High Strength Concrete

According to Chen, W.F. (1982), Poisson's ratio ranges from 0.15 to 0.22 for normal-strength concrete until approximately 80% of the maximum strength, at which point the ratio starts to increase. For high-strength concrete, Ahmad and Shah (1987) conclude that Poisson's ratio seems compatible with the expected range of values for normal strength concrete in the elastic range (0.18-0.24), and it is likely to be lower in the inelastic range because of the smaller relative increase in lateral strains for high-strength concrete due to less micro-cracking, specially in the post peak region.

Table 2.1 Main Variables Found in the Specimens Tested in the Literature

Reference	Specimen Type	Column Width (mm)	Floor Thickness (mm)	Column Strength (MPa)	Floor Strength (MPa)	Vertical Reinforcement		
						Yield Strength (MPa)	Ratio (%)	Diameter (mm)
Ospina and Alexander	IJ	175-250	100-250	89-120	15-46	400	1.3-4.0	16
	EJ	230	170-230	107-108	31-35	400	3.0	16
	SC	250	75-250	105-107	17	400	1.3	16
Shu and Hawkins	SC	152	25-458	39-51	7-49	439-501	1.2	9.5
Kayani	SC and EJ	254	178	89-104	25-40	414	1.8-3.6	19
Gamble and Klinar	IJ	254	127-178	72-97	17-43	486	1.8	19
	EJ	254	127-178	79-96	16-46	486	1.8	19
Bianchini et al.	IJ	279	178-508	23-51	12-24	259-323	1.5	19
	EG	279	178-508	13-52	10-24	294-322	1.5	19
	CJ	279	178	16-52	9-25	294-319	1.5	19
	SC	279	178	21-37	14-15	299-333	1.5	19

Floor thickness includes thickness of the slab, drop panels and beams if any.

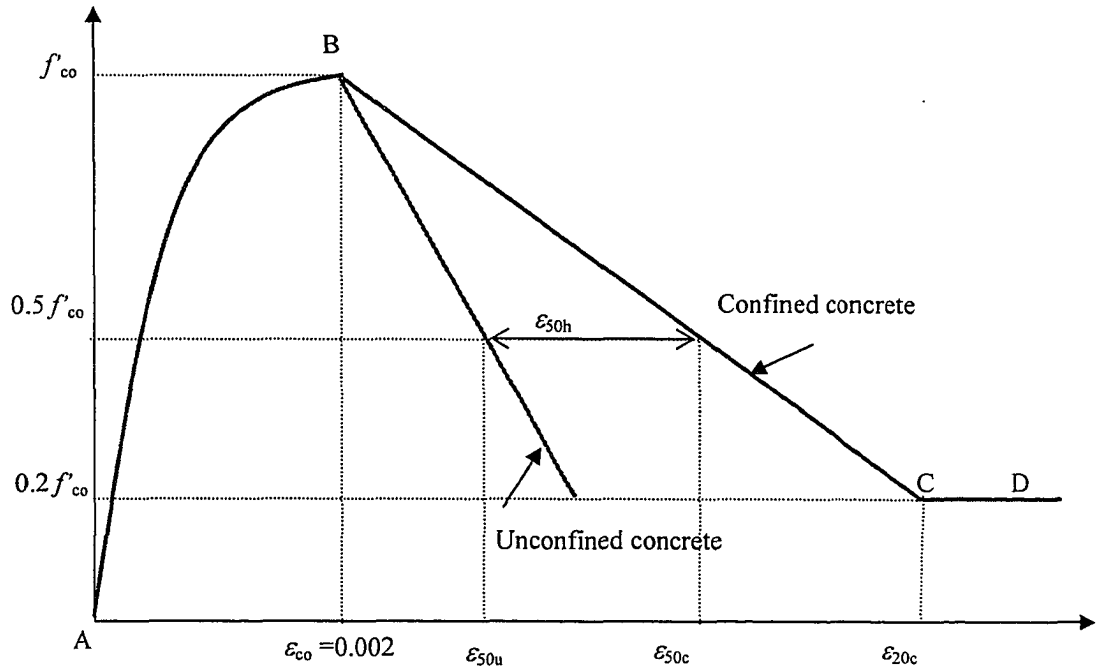

Figure 2.1. Stress-Strain Model by Kent and Park (1971) for Unconfined and Confined Concretes

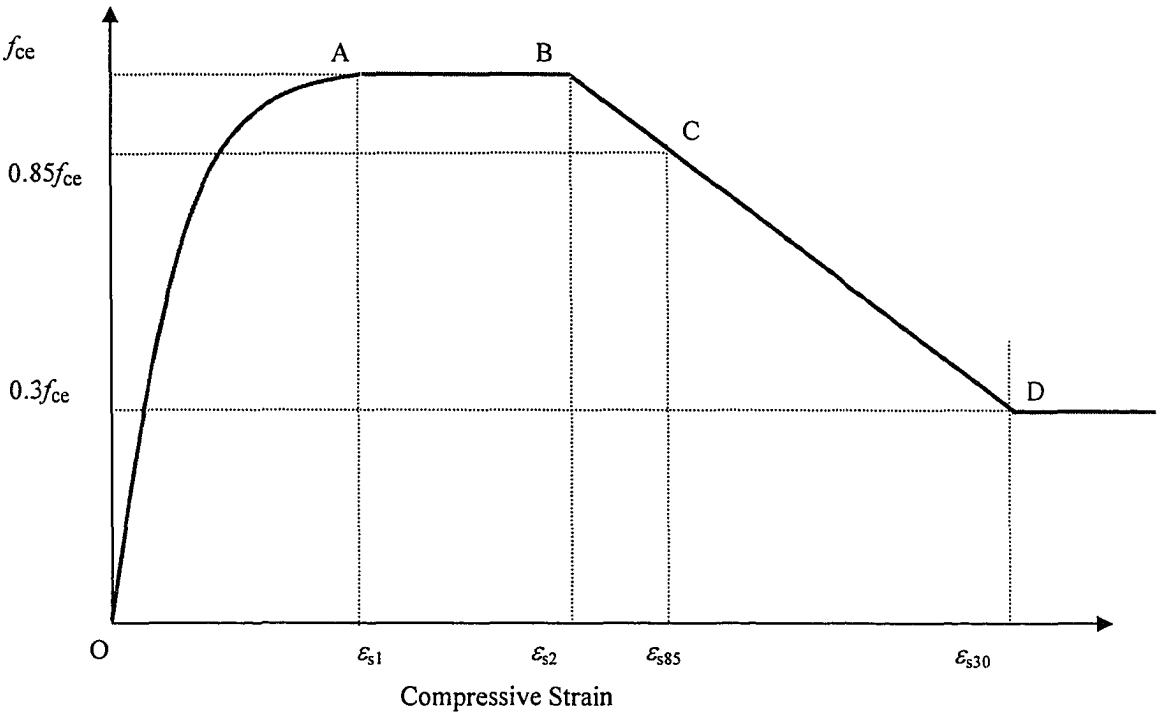

Figure 2.2. Stress-Strain Model by Sheikh and Uzumeri (1982) for Monotonic Loading for Confined Concrete

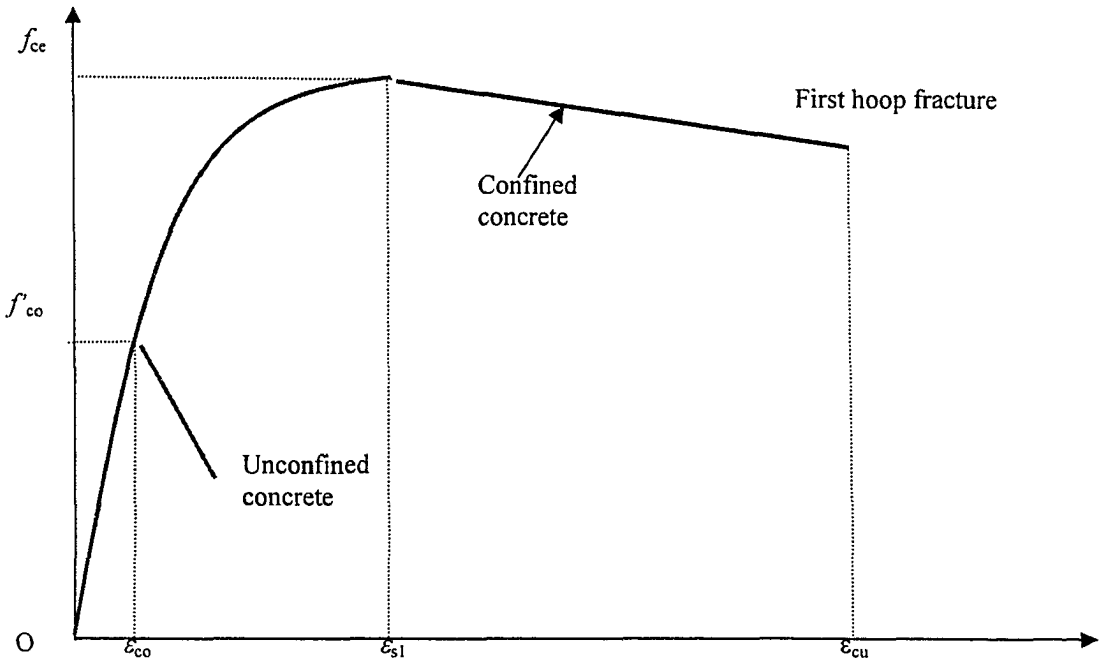

Figure 2.3. Stress-Strain Model by Mander at al. (1988) for Monotonic Loading for Confined Concrete

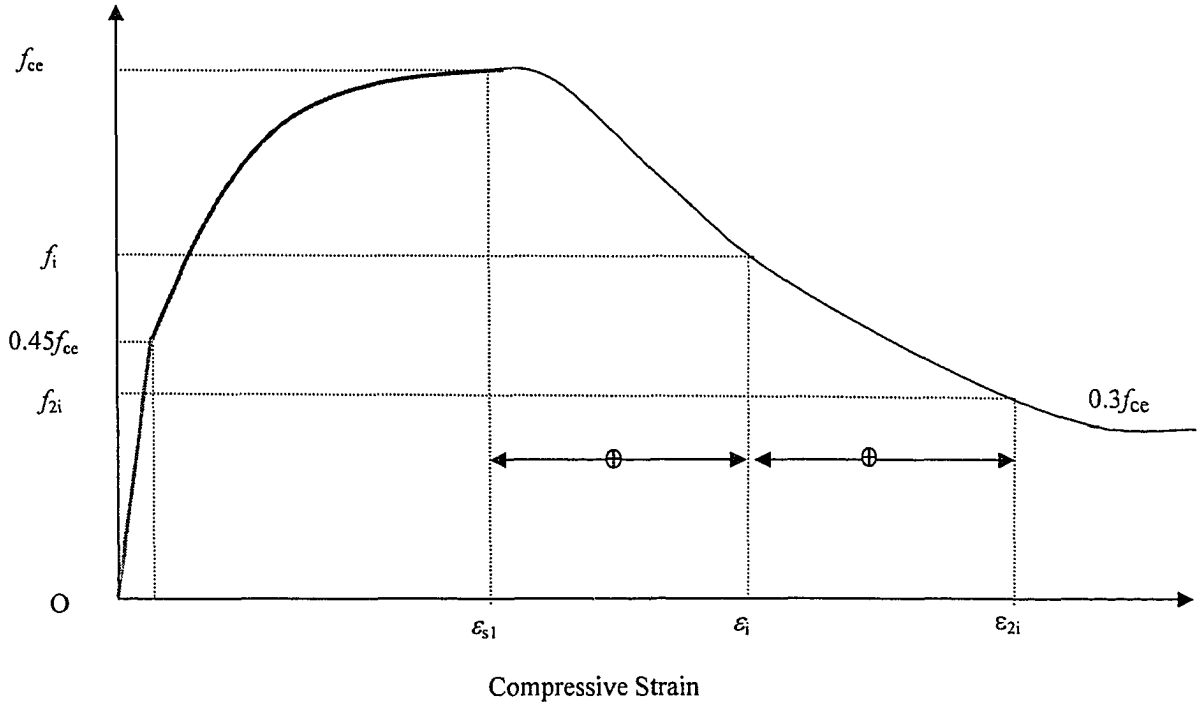

Figure 2.4. Stress-Strain Model by Yong at al. (1988) for Monotonic Loading for Confined Concrete

3 SPECIMEN PREPARATION AND TESTING

3.1 Introduction

This chapter covers specimen design and outlines the variables studied in this research. The chapter covers also fabrication and instrumentation of the specimens.

3.2 Specimen Design

The confinement provided by the floor to the joint depends on the joint type and the surrounding floor system. The top reinforcement of the floor, which is in most cases flexurally continuous, is actively pulling the joint apart; a critical case for an interior joint in a flat-plate system. Conversely, the bottom reinforcement and the floor concrete are adding more confinement to the joint. For a corner joint or an edge joint, bottom of the joint is under biaxial compression state that accelerates the dilation of the concrete in the unconfined direction.

To combine the entire confining problems- related to the intervening floors- in a single joint type, an interior joint between a column and a floor made of one-way slab and unidirectional beams is used in this research. The beam spans along the column longer dimension and the joint is unconfined perpendicular to the axis of the beam. From the design perspective, this joint has very poor confinement and so it has the most to gain from any strengthening technique. From a testing point of view, the joint is convenient because the floor loading can be applied symmetrically around the column. While an edge or corner column presents a similar lack of confinement to the joint, applying a floor load to such a specimen introduces asymmetry around the column. Testing edge or corner columns, therefore, would result in complications to the testing frame. Finally, there are no other tests of joints between high strength concrete (HSC) columns and one-way slab-beam floors.

The panel dimensions of the prototype structure under investigation are 4200 and 9600 mm with a 150mm-slab. The beam dimensions are 375 and 540 mm and the

columns are 375 and 525 mm. The different elements were designed according to the CSA A23.3-94 provisions. The design was based on a mean cylinder strength of floor concrete (f'_{cs}) of 20 MPa, a mean cylinder strength of column concrete (f'_{cc}) of 80 MPa, and elastic perfectly plastic reinforcing steel with a mean value of yield strength of 400 MPa. The column dimensions were determined based on the column concrete strength assuming the joint of bigger effective strength.

Sizing of the test specimens required a compromise between two opposing constraints: testing large cross sections for meaningful results and capacity of the testing machine needed to test such specimens to failure. With a two thirds reduction factor, the scaled-down structure, seen in figure 3.1, has panel dimensions of 2800 and 6400 mm with 100mm-slab. The beam dimensions are 250 x 360 mm and the columns are 250 x 350 mm. Figure 3.2 shows a typical specimen that has floor dimensions 1400 x 3350 mm, encircled by the points of contra flexure. The top and bottom columns were made long enough to create two segments free of boundary effects to ensure uniform and natural stress in such zones.

3.3 Main Differences in Fabrication of Specimens

All seven specimens tested in this research were identical in dimensions and reinforcement details with a few differences related to type of concrete inside the joint and debonding the beam top reinforcement through the joint. As for the joint concrete: it was either of normal strength, cast with the floor, or of high strength, cast with the top column. As shown in figure 3.2, area of HSC inside the joint was 74% of the joint cross-sectional area. This was achieved by blocking out the floor concrete from the core of the joint region. The blocked out region was filled in later when the top column was cast.

Table 3.1 shows matrix of the variables tested in this research. Specimens SP1 and SP2 had normal strength concrete (NSC) joints with bonded beam reinforcement; SP3 and SP4 had HSC cores in the joints with bonded beam reinforcement; SP5 and SP6 had NSC joints with the top beam reinforcement partially debonded within the joint using PVC pipes; and SP7, the control specimen, was made of NSC columns with bonded beam reinforcement. The loading type in table 3.1 will be discussed in chapter 4.

3.4 Materials and Specimen Preparation

3.4.1 Reinforcement

3.4.1.1 Material

Four different reinforcement sizes were used for preparing the specimens. M15 deformed bars of Grade G30.12 M 400 were used for beam and column main reinforcement. The M15 rebar for SP7 came from a different heat. M10 deformed bars of Grade G30.12 M 400 were used for beam stirrups and column ties. Bars having diameter of 9 mm were used for the slab top reinforcement. Bars with diameter of 6 mm were used as crack control rebars on sides of the beam, for slab bottom reinforcement, and for slab secondary reinforcement.

The yield and ultimate strengths of all reinforcement, summarized in table 3.2, were established by tension tests according to ASTM A370-94. Tension coupon tests were performed on three 14-inch long samples from each heat. Each sample was instrumented with an extensometer of 2-inch gauge length and two foil strain gauges-mounted on opposite sides of the coupon. Figures 3.3 to 3.7 show typical stress-strain curves for each type of reinforcement steel. The loading was stopped at two intervals, during yield and near the maximum load, to obtain the static yield strength and the static ultimate tensile strength.

3.4.1.2 Cages

Reinforcement for each specimen consisted of two cages: floor cage, figure 3.8, and column cage, figure 3.9. Plastic chairs were placed outside the test regions as shown in photos in appendix A. Column rebars were welded to a thick base plate. Column ties were composed of an outer rectangular tie and an inner diamond-shape one. This configuration is convenient for research because it provides un-congested column core to facilitate casting and vibrating the concrete without damaging the internal instrumentation. Spacing between the two ties right below the beam was half that in the test region to avoid getting failure due to an interactive response of the joint and bottom column. Thus, failure of the joint would be independent of the bottom column behaviour and failure of the bottom column would be independent of the joint behaviour. Stresses

from handling and storing of the specimens were checked and found within the elastic range.

3.4.2 Concrete

3.4.2.1 Ingredients and Mix Proportions

Two types of cement were used in concrete mixtures. Normal Portland cement CSA type 10 was used for the 20 MPa mixtures while high-early-strength Portland cement CSA type 30 was used for the 80 MPa mixtures. The sand and the coarse aggregates used in making the mixtures were taken from a local pit; one size distribution (5-14 mm) crushed coarse aggregates was used. Super plasticizer was used in all the mixtures while silica fume was used only in the 80 MPa mixtures.

Preparation of the concrete mixtures and curing of the fresh concrete was done in accordance with CSA test methods A23.2. While a commercial ready-mix plant supplied the floor concrete mixtures, the column concrete mixtures were developed through trial batching. Table 3.3 shows typical mix design for HSC.

The column concrete was made in a nine cubic-foot mixer. After washing the mixer, the materials were charged in the order: sand, cement, silica fume, water and super plasticizer. These materials were mixed together for three to five minutes before adding the coarse aggregates. Mixing time after adding the coarse aggregates was five to ten minutes.

3.4.2.2 Casting

Concrete was placed into the forms after a slump test was performed. Slump values of the fresh concretes ranged from 70 to 100 mm. Column and floor concretes were consolidated using a pencil vibrator. A total of eight 4-inch control cylinders were made from each high-strength-concrete mixture and were consolidated using a vibrating table. For normal-strength-concrete, eight 6-inch cylinders and two 4-inch cylinders were made and consolidated using a steel rod.

For the nominal characteristics, half the control cylinders were moist-cured and tested at an age of 28 days. The remaining cylinders were field-cured alongside the specimens and tested concurrently with them.

3.4.2.3 Curing

Exposed surfaces of the fresh concrete, in forms and cylinders, were covered with plastic sheets 3-4 hours after casting. Stripping of the column forms was done 48 hours after casting. The columns and their cylinders were wrapped with plastic sheets for three more days. The floors and their cylinders were kept covered till stripping of the forms, one week after casting.

3.4.2.4 Cylinder Testing

Table 3.4 shows the compressive strength of the control cylinders tested on the 28^{th} day age and on the day of testing each specimen, which varied from 34 to 171 days. Normal-strength-concrete cylinders were capped with molten sulphur while high-strength-concrete cylinders were faced, using a grinder and a lathe, to ensure flat surfaces perpendicular to the cylinder axis. Field and moisture-cured cylinders achieved almost the same strength.

Figures 3.10 and 3.11 show typical stress-strain curves obtained by testing the control cylinders under compression. With the applied control system, it was possible to obtain smooth and continuous descending branches. In addition to its higher strength, high-strength concrete showed stiffer loading curve and steeper unloading branch as compared to NSC. Cracks appeared first in central region of the cylinders and propagated into the end zones. Conical rupture was observed.

3.4.2.5 Young's Modulus and Poisson's Ratio

At 28-day age, Young's modulus ranged from 19000 to 27000 MPa for normal-strength-concrete and from 36000 to 43000 MPa for HSC. Poisson's ratio ranged from 0.18 to 0.24 for NSC and from 0.19 to 0.23 for HSC. These numbers conform well to findings by Chen, W.F. (1982) about NSC and by Ahmad et al. (1987) about HSC.

3.5 Instrumentation for Loading and Deformation

3.5.1 Loading Apparatus

All applied loads during the test are shown in figure 3.12. Loads on the column (P_c) were provided through the 6000 kN universal testing machine (UTM). The column

was fitted in steel shoes to avoid concrete crushing at the cut off points of the column reinforcement, and to facilitate alignment of the column under the UTM. Floor loads (P_f) were applied using a 30-ton and a 60-ton hydraulic jacks (HJ) on each side of the column. The jacks were connected together to the same hydraulic pump so that the outer load was always twice the inner one and there was always symmetrical loading. The jacks were positioned such that straining actions produced on the slab and on the beam are equal to those calculated in the scaled-down structure. The jacks were attached to the strong floor via a setup of metallic beams and threaded rods, as seen in figures 3.13 and 3.14. Five load cells monitored the applied loads: one for the UTM and four for the jacks. In case a considerable difference occurred between both sides of the floor, the test would stop and would be resumed after checking the cause and fixing the problem.

To ensure the safety and adequacy of the loading and measuring devices, the expected capacity of each specimen was calculated assuming a probable variation of 5 mm in any dimension, a 10% variation in the reinforcement yield strength, and a 20% variation in the concrete nominal strengths.

3.5.2 Instrumentation for Measuring Deformation

3.5.2.1 Strain Gauges

As described below, five sets of strain gauges were mounted on the different elements of each specimen to monitor the strain change under loads. Each specimen was provided with redundant strain gauges to reduce the risk of losing important data because of failed gauges. For step by step instructions on making consistently successful strain gauge installations, reference is made to M-M (M-line accessories).

Group A, *strain gauges embedded in the concrete core*: a total of nine gauges per specimen were used to measure strains along the column axes. As shown in figure 3.15, a set of three orthogonal 4-inch gauges was used at the joint between the two ties and two other sets were located in the testing zones of the columns.

Group B, *foil strain gauges on vertical rebars*: a total of 20 gauges per specimen, shown in figure 3.16, were used as follows: 6 gauges for the bottom column, 6 gauges for the top column, and 8 gauges for the joint. They were mounted at mid-height between

the ties, on level with group-A gauges.

Group C, *foil strain gauges on ties*: a total of 12 gauges per specimen were mounted in the middle of each tie leg as shown in figure 3.17.

Group D, *foil strain gauges on the beam longitudinal-reinforcement*: a total of 14 gauges were used to measure strain at the column face and in the joint core: four gauges for the bottom reinforcement, seen in figure 3.18; four gauges for the side reinforcement, seen in figure 3.19; and six gauges for the top reinforcement, seen in figure 3.20.

Group E, *foil strain gauges on the slab reinforcement*: a total of four strain gauges, shown in figure 3.21, were mounted on two bars passing through the joint and two bars beside the joint. The four gauges were mounted at the column face except in SP7, where they were mounted along the beam axis.

Certain measures were done to obtain good results. Each column rebar was oriented in the cage such that the flexural effect due to internal lateral pressure would not distort the measured strain values. It was not possible, though, to avoid some flexural effect in corner rebars due to the bilateral flexural behaviour. For ties, eliminating the flexural effect was done either by carefully choosing the foil gauge locations or by mounting gauges on opposite sides of the same tie-leg and taking their average. Strain gauge installations are mentioned in appendix A.

3.5.2.2 LVDT and RVDT

Axial shortening of the specimen was recorded using three vertical *LVDT* devices, as in figure 3.22. Deflection of the beams was measured by three *LVDT*'s mounted at the loading points as seen in figure 3.22. Rotation of the beam fixed ends, under the floor loads, was monitored by two rotational variable differential transformers (RVDT) glued on each fixed end of the beam, as seen in figure 3.23. Horizontal strain values were recorded by two horizontal *LVDT*'s for each column and by three horizontal *LVDT*'s for the joint region, as shown in figure 3.24. Each LVDT was used in every test at the same location of the specimen in order to detect and correct any systematic error. Data measured by strain gauges, *LVDT*'s, *RVDT*'s and load cells were recorded by 130-channel Fluke data acquisition system.

Table 3.1. Matrix of Tested Variables

Specimen	*NSC Column*	*HSC Joint*	*Debonding*	*Loading Type*
SP1	---	---	---	*II*
SP2	---	---	---	*I*
SP3	---	Yes	---	*II*
SP4	---	Yes	---	*I*
SP5	---	---	Yes	*I*
SP6	---	---	Yes	*II*
SP7	Yes	---	---	*I*

Table 3.2. Properties of Steel Reinforcement

Bar Diameter (mm)	Bar Designation	Bar Area (mm^2)	Yield strength* (MPa)	Ultimate strength (MPa)	Remarks
16	No. 15M	200	409	613	In SP1 through SP6
16	No. 15M	200	442	700	In SP7 only
11	No. 10M	100	458	618	In all specimens
9		63.6	500	700	In all specimens
6		28.3	418	538	In all specimens

* Based on 0.2% strain offset

Table 3.3. Typical Mix Design for the High Strength Concrete (per cubic meter)

Cement (Type III), kg	491
Silica fume, kg	27
Coarse aggregate (SSD), kg	1059
Fine aggregate (SSD), kg	611
Superplasticizer, litres	16
Total water, kg	128
Water / Cement ratio	0.26
Water / Total Cementitious ratio	0.25

Note: SSD = saturated surface dry

Table 3.4. Compressive Cylinder Strength of Concrete (MPa)

Specimen	At 28 days				At time of test			
	Bottom Column	Floor	Joint	Top Column	Bottom Column	Floor	Joint	Top Column
SP1	79.1	13.3	13.3	69.8	84.6	18.0	18.0	72.8
SP2	82.2	17.9	17.9	77.1	86.6	20.4	20.4	93.0
SP3	82.0	27.8	27.8+81.2	81.2	89.2	31.8	31.8+90.7	90.7
SP4	81.2	15.7	15.7+63.5	63.5	90.7	17.6	17.6+66.7	66.7
SP5	63.5	18.5	18.5	91.3	66.7	19.8	19.8	95.5
SP6	89.6	18.9	18.9	91.4	93.7	20.6	20.6	94.9
SP7	17.8	17.8	17.8	28.2	18.7	18.7	18.7	28.2

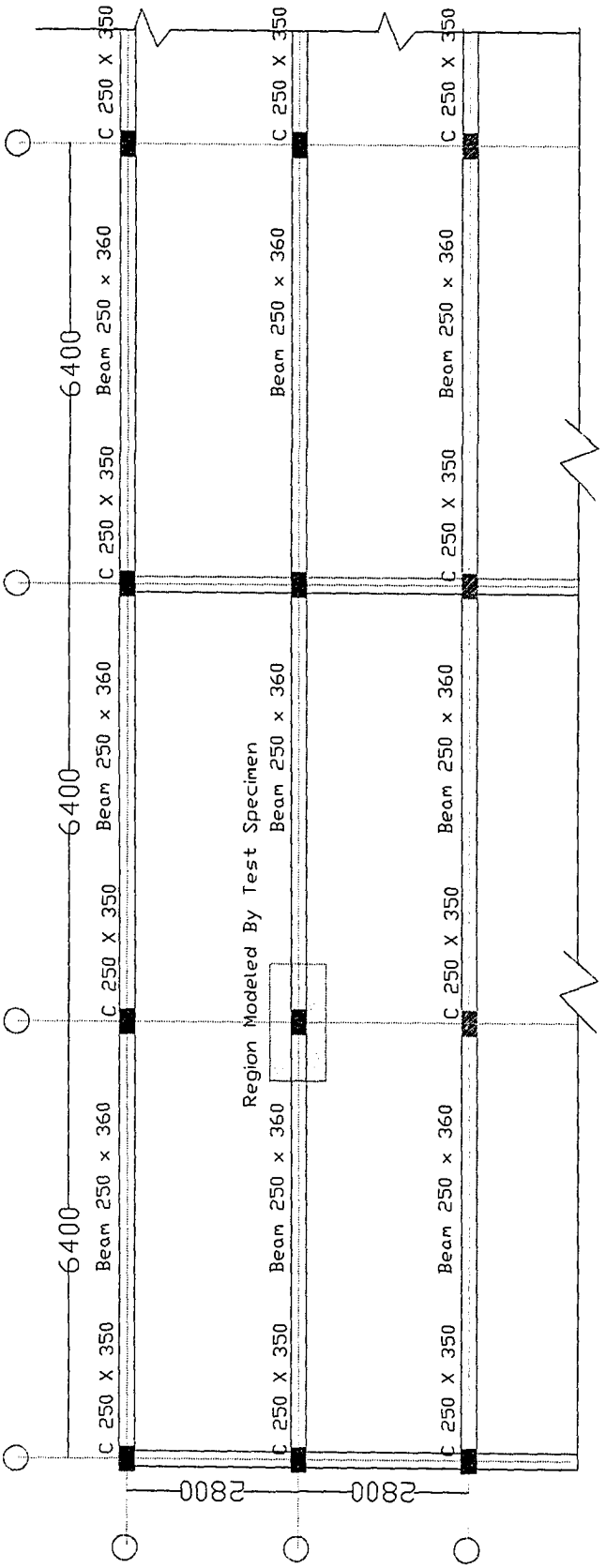

Figure 3.1. Plan of a Typical Floor in a Scaled Down Structure

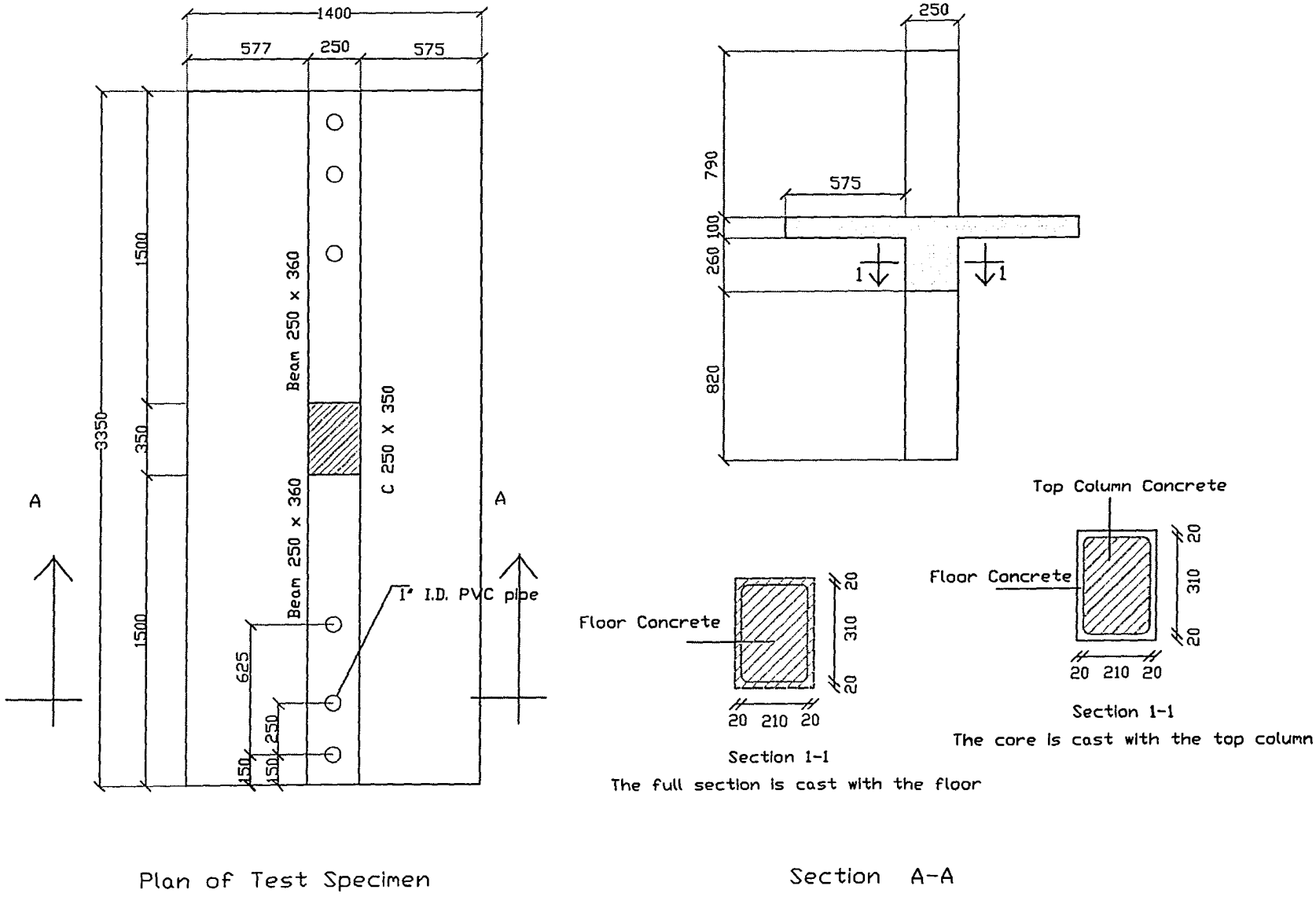

Figure 3.2. Concrete Dimensions (in mm) of a Typical Test Specimen

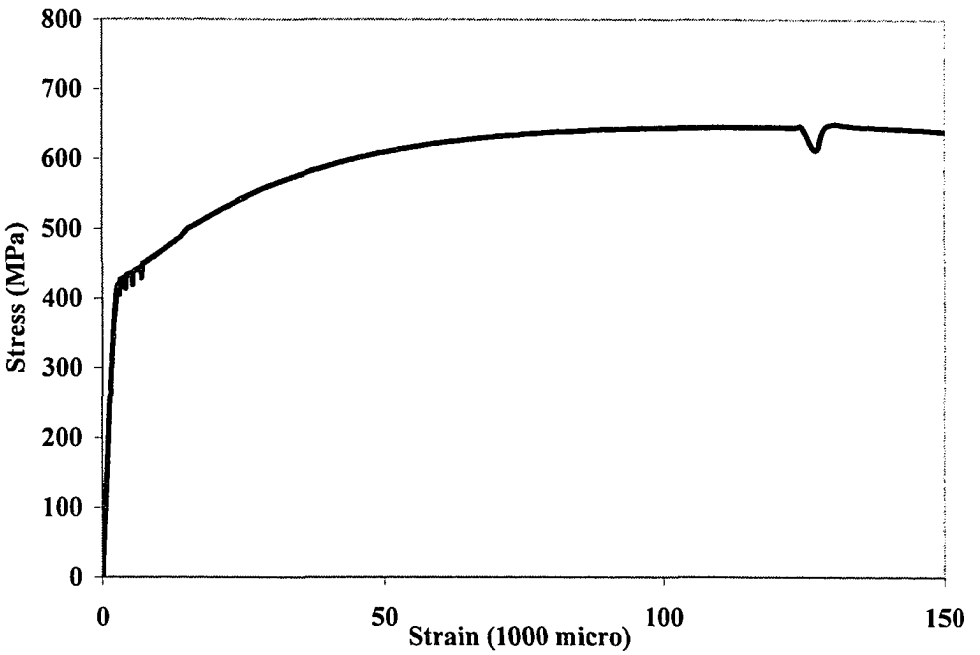

Figure 3.3. Stress- Strain Curve for M15 Rebars Used in SP1-SP6

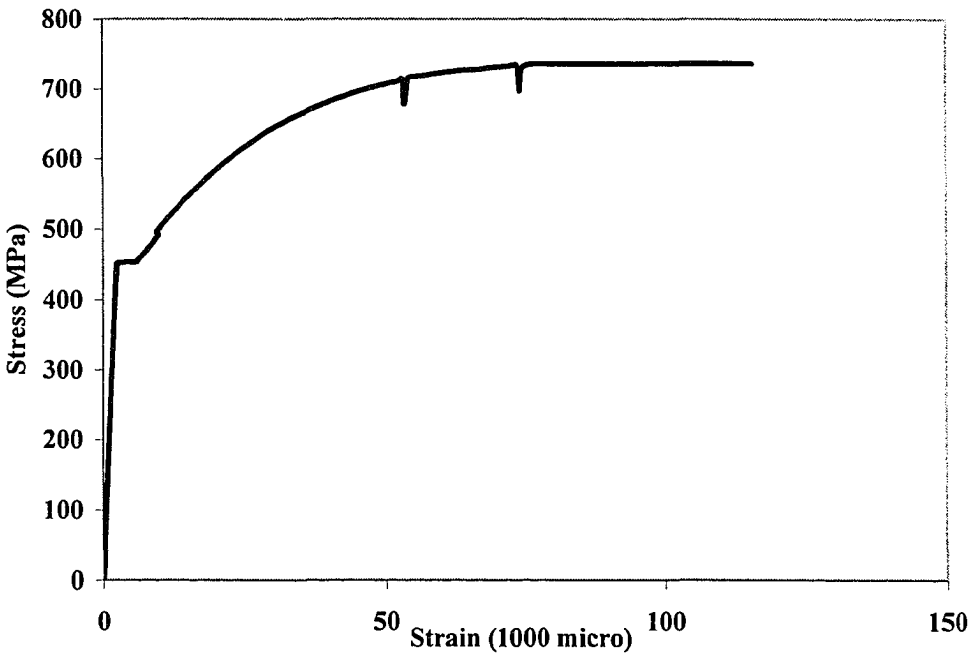

Figure 3.4. Stress- Strain Curve for M15 Rebar Used in SP7

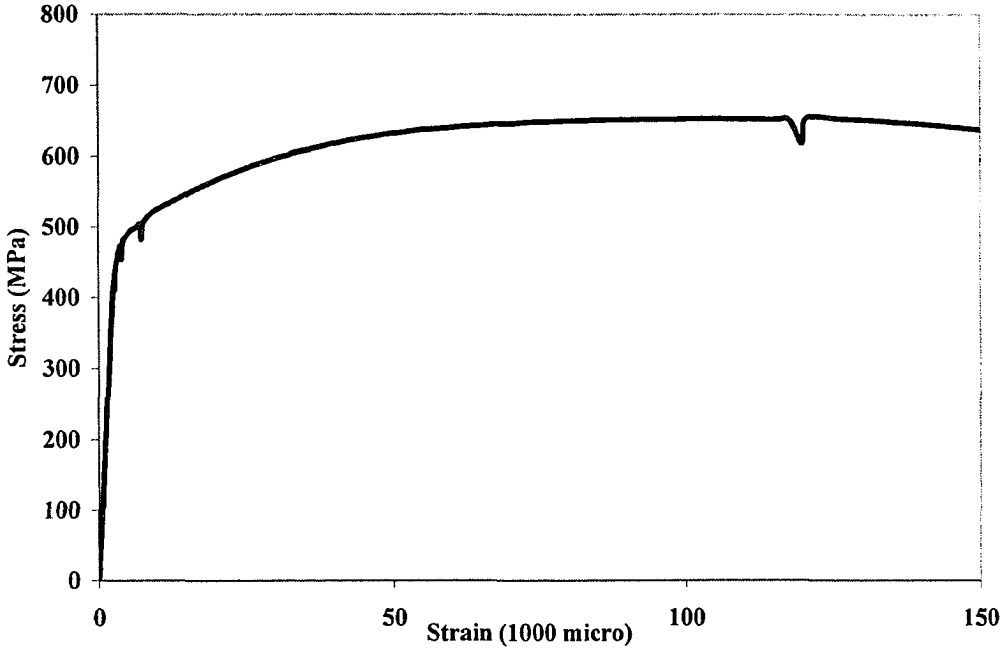

Figure 3.5. Stress-Strain Curve for M10 Rebars

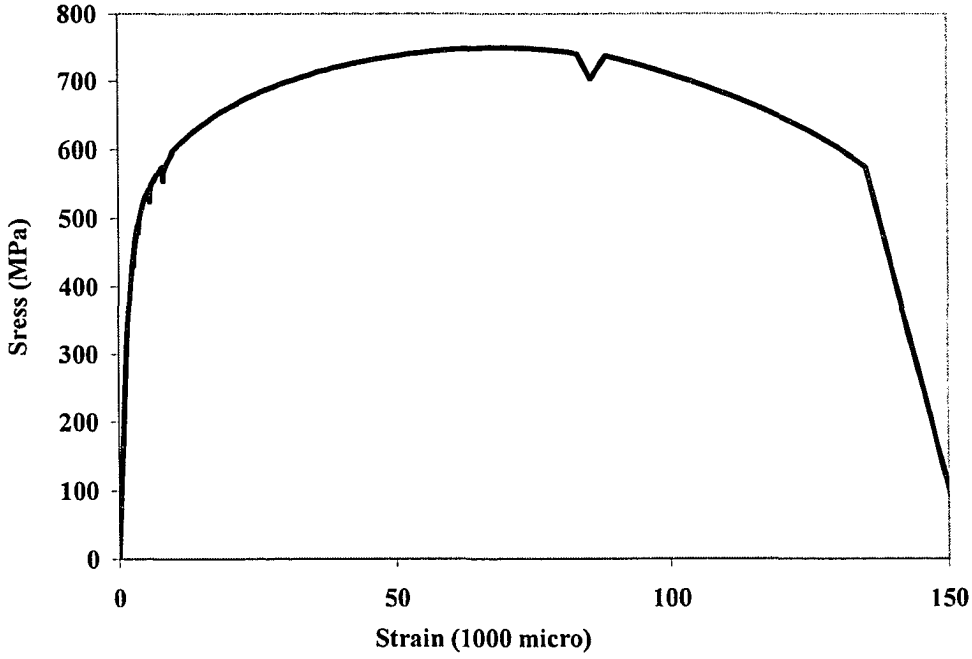

Figure 3.6 Stress-Strain Curve for 9 mm Rebars

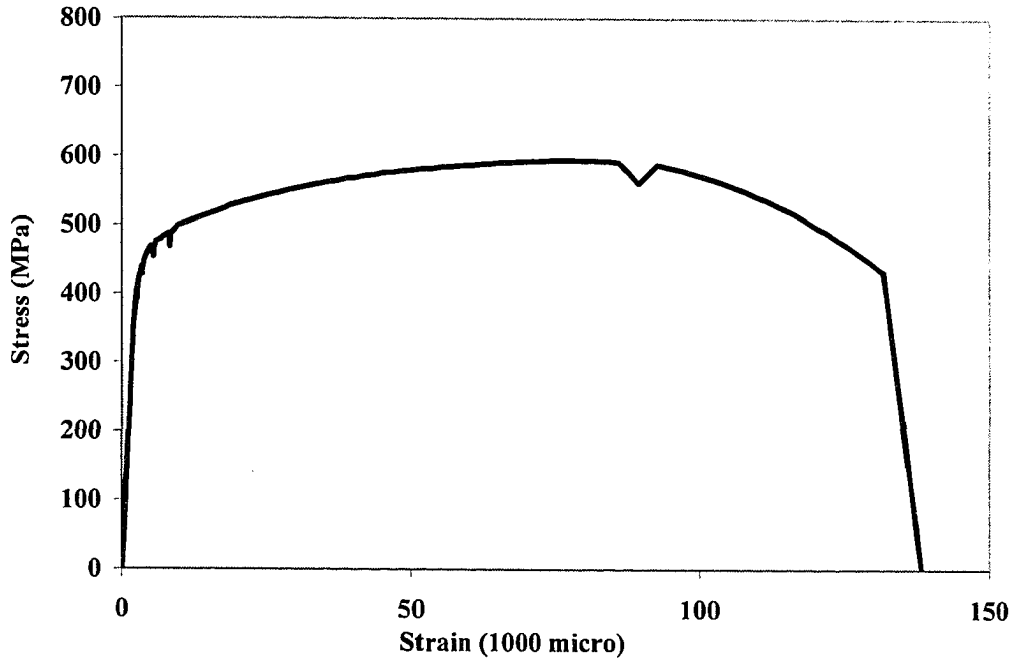

Figure 3.7. Stress-Strain Curve for 6 mm Rebars

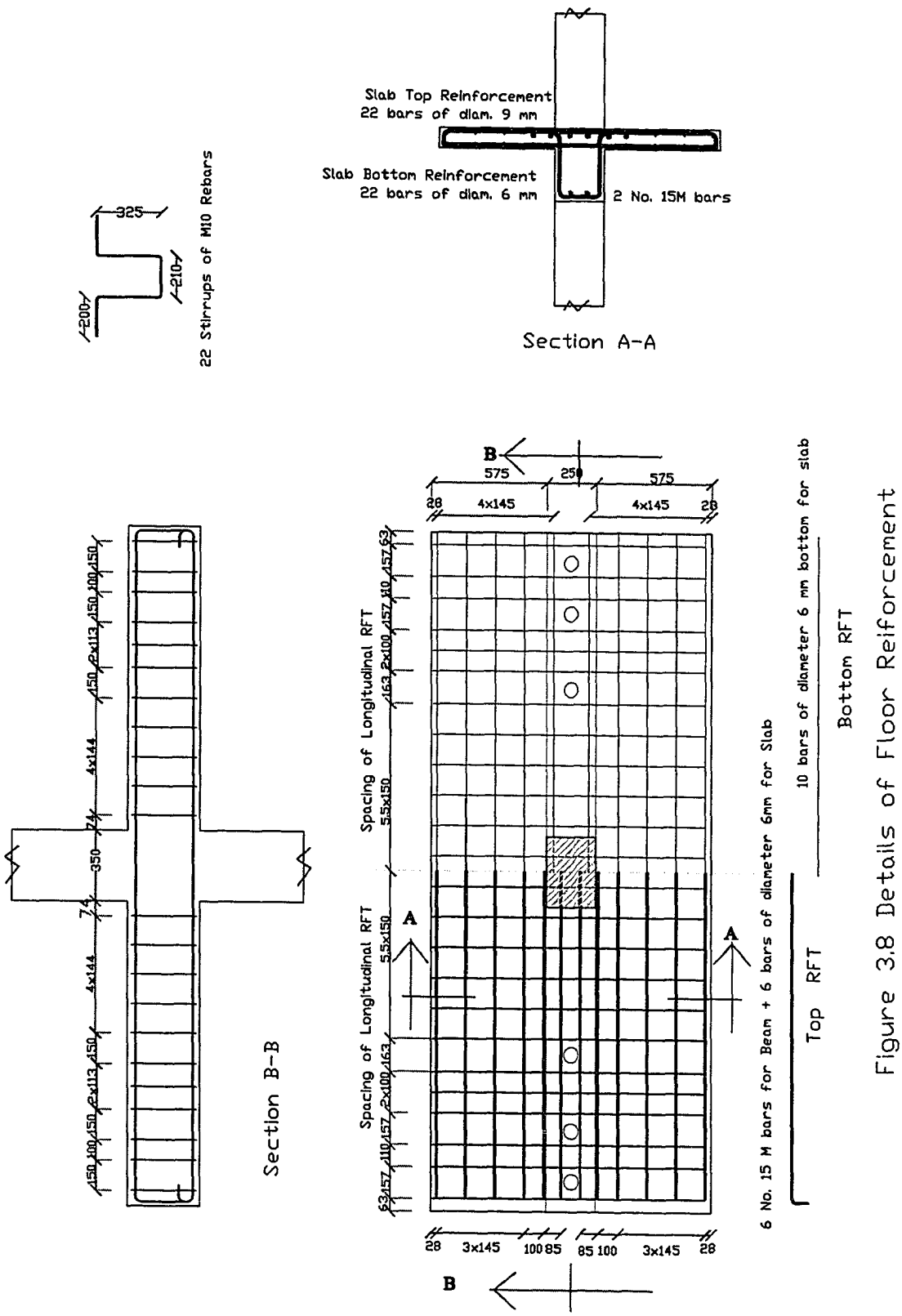

Figure 3.8 Details of Floor Reiforcement

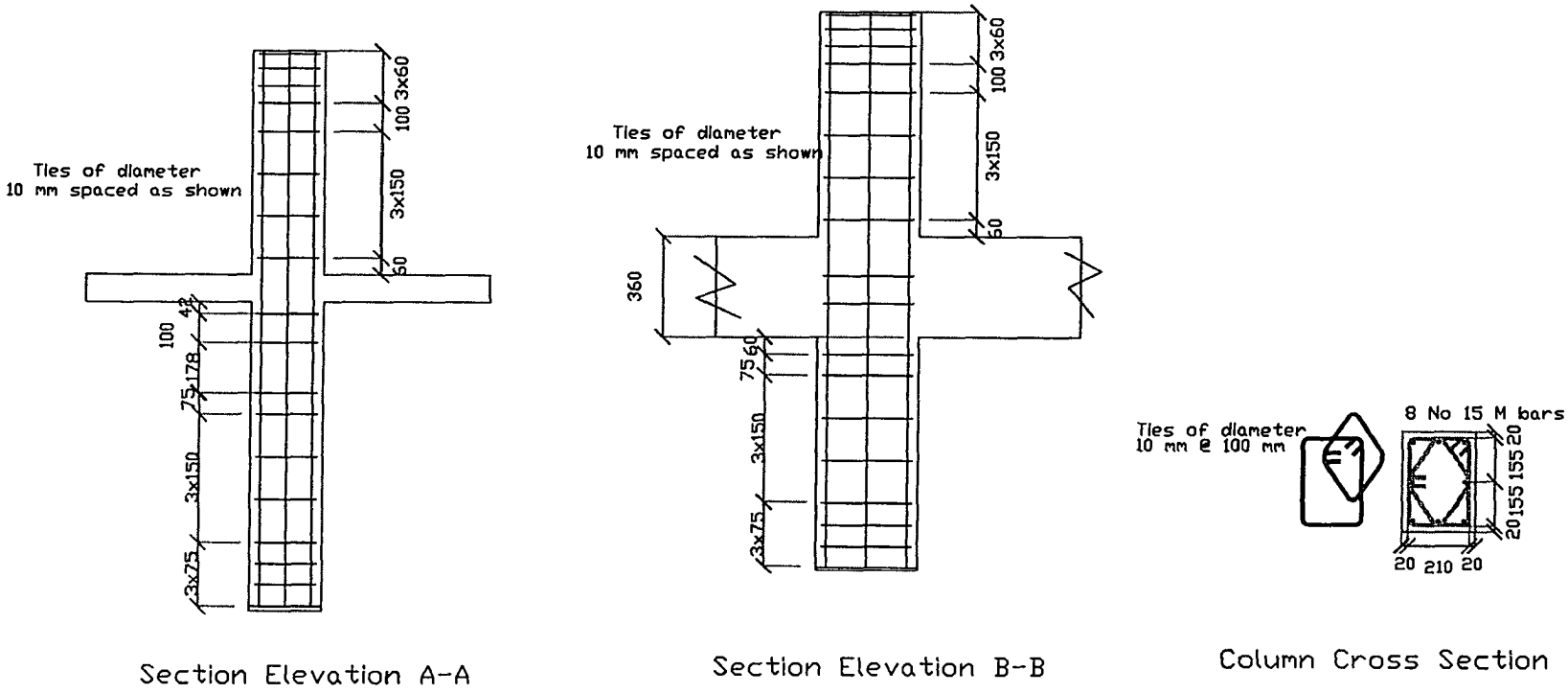

Figure 3.9. Details of Column Reinforcement

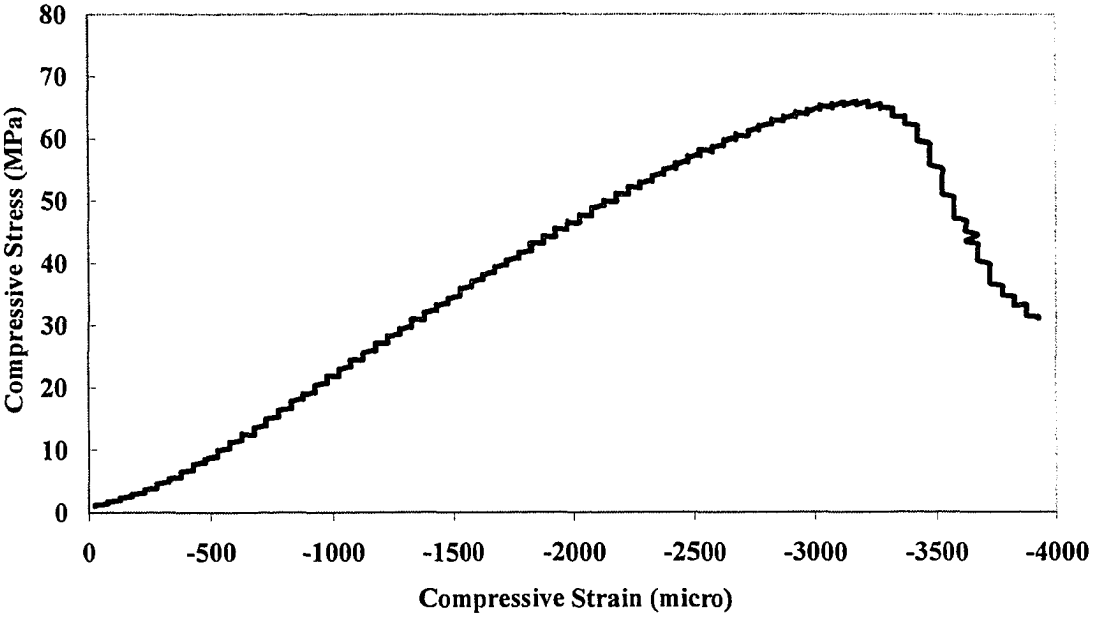

Figure 3.10. Stress-Strain Curve for High Strength Concrete Cylinder

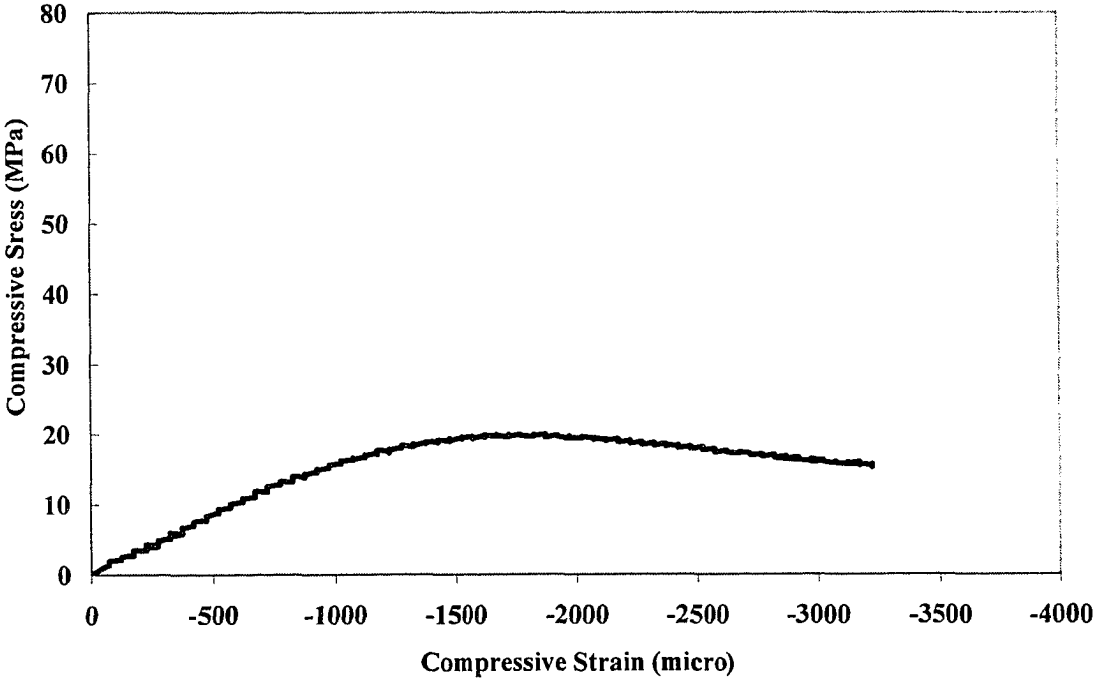

Figure 3.11. Stress-Strain Curve for Normal Strength Concrete Cylinder

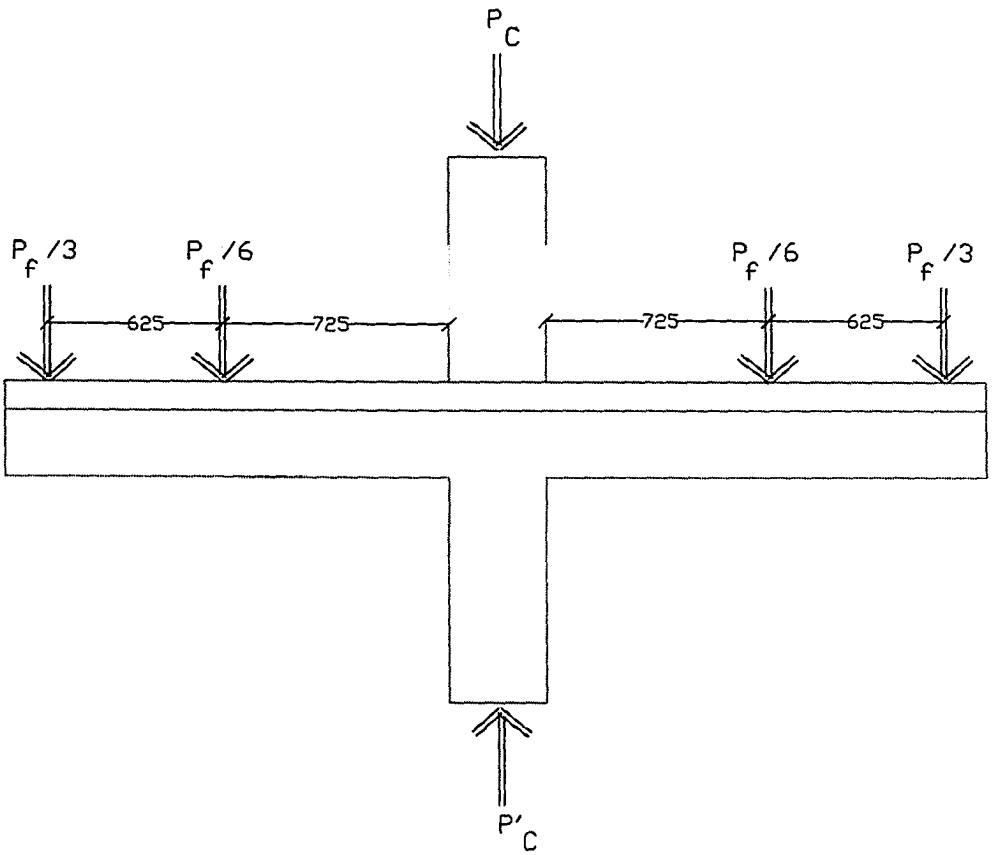

Elevation View

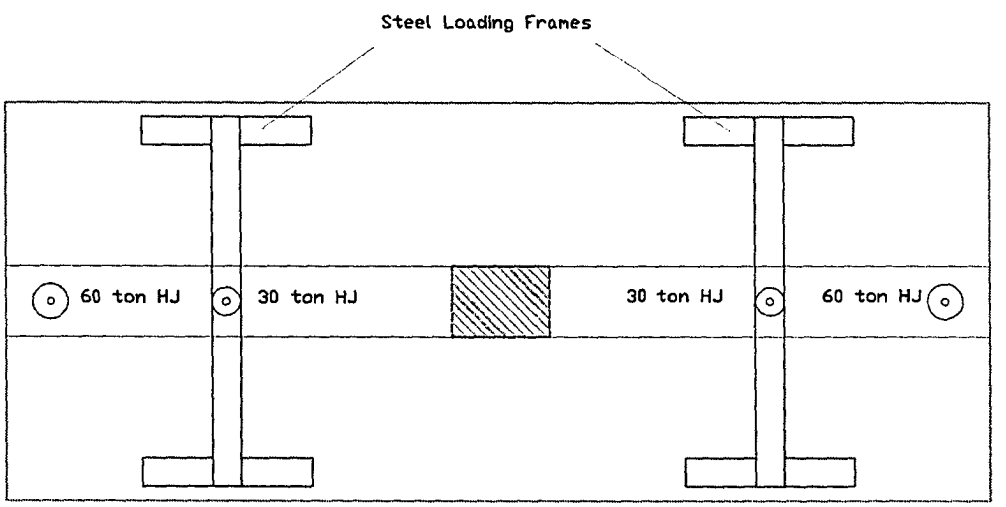

Plan View

Figure 3.12. Applied Loads During The Test

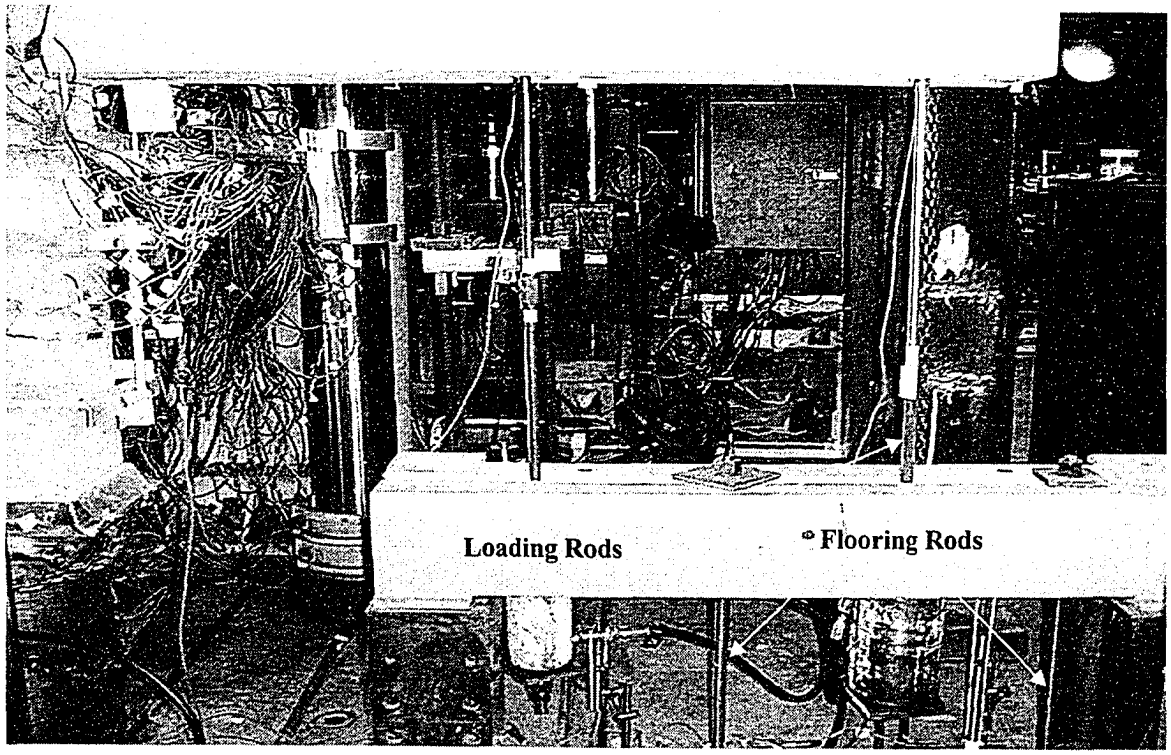

Figure 3.13. Load and Deformation Devices on One Side of Floor

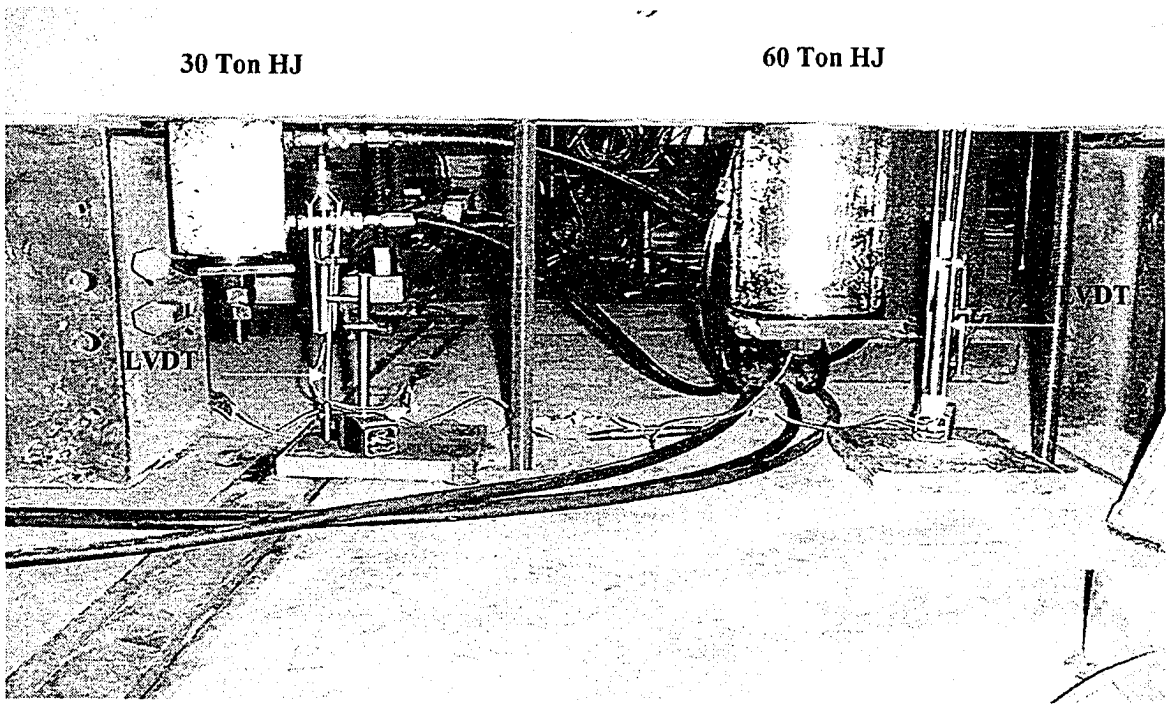

Figure 3.14. Load Transfer from Specimen to Lab-Strong Floor

Labeling of Concrete Gages:

	Vertical	Horizontal N-S	Horizontal E-W
BOTTOM	7	8	9
JOINT	38	39	40
TOP	20	21	22

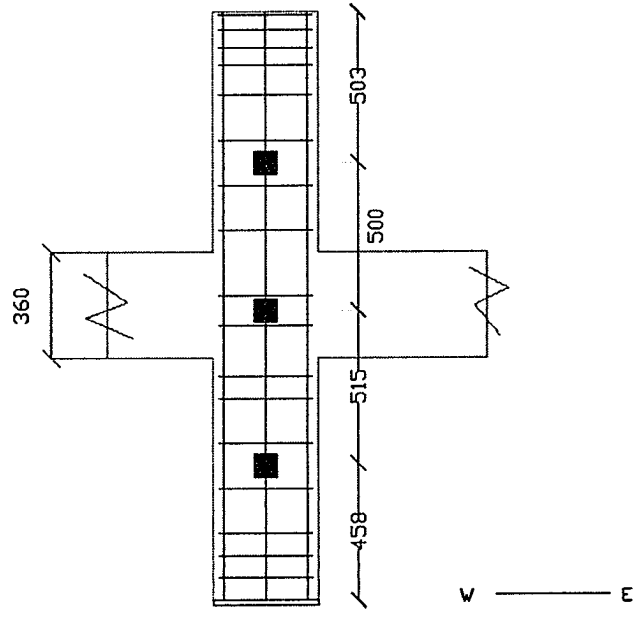

Figure 3.15. Locations of Concrete Embedded Gages (Group A)

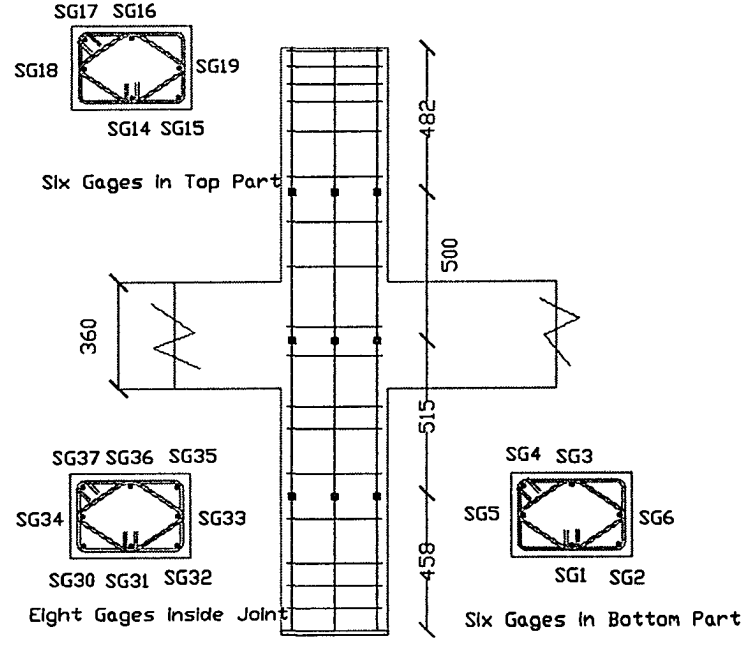

Figure 3.16. Location of Strain Gages on Column Vertical Rebars (Group B)

Labeling of Strain Gages:

	A1	A2	A3	B1	B2	C1	C2
BOTTOM	10	11	13				12
JOINT				44	45	46	47
TOP	23	25	26				24

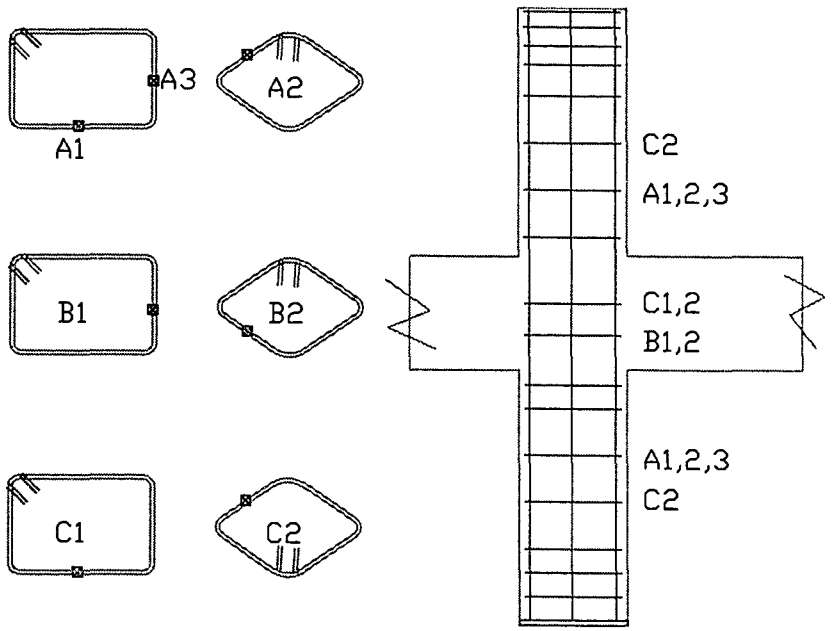

Figure 3.17. Locations of Strain Gages on Ties (Group C)

Note: The missing gage numbers (27, 28, 29, 41, 42 & 43) refer to gage locations that were abandoned from the initial plan

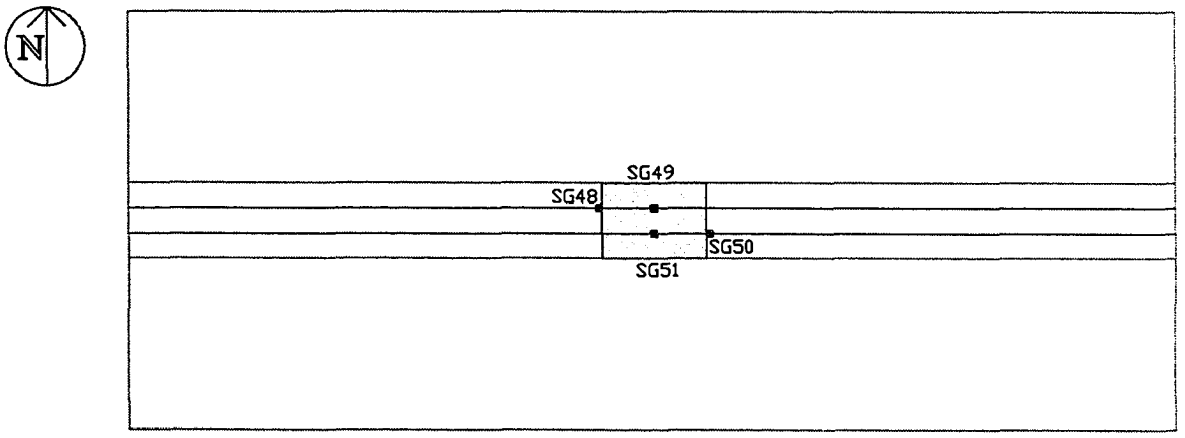

Figure 3.18. Locations of Strain Gages on Beam Bottom Rebars (Group D)

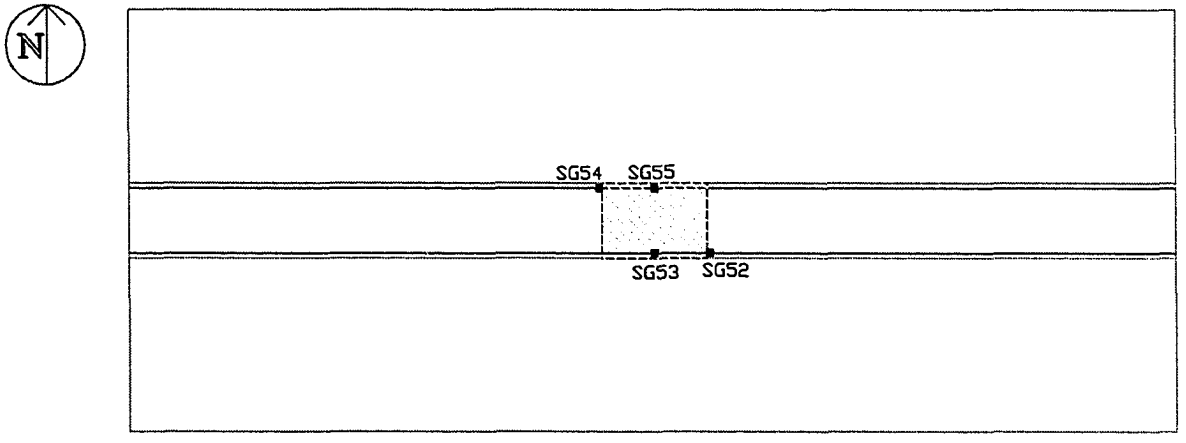

Figure 3.19. Location of Strain Gages on Beam Side Rebars (Group D)

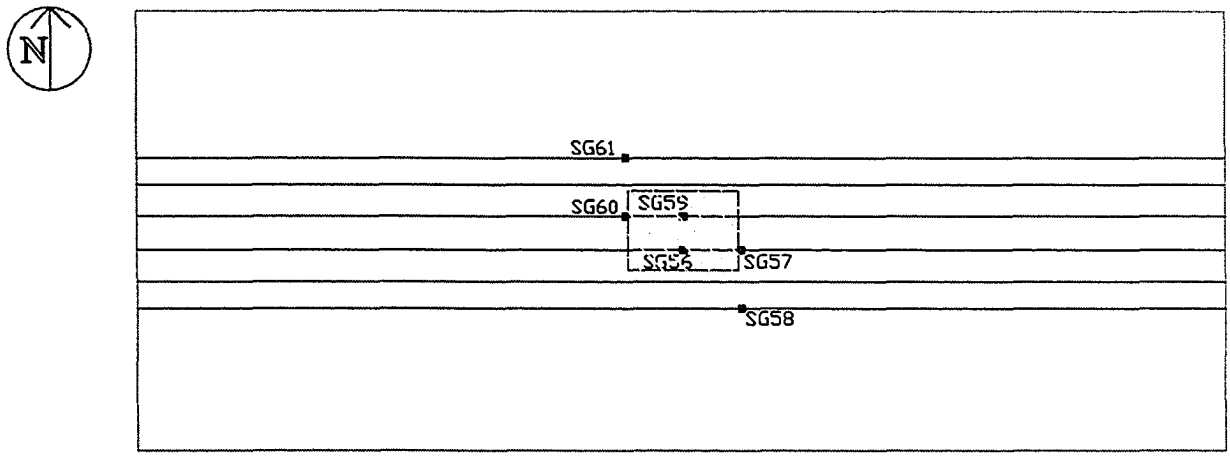

Figure 3.20. Location of Strain Gages on Beam Top Rebars (Group D)

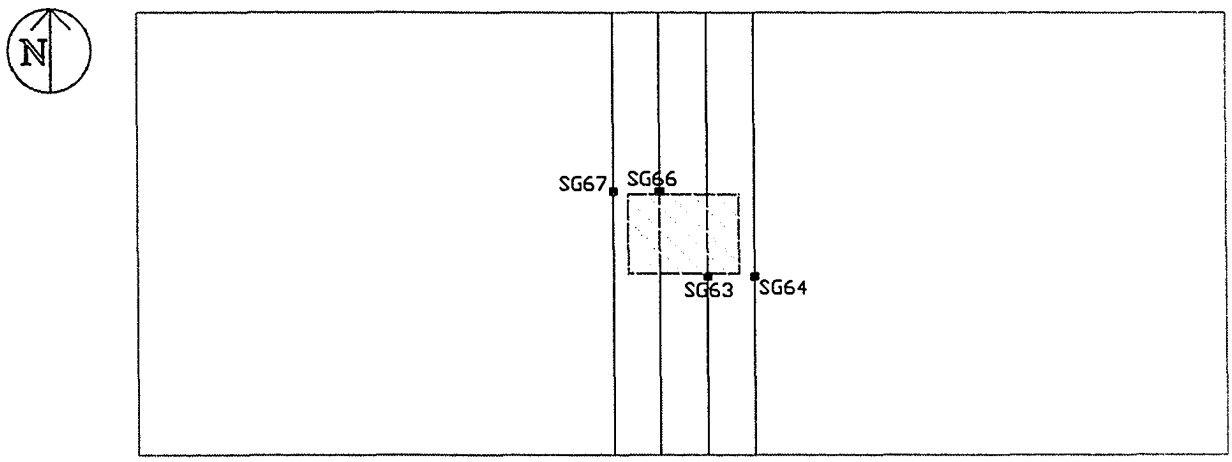

Figure 3.21. Location of Strain Gages on Slab Main Rebars (Group E)

Note: The missing gage numbers (62 & 65) refer to gage locations that were abandoned from the initial plan

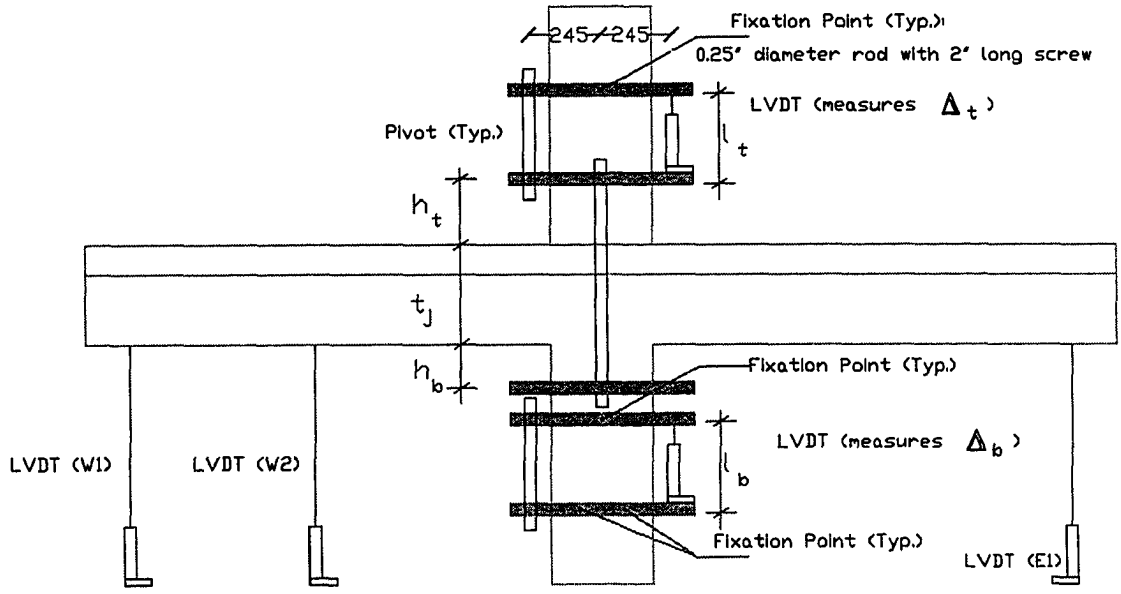

South View

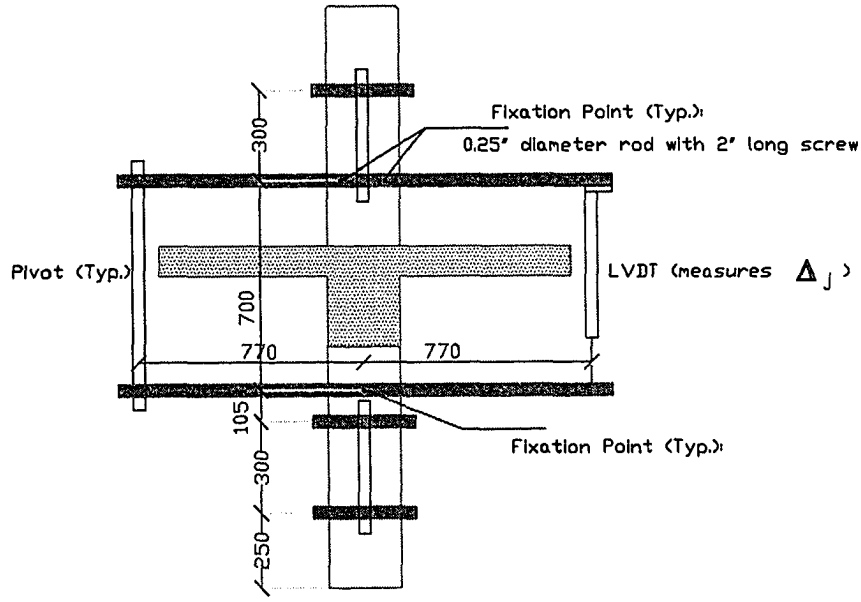

West View

Figure 3.22. LVDT Set-up for Average Vertical Strain Measurements

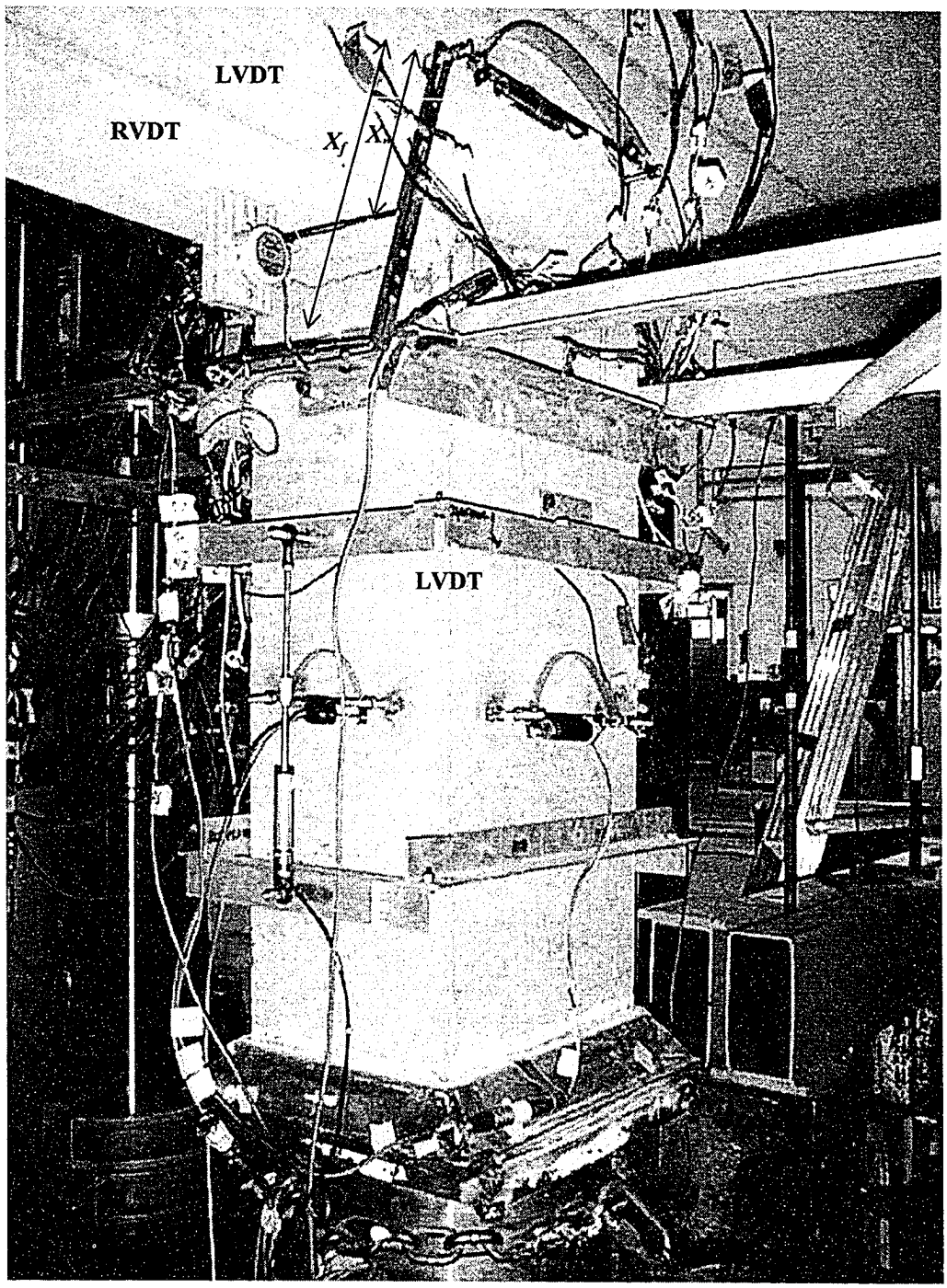

Figure 3.23. External Instrumentation for Measuring Deformation

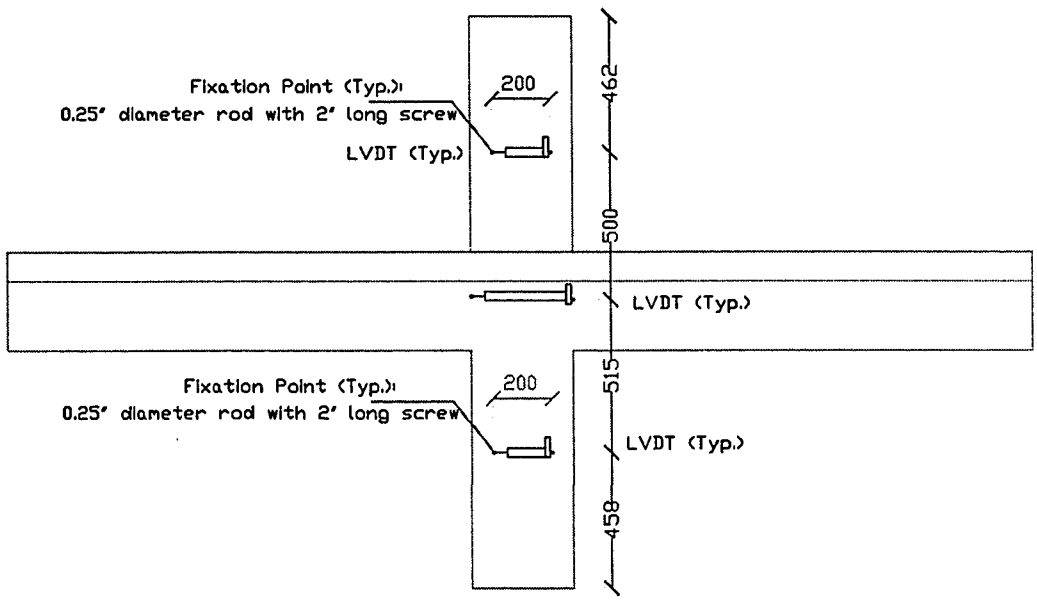

North View

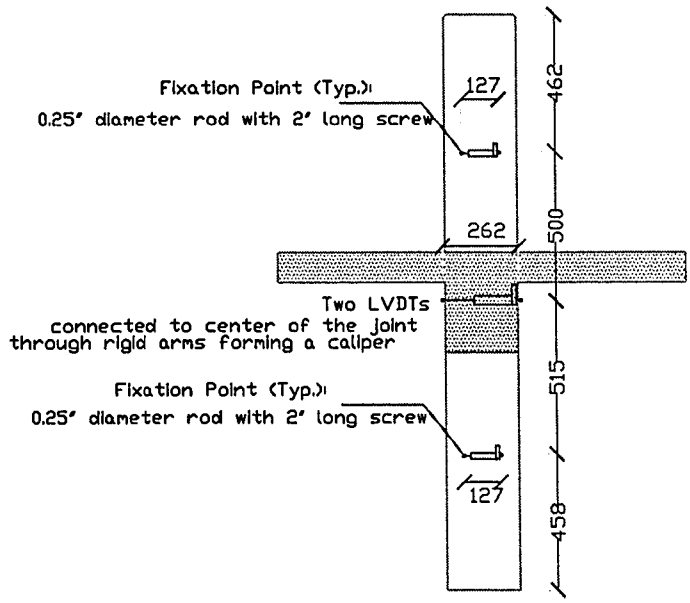

East-Side View

Figure 3.24. LVDT Set-up for Average Horizontal Strain Measurements

4 TEST PROTOCOL, RESULTS AND OBSERVATIONS

4.1 Introduction

This chapter outlines the protocol followed in conducting the seven tests, observations of each test and description of the general modes of failure.

4.2 Test Protocol

4.2.1 General

Prior to testing, shrinkage cracks were marked to distinguish them from cracks formed during the test. Upon reaching a loading stage, the actuators were stopped to allow for inspection and to obtain static readings. During the test, loading and deformation were monitored for checking symmetry in the response of the floor.

The seven tested specimens can be grouped into two sets based on the loading case. Type-I loaded specimens included SP2, SP4, SP5, and the control specimen SP7; each was loaded with full service load on the floor and ultimate load on the column. Type-II loaded specimens included SP1, SP3 and SP6; each was loaded with full service load on the column and ultimate load on the floor. For a floor with strength lower than the nominal, this case of loading can likely occur and seriously damage the joint or the floor. After collapse of the floors, the columns were loaded until the specimens failed.

The service load is defined as the unfactored load. It represents the dominant load through the lifespan of the structure. According to the CSA standards, a dead service load is 1/1.25 of the factored dead load used in design; a sustained live load is 1/1.5 of the factored live load used in design; a full service load is the sum of both values. The fraction of the full service load to the total factored load depends on the ratio between the dead and live unfactored loads. For a case of 60% dead load and 40% live load, the full service load is expected to be about 75% of the total factored load.

4.2.2 Load Expectation

The expected axial capacity of each specimen was calculated based on nominal characteristics using equations 2.4, 2.7, 2.22 and 2.30. Except for SP7, the failure of the

specimen under load of the universal testing machine 6000 (UTM) was expected to happen in the joint region. As for SP7, the bottom column was the weakest part in the load path and therefore more likely to fail before the joint or the top column.

4.2.3 Pre-Compression and Loading Scenario

With reference to figure 3.14, each specimen was subjected to a primary load (P_c) applied to the column via the UTM and a secondary load (P_f) applied to the floor through the hydraulic jacks (HJ). The values for P_f reported here are the sum of HJ loads on both sides of the column.

The loading strategy was intended to simulate the usual loading sequence of a column in a high-rise structure, with some adjustment to suit the nature of testing. Figures 4.1 and 4.2 show schematic loading sequences for type-I and type-II loaded specimens.

The following sequence of loading was followed for type-I and type-II loaded specimens. It is shown in figures 4.1 and 4.2 as a shaded area. First, P_c was brought up to 400 kN to ensure all the measuring devices working properly. Next, P_f was increased by an amount equivalent to self weight of the floor plus construction loads from upper floors. This was followed by reducing P_f to match the self weight of the floor, simulating the removal of the scaffolding system. Then P_c was raised to a value simulating the total dead weight from the above floors. P_f was then increased to match the service load of the floor. P_c was then raised until the estimated service loading value on the column.

As seen in figure 4.1, P_c was then raised for a type-I loaded specimen until failure of the column while maintaining the loads on the floor at service level.

As seen in figure 4.2 for a type-II loaded specimen, P_f was raised until floor collapse and P_c was then increased until failure of the column to see how much the axial strength of the joint would decrease due to failure of the surrounding floor.

For all the specimens, testing the column was planned to continue until P_c dropped to 50% of the attained peak load.

4.2.4 Estimation of Column Service Load for Type-II Loaded Specimens

Type-II loaded specimens required the load on the column to be at service level. This was assumed to be in the range of 0.7-0.8 of the estimated column failure load.

Using the available design equations and accounting for variations in the material properties resulted in a substantial range of the estimated failure loads, and so of the service loads. Because of the uncertainty in these estimated values, additional criteria were established.

Two criteria, based on initial analysis of the strain values recorded for type-I specimens previously tested, were adopted to determine P_c corresponding to full service load on column. The service load was considered reached at the earliest occurrence of: strain of any diamond-shape tie, or any lateral concrete gauge, reaching 1200 με, or the joint cracking similar to that appearing at 80% of the ultimate loads on type-I specimens.

4.2.5 Rate of Column Loading

Loading rate of the UTM was based on the following: the loading rates commonly used in testing specimens under static monotonic loads, the expected total shortening of the specimen and the available testing time. The minimum UTM loading rate used in this research was 0.225 mm/min. Occasionally, this rate was reduced to zero for inspecting the specimen or increased to 0.45mm/min while unloading. The strain rate of each test was very low as compared to that for a uniaxial cylinder test. According to MacGregor and Bartlett (2000), a corresponding actual unconfined compressive strength of the concrete was expected to be about 0.85 that of the control cylinder.

4.3 Test Records and Observations

Table 4.1 shows a summary of the maximum values of P_c and P_f. Figures 4.3 to 4.9 show P_c and P_f plotted against the stroke of the UTM for the specimens SP1 to SP7 respectively. Because it includes deflection of the loading frame, the stroke of the UTM does not exactly match the total axial deformation of the specimen. Nevertheless, it provides a useful testing record. Figures 4.10 to 4.16 show the specimens after the test. Comprehensive records of test observations are shown in tabular form in appendix B.

The following subsections cover the main observations recorded during each test. The number in parentheses after each load value is the percentage ratio of the achieved load compared to the maximum static load recorded during the test. SG is the foil strain gauge mounted on reinforcement, and CG is the embedded concrete gauge placed in the

column core. The directions mentioned hereinafter are those of the specimens while being tested: east-west was the direction parallel to the beam longitudinal axis and north-south was the direction parallel to the transverse axis.

4.3.1 Test Observations of SP1 (Type-II)

Figure 4.3 shows the load against stroke for SP1. At P_f of 108 kN (31%), hairline cracks were observed on top of the slab. At P_f of 160 kN (46%), maximum strain in the beam top reinforcement (flexural strain) was +2000 μ ε (SG57). AT P_f of 280 kN (82%), the beam bottom cover started to peal at its contact with the column.

P_c was stopped at 2800 kN (77%) when the cover of the joint started to peal off. Maximum strain in the vertical rebars (vertical strain) was –8900μ ε (SG37) and maximum beam flexural strain was +4860 μ ε (SG57).

At P_f of 325 kN (95%), the beam bottom-cover started to spall at its connection with the column. At P_f of 342 kN (100%), the floor collapsed. The joint cover started to spall and wide longitudinal cracks were observed extending from the beam-column interface indicating buckling of the beam bottom rebars.

The peak P_c value was 3636 kN (100%). South cover of the joint was lost completely and joint concrete started falling simultaneously with buckling of the vertical rebars. Maximum vertical strain was –20000 μ ε (SG33). The specimen was unloaded at the end of the test when P_c was about 2000 kN (55%).

Figure 4.10 shows SP1 after the test. After-collapse inspection showed that the south-west vertical rebar buckled in two locations (at top and bottom of the joint), the south vertical rebar buckled at the bottom of the joint, and the south-east vertical rebar buckled between ties in the joint.

4.3.2 Test Observations of SP2 (Type-I)

Figure 4.4 shows the load against stroke for SP2. At P_f of 108 kN, hairline cracks appeared on the slab top surface as in previous test. At P_c of 3457 kN (75%), cracks started on the joint. At P_c of 3800 kN (82%), cover of the joint started to spall. The maximum vertical strain was –7300 μ ε (SG36).

UTM loading reached the peak at 4605 kN (100%). Vertical rebars buckled at the joint-interface with the bottom column. The top column did not crack. The test was continued until UTM unloaded to 30 % of the peak load. Figure 4.11 shows SP2 after the test.

4.3.3 Test Observations of SP3 (Type-II)

Figure 4.5 shows the load against stroke for SP3. At P_f of 160 kN, maximum flexural strain was +1697 μ ε. Hairline cracks appeared on the slab top surface as in previous tests. The maximum flexural strain reached +2000 μ ε at P_f of 194 kN.

At P_c of 5037 kN (75%), hairline cracks were noticed on the joint and on the top column at its south-west corner with the slab.

At P_f of 274 kN, maximum flexural strain was +2770 (SG60). Cracks appeared on the slab bottom surface; shear cracks extended slightly; and previously marked cracks widened a bit on the slab top surface. Maximum flexural crack width was about 0.4 mm near the column face.

The floor failed at P_f of about 408 kN. Maximum flexural crack width was 3.0 mm. Maximum shear crack width was 1.5 mm. Vertical strain in the joint did not change much due to loading the floor.

At P_c of 6400 kN (95%), there was an interrupt in loading due to user introduced problem.

The top column collapsed explosively at P_c of 6700 kN (100%) when a tie snapped and the vertical rebars buckled consequently. Figure 4.12 shows the tested SP3.

4.3.4 Test Observations of SP4 (Type-I)

Figure 4.6 shows the load against stroke for SP4. At P_f of 108 kN, hairline cracks appeared on top of the slab as in previous tests and the flexural strain was +1080 μ ε.

At P_c of 4200 kN (75%), hairline cracks appeared on the top column, right above the slab, and vertical strain was –3500 μ ε (SG31).

The maximum P_c was 5583 kN (100%) and the corresponding maximum vertical strain was–8300 μ ε (SG33). The maximum P_c stabilized for a while then started to

soften with spalling of the cover at the joint-interface with the bottom column. The vertically cracked south cover was almost detached when the crack-line was suddenly intercepted by a horizontal crack, which extended across the width of the south face indicating buckling of rebars.

While unloading from 5316 (95%) to 3560 kN (64%), north-cover of the bottom column was detached suddenly indicating buckling of rebars in the bottom column. Lateral strain values changed abruptly by about +3000 μ ε and vertical strain values changed by about -7000 μ ε. The test ended when P_c reached a load of 2000 kN. No visible cracks were observed in the top column. Figure 4.13 shows SP4 after the test.

4.3.5 Test Observations of SP5 (Type-I)

Figure 4.7 shows the load against stroke for SP5. At P_f of 90 kN, hairline cracks were observed on the slab top surface as in previous tests.

At P_c of 4400 kN (97%), radial cracks on the slab top surface expanded and circumferential cracks around the column widened. Some cracks appeared on the top column. The maximum P_c was 4558 kN (100%) and the corresponding maximum vertical strain was –26000 μ ε.

At about UTM degrading load of 4400 kN, a bang was heard accompanying a sudden drop in P_c to about 3800 kN. Figure 4.14 shows a picture of SP5 after the test.

4.3.6 Test Observations of SP6 (Type-II)

Figure 4.8 shows the load against stroke for SP6. At P_f of 92 kN, hairline cracks appeared on the slab top surface as in previous tests.

At P_c of 2400 kN (58%), hairline shear cracks appeared on the beam, and more flexural cracks appeared on the slab top surface. Transverse cracks were observed on bottom of the slab right under those on the top. These cracks started under supports of the distributor beams and extended inwards.

At P_c of 3000 kN (72%), vertical hairline cracks were observed on the joint north-face and maximum vertical rebar strain was –3600μ ε (SG37).

The floor collapsed when P_f reached 376 kN (100%) with side-bars yielding at the column face. Nothing happened to the bottom column except widening of some cracks. Vertical strain in the joint, though, did not change much by increasing the floor load.

The ultimate P_f was expected to be about 360 kN based on the comparison between floor strengths in SP6 and SP1, ignoring the effect of debonding the beam top reinforcement. Having failed at 376 kN, floor of SP6 did not lose its flexural strength due to partial debonding of the beam top reinforcement.

At P_c of 3600 kN (86%), joint cover started to spall. The crack control rebars (side rebars) yielded inside the core and their strain values were increasing with the increase in P_c.

In an effort to capture peak P_c values unaffected by pauses in loading, the specimen was loaded continuously until after the peak region. There was a UTM loading plateau and the maximum P_c was 4167 kN (100%) with no second peak value. South-rebars buckled at the joint-interface with the bottom column. Maximum rebar strain in the joint was–14500 με (SG35) while the columns showed maximum strain of –2100 με.

While the bottom column was mostly damaged on the south side, the top column was mostly damaged on the north side. During unloading, the damaged zone of the joint north-face was within the upper third while the damaged zone of the joint south-face was all over the joint but it was more pronounced in the lower third (closer to the interface). The test stopped when P_c reached 1880 kN (45%). Figure 4.15 shows SP6 after the test.

4.3.7 Test Observations of SP7 (Type-I)

Figure 4.9 shows the load against stroke for SP7. At P_f of 90 kN, hairline cracks appeared on the slab top surface as in previous tests.

At P_c of 2200 kN (79%), vertical cracks started to appear on the top column and maximum vertical strain was –2300 με (CG20). At P_c of 2670 kN (96%), a single hairline crack was noticed in the joint.

The maximum P_c was 2783 kN (100%). The UTM loading was continuously applied and no second peak value was observed. At failure, particles of the bottom column were falling down and the cracks extended diagonally and horizontally from

north-west corner until they reached the adjacent corners. Figure 4.16 shows SP7 after the test.

4.4 Performance of the Strain Gauges

Fifty foil strain gauges (SG) and nine concrete gauges (CG) were used in each specimen. The number of gauges that were working at the start of testing was as follows: 44 SG and nine CG for SP1, 37 SG and nine CG for SP2, 46 SG and nine CG for SP3, 42 SG and eight CG for SP4, 39 SG and seven CG for SP5, 41 SG and nine CG for SP6, and 42 SG and six CG for SP7.

Figures 4.17 to 4.36 show the vertical loads applied to the columns against strain values measured by the concrete gauges and the foil gauges mounted on the column reinforcement. The rest of the test results are shown in appendix B. The figures are classified according to direction of the measured strain and location of the gauge in the specimen. The figures show consistency between readings of the different gauges at the same section, regardless of some variation through the entire test.

Maximum vertical strain for the high-strength-concrete (HSC) columns was less than -5000με and maximum vertical strain for the normal-strength-concrete (NSC) joints was in excess of -50000με. Maximum lateral strain for HSC columns was less than +1000 με and maximum lateral strain for NSC joints was over +15000 με. Maximum lateral strain in the bottom column of SP7 was almost five times that in HSC columns. Ties yielded in the joints- except in SP3 and SP7- and in the bottom column of SP7.

4.5 Mechanism of Failure

4.5.1 Failure of Type-I Loaded Specimens

Type-I loaded specimens with NSC joints failed by crushing of the joint concrete and buckling of the vertical rebars after falling of the concrete covers. The beams were relatively intact. The behaviour of SP5 was similar to that of SP2. SP4 failed in both the joint and the bottom column with buckling of the column reinforcement in both regions. SP7, with NSC throughout, failed in the weaker column.

4.5.2 Failure of Type-II Loaded Specimens

The actual service loads for SP1, SP3 and SP6 were 80% of the maximum loads applied to the joints (equivalent to 75% of the maximum P_c).

The floor collapsed in flexure with the top reinforcement yielding. There was a well-developed compression fan. Crushing of the compression block was accompanied by buckling of the beam bottom reinforcement. The specimens showed substantial loss of section in the beam.

Failure of the joint of type-II specimens was similar to that of type-I loaded specimens. But, failure of the top column of SP3 was a shear plane failure accompanied by rupturing of the lateral steel and buckling of the longitudinal reinforcement.

4.5.3 General

The joints started to crack at an average of 75% of the maximum P_c. The first crack was vertical centered within the joint under the slab and extended upwards and downwards. Horizontal cracks then started to show up. An exception was for SP4 and SP7, whose first cracks were on the top column at the interface with the slab.

Concrete failure, in the joint or column, was noticed to be either conical shear failure or plane shear failure similar to cylinders under uniaxial compression.

In specimens with NSC joints, the failure happened at the joint-interface with the bottom column regardless of how much load was applied on the floor. The joint failed when ties yielded. This demonstrates the importance confinement played inside the joint.

Having high strength concrete in the joint increased its axial capacity. Failure of SP3 was in the top column and failure of SP4 occurred simultaneously in two zones: at the joint-interface with the bottom column, and in the bottom column.

Capacity of the joint depends on the confinement provided by the floor elements and the end conditions. Failure of SP7 happened in the bottom column that had the same concrete of the joint, 18.7 MPa. The joint was very slightly cracked while the top column, of 28.2 MPa, experienced much damage. Accordingly, the floor plays a vital role in strengthening the joint.

Table 4.1. Summary of the Maximum Loads Applied During the Tests

SP#	P_c (kN)	P_f (kN)	$P_{f,res}$ (kN)
1	3636	342	79
2	4605	158	158
3	6700	408	---
4	5583	158	158
5	4558	151	151
6	4167	376	174
7	2783	143	143

P_c is the maximum applied load on the column (UTM load)
P_f is the maximum applied load on the floor (HJ loads)
$P_{f,res}$ is the residual floor load corresponding to P_c

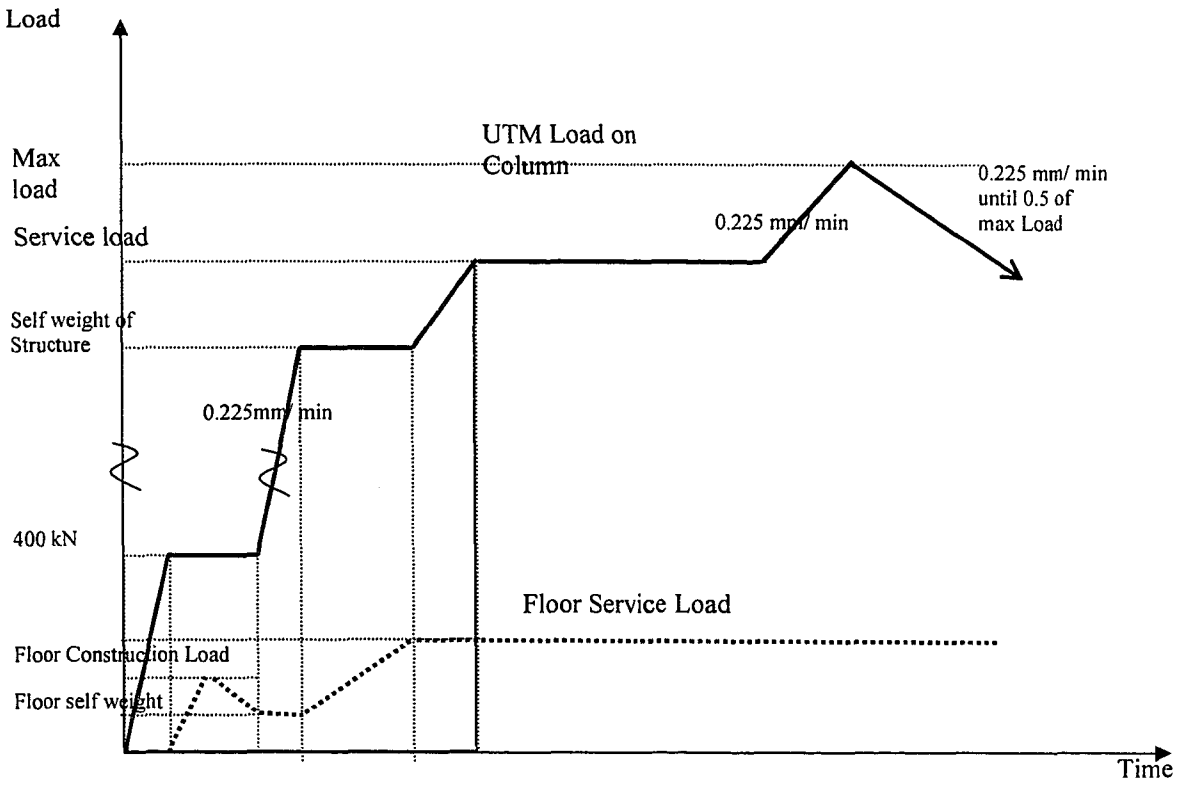

Figure 4.1. Schematic Loading Scenario for Type-I Loaded Specimens (SP2, SP4, SP5 and SP7)

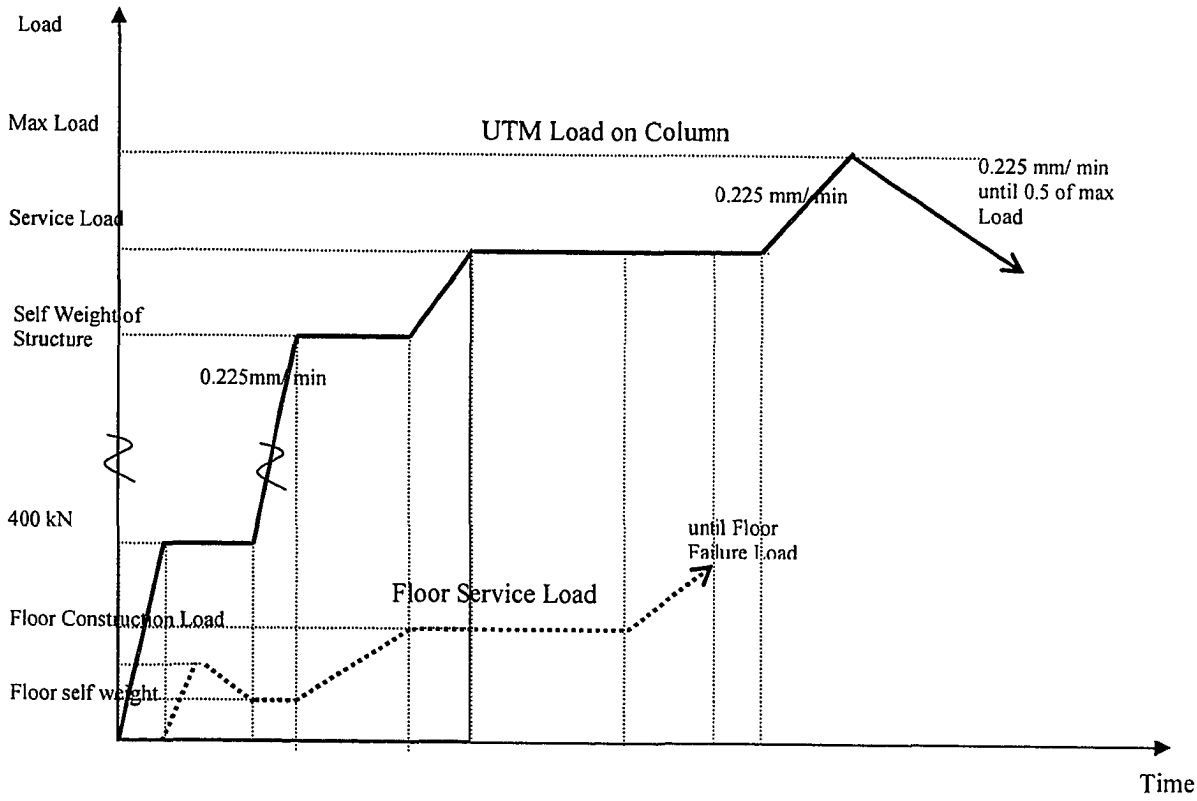

Figure 4.2. Schematic Loading Scenario for Type-II Loaded Specimens (SP1, SP3 and SP6)

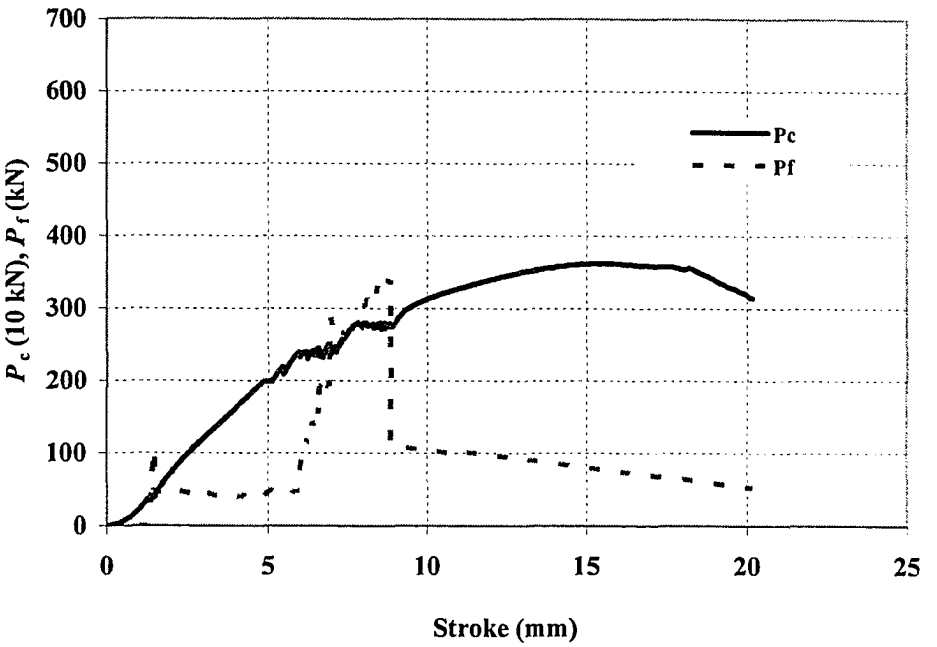

Figure 4.3. Column Load (P_c) and Floor Loads (P_f) vs. Stroke for SP1 (Type-II Loading)

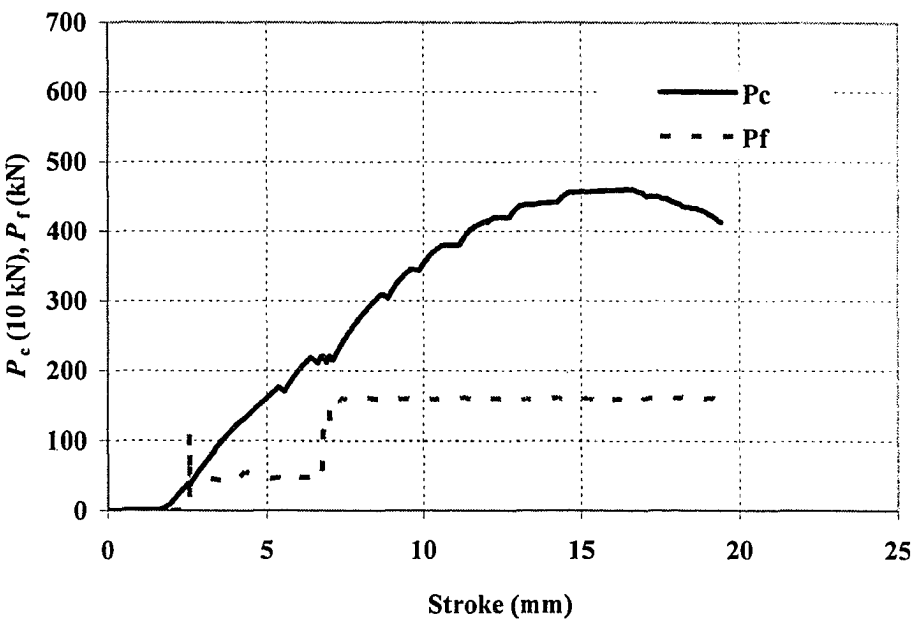

Figure 4.4. Column Load (P_c) and Floor Loads (P_f) vs. Stroke for SP2 (Type-I Loading)

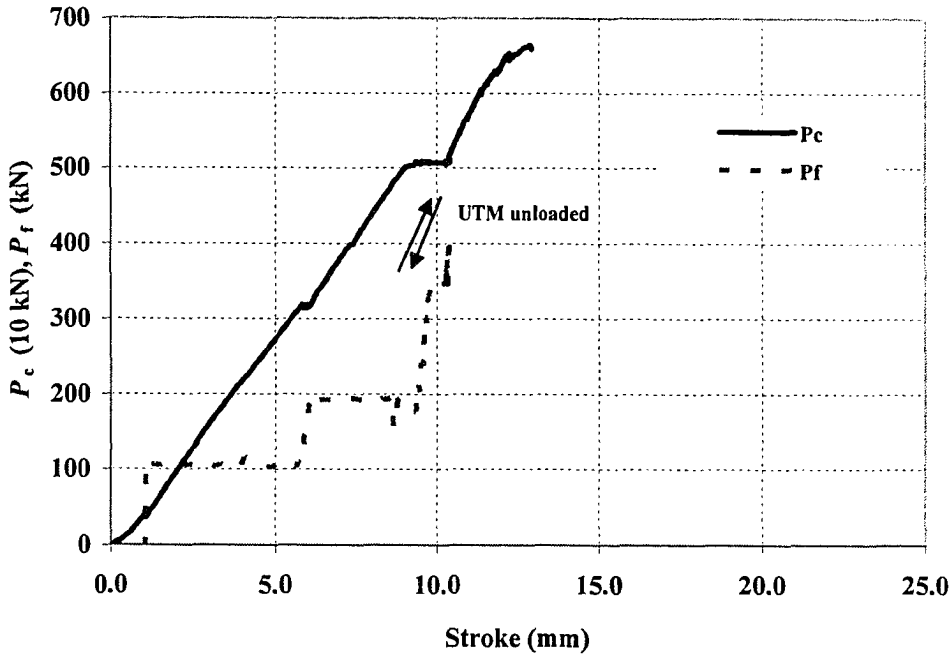

Figure 4.5. Column Load (P_c) and Floor Loads (P_f) vs. Stroke for SP3 (Type-II Loading)

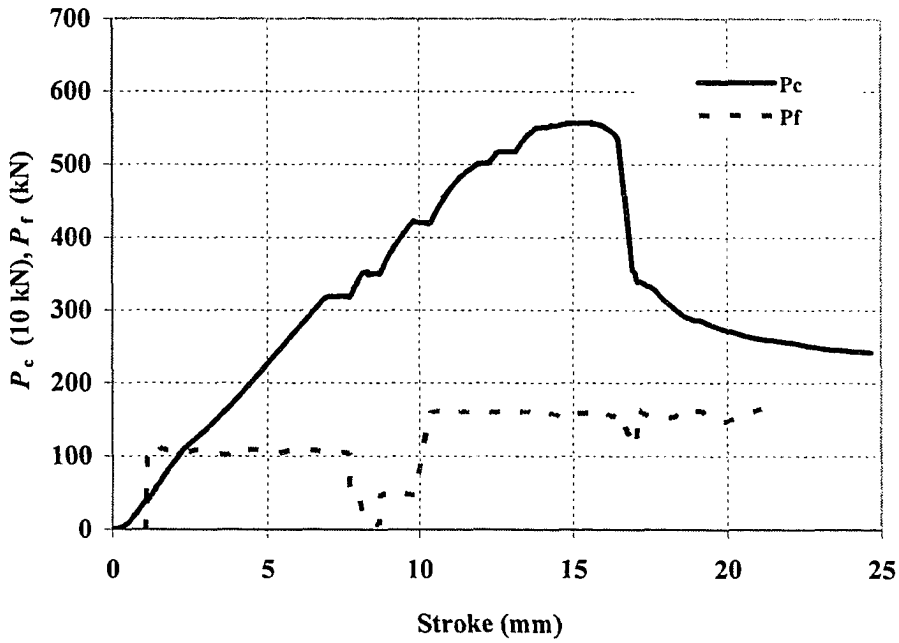

Figure 4.6. Column Load (P_c) and Floor Loads (P_f) vs. Stroke for SP4 (Type-I Loading)

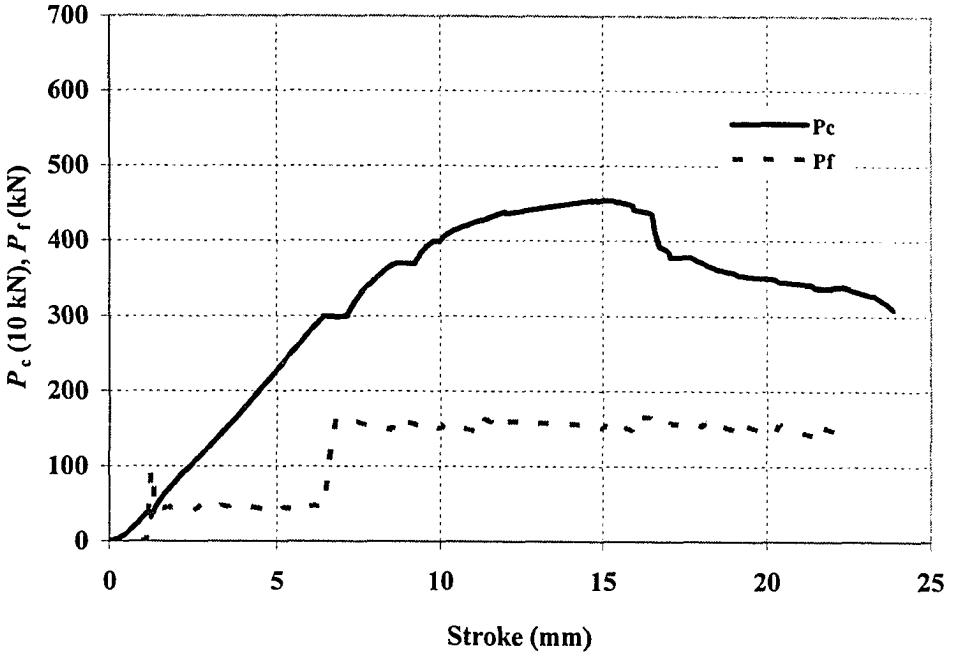

Figure 4.7. Column Load (P_c) and Floor Loads (P_f) vs. Stroke for SP5 (Type-I Loading)

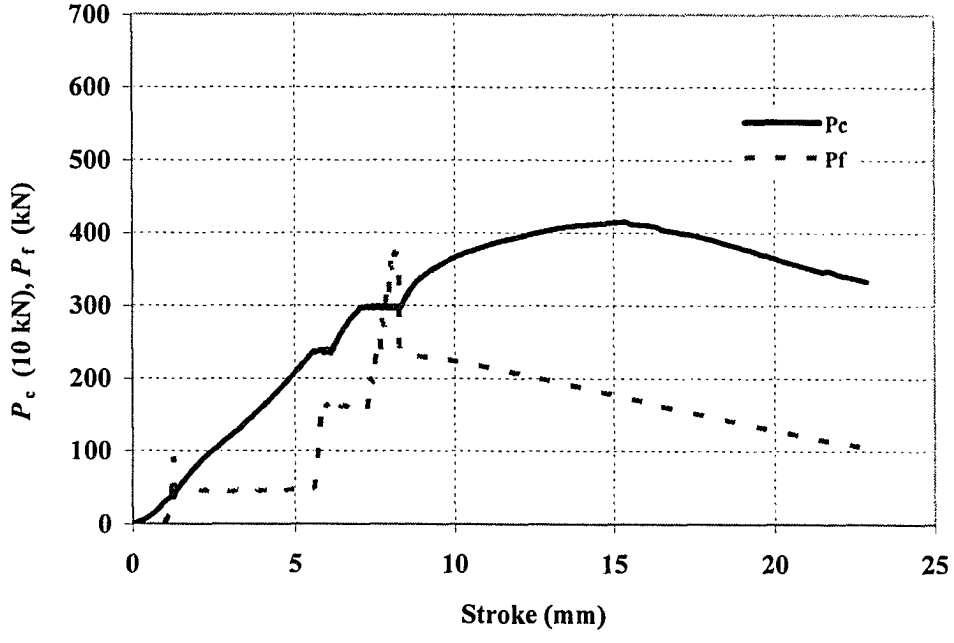

Figure 4.8. Column Load (P_c) and Floor Loads (P_f) vs. Stroke for SP6 (Type-II Loading)

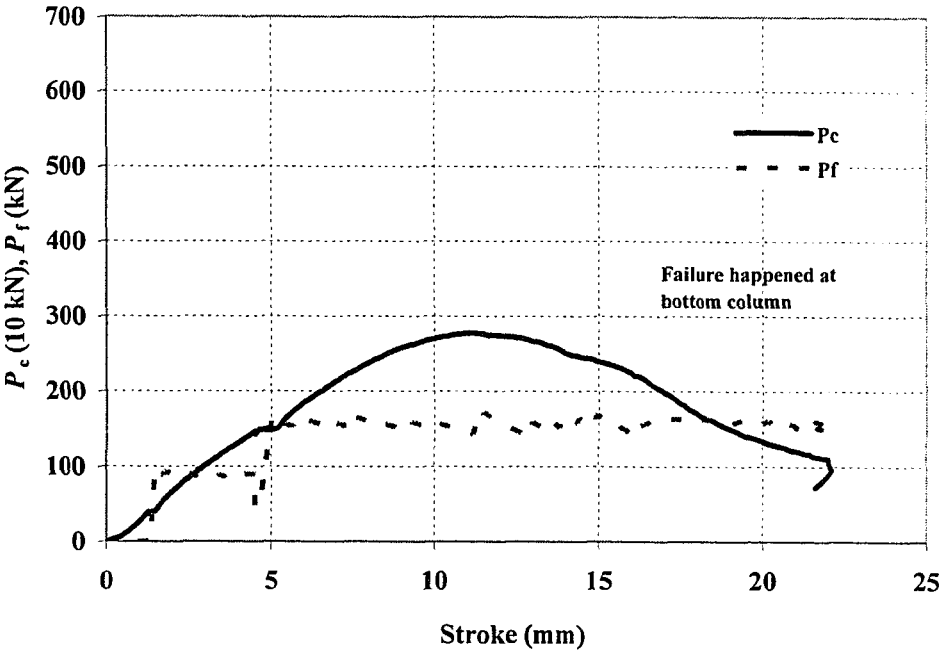

Figure 4.9. Column Load (P_c) and Floor Loads (P_f) vs. Stroke for SP7 (Type-I Loading)

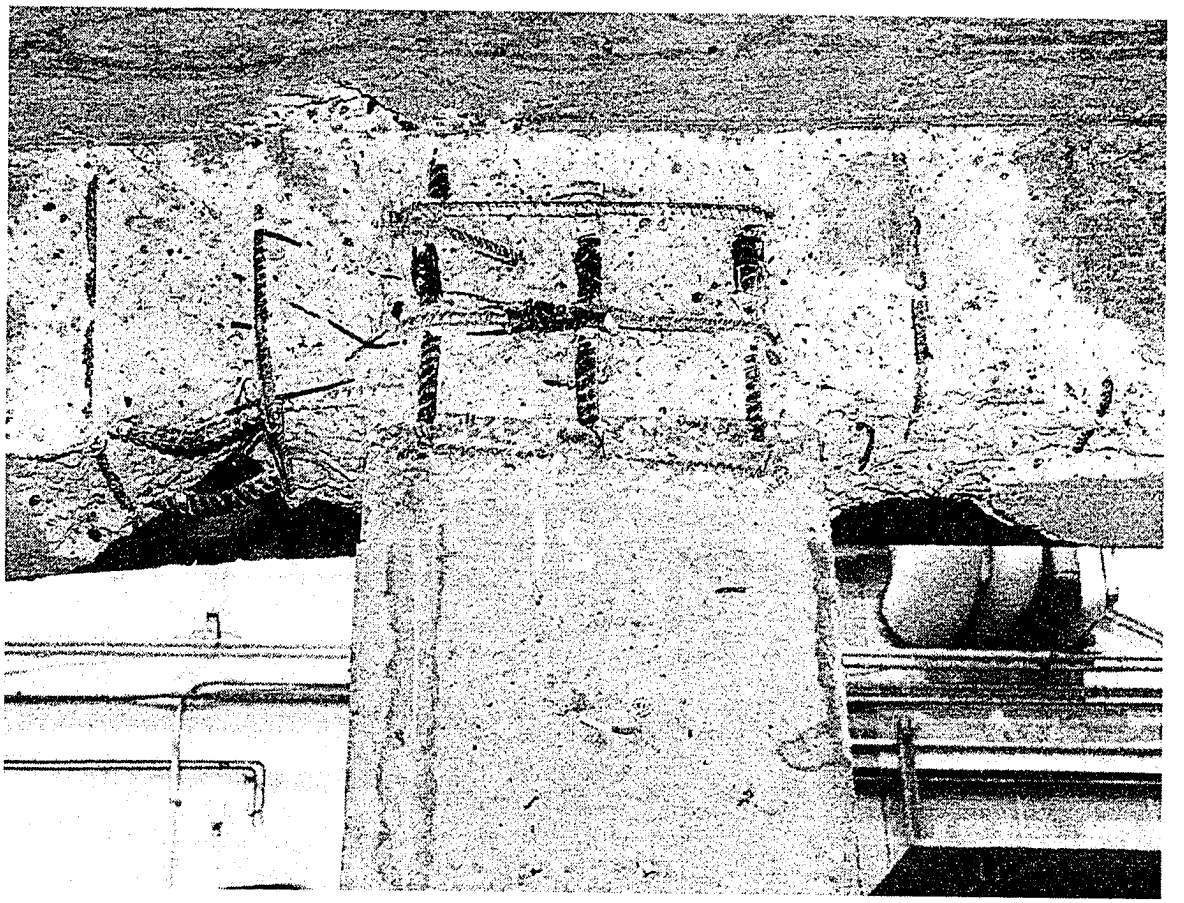

Figure 4.10. SP1-South View of the Column – Beam after the Test

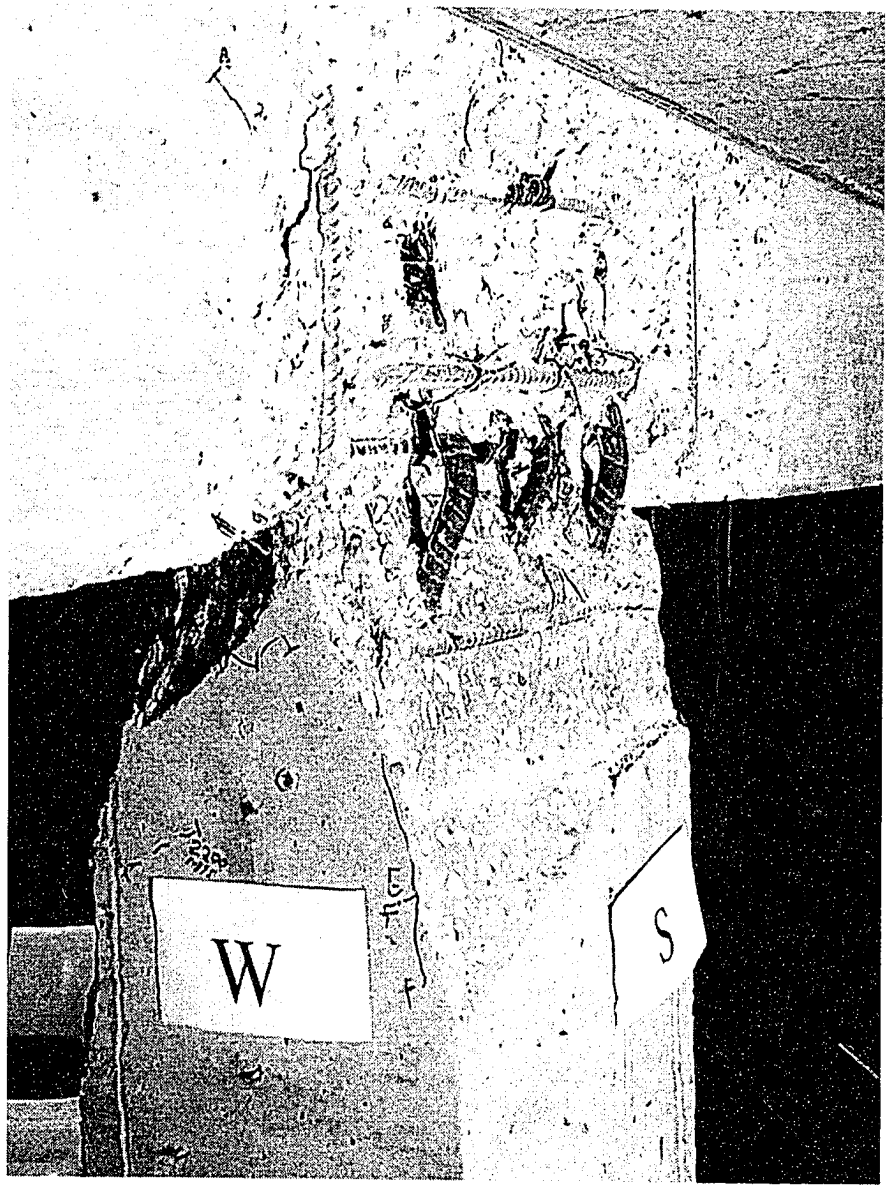

Figure 4.11. SP2-South West View of Beam-Column after the Test

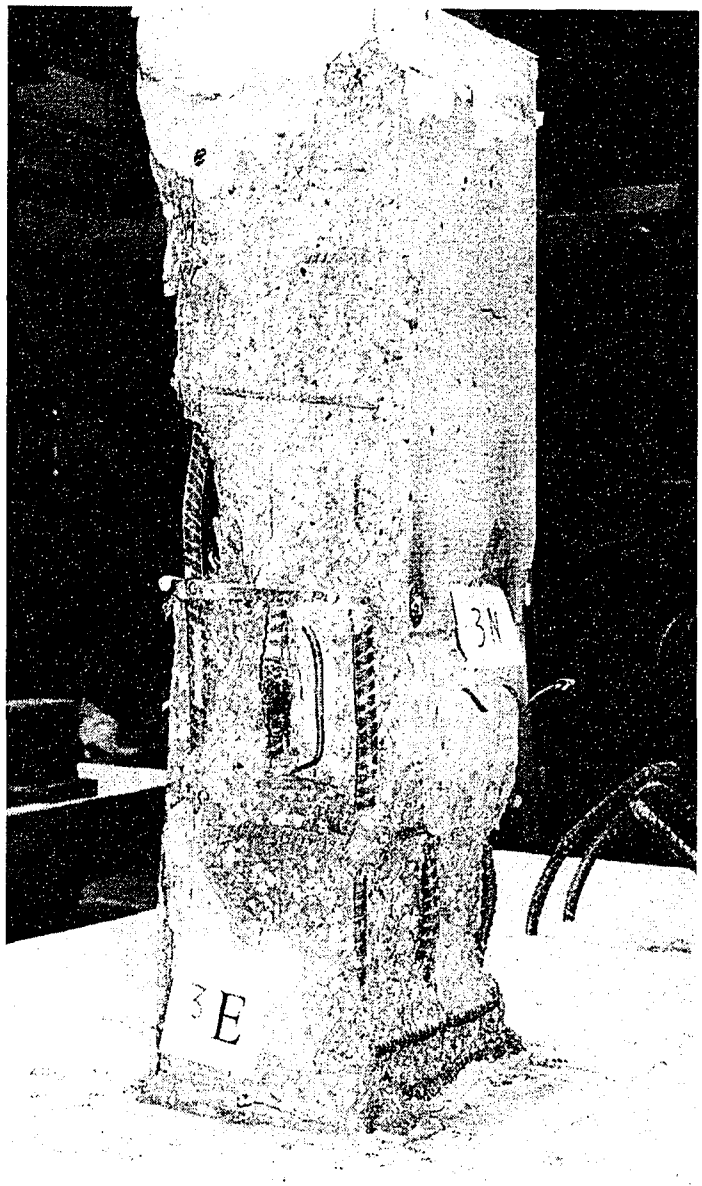

Figure 4.12. SP3-North East View of the Top Column after the Test

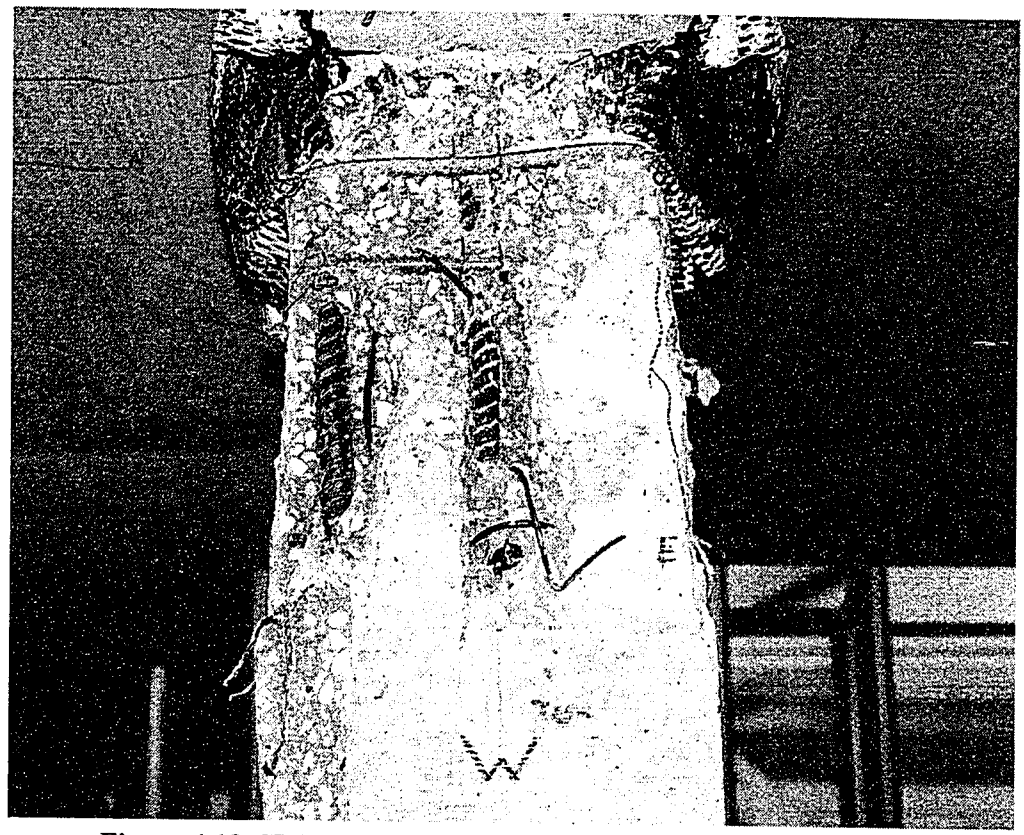

Figure 4.13. SP4- West View of the Bottom Column after the Test

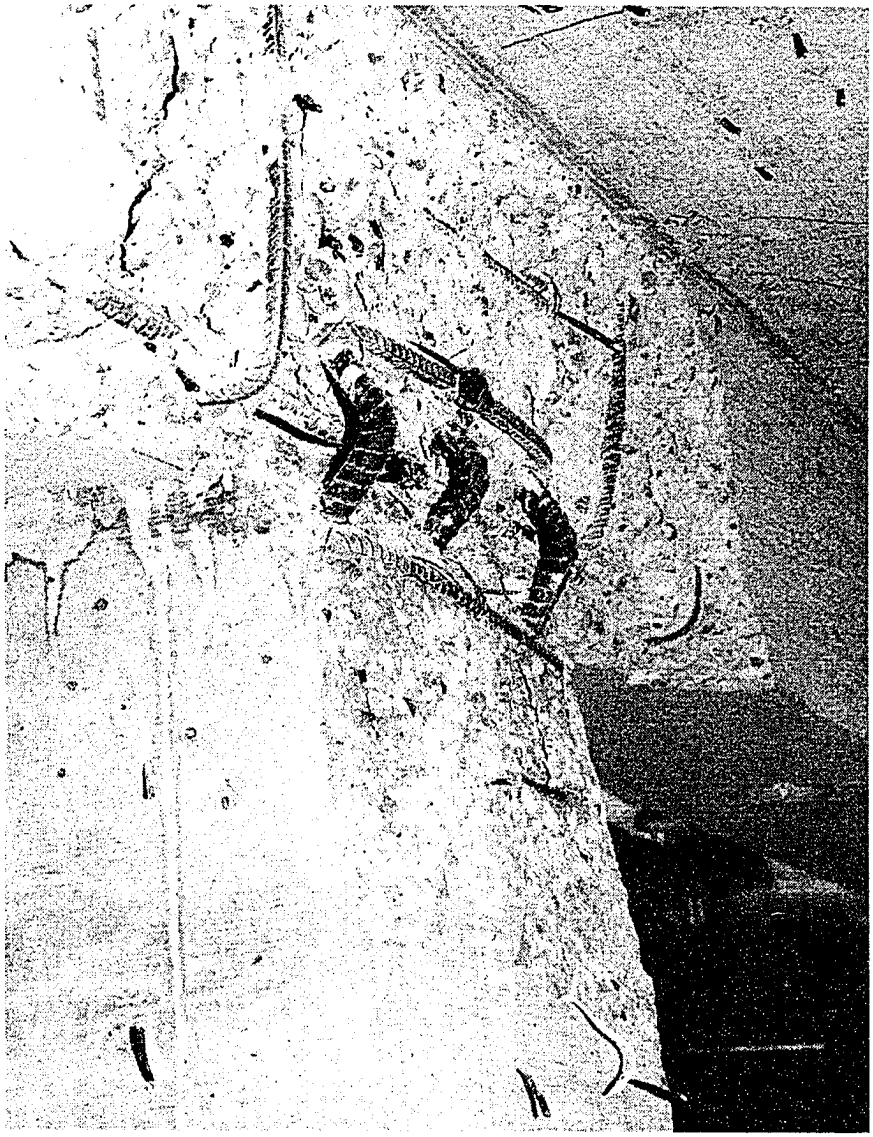

Figure 4.14. SP5-South West View of the Joint after the Test

Figure 4.15. SP6-South East View of Beam-Column after the Test

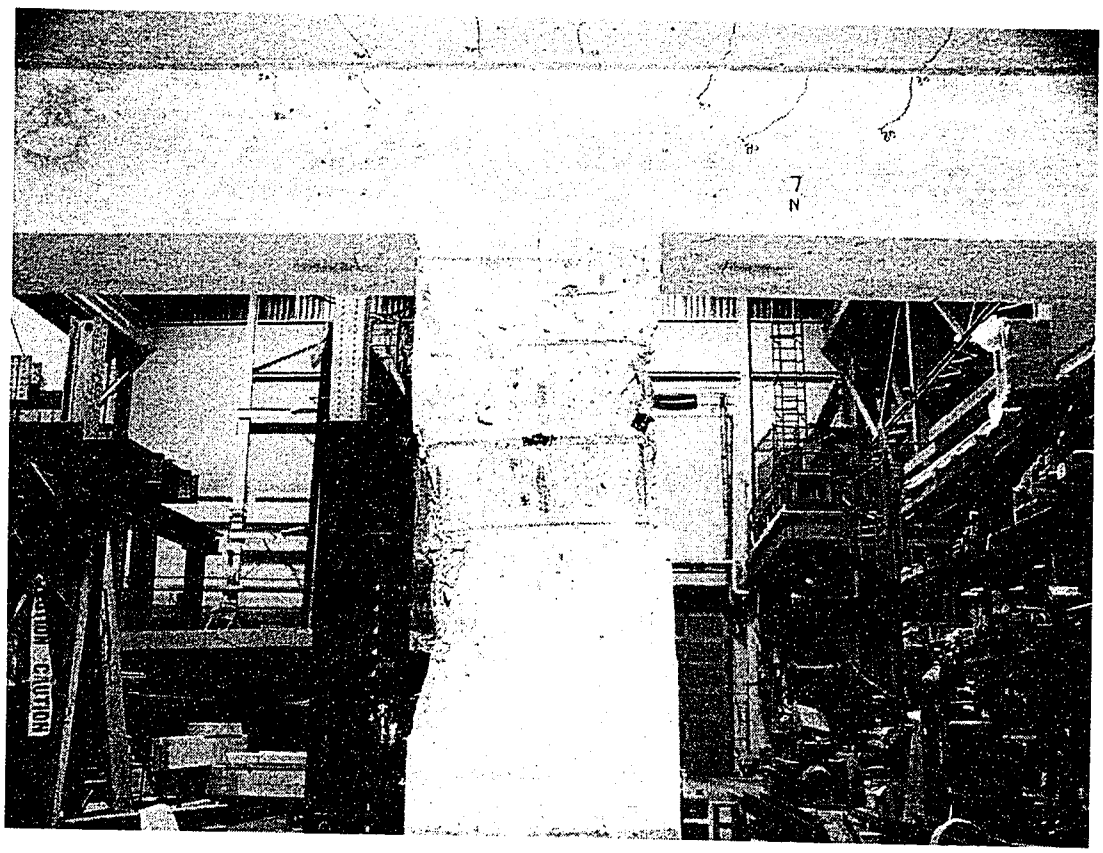

Figure 4.16. SP7-North View of the Column-Beam after the Test

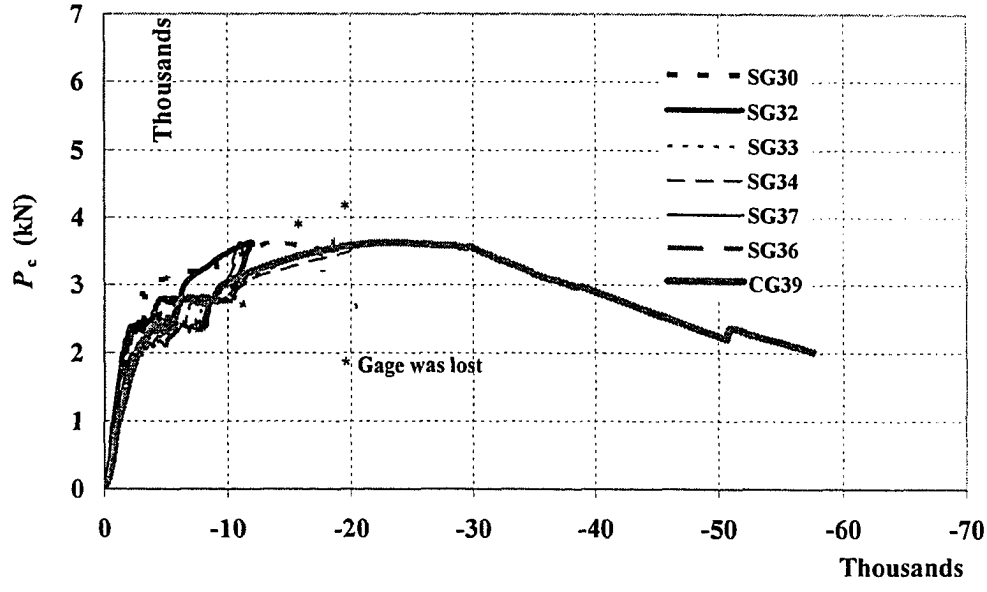

Figure 4.17. Column Load (P_c) vs. Vertical Strain Values in SP1-Joint

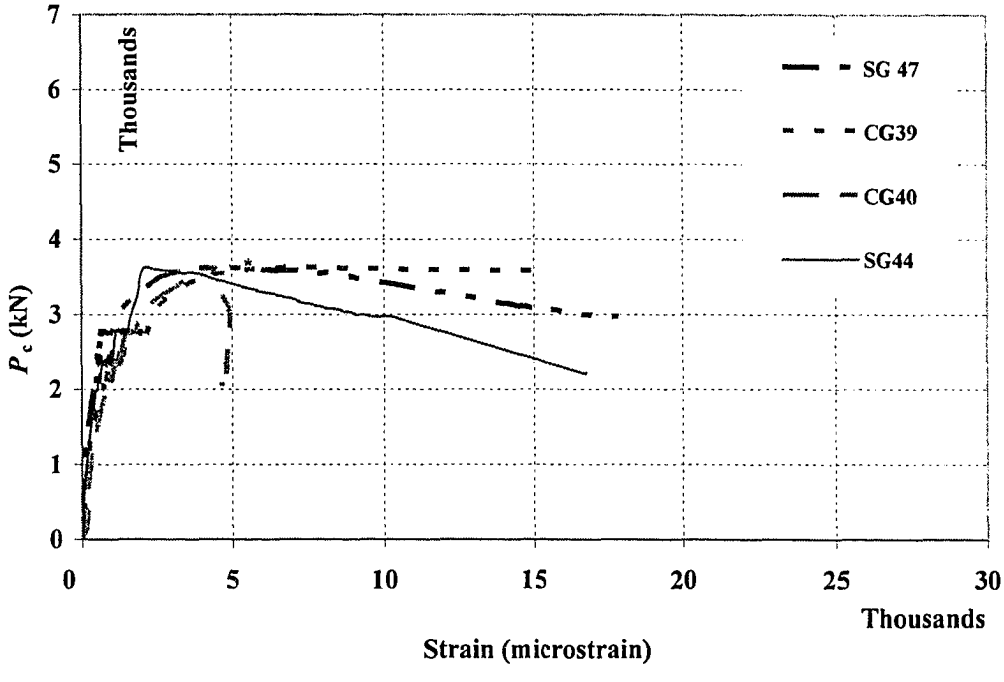

Figure 4.18. Column Load (P_c) vs. Lateral Strain Values in SP1-Joint

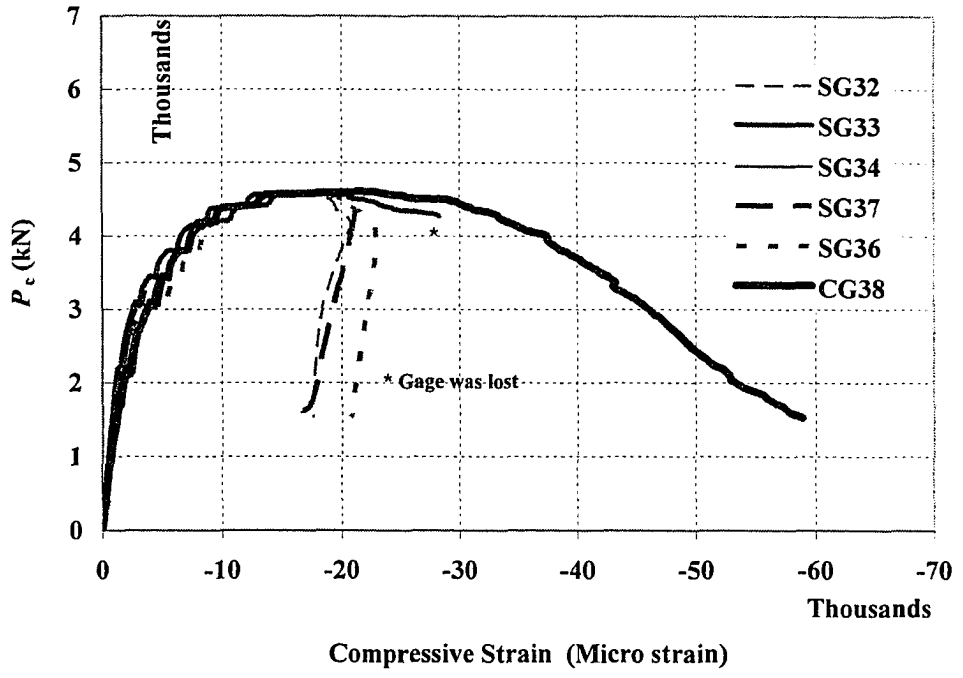

Figure 4.19. Column Load (P_c) vs. Vertical Strain Values in SP2-Joint

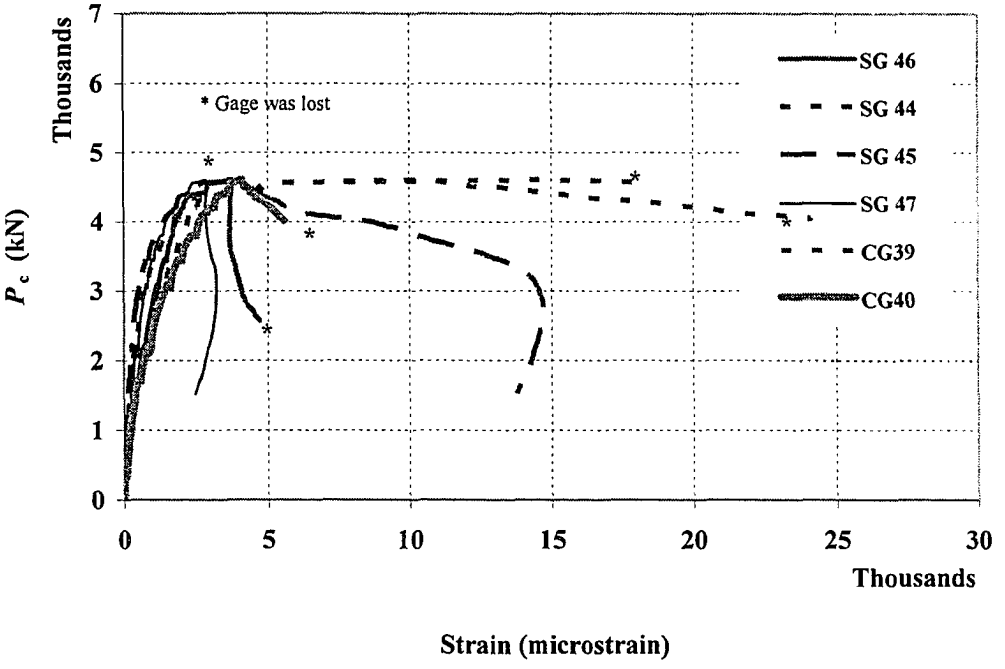

Figure 4.20. Column Load (P_c) vs. Lateral Strain Values in SP2-Joint

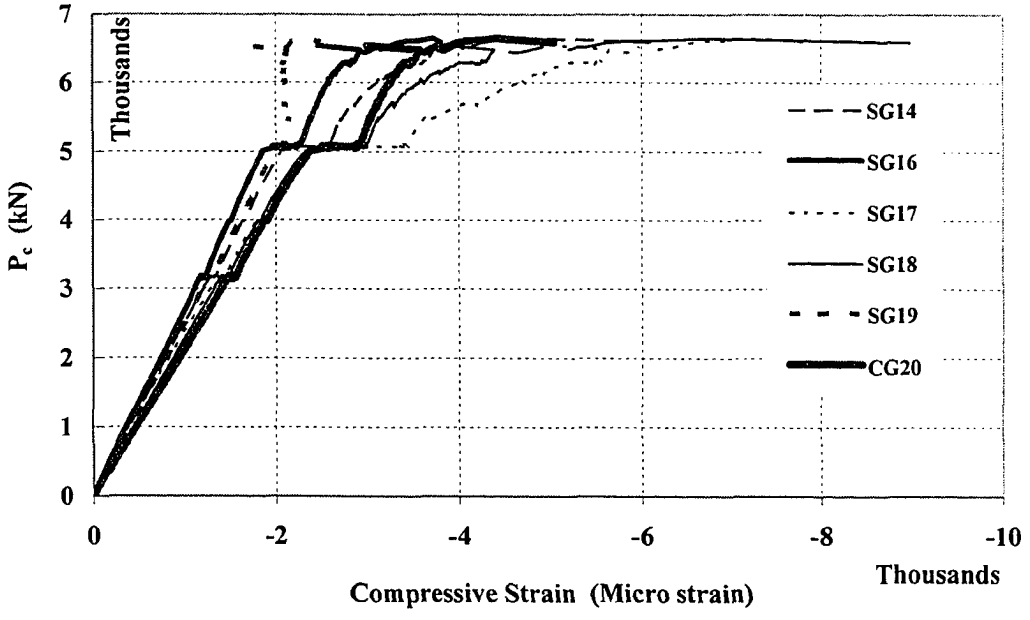

Figure 4.21. Column Load vs. Vertical Strain Values in Top Column of SP3

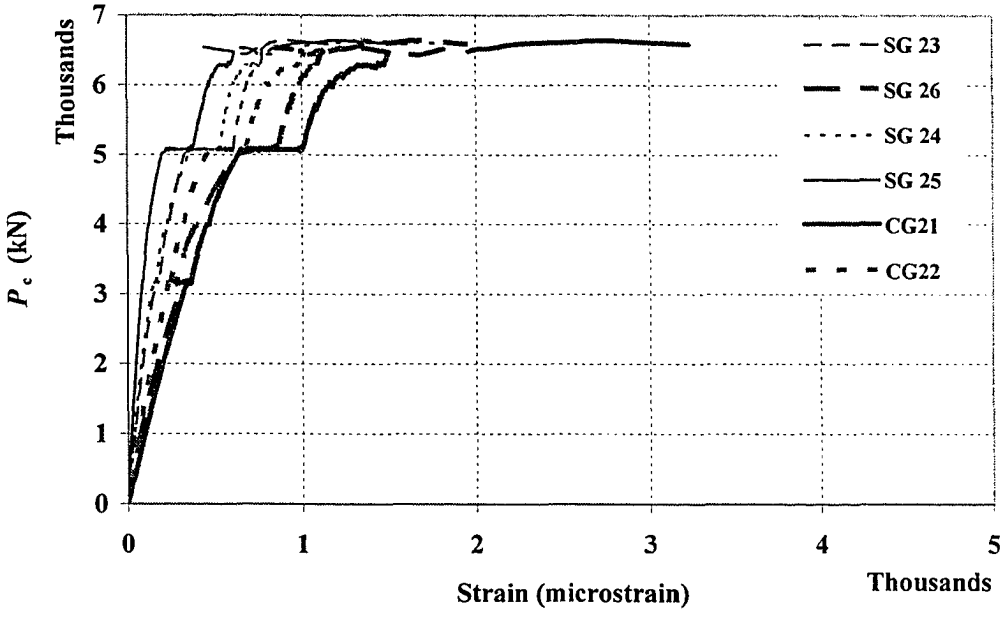

Figure 4.22. Column Load (P_c) vs. Lateral Strain Values in Top Column of SP3

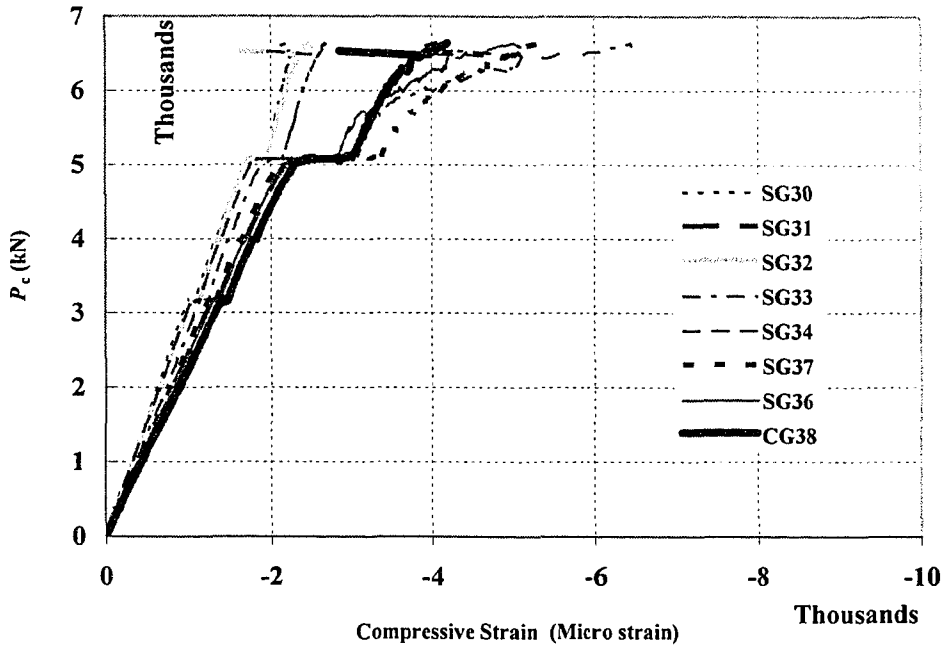

Figure 4.23. Column Load (P_c) vs. Vertical Strain Values in SP3-Joint

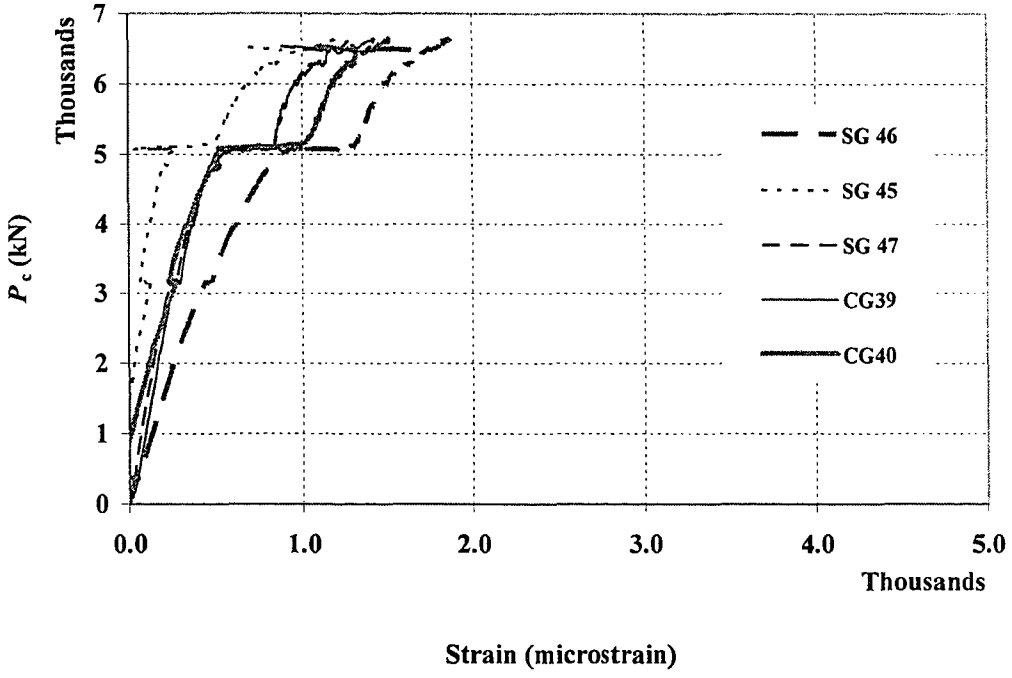

Figure 4.24. Column Load (P_c) vs. Lateral Strain Values in SP3-Joint

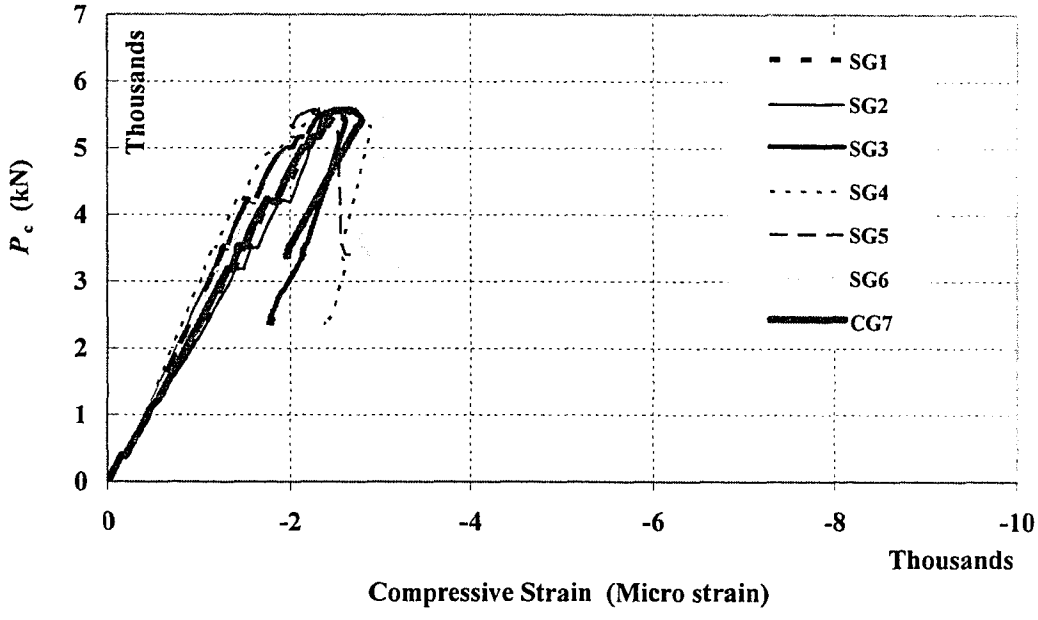

Figure 4.25. Column Load (P_c) vs. Vertical Strain Values in Bottom Column of SP4

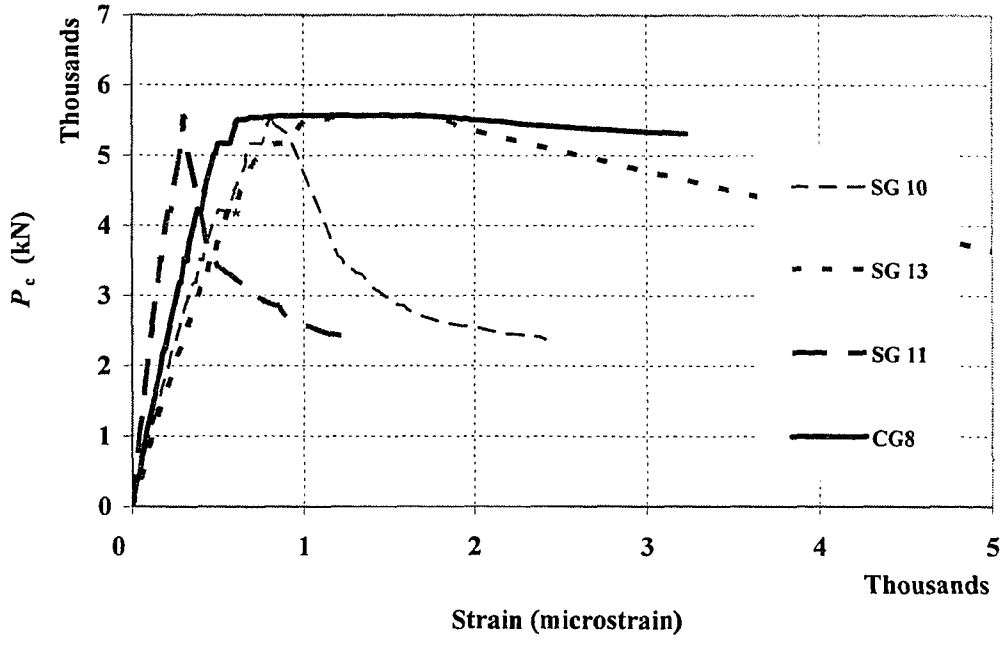

Figure 4.26. Column Load (P_c) vs. Lateral Strain Values in Bottom Column of SP4

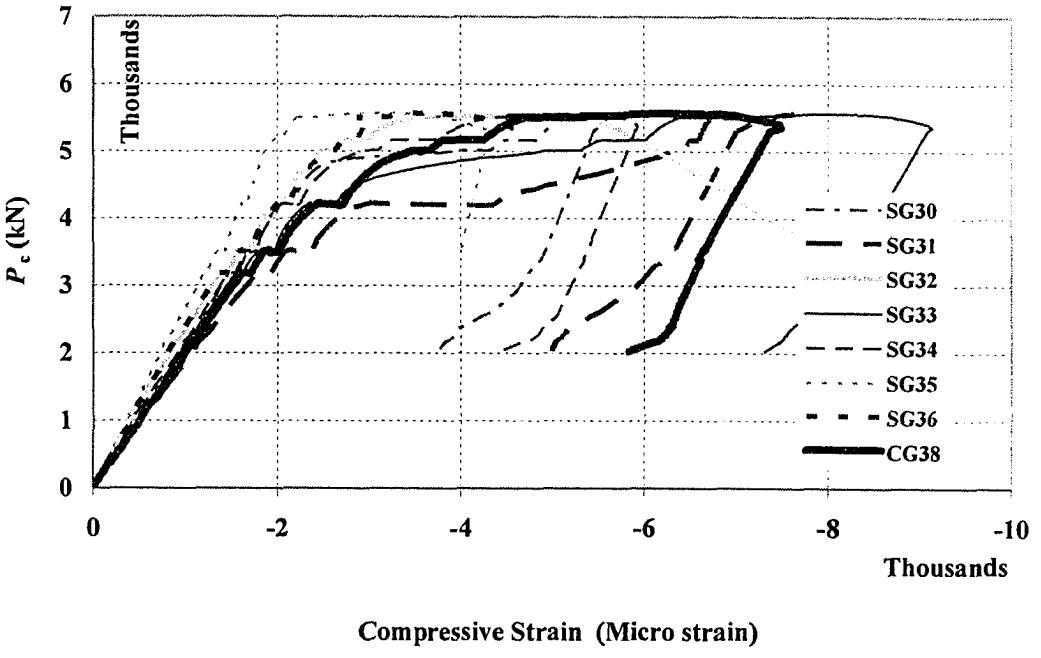

Figure 4.27. Column Load (P_c) vs. Vertical Strain Values in SP4-Joint

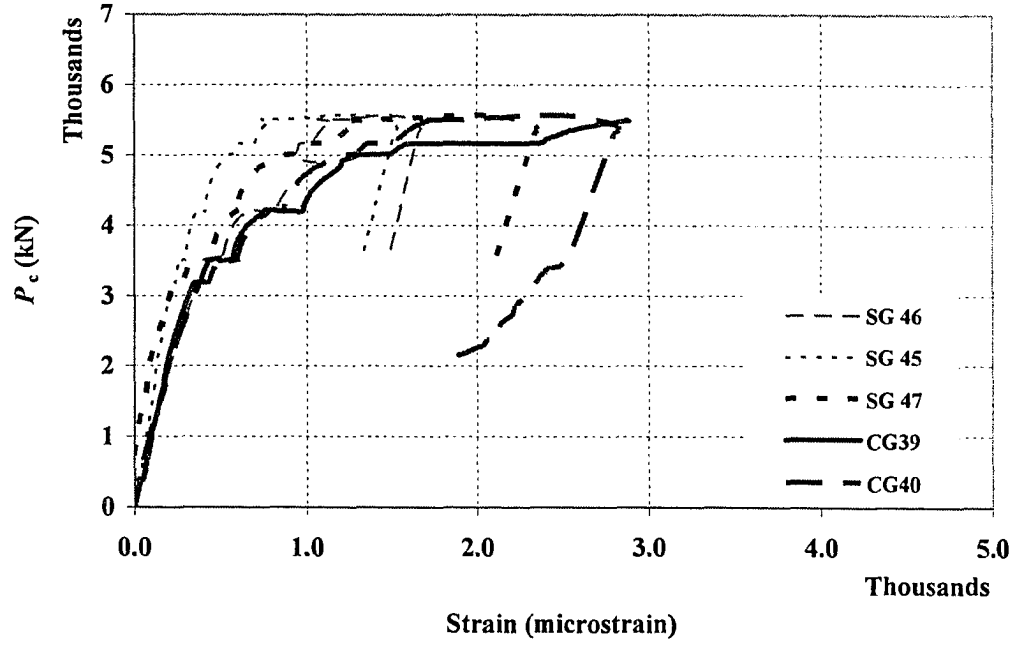

Figure 4.28. Column Load (P_c) vs. Lateral Strain Values in SP4-Joint

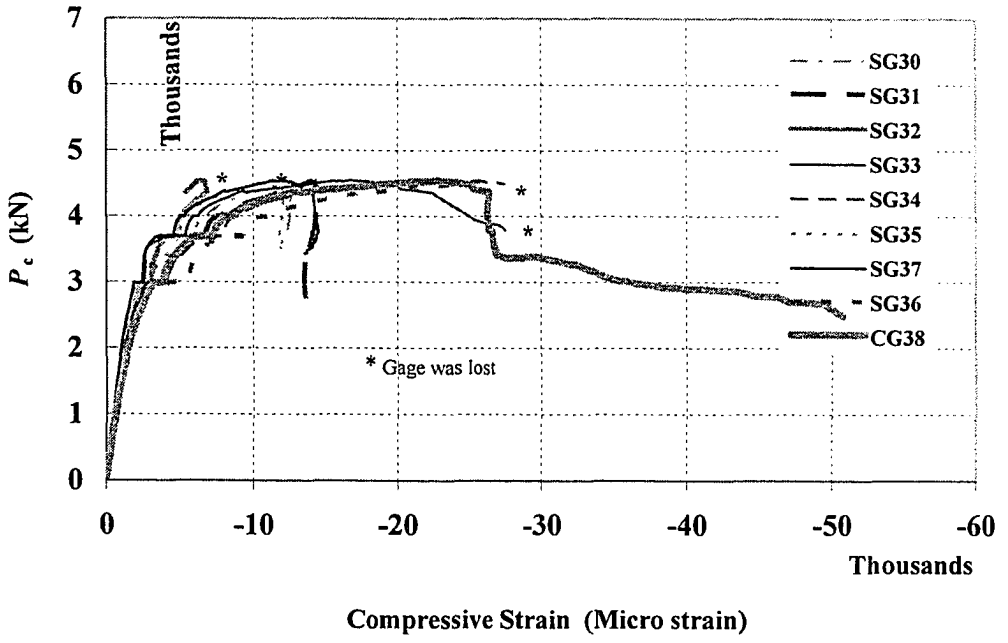

Figure 4.29. Column Load (P_c) vs. Vertical Strain Values in SP5-Joint

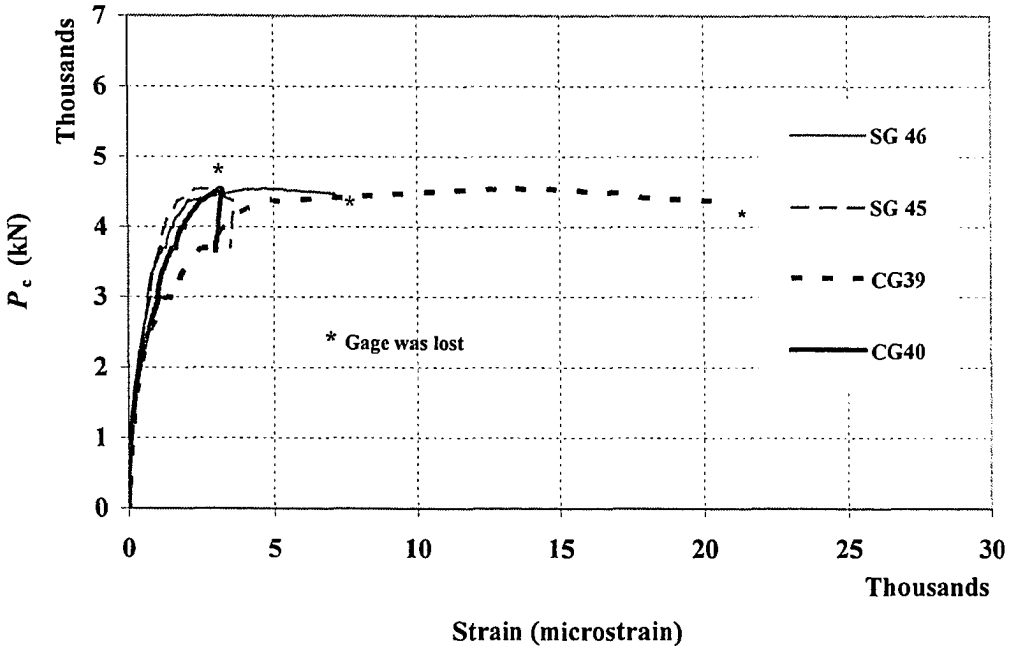

Figure 4.30. Column Load (P_c) vs. Lateral Strain Values in SP5-Joint

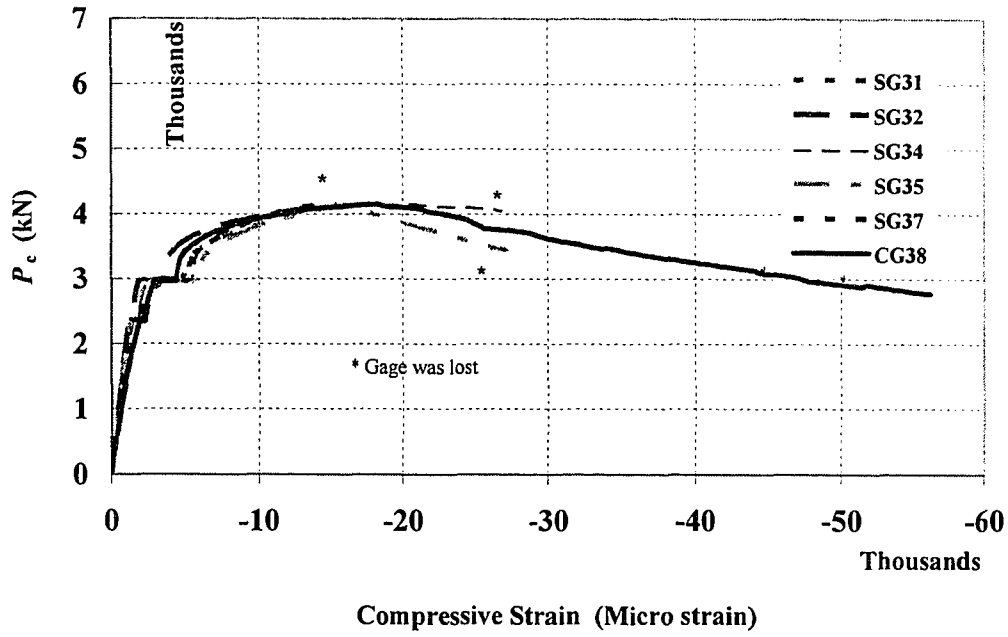

Figure 4.31. Column Load (P_c) vs. Vertical Strain Values in SP6-Joint

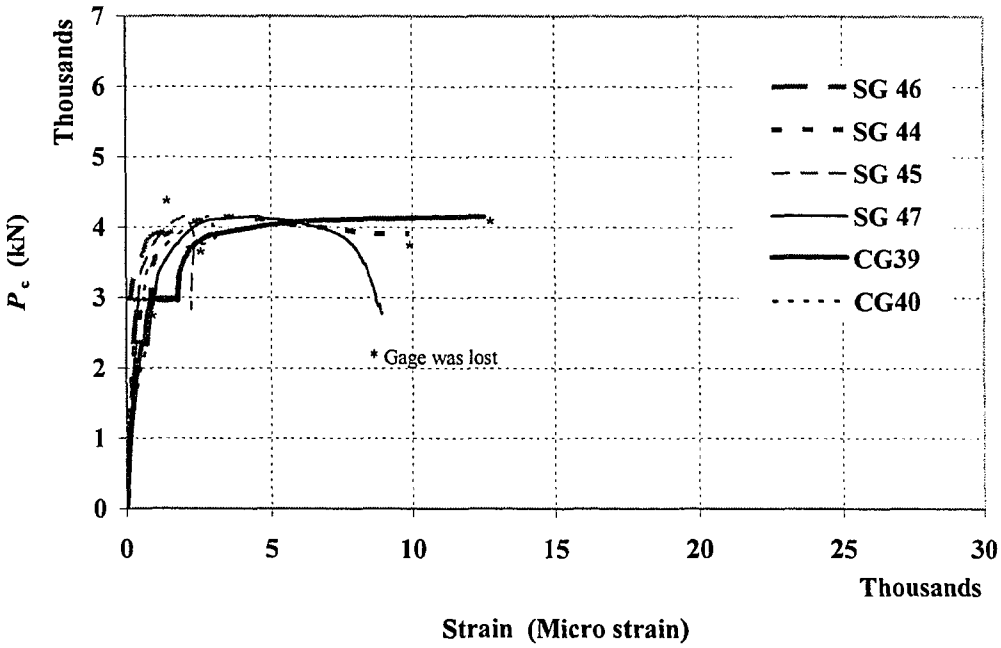

Figure 4.32. Column Load (P_c) vs. Lateral Strain Values in SP6-Joint

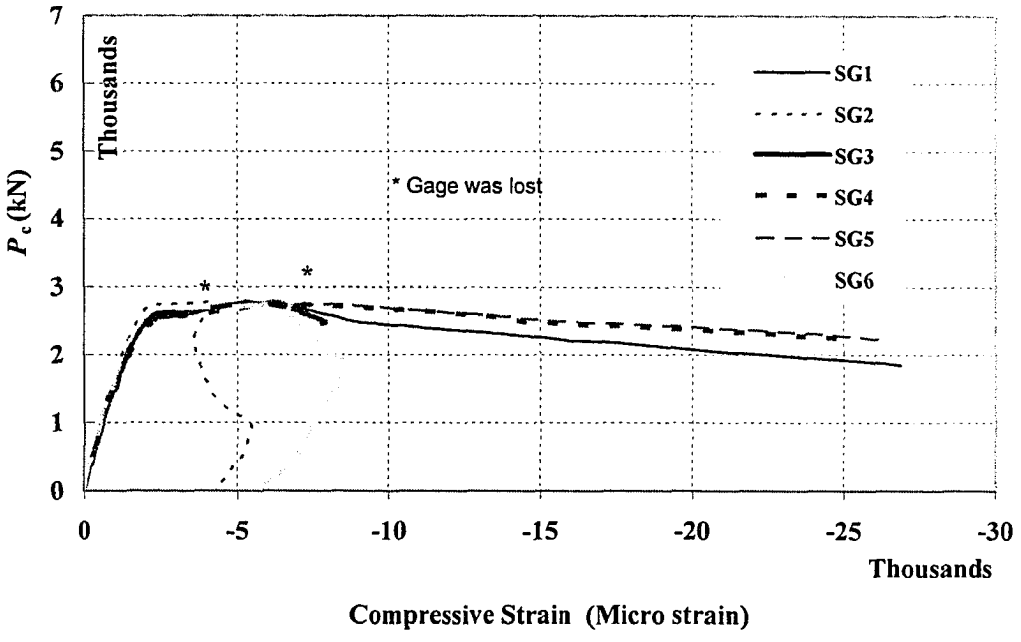

Figure 4.33. Column Load (P_c) vs. Vertical Strain in Bottom Column of SP7

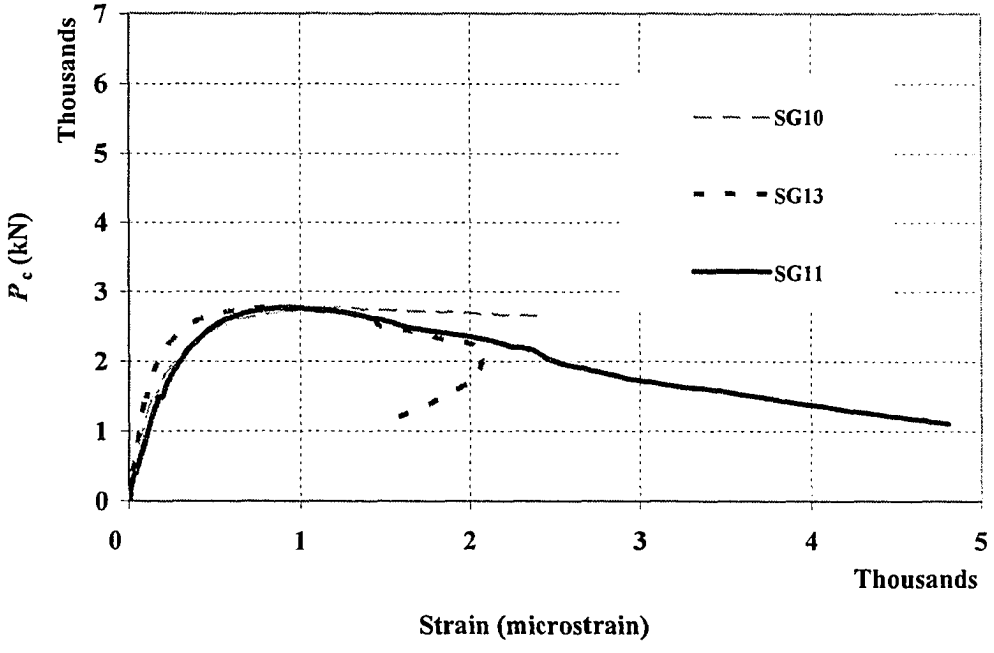

Figure 4.34. Column Load (P_c) vs. Lateral Strain in Bottom Column of SP7

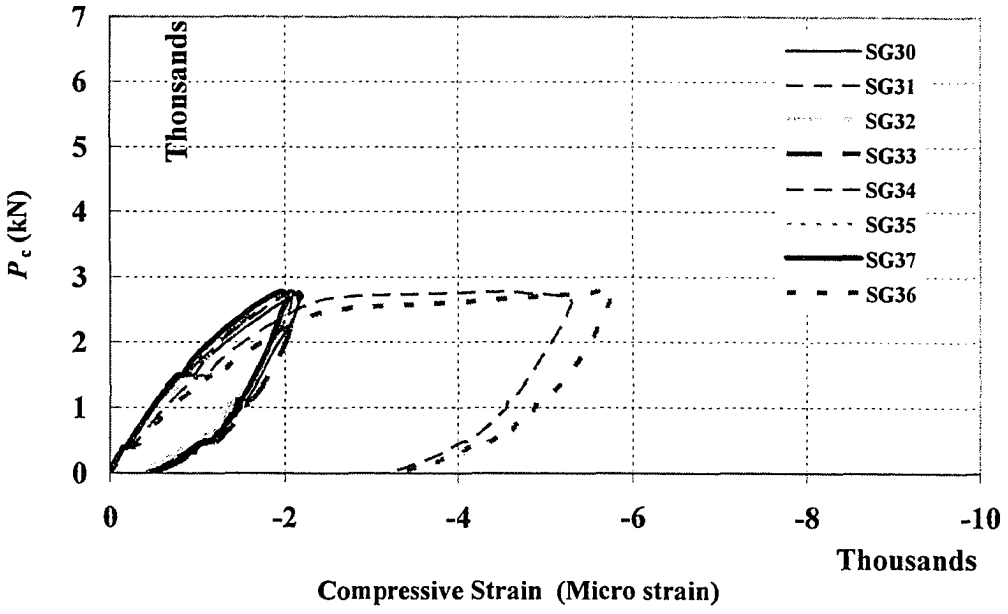

Figure 4.35. Column Load (P_c) vs. Vertical Strain Values in SP7-Joint

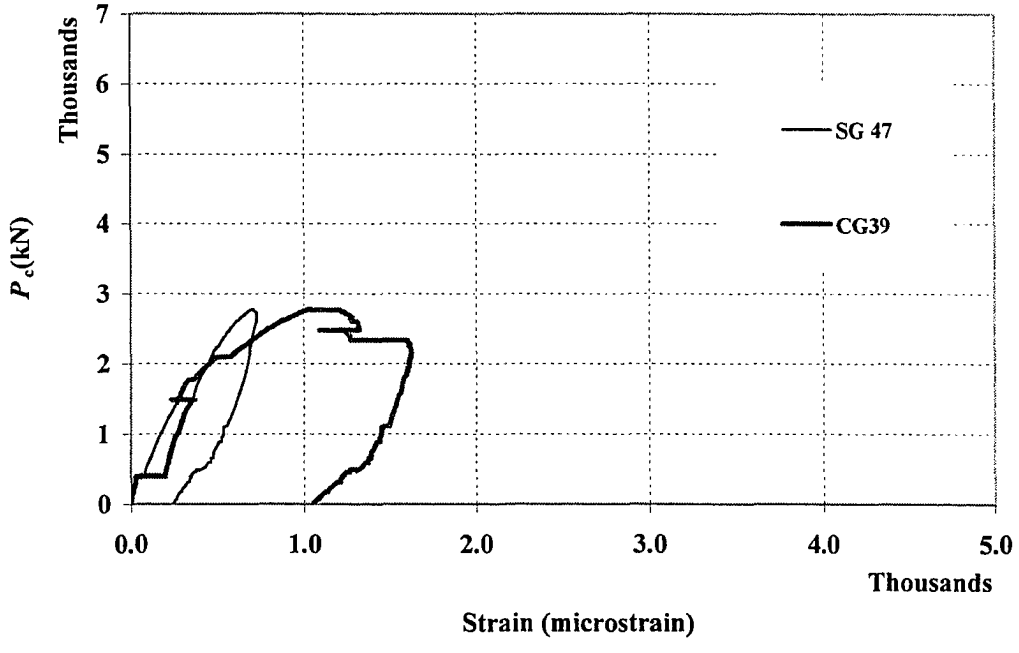

Figure 4.36. Column Load (P_c) vs. Lateral Strain Values in SP7-Joint

5 ANALYSIS OF TEST RESULTS

5.1 Introduction

This chapter covers processing the data and analysis of the behaviour and the failure of each specimen. The test results are compared to the prediction of the empirical equations and analytical models available in literature. The chapter concludes by discussing the influence of the applied loads on behaviour of the different floor elements.

5.2 Analysis of Strain Readings of the Column and Joint Elements

5.2.1 Calculation of LVDT-Based Strain Values

Vertical deformations recorded by LVDT for top and bottom columns were processed as in equation 5.1 to obtain the average vertical strain values in the joint.

$$\varepsilon_j = \frac{\Delta_j - (\frac{\Delta_b}{l_b} h_b + \frac{\Delta_t}{l_t} h_t)}{t_j} \qquad [5.1]$$

With reference to figure 3.24: Δ_b, Δ_j and Δ_t are the total deformations recorded by the bottom, the middle and the top vertical LVDTs respectively and projected at the column axis; l_b and l_t are original distances between the fixation points of the top and bottom LVDTs; h_b is the vertical distance from the lower pinned frame of the middle LVDT to the beam-bottom level; h_t is the vertical distance from the upper fixed frame of the middle LVDT to the slab top level; and t_j is the joint thickness.

LVDT-based lateral strain values were calculated directly for top and bottom columns as the deformation divided by the original length. In the beam direction, lateral strain values of the joint were calculated similarly. Strain values in the transverse (unconfined) direction of the joint were calculated using equation 5.2.

$$\varepsilon_{j;t} = \varepsilon_f - \frac{(\varepsilon_f - \varepsilon_n)}{(1 - x_n / x_f)} \qquad [5.2]$$

With reference to figure 3.25, $\varepsilon_{j;t}$ is the strain value at the joint centreline through the beam thickness, ε_f and ε_n are the strain values calculated from the far and near LVDT devices fixed in the transverse direction of the joint, and x_f and x_n are the distances between the joint centerline and far and near LVDT devices respectively.

5.2.2 Comparison of Vertical Strain Values

Strain values in the joints were bigger than in the columns, except for SP7. Rebars yielded in joint region of all the specimens and in the columns of SP3, SP4, and SP7.

Averaging the recorded strain values of gauges at the same location was reasonable up to the peak load because there was no significant difference between them. Only at higher loads, variation of the strain values was observed because of the uneven spalling of the concrete cover and because of the unavoidable flexural effect on the corner rebars. After the peak load, some rebars buckled or some gauges delaminated.

Strain in the vertical rebars was slightly higher than in the high-strength-concrete (HSC) core. The rebar strain was equal to that in normal-strength-concrete (NSC) until rebars yielded. Figures 5.1 to 5.7 demonstrate the consistency between foil-gauge readings, concrete-gauge readings and LVDT-based strain values. As seen in figures 5.3, 5.4 and 5.7, foil-gauge strain values can be used to estimate rebar stresses for the entire tests of SP3, SP4 and SP7, without extrapolation. For other specimens, it is necessary to extrapolate the rebar strain values shown in figures 5.1, 5.2, 5.5 and 5.6 by using either values from the concrete embedded gauges or the LVDT, depending on which is closer to the average rebar strains.

Figure 5.8 shows the column load (in 10 kN) and the floor load (in kN) against the average vertical strain in the joint of SP2, other figures are shown in appendix C. The column load was the main cause of vertical strain values in the joint region; the floor load effect was a result of its being a fraction of the total applied loads.

5.2.3 Comparison of Lateral Strain Values

Similar to vertical strains, there was no substantial difference between lateral strain values at the same location under small column loads but the small difference

increased with increasing the loads. Strain in the joints was bigger than in the columns, except for SP7. Ties yielded in the joints of all specimens except in SP3 and SP7.

Figure 5.9 shows the column load (in 10 kN) and the floor load (in kN) against the lateral joint-strain measured by the concrete embedded gauges. Lateral strain values of embedded concrete gauges were bigger than those of the tie gauges. The difference increased with the load because the concrete gauges were mounted at mid-elevation between the ties. Therefore, while the gauges on the ties measured strain at the most confined section, the concrete gauges measured strain at the least confined section. Strain values measured by the embedded gauges in the transverse direction were increasing while those in the beam direction stabilized/decreased because of their location under the level of the beam neutral axis.

Figure 5.10 shows the column load (in 10 kN) and the floor load (in kN) against the strain in the ties. The difference between the strain values in outer ties is attributed to their rectangularity and their location relative to the neutral axis of the beam. To check the difference in strain due to flexural effect, some gauges were mounted on the inner and outer points of the long leg of a tie in the column and a tie in the joint. In columns, the inner gauges recorded negative strain values while the outer gauges recorded positive strain values at low column loads and the maximum strain difference was only 120 με. That difference vanished at higher loads due to the concrete dilation. In the joints, some of the instrumented ties were placed below the beam neutral axis and the rest were placed above the neutral axis. For ties below the neutral axis, flexural compression added negative strain to the long leg of the tie reducing the column loading effect, and added positive strain to the short leg. Gauges in ties located above the neutral axis did not show any difference because the expansion caused by the flexural tension in the beam diminished the flexural effect in ties.

5.3 Calculation and Analysis of the Concrete Effective Strength

5.3.1 Calculation of Rebar Stresses

To estimate the concrete effective strength, it is essential to exclude the load carried by the rebars from the total load carried by the section. To do that, rebar stresses are calculated, based on the average measured strain values, by using the non-linear

constitutive models developed for the steel reinforcement and shown in appendix C. Table 5.1 shows average rebar stresses (f_{st}) in the joint region at failure of specimen.

5.3.2 Calculation of the Effective Concrete Strength

Table 5.1 shows results of the joint effective strength (f_{ce}) for the seven specimens tested in this research using equation 2.2 by Bianchini et al. (1960). The actual effective strengths in joints of SP3 and SP7, both of which failed outside the joint, are higher than those shown in the table.

Figure 5.11 shows the relation between the effective strength ratio at failure, f_{ce}/f'_{cs}, and the differential strength, f'_{cc}/f'_{cs}. The value of f'_{cc} is the smaller of the two column strengths. The equation for nominal column strength is represented in the figure by the solid line that has a slope of 1:1. The strength equation for edge joints- mentioned in the Canadian and American standards- is shown by the horizontal line at an f_{ce}/f'_{cs} of 1.4. The f_{ce} values of all the specimens were bigger than the strengths predicted by the edge-joint equation but they were less than the column strengths, except for SP7.

5.3.3 Comparison between Actual and Estimated Effective Concrete Strengths

Table 5.2 shows values of the actual f_{ce} and other values using the equations from literature. Values using the empirical equations for edge joints are smaller than the actual values in general. Using the equation by Gamble et al. (1991) results in the best estimate of f_{ce} except for SP3, SP4 and SP7. Using the analytical models that were developed for columns produces the best estimate for SP3, SP4 and SP7, which failed in the columns. More discussion on the effective strength is given in chapter 6.

5.3.4 Calculation of Tie Confining Stresses

Table 5.3 shows average stresses in the rectangular and diamond ties when the specimens failed and the confining stresses due to ties. Stresses in ties are based on the average strain values and the non-linear constitutive model shown in appendix C. The passive confining stress imposed by the ties on the concrete is estimated by equation 5.5. Except in SP3, SP4, and SP7, average tie stress at specimen failure exceeded the yielding.

$$f_l = \frac{(Af)_{s;o}}{A_o} + \frac{(Af)_{s;i}}{A_i} \qquad [5.5]$$

where f_l is the confining stress of ties; $(Af)_{s;o}$ and $(Af)_{s;i}$ are the confining forces produced by the rectangular and diamond ties respectively; each equals the product of tie average-stress times tie cross-sectional areas at plane of failure; A_o and A_i are the core surface areas confined by the rectangular (outer) and diamond (inner) ties respectively.

As seen in table 5.3,valu es of f_l using equation 5.5 are very close to those calculated using equation 2.31 by Mander et al. (1988). The results could have been closer if an elastic perfectly-plastic constitutive stress-strain model was adopted for ties.

Table 5.3 also shows the gain in concrete strength, Δf_{ce}, as the difference between f_{ce} and f'_{cs}, and the $\Delta f_{ce}/f_l$ ratio. The negative gain in effective strength in SP3 reflects the failure of the specimen before reaching nominal unconfined concrete strength. Tie stresses in the joint of SP3 were almost double that in the top column but they were still far below yielding. Tie stresses in the bottom column of SP4 were smaller than in the joint. Tie stresses in the joint of SP7 were less than in the bottom column, indicating more potential for resisting bigger lateral pressure. The scatter in the $\Delta f_{ce}/f_l$ values indicates that there are more confining factors to consider other than the ties.

5.3.5 Effect of Column and Floor Cases of Loading

Comparing the slope of SP1 vs. SP2, SP3 vs. SP4 and SP5 vs. SP6 in figure 5.11 reveals that the amount of floor loading had some effect on f'_{ce}. Type-I loaded specimens demonstrate higher strengths than type-II loaded specimens. The lowest effective strength ratios are for the type-II loaded specimens with NSC joints (SP1 and SP6).

After collapse of the floor, the effect of floor confinement was lost but the columns still sustained higher loads than those estimated by ACI or CSA equations. Generally, this means that: (1) existence of the floor improves the joint capacity compared to sandwich columns, (2) Overloading the floor will not seriously damage the joint as long as the column load is at service level, (3) the detrimental effect of floor overloading is restricted to the floor, not to the whole structure.

5.3.6 Effect of Using High Strength Concrete in the Joint

As seen from points SP3 and SP4 in figure 5.11, providing sufficient amount of high strength concrete (HSC) in the joint can utilize the full strength of the column.

Specimens SP3 and SP4 developed almost the full strength of the weaker of the two columns framing into the joint although the area of HSC inside the joint was 74% of the column cross section. Increasing the amount of HSC in the joint should increase its effective strength.

5.3.7 Effect of the Differential Strength (f'_{cc}/f'_{cs})

With the same geometry, reinforcement details and loading level, the increase in differential strength, in terms of f'_{cc}/f'_{cs}, increases f_{ce}. SP2 had f'_{cc}/f'_{cs} of 4.2, with f'_{cs} of 20.4 MPa and f'_{cc} of 86.6 MPa, failed when f_{ce} was 45.9 MPa. SP4 had f'_{cc}/f'_{cs} of 1.2, with average f'_{cs} of 0.74x66.7+0.26x17.6=53.9 MPa and with f'_{cc} of 66.7 MPa, failed when f_{ce} was 57.9 MPa. The change of f'_{cc}/f'_{cs} from 1.2 to 4.2 caused f'_{cc}/f'_{cs} to increase from 1.07 to 2.25.

5.3.8 Effect of Partial Debonding of Floor Main Reinforcement

As seen from figure 5.11, comparing SP6 to SP1 reveals that partial debonding has no effect on f_{ce} for type-II loaded specimens. The ratio f_{ce}/f'_{cs} had a value of 1.9 and 2.0 for SP1 and SP6 while f'_{cc}/f'_{cs} was 4.0 and 4.5 respectively. The enhancement in f_{ce}/f'_{cs} for SP6 over SP1 is only due to the difference of the effect of end confinement.

Partial debonding had some potential to improve f_{ce} as long as the floor did not fail. As seen from table 5.1 and figure 5.11, comparing SP2 to SP5, the ratio f_{ce}/f'_{cs} has the same value (2.3) while the ratio of f'_{cc}/f'_{cs} is 4.2 and 3.4 respectively. Although the effect of end confinement is bigger for SP2, the enhancement in f_{ce} of SP5 is almost the same owing to debonding the floor reinforcement.

5.4 Analysis of the Concrete Behaviour

5.4.1 Overall Behaviour

Figures 5.12 through 5.18 demonstrate that NSC joints reached the peak stress at strains much higher than those experienced in joints made of HSC. In the former, the peak stress occurred at a strain in excess of 1.5 percent and there was a significant descending (softening) part, indicating that most of the axial deformation of the column was localized in the joint. Because neither SP3 nor SP7 failed in the joint, there was no softening. Results of SP4-joint showed an incomplete stress plateau suggesting that the

ultimate strength of the joint was reached but failure of the bottom column resulted in unloading before the joint exhibited full softening.

Crushing of the joint concrete- observed in SP1, SP2, SP5 and SP6- was marked by a significant increase in transverse strain, demonstrated by long plateau in the vertical stress-lateral strain curves. Transverse strains in the joints of SP3, SP4, and SP7 were substantially smaller.

The very large longitudinal strains in NSC joints would be more than enough to yield even prestressing steel. This suggests the possibility of considering high strength steel for strengthening NSC joints. Using high strength steel for dowels would reduce reinforcement congestion in the joint and make this design option more practical.

Similarly, the very large lateral strains in NSC joints would be more than enough to yield ties made of high strength steel. This suggests a possible benefit from using high strength steel for confining NSC joints.

As seen in figures 5.12 to 5.18, the overall behaviour can be divided into five stages. (1) The linear ascending stage starts from zero stress until yielding of vertical rebars (f_y). This is not truly linear but close enough to be considered linear. (2) The non-linear ascending stage ends when the cover starts spalling, at about 70-75% of f_{ce} and tie-stresses at 40-50% of f''_y. The concrete effective cross-sectional area is believed to remain unchanged over the entire stage. The concrete stress state changes from biaxial under floor and column loads, to triaxial status due to the tie passive confinement. (3) The cover-spalling stage continues until onset of the peak stage. Spalling of the cover concrete reduces the effectively confined core area until the area stabilizes. What keeps increasing f_{ce} is the increasing confinement stress provided by the reinforcement. (4) The peak plateau stage starts when ties reach maximum stress and continues till softening of the stress starts when the effectively confined core starts to collapse or a tie ruptures. (5) The strain-softening stage is characterized by strain localization or localized failure. The inclination of this part depends on the amount of damage to the section and on the remaining confinement.

5.4.2 Interaction between the Concrete and the Reinforcement at Failure

This section describes the failure mechanism of the different specimens by studying vertical stresses in the concrete (f_c) vs. stresses in the vertical reinforcement (f_{st}). As shown in figures 5.19 through 5.26, three modes of failure can be observed: the

concrete crushes before the rebars buckle, the rebars buckle before the concrete crushes, or the failure combines crushing of the concrete and buckling of the rebars.

For the joint of SP1, figure 5.19, concrete and rebars reached maximum stresses simultaneously. Collapse happened in the concrete before the rebars buckled. For the joint of SP2, figure 5.20, stresses in the concrete and steel were proportionally increasing until the vertical rebars yielded. This was followed by sharp increase in concrete stress that reached maximum and the concrete started to crush while f_{st} was increasing until the rebars buckled. For the column of SP3, figure 5.21, f_c increased almost linearly with the increase in f_{st} until the concrete reached a stress of 50 MPa. Rebar stress stabilized at 400 MPa while f_c was escalating until the sudden failure.

As in figure 5.22, f_c in the joint of SP4 remained at maximum until rebars reached maximum stress. While the concrete was crushing, f_{st} remained at maximum until local buckling of rebars. For SP4-bottom, figure 5.23,t he concrete reached maximum stress slightly after reinforcement. Some rebars buckled upon yielding. Buckling of the rebars in the bottom column occurred after joint concrete started to crush. The axial load, while decreasing, was transmitted from top to bottom columns through vertical rebars. Tie spacing in the columns was fifty percent longer than in the joint and therefore the rebars buckled consecutively in the bottom column with deterioration of the joint concrete.

As seen in figures 5.24 and 5.25, f_c and f_{st} in the joints of SP5 and SP6 increased proportionally until the rebars yielded. The concrete stress, then, increased sharply up to its maximum value before localized crushing in combination with buckling of rebars.

Figure 5.26 shows that the concrete of SP7 crushed before the rebars buckled.

Slight differences could be observed in the failure of SP5 and SP6. Studying SP5 processed data and figure 5.16 revealed that ties yielded very close to the maximum effective stress (f_{ce}) and failure of the joint started right after. This was marked by sudden drops in the concrete stress and tie stresses. This resulted from a localized crushing of the effectively confined core at tie level, causing partial unloading of the ties. As seen from the processed data of SP6 and from figure 5.17, the tie stress was increasing while the concrete stress was gradually softening. This resulted from gradual crushing of the effectively confined core between ties, with no localized failure at tie level.

5.4.3 Failure of SP3- Top Column

Failure of the column was explosive because the load at failure exceeded the nominal capacity of the UTM. Huge strain energy was stored in the UTM until the shear failure formed in the concrete. After the shear failure caused the tie to snap, the strain energy released by the UTM as the load dropped exceeded the energy that the specimen could absorb. This is similar to the explosive failure of HSC cylinders.

It is difficult to determine whether failure of the concrete in the top column occurred before or after rupture of the second tie above the slab. The possibility that the tie fractured before the concrete because of a flaw in the tie cannot be verified either.

The bottom column of SP3 had about 6% more load than the top column. The difference in strength between the bottom and top columns (89.2 MPa compared to 90.7MPa) is well within the normal scatter between various "identical" columns.

5.4.4 Comparison to Models from Literature

Figures 5.27 to 5.33 show the experimental stress-strain curves compared with those predicted using the models mentioned in chapter 2. The curves predicted by the models are not in good agreement with the actual ones except for SP3, SP4 and SP7. The models by Sheikh and Uzumeri, and Mander et al. (1988) are close to each other and closer to the actual curves than the model by Yong et al. (1988). The model by Sheikh and Uzumeri showed unjustified reversal in the peak of SP3 and SP4, joints of HSC. For SP1, SP2, SP5 and SP6, there is a big difference between the actual and modeled curves in terms of strength and in ductility. This reflects the substantial increase in strength and ductility of the joint as compared to a column section with similar reinforcement.

Figures 5.27, 5.28, 5.31 and 5.32 show kinks in the actual stress-strain curves corresponding to the peak stresses predicted by the models. While the peaks in the models correspond to the cover spalling, the kink in the actual curves is bigger for type-II loaded specimens than for type-I loaded. As the pause in column loading was longer for type-II, the kink of the peak is related to structure behaviour and loading sequence.

5.5 Behaviour of the Floor Elements

This section describes the effect of column load and floor loads on the strain

values measured through the gauges mounted on the floor reinforcement.

Figures 5.34 to 5.41 show effect of the column and floor loading on strain values of the floor reinforcement at the face and core of each joint; the rest of the figures are shown in appendix B. Figures 5.34 and 5.35 cover behaviour of the beam bottom reinforcement, figures 5.36 and 5.37 cover behaviour of the beam side reinforcement, figures 5.38 and 5.39 cover behaviour of the beam top reinforcement, and figures 5.40 and 5.41 cover behaviour of the slab top reinforcement.

Strain in the side rebars at peak load was equal to that in top rebars of the beam despite the difference in their distance from the neutral axis. The increase in the strain values of the side rebars above that caused by the flexural action of the beam is attributed to the development of a strut-tie mechanism in the joint. The core strain values were increasing at higher rate than those at the face. This was not the case in SP3, SP4 or SP7 because their joints were not the weakest parts, and so no strut-tie mechanism developed.

5.5.1 Effect of the Column Load

The column load caused dilation of the joint, adding tension strain to the floor reinforcement. The effect was small on strain values measured at face of the joint and vanished after failure of the floor. Below the full service load on the floor, the column load added more tension strain to the bottom rebars than to the top or side rebars. At higher loads on type-I loaded specimens, the added strain was the same on all rebars, with the exception of partially debonded rebars, which were unaffected. The added strain was substantial in SP2, having the weakest joint and slight in SP4 and SP7.

5.5.2 Effect of the Floor Load

The floor load added tension strain to the top reinforcement at face and core of the joint. Gauges at the face recorded larger strain than those in the core because of the flexural action of the beam. The added strain was minor for specimens with bonded reinforcement and major for specimens with partially debonded reinforcement.

The floor load added compression strain to the bottom reinforcement, except for SP5. Strain values in the bottom rebars of SP5 changed from compression to tension at low floor loads due to dilation of the concrete but, surprisingly, the tension strain

increased with increasing the floor load. A possible reason for this observation is that the foil gauge was facing the unconfined face of the joint.

The floor load was the main cause of tension strain in side bars of the beam till service load level, above which the increase in strain values was only due to column load except for type-II loaded specimens. For partially debonded specimens, there was no effect of the floor load on strain in side reinforcement until service load and even then there was only a minor effect at higher floor loads until collapse of the SP6 floor.

5.6 Floor Moment – Curvature Relation

Figures 5.42 and 5.43 show effect of the specimen loading on curvature of the beam for SP2 and SP3. The column load, P, is normalized with the peak load, P_c. The bending moment, M, is calculated at the face of the column and normalized with the factored moment of resistance of the beam, M_r, which is calculated according to the CSA A23.3-94. The curvature (ϕ) is based on strain measurements on the top and bottom beam reinforcement at the face of the column and is calculated as in equation 5.6. The beam of SP2 was loaded to half its flexural capacity under type-I loading while the beam of SP1 was loaded to its full flexural capacity under type-II loading.

$$\phi = \left(\frac{\varepsilon_{t,ave} - \varepsilon_{b,ave}}{d - d_2} \right) \qquad [5.6]$$

Where: $\varepsilon_{t,ave}$ and $\varepsilon_{b,ave}$ are the average strain values of top and bottom beam reinforcement at face of the column, d is the flexural depth, (d-d_2) is the center to center distance between top and bottom reinforcement, A_s is area of the beam flexural reinforcement, f_y is yield strength of the beam flexural reinforcement, f'_{cs} is the specified compressive strength of the floor, and b_w is the beam width.

Increasing the column load decreases the curvature at low loads owing to the upward curling of the floor. The expansion of the joint was more restrained at the top than at the bottom because the top reinforcement was more than the bottom (as reported by Gamble et al). The curvature increases at higher column loads due to the plastic deformation in the floor top reinforcement.

Debonding of the beam top reinforcement allows higher strains to be mobilized in the top steel with limited damage to the concrete. This could be inferred by comparing the maximum flexural strain of the beam reinforcement of SP1, SP3 and SP6, by comparing the lateral strain measured by the concrete gauges to that measured by foil gauges of SP6, and by observing fewer cracks on the slab of SP6 than that of SP1.

The curvature of type-II loaded floors is about 10 times that of type-I loaded floors. The maximum curvature, though, is very little (0.2 radians) because of the relatively high reinforcement ratio of the beam, which was selected to satisfy the flexural needs of the first internal joint of the prototype structure without allowing for moment redistribution.

Curvature of a beam was much smaller for specimens with monolithic NSC joints than for specimens with HSC cores or specimens with debonded reinforcement (compare SP1 vs. SP3, SP2 vs. SP4, SP2 vs. SP5, and SP2 vs. SP7, figures 5.42, 5.43 and figures C57 to C61). For SP3, SP4 and SP7, the confinement was negligible because the relative concrete strength ratio, f'_{cc}/f'_{cs}, is small while it is much bigger for SP1 and SP2. There was no restraint at all for the case of debonded negative reinforcement (SP5 and SP6). This suggests that floors with monolithic joints have less end rotation than others, especially when f'_{cc}/f'_{cs} is large. As well, it demonstrates that floors with non-monolithic joints or floors with debonded reinforcement have enough rotational capacity.

According to the variables tested in this research, three factors are believed to affect the beam curvature: the bond between the beam top reinforcement and the joint concrete; the axial stress level, which can be defined as the ratio of f_c at the time of floor collapse, to f_{ce}; and the f'_{cc}/f'_{cs} ratio. The combination of these factors determines the amount of restraint imposed on the beam reinforcement within the joint. The restraining force or the rotational stiffness decreases by debonding the beam top reinforcement, by increasing the axial stress level and by decreasing the differential strength.

5.7 Discussion

5.7.1 Unloading and Reloading During Test

As the UTM load was suddenly dropped to zero before the peak load of SP3 was

reached, it was necessary to investigate the unloading/ reloading effect. According to W.F. Chen (1982), the stress-strain curve for monotonic loading serves as a reasonable envelope for the peak value of stress for concrete under cyclic loading. James et al. (2001) concluded the same for HSC. This was experimentally verified in this research by unloading/ reloading some concrete cylinders after reaching different loading values and comparing their behaviour to the monotonically loaded cylinders of the same batch. The unloading/ reloading incidences did not affect the test results.

5.7.2 Peak Load or Peak Stress Values, One or Two?

The peak plateau shown in the stress-strain relation in figures 5.12 to 5.18 does not contradict the possibility of observing two peaks: a first peak load or stress that is marked by the cover spalling, and another peak, maybe different in magnitude than the first peak, depends on the gain in strength by confinement whether it can overweigh the loss in strength due to cover spalling. For well-confined sections, distributed triaxial stress state develops in the core between ties while it develops only at the tie level for poorly confined sections. The axial stress regained by the triaxial effect at the tie level can not compensate the strength loss caused by the localized failure of the concrete between ties. For specimens tested in this research, the gain in strength started simultaneously with spalling of the joint cover and there was a continuous compensation of the strength loss. Because the total gain in strength was equal to the total loss in strength, the two strength peaks merged into a broad one[1].

As for the load peaks, compared to the stress peaks, one should be aware of the "fake" peak caused by the dynamic effect of the loading. Among the criteria that influence the dynamic loading effect are: the loading rate of the UTM, the UTM load fluctuation, number and duration of pauses of the UTM loading, and the at-stoppage load relative to the peak load. Stopping the UTM loading at the peak value brings the curve a little down and then by resuming the load it rises up, which might falsely indicate two peaks. The peak load value should not be estimated based on UTM load alone unless for the top column. Rather, it should be based on the UTM load plus the floor loads.

---

[1] Spirally reinforced columns often exhibit two peaks, the first at spalling of the cover and the second when the spiral is fully mobilized. Sometimes the two peaks merge, as noted here.

Table 5.1. Results of the Effective Concrete Strength in the Joint

SP#	P_c kN	P_f kN	P_{ult} kN	f'_{cs} MPa	f'_{cc} MPa	f_{st} MPa	f_{ce} MPa	f_{ce}/f'_{cs}	f'_{cc}/f'_{cs}
1	3636	79	3689	18.0	72.8	454	34.4	1.91	4.0
2	4605	158	4711	20.4	86.6	466	45.9	2.3	4.2
3	6700	—	6669	31.8	89.2	352	70.8	2.2	2.8
4	5583	158	5689	17.6	66.7	422	57.9	3.3	3.8
5	4558	151	4659	19.8	66.7	462	45.5	2.3	3.4
6	4167	174	4284	20.6	93.7	465	41.1	2.0	4.6
7	2783	143	2879	18.7	18.7	445	26.5	1.4	1.0

❖To account for the effect of floor load on the effective strength of the joint, the value of P_{ult} is taken as $P_c+2/3P_f$, where P_c is the column load and P_f is the floor load at column failure.

❖f'_{cs} is the nominal strength of the floor; f'_{cc} is the nominal strength of the column; f_{st} is the stress in longitudinal reinforcement at peak load; and f_{ce} is the effective concrete strength.

❖The equivalent f'_{cs} value for SP3 is the 0.74x89.2+0.26x31.8= 74.3 MPa, and the equivalent f_{cs} value for SP4 is the 0.74x66.7+0.26x17.6= 53.9 MPa.

Table 5.2. Comparison of the Concrete Effective Strength Values (MPa)

SP#	f'_{co} MPa	Actual f_{ce}	Edge-Joint Empirical Equations				Analytical Strength Model for Columns		
			CSA A23.3-94	ACI 318-02	Kayani 1992	Gamble 1991	Sheikh 1982	Mander 1988	Yong 1988
1	18.0	34.4	25.2	25.2	28.9	38.6	24.3	26.5	19.6
2	20.4	45.9	28.6	28.6	33.0	45.1	26.7	29.0	22.2
3	74.3	70.8	44.5	44.5	46.9	55.6	80.5	83.9	81.7
4	53.9	57.9	24.6	24.6	27.9	36.3	60.2	63.4	59.2
5	19.8	45.5	27.7	27.7	30.5	38.2	26.1	28.4	21.6
6	20.6	41.1	28.8	28.8	33.8	47.5	26.9	29.2	22.4
7	18.7	26.5	18.7	18.7	18.7	18.7	25.0	27.2	20.4

Table 5.3. Actual and Estimated Values of Tie-confining Stress at Failure

SP#	*Actual* $f''_{s,o}$ MPa	*Actual* $f''_{s,i}$ MPa	f_l^1 MPa	f_l^2 MPa	$f'_{cs}{}^3$ MPa	f_{ce} MPa	$\Delta f_{ce}{}^4$ MPa	$\Delta f_{ce} / f_l$
1	(457+467)/2	467	1.7	1.4	18.0	34.4	16.4	9.6
2	(488+464)/2	462	1.7	1.4	20.4	45.9	25.5	14.8
3	(65+49)/2	(75+52)/2*	0.2	1.4	74.3	70.8	-3.5	N/A
4	313	347**	1.2	1.4	53.9	57.9	4.0	3.2
5	467	459	1.7	1.4	19.8	45.5	25.7	15.1
6	465	444	1.7	1.4	20.6	41.1	20.5	12.3
7	(176+248)/2	196***	1.1	1.4	18.7	26.5	7.80	7.3

Notes:

$f''_{s;o}$ and $f''_{s;i}$ are average stresses in the rectangular and diamond-shape ties respectively at failure of the section;

1 is the actual confining stress of ties

2 Tie confining stress as calculated by Mander et al. (1988).

3 The equivalent nominal strength (f'_{cs}) is calculated as the sum of the product of nominal strength and % area of the concretes constituting the section.

4 Strength gain is calculated as the difference between concrete effective and concrete nominal strengths.

* Shown are stresses in top ties. Stresses in joint ties are (153+143) MPa for short-leg and long-leg rectangular ties, and (79+101) MPa for diamond ties.

** Shown are stresses in joint ties. Stresses in bottom ties are (355+175) MPa for short-leg and long-leg rectangular ties, and (62) MPa for diamond ties.

*** Shown are stresses in bottom ties. Stresses in joint ties are (109+147) MPa for short-leg and long-leg rectangular ties, and (47) MPa for diamond ties.

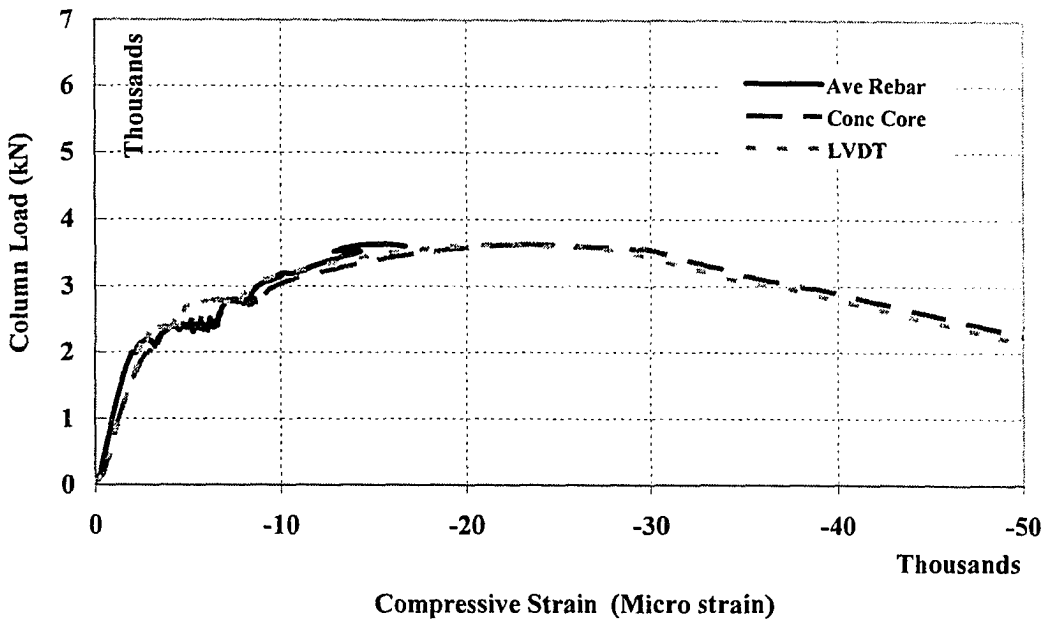

Figure 5.1. Column Load vs. Average Vertical Strain Values at SP1-Joint

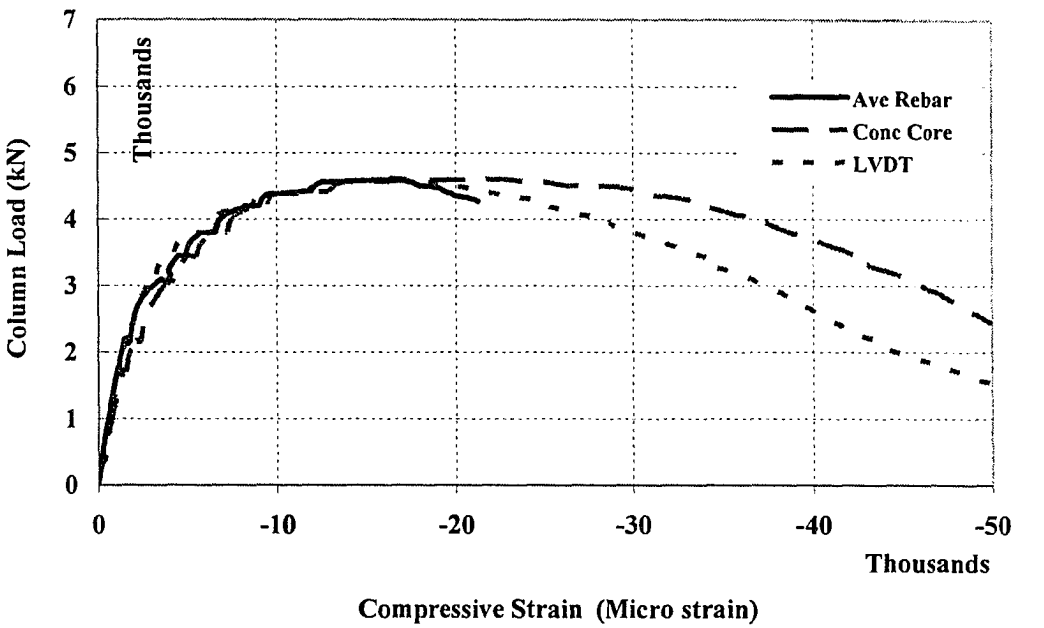

Figure 5.2. Column Load vs. Average Vertical Strain Values at SP2-Joint

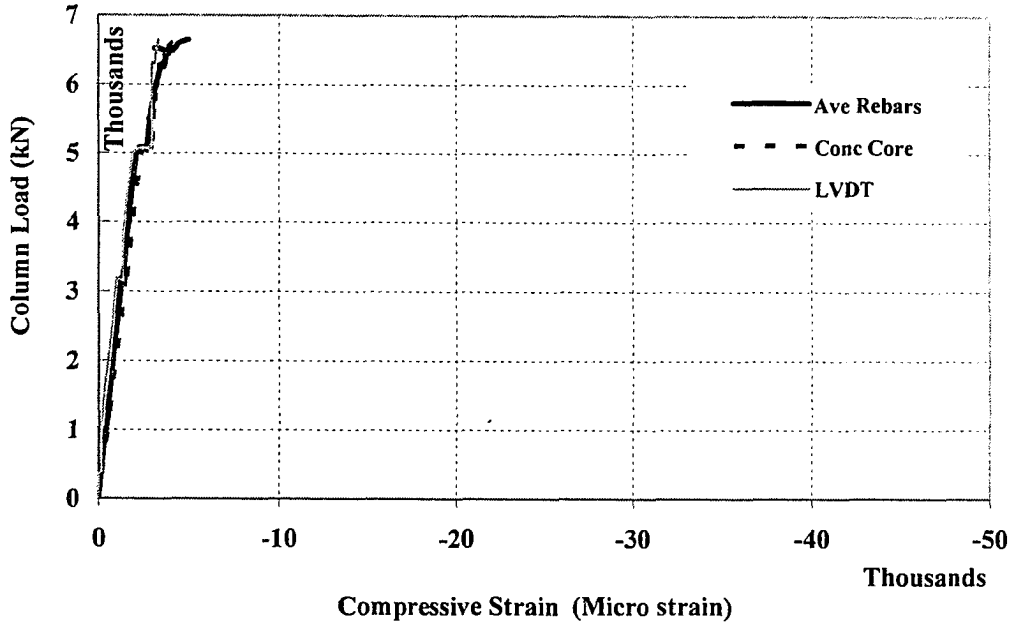

Figure 5.3. Column Load vs. Average Vertical Strain Values at SP3-Top Column

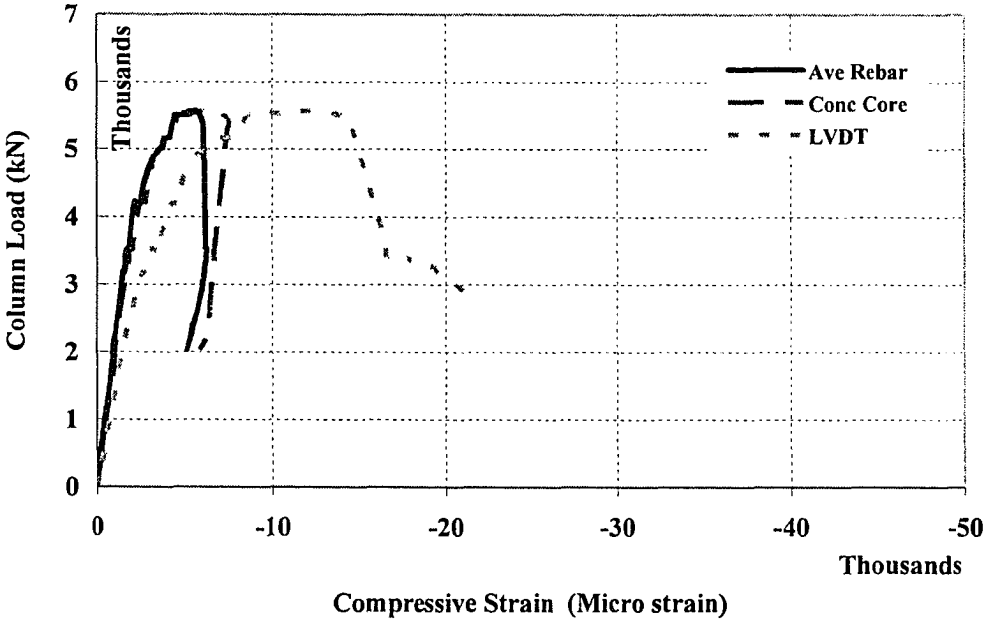

Figure 5.4. Column Load vs. Average Vertical Strain Values at SP4-Joint

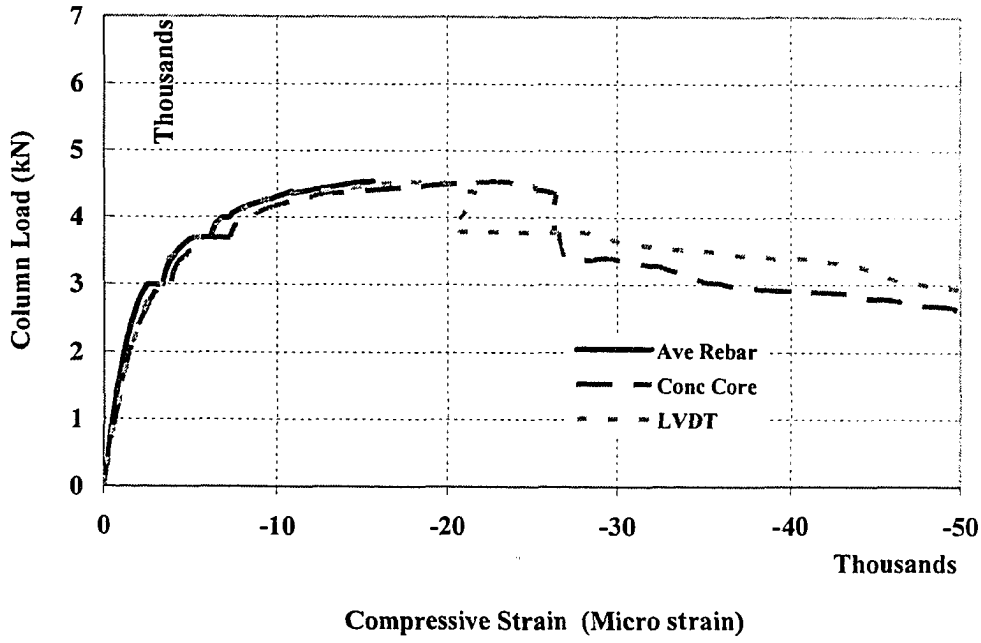

Figure 5.5. Column Load vs. Average Vertical Strain Values at SP5-Joint

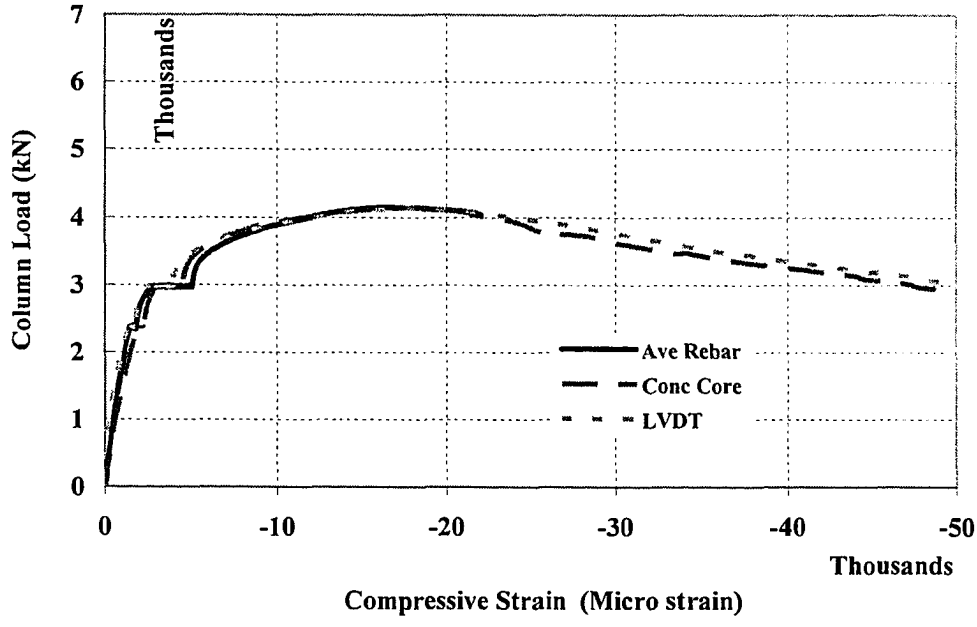

Figure 5.6. Column Load vs. Average Vertical Strain Values at SP6-Joint

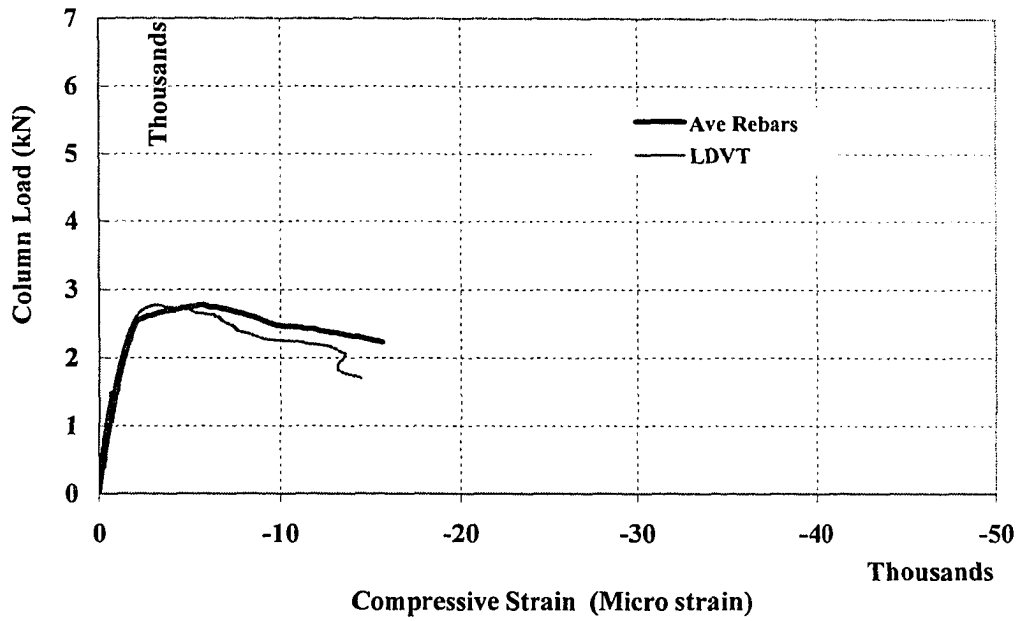

Figure 5.7. Column Load vs. Average Vertical Strain at SP7-Bottom Column

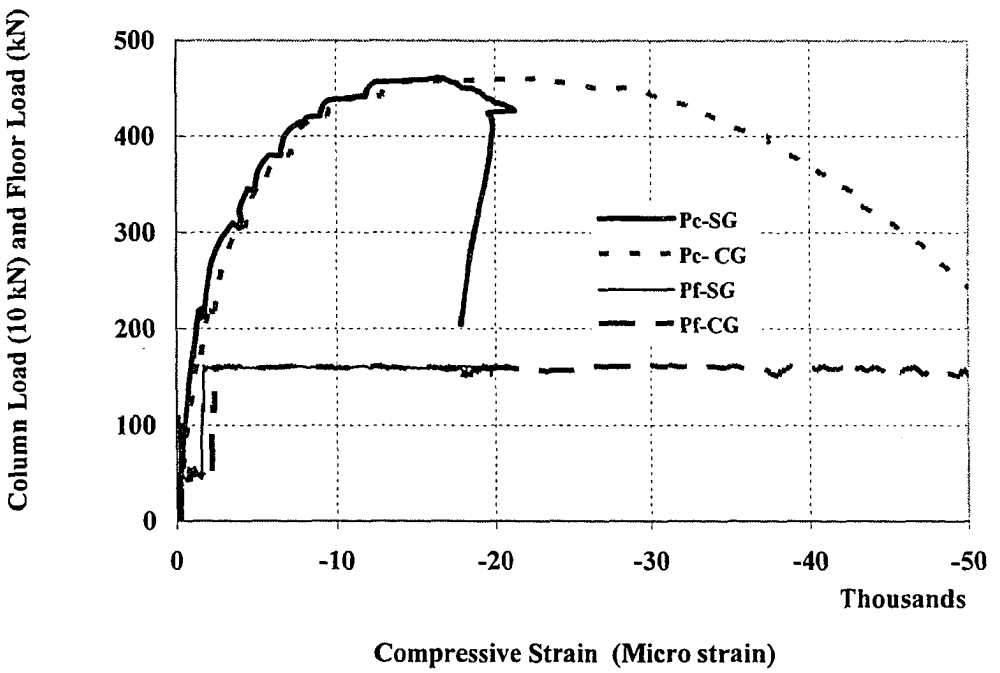

Figure 5.8. Effect of Column and Floor Loads on SP2-Vertical Strain

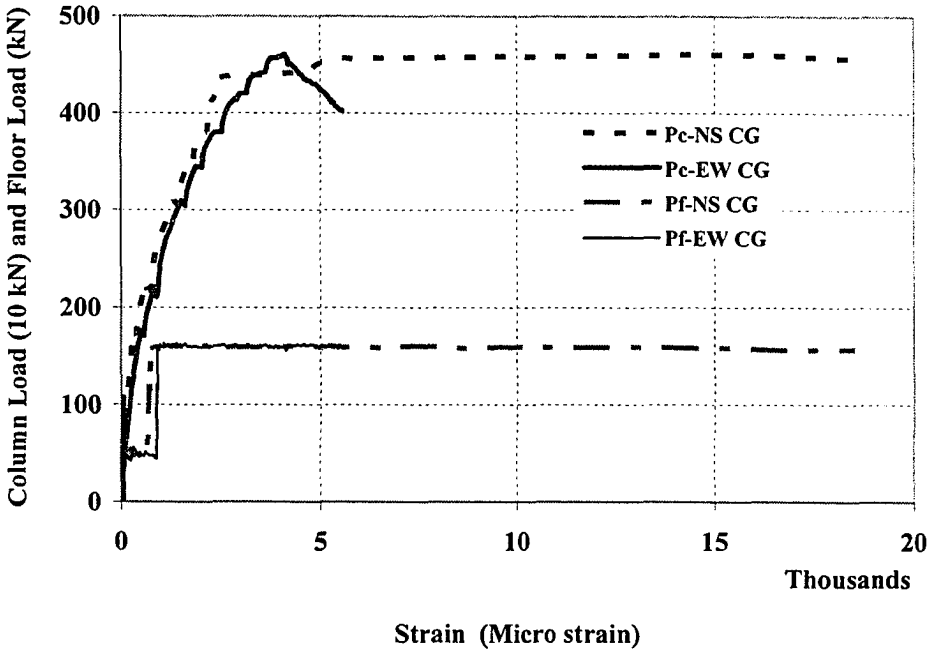

Figure 5.9. Effect of Column and Floor Loads on Lateral Strain of SP2-Joint Core

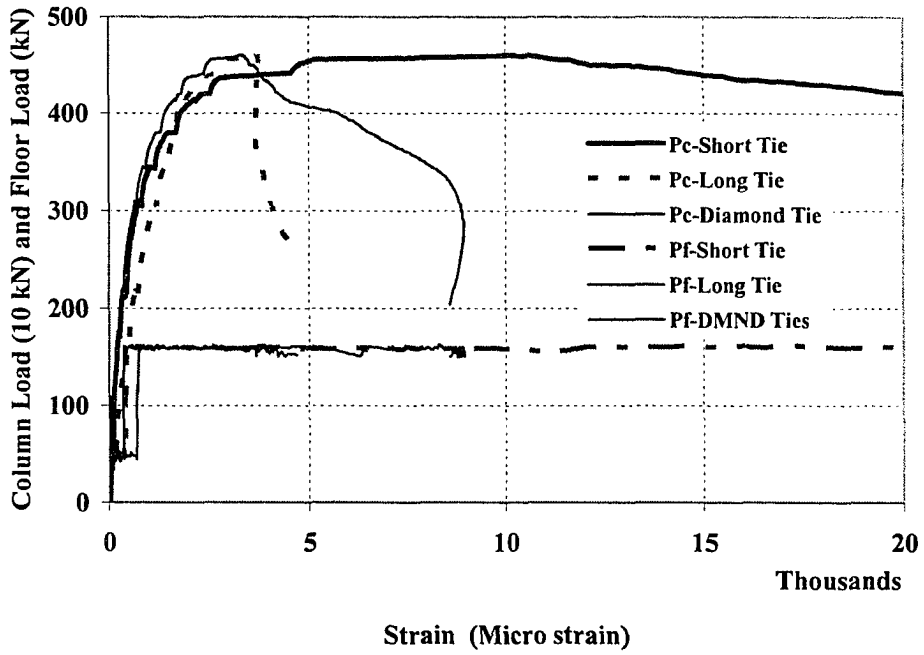

Figure 5.10. Effect of Column and Floor Loads on Strain of SP2-Joint Ties

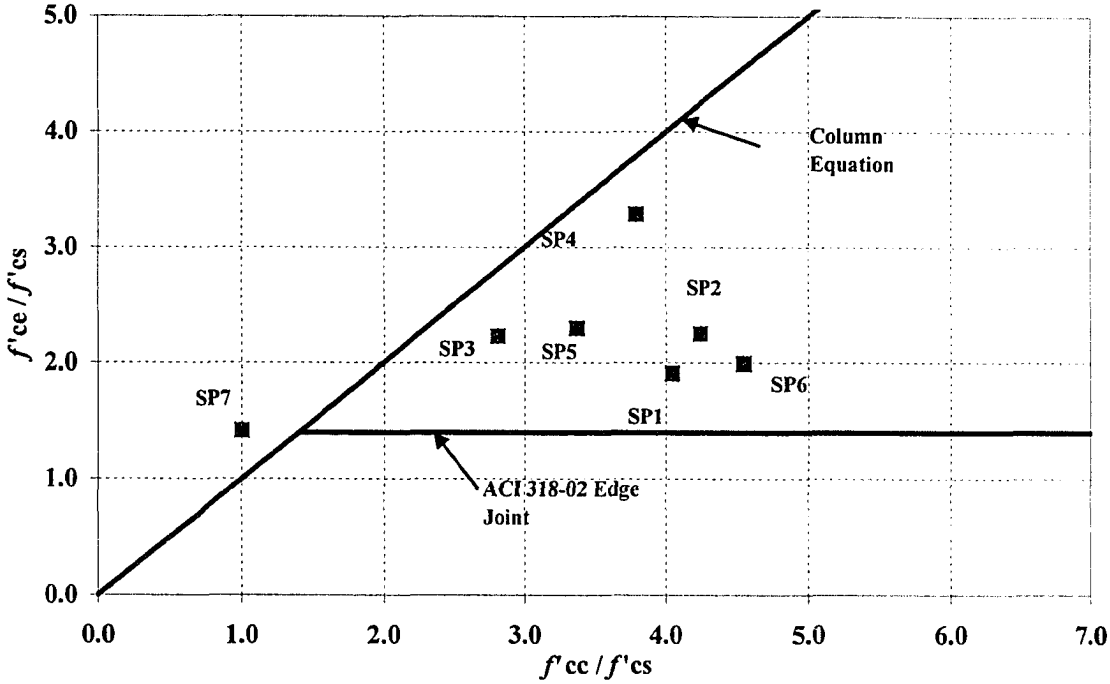

Figure 5.11. f'_{ce}/f'_{cs} vs. f'_{cc}/f'_{cs} for Test Results of This Research

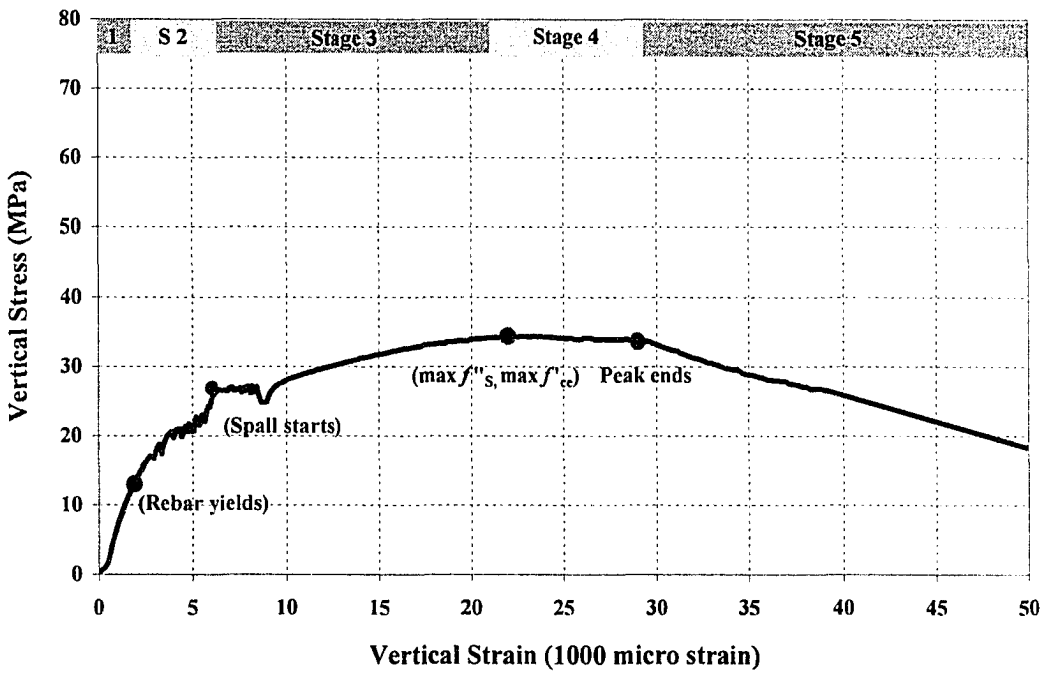

Figure 5.12. Vertical Stress vs. Vertical Strain for SP1-Joint

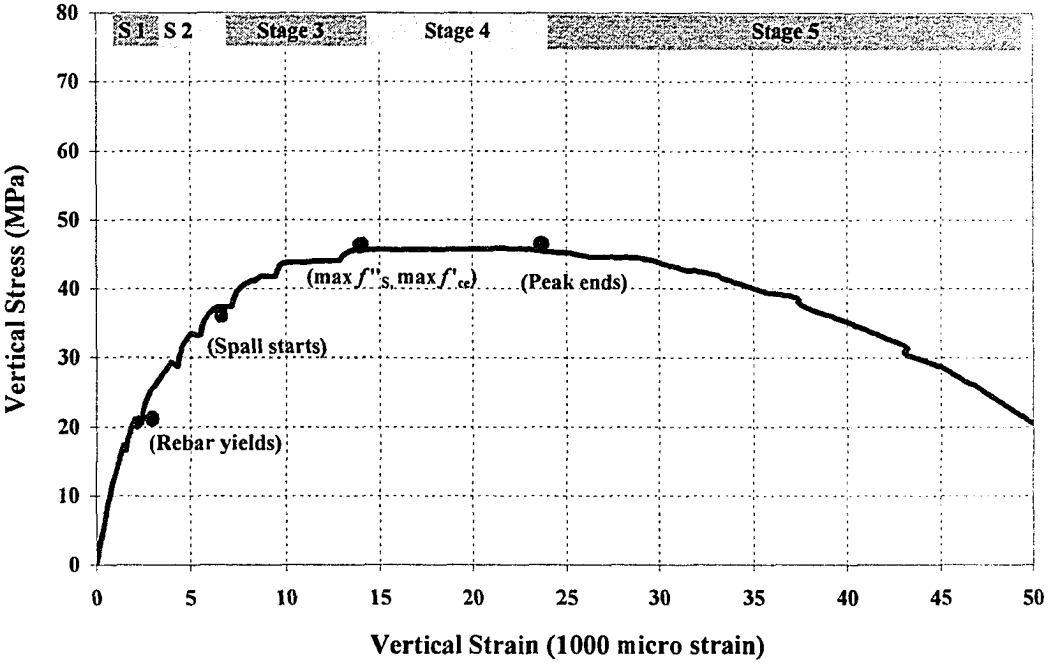

Figure 5.13. Vertical Stress vs. Vertical Strain for SP2-Joint

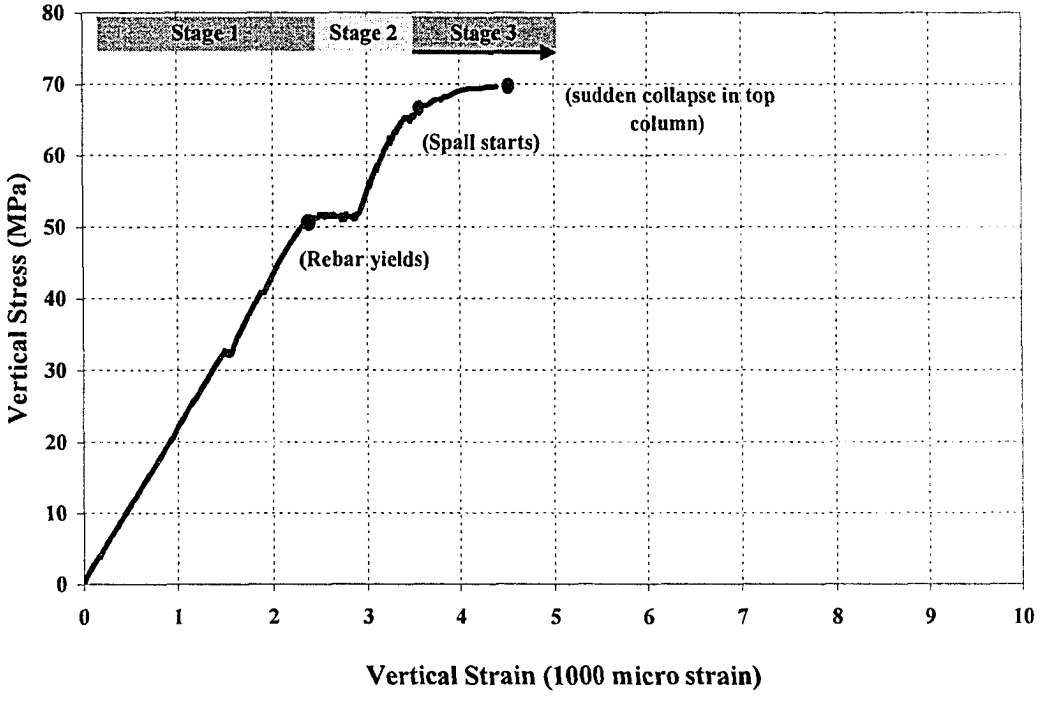

Figure 5.14. Vertical Stress vs. Vertical Strain for SP3-Joint

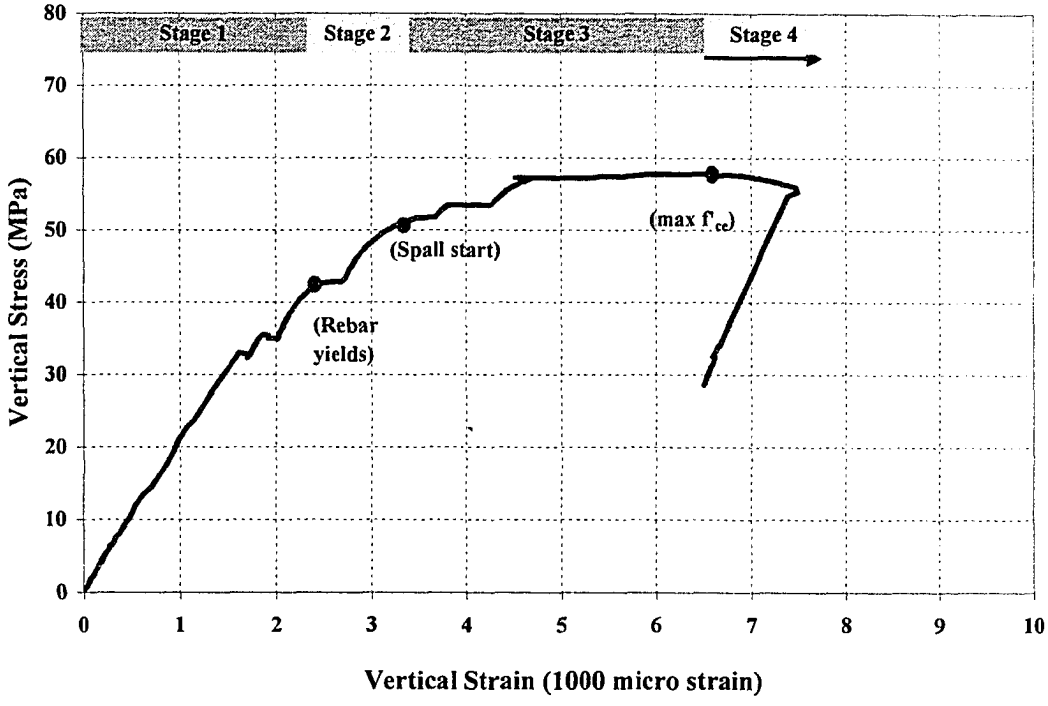

Figure 5.15. Vertical Stress vs. Vertical Strain for SP4-Joint

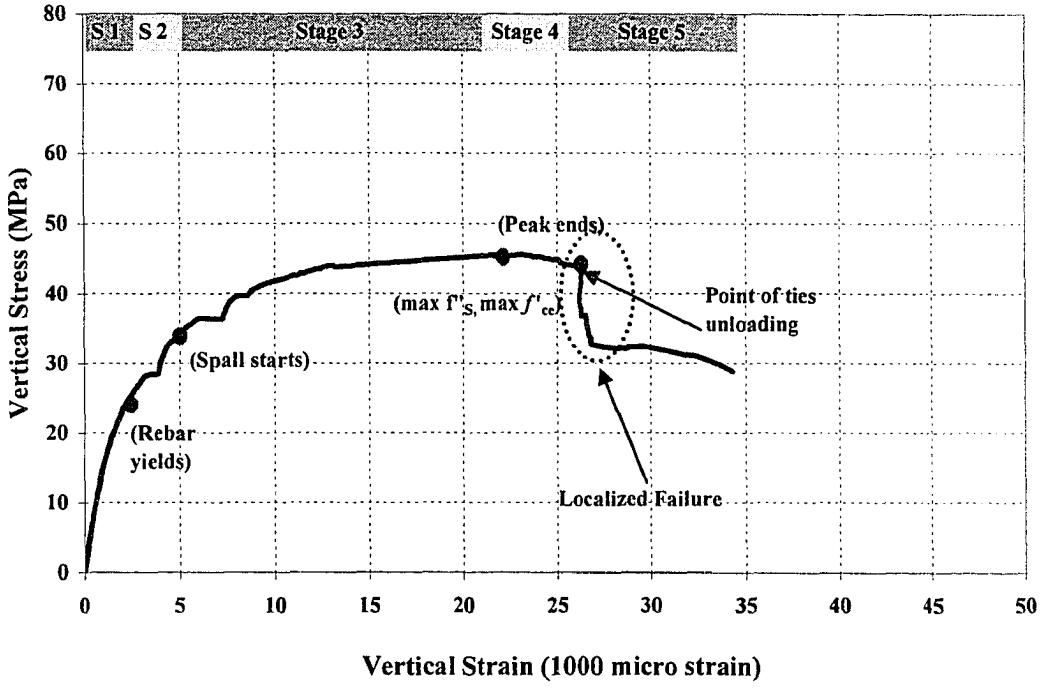

Figure 5.16. Vertical Stress vs. Vertical Strain for SP5-Joint

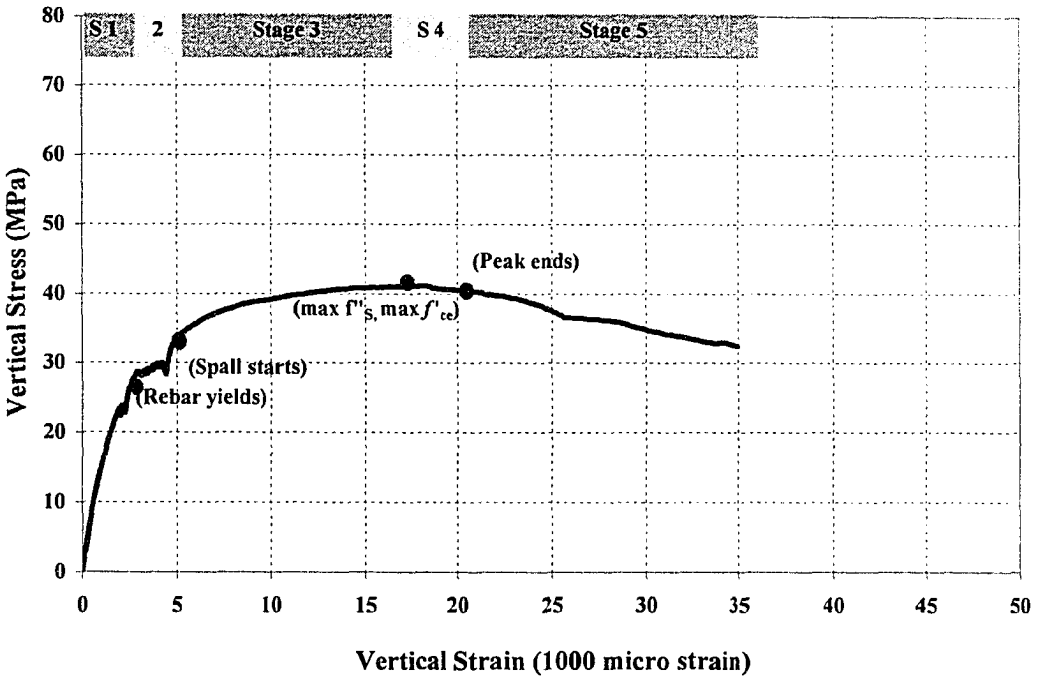

Figure 5.17. Vertical Stress vs. Vertical Strain for SP6-Joint

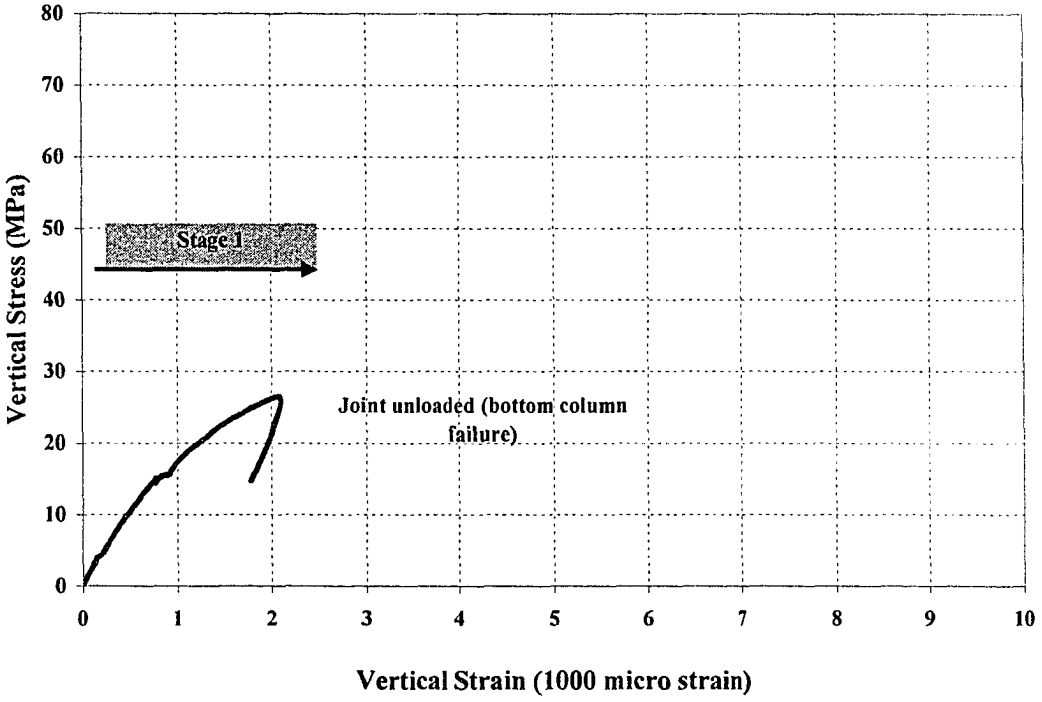

Figure 5.18. Vertical Stress vs. Vertical Strain for SP7-Joint

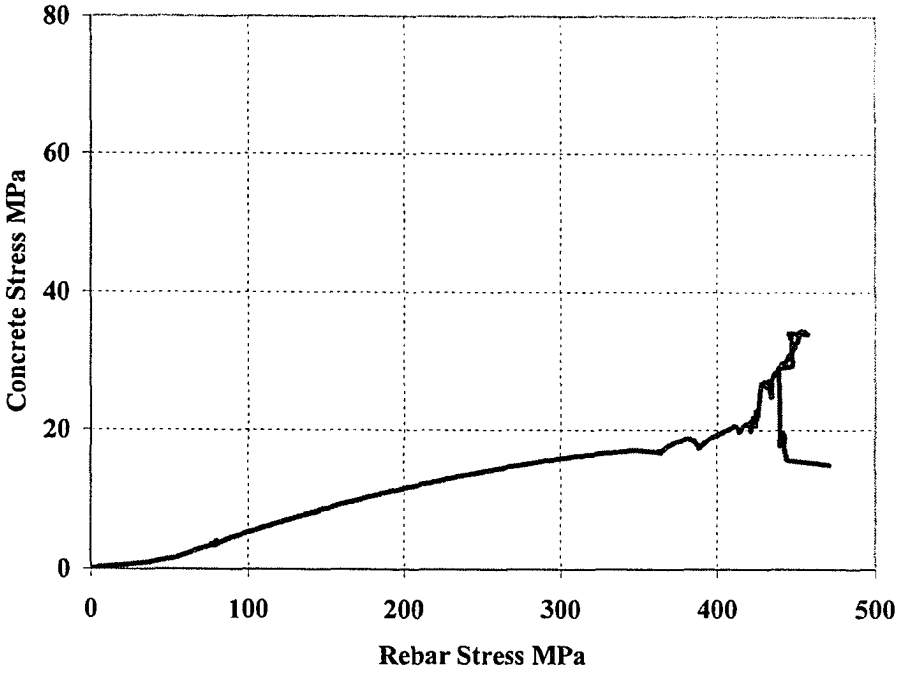

Figure 5.19. Vertical Concrete Stress-Rebar Stress Relation for SP1-Joint

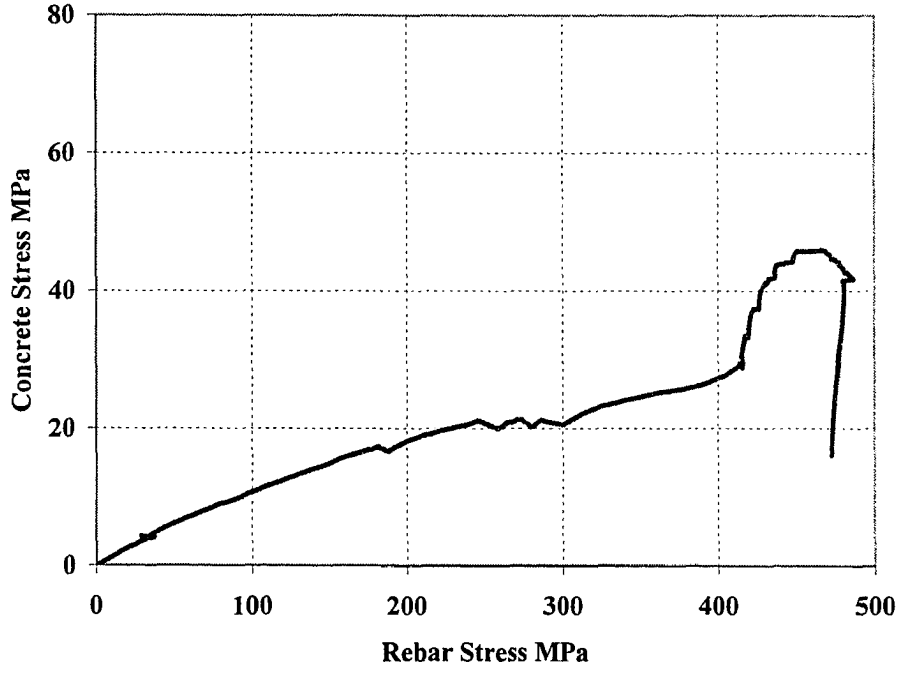

Figure 5.20. Vertical Concrete Stress-Rebar Stress Relation for SP2-Joint

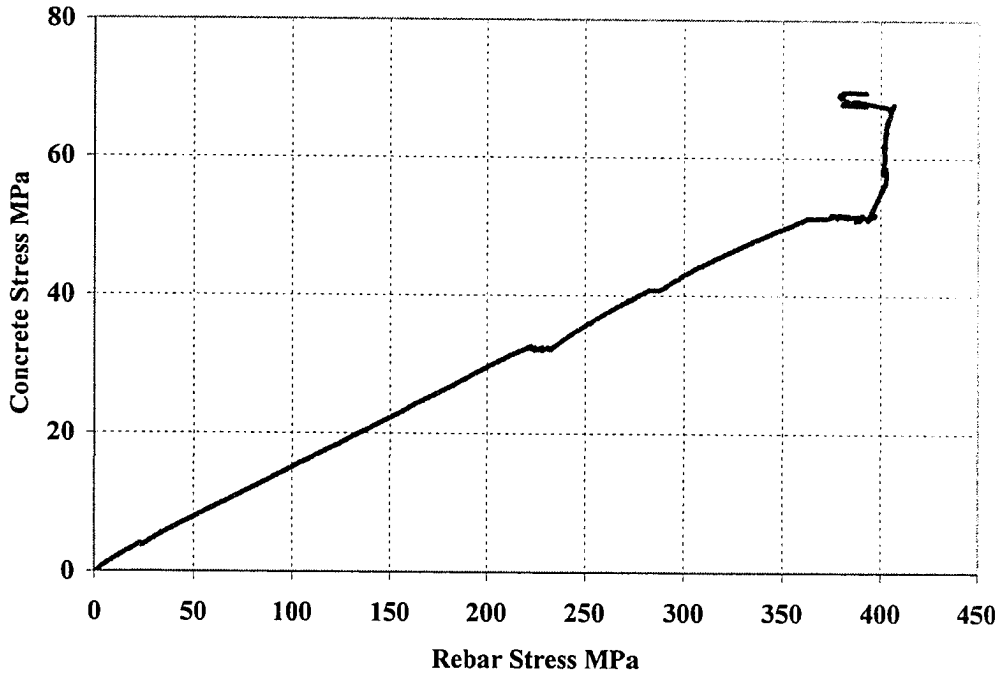

Figure 5.21. Vertical Concrete Stress-Rebar Stress Relation for SP3-Top Column

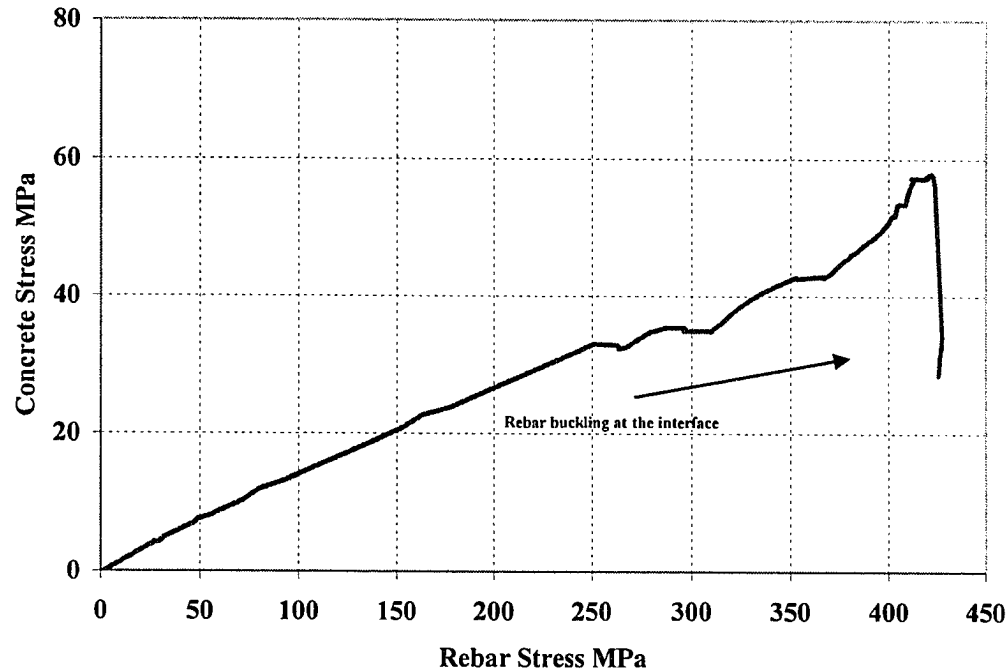

Figure 5.22. Vertical Concrete Stress-Rebar Stress Relation for SP4-Joint

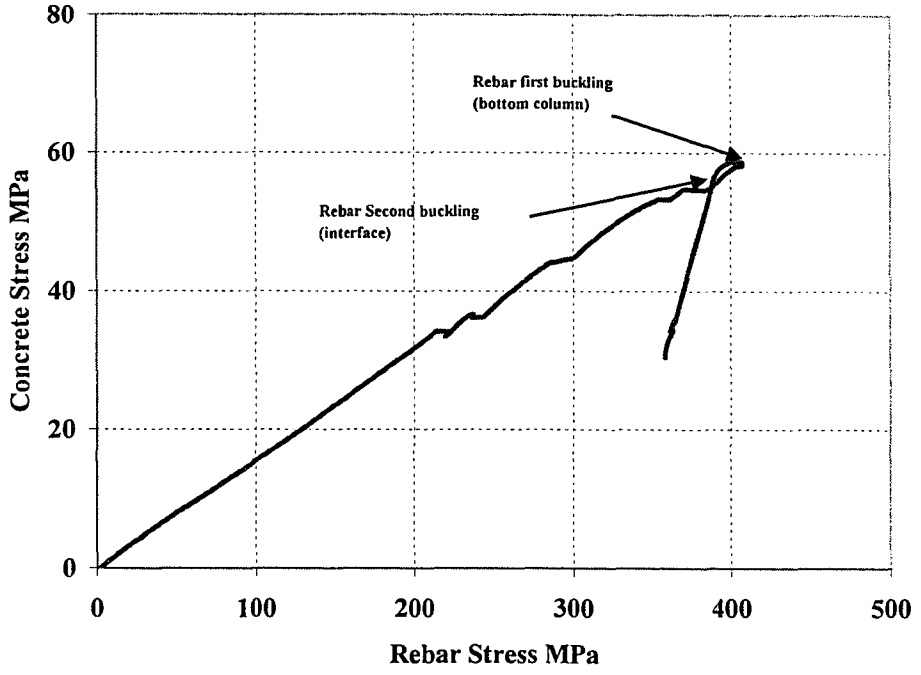

Figure 5.23. Vertical Concrete Stress-Rebar Stress Relation for SP4-Bottom Column

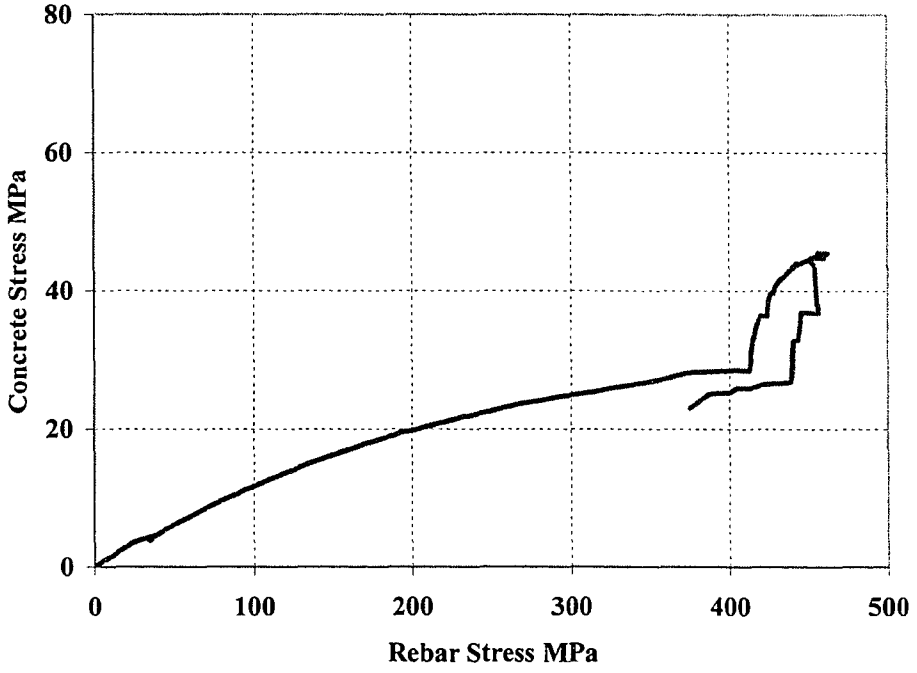

Figure 5.24. Vertical Concrete Stress-Rebar Stress Relation for SP5-Joint

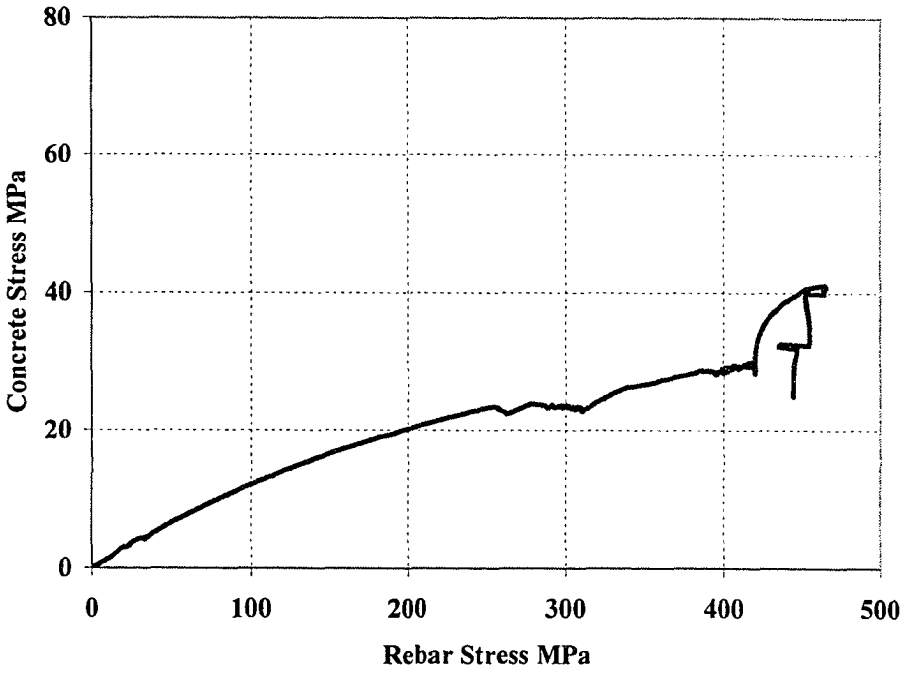

Figure 5.25. Vertical Concrete Stress-Rebar Stress Relation for SP6-Joint

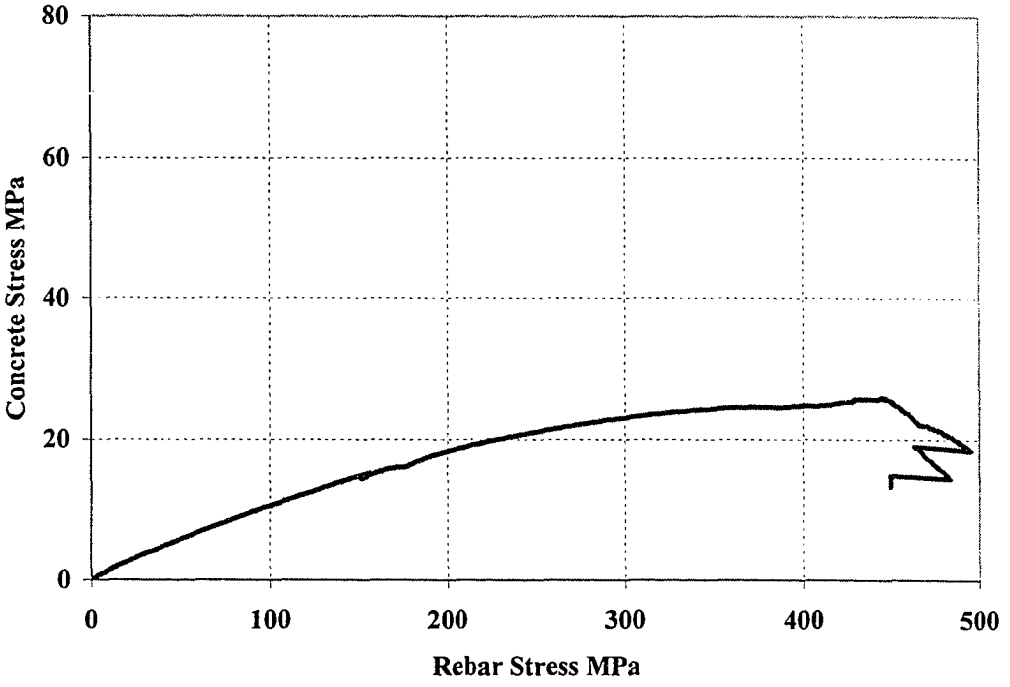

Figure 5.26. Vertical Concrete Stress-Rebar Stress Relation for SP7-Bottom Column

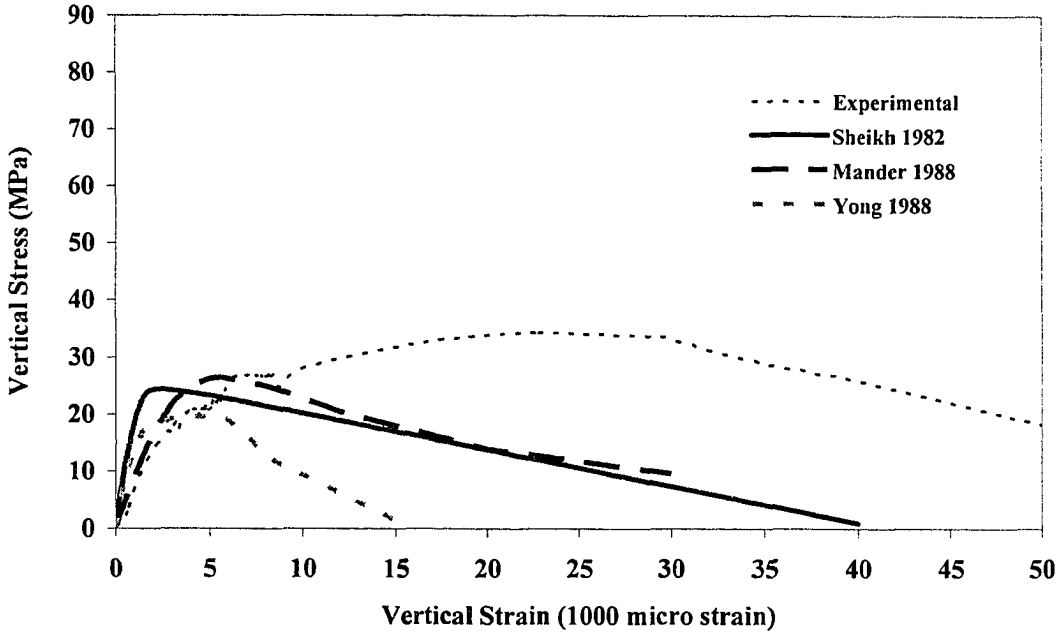

Figure 5.27. Comparison between Experimental and Analytical Compressive Stress-Strain Models for SP1-Joint

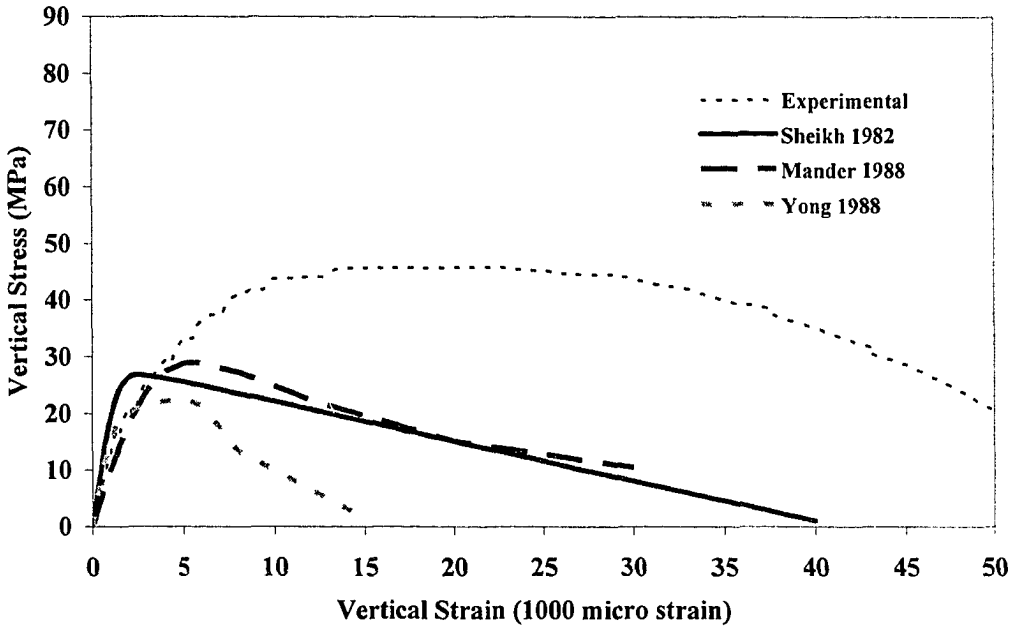

Figure 5.28. Comparison between Experimental and Analytical Compressive Stress-Strain Models for SP2-Joint

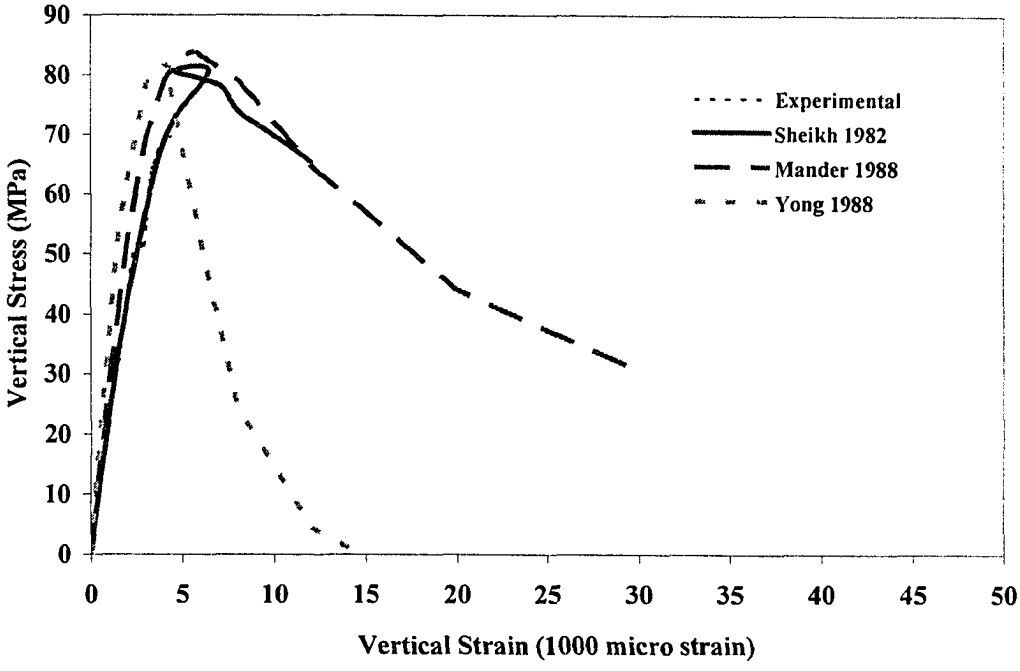

Figure 5.29. Comparison between Experimental and Analytical Compressive Stress-Strain Models for SP3-Top

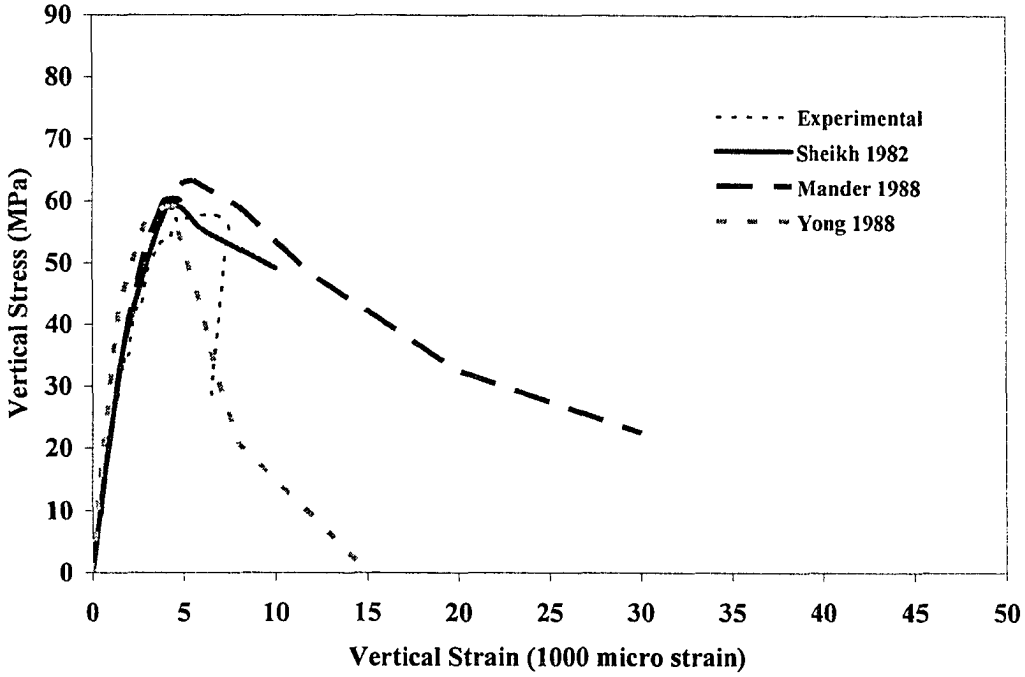

Figure 5.30. Comparison between Experimental and Analytical Compressive Stress-Strain Models for SP4-Joint

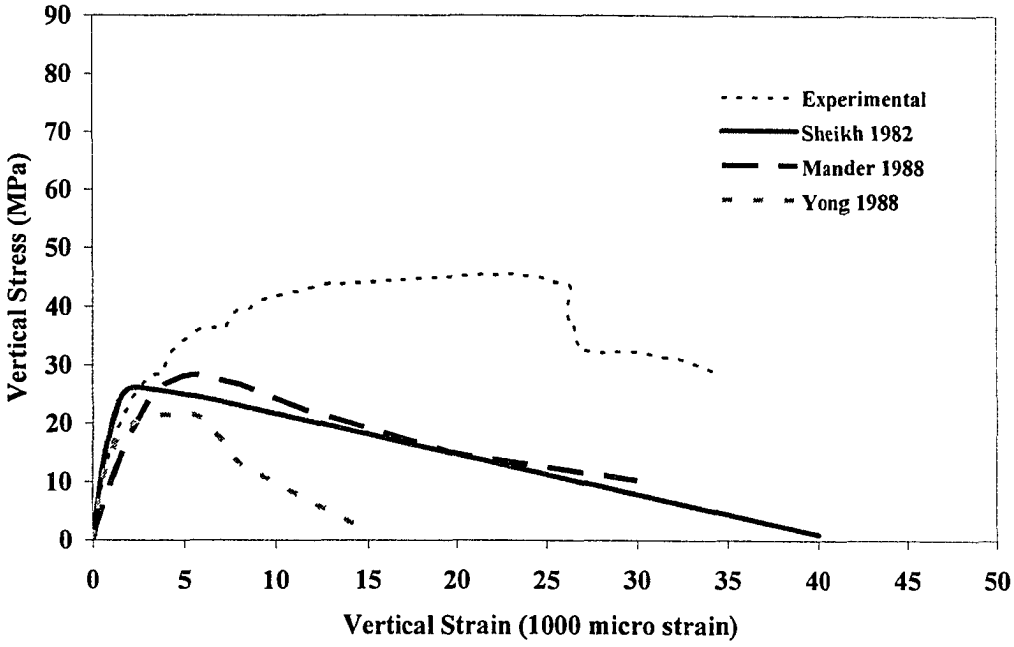

Figure 5.31. Comparison between Experimental and Analytical Compressive Stress-Strain Models for SP5-Joint

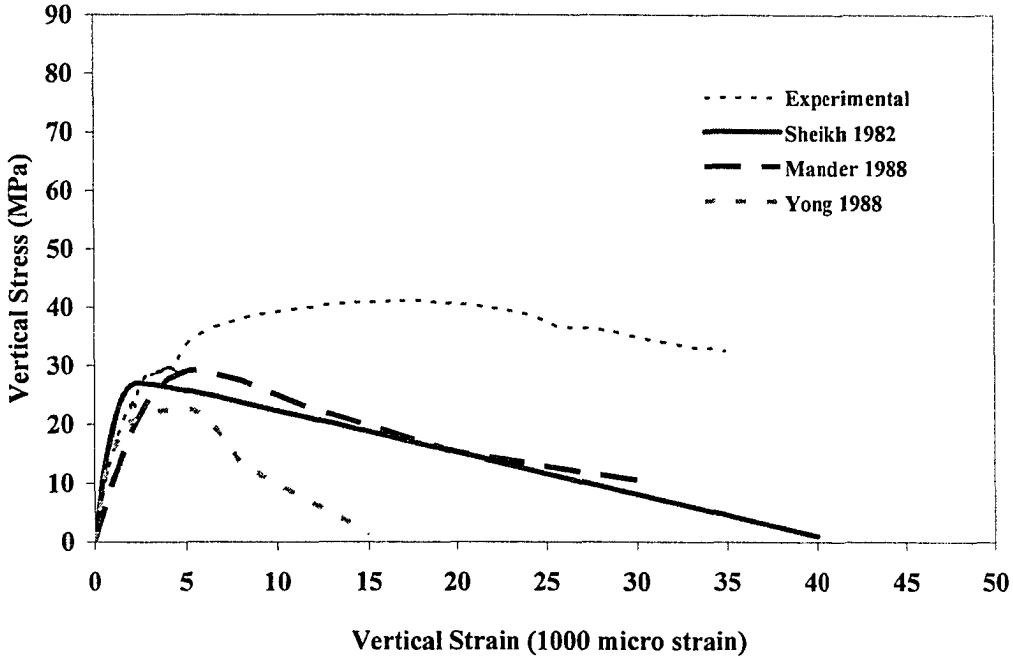

Figure 5.32. Comparison between Experimental and Analytical Compressive Stress-Strain Models for SP6-Joint

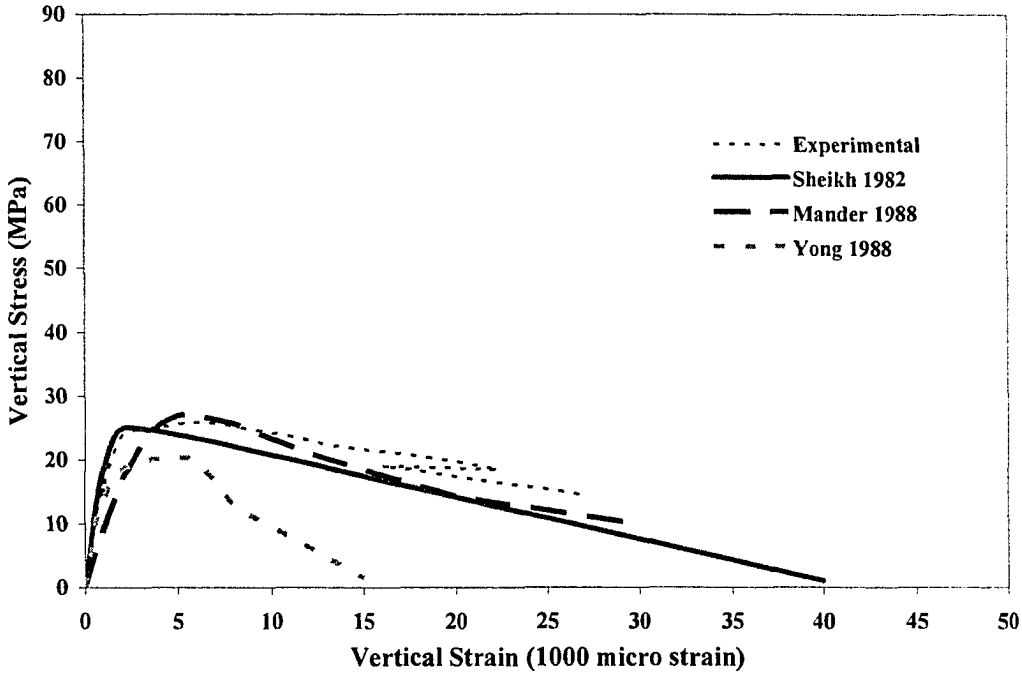

Figure 5.33. Comparison between Experimental and Analytical Compressive Stress-Strain Models for SP7-Bottom

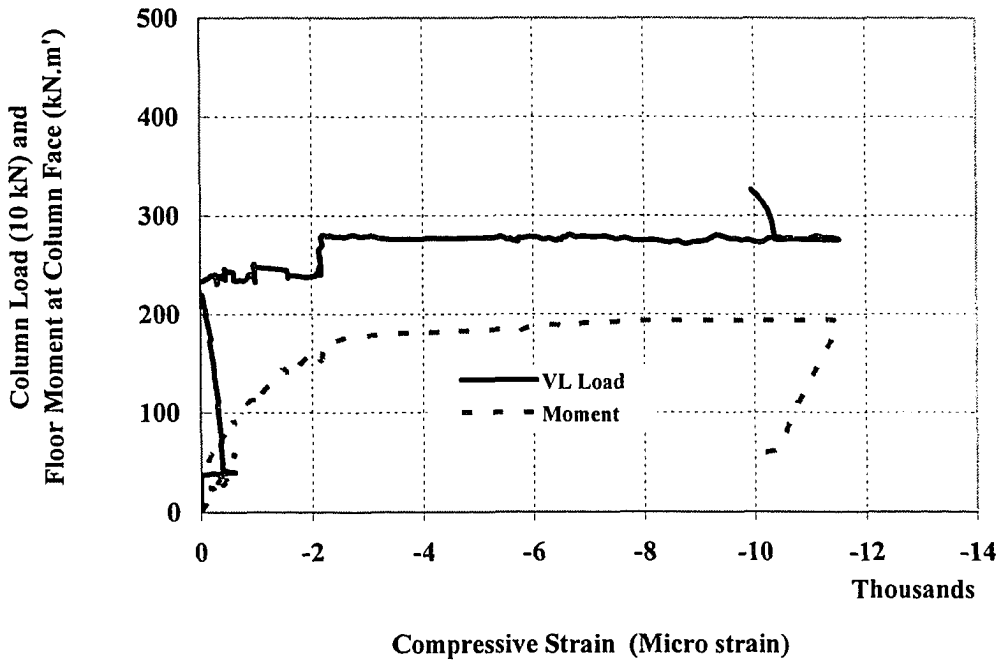

Figure 5.34. Effect of Column and Floor Loads on Strain of Beam Bottom Reinforcement at Face of SP1-Joint

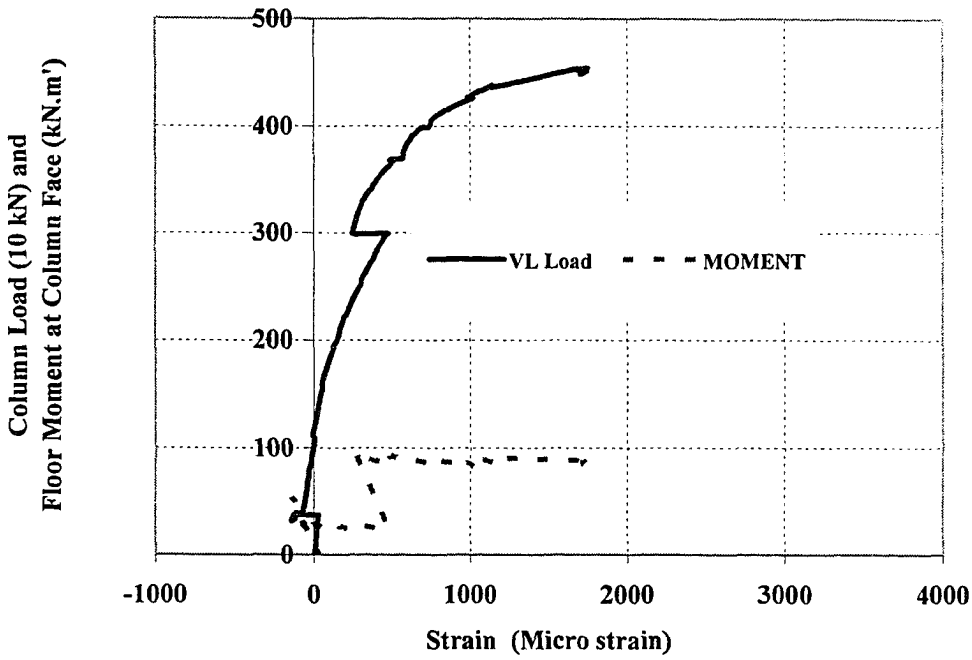

Figure 5.35. Effect of Column and Floor Loads on Strain of Beam Bottom Reinforcement at Core of SP5-Joint

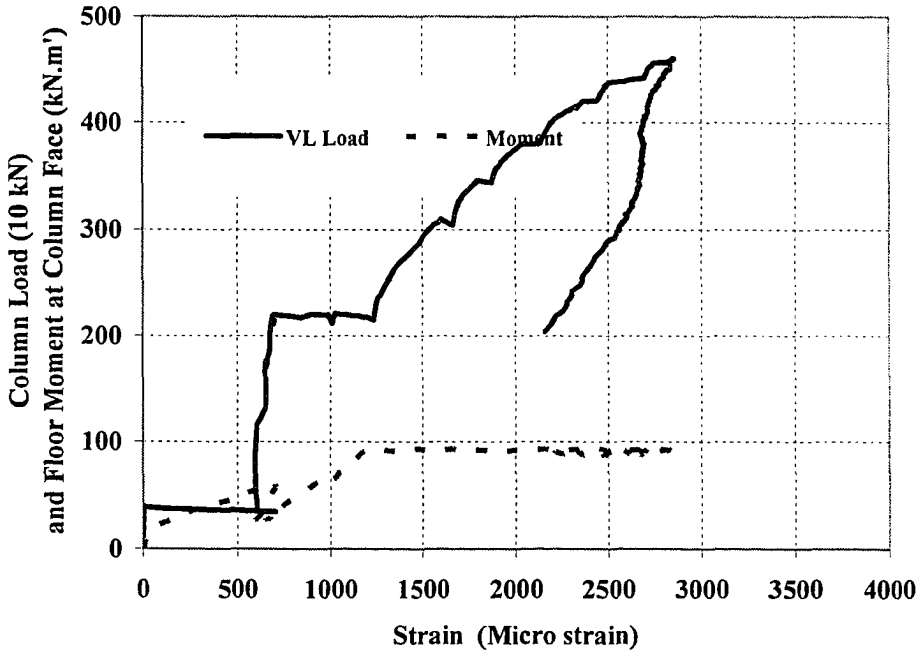

Figure 5.36. Effect of Column and Floor Loads on Strain of Beam Side Reinforcement at Face of SP2-Joint

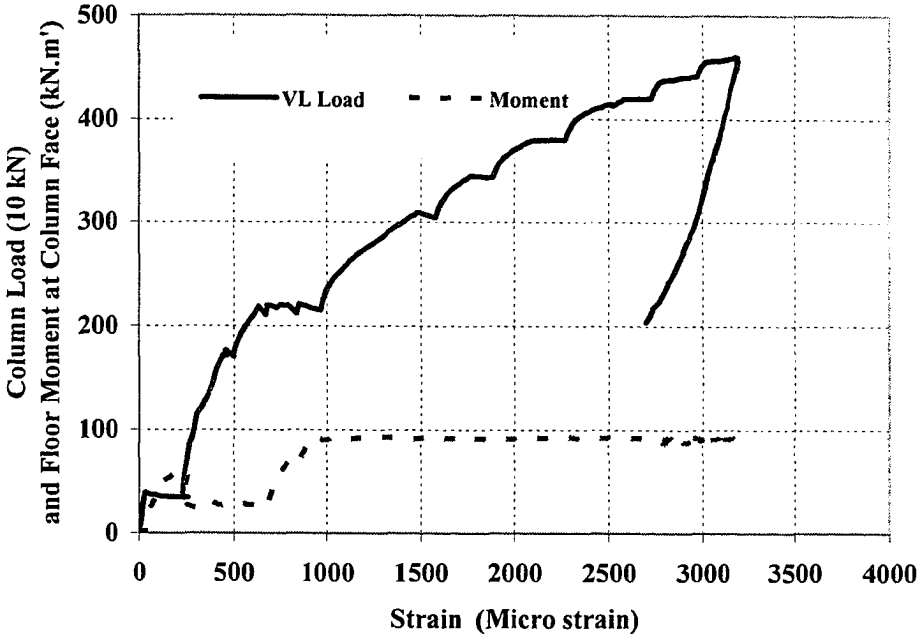

Figure 5.37. Effect of Column and Floor Loads on Strain of Beam Side Reinforcement at Core of SP2-Joint

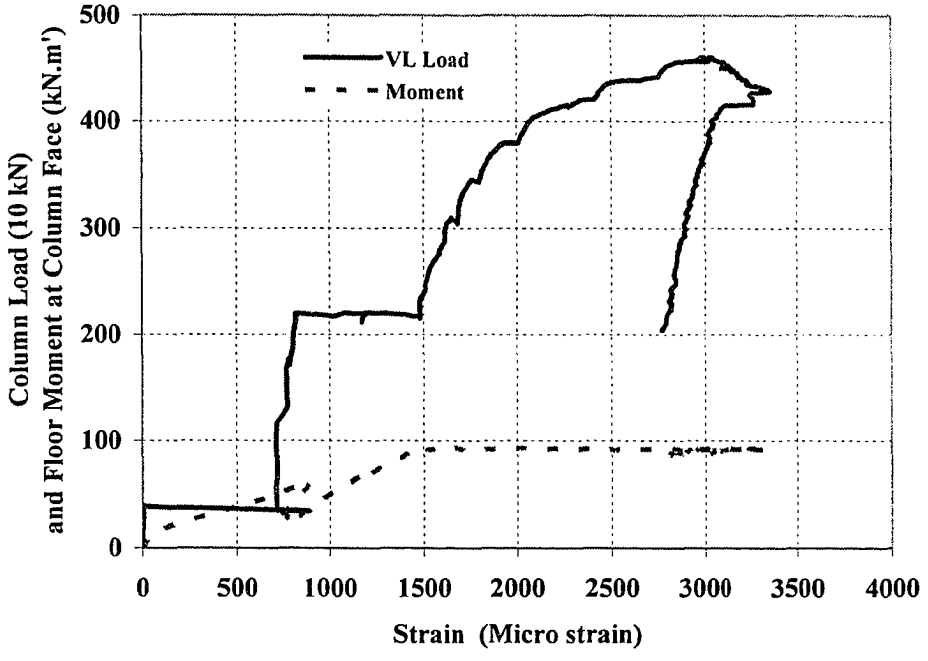

Figure 5.38. Effect of Column and Floor Loads on Strain of Beam Top Reinforcement at Face of SP2-Joint

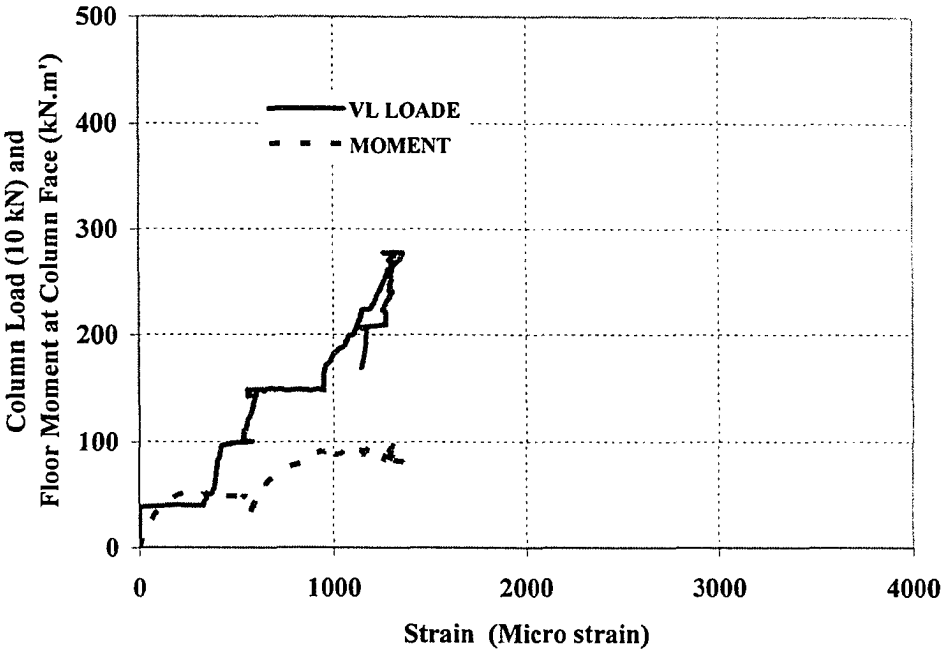

Figure 5.39. Effect of Column and Floor Loads on Strain of Beam Top Reinforcement at Core of SP7-Joint

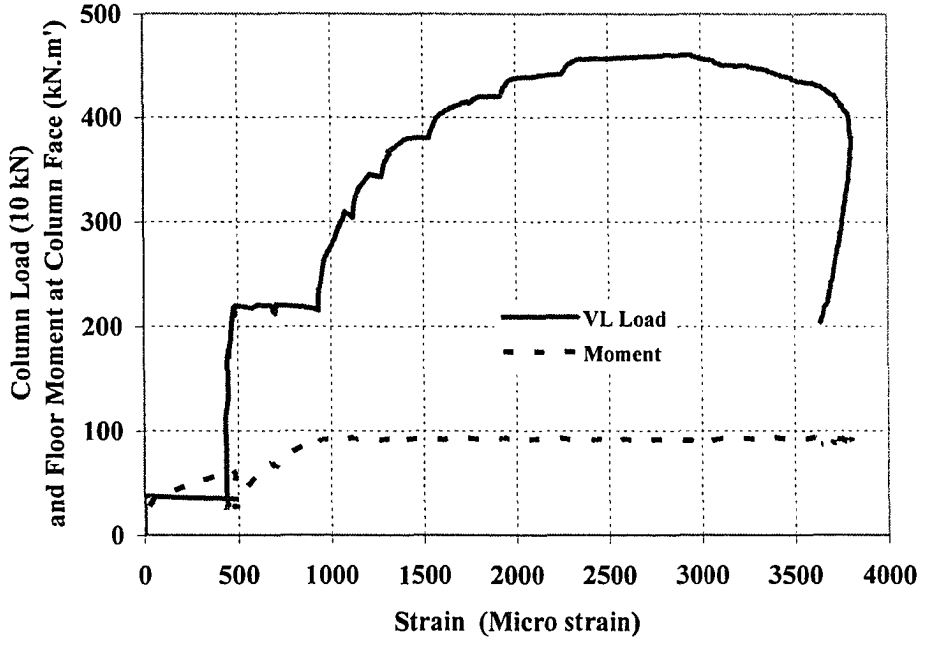

Figure 5.40. Effect of Column and Floor Loads on Strain of Slab Top Reinforcement at Face of SP2-Joint

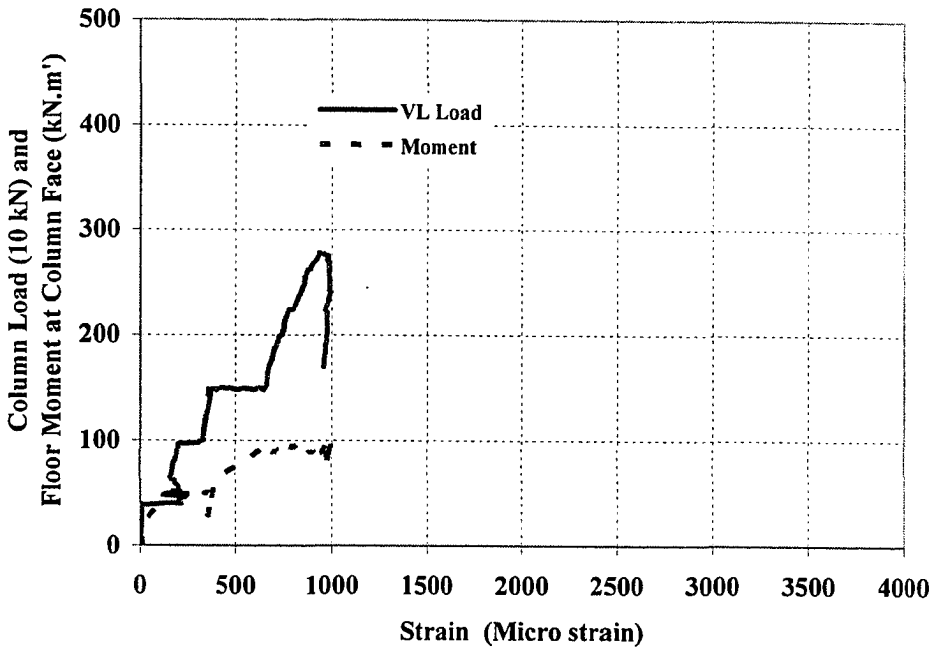

Figure 5.41. Effect of Column and Floor Loads on Strain of Slab Top Reinforcement at Core of SP7-Joint

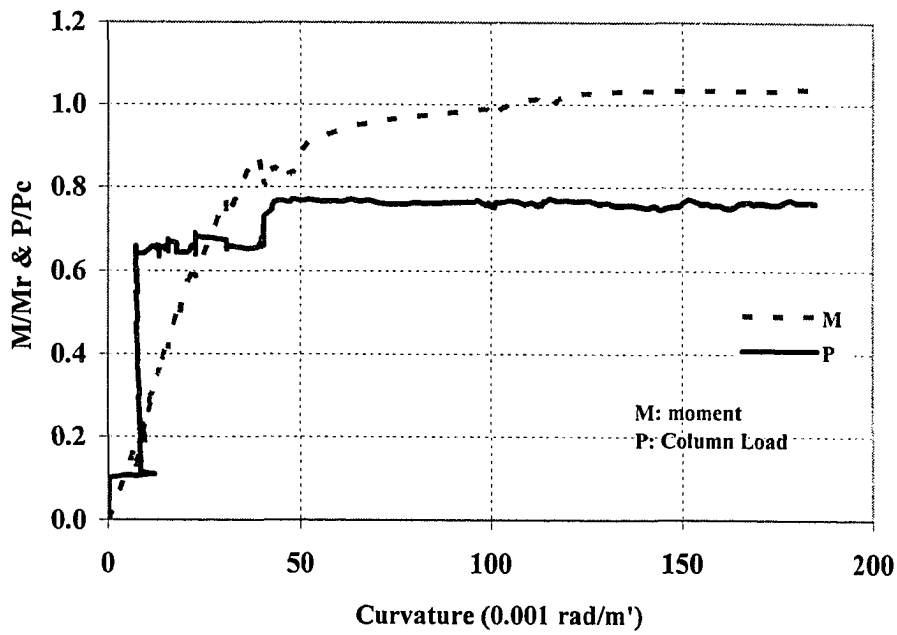

Figure 5.42. Effect of Specimen Loading on Floor Curvature for SP1

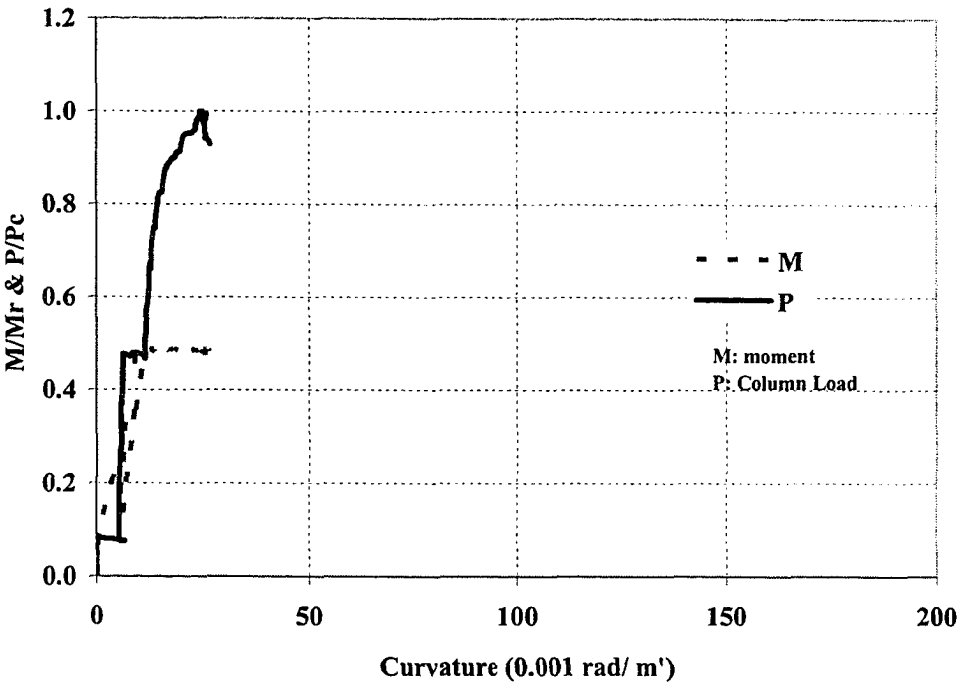

Figure 5.43. Effect of Specimen Loading on Floor Curvature for SP2

6 MODELING THE JOINT STRESS-STRAIN BEHAVIOUR

6.1 Introduction

The purpose of this chapter is to model the axial stress-strain relation of confined concrete sections under concentric axial loads. The chapter starts by identifying the main parameters for the modeling process and how to evaluate them. The chapter presents a detailed method for estimating the concrete effective compressive strength (f'_{ce}) for design and model purposes. The developed design equation and the developed stress-strain model are validated against actual results of different types of column-floor joints.

6.2 Generalized Vertical Stress-Vertical Strain Relation

A five-stage model of the axial stress-strain curve is shown in figure 6.1. The model is very like those proposed by Kent and Park (1971) and by Sheikh and Uzumeri (1982). The first stage is a straight line between point O and point A, which represents the yielding point of the vertical rebars. The second stage is a slightly curved line between point A and point B, at which point the cover starts to spall. The third stage is a more curved line between points B and C_1 (f_{ce}, ε_{s1}), where the peak stress is attained. The fourth stage is a straight line between points C_1 and C_2 (f_{ce}, ε_{s2}). In general, stress at point C_1 could be bigger, equal to or smaller than that at point C_2, depending on the gain in strength by confinement compared to the decrease in strength due to cover spalling, as explained in chapter 5. After reaching point C_2, the tie ruptures or concrete starts failing locally. The fifth stage is a straight declining line from C_2, where the damaged zone increases rapidly, till end of the test.

For modeling the stress-strain curve, the five points are not all needed. Points C_1 and C_2, are sufficient to define the behaviour till the start of post-peak failure, after which only the slope of the descending line is required. The proposed model consists of two parts: part O-C_1-C_2 covers the ascending and peak stages, and part C_2-E is the descending stage. The slope of the descending line is function of the degree of confinement remaining around the effective section.

6.3 Calculation of the Maximum Effective Stress (the Strength Model)

One could look at a floor-column joint as a column section equipped with more confining elements other than the lateral reinforcement. Mostly these elements are related to the joint type, the flooring system, the floor geometry, the degree of floor loading, and construction techniques. The idea here is to quantify the effect of all the elements contributing to the confinement and to put them in a form suitable to all kinds of concrete sections, columns or joints, subject to axial loads. The effective compressive strength (f_{ce}) of a floor-column joint can be written in the general form as function of the floor concrete strength (f'_{cs}) as in equation 6.1.

$$f_{ce} = f'_{cs}\,(1 + k_{STR;Conf} + k_{Floor;Res} + k_{Floor;Deb} + k_{HSC;Core} + k_{End;Conf}) \qquad [6.1]$$

$k_{STR;Conf}$ accounts for strength enhancement by the interacted confinement of column reinforcement and floor. It considers the integrated effect of geometry and reinforcement details. $k_{STR;Conf}$ applies to both joint and column sections; the remaining k-factors apply only to joint sections. $k_{Floor;Res}$ accounts for strength enhancement by the floor reserve strength, which is the flexural strength above that needed to carry the flooring loads. $k_{Floor;Deb}$ accounts for strength enhancement by debonding of the floor negative reinforcement. $k_{HSC;Core}$ accounts for strength enhancement by the high-strength-concrete (HSC) inside the joint, that is the composite section effect. $k_{End;Conf}$ accounts for strength enhancement because of the confinement of ends of the joint between the columns. The following subsections outline the procedures of calculating each k-factor.

6.3.1 Evaluating the Integrated Effect of Geometry and Reinforcement Details

This section describes how to compute $k_{STR;Conf}$, the integrated confining action of joint reinforcement and the floor surrounding the joint. By setting equation 6.1, applied for columns, equal to equation 2.24 (chapter 2),a formula to estimate $k_{STR;Conf}$ is obtained as $k_{STR;Conf} = k_s - 1 = A_{ce}(\rho'' f''_y)^{0.5}/(140 P_{occ})$.

As seen in equation 6.2, a modification is introduced into the expression for $k_{STR;Conf}$ to overcome the shortcomings outlined in section 2.4.6. The term $\rho''f''_y$ is replaced with the term $(\rho'' f''_s + \kappa\rho f_y)$ to reflect the interaction between vertical and lateral reinforcement. The new term is a function of the maximum expected stress in ties

at failure of the section (f''_s). To reflect the experimental observations, f''_s is estimated by equation 6.3 as function of the tie yield strength (f''_y) and the concrete strength. The factor (κ) is constant and is found to yield good results if taken as 0.2. Contribution of the vertical rebars in confining the section is less than contribution of the lateral reinforcement, which has larger stiffness. The tie-volumetric ratio, ρ'', is simply calculated as ratio of volume of ties to the gross volume of the confined concrete.

$$k_{STR;Conf} = \frac{6.7 A_{ce}}{f_{cs} A_{cg}} (\rho'' f''_s + 0.2 \rho f_y)^{0.5} \qquad [6.2]$$

$$f''_s = f''_y \qquad \text{for } f'_{cs} < 0.10 f''_y \qquad [6.3.a]$$

$$f''_s = 1.5 f''_y - 5 f'_{cs} \qquad \text{for } f'_{cs} \geq 0.10 f''_y \qquad [6.3.b]$$

Where: A_{ce} is the effectively confined core area at the critical section between ties and A_{cg} is the gross confined area. f_y is the yield strength of vertical rebars. ρ'' and ρ are the tie volumetric ratio and reinforcement ratio respectively.

To calculate the effectively confined area in a way suitable for both columns and joints, the definitions of some terms in Sheikh and Uzumeri (1982) are adapted.

$$A_{cg} = B \times H \qquad [6.4]$$

$$A_{ce} = \zeta A_{co} \qquad [6.5]$$

$$\zeta = 1 - \frac{\sum_{1}^{m} C_i^2}{\alpha A_{co}} \qquad [6.6]$$

$$A_{co} = (B - 0.5S \tan\theta)(H - 0.5S \tan\theta) \qquad \text{for column-section} \qquad [6.7.a]$$

$$A_{co} = (B - 0.5S \tan\theta)H \qquad \text{for joint-section confined along H-dimension} \qquad [6.7.b]$$

$$A_{co} = B \times H \qquad \text{for interior joint confined in all directions} \qquad [6.7.c]$$

B and H are dimensions of the section minus thickness of the unconfined cover at tie level. A_{co} is the core area at tie level. ζ is ratio of the effectively confined concrete area to the core area at tie level. The term ($\sum C_i^2/\alpha$) is the unconfined area between longitudinal bars. C_i is the center to center distance between longitudinal bars along the unconfined sides. m is number of arcs between longitudinal bars along the unconfined sides. α is a constant taken, in most strength models found in literature, equal to 5.5. θ is

angle of the curve separating the tension and compression zones, which observed to be 45°. S is the smaller of the tie spacing (s'') or the vertical rebar spacing.

An example is used to demonstrate the difference in computing A_{ce} for a column and for a column-floor joint. For the case shown in figure 6.2, the column dimensions are 250x350mm, clear cover is 20 mm, and ties are made of M10 bars spaced at 100 mm center to center. The variable m equals 8 for the column-section and equals 4 for the joint-section confined by two beams on the short opposite sides.

For the column section:

$$\sum_{1}^{m=8} C_i^2 = 4(86\text{^}2 + 136\text{^}2) = 103568 \text{ mm}^2$$

B= 250-2x20-11=199 mm

H= 350-2x20-11=299 mm

A_{co} =(199-0.5x100xtan45)x(299-0.5x100xtan45)= 37101 mm^2

$$\zeta = 1 - \frac{103568}{5.5 \times 37101} = 0.492$$

A_{ce} = 0.492x37101= 18270 mm^2

For the joint section:

$$\sum_{1}^{m=4} C_i^2 = 4 \times 136\text{^}2 = 73984 \text{ mm}^2$$

B= 250-2x20-11=199 mm

H= 350 mm

A_{co} = (199-0.5x100xtan45)x350 = 52150 mm^2

$$\zeta = 1 - \frac{73984}{5.5 \times 52150} = 0.742$$

A_{ce} = 0.742x52150 = 38698 mm^2

6.3.2 Derivation of the Joint-Related Strength Terms (k-Factors)

6.3.2.1 Assumptions Considered in Deriving the k-Factors

In deriving equations of the other strength terms "$k_{Floor;Res}$, $k_{Floor;Deb}$, $k_{HSC;Core}$, and $k_{End;Conf}$", each term is evaluated as the enhancement in the effective strength, Δf_{ce},

divided by f'_{cs} where $\Delta f_{ce}=f_{ce}-f'_{cs}$. The equation of any k-factor is derived in the form: $k=f(f'_{cc}, f'_{cs}, \eta, \lambda, h/c, \gamma, \psi)$.

The variable η represents the reserve strength or reserve strain of the floor. A linear relation is assumed between Δf_{ce} and η. For the specimens of this research: η is zero for specimens with ultimately loaded floors (SP1, SP3 and SP6); and η is taken as unity for specimens with floors loaded at service level (SP2, SP4, SP5 and SP7). The value of η can be estimated in four ways: as the normalized difference between yield strain of the floor reinforcement (ε_y) and the maximum expected strain (ε), as in equation 6.8.a; as the normalized difference between the floor moment of resistance (M_r) and the maximum expected moment (M), as in equation 6.8.b; as the normalized difference between the floor load-capacity (w_u) and the maximum expected floor load (w), as in equation 6.8.c; or as the normalized difference between the chosen reinforcement for the floor (ρ_{act}) and the required floor reinforcement (ρ_{req}), as in equation 6.8.d.

$$\eta = 5(1-\frac{\varepsilon}{\varepsilon_y}) \qquad [6.8.a]$$

$$\eta = 5(1-\frac{M}{M_r}) \qquad [6.8.b]$$

$$\eta = 5(1-\frac{w}{w_u}) \qquad [6.8.c]$$

$$\eta = 5(\frac{\rho_{act}}{\rho_{req}}-1) \qquad [6.8.d]$$

$$\rho_{bal} \geq \rho_{act} \geq \rho_{req}$$

A linear relation is assumed between Δf_{ce} and the degree of confinement by the surrounding floor or the joint type. λ is introduced as the ratio of the perimeter confined by the floor to the total perimeter. For the specimens of this research, slab-beam floor, one can identify two sub-joints between the floor and the column: a sub-joint that is confined from all directions by the slab (an interior joint) with $\lambda = 1.0$, and a sub-joint that is confined in two opposing directions by the beam stem (an edge joint) with $\lambda = 250x2/[2x(250+350)] = 0.42$; the beam-column joint is more critical.

To determine the joint aspect ratio, h/c, the value c is the column smaller dimension and the value h is the joint vertical thickness. For flat plate floors, h is the

floor thickness. For slab-beam floor system, two values of h are identified: the slab thickness for the slab-column sub-joint, and the beam-stem for the beam-column sub-joint. For the specimens of this research: the slab-column sub-joint has an h = 100 mm, and the beam-column sub-joint has an h = 360-100 = 260 mm. The beam-column sub-joint is more critical. The beam-column sub-joint for the specimens in this research governs the overall capacity.

The variable γ is the ratio between the area of HSC in the joint and the joint cross-sectional area (γ = 0.74 for SP3 and SP4).

The variable ψ represents fraction of the main reinforcement of the floor debonded within the joint: ψ = 1 if all the floor main reinforcement is debonded, and ψ = 0 if the floor main reinforcement is bonded.

6.3.2.2 Assumptions for Deriving Basic Equations of the Different Specimens

For joints such as those tested in this research, f_{ce} is assumed equal to f'_{cc} for f'_{cc}/f'_{cs} values below or equal to 1.4. This assumption is supported by the consensus between design equations found in CSA A23.3 (84), CSA A23.3 (94) and ACI 318-02 and is in reasonable agreement with test results from literature.

Figure 6.3 shows results of the seven tests of this research as discrete points connected to point A (1.4, 1.4) by straight lines. By assuming that each test result correctly represents a case, a design equation can be derived for each case as an equation of a line segment between that test result and point A. The difference between any two derived equations is strictly a function of the variations between the specimens. Therefore, the effect of each individual parameter or their combination, such as HSC or debonding, can be seen as rotational transition from one line to another about point A.

6.3.2.3 Setting Basic Strength Equations for the Different Specimens

Following the assumptions stated in the previous section, five equations can be used to estimate the effective strength of an edge joint. Each equation represents a line shown in figure 6.3 and is written in the form: $f_{ce} = a f'_{cs} + b f'_{cc}$. Values of a and b for each specimen is shown in table 6.1. Equations 6.9 to 6.13 contain a and b expressed in

terms of the variables γ and ψ tested in this research. Using equations 6.9 to 6.13, the gain in f'_{ce} due to any factor is expressed in the form: ($\Delta f_{ce} = c f'_{cs} + d f'_{cc}$).

$$f_{ce} = 1.13 f'_{cs} + 0.19 f'_{cc} \quad \text{for SP1 and SP6} \quad [6.9]$$

$$f_{ce} = 0.98 f'_{cs} + 0.30 f'_{cc} \quad \text{for SP2} \quad [6.10]$$

$$f_{ce} = 1.13(1 - 0.65\gamma) f'_{cs} + 0.19(1 + 2.84\gamma) f'_{cc} \quad \text{for SP3} \quad [6.11]$$

$$f_{ce} = 0.98(1 - 0.95\gamma) f'_{cs} + 0.30(1 + 2.21\gamma) f'_{cc} \quad \text{for SP4} \quad [6.12]$$

$$f_{ce} = 0.98(1 - 0.20\psi) f'_{cs} + 0.30(1 + 0.52\psi) f'_{cc} \quad \text{for SP5} \quad [6.13]$$

6.3.2.4 Reserve Strength of the Floor

The gain in f_{ce} due to reserve strength of the floor is estimated as the difference between equations 6.9 and 6.10 for specimens with normal strength concrete (NSC) joints and as the difference between equations 6.11 and 6.12 for joints with HSC cores. This gain can be estimated as $\Delta f_{ce} = 0.1[(1.1+1.2\gamma) f'_{cc} - (1.5+2.0\gamma) f'_{cs})]$. From this, equation 6.14 for $k_{Floor;Res}$ is derived and the variable η is included to match any loading level and λ is reflecting the observation in Ospina and Alexander (1997).

$$k_{Floor;Res} = 0.1[(1.1 + 1.2\gamma) f'_{cc} / f'_{cs} - 1.5 - 2.0\gamma]\eta\lambda \geq 0 \quad [6.14]$$

6.3.2.5 Debonding the Floor Reinforcement

The gain in f_{ce} due to partially debonded floor reinforcement can be estimated as $\Delta f_{ce} = (-0.2 f'_{cs} + 0.16 f'_{cc})]\psi$ which is the difference between equations 6.10 and 6.13. This effect would vanish if the floor collapsed before the column, as for SP6.

$$k_{Floor;Deb} = (0.16 f'_{cc} / f'_{cs} - 0.2)\psi \geq 0 \quad [6.15]$$

The gain in f_{ce} due to debonding the floor-negative reinforcement through NSC joints could be different than through HSC joints because of the difference in the released bond stress that was to develop between the floor reinforcement and the joint concrete. This gain is believed to be bigger for HSC joints than for NSC joints, which would make equation 6.15 conservative when applied to joints made of HSC.

6.3.2.6 High-Strength-Concrete Core

The difference between equations 6.9 and 6.11 gives an estimate of Δf_{ce} due to HSC core for a joint of type-II loaded specimens while the difference between equations

6.10 and 6.12 gives a corresponding estimate for a joint of type-I loaded specimens. Both estimates of $\Delta f'_{ce}$ can be expressed in a general form as function of the floor loading level or deformation by the variable (η). This effect can be expressed as $\Delta f_{ce} = [(-0.73-0.2\eta) f'_{cs} + (0.54+0.12\eta) f'_{cc})]\gamma$. Accordingly, equation 6.16 can be used for calculating $k_{HSC;Core}$.

$$k_{HSC;Core} = [(0.54 + 0.12\eta) f'_{cc} / f'_{cs} - 0.73 - 0.2\eta]\gamma \geq 0 \qquad [6.16]$$

6.3.2.7 End Confinement and the Aspect Ratio

After calculating $k_{STR;Conf}$, $k_{Floor;Res}$, $k_{Floor;Deb}$ and $k_{HSC;Core}$ for SP1, SP2, SP5 and SP6 using the equations developed above, the only unknown remaining in equation 6.1 is $k_{End;Conf}$. Values of $k_{End;Conf}$ can be obtained by setting equation 6.1 equal to equations 6.9, 6.10, and 6.13. The average $k_{End;Conf}$ can be estimated as $k_{End;Conf} = 0.11(f'_{cc}/f'_{cs} - 1)$.

The effect of the joint aspect ratio is analogous to that of the concrete cylinders on their apparent strengths. Neville (1981) shows that the apparent strength of a concrete cylinder is affected by the rigidity of the platens of the testing machine and the cylinder aspect ratio (defined as height/diameter of the cylinder). The correction factor based on results in Neville follows a nonlinear relation in the aspect ratio with maximum value of 2, minimum value of 0.9.

To match the results of this research and the results in Neville, a quadratic polynomial in h/c defined as $k_{End;Conf} = [1 - 1.24(h/c) + 0.37(h/c)^2](f'_{cc}/f'_{cs} - 1)$ is proposed. $k_{End;Conf}$ is rewritten in equation 6.17 after including a factor of 0.85 before the ratio f'_{cc}/f'_{cs}, resulted from regression analysis. A linear relation is assumed between $k_{End;Conf}$ and percentage of the joint area that is made of NSC because $k_{End;Conf}$ vanishes when the joint is totally made of HSC. For h/c value greater than 2.0, $k_{End;Conf}$ is taken as zero.

$$k_{End;Conf} = [1 - 1.24(\frac{h}{c}) + 0.37(\frac{h}{c})^2](0.85 f'_{cc} / f'_{cs} - 1)(1 - \gamma) \qquad [6.17]$$

$$1.0 \geq k_{End;Conf} \geq -0.1$$

6.3.3 Determining the Effects of Geometry and Reinforcement Details

To estimate the joint effective strength using equation 6.1, one has to use equations 6.2 through 6.7 to evaluate the term $k_{STR;Conf}$, which are not convenient for design purposes. A simpler approach is needed. $k_{STR;Conf}$ reflects effect of the structure

and so the effect of joint reinforcement cannot be separated from the flooring effect. To evaluate the effective strength for design purposes, $k_{STR;Conf}$ is broken down into two terms as shown in equation 6.18: $k_{RFT;Conf}$ is the relative enhancement provided by the joint reinforcement and $k_{Floor;Conf}$ is the relative enhancement provided by the floor.

$$k_{STR;Conf} = k_{RFT;Conf} + k_{Floor;Conf} \quad [6.18]$$

For an NSC joint with collapsed floor (SP1 and SP6), $k_{Floor;Deb}$, $k_{Floor;Res}$ and $k_{HSC;Core}$ are zero, and so equation 6.1 will contain only $k_{STR;Conf}$ and $k_{End;Conf}$. By setting equation 6.1 equal to equation 6.9, equation 6.19 is produced. By substituting for $k_{End;Conf}$, $k_{STR;Conf}$ can be obtained as a function of f'_{cc}/f'_{cs}, as in equation 6.20.

$$f_{ce} = 1.13f'_{cs} + 0.19f'_{cc} = f'_{cs}(1 + k_{STR;Conf} + k_{End;Conf}) \quad [6.19]$$

$$k_{STR,Conf} = 0.08f'_{cc} / f'_{cs} + 0.24 \quad [6.20]$$

To evaluate the two terms, $k_{RFT;Conf}$ and $k_{Floor;Conf}$, table 6.2 is presented. In this table, $k_{Conf;Test}$ is the ratio of the actual f_{ce} to the equivalent f'_{cs} minus unity. The equivalent f'_{cs} is the sum of the products of the concrete strengths times areas of the concretes inside the joint, divided by the joint area. $k_{RFT;Conf}$ is estimated as $k_{STR;Conf}$ for a column section. $k_{Floor;Conf}$ is obtained as the difference between $k_{STR;Conf}$ values of an edge joint and its column respectively. The last column of the table contains *other effects* which is obtained by subtracting $k_{STR;Conf}$, for joints, from $k_{Conf;Test}$.

Other effects in table 6.2 includes, where applicable, the loading effect for all specimens failed in the joint, the debonding effect for joints with partially debonded floor reinforcement, and the effect of HSC inside the joints. As shown in table 6.2, the average $k_{RFT;Conf}$ is 0.32 and the average $k_{RFT;Conf}$ is 0.12. Therefore, $k_{RFT;Conf}$ is 72% of $k_{STR;Conf}$ and $k_{Floor;Conf}$ is 28% of $k_{STR;Conf}$, calculated in equation 6.20. After some iterations to best-match the different types of concrete sections from literature, the final expressions of the cage and floor confining effects can be evaluated using equations 6.21 and 6.22.

$$k_{RFT;Conf} = 0.025(\rho'' f''_s + 0.2\rho f_y)(1 + 0.55f'_{cc} / f'_{cs}) \quad [6.21]$$

$$k_{Floor;Conf} = 0.02\lambda(3 + f'_{cc} / f'_{cs})(1 - \gamma) \quad [6.22]$$

Comparing $k_{Conf;act}$ to $k_{STR;Conf}$ for SP4 and SP7 reveals that equation 6.2, used to evaluate $k_{STR;Conf}$, works well. According to equation 6.2, actual $k_{Conf;act}$ for the column of

SP3 would have been 13% higher if the top column collapsed smoothly, yet it would not have failed in the joint.

6.3.4 Summary of Terms of the Strength Model

$$f_{ce} = f'_{cs}(1 + k_{STR;Conf} + k_{Floor;Res} + k_{Floor;Deb} + k_{HSC;Core} + k_{End;Conf}) \quad [6.23.a]$$

$$f_{ce} = f'_{cs}(1 + k_{RFT;Conf} + k_{Floor;Conf} + k_{Floor;Res} + k_{Floor;Deb} + k_{HSC;Core} + k_{End;Conf}) \quad [6.23.b]$$

$$k_{STR;Conf} = \frac{6.7 A_{ce}}{f_{cs} A_{cg}} (\rho'' f_s'' + 0.2\rho f_y)^{0.5}$$

$(\rho f_y)_{eq} = (\rho f_y)_1 + (\rho f_y)_2 + \ldots$ if two or more grades of rebars are used,

$$A_{cg} = B \times H$$

$$A_{ce} = \zeta A_{co}$$

$$\zeta = 1 - \frac{\sum_{i}^{m} C_i^2}{\alpha A_{co}}$$

$A_{co} = (B - 0.5S\tan\theta)(H - 0.5S\tan\theta)$ for column-section

$A_{co} = (B - 0.5S\tan\theta)H$ for joint-section confined along H-dimension

$A_{co} = B \times H$ for interior joint confined in all directions

$$k_{RFT;Conf} = 0.025(\rho'' f''_s + 0.2\rho f_y)(1 + 0.55 f'_{cc} / f'_{cs})$$

$$k_{Floor;Conf} = 0.02\lambda(3 + f'_{cc} / f'_{cs})(1 - \gamma)$$

$$k_{Floor;Res} = 0.1[(1.1 + 1.2\gamma) f'_{cc} / f'_{cs} - 1.5 - 2.0\gamma]\eta\lambda$$

$$1 \geq k_{Floor;Res} \geq 0$$

$$k_{Floor;Deb} = (0.16 f'_{cc} / f'_{cs} - 0.2)\psi$$

$$1.0 \geq k_{Floor;Deb} \geq 0$$

$$k_{HSC_{core}} = [(0.54 + 0.12\eta) f'_{cc} / f'_{cs} - 0.73 - 0.2\eta]\gamma$$

$$k_{End;Conf} = [1 - 1.24(\frac{h}{c}) + 0.37(\frac{h}{c})^2](0.85 f'_{cc} / f'_{cs} - 1)(1 - \gamma)$$

$$1.0 \geq k_{End;Conf} \geq -0.1$$

6.4 Obtaining Strain Values ε_{s1} and ε_{s2}

Similar to the modified model by Hognested et al. (1951), equations 6.24 and 6.25 are proposed to calculate strain values at peak stresses but with two differences: f'_{co} is

replaced by f_{ce} and the elastic modulus of the cracked section (E_{cr}) is used instead of that for uncracked section (E_c). To conform to the experimental observations, E_{cr} is proposed as a function of f''_s/f''_y. If the section has enough confinement and is made of NSC, ties will yield and localized failure will follow. Two values of E_{cr} are proposed in equations 6.26 and 6.27: E_{cr1} at point C_1, and E_{cr2} at C_2. E_{cr2} is assumed 10% less than E_{cr1}. The more the section is damaged, the higher the strain in ties and subsequently the less stiff is the section.

$$\varepsilon_{s1} = 1.8 f_{ce} / E_{cr1} \quad [6.24]$$

$$\varepsilon_{s2} = 1.8 f_{ce} / E_{cr2} \quad [6.25]$$

$$E_{cr1} = E_c[0.2 + 0.8(1 - \frac{f''_s}{f''_y})] \quad [6.26]$$

$$E_{cr2} = 0.9 E_{cr1} \quad [6.27]$$

6.5 Modeling the Pre-peak and Peak Behaviour

With slight modification, the model developed by Mander et al. (1988) yields the best fit for the ascending branch of the stress-strain curve (part O-C_1-C_2 in figure 6.1). The stress, f_c, at any strain value, ε_c, can be estimated using equations 6.28 through 6.31.

$$f_c = \frac{f_{ce} x r}{r - 1 + x^r} \quad [6.28]$$

$$x = \frac{\varepsilon_c}{\varepsilon_{s1}} \quad [6.29]$$

$$r = 1.05 \frac{E_c}{E_c - E_{sec}} \quad [6.30]$$

$$E_{sec} = \frac{f_{ce}}{\varepsilon_{s1}} \quad [6.31]$$

6.6 Modeling the Post Peak Behaviour

The post peak model is described by equations 6.32 through 6.34. Equation 6.32 is proposed to determine the slope of the descending part. It is similar to that developed by Kent and Park with a few additions to account for the column rectangularity, the floor reserve strength, and debonding of floor main reinforcement. The dimension B is the

smaller unconfined dimension. The term (η) reflects contribution of the reserve strength of the floor to the joint ductility in terms of reducing the rate of failure. Similarly, the term (5ψ) reflects the level of lateral strain relief provided to the joint by partial debonding. The stress f_c at any strain value ε_c beyond ε_{s2} is given by equation 6.34.

$$z = \frac{0.5}{\frac{3}{4}\rho'' \sqrt{\frac{B}{s''}} + \varepsilon_{50u} - \varepsilon_{s2}} - \eta - 5\psi \qquad [6.32]$$

$$\varepsilon_{50u} - \varepsilon_{s2} = \frac{1 + 5\varepsilon_{cs} f_{cs}}{f_{cs} + 100} \qquad [6.33]$$

$$f_c = f_{ce}[1 - z(\varepsilon_c - \varepsilon_{s2})] \qquad [6.34]$$

Matching with the experimental results, equation 6.32 suggests that the unloading part of the stress–strain curve is steeper if the volumetric ratio of lateral reinforcement is lower and if the tie spacing is bigger. As well, equation 6.32 suggests that the unloading part is flatter if the floor load is within serviceability and/or if the floor negative reinforcement is debonded.

6.7 Validating the Proposed Behaviour Model

Validation of the proposed model was done by comparing the estimated against the actual test results of twenty interior joints, thirteen edge joints and four sandwich columns. The data used in the comparison are those from this research and from Ospina and Alexander (1997).

6.7.1 Validating the Strength Model

Table 6.3 shows results of f_{ce} using equations 6.23.a and 6.23.b vs. actual effective strength, $f_{ce,\,test}$, for the thirty-seven specimens. The table shows values of the k-factors and ratios of predicted to actual f_{ce} using both equations. From that table, the average and coefficient of variation values of this ratio using equation 6.23.a are 1.02 and 0.13 respectively. The corresponding values using equation 6.23.b are 1.05 and 0.17 respectively. The comparison reveals accuracy of both equations to estimate the effective strength of any type of floor-column joint. Each equation can be used in place of the other but equation 6.23.b will be convenient for design purposes.

6.7.2 Comparing Model-Predicted to Actual Joint Behaviour

6.7.2.1 Tests of This Research

As seen in figures 6.4 through 6.10 for the seven specimens tested in this research, the model can capture the overall behaviour with a reasonable accuracy as long as there is no localized failure. Except in figure 6.10, concrete strain values are the average strain readings measured by the concrete embedded gauges. In figure 6.10, each strain value is the average of the eight strain readings from the mounted foil gauges.

6.7.2.2 Interior Specimens (Series A and B) by Ospina and Alexander

In general, there is good agreement between the predicted and the actual curves for all the twelve specimens of series A despite the fact that five specimens failed outside the joints. For specimens failing in the joint, the actual post-peak behaviour is much flatter than the predicted. This is attributed to spalling concrete, which affected the LVDT readings. Figures 6.11 through 6.13 show the actual and predicted stress-strain curves for specimens A1C, A3C and A4C respectively. The rest of figures are shown in appendix D.

There is a good fit between the predicted and the actual curves for specimens B1 to B4 while specimens B5 to B8 show the worst match. Three reasons are believed attributing to the worst match: (1) reinforcement ratio of the vertical rebars was fixed at 1.28%, very close to the minimum recommended by the codes of design, which would not represent a common design practice for columns of high rise buildings; (2) values of f'_{cs} were 15 and 19 MPa when the specimens were tested at age of three weeks, similar to what Shu and Hawkins observed; (3) the f'_{cc} / f'_{cs} ratio exceeded 6.0; the model could be conservative with respect to f'_{cc} / f'_{cs} ratio. Figures 6.14 and 6.15 show the actual and predicted stress-strain curves for specimens B1 and B3. The rest of figures are shown in appendix D.

6.7.2.3 Edge Specimens (Series C) by Ospina and Alexander

Figures 6.16 through 6.18 show good match between the actual and predicted stress-strain curves for specimens C1B, C2B and C2C; the predicted curves for specimens C1A, C1C and C2A are slightly above the actual ones. As reported by Ospina and Alexander, average strain values of the slab reinforcement included strain

measurements away from the column face. Using exact strain values in the model would have lessened the gap between the predicted and actual curves. Two more things attributed to the deviation between the actual and predicted curves: the method of slab loading, which included some eccentricity on the column, and the boundary conditions of the tested specimens, which were widely different from those of the current research.

6.7.2.4 Sandwich Specimens (Series D) by Ospina and Alexander

Figures 6.19 and 6.20 show good match between the actual and predicted stress-strain curves for SC3 and SC4; the predicted curves for specimens SC1 and SC2 are slightly above the actual ones. A combination of the reasons mentioned in the previous subsections applies here.

6.7.3 Limitations of Comparing Data from Different Sources

The degree of agreement between model-predicted and actual responses does not depend solely on the model accuracy. Design and control of the test setup can affect the results and consequently the honest judgment about the model. Palmquist and Jansen (2001) observed that the constants found in any empirical equation are set to match group of tests conducted by the modeller to derive the tests.

Judging the curacy of a model by comparing its results to actual results from different sources is extremely difficult. When applying a model against different set of tests, variation could be observed because of material variability or difference in specimen size (Palmquist and Jansen). James et al. (2001) adds that the variation could be because of the different lengths of gauges used and the different location of strain measurement among researchers.

Regarding the test results of Ospina and Alexander, some points are worth mentioning. Calculation of stresses was based on LVDT readings, which were affected by spalling of the cover concrete. This would lead to an overestimate of rebar stresses and consequently less f_{ce} values. Moreover, the floor loading was controlled based on the measured strain values of the slab top reinforcement. Such strain values were monitored through the working foil gauges regardless of their location relative to the load points, which was irregular in the case of edge specimens. Although the floor loads reached in

some cases seven percent of the maximum applied column loads, it was not accounted for in calculation of the actual stresses.

6.8 Advantages and Disadvantages of the Proposed Model

6.8.1 Advantages

- Equations 6.23.a and 6.23.b are suitable for predicting the concrete effective strength for columns and joints.
- Both equations account for the effect of reinforcement details, debonding of floor reinforcement and floor loading level.
- Both equations provide transparency to the design of floor-column joints such that the designer can expect the change made by controlling the different parameters.
- Both equations provide flexibility to the designer to choose from different measures to upgrade the joint strength.
- The stress-strain model is proved good at replicating behaviour of all types of joints under any scheme of loading.

6.8.2 Disadvantages

- Both equations are incapable of differentiating between corner and edge columns that are framing into beams from two sides only.
- Like all mathematical models, the proposed model is incapable of capturing "localized failure phenomenon" between the peaks, if more than one, or at the end of the peak period.

Table 6.1. Values of a and b for the strength equation $f_{ce} = a f'_{cs} + b f'_{cc}$

SP#	a	b
SP1	1.13	0.19
SP2	0.98	0.30
SP3	0.58	0.59
SP4	0.29	0.79
SP5	0.76	0.45
SP6	1.13	0.19

Table 6.2. Breakdown of the Confinement Effect

Specimen number	$k_{Conf,\ test}$ $= (f_{ce}/f'_{cs} - 1)$	$k_{STR;Conf}$ Column	$k_{STR;Conf}$ Edge Joint	Cage Effect $K_{RFT;Conf}$	Floor Effect $K_{Floor;Conf}$	Other Effects
1	0.91	0.46	0.61	0.46	0.15	0.30
2	1.25	0.41	0.54	0.41	0.13	0.71
3	-0.05(top-tie snapped)	0.08	0.12	0.08	0.04	-0.17
4	0.07 (bottom)	0.11	0.17	0.11	0.06	-0.10
5	1.30	0.42	0.56	0.42	0.14	0.74
6	1.00	0.40	0.54	0.40	0.14	0.46
7	0.42 (bottom)	0.39	0.59	0.39	0.20	-0.17
			Average	= 0.32	0.12	

Table 6.3. Predicted vs. Actual Effective Concrete Strength (MPa) Using Equation 6.23

Test ID	f'_{cc} (MPa)	f'_{cs} (MPa)	$f_{ce,\,test}$ (MPa)	$k_{STR;Conf}$	$k_{End;Conf}$	$k_{Floor;Res}$	$k_{Floor;Deb}$	$k_{HSC;Core}$	$k_{RFT;Conf}$	$k_{Floor;Conf}$	Equation (a)		Equation (b)	
											f_{ce} (MPa)	Ratio*	f_{ce} (MPa)	Ratio*
SP1	72.8	18	34.4	0.61	0.27	0.00	0.00	0.00	0.71	0.06	33.9	0.99	36.7	1.07
SP2	86.6	20.4	45.9	0.54	0.29	0.13	0.00	0.00	0.74	0.06	40.0	0.87	45.2	0.99
SP3	89.2	31.8	70.8	0.30	0.04	0.00	0.00	0.76	0.42	0.05	61.1	0.86	64.8	0.91
SP4	66.7	17.6	57.9	0.60	0.06	0.19	0.00	1.16	0.63	0.06	53.2	0.92	53.9	0.93
SP5	66.7	19.8	45.5	0.56	0.21	0.09	0.34	0.00	0.63	0.05	43.5	0.96	45.9	1.01
SP6	93.7	20.6	41.1	0.54	0.32	0.00	0.00	0.00	0.77	0.06	38.2	0.93	44.3	1.08
SP7	18.7	18.7	26.5	0.60	0.00	0.00	0.00	0.00	0.35	0.03	29.5	1.11	25.5	0.97
A1-A	105	40	100.3	0.33	0.58	0.69	0.00	0.00	0.24	0.11	104.4	1.04	105.2	1.05
A1-B	105	40	94.0	0.33	0.58	0.35	0.00	0.00	0.24	0.11	90.7	0.97	91.6	0.97
A1-C	105	40	90.2	0.33	0.58	0.01	0.00	0.00	0.24	0.11	77.1	0.85	77.9	0.86
A2-A	112	46	97.4	0.29	0.51	0.59	0.00	0.00	0.23	0.11	109.7	1.13	112.0	1.15
A2-B	112	46	98.0	0.29	0.51	0.30	0.00	0.00	0.23	0.11	96.4	0.98	98.7	1.01
A2-C	112	46	92.2	0.29	0.51	0.01	0.00	0.00	0.23	0.11	83.1	0.90	85.4	0.93
A3-A	89	25	85.7	0.53	0.56	1.21	0.00	0.00	0.29	0.13	82.5	0.96	79.8	0.93
A3-B	89	25	80.0	0.53	0.56	0.61	0.00	0.00	0.29	0.13	67.7	0.85	64.9	0.81
A3-C	89	25	53.6	0.53	0.56	0.02	0.00	0.00	0.29	0.13	52.8	0.99	50.1	0.93

Test ID	f'_{cc} (MPa)	f'_{cs} (MPa)	$f_{ce,test}$ (MPa)	$k_{STR;Conf}$	$k_{End;Conf}$	$k_{Floor;Res}$	$k_{Floor;Deb}$	$k_{HSC;Core}$	$k_{RFT;Conf}$	$k_{Floor;Conf}$	Equation (a)		Equation (b)	
											f_{ce} (MPa)	Ratio*	f_{ce} (MPa)	Ratio*
A4-A	106	23	80.6	0.58	0.81	1.78	0.00	0.00	0.35	0.15	96.0	1.19	94.2	1.17
A4-B	106	23	72.2	0.58	0.81	0.91	0.00	0.00	0.35	0.15	75.8	1.05	74.0	1.02
A4-C	106	23	56.4	0.58	0.81	0.03	0.00	0.00	0.35	0.15	55.6	0.99	53.8	0.95
C1-A	107	32	59.8	0.26	0.53	0.54	0.00	0.00	0.25	0.06	74.5	1.25	76.2	1.28
C1-B	107	35	56.4	0.23	0.46	0.01	0.00	0.00	0.23	0.06	59.4	1.05	61.6	1.09
C1-C	107	34	54.8	0.24	0.48	0.00	0.00	0.00	0.24	0.06	58.5	1.07	60.5	1.10
C2-A	108	31	52.7	0.26	0.25	0.58	0.00	0.00	0.25	0.06	65.0	1.24	66.7	1.27
C2-B	108	34	50.2	0.24	0.22	0.25	0.00	0.00	0.23	0.06	58.2	1.16	60.2	1.20
C2-C	108	33	46.3	0.24	0.23	0.00	0.00	0.00	0.24	0.06	48.7	1.05	50.6	1.09
B-1	104	42	74.4	0.28	0.14	0.39	0.00	0.00	0.18	0.11	76.1	1.02	76.6	1.03
B-2	104	42	98.0	0.31	0.43	0.31	0.00	0.00	0.22	0.11	86.0	0.88	86.9	0.89
B-3	113	44	93.4	0.23	0.08	0.65	0.00	0.50	0.14	0.06	108.1	1.16	106.6	1.14
B-4	113	44	114	0.29	0.46	0.66	0.00	0.00	0.22	0.11	106.3	0.93	108.1	0.95
B-5	95	15	48.2	0.79	0.57	0.72	0.00	0.00	0.35	0.19	46.1	0.96	42.3	0.88
B-6	95	15	66.8	0.86	1.00	0.58	0.00	0.00	0.42	0.19	51.6	0.77	47.8	0.72
B-7	120	19	50.3	0.63	-0.07	1.12	0.00	0.00	0.35	0.19	50.8	1.01	49.1	0.98
B-8	120	19	74.4	0.68	0.91	0.98	0.00	0.00	0.42	0.19	68.0	0.91	66.5	0.89

Test ID	f'_{cc} (MPa)	f'_{cs} (MPa)	$f_{ce,\,test}$ (MPa)	$k_{STR;Conf}$	$k_{End;Conf}$	$k_{Floor;Res}$	$k_{Floor;Deb}$	$k_{HSC;Core}$	$k_{RFT;Conf}$	$k_{Floor;Conf}$	Equation (a)		Equation (b)	
											f_{ce} (MPa)	Ratio*	f_{ce} (MPa)	Ratio*
SC1	105	17	21.0	0.07	0.55	0.00	0.00	0.00	0.34	0.00	27.6	1.31	32.2	1.53
SC2	105	17	26.6	0.08	1.00	0.00	0.00	0.00	0.41	0.00	35.3	1.33	40.9	1.54
SC3	107	17	31.9	0.08	1.00	0.00	0.00	0.00	0.44	0.00	35.4	1.11	41.4	1.30
SC4	105	17	37.4	0.08	1.00	0.00	0.00	0.00	0.49	0.00	35.4	0.95	42.3	1.13
											Average = 1.02			=1.05
											Standard Deviation = 0.13			=0.18
											Coefficient of Variation = 0.13			=0.17

* Ratio is obtained by dividing f'_{ce} calculated using equation 6.23.a or 6.23.b by $f_{ce,\,test}$.

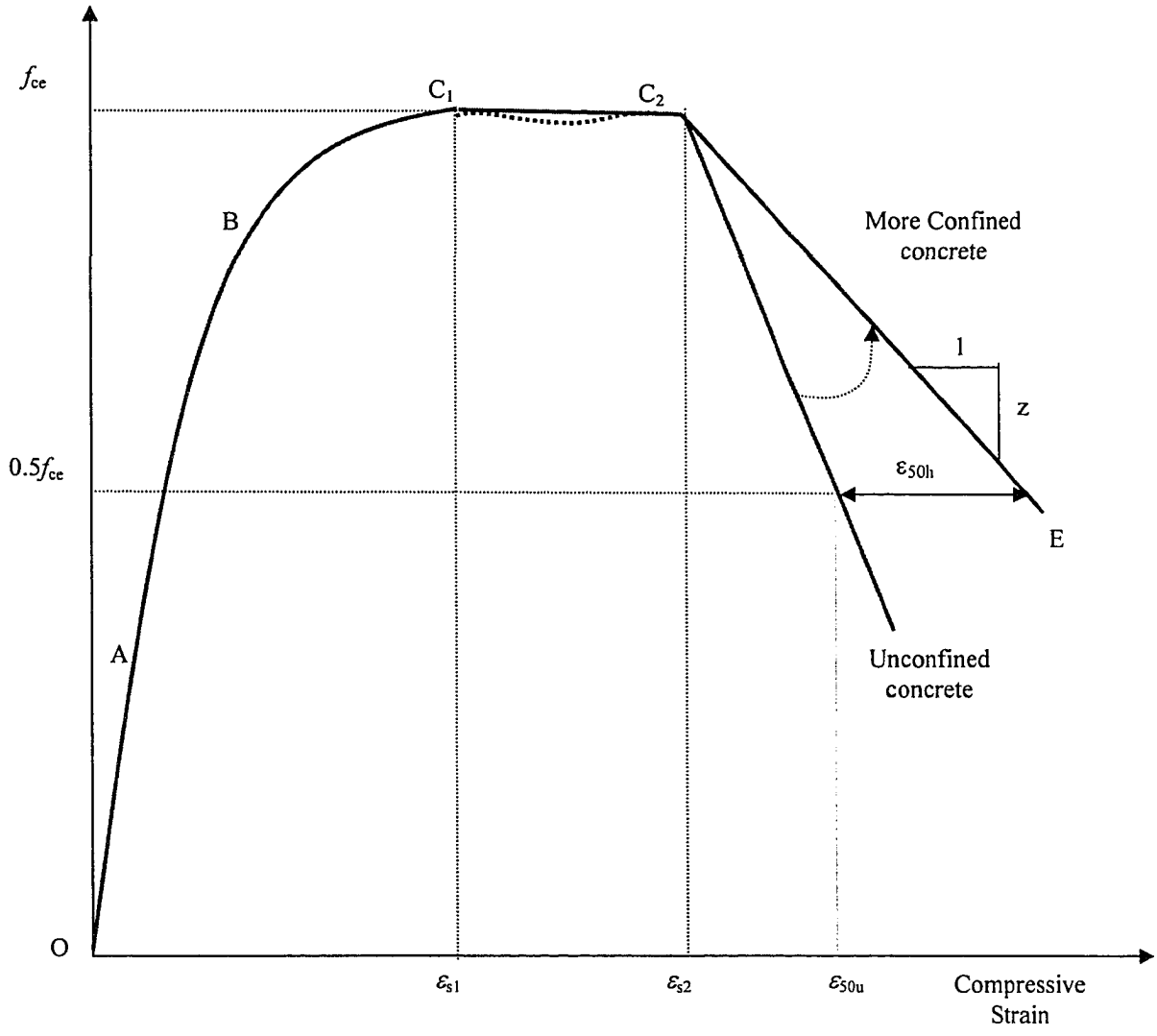

Figure 6.1. Schematic Axial Stress-Strain Behaviour

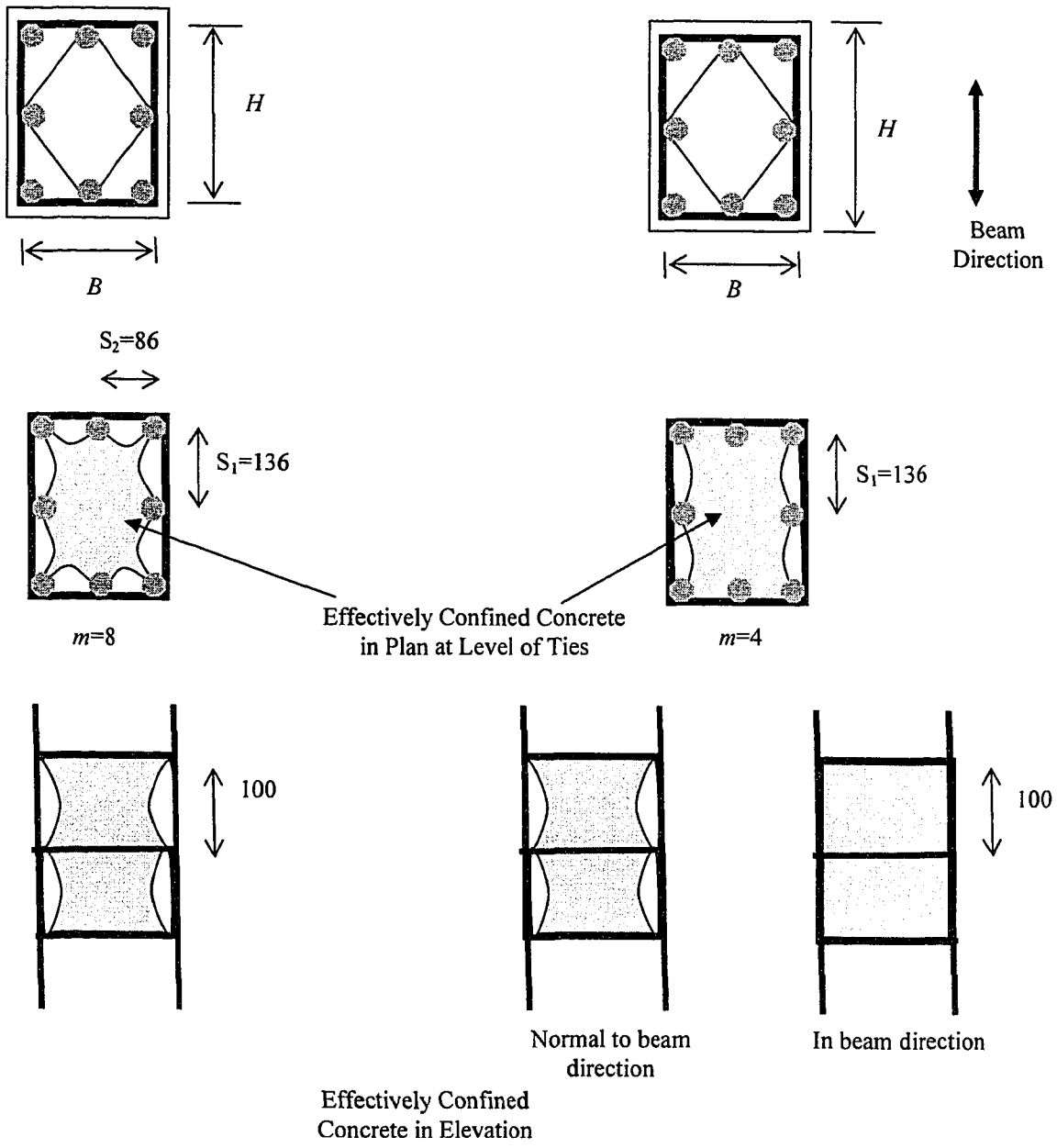

Figure 6.2. Confined Area between Levels of Ties for Column and Joint Sections

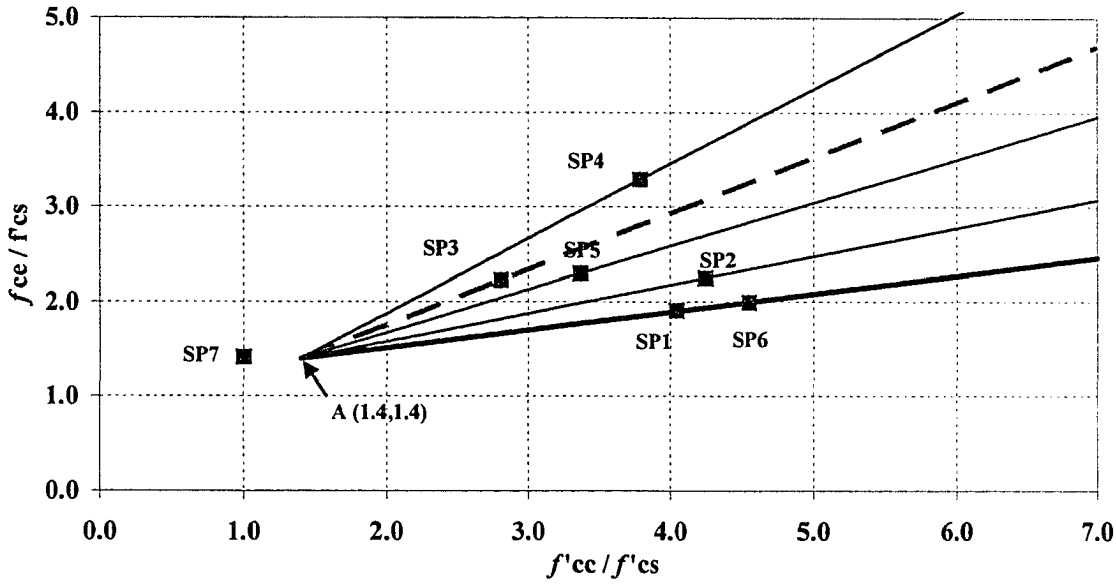

Figure 6.3. $f'ce / f'cs$ vs. $f'cc / f'cs$ for Results of This Research

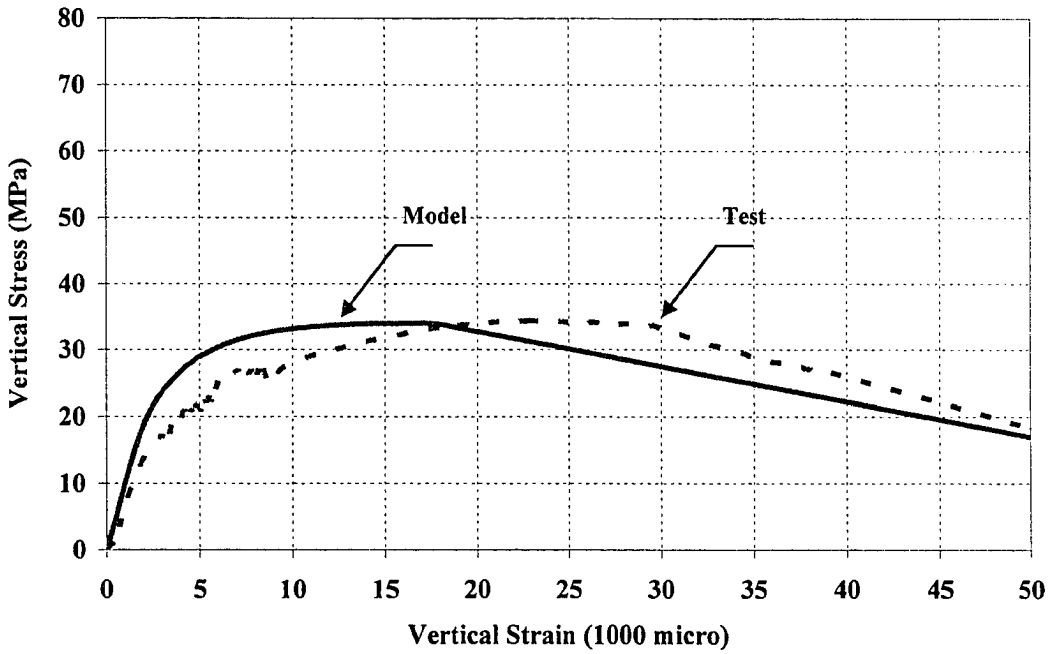

Figure 6.4. Comparison of Experimental and Analytical Compressive Stress-Strain Curves for SP1-Joint

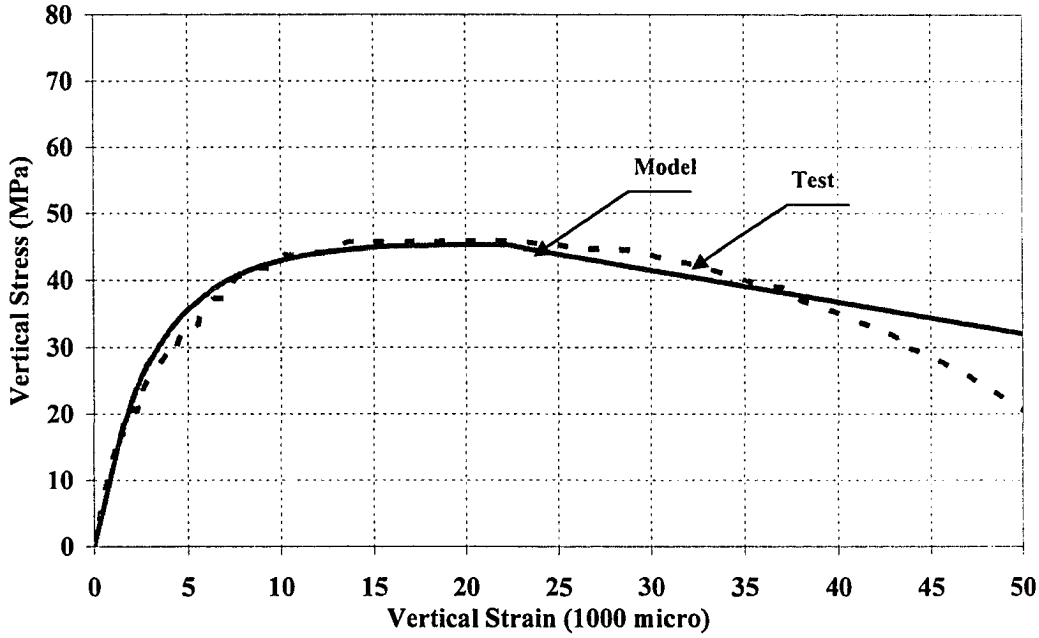

Figure 6.5. Comparison of Experimental and Analytical Compressive Stress-Strain Curves for SP2-Joint

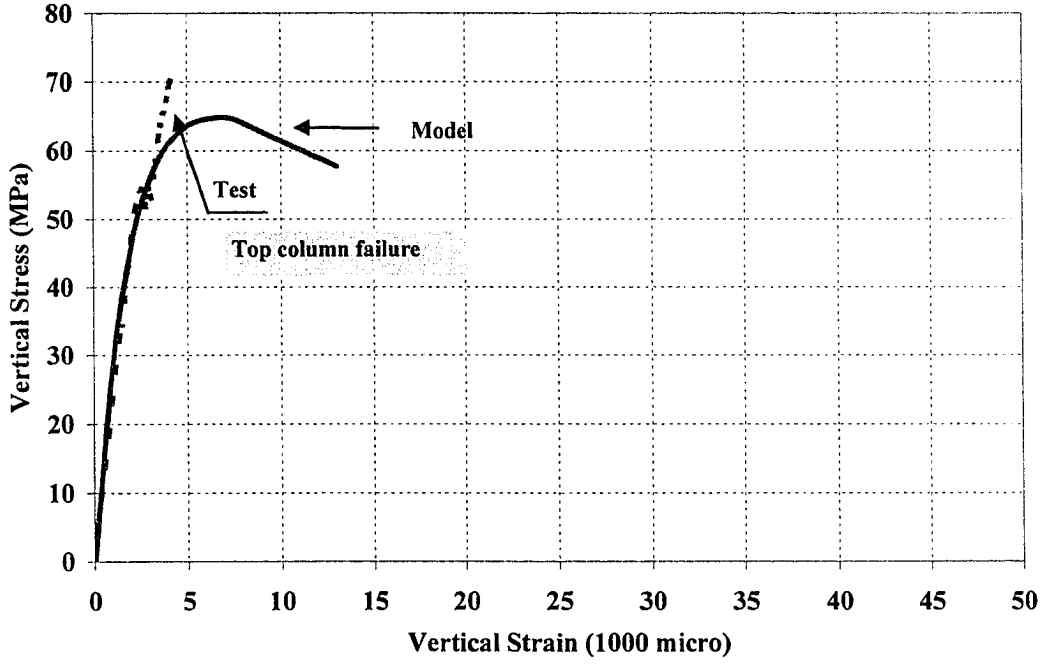

Figure 6.6. Comparison of Experimental and Analytical Compressive Stress-Strain Curves for SP3-Joint

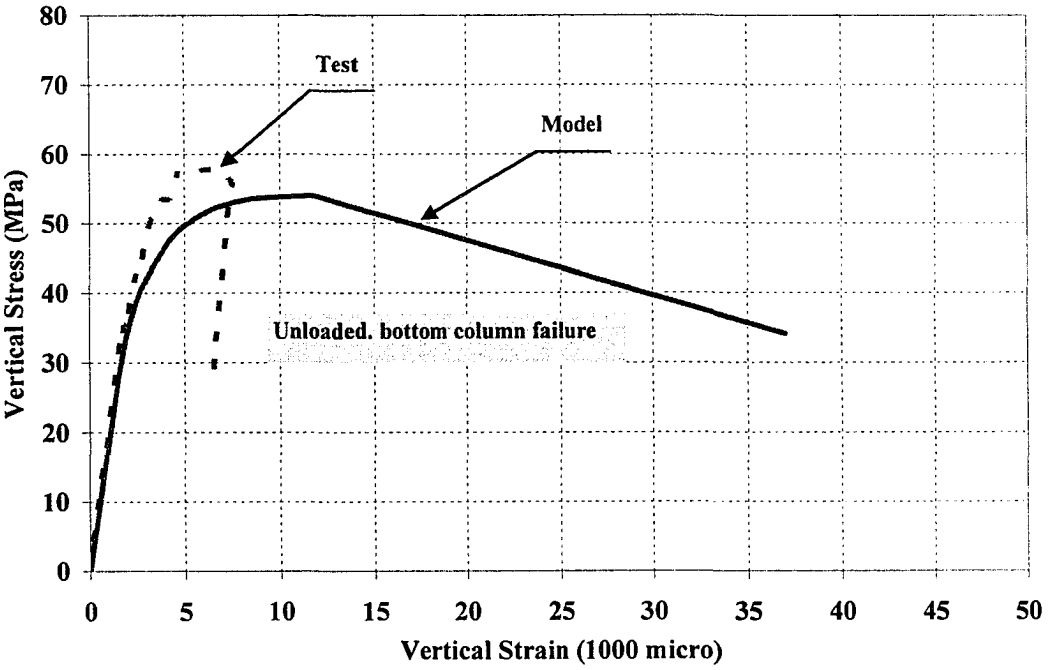

Figure 6.7. Comparison of Experimental and Analytical Compressive Stress-Strain Curves for SP4-Joint

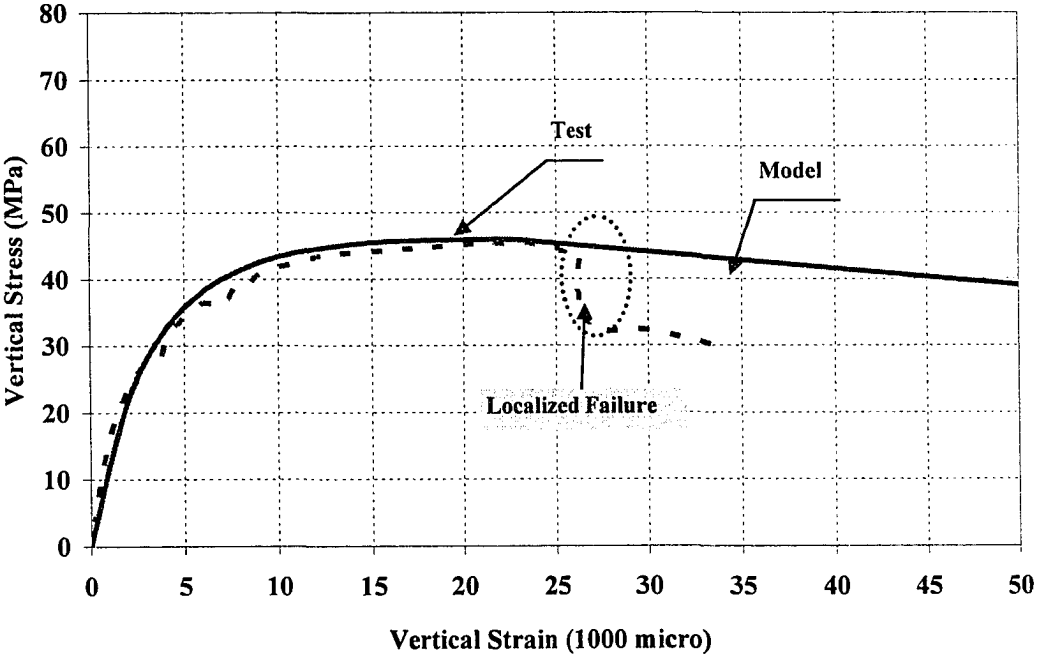

Figure 6.8. Comparison of Experimental and Analytical Compressive Stress-Strain Curves for SP5-Joint

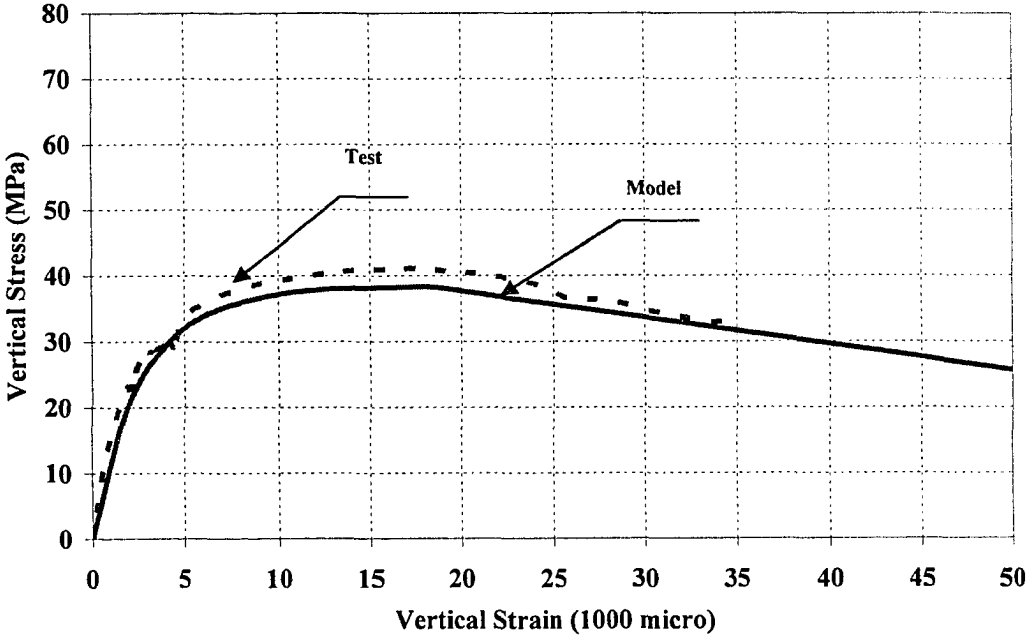

Figure 6.9. Comparison of Experimental and Analytical Compressive Stress-Strain Curves for SP6-Joint

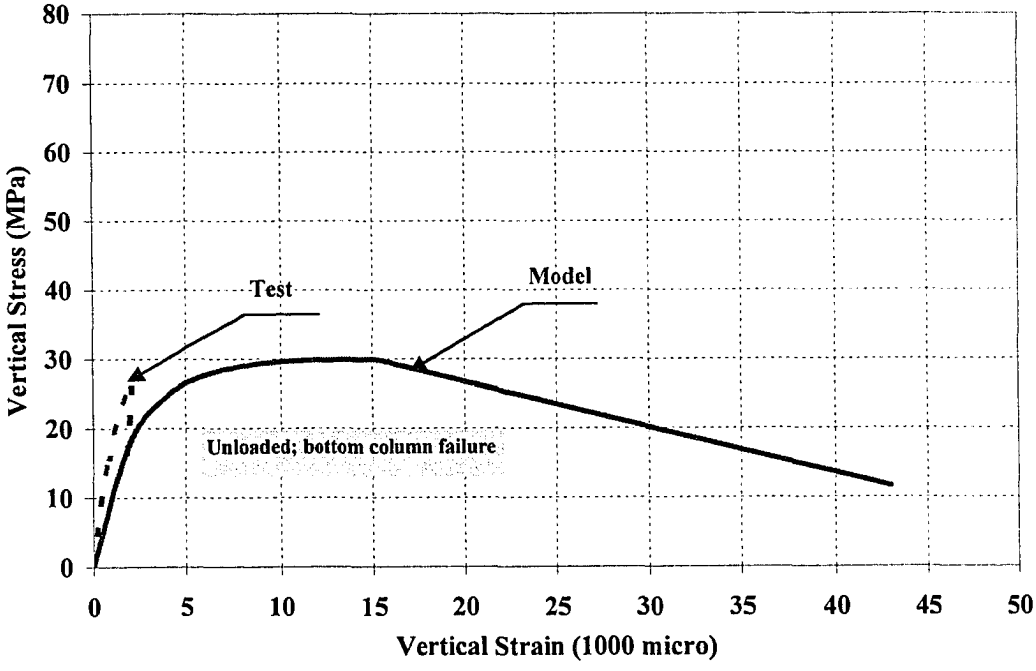

Figure 6.10. Comparison of Experimental and Analytical Compressive Stress-Strain Curves for SP7-Joint

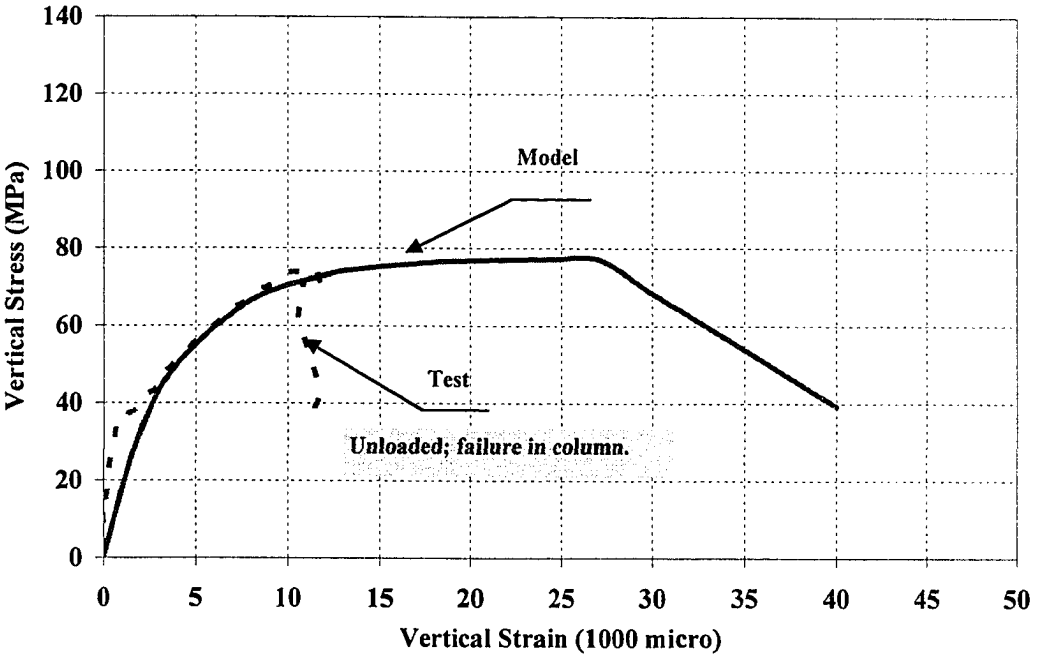

Figure 6.11. Comparison of Experimental and Analytical Compressive Stress-Strain Curves for A1C-Joint

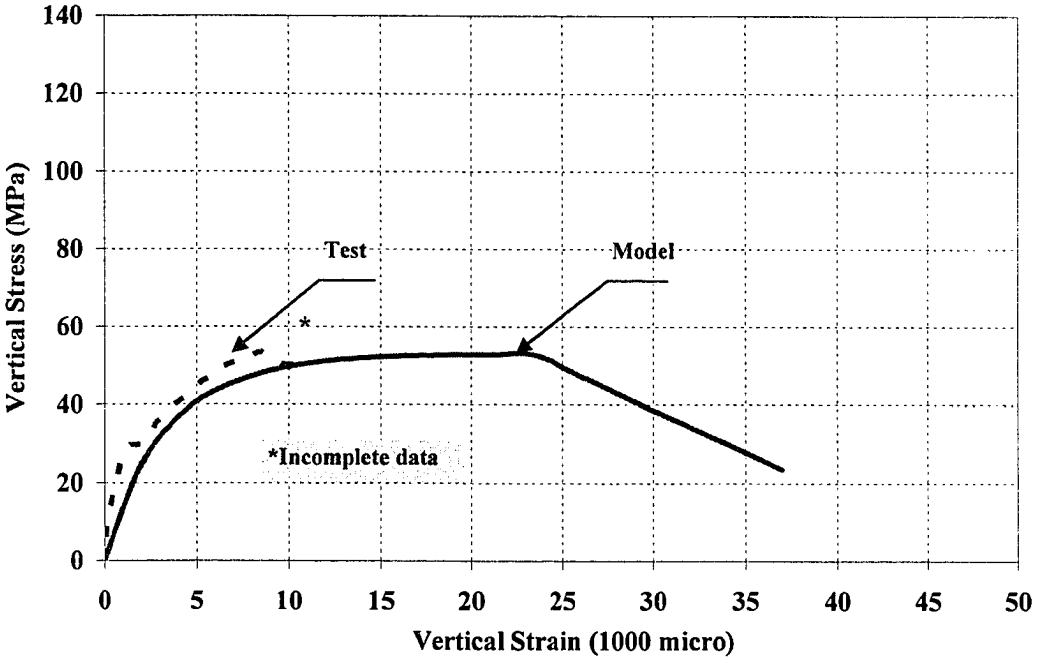

Figure 6.12. Comparison of Experimental and Analytical Compressive Stress-Strain Curves for A3C-Joint

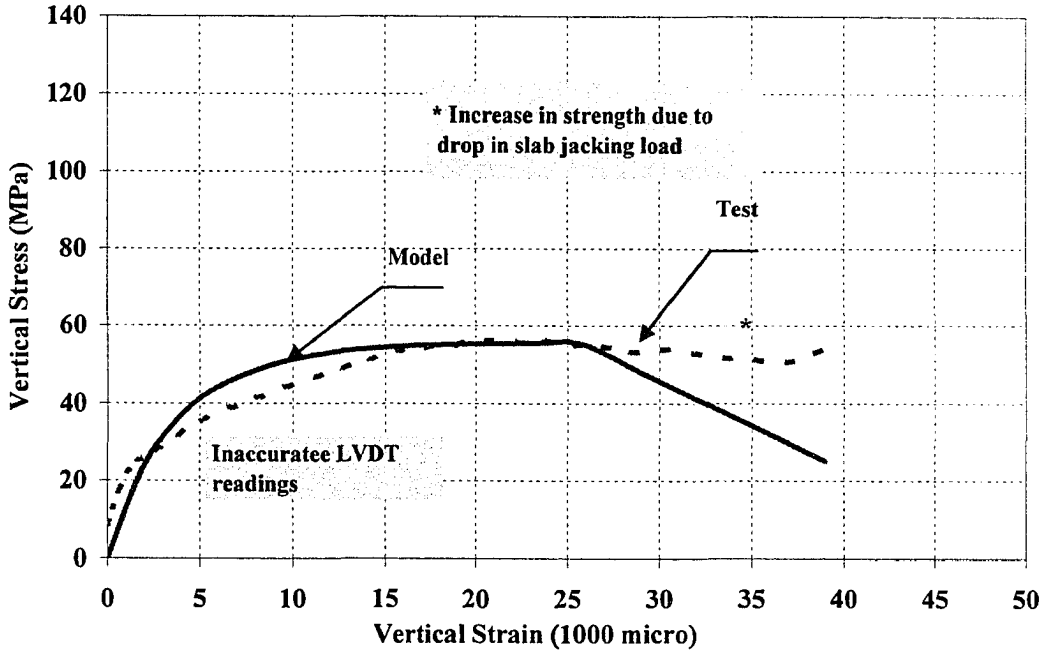

Figure 6.13. Comparison of Experimental and Analytical Compressive Stress-Strain Curves for A4C-Joint

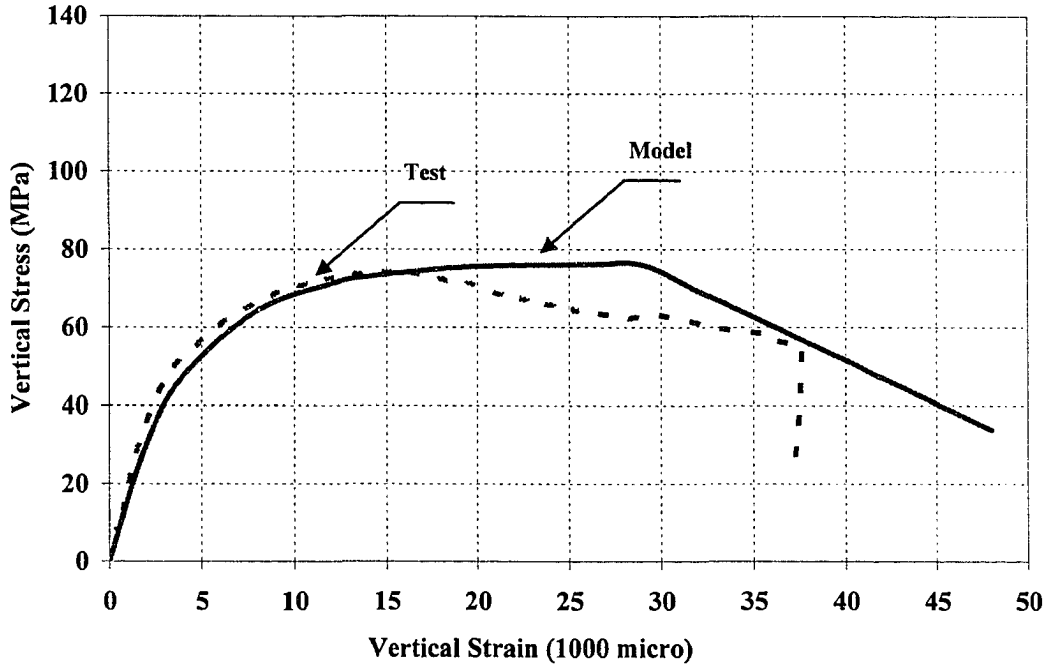

Figure 6.14. Comparison of Experimental and Analytical Compressive Stress-Strain Curves for B1-Joint

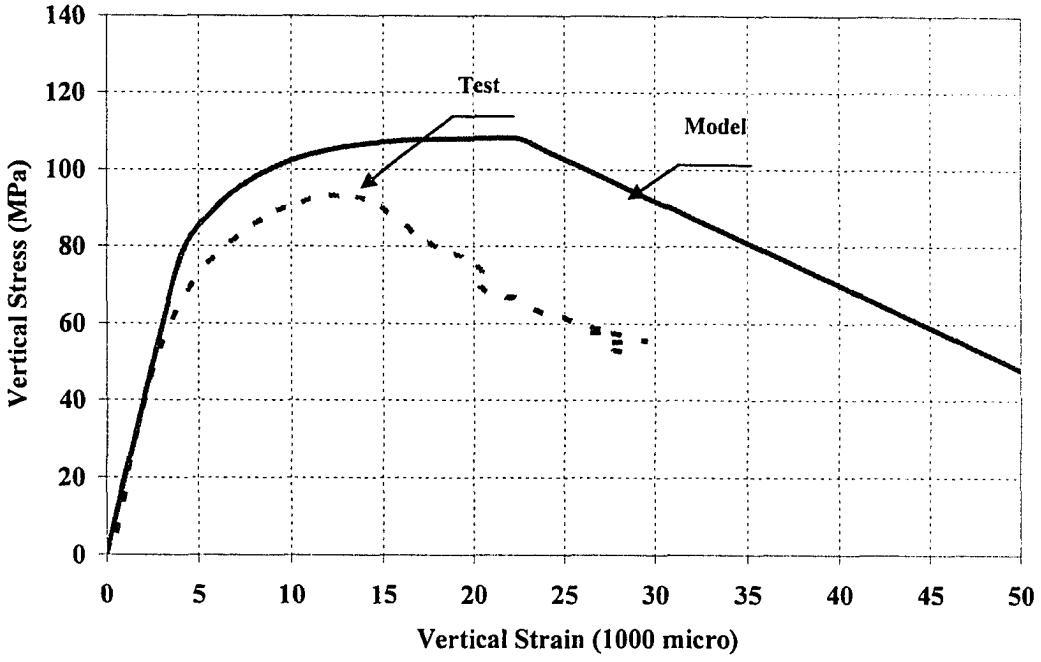

Figure 6.15. Comparison of Experimental and Analytical Compressive Stress-Strain Curves for B3-Joint

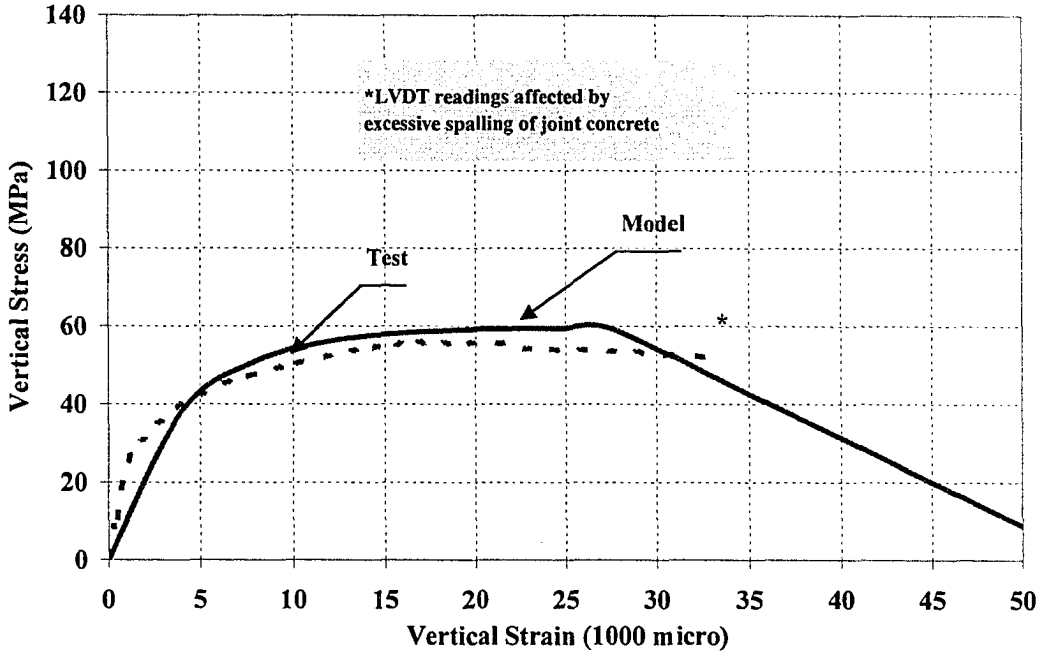

Figure 6.16 Comparison of Experimental and Analytical Compressive Stress-Strain Curves for C1B-Joint

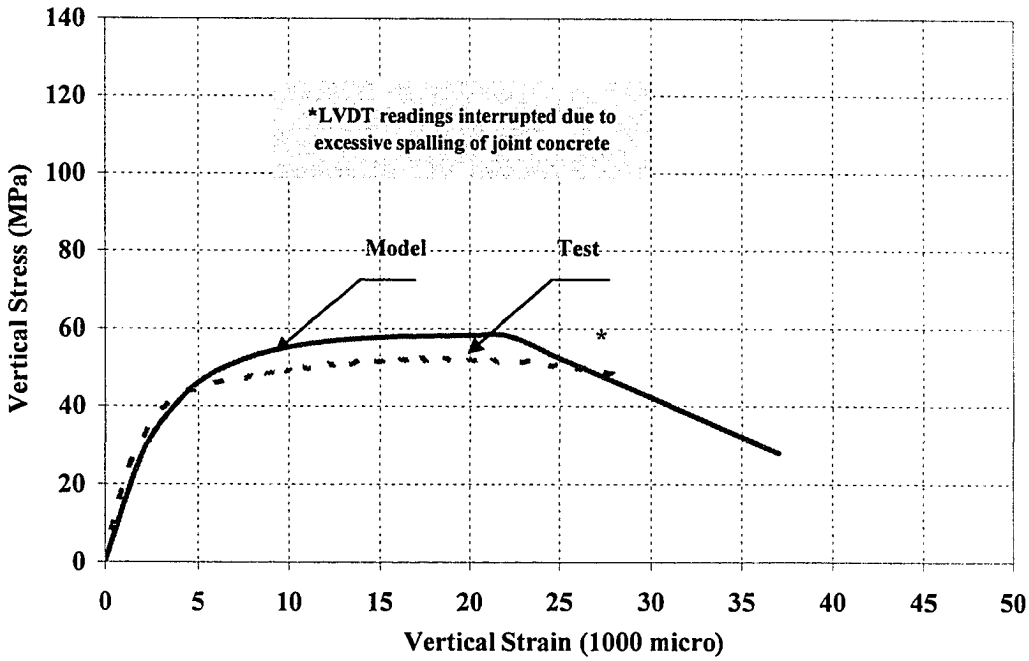

Figure 6.17. Comparison of Experimental and Analytical Compressive Stress-Strain Curves for C2B-Joint

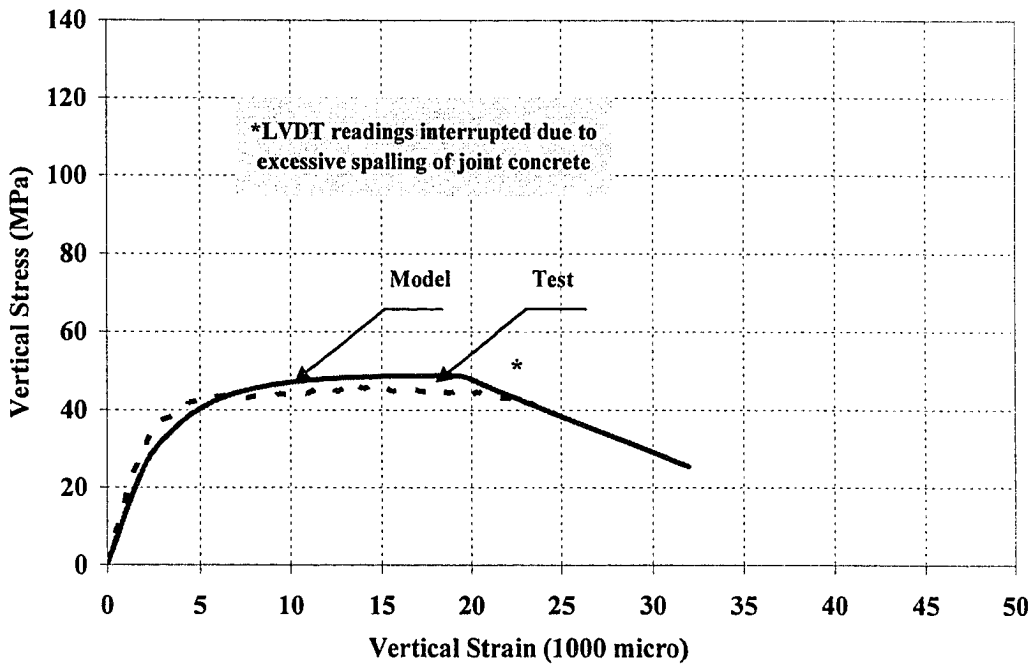

Figure 6.18 Comparison of Experimental and Analytical Compressive Stress-Strain Curves for C2C-Joint

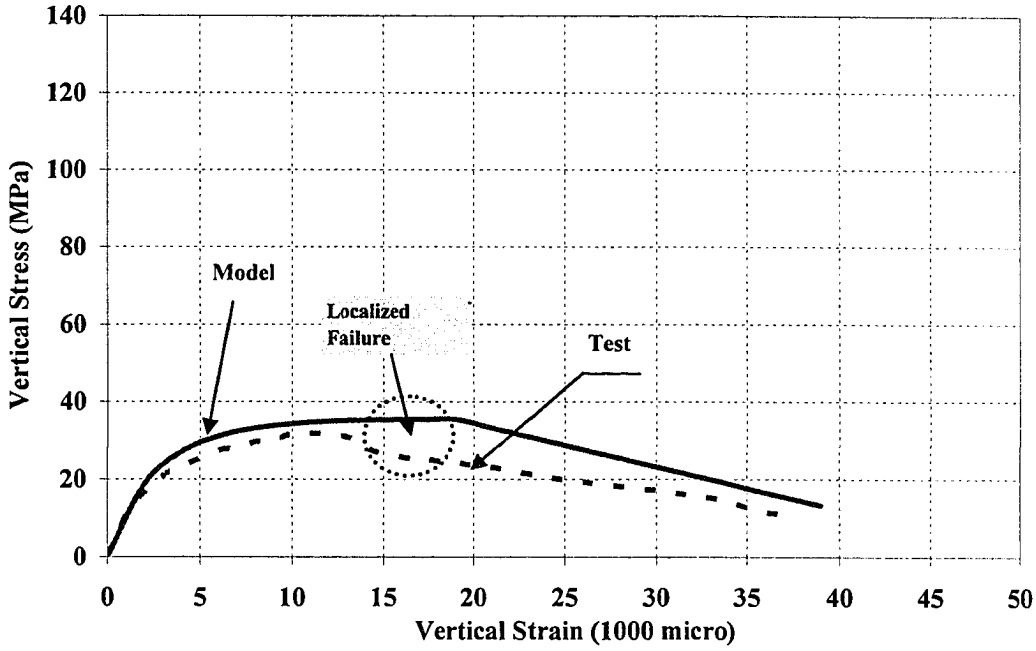

Figure 6.19. Comparison of Experimental and Analytical Compressive Stress-Strain Curves for SC3-Joint

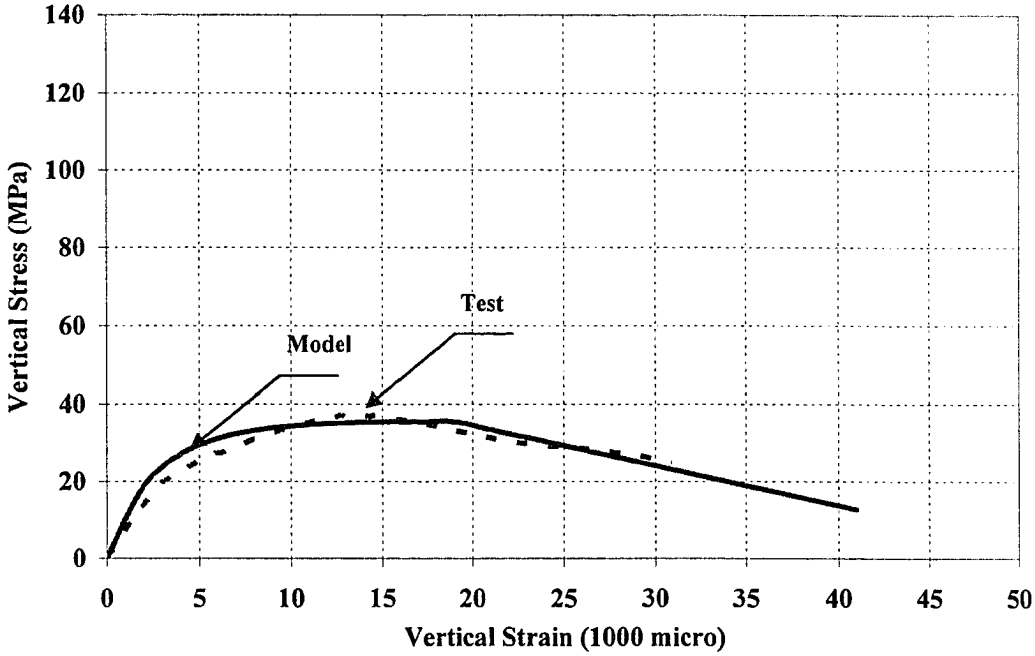

Figure 6.20. Comparison of Experimental and Analytical Compressive Stress-Strain Curves for SC4-Joint

7 PROPOSED DESIGN PROVISIONS

7.1 Introduction

The first step in column design is to estimate the required size. For high strength columns with intervening normal strength concrete floors, the required column area depends mainly on the effective strength of the weakest part- the joint.

In this chapter, in addition to equation 6.23.b that was introduced in a form convenient for design purposes (design-oriented), a simplified empirical method is proposed for possible design provisions. The output of both methods is compared to those using current design codes and other empirical design equations from the literature.

7.2 The Simplified Equations

The effective concrete strength of a joint can be determined using equation 7.1 for f'_{cc}/f'_{cs} ratio above or equal to the limiting values: 1.4 for interior and edge joints and 1.0 for corner joints. For using the simplified equations, a joint is said to be an interior joint when it is laterally confined from all sides by floor elements of equal depths; a joint is said to be an edge joint when it is laterally confined from two opposite sides by floor elements of equal depths; a joint is said to be a corner joint when it is not laterally confined from any opposite sides. To account for the effect of high-strength-concrete inside the joint, f'_{cs} is weighted strength of the concretes inside the joint.

$$f_{ce} = (A - \frac{B}{h/c}) f'_{cs} + \frac{C}{h/c} f'_{cc} \qquad [7.1]$$

$$f_{ce} \leq f'_{cc}$$

For Interior joints:	A= 1.4,	B= 0.56,	C=0.40
For Edge joints:	A= 1.4,	B= 0.28,	C=0.20
For Corner joints:	A= 1.0,	B= 0.15,	C=0.15

7.3 Comparison between the Detailed and the Simplified Methods

Table 7.1 compares results of f_{ce} using equation 6.23.b and equation 7.1. Using equation 6.23.b, the average and coefficient of variation for ratios of predicted to actual effective strength are 1.05 and 0.17 respectively. Using equation 7.1, the corresponding

statistical values are 1.07 and 0.19 respectively. A small difference can be noticed in the average but equation 6.23.b produces less scattered results.

Equation 6.23.b can be used for any f'_{cc}/f'_{cs} ratio equal or above unity and is suitable for any type of joints under any loading and/or construction condition. Unlike equation 6.23.b, the simplified equation 7.1 do not account for the debonding of floor reinforcement or for the effect of reinforcement details.

7.4 Comparison between the Different Available Design Equations

This section compares results using the proposed equations with all equations available in the literature. In total, there are 140 specimens including: 46 interior specimens, 37 edge specimens, 9 corner specimens and 48 sandwich column specimens.

As shown in figure 7.1, the upper and lower limits of equation 6.23.b embraces almost all the data found in literature.

Figures 7.2 to 7.4 show the CSA and ACI equations each as one line while the simplified equation is represented by three lines corresponding to h/c of 1/3, one, and three. Equation 7.1 yields values of f_{ce} larger than those using the CSA equation for edge and corner joints, and larger than those using the ACI equation for edge joints.

Statistical analysis of the results is shown in tables 7.2 to 7.4. Table 7.2 shows statistical analysis for ratios of predicted to actual f_{ce} using the proposed methods. Table 7.3 shows the corresponding values using CSA A23.3-94 and ACI 318-02 design equations. Table 7.4 shows the corresponding values using all the empirical equations from literature.

Figures 7.5 to 7.14 illustrate the differences between the proposed equations and the equations in CSA and ACI. Figures 7.5 to 7.8 compare the actual f_{ce} with the predicted f_{ce} in the range from 25 to 125 MPa. Shown on the same graphs are the ideal relations, represented by 1:1 lines, and their 20% offsets. Figures 7.9 to 7.11 exhibit the same data in a different way to demonstrate the effect of f'_{cc}/f'_{cs}. Each figure shows ratios of predicted to measured f_{ce} drawn against f'_{cc}/f'_{cs}. Similarly, figures 7.12 to 7.14 show ratios of predicted to measured f_{ce} drawn against h/c. The scatter above the horizontal axis indicates unconservative results.

7.4.1 All Literature Data

The results of using the proposed equations and equations of the codes are shown in tables 7.2 and 7.3. Using equation 6.23.b, the average, and coefficient of variation for ratios of predicted to actual f_{ce} for all the literature are 0.98 and 0.19 respectively. The corresponding values using equation 7.1 are 0.95 and 0.18 respectively. Using CSA A23.3-94 results in corresponding values of 0.75 and 0.21 respectively. The corresponding values using ACI 318-02 equations are 0.90 and 0.21 respectively.

Comparing figures 7.5 and 7.6 to 7.7 and 7.8 demonstrates that using the proposed equations result in less scatter of the values outside the 20% margin. The CSA-A23.3-94 results in conservative values for all types of joints, leading to bigger sections. The ACI 318-02 is unconservative for interior joints but conservative for the rest especially at low values of column strengths.

7.4.2 Interior Joints Data

As seen in tables 7.2 and 7.3, the average and coefficient of variation for ratios of predicted to actual f_{ce} are 0.93 and 0.17 respectively using equation 6.23.b, 0.96 and 0.13 respectively using equation 7.1, 0.77 and 0.14 respectively using CSA A23.3 94, and 0.90 and 0.17 respectively using ACI 318-02. Equation 6.23.b is sufficiently accurate yet conservative. It maintains good degree of safety with less degree of conservatism. The simplified equation leads to the best estimate of f_{ce}. The proposed equations are conservative for predicting f_{ce} for joints made of fibre reinforced concrete like those tested by McHarg et al. (2000).

Figure 7.9 shows that: the results using the proposed methods are evenly distributed around the horizontal axis; the ratio of predicted to actual f_{ce} using ACI 318-02 is about unity for f'_{cc}/f'_{cs} ratio below 2.0, after which the predicted to actual f_{ce} ratios decrease by increasing f'_{cc}/f'_{cs} ratio. The CSA A23.3-94 equation is always conservative.

As seen in table 7.4, the average, and coefficient of variation for ratios of predicted to actual f_{ce} are 0.87, and 0.16 respectively using the equation by Gamble and Klinar; 0.79 and 0.16 respectively using the equation by Kayani; and 0.82 and 0.12 respectively using the equation by Ospina and Alexander; the latter equation gives the least scatter.

7.4.3 Edge Joints Data

As seen in tables 7.2 to 7.3: the average, and coefficient of variation for ratios of predicted to actual f_{ce} using equation 6.23.b for edge joints are 1.08 and 0.17 respectively. The corresponding values using the equation 7.1 are 1.02 and 0.14 respectively, almost the same as the detailed method. Using CSA A23.3-94 or ACI 318-02 results in corresponding values of 0.82 and 0.21 respectively, more conservative than the proposed methods, but with bigger scatter in values. Although the average of the results for edge joint using equation 6.23.b is 1.08, the highest value of the entire population is lower than the highest of the other equations.

Figure 7.10 shows that: using equation 7.1 results in the least scatter, followed by equation 6.23.b. The ratio of predicted to actual f_{ce} using ACI 318-02 and CSA A23.3-94 for edge joints is below unity for f'_{cc}/f'_{cs} ratios below 3.0 and decreases slightly with increasing f'_{cc}/f'_{cs} afterwards.

As seen in table 7.4, the average, and coefficient of variation values for edge joints using the equation by Gamble and Klinar are 1.01 and 0.17 respectively. The equation by Kayani leads to corresponding values of 0.84 and 0.18 respectively while the equation by Shu and Hawkins results in 0.99 and 0.15 respectively.

7.4.4 Sandwich Column Data

More experiments are needed for testing the behaviour of corner joints. Except the nine corner-plate specimens tested by Bianchini et al. (1960), there is no test in literature, so far according to the author's knowledge, on corner joints. The other 48 tests found in literature are for sandwich columns with no floor confinement or floor loading. This can be the main reason for the big scatter in values. The big scatter could be also attributed to the wide variation in material properties, specimen sizes, or instrumentation.

As seen in tables 7.2 and 7.3, the average, and coefficient of variation for ratios of predicted to actual f_{ce} for sandwich columns are 0.94 and 0.22 respectively using equation 6.23.b, 0.92 and 0.24 respectively using equation 7.1, 0.70 and 0.24 respectively using CSA A23.3-94, and 0.94 and 0.22 respectively using ACI 318-02.

Figure 7.11 shows undefined trend of the ratio of predicted to actual f_{ce}. The scatter of results is big among all the methods. While the CSA gives conservative results always, the ACI gives conservative f_{ce} results for f'_{cc}/f'_{cs} values over 4.0.

As seen in table 7.4, the average, and coefficient of variation values for sandwich columns using the equation by Kayani are 0.84 and 0.21 respectively. The equation by Shu and Hawkins leads to corresponding values of 1.10 and 0.33 respectively while the equation by Ospina and Alexander results in 0.83 and 0.22 respectively.

7.4.5 Discussion

Although in some cases, the predicted effective strength using the proposed equations was bigger than actual effective strength, the effective strength using the proposed equations is smaller than the actual value with consideration of the resistance reduction factors used in the design.

Following ACI and CSA equations, compared to the proposed equations, could result for some cases in reducing the usable area of the floor, such as seating capacity, and wasting the construction materials. By comparing one by one result in figures 7.9 to 7.11, the predicted f'_{ce} using the CSA standards can be as low as 20% of the actual f_{ce}.

Figures 7.15 to 7.18 show the histograms of the ratios of predicted to actual f_{ce} using the four methods. The figures summarize the previous discussion indicating that: the CSA equation for interior joints can be the best empirical equation if its factors are multiplied by an offset factor of 1.3; the proposed equations together with the ACI equation have the best distribution for interior joints; and the proposed equations have the best distribution for edge joints.

As seen in figures 7.12 through 7.14, the effect of (h/c) on ratios of predicted to actual f_{ce} was found similar to that of f'_{cc}/f'_{cs}. The results using the proposed equations are evenly distributed around the horizontal axis unlike the case of using the CSA and ACI equations, which give unidentified pattern. The ACI equations give conservative estimation of f_{ce} for h/c ratio above 0.5 for interior joints, and unconservative estimation of f_{ce} for h/c ratio above 2.0 for corner joints. For corner joints with h/c values below 0.5,

the simplified equation may give unconservative estimation of f_{ce} unlike equations of the codes.

To complement this study, further experimental research is needed to fill the gap shown in figures 7.9 to 7.14 as follows: on interior joints with f'_{cc}/f'_{cs} values from 3.5-4.5 and from 5-6 and with *h/c* values above 1.5; on edge joints with f'_{cc}/f'_{cs} values above five and with *h/c* values above 1.3; on corner joints with f'_{cc}/f'_{cs} values from 3.5-5.5 and with *h/c* values from 1-2 and from 2-3.

Table 7.1 Predicted vs. Actual f_{ce} using Detailed and Simplified Methods

Test ID	f'_{cc} (MPa)	f'_{cs} (MPa)	$f_{ce\ actual}$ (MPa)	$f_{ce\ detailed}$ (MPa)	$f_{ce\ Simplified}$ (MPa)	Detailed to Actual Ratio	Simplified To Actual Ratio
SP1	72.8	18.0	34.4	36.7	37.1	1.07	1.00
SP2	86.6	20.4	45.9	45.2	43.3	0.99	0.87
SP3	89.2	31.8	70.8	64.8	66.5	0.91	1.08
SP4	66.7	17.6	57.9	53.9	46.1	0.93	1.27
SP5	66.7	19.8	45.5	45.9	36.8	1.01	0.77
SP6	93.7	20.6	41.1	44.3	45.6	1.08	1.01
SP7	18.7	18.7	26.5	25.5	21.5	0.97	0.71
A1-A	105	40	100.3	105.2	80.0	1.05	0.95
A1-B	105	40	94.0	91.6	80.0	0.97	1.01
A1-C	105	40	90.2	77.9	80.0	0.86	1.06
A2-A	112	46	97.4	112.0	88.5	1.15	1.05
A2-B	112	46	98.0	98.7	88.5	1.01	1.05
A2-C	112	46	92.2	85.4	88.5	0.93	1.11
A3-A	89	25	85.7	79.8	59.4	0.93	0.74
A3-B	89	25	80.0	64.9	59.4	0.81	0.80
A3-C	89	25	53.6	50.1	59.4	0.93	1.19
A4-A	106	23	80.6	94.2	64.3	1.17	0.89
A4-B	106	23	72.2	74.0	64.3	1.02	0.99
A4-C	106	23	56.4	53.8	64.3	0.95	1.27
C1-A	107	32	59.8	76.2	59.3	1.28	1.03
C1-B	107	35	56.4	61.6	61.9	1.09	1.15
C1-C	107	34	54.8	60.5	61.0	1.10	1.16
C2-A	108	31	52.7	66.7	58.8	1.27	1.07
C2-B	108	34	50.2	60.2	61.3	1.20	1.19
C2-C	108	33	46.3	50.6	60.5	1.09	1.26
B-1	104	42	74.4	76.6	81.5	1.03	1.03

Test ID	f'_{cc} (MPa)	f'_{cs} (MPa)	$f_{ce\ actual}$ (MPa)	$f_{ce\ detailed}$ (MPa)	$f_{ce\ Simplified}$ (MPa)	Detailed to Actual Ratio	Simplified To Actual Ratio
B-2	104	42	98.0	86.9	81.5	0.89	0.91
B-3	113	44	93.4	106.6	121.6	1.14	0.18
B-4	113	44	114.0	108.1	87.0	0.95	0.84
B-5	95	15	48.2	42.3	52.3	0.88	1.05
B-6	95	15	66.8	47.8	52.3	0.72	1.05
B-7	120	19	50.3	49.1	66.1	0.98	1.05
B-8	120	19	74.4	66.5	66.1	0.89	0.94
SC1	105	17	21.0	32.2	33.8	1.53	1.44
SC2	105	17	26.6	40.9	33.8	1.54	1.47
SC3	107	17	31.9	41.4	34.2	1.30	1.38
SC4	105	17	37.4	42.3	33.8	1.13	1.63
					Average = 1.05		=1.07
					Standard Dev. = 0.18		= 0.20
					C. of Variation = 0.17		= 0.19

Table 7.2 Predicted and Actual f'_{ce} Ratios Using the Proposed Design Equations

Category	Equation	Average	Standard Deviation	Coef. of Variation
ALL JOINTS	Detailed	0.98	0.19	0.19
	Simplified	0.95	0.17	0.18
INTERIOR JOINTS	Detailed	0.93	0.16	0.17
	Simplified	0.96	0.13	0.13
EDGE JOINTS	Detailed	1.08	0.18	0.17
	Simplified	1.02	0.15	0.14
SANDWICH COLUMNS	Detailed	0.94	0.20	0.22
	Simplified	0.90	0.20	0.23

Table 7.3 Predicted to Actual f'_{ce} Ratio Using the Codes Design Equations

Category	Equation	Average	Standard Deviation	Coefficient of Variation
ALL JOINTS	CSA (1994)	0.75	0.16	0.21
	ACI (2002)	0.90	0.19	0.21
INTERIOR JOINTS	CSA (1994)	0.77	0.11	0.14
	ACI (2002)	0.90	0.15	0.17
EDGE JOINTS	CSA (1994)	0.82	0.17	0.21
	ACI (2002)	0.82	0.17	0.21
SANDWICH COLUMNS	CSA (1994)	0.70	0.17	0.24
	ACI (2002)	0.94	0.21	0.22

Table 7.4 Predicted to Actual f'_{ce} Ratio Using Literature Equations

Category	Equation	Average	Standard Deviation	Coefficient of Variation
INTERIOR JOINTS	Gamble and Klinar (1991)	0.87	0.14	0.16
	Kayani (1992)	0.79	0.12	0.16
	Shu and Hawkins (1992)	----------	----------	----------
	Ospina and Alexander (1997)	0.82	0.10	0.12
EDGE JOINTS	Gamble and Klinar (1991)	1.01	0.17	0.17
	Kayani (1992)	0.84	0.15	0.18
	Shu and Hawkins (1992)	0.99	0.15	0.15
	Ospina and Alexander (1997)	----------	----------	----------
SANDWICH COLUMNS	Gamble and Klinar (1991)	----------	----------	----------
	Kayani (1992)	0.84	0.18	0.21
	Shu and Hawkins (1992)	1.10	0.37	0.33
	Ospina and Alexander (1997)	0.83	0.18	0.22

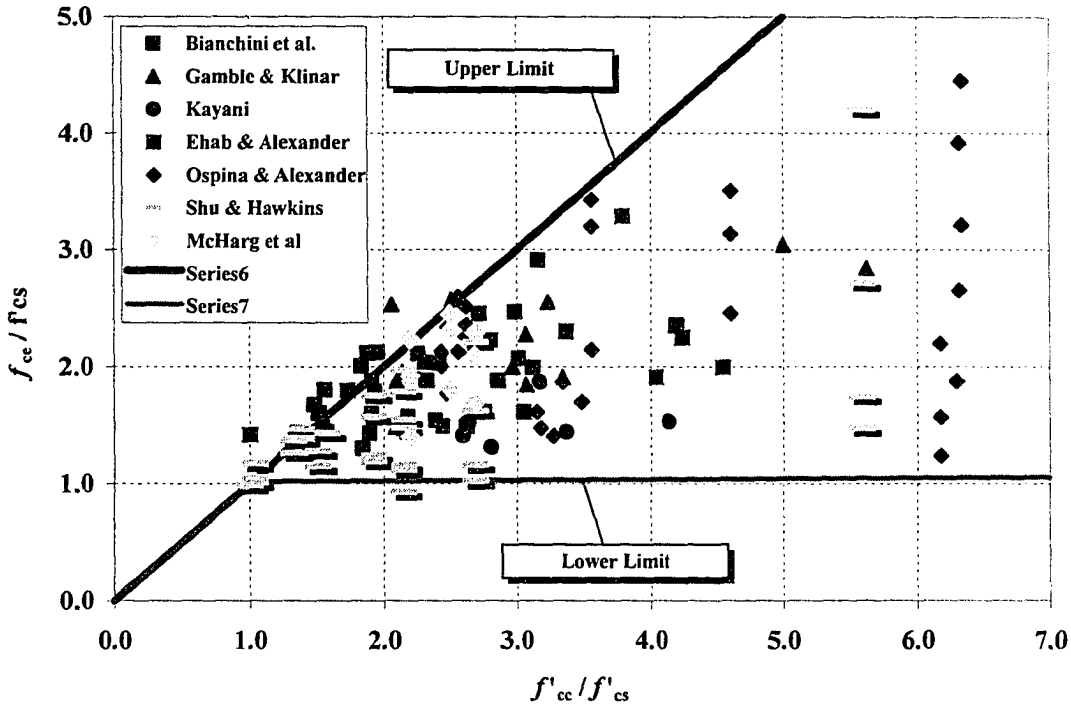

Figure 7.1 Actual Experimental Results vs. Limits of The Proposed Detailed Equation

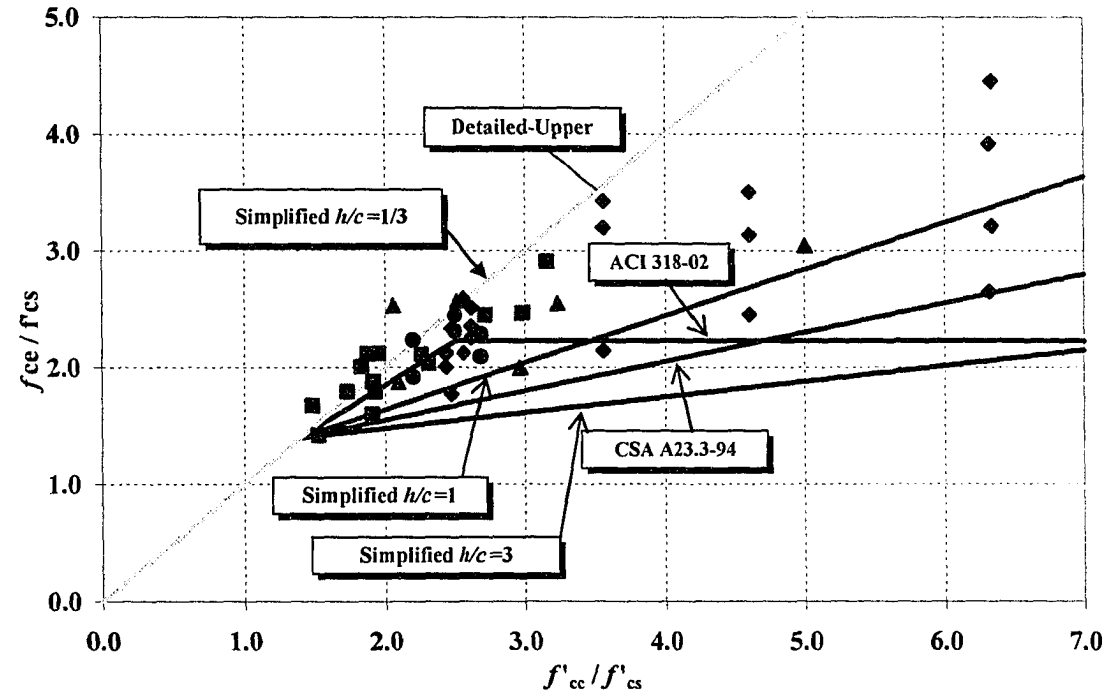

Figure 7.2. Existing Design Provisions vs. Proposed Equations for Interior Joints

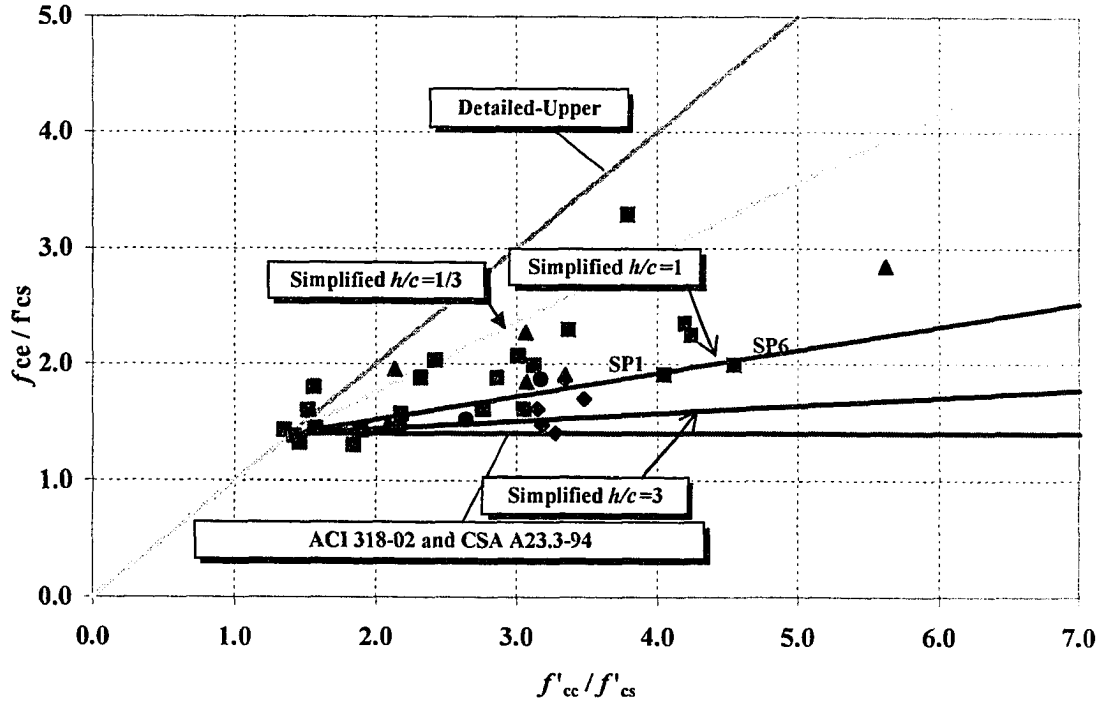

Figure 7.3. Existing Design Provisions vs. Proposed Equations for Edge Joints

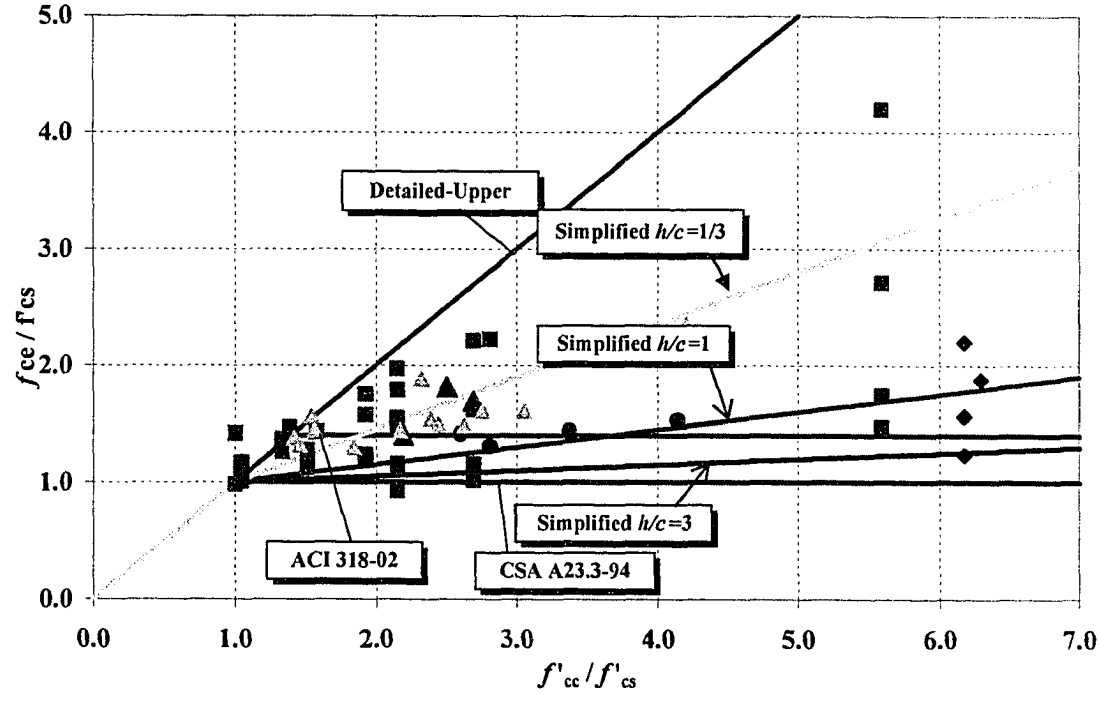

Figure 7.4. Existing Design Provisions vs. Proposed Equations for Corner Columns

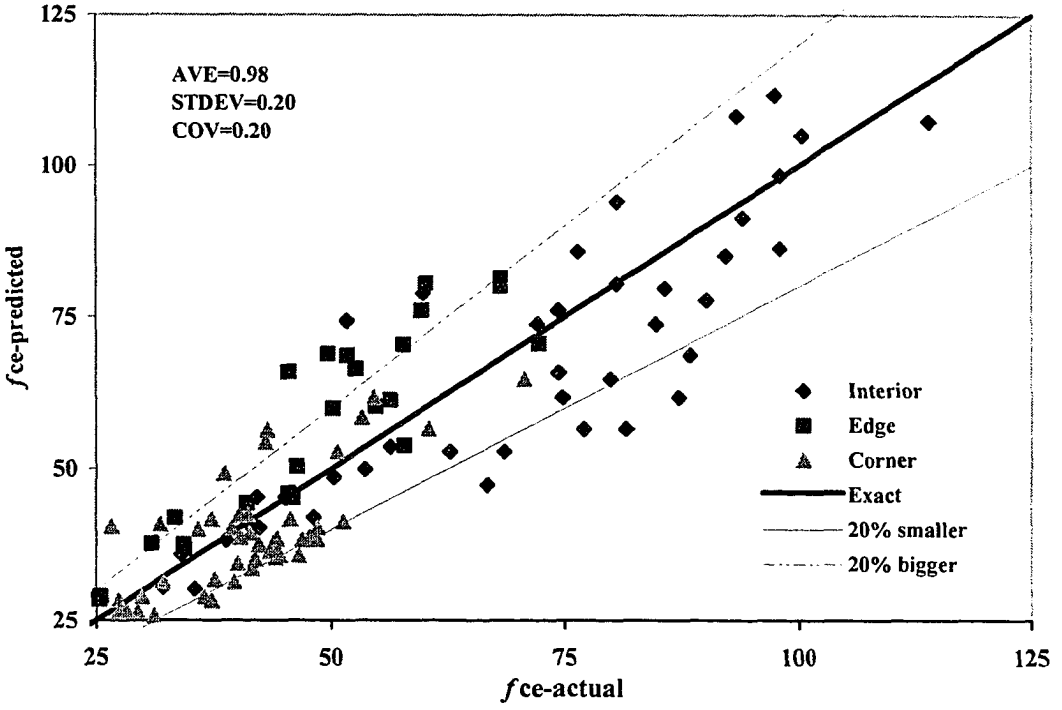

Figure 7.5. Predicted vs. Actual Joint Effective Strength for All Data Using the Detailed Equation

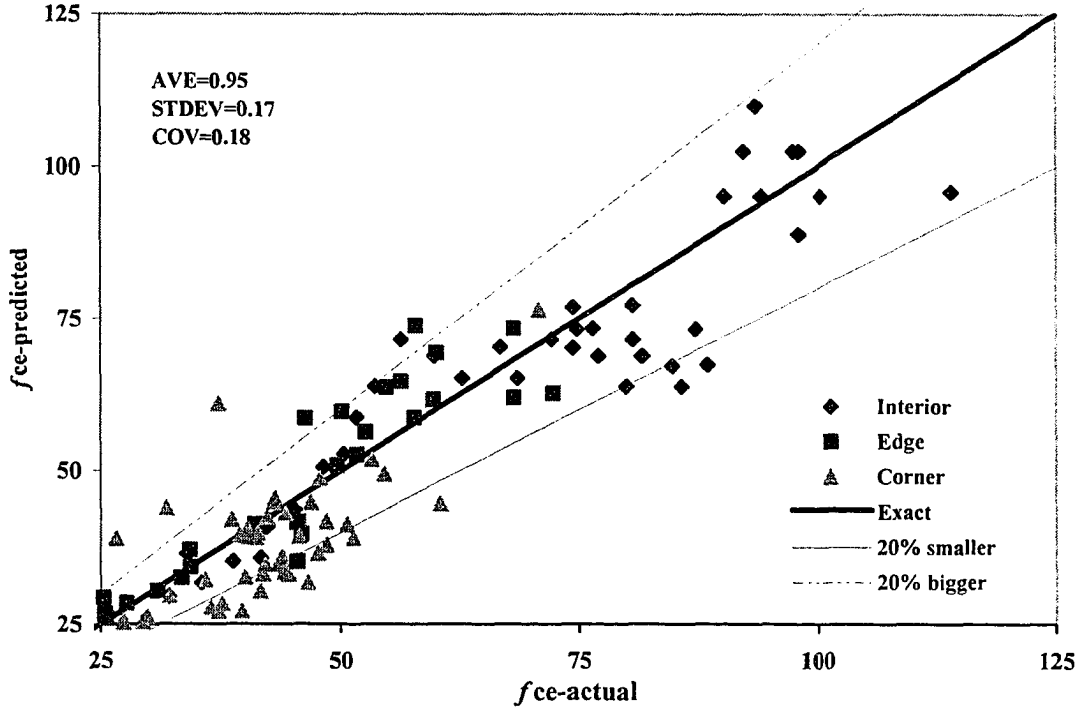

Figure 7.6. Predicted vs. Actual Joint Effective Strength for All Data Using the Simplified Equations

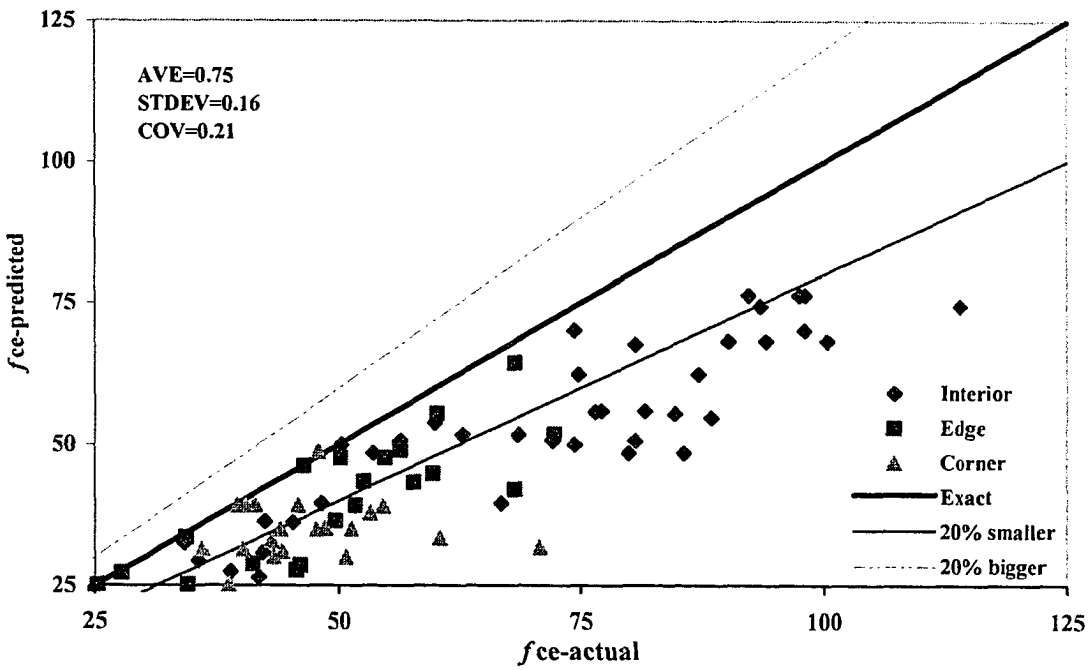

Figure 7.7. Predicted vs. Actual Joint Effective Strength for All Data Using the CSA A23.3 (1994)

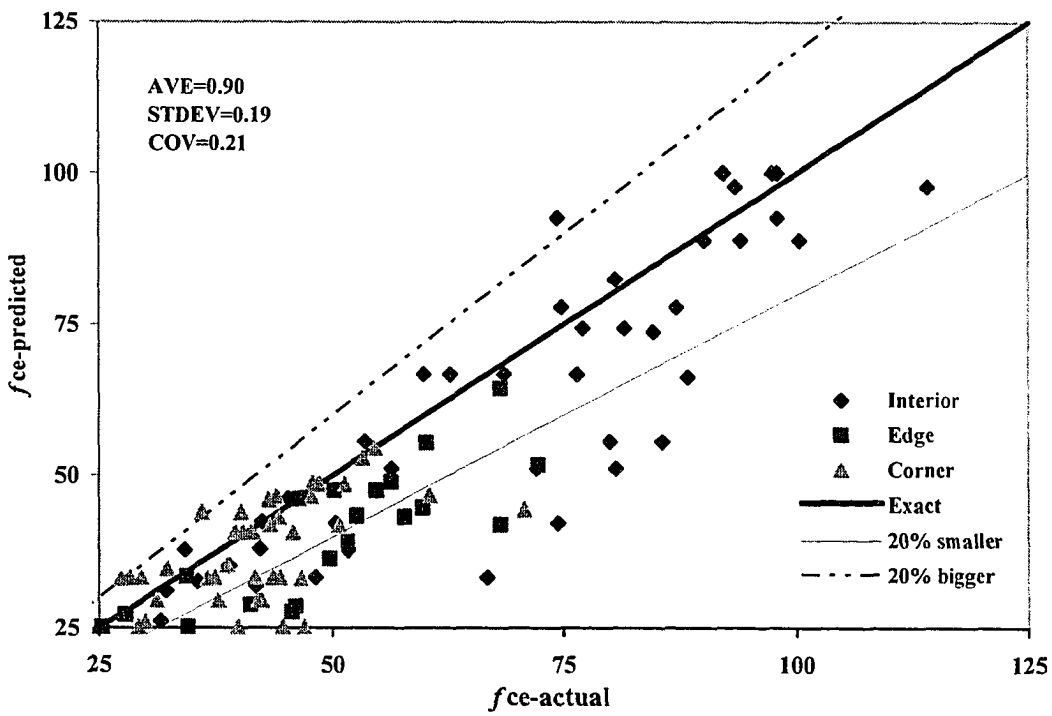

Figure 7.8. Predicted vs. Actual Joint Effective Strength for All Data Using the ACI-318 (2002)

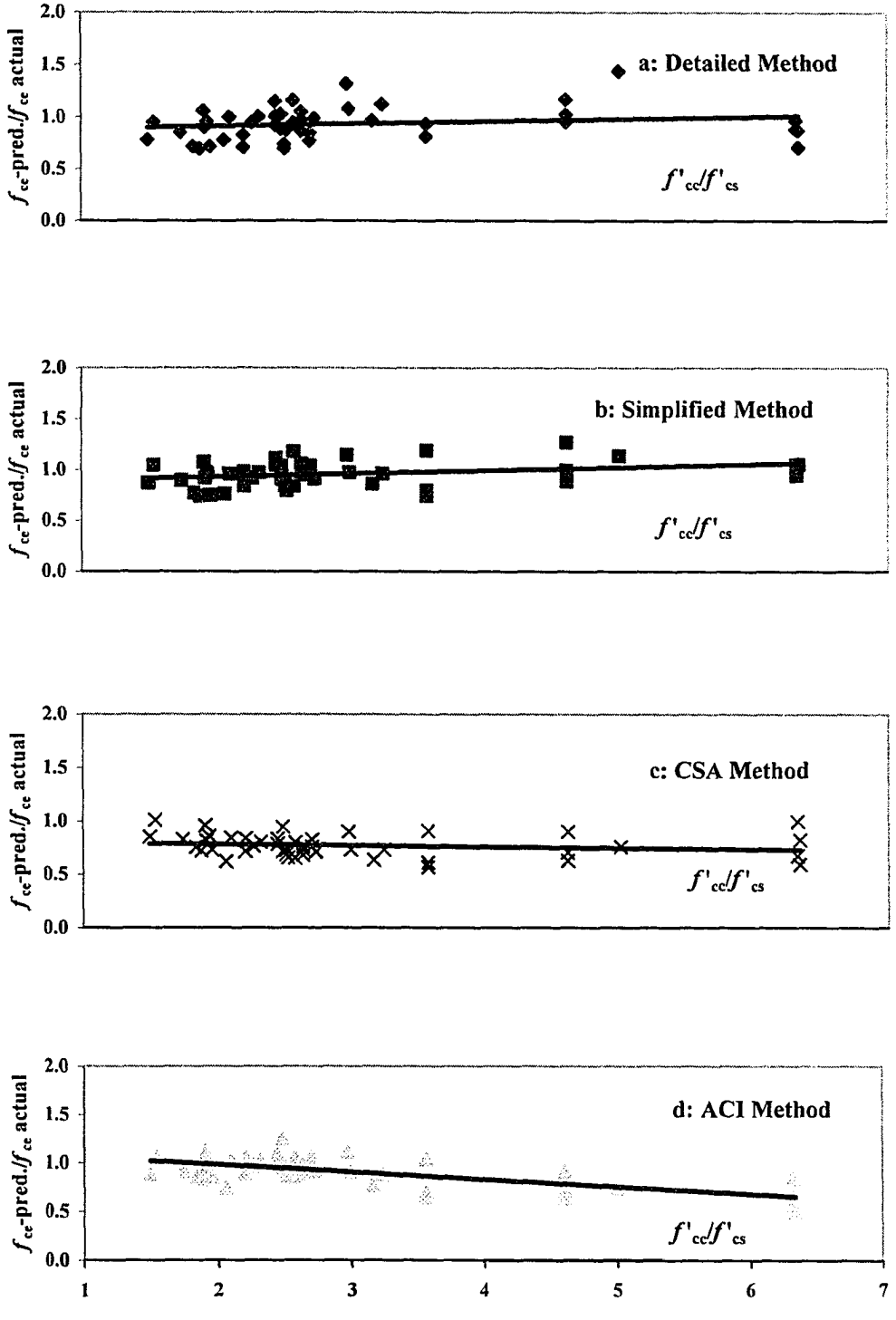

Figure 7.9. Ratio of Predicted to Actual f'_{ce} vs. f'_{cc}/f'_{cs} for Interior Joints

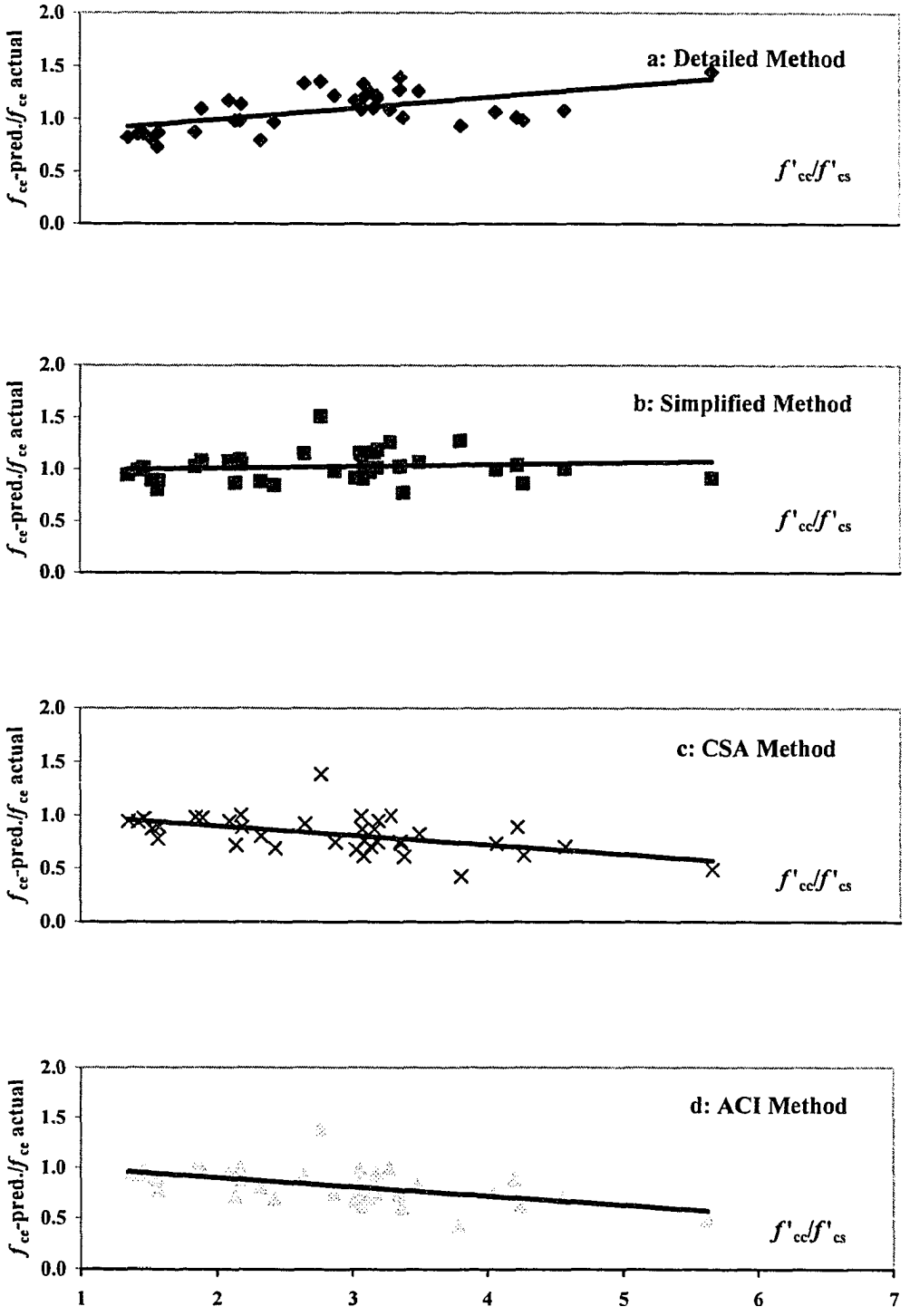

Figure 7.10. Ratio of Predicted to Actual f'_{ce} vs. f'_{cc}/f'_{cs} for Edge Joints

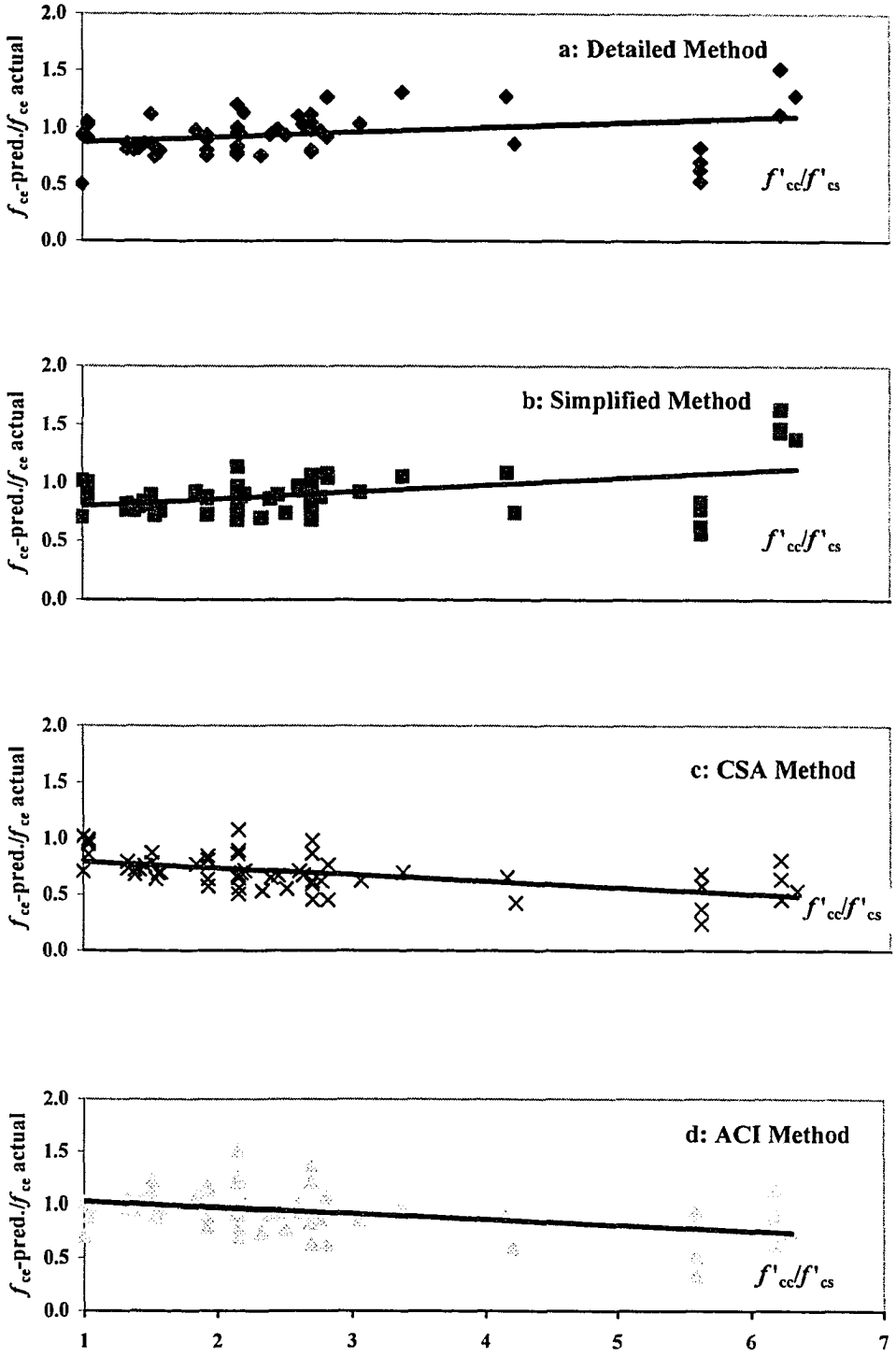

Figure 7.11. Ratio of Predicted to Actual f'_{ce} vs. f'_{cc}/f'_{cs} for Corner Joints

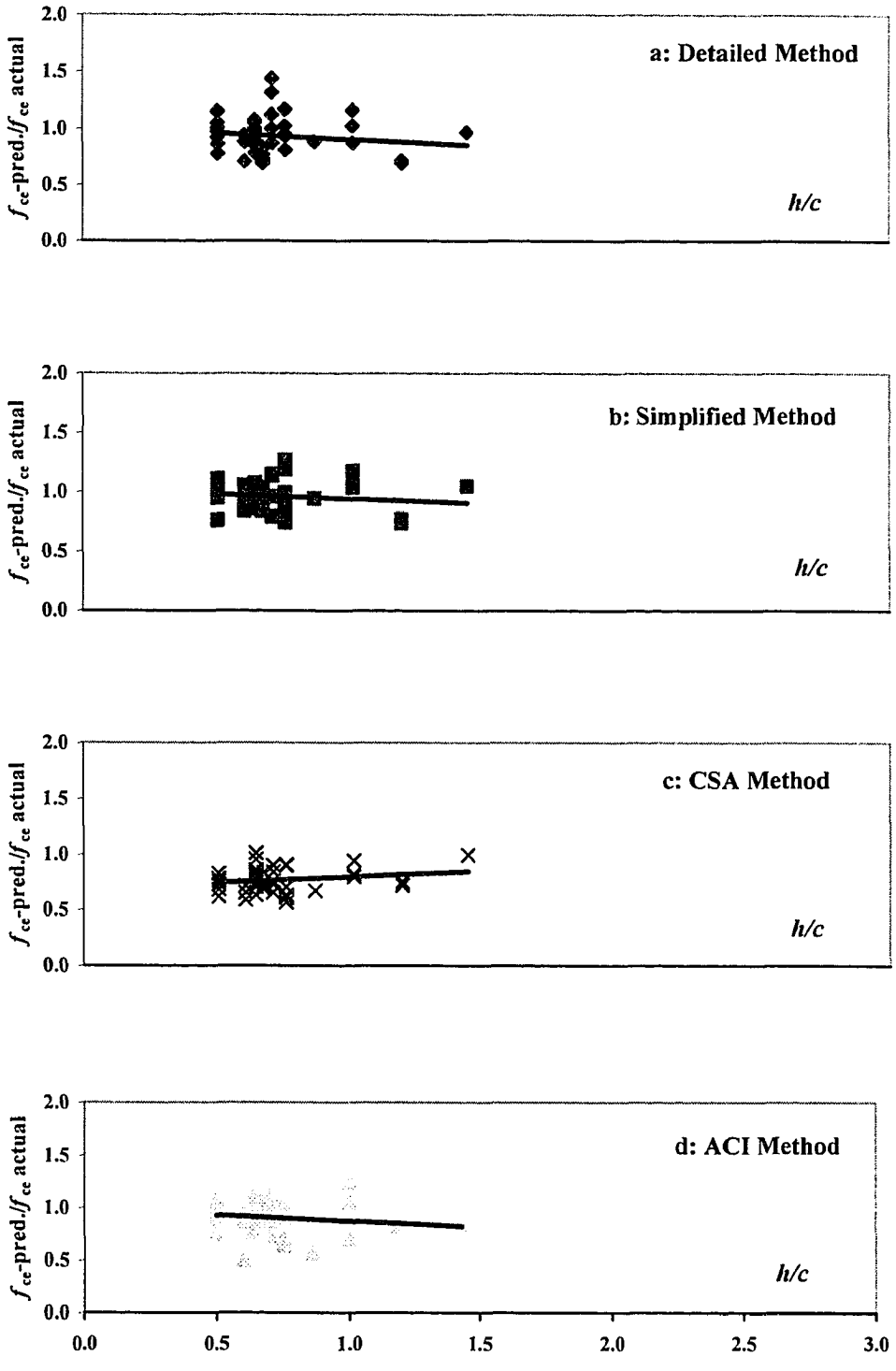

Figure 7.12. Ratio of Predicted to Actual f'_{ce} vs. *h/c* for Interior Joints

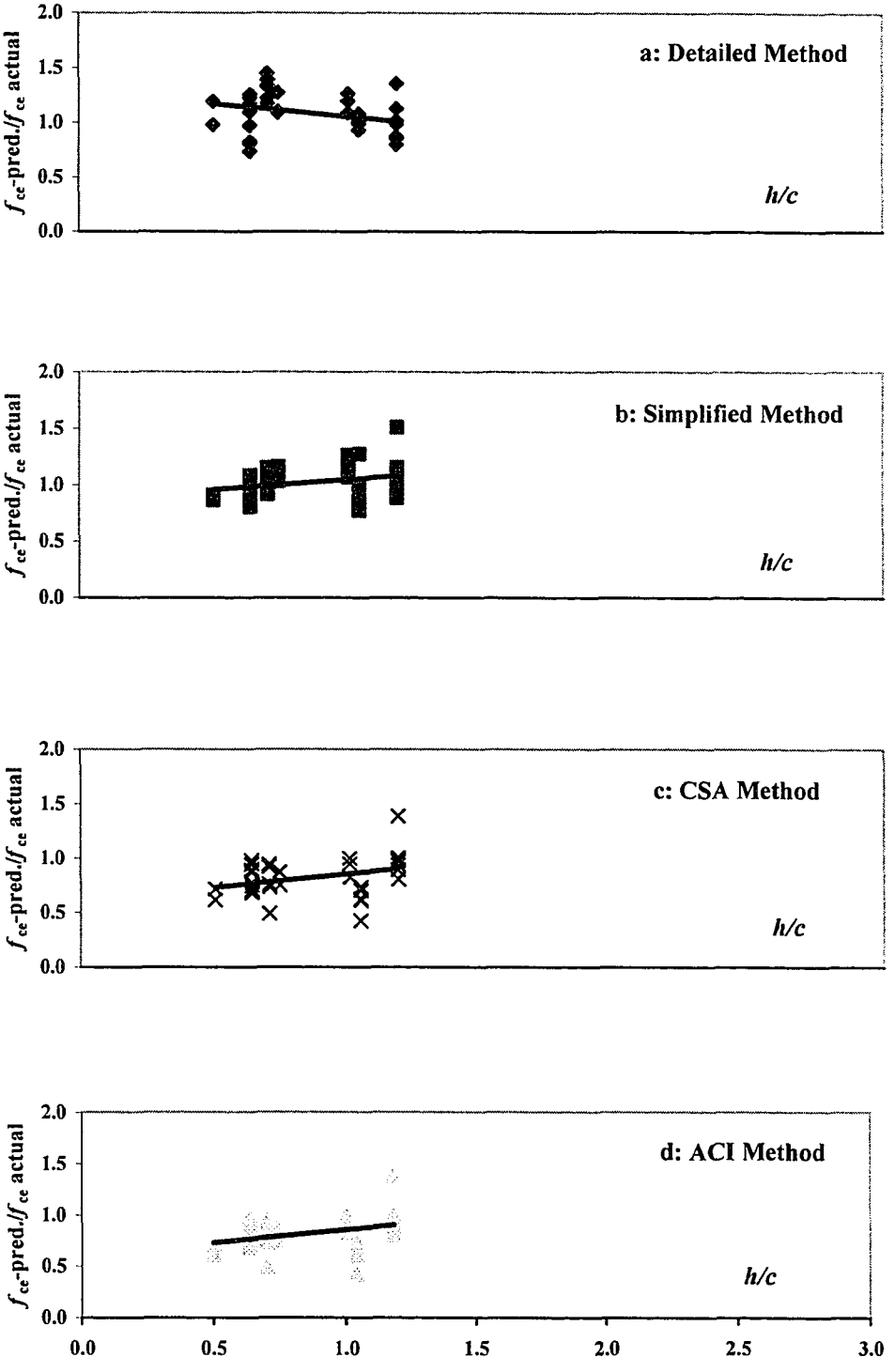

Figure 7.13. Ratio of Predicted to Actual f'_{ce} vs. *h/c* for Edge Joints

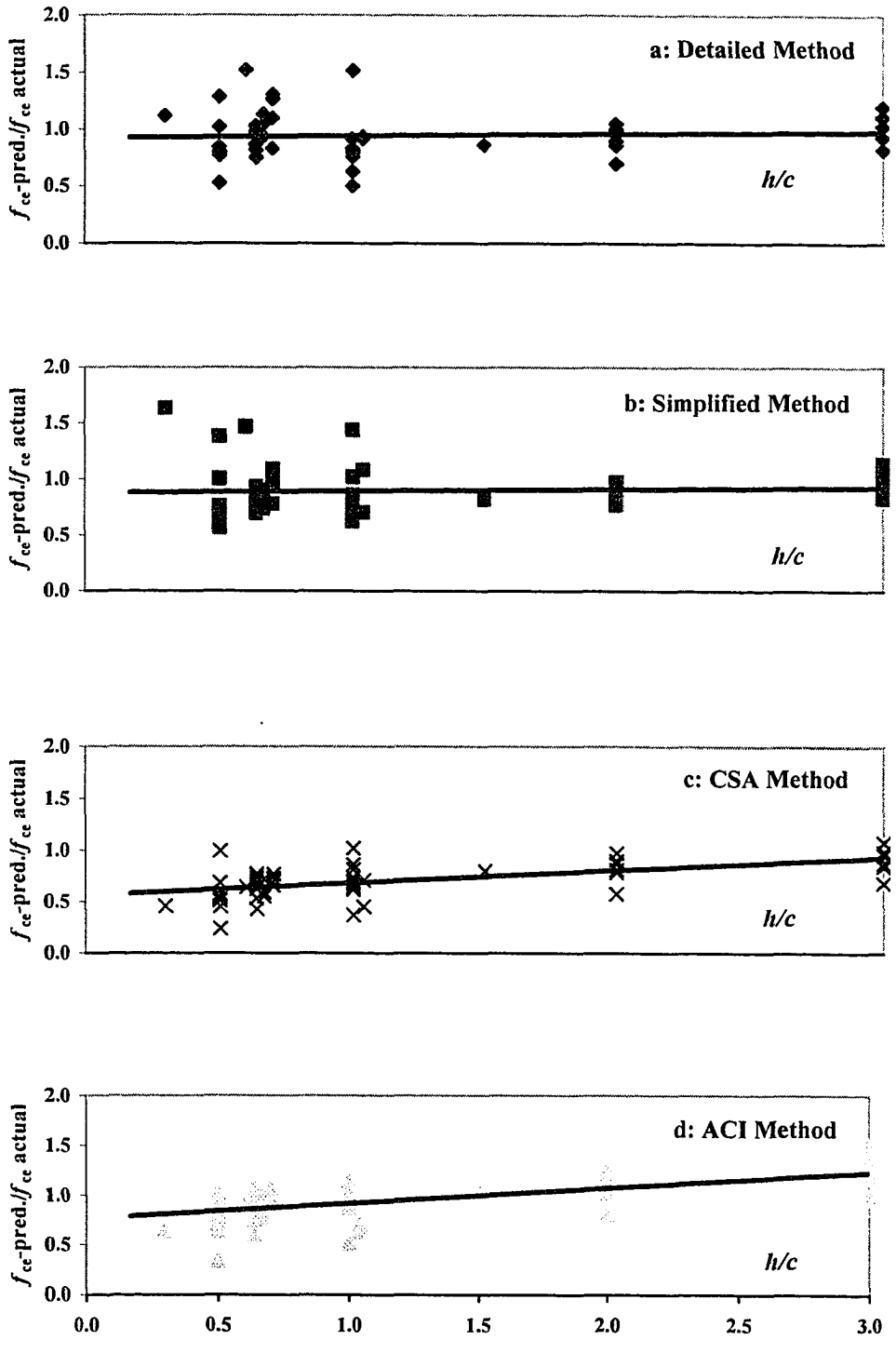

Figure 7.14. Ratio of Predicted to Actual f'_{ce} vs. *h/c* for Corner Joints

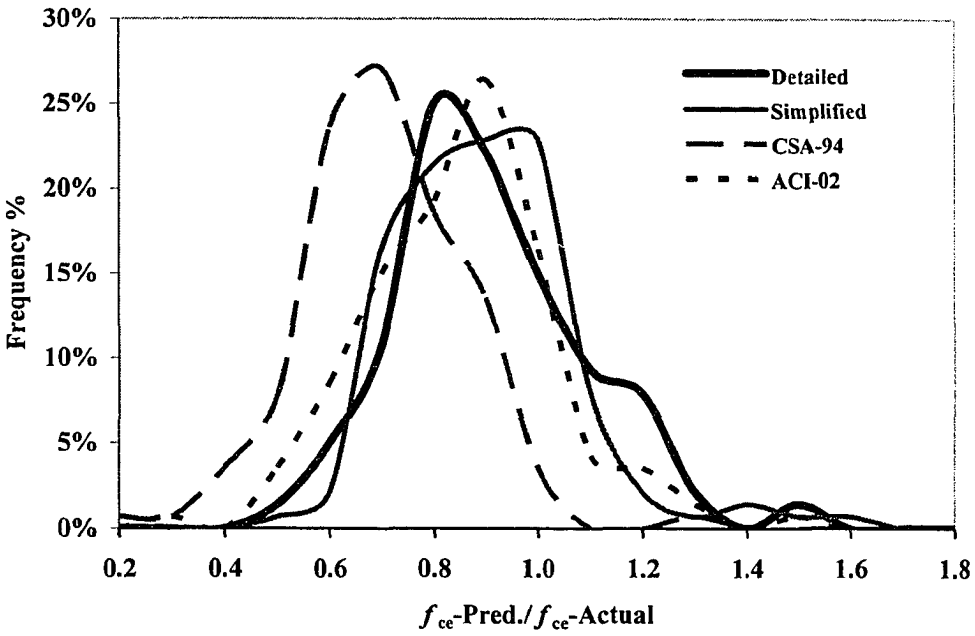

Figure 7.15. Histograms of Ratios of Predicted to Actual Effective Strength for All Joints

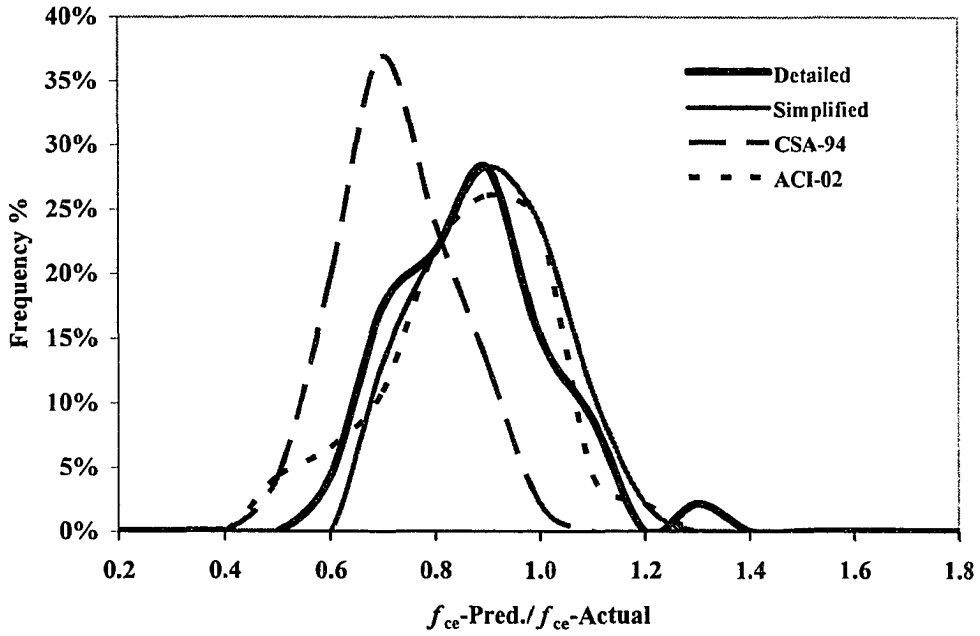

Figure 7.16. Histograms of Ratios of Predicted to Actual Effective Strength for Interior Joints

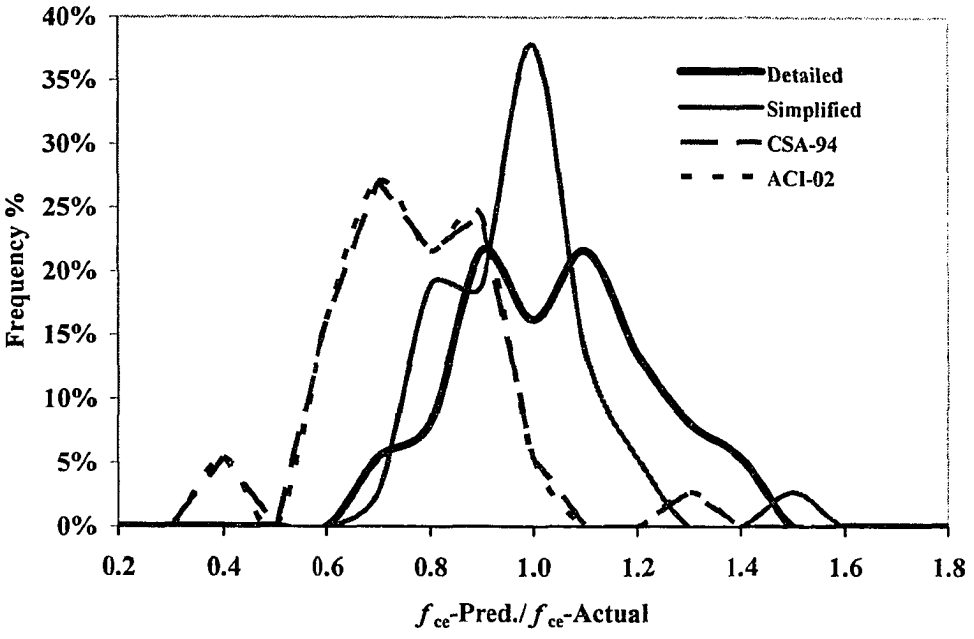

Figure 7.17. Histograms of Ratios of Predicted to Actual Effective Strength for Edge Joints

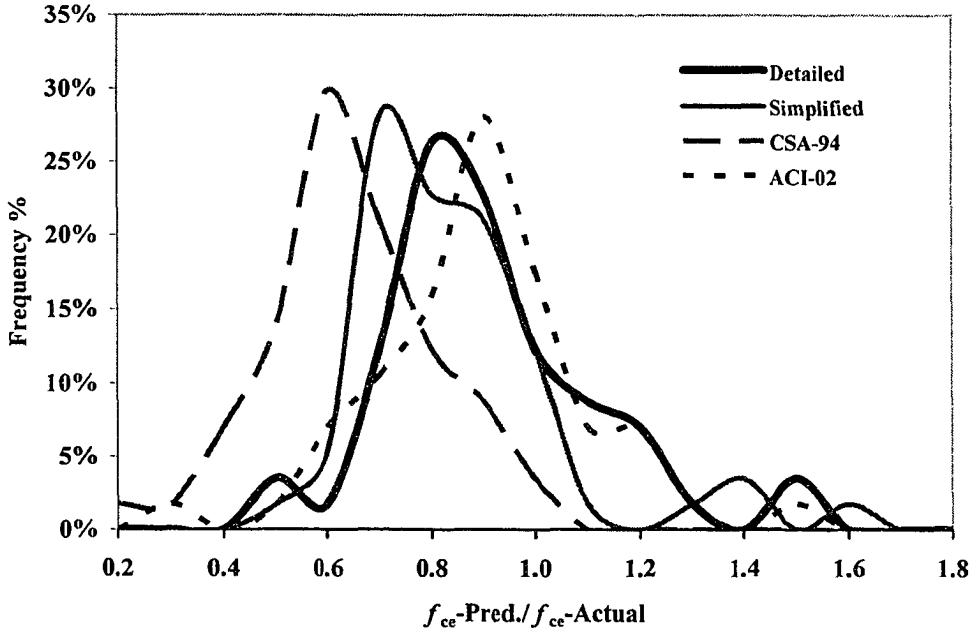

Figure 7.18. Histograms of Ratios of Predicted to Actual Effective Strength for Sandwich Columns

8 SENSITIVITY STUDY

8.1 Introduction

The model proposed in chapter 6 is used in this chapter to conduct a sensitivity study of the effective strength and behaviour of floor-column joints for structures that would be difficult to model experimentally, such as large scale specimens. Where applicable, the results of this study are compared to available results from literature, mostly on columns under similar loading conditions. A design example concludes this chapter.

8.2 Parameters to Consider in Upgrading the Effective Strength

The parameters affecting strength and behaviour of floor-column joints can be placed in four categories related to geometry, material, loading and deformation. Geometric variables include joint type, flooring system, and joint dimensions. Material variables include: column and floor concrete strengths; reinforcement ratio, diameter, and spacing of vertical rebars; volumetric ratio, diameter, and spacing of ties; bond between floor reinforcement and joint concrete; and percentage of column concrete inside the joint. Loading parameters include the column and the floor loads. Deformation parameters include axial and rotational capacity of the joint.

8.3 Selecting a Prototype for the Sensitivity Study

The prototype for this sensitivity study has a 150 mm thick slab. The beam dimensions are 450 by 600 mm and the columns are 600 by 600 mm. The floor-column joint is subdivided into two sub-joints: a column-slab sub-joint with an aspect ratio of 0.25 and a column-beam sub-joint with an aspect ratio of 0.50. For this structure, the beam-column sub-joint has the more critical aspect ratio and, with all other factors being equal, will govern the strength of the joint. The concrete strengths are 20 MPa for the floor and 80 MPa for the column. The column reinforcement consists of 8-M35 vertical rebars spaced at 256 mm center to center (reinforcement ratio of 2.2%) and No. 10M ties spaced at 150 mm center to center (volumetric ratio of 0.8%), even through the joint. Reinforcement is assumed to have elastic-perfectly-plastic stress-strain relation. No

partially-debonded floor reinforcement or high strength concrete is assumed inside the joint. The floor is assumed to have a moment of resistance 1.20 times the factored moment. The floor is assumed to have been adequately designed for shear.

8.4 Effect of the Different Parameters

Table 8.1 summarizes the range of the investigated parameters, except the various arrangements of floor confinement (joint type), and the predicted variations in f_{ce}/f'_{cs}. The prototype cases can be identified in table 8.1 by its darkened cells.

Complete stress-strain curves of both joint and column are shown in figures 8.2 through 8.16 assuming that each the joint and the column act independently.

8.4.1 Floor Physical Effect (Joint Type)

The five cases to be examined are illustrated in figure 8.1. These range from an unconfined joint to a joint confined in all sides. If the column reinforcement is constant, any change in $k_{STR;Conf}$ would actually reflect the floor physical effect. As seen from the strength model, the value of f_{ce} increases by increasing λ.

Figure 8.2 shows that the maximum change in the total gain in f_{ce} by changing joint type from unconfined to a totally confined one is $0.47 f'_{cs}$. The total gain is significant for the case of interior joints. Compared to case A in figure 8.1, the corresponding gain is 0.09, 0.19, and 0.32 for cases B, C, and D respectively.

8.4.2 Thickness of Concrete Cover

According to equation 6.23a, increasing the cover reduces the effectively confined area, and consequently decreases the post-cover-spalling effective strength, except for interior joints. This suggestion of the equation is supported by observations from Cusson et al. (1994), Foster et al. (1999) and Liu et al. (2000).

8.4.3 Arrangement of Reinforcement

In this subsection, the reinforcement ratio of the vertical rebars is kept constant at 2.2% while different arrangements of rebars, shown in figure 8.3, are investigated. The sets of reinforcements are: 16 M25, 12 M30, 8 M35, and 4 M55.

The model predicts almost no effect of changing diameter and spacing of the vertical rebars without changing the reinforcement ratio in the joint. As seen in figure 8.4, only one curve is resulted.

8.4.4 Ratio and Diameter of Vertical Reinforcement

Combinations of reinforcement diameter and reinforcement spacing are limited to those satisfying the maximum and minimum reinforcement ratio found in CSA A23.3-94.

As seen in table 8.1, the effect of the reinforcement ratio is investigated in the range from 1.1% to 3.3%, corresponding to increasing the size of vertical reinforcement from 8 M25 bars to 8 M45 bars. The corresponding increase in f_{ce}/f'_{cs} ratio is 0.11, 0.12 and 0.13 for corner, edge and interior joints respectively. Increasing the reinforcement ratio by increasing the size of rebars increases the confinement of the concrete core and increases the strength and ductility of the joint as seen in figure 8.5.

8.4.5 Ratio and Spacing of Vertical Reinforcement

As seen in table 8.1, increasing the reinforcement ratio from 1.1 to 4.4 percent, corresponding to increasing the number of rebars from 4 M35 to 16 M35 and decreasing their spacing, increases f_{ce}/f'_{cs} ratio by 0.11, 0.15 and 0.19 for corner, edge and interior joints respectively. Decreasing the reinforcement spacing increases the confinement of the concrete core and increases the strength and ductility of the joint as seen in figure 8.6. These suggestions match well with findings of Sheikh and Uzumeri and Nehikhare et al.

8.4.6 Yield Strength of Vertical Reinforcement

In this section, yield strength values are 400, 550, 835, 1080 and 1420 MPa. The first two cases are based on using 8 M35 bars while the other cases are based on using DYWIDAG® bars of diameter 36 mm.

Using high yield strength reinforcement in the joint will result in considerable gain in f_{ce} and in increasing the load capacity carried by the reinforcement itself. As seen in table 8.1, f_{ce}/f'_{cs} ratio increases by 0.23, 0.26 and 0.29 for corner, edge and interior joints respectively by increasing the yield strength of vertical rebars from 400 MPa to 1420 MPa. As seen in figure 8.7, using high strength reinforcement shifts the stress-strain curve upward, reaching bigger strength, and sideways, achieving more ductility. This

benefit is achievable in joints as their expected compressive strain at ultimate stress exceeds the yield strain of the reinforcement.

8.4.7 Tie Diameter and Volumetric Ratio

As seen in figure 8.8, using larger tie diameter improves the strength and ductility of the joint. As seen in table 8.1, f_{ce}/f'_{cs} ratio increases by 0.80, 0.60 and 0.42 for corner, edge and interior joints respectively by increasing the tie diameter from zero (no tie) to 16 mm, which corresponds to a change in tie volumetric ratio from 0% to 1.6%. The findings of the effect of tie volumetric ratio match well with findings of Mander et al., Bing et al., James et al. (2001), Assa et al. (2002) and Saatcioglu et al. (2002).

8.4.8 Tie Spacing and Volumetric Ratio

As seen in figure 8.9, using closely spaced ties improves the strength and ductility of the joint. As seen in table 8.1, f_{ce}/f'_{cs} ratio increases by 1.0, 0.75 and 0.51 for corner, edge and interior joints respectively by decreasing the tie spacing from 600 to 60 mm. The findings of the model match well with findings of the research work mentioned in subsection 8.4.7. Tie spacing can be adjusted more easily than tie diameter.

8.4.9 Tie Yield Strength

In this subsection, yield values ranges from zero, case of no ties, to 1318 MPa. The upper value is reported in tests done by Bing et al. (2001). As seen in the strength model, the maximum stress in a tie depends on its yield strength compared to the concrete strength. In addition, the maximum stress in a tie is limited by the ability of the reinforcement arrangements to prevent local failure of the effectively confined core.

As seen in figure 8.10, using ties made of high strength steel in normal strength concrete joints will increase stress and strain values at the peak point, more strength and ductility, owing to the greater confinement provided by the ties. As seen in table 8.1, adding grade 400 ties to the joint increases f_{ce}/f'_{cs} ratio by 0.63, 0.41 and 0.21 for corner, edge and interior joints respectively compared to the case of no ties. If ties of grade 1320 MPa are used instead, f_{ce}/f'_{cs} ratio increases in total by 0.98, 0.80 and 0.64 for corner, edge and interior joints respectively. This suggests that using high yield strength ties inside and around the joint will result in considerable gain in f_{ce}. The predictions of this

model are in good match with findings of Mander et al. (1988), Cusson et al. (1994), and Bing et al. (2001) who concludes that strength and ductility of the confined concrete are significantly enhanced when using ultra high yield strength ties.

8.4.10 Column Strength

f'_{cc}/f'_{cs} is the main parameter in determining the effective strength of a joint. As seen in figure 8.11, increasing f'_{cc}/f'_{cs} ratio increases the strength and ductility of the joint. As seen in table 8.1, increasing f'_{cc}/f'_{cs} ratio from 2.0 to 4.0, by increasing f'_{cc} from 40 MPa to 80 MPa, increases f_{ce}/f'_{cs} ratio by 0.83, 0.92 and 1.0 for corner, edge and interior joints respectively. Increasing f'_{cc}/f'_{cs} ratio from 2.0 to 6.0 increases f_{ce}/f'_{cs} ratio by 0.89, 1.00 and 1.11 for corner, edge and interior joints respectively. Optimum f'_{cc}/f'_{cs} ratio need not be the biggest all the time.

8.4.11 Floor Strength

As seen in figure 8.12, increasing the floor strength improves the effective strength and ductility of the joint. As seen in table 8.1, the higher f'_{cs}, the higher is the effective strength of the joint. As f'_{cs} increases from 20 MPa to 80 MPa, corresponding f'_{cc}/f'_{cs} ratio decreases from 4.0 to 1.0, f_{ce}/f'_{cs} ratio decreases by 1.72, 1.86 and 1.99 for corner, edge and interior joints respectively corresponding to increasing f_{ce} to 82 MPa. Out of this total gain, the change in $k_{End;Conf}$ vanishes and $k_{STR;Conf}$ drops from 0.6 to 0.1 as the maximum tie stress decreases. The findings compare well with that in Cusson et al.

8.4.12 Aspect Ratio

The aspect ratio is affected by changing the floor height or the smaller column dimension. Changing the slab thickness or beam height affects only the aspect ratio and consequently the end confinement effect. Changing the column dimension affects not only the end confinement but also has implications for the reinforcement arrangement.

As seen in figure 8.13, a joint with smaller aspect ratio is expected to have bigger strength and more ductility than a joint with big aspect ratio. As seen in table 8.1, decreasing h/c from 2.0 to 0.5 increases the gain in f_{ce} by $1.0 f'_{cs}$. This gain is independent of type of the joint.

8.4.13 Floor Reserve Strength

As seen in figure 8.14, the floor reserve strength affects strength and ductility of the joint. As shown in table 8.1, f_{ce}/f'_{cs} ratio increases by 0.73, 1.09 and 1.45 for corner, edge and interior joints respectively for unloaded floors compared to fully loaded ones. Fully loaded floors have no remaining capacity in the floor reinforcement to restrain the joint lateral dilation under the column loads.

Within practical margins, the floor reserve strength can be in the range of 40%. With using permissible moment redistribution, the floor reserve strength can reach 20%. The former case compared to fully loaded floor results in a gain in f_{ce}/f'_{cs} ratio of 0.29, 0.43 and 0.58 for corner, edge and interior joints respectively, as seen in table 8.1.

8.4.14 Partial Debonding of Floor Reinforcement

As seen in figure 8.15, partial debonding of floor negative reinforcement improves the effective strength and ductility of the joint. As seen in table 8.1, partial debonding of the floor reinforcement passing through the joint, compared to bonded reinforcement, increases f_{ce}/f'_{cs} by 0.44. This is a considerable gain at almost no cost. This technique suits best the case of slab-beam floors. For heavily reinforced joints, especially in flat plate floors, partial debonding could weaken the joint, rather than strengthening it, by creating delamination in the concrete.

8.4.15 High Strength Concrete in the Joint

As equation 6.23 implies, the more the high-strength-concrete into the joint, the bigger is the value of f_{ce}. Adding high-strength-concrete into the joint increases $k_{HSC;Conf}$ and $k_{Floor;Res}$ but compromises $k_{End;Conf}$ and the effect of ties by decreasing f''_s.

As seen in table 8.1, the case of f'_{cs} equals f'_{cc} of 80 MPa, discussed in subsection 8.4.10, gives higher values of f_{ce} than the case of pouring the joint with the column (HSC/NSC =1). The difference is small for the case of interior joints (1.04x80 MPa compared to 3.91x20 MPa), bigger for edge joints (1.04x80 MPa compared to 3.71x20 MPa), and the biggest for corner joints (1.04x80 MPa compared to 3.51x20 MPa). This difference (maximum of 15%) suggests that the estimation of $k_{HSC;Conf}$ can be

conservative. The difference in behaviour for edge joints can be seen from comparing figure 8.12 to figure 8.16.

8.4.16 Discussion

The most significant parameters affecting the strength of confined concrete columns are the volumetric ratio, yield strength, and arrangement of vertical and lateral reinforcement. For floor-column joints, the list of the significant parameters widens to include the joint type, the floor system, aspect ratio, high-strength-concrete core, reserve strength of the floor, and debonding of the floor main reinforcement in the joint.

Other than making the joint of high strength concrete, there is no single practical parameter that can develop an effective strength in the joint equal to that of the column.

Closely spaced reinforcements should be provided for corner joints and generally for all columns to improve their performance. This suggestion matches well with conclusions made by Bing et al. (2001) and Nehikhare et al. (2001) However, selecting closely spaced reinforcements of equivalent volumetric ratio may result in small reinforcement diameters. To guarantee safety against local buckling of reinforcement, spacing between the ties should be limited to (8) times the diameter of the vertical rebars.

Increasing the ratio and yield strength of both vertical and lateral reinforcement improve the effective strength and ductility of the joint. The effect of lateral reinforcement is five times that of vertical reinforcement. Besides being based on the strength model, this is logical because the confinement provided to the core by vertical rebars, being under compression and lateral loads, is less than that due to ties.

A practical solution is to add to the joint DYWIDAG® bars as vertical reinforcement, with enough anchorage length, and to confine the joint area with closely spaced ties of the same grade as those used in the columns.

There is an advantage of using high-strength ties inside the joints but there could be a problem of misplacing them with the ties in the columns. Therefore, it is better to use ties of the same grade in the columns and through the joints. Confinement failure when using high-strength ties is more dangerous than when using normal-strength ties. In the former case, failure is sudden, violent, and explosive (James et al.).

Increasing the floor reserve strength, by adding more negative reinforcement is a suitable solution in non-seismic areas. Over-reinforced section should be avoided, especially in slab-beam floors in seismic areas. Additional floor reinforcement means additional cost per floor besides expected congestions problems.

The descending part of the stress-strain curve reflects the post-peak ductility, which is very useful in estimating the rotational capacity of the joint under seismic loads. It is also useful to check whether there is a margin for redistributing the loads if a joint (or a column) fails under axial load. Slope of the descending part decreases, more ductile, by increasing the volumetric ratio of and decreasing spacing between the lateral reinforcement. The slope increases, less ductile, by increasing the concrete strength of the joint and by increasing the joint aspect ratio.

For each investigated parameter the stress-strain curves are identical up to a compressive strain value that corresponds to the yield strain of the vertical rebars. Afterwards, the curves diverge indicating the end of the material-dependent phase. The subsequent behaviour is structure-dependent.

8.5 Design Example

Figure 8.17 shows a sectional plan and a sectional elevation of an edge connection with the following characteristics: slab thickness is 150 mm, edge beam dimensions are 500 mm x 500mm, column dimensions must be 600 x 600 mm, floor concrete strength, f'_{cs}, is 25 MPa or greater, column concrete strength, f'_{cc}, is 100 MPa or smaller. Available are reinforcement of grade 400 and DYWIDAG bars of diameter 36mm and grade 1080/1230. It is required to design the edge column and its joint with the floor to carry a total factored axial load of 15000 kN. Design should satisfy CSA A23.3-94.

Design of the Column Section

For a 600 x 600 mm column of f'_{cc} = 100 MPa provided with 8 M 30 bars of f_y = 400 MPa and confined with an outer rectangular and inner diamond ties of No. 10M bars of grade 400 spaced at 250 mm.

Check minimum tie diameter of 0.3 * 25.2 = 7.5 mm < 10.3mm OK
Check maximum tie spacing = 0.75 x 48 x 7.5 = 270 mm > 250 mm OK
Or maximum tie spacing = 0.75 x 16 x 25 = 300 mm > 250 mm OK

$$P_r = \alpha_1 * \phi_c * f'_{cc} * (A_g - A_{st}) + \phi_s * f_y * A_{st}$$

P_r = [(0.85-0.0015*100)*0.6 * 100 MPa * (1-0.015) + 0.85 *400 MPa* 0.015]

*600 mm*600 mm*10^{-3}= 16783 kN.

$P_r > P_f$ (15000 kN) OK

Design of the Joint Section Using CSA A23.3 (94)

According to the CSA A23.3 (94), this is an edge joint having f'_{cc} greater than $1.4f'_{cs}$. Thus, f_{ce} is 35 MPa for any floor system. f_{ce} will not change by increasing or decreasing the amount of vertical reinforcement or lateral reinforcement.

Options:

1- The joint is reinforced as the column, then f_{ce} = 35 MPa, f_y = 400 MPa

P_r = 7890 kN < P_f UNSAFE

2- Increase the reinforcement in the joint to ρ= 6.5%, then f_{ce} = 25 MPa, f_y = 400 MPa

P_r = 12000 kN < P_f UNSAFE

The maximum reinforcement ratio in any section is not to exceed 8%. With 3% reinforcement ratio in the joint from the bottom and top columns, the additional reinforcement that can be placed in the joint cannot exceed 5% of the cross sectional area. The maximum total reinforcement ratio in the joint is, therefore, 6.5%.

The option of strengthening the joint by adding reinforcement (or dowels in ACI 318-02) based on f'_{cs}, not $1.4f'_{cs}$, is unduly conservative. This unjustifiable ignorance of the strength enhancement is believed illogical. Even with violating that conservative condition, that is to consider f_{ce} = 35 MPa when ρ is increased to 6.5%, P_r will be equal to 13600 kN (UNSAFE).

3- Puddle the two concretes when casting the floor, then f_{ce} = 100 MPa, f_y = 400 MPa

$P_r > P_f$ (15000 kN) OK

Design of the Joint Section Using the Design-Oriented Method

By looking at figure 8.17, there are two sub-joints: one between the slab and the column and the other between the beam stem and the column. One can judge which of them is more critical by comparing their aspect ratios, their concrete design strengths (if different), and the degree of physical confinement provided by the floor element, either slab or beam. As seen in the figure, the beam-column sub-joint is the critical one.

h/c = (500-150)/600 = 0.58

λ= 2x500/(4x600) = 0.42

Scenario I: the joint is totally made of high strength concrete

The maximum tie tensile stress (f''_s), contributing to the effective strength enhancement, can be estimated as: $f''_s = 1.5*400 - 5*(1.0*100 + 0*25) = 100$ MPa. Each k-factor shown in equation 6.23b is calculated as follows:

$k_{Floor;Res} = 0.5*[(1.1+1.2*1)*100/25 - 1.5 - 2*1]*0.2*0.42 = 0.24$ (equation 6.14)

$k_{Floor;Deb} = (0.8*100/25 - 1)0.2*0 = 0$ (equation 6.15)

$k_{HSC;Core} = [(0.54 + 0.6*0.2)*100/25 - 0.73 - 1*0.2]*1.0 = 1.71$ (equation 6.16)

$k_{End;Conf} = [1 - 1.24(0.58) + 0.37(0.58)^2](0.85*100/25 - 1)(1-1) = 0$ (equation 6.17)

$k_{RFT;Conf} = 0.025(0.2*0.015*400 + 100*0)(1 + 0.55\frac{100}{25}) = 0.1$ (equation 6.21)

$k_{Floor;Conf} = 0.02*0.42*(3 + 100/25)*(1-1) = 0.0$ (equation 6.22)

$f_{ce} = f'_{cs}(1 + 0.24 + 0 + 1.71 + 0 + 0.1 + 0) = 76.2$ MPa

P_r = [(0.85-0.0015*f_{ce})*0.6 * f_{ce} * (1-0.015) + 0.85 *400 MPa* 0.015]*

600 mm*600 mm*10^{-3} = 13671 kN.

$P_r < P_f$ (15000 kN) UNSAFE

Now if ratio of the vertical reinforcement (ρ) is increased to 4% (2.5% more reinforcement in the joint) then $k_{RFT;Conf}$ will increase to 0.26 and the effective strength would be 80.2 MPa.

P_r = [(0.85-0.0015*f_{ce})*0.6 * f_{ce} * (1-0.04) + 0.85 *400* 0.04]*600*600*10^{-3}= 17031 kN.

P_r= 17031 kN > P_f (15000 kN) OK

Scenario II: half of the joint is made of high strength concrete

To maximize the joint capacity, ρ will be increased to 4% and ties of grade 400 will be added inside the joint. Practically, a maximum of three sets of ties can be placed in the joint along the beam stem. Volumetric ratio of the ties (ρ'') will be 0.011 if No. 10M bars are used. f''_s can be estimated as:

$f''_s = 1.5*400 - 5*(0.5*100 + 0.5*25) = 288$ MPa

$k_{Floor;Res} = 0.5*[(1.1+1.2*0.5)*100/25 - 1.5 - 2*0.5]*0.2*0.42 = 0.18$

$k_{Floor;Deb} = (0.8*100/25 - 1)0.2*0 = 0$

$k_{HSC;Core} = [(0.54 + 0.6*0.2)*100/25 - 0.73 - 1*0.2]*0.5 = 0.86$

$$k_{End;Conf} = [1 - 1.24(0.58) + 0.37(0.58)^2](0.85 * 100/25 - 1)(1 - 0.5) = 0.49$$

$$k_{RFT;Conf} = 0.025(0.2 * 0.04 * 400 + 288 * 0.011)(1 + 0.55\frac{100}{25}) = 0.51$$

$$k_{Floor;Conf} = 0.02 * 0.42 * (3 + 100/25) * (1 - 0.5) = 0.03$$

$$f_{ce} = f'_{cs}(1 + 0.18 + 0 + 0.86 + 0.49 + 0.51 + 0.03) = 76.7 \text{ MPa}$$

$P_r = 16585$ kN > P_f (15000 kN) OK

Scenario III: the joint is made of normal strength concrete

Starting with having 4% reinforcement ratio of vertical rebars of grade 400 and 1.1% volumetric ratio of ties of grade 400, calculation of the capacity of the joint will be as follows:

$$f''_s = f''_y = 400 \text{ MPa}$$

$$k_{Floor;Res} = 0.5 * [1.1 * 100/25 - 1.5] * 0.2 * 0.42 = 0.12$$

$$k_{Floor;Deb} = (0.8 * 100/25 - 1)0.2 * 0 = 0$$

$$k_{HSC;Core} = [(0.54 + 0.6 * 0.2) * 100/25 - 0.73 - 1 * 0.2] * 0 = 0$$

$$k_{End;Conf} = [1 - 1.24(0.58) + 0.37(0.58)^2](0.85 * 100/25 - 1) = 0.97$$

$$k_{RFT;Conf} = 0.025(0.2 * 0.04 * 400 + 400 * 0.011)(1 + 0.55\frac{100}{25}) = 0.61$$

$$k_{Floor;Conf} = 0.02 * 0.42 * (3 + 100/25) * (1 - 0) = 0.06$$

$$f_{ce} = f'_{cs}(1 + 0.12 + 0 + 0 + 0.97 + 0.61 + 0.06) = 69.0 \text{ MPa}$$

$P_r = 15577$ kN > P_f (15000 kN) OK

Scenario III is the easiest to apply and the least in terms of cost. Three remaining options can be used to improve f_{ce}. The first one is to replace the added vertical rebars with DYWIDAG bars that has f_y= 1080 MPa.

$$(\rho f_y)_{eq} = (0.015 * 400)_1 + (0.025 * 1080_y)_2 = 0.04 * 825 MPa$$

The second option is to debond the top reinforcement of the beam through the joint. The third option is to increase the floor reserve strength by increasing the moment of resistance of the beam, by increasing the grade or the ratio of the beam top reinforcement. Caution should be taken to avoid shifting the location of the plastic hinge from the beam to the column.

Table 8.1. Summary of the change in f_{cc}/f'_{cs} ratio with the different parameters

Factors Investigated							f_{cc}/f'_{cs} ratio																	
Factor	Values						Corner Joints						Edge Joints						Interior Joints					
Rebars Arrangement *	SH1	SH2	SH3	SH4			2.75	2.74	2.76	2.78			2.89	2.88	2.90	2.91			3.04	3.04	3.04	3.04		
Rebars Diameter & Volumetric Ratio (%)	M25(1.1)	M30 (1.5)	M35 (2.2)	M45 (3.3)			2.70	2.72	2.76	2.81			2.83	2.86	2.90	2.95			2.97	2.99	3.04	3.10		
Rebars Spacing & Volumetric Ratio (%)	580 (1.1)	265 (2.2)	194 (3.3)	167 (3.9)	146 (4.4)		2.72	2.76	2.79	2.80	2.83		2.84	2.90	2.94	2.97	2.99		2.97	3.04	3.10	3.13	3.16	
Rebars Yield Strength (MPa)	400	550	835	1080	1420		2.76	2.80	2.87	2.92	2.99		2.90	2.94	3.02	3.08	3.16		3.04	3.09	3.17	3.24	3.32	
Ties Diameter & Volumetric Ratio (%)	0 (0.0)	M10 (0.8)	M15 (1.6)				2.13	2.76	2.93				2.49	2.90	3.09				2.83	3.04	3.25			
Ties Spacing & Volumetric Ratio (%)	0	250 (0.5)	150 (0.8)	120 (1.0)	60 (2.0)		2.13	2.57	2.76	2.84	3.13		2.49	2.75	2.90	2.97	3.23		2.83	2.94	3.04	3.10	3.34	
Ties Yield Strength (MPa)	0	400	550	1318			2.13	2.76	2.83	3.11			2.49	2.90	2.97	3.29			2.83	3.04	3.12	3.47		
Column Concrete Strength (MPa)	40	60	80	100	120		1.98	2.44	2.76	2.81	2.87		2.06	2.55	2.90	2.98	3.06		2.15	2.66	3.04	3.15	3.26	
Floor Concrete Strength (MPa)	20	40	80				2.76	1.67	1.04				2.90	1.72	1.04				3.04	1.77	1.04			
Aspect Ratio (h/c)	0.50	1.00	1.50	2.00			2.76	2.15	1.68	1.76			2.90	2.29	1.81	1.90			3.04	2.43	1.95	2.04		
Floor Reserved Strength (%)	0	20	40	60	80	100	2.61	2.76	2.90	3.05	3.19	3.34	2.68	2.90	3.11	3.33	3.55	3.77	2.75	3.04	3.33	3.62	3.91	4.20
Partial Debonding of Floor RFT (%)	0	20	40	60	80	100	2.76	2.85	2.93	3.02	3.11	3.20	2.90	2.99	3.07	3.16	3.25	3.34	3.04	3.13	3.21	3.30	3.39	3.48
HSC/ NSC ratio inside the Joint (%)	0	20	40	60	80	100	2.76	3.04	3.10	3.24	3.38	3.51	2.90	3.19	3.25	3.41	3.56	3.71	3.04	3.34	3.41	3.58	3.75	3.91

RFT: Reinforcement
HSC: High Strength Concrete
NSC: Normal Strength Concrete

* See figure 8.3

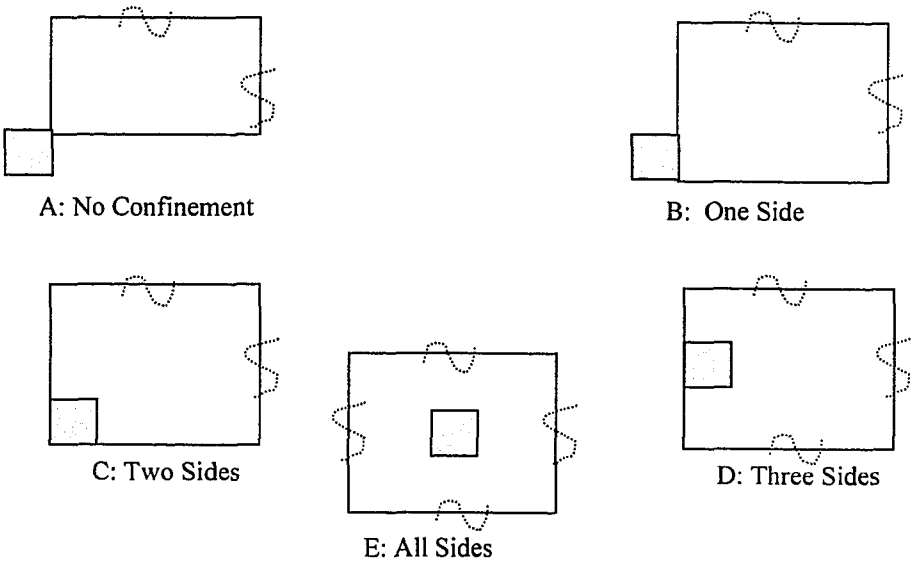

Figure 8.1. Different Cases of Floor Confinement

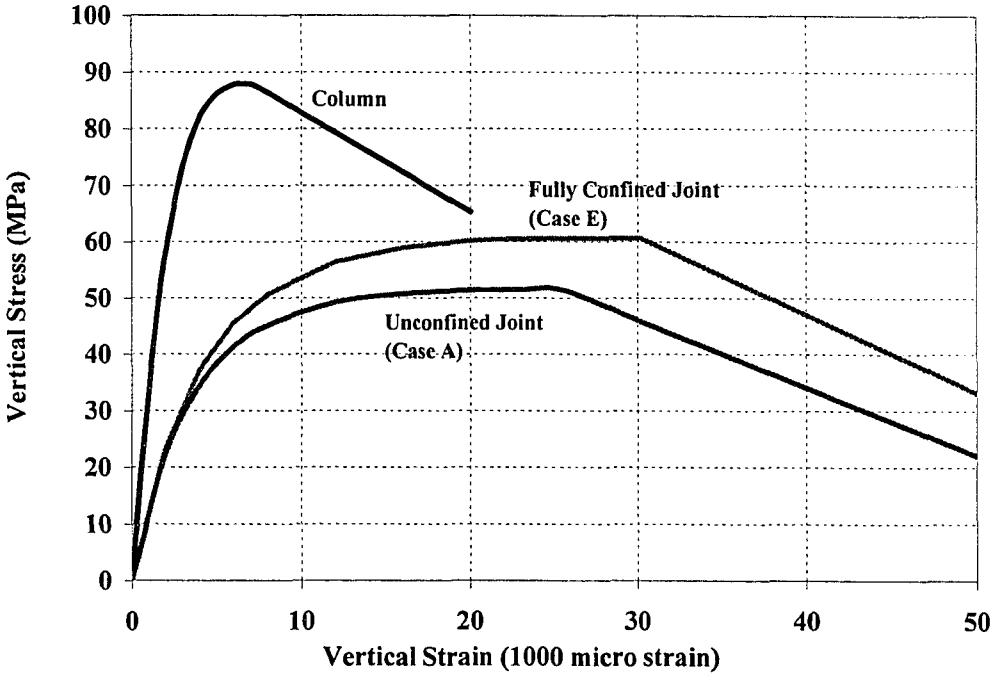

Figure 8.2. Effect of The Floor Confinment on the Behaviour of an Edge Joint

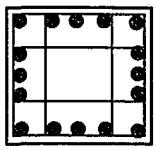

SH1: 16M25mm

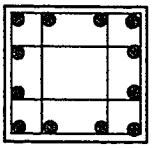

SH2: 12M30

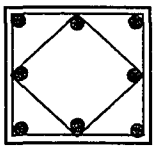

SH3: 8M35mm

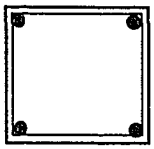

SH4: 4M55mm

The Control Specimen has the Following Characteristics:
Rectangular Column of 600x600 mm; 8-M35 rebars with diamond ties; 2.2% reinforcement ratio and yield strength 400 MPa; ties of M10 bars spaced every 150 mm with volumetric ratio of 0.8 and yield strength of 400 MPa; column concrete strength of 80 MPa and floor concrete strength of 20 MPa; floor to column aspect ratio of 0.50; 20% floor reserve strength; no debonded floor reinforcement and no high strength concrete inside the joint.

Figure 8.3. Different Cases of Rebars Arrangement Covered in the Sensitivity Study

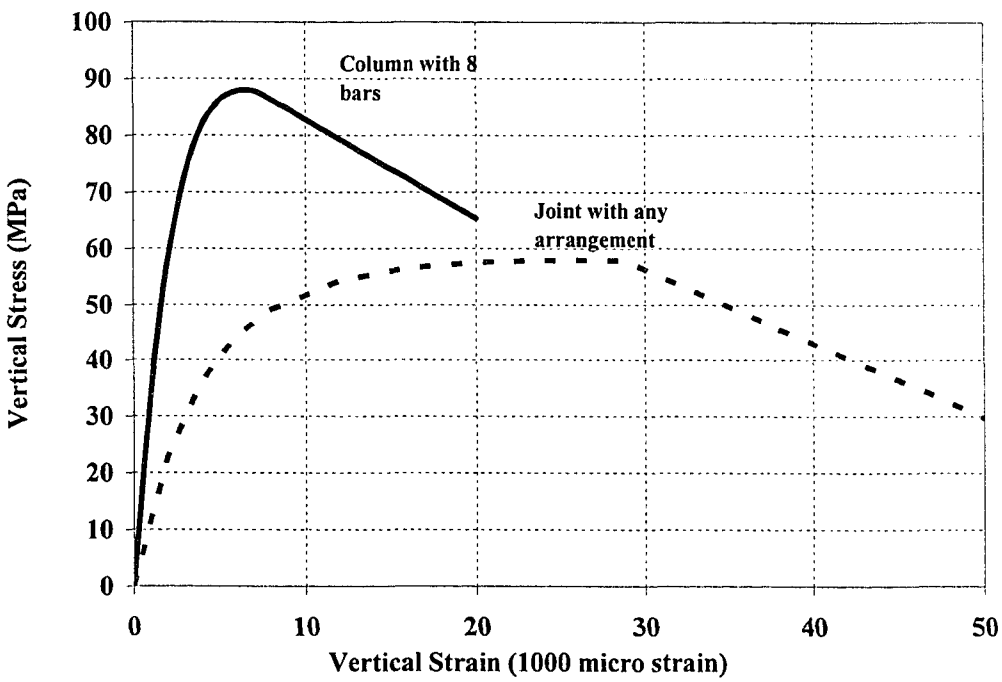

Figure 8.4. Effect of Rebar Arrangement on the Behaviour of an Edge Joint

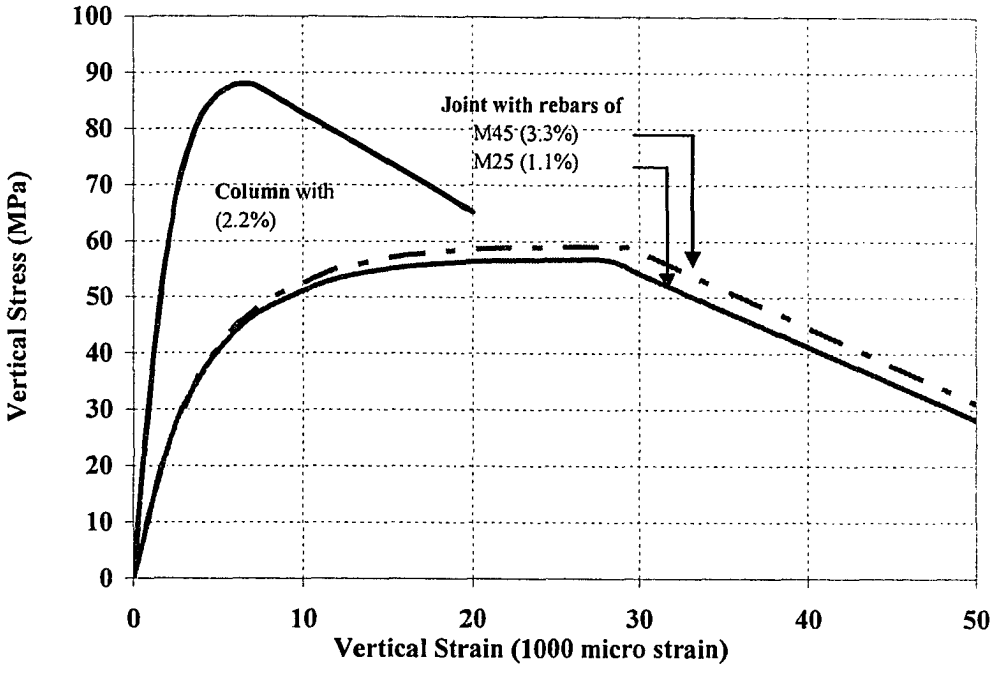

Figure 8.5. Effect of Rebar Diameter and Reinforcement Ratio (%) on the Behaviour of an Edge Joint

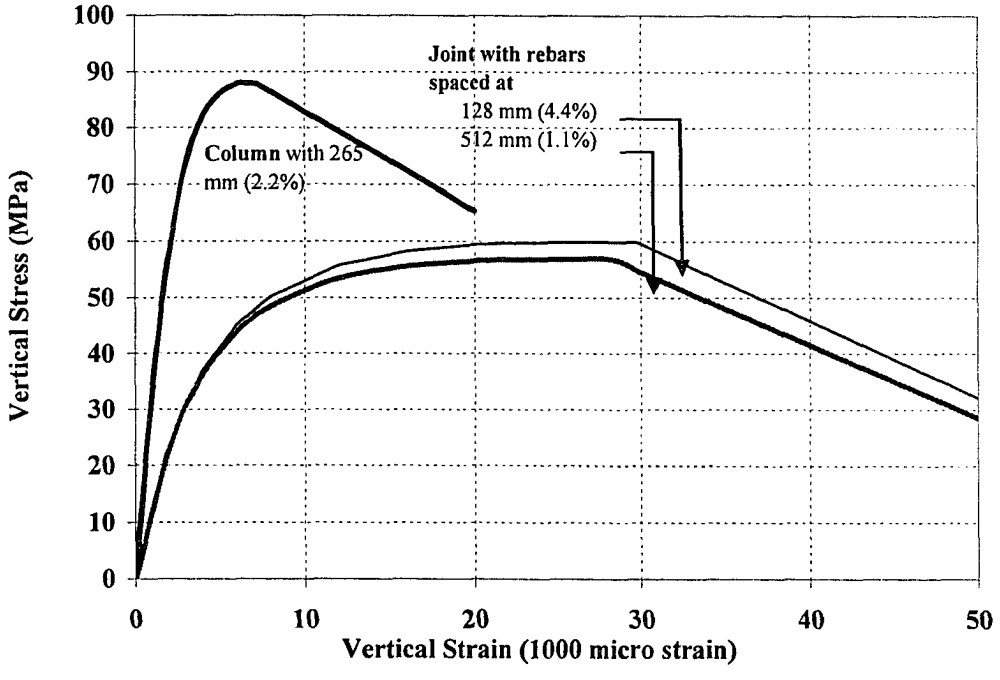

Figure 8.6. Effect of Rebar Spacing and Reinforcement Ratio (%) on the Behaviour of an Edge Joint

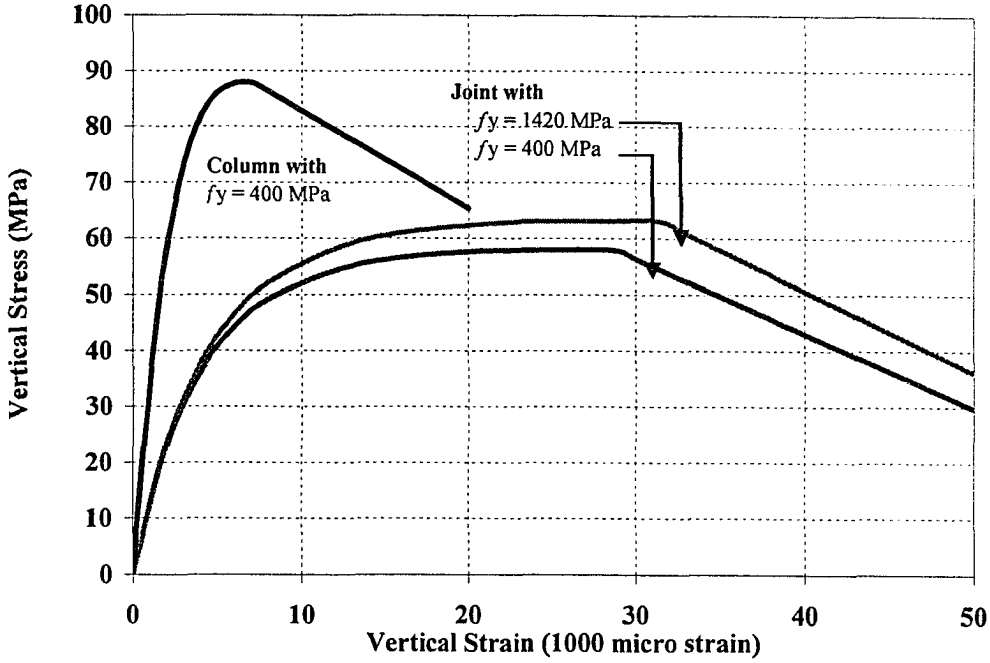

Figure 8.7. Effect of Rebar Yield Strength (MPa) on the Behaviour of an Edge Joint

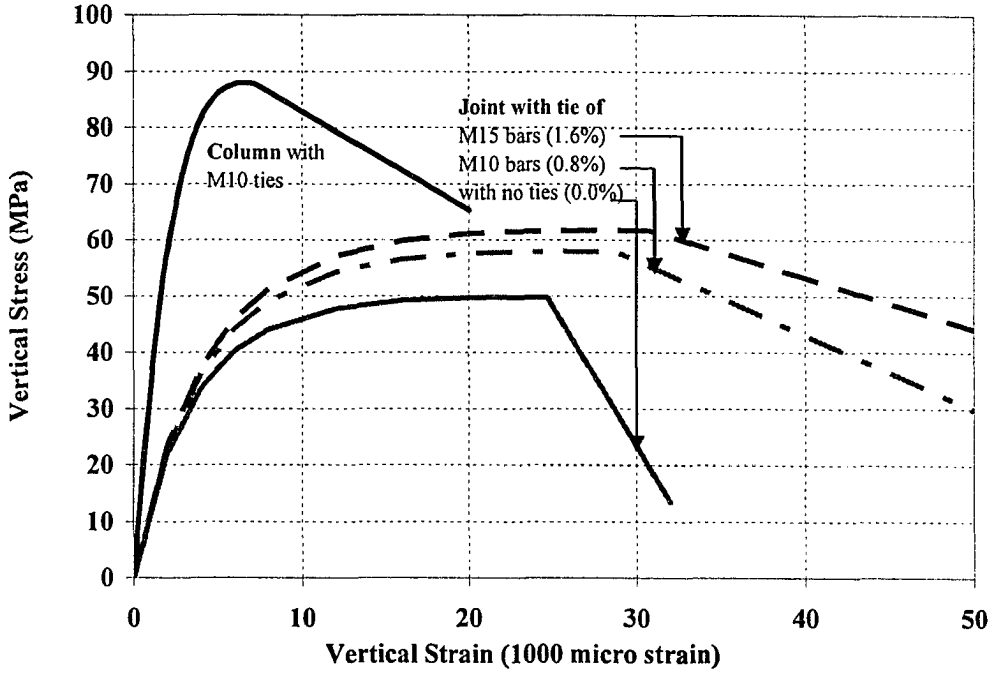

Figure 8.8. Effect of Diameter and Volumetric Ratio of Ties on the Behaviour of an Edge Joint

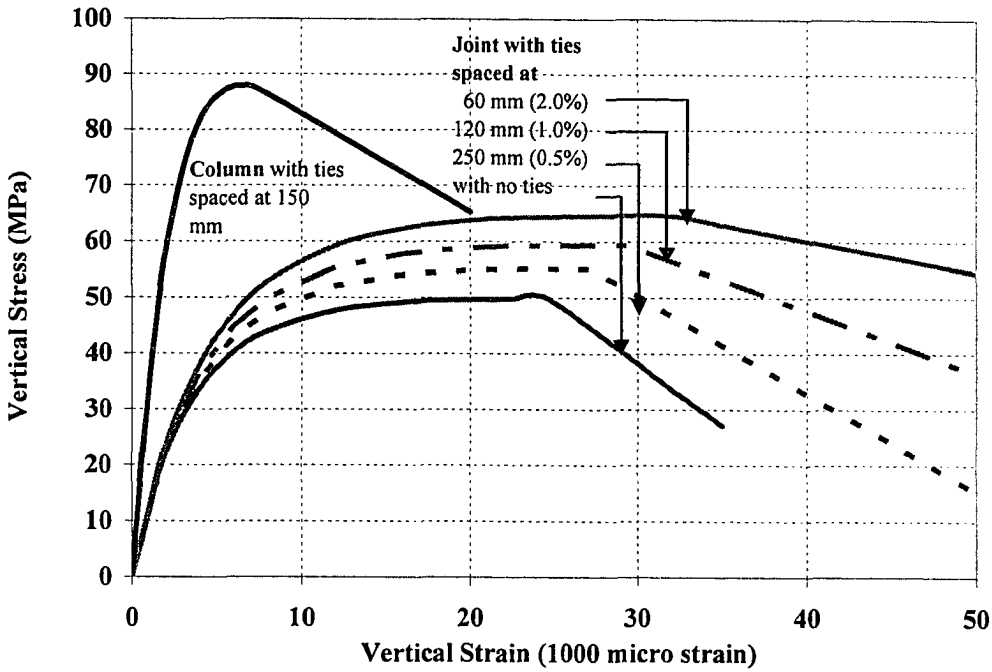

Figure 8.9. Effect of Spacing and Volumetric Ratio of Ties on the Behaviour of an Edge Joint

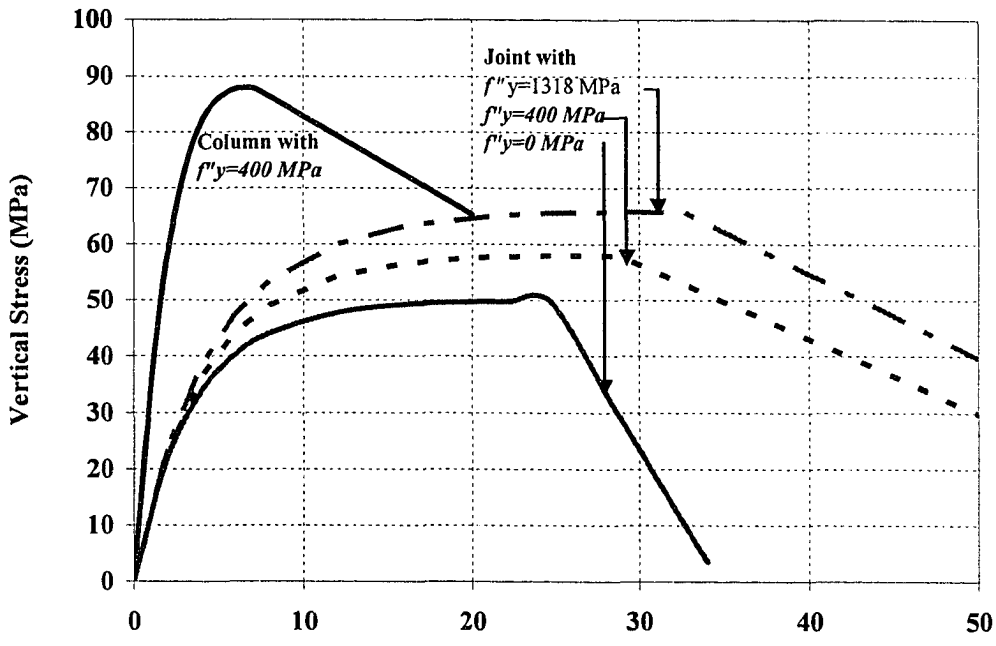

Figure 8.10. Effect of Tie Yield Strength (MPa) on the Behaviour of an Edge Joint

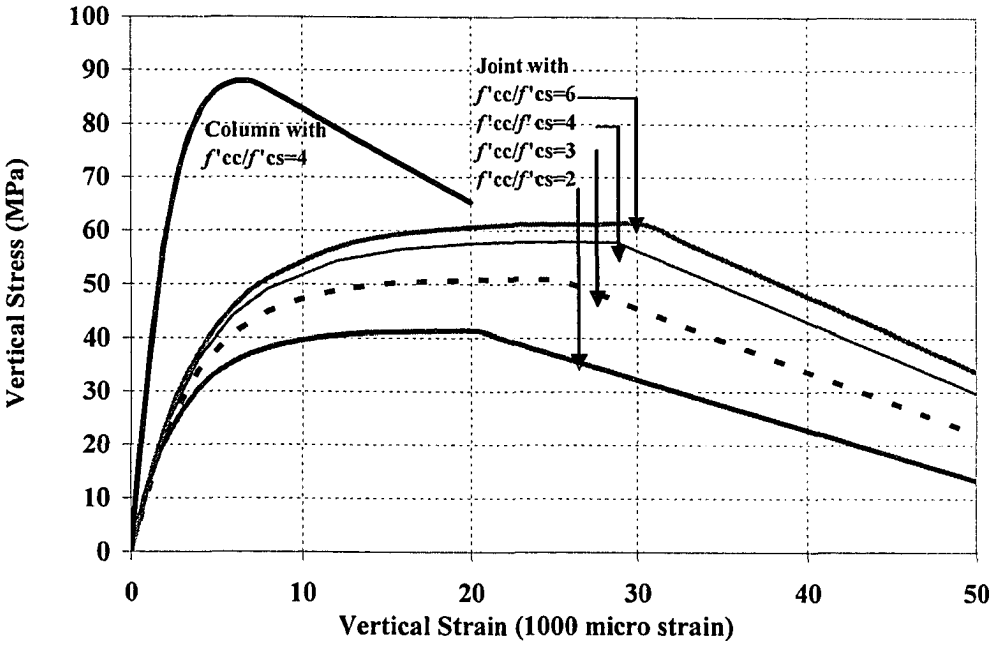

Figure 8.11. Effect of Column Concrete Strength on the Behaviour of an Edge Joint

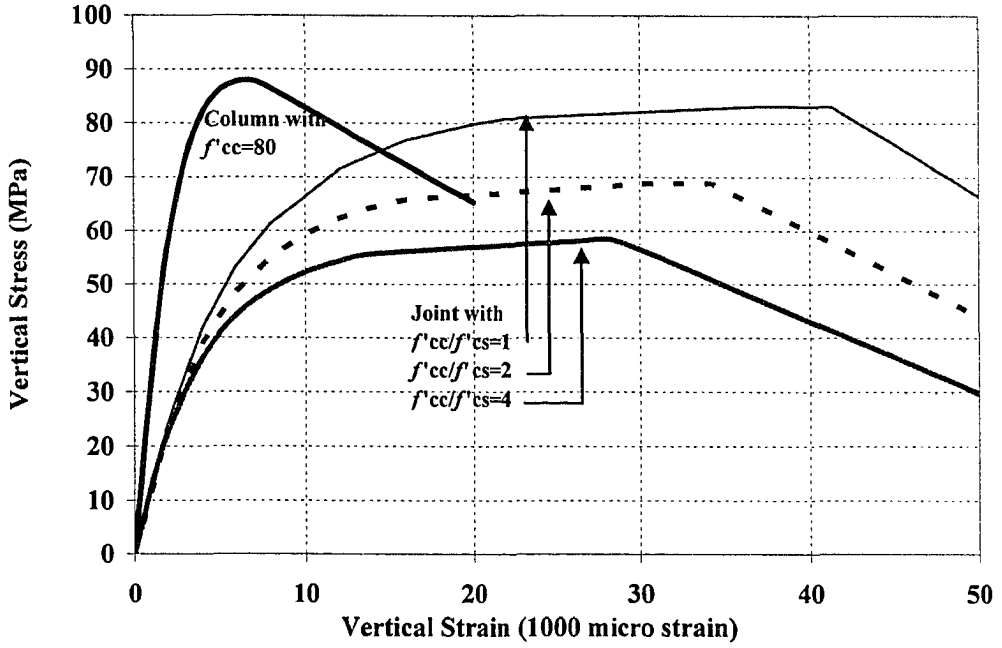

Figure 8.12. Effect of Floor Concrete Strength on the Behaviour of an Edge Joint

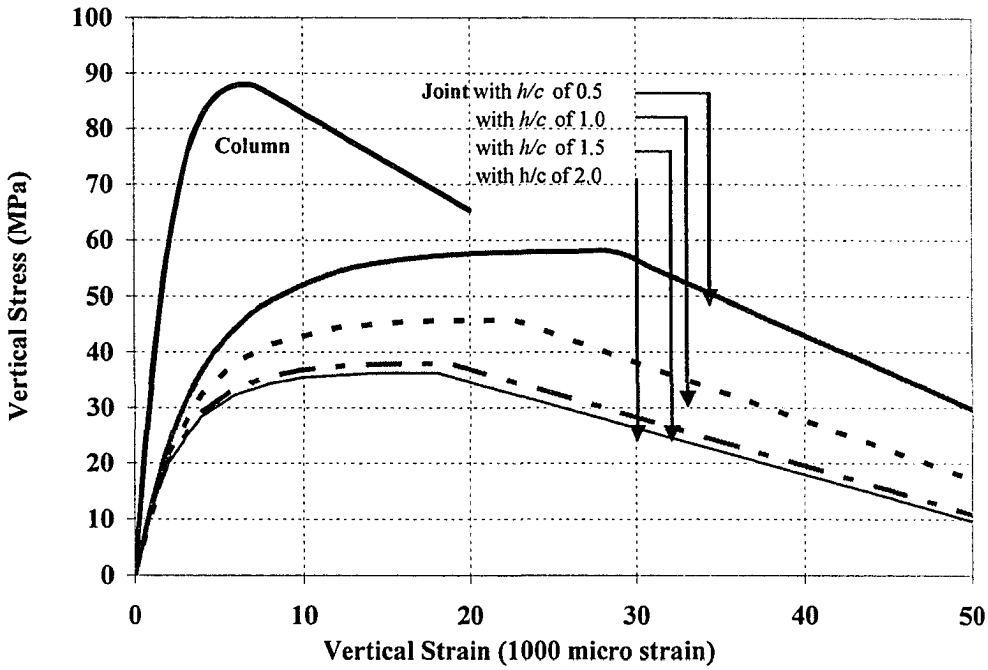

Figure 8.13. Effect of Joint Aspect Ratio on the Behaviour of an Edge Joint

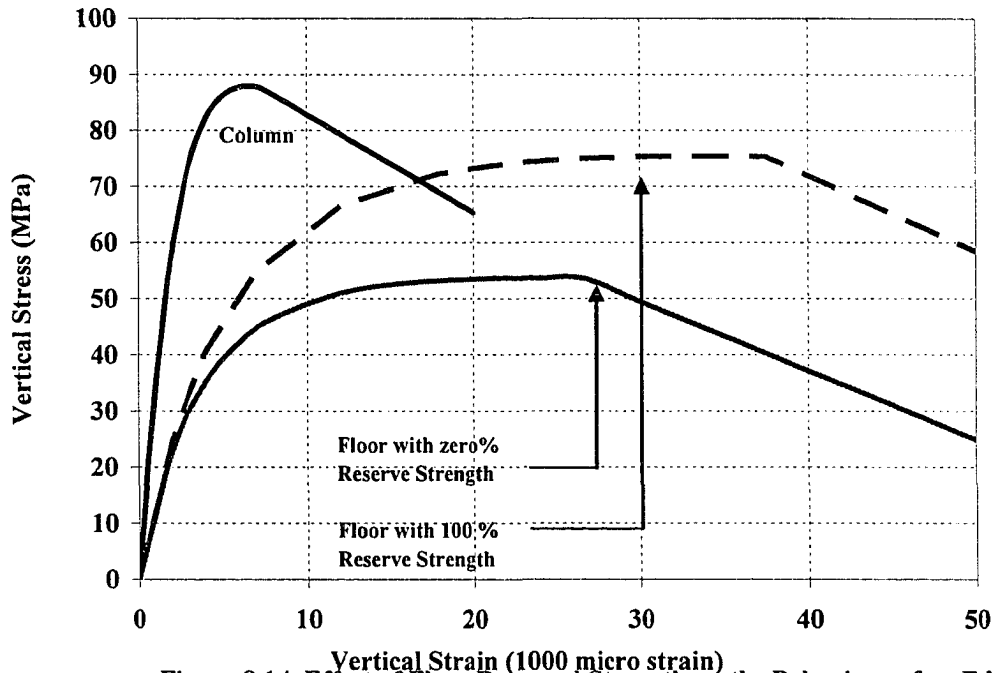

Figure 8.14. Effect of Floor Reserved Strength on the Behaviour of an Edge Joint

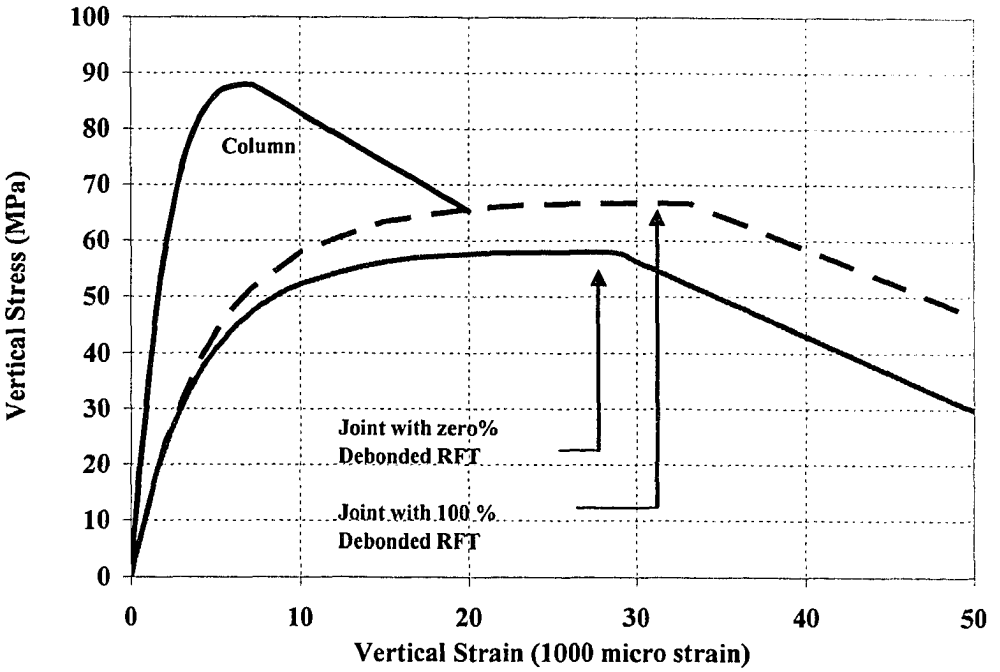

Figure 8.15. Effect of Debonded Floor Reinforcement on the Behaviour of an Edge Joint

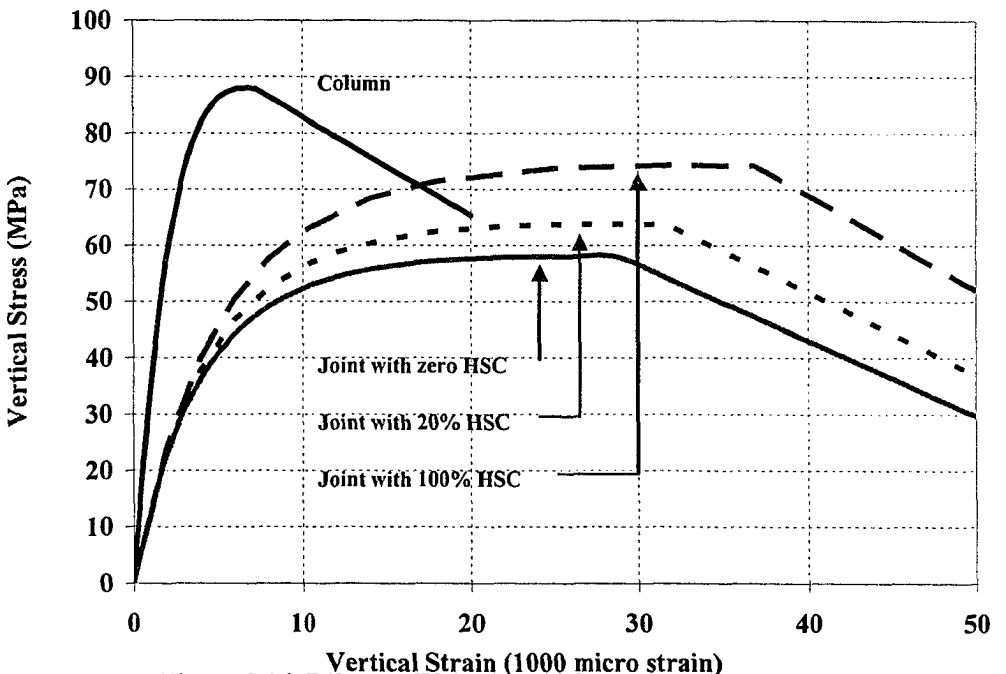

Figure 8.16. Effect of HSC Area to Total Area on the Behaviour of an Edge Joint

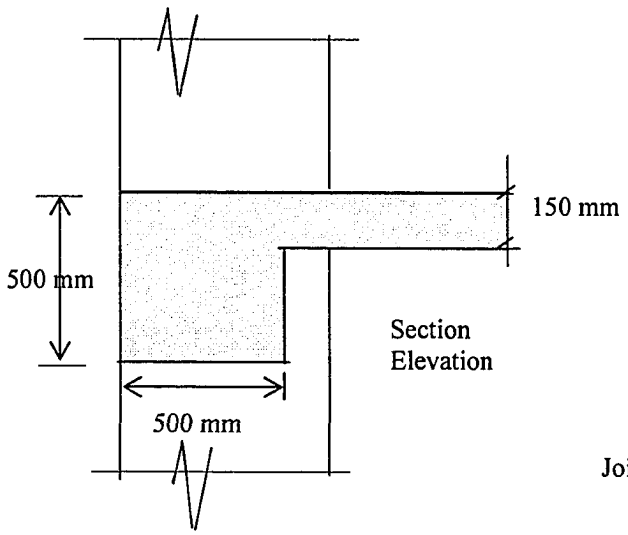

Joint (1) between slab and column:

$\lambda = (3 \times 600) / (4 \times 600) = 0.75$

$h/c = 150/600 = 0.25$

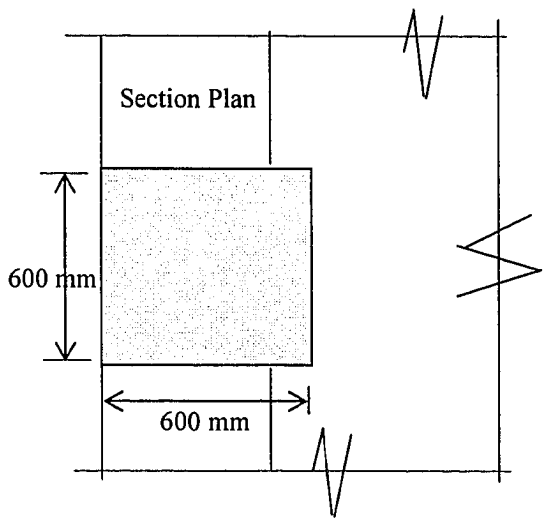

Joint (2) between column and beam-stem:

$\lambda = (2 \times 500) / (4 \times 600) = 0.42$

$h/c = (500-150)/600 = 0.58$

Joint (2) is more critical than joint (1)

Figure 8.17. Design Example. Sections

9 SUMMARY, CONCLUSIONS AND RECOMMENDATIONS

9.1 Summary of Previous Research

Past researchers have attributed the joint restraint effect to the slab concrete around the joint periphery and to the high-strength concrete (HSC) column ends framing into the normal-strength-concrete (NSC) joint. The value of effective concrete strength, f_{ce}, was found dependent on f'_{cc}/f'_{cs} ratio, and the aspect ratio of the joint, h/c. To account for the effect of the surrounding floor, an empirical equation was proposed for each type of joint. The difference between these equations relies on the factor before the variables f'_{cc} and f'_{cs}. Of all the proposed equations to estimate f_{ce}, none accounts for the level of floor loading, the presence of debonded floor reinforcement or the presence of more than one type of concrete in the joint. There is no analytical method to model the behaviour of edge or corner floor-column joints. The model by Lokuge et al. includes sets of conditional equations developed for interior joints only.

Evaluation of the concrete confinement provided by lateral reinforcement to NSC and HSC columns has been investigated for decades. Many empirical equations and analytical models have been developed to estimate the increase in axial strength and ductility as function of the confining pressure.

9.2 Summary of This Research

This research aimed at providing a tool for estimating f_{ce} of any joint between HSC columns and NSC floors. Seven near-full-scale specimens were made and tested to investigate the behaviour of column-floor joints under different loading combinations. Each specimen represents an interior joint between a column and a floor made of one-way slab and unidirectional beams that span along the column longer dimension.

Vertical and lateral strain values in the joint and in the columns were monitored through nine embedded concrete gauges in the cores and thirty two foil gauges mounted on the vertical and lateral reinforcement at three locations: bottom column, joint and top column. Additional eighteen foil gauges were used to monitor strain values in the floor

reinforcement. Specimens were tested at ages between 34 to 171 days when the average cylinder strength was 20 MPa for the floor and 80 MPa for the columns.

The research investigated the effect of a new construction technique and the role of partial debonding of the beam top reinforcement in alleviating the flooring action of pulling the joint concrete apart.

Two loading scenarios were designed to cover the extreme combinations of loading the columns and floors. Under type-I loading, the axial compressive strength of the joint was tested with the floor under service load. With type-II loading, the joint was tested under service column load and ultimate floor load. No joint failed as a result of extreme loading on the floor. Compared to type-I, type-II loaded specimens showed substantial loss of section in the beam and buckling of the beam compression reinforcement. The failure of the beam did not seriously compromise the strength of the joint under column load. Failure of the specimens under axial loads was marked by crushing of the concrete and by buckling of the longitudinal reinforcement.

Maximum vertical strain values for HSC columns were less than -5000με and maximum vertical strain values for NSC joints were in excess of -50000με. Maximum lateral strain recorded in HSC columns were less than +1000 με, one fifth of that in NSC column of the control specimen and maximum lateral strain values for NSC joints were in excess of +15000 με.

For specimens with NSC joints, the peak stress occurred at an axial strain in excess of 1.5 percent and there was a significant descending (softening) part in each stress-strain curve. The tie maximum stress was fully activated at the peak load when no localized failure happened before.

For specimens with HSC joints, the peak stress occurred at an axial strain below 0.5 percent. The ties did not yield.

In specimens with NSC joints, the failure happened at the joint-interface with the bottom column. The joint reached failure when ties yielded. Failure of NSC sections was noticed to be conical shear failure similar to cylinders under uniaxial compression. Failure of HSC sections was a shear plane failure.

This research presents a detailed equation and a simplified equation for estimating f'_{ce}. The detailed equation accounts for mechanical properties of the concrete and steel reinforcement, geometrical characteristics of the joint and reinforcement arrangement. The simplified equation accounts for the joint type and the aspect ratio. Both equations are more accurate and more consistent than other available equations.

An axial stress-strain model was developed, to predict the behaviour of floor-column joints, by defining the stress-strain curve as a continuous function covering the pre-peak and peak zones. The post-peak behaviour is reasonably represented by a linear equation that reflects the softening. The model presented here was found good at replicating behaviour of different types of joints under any scheme of loading.

9.3 Conclusions from Test Program

The seven tested specimens behaved in a way similar to an edge joint between HSC columns and NSC floor. For one-way slab-beam system or edge column case, the critical zone is the interface between the joint and bottom column where the section is under biaxial compression-compression loads.

The very large longitudinal and lateral strains in joints made of normal strength concrete suggest that there is benefit in considering high strength steel for strengthening joints between HSC columns and NSC floors.

The level of floor loading had some effect on f_{ce}. The combination of extreme floor loading and service column loading will not fail the joint but type-I loaded specimens demonstrate higher strengths than type-II loaded specimens.

Capacity of the joints provided with 74% high-strength-concrete was nearly equal to the capacity of full HSC section. The HSC inside the joint limits the effect of column loads on strain of the beam reinforcement.

Partial debonding of the beam top reinforcement improves the joint effective strength without causing any reduction of the floor flexural capacity.

According to the variables tested in this research, three factors are believed to affect the beam curvature: the bond strength between beam reinforcement and joint

concrete; the axial stress level, defined as the ratio of the axial stress at the time of floor collapse to the joint effective strength; and f'_{cc}/f'_{ce} ratio.

Adding shrinkage control reinforcement (side) reinforcement to the beam helps in bridging part of the axial compressive load to the bottom column from the top column.

9.4 Conclusions based on Behaviour Model

The most significant parameters affecting the strength and behaviour of floor-column joints are the volumetric ratio, yield strength and arrangement of vertical and lateral reinforcement, the aspect ratio of the joint, adding HSC in the joint, debonding of the floor top reinforcement, and the reserve strength of the floor.

The arrangement of rebars is not crucial for floor-column interior joints as long as rebar reinforcement ratio remains constant. Increasing the reinforcement ratio of vertical rebars increases the effective strength and is substantially useful for the overall section capacity.

The effect of increasing tie-volumetric ratio on the effective strength is five times that of the vertical rebars. Increasing the tie volumetric ratio by decreasing the tie spacing is of similar effect to increasing the volumetric ratio by increasing the tie diameter. Tie volumetric ratio has a substantial effect on the shape of the softening part.

Using high yield-strength reinforcement in the joint can improve the effective strength and ductility of the joint.

9.5 General Design Recommendations

- Joints or sub-joints not confined in all directions should be provided with ties.
- Column ties should be provided as close as possible to the interface between the column and the floor elements.
- For best utilization (most efficient use) of lateral reinforcement, yield strength of ties should be at least equal to ten times the nominal unconfined concrete strength.
- Compression reinforcement of the beam should not be considered in the flexural strength calculations. If considered, the maximum unsupported length of the rebars through the joint should be safe against buckling.

- When selecting closely spaced rebars of equivalent reinforcement ratio, caution should be taken to guarantee safety against rebar local buckling.

9.6 Recommendations for Further Research Work

Further research work is required to investigate the effect of the following on the behaviour of floor-column joints:

- Using high yield strength reinforcement in the joint.
- Using precast high strength cores in the joint.
- Using high strength concrete filled tube in the joint.
- High-strength-concrete joints with debonded floor reinforcement.
- Interior joints with f'_{cc}/f'_{cs} values from 4-6 and h/c values above 1.5
- Edge joints with f'_{cc}/f'_{cs} values above five and h/c values above 1.3
- Corner joints with f'_{cc}/f'_{cs} values from 3.5-5.5 and h/c values from 1-2 and from 2-3
- Debonding the top and bottom floor reinforcement.
- The effective width of debonding of the top reinforcement of flat plates.
- Combination of axial and lateral loadings.
- Developing strut-tie mechanism through beam-column joints.

In addition, further research work could be needed to study the effect of having a joint made totally of HSC on the punching strengths of the floor during construction and exploitation phases.

In addition, a finite element study, with "progressive fracture models", is needed to capture the localized failure phenomenon.

REFERENCES

Abdel Wahab, E.A.W., and Alexander, S.D.B. (2004), "High Strength Concrete Columns with Intervening Normal Strength One-Way Slab and Beam Floors", Research and Development Bulletin RD serial no. 2622, *Portland Cement Association,* Skokie, Illinois, U.S.A.,39p.

ACI Committee 318 (2002), "Building Code Requirements for Reinforced Concrete (ACI 318M-02) and Commentary (ACI 318RM-02)," *American Concrete Institute,* Farmington Hills, Mich.,443 p.

ACI-ASCE Committee 441 (1997), "High-Strength Concrete Columns: State of The Art," *ACI Structural Journal,* Vol. 94, No. 3, May-June, pp. 323-335.

Ahmad, S.H., and Shah, S.P. (1982), "Complete Tri-Axial Stress Strain Curves for Concrete," *Journal of the Structural Division, ASCE,* Vol. 108, No. 4, April, pp.728-741.

Ahmad, S.H., and Shah, S.P. (1987), "High Strength Concrete - A New Material," Conf. Proceed., Materials and Member Behavior, *ASCE,* Orlando, FL, USA, pp.421-434.

Assa, B., Nishiyama, M., and Watanabe, F. (2001), "New Approach for Modeling Confined Concrete. II: Rectangular Columns," *Journal of Structural Engineering, ASCE,* Vol. 127, No.7, April, pp.751-758.

Assa, B., and Dhanasekar, M. (2002), "The Significance of Transverse Steel Configurations to the Behaviour of RC Columns," Conf. Proceed., *Advances in Mechanics of Structures and Materials,* Loo, Chowdhury and Fragomeni (eds.), Swets and Zeitlinger, Lisse, ISBN 9058093867, PP. 139-144.

Attard, M.M., and Setung, S. (1996), "Stress-Strain Relationship of Confined and Unconfined Concrete," *ACI Materials Journal,* Vol. 93, No.5, Sept.-Oct., pp. 432-442.

Avram, C., Facaoaru, I., Filimon, O. and Tertea, I., (1981), "Concrete Strength and Strains," *Elsevier Scientific Publishing Company*, Amsterdam, 558 p.

Bianchini, A.C., Woods, R.E. & Kesler, C.E. (1960), "Effect of Floor Concrete Strength on Column Strength," *ACI Structural Journal,* Vol. 31, No. 11, pp.1149-1169.

Bing, Li, Park, R., and Tanaka, H. (2001), "Stress-Strain Behaviour of High-Strength Concrete Confined by Ultra-High- and Normal Strength Transverse Reinforcements," *ACI Structural Journal,* Vol. 98, No. 3, pp.395-406.

Chen, W.F. (1982), "Plasticity in Reinforced Concrete," N.Y., *McGraw-Hill,* 474 p.

Cheong, H.K., and Zeng, H. (2002), "Stress Strain Relationship for Concrete Confined by Lateral Steel Reinforcement," *ACI Material Journal,* Vol. 99, No. 3, pp.250-255.

CSA Technical Committee (1994), "Design of Concrete Structures for Buildings," CAN3-A23.3-M94, *Canadian Standards Association,* Rexdale, Ontario, 199 p.

Cusson, D., and Paultre, P. (1994), "High Strength Concrete Columns Confined by Rectangular Ties," *Journal of Structural Engineering, ASCE,* Vol. 120, No.3, pp. 783-804.

Cusson, D., and Paultre, P. (1995), "Stress Strain Model for Confined High Strength Concrete," *Journal of Structural Engineering, ASCE,* Vol. 121, No 5, pp. 468-477.

Fafitis, A., and Shah, S. P. (1985), "Lateral Reinforcement for High-Strength Concrete Columns," *High-Strength Concrete, SP-87, ACI,* Farmington Hills, Mich., pp. 213-232.

Foster, S.J. (2001), "On Behaviour of High Strength Concrete Columns: Spalling, Steel Fibres, and Ductility," *ACI Structural Journal,* Vol. 98, No. 4, pp.583-589.

Foster, S.J., Liu, J., and Sheikh S.A. (1998), "Cover Spalling in HSC Columns Loaded in Concentric Compression," *Journal of Structural Engineering, ASCE,* Vol. 124, No. 12, pp. 1431-1437.

Gamble, W.L., and Klinar, J.D. (1991), "Tests on High Strength Concrete Columns with Intervening Floor Slabs," *Journal of Structural Engineering, ASCE,* Vol. 117, No. 5, pp.1462-1476.

Harries, K.A., and Kharel, G. (2002), "Behaviour and Modeling of Concrete Subject to Variable Confining Pressure," *ACI Structural Journal,* Vol. 99, No. 2, pp.181-189.

James, V.C., and Hailing, Y. (2001), "Radial Elastic Stiffness Associated with Bond between Steel Bars and Concrete," *ACI Structural Journal,* Vol. 98, No. 1, pp.16-26.

Kayani, M.K. (1992), "Load Transfer from High Strength Concrete Columns through Lower Strength Concrete Slabs," Ph.D. Thesis, Dept of Civil Eng., *U. of Illinois, Urbana Champaign,* 111p.

Kent, D.C., and Park, R. (1971), "Flexural Members with Confined Concrete," *Journal of Structural Division, ASCE,* Vol. 97, No. ST7, PP. 1969-1990.

Khaloo, A.R., and Bozorgzadeh, A. (2001), "Influence of Confining Hoop Flexural Stiffness on Behaviour of High-Strength Lightweight Concrete Columns," *ACI Structural Journal,* Vol. 98, No. 5, pp.657-664.

King, J.W.H. (1946), "The Effect of Lateral Reinforcement in Reinforced Concrete Column," *The Structural Engineering (London),* Vol. 24, No.7, pp. 355-388.

Liu, J., Foster, S.J., and Attard, M.M. (2000), "Strength of Tied High-Strength Concrete Columns Loaded in Concentric Compression," *ACI Structural Journal,* Vol. 97, No. 1, pp.149-156.

Lokuge, W.P., Setunge, S., Mendis, P., and Sanjayan, J.G. (2002), "Prediction of Strength of Interior High-Strength Concrete Column-Slab Joints," Conf. Proceed., *Advances in Mechanics of Structures and Materials,* Loo, Chowdhury and Fragomeni (eds.), Swets and Zeitlinger, Lisse, PP. 185-190.

MacGregor, J.G., and Bartlett, F.M. (2000), "Reinforced Concrete Mechanics and Design," First Canadian Edition, *Prentice Hall,* Scarborough, Ontario.

Mander, J.B., Priestley, M.J.N., and Park, R. (1988), "Observed Stress-Strain Behaviour of Confined Concrete," *Journal of Structural Engineering, ASCE,* Vol. 114, No.8, pp. 1827-1849.

Mander, J.B., Priestley, M.J.N., and Park, R. (1988), "Theoretical Stress-Strain Model for Confined Concrete," *Journal of Structural Engineering, ASCE,* Vol. 114, No.8, pp. 1804-1826.

Mau, S.T., Holland, J.M., and Hong, L. (1998), "Small Column Compression Tests on Concrete Confined by WWF," *Journal of Structural Engineering, ASCE,* Vol. 124, No.3, Mar., pp. 252-261.

Mau, S.T., and El-Mabsout, M. (1989), "Inelastic Buckling of Reinforcing Bars," *Journal of Engineering Mechanics, ASCE,* Vol. 115, No.1, January, pp. 1-17.

McHarg, P.J., Cook, W., Mitchell, D., and Yoon, Y. (2000), "Improved Transmission of High-Strength Concrete Column Loads through Normal Strength Concrete Slabs," *ACI Structural Journal,* Vol. 97, No. 1, pp.157-165.

Micro Measurements, "Strain Gauge Installations with M-Bond 200 and AE-10 Adhesive Systems," *M-Line Accessories,* Student Instructions Bulletin, 7p.

Nehikhare, A.L. and Tabsh, S.W. (2001), "Confinement of High Strength Concrete with Welded Wire Reinforcement," *ACI Structural Journal,* Vol. 98, No. 5, pp.677-685.

Neville, A.M. (1981), "Properties of Concrete," 3rd edition, London, Marshfield, MA, *Pitman Pub.*, 779 p.

Ospina, C.E. and Alexander, S.D.B. (1997), "Transmission of High Strength Concrete Column Loads through Concrete Slabs," Structural Engineering Report 214, *Dept. of Civil and Env. Eng., U. of Alberta,* Edmonton, Canada.

Ospina, C.E. and Alexander, S.D.B. (1998), "Transmission of Interior Concrete Column Loads through Floors," *Journal of Structural Engineering, ASCE,* Vol. 124, No.6, Mar. pp. 602-610.

Palmquist, S.M., and Jansen, D.C. (2001), "Post-Peak Stress-Strain Relationship for Concrete in Compression," *ACI Material Journal,* Vol. 98, No. 3, pp. 213-219.

Paultre, P., L'egeron, F., and Mongeau, D. (2001), "Influence of Concrete Strength and Transverse Reinforcement Yield Strength on Behaviour of High-Strength Concrete Columns," *ACI Structural Journal,* Vol. 98, No. 4, pp.490-501.

Razvi, S., and Saatcioglu, M. (1999), "Confinement Model for High-Strength Concrete," *Journal of Structural Eng., ASCE,* Vol. 125, No.3, Mar. pp. 281-289.

Razvi, S.R., and Saatcioglu, M. (1994), "Strength and Deformability of Confined High-Strength Concrete Columns," *ACI Structural Journal,* Vol. 91, No. 6, pp. 678-687.

Razvi, S.R., and Saatcioglu, M. (1999), "Stress-Strain Relationship for Confined High Strength Concrete," *Journal of Structural Eng., ASCE,* Vol. 125, No. 3, pp. 281-289.

Saatcioglu, M., and Grira, M. (1999), "Confinement of Reinforced Concrete Columns with Welded Reinforcement Grids," *ACI Structural Journal,* Vol. 96, No. 1, pp. 29-39.

Saatcioglu, M., and Razvi. S.R. (1998), "High Strength Concrete Columns, with Square Sections," *Journal of Structural Eng., ASCE,* Vol. 124, No. 12, pp. 1438-1447.

Saatcioglu, M., and Razvi, S.R. (2002), "Displacement-Based Design of Reinforced Concrete Columns for Confinement," *ACI Structural Journal,* Vol. 99, No. 1, pp. 3-11.

Saatcioglu, M., and Razvi, S.R. (1992), "Strength and Ductility of Confined Concrete," *Journal of Structural Eng., ASCE,* Vol. 118, No. 6, pp.1590-1607.

Scott, B.D., Park., R., and Priestley, M.J.N. (1982), "Stress-Strain Behaviour of Concrete Confined by Overlapping Hoops at High and Low Strain Rates," *ACI Journal,* Vol. 79, No. 1, Jan.-Feb., pp 13-27.

Sheikh, S.A. (1982), " A Comparative Study of Confinement Models," *ACI Journal,* Vol. 79, No. 4, pp. 296-306. Discussion (1983), *ACI Journal,* Vol. 80, No. 3, pp. 260-265.

Sheikh, S.A., and Uzumeri, S.M. (1980), "Strength and Ductility of Tied Concrete Columns," *Journal of Structural Engineering, ASCE,* Vol. 106, No. 5, pp. 1079-1102.

Sheikh, S.A., and Uzumeri, S.M. (1982), "Analytical Model for Concrete Confinement in Tied Columns," *Journal of the Structural Division, ASCE,* Vol. 108, No. 12, pp. 2103-2122.

Sheikh, S.A., Shah, D.V., and Khoury, S.S. (1994), "Confinement of High-Strength Concrete Columns," *ACI Structural Journal,* Vol. 91, No. I, Jan.- Feb., pp. 100-111.

Shu, C.C., and Hawkins, N.M. (1992), "Behaviour of Columns Continuous through Concrete Floors," *ACI Structural Journal,* Vol. 89, No. 4, July-August, pp. 405-414.

Yong, Y., Nour, M.G., and Nawy, E.G. (1988), "Behaviour of Laterally Confined High-Strength Concrete under Axial Loads," *Journal of Structural Engineering, ASCE,* Vol. 114, No. ST 2, pp. 332-351.

APPENDIX A

APPENDIX A.1

Fabrication of Specimens

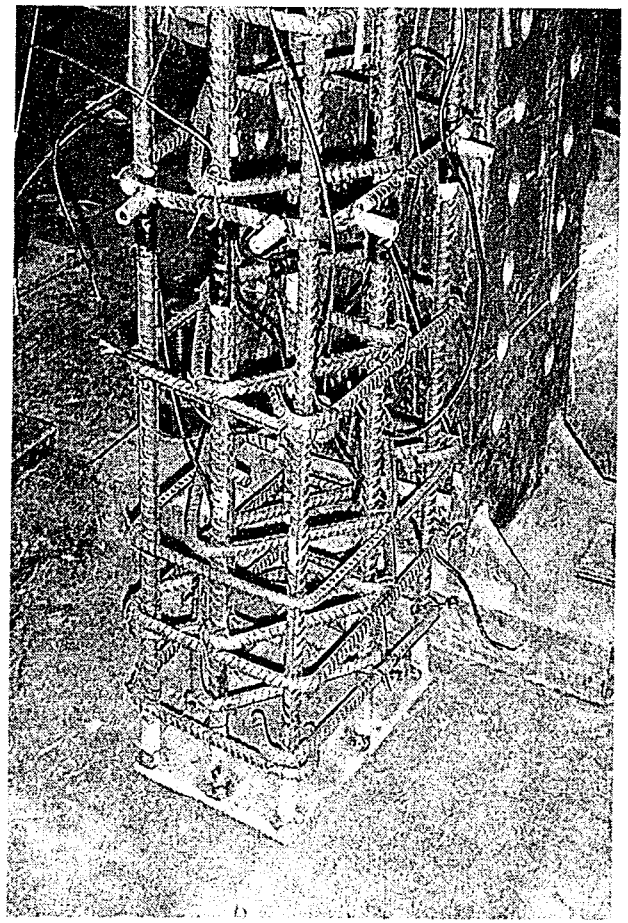

Figure A.1. Column Cage after Assembled

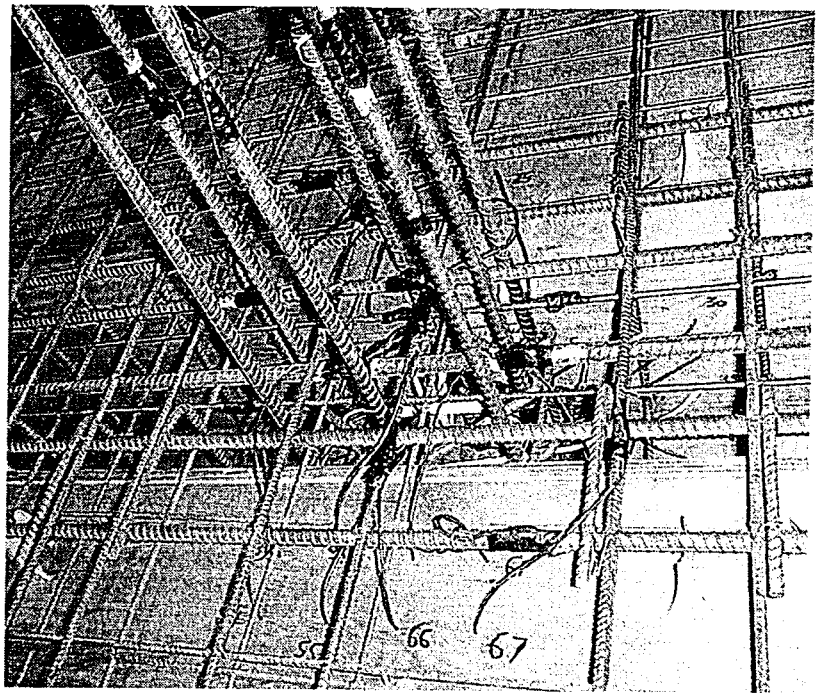

Figure A.2. Slab RFT and Different Gages inside the Joint

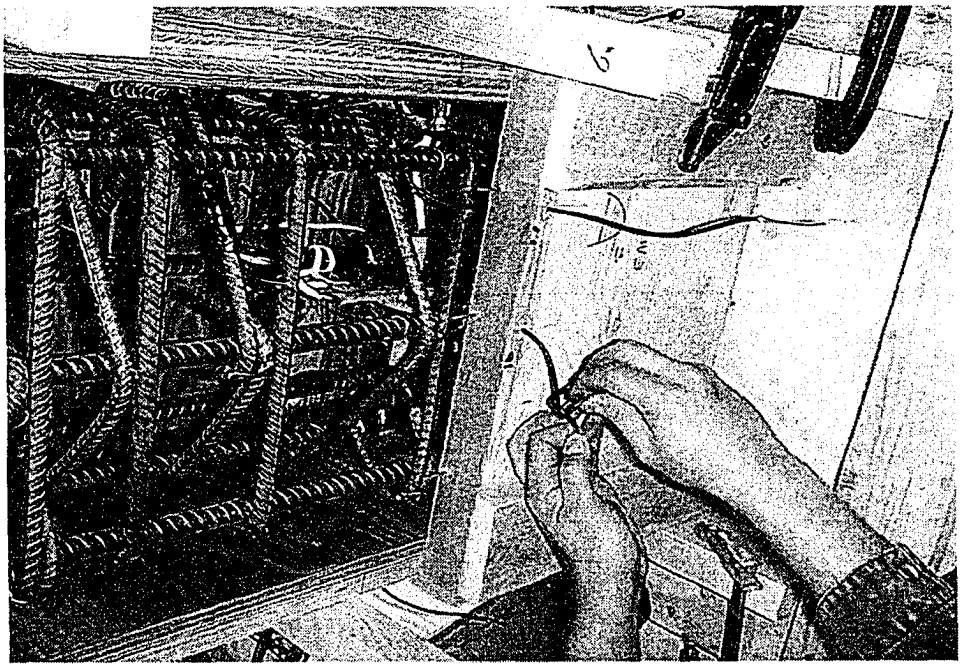

Figure A.4. Top Column Form Assembling

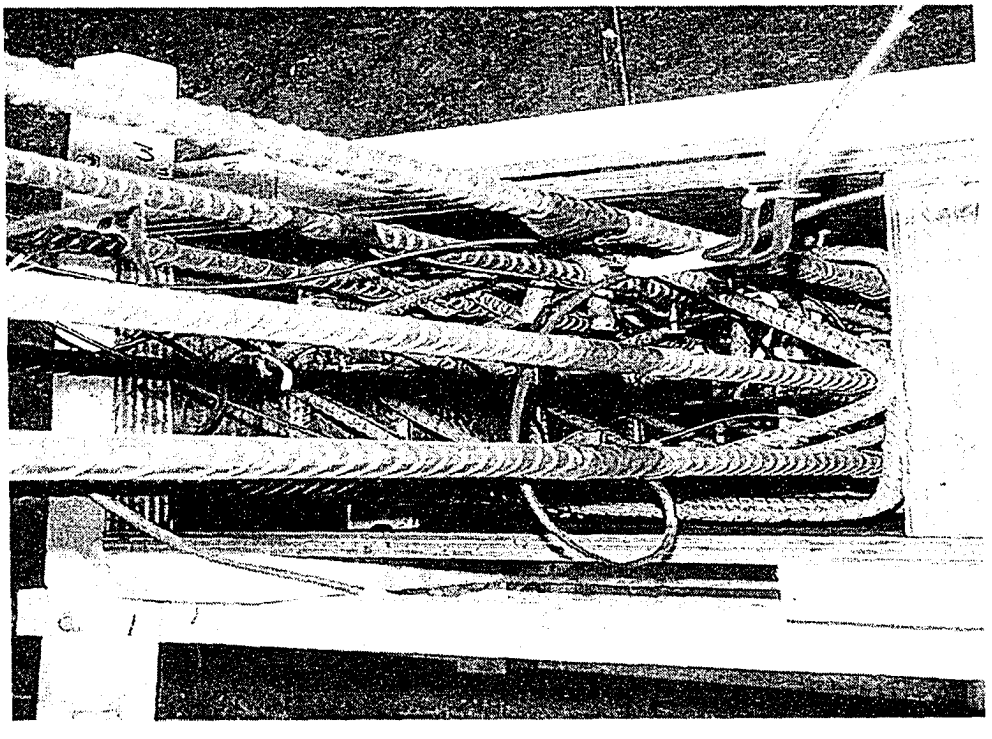

Figure A.3. Bottom Column after Form Assembling

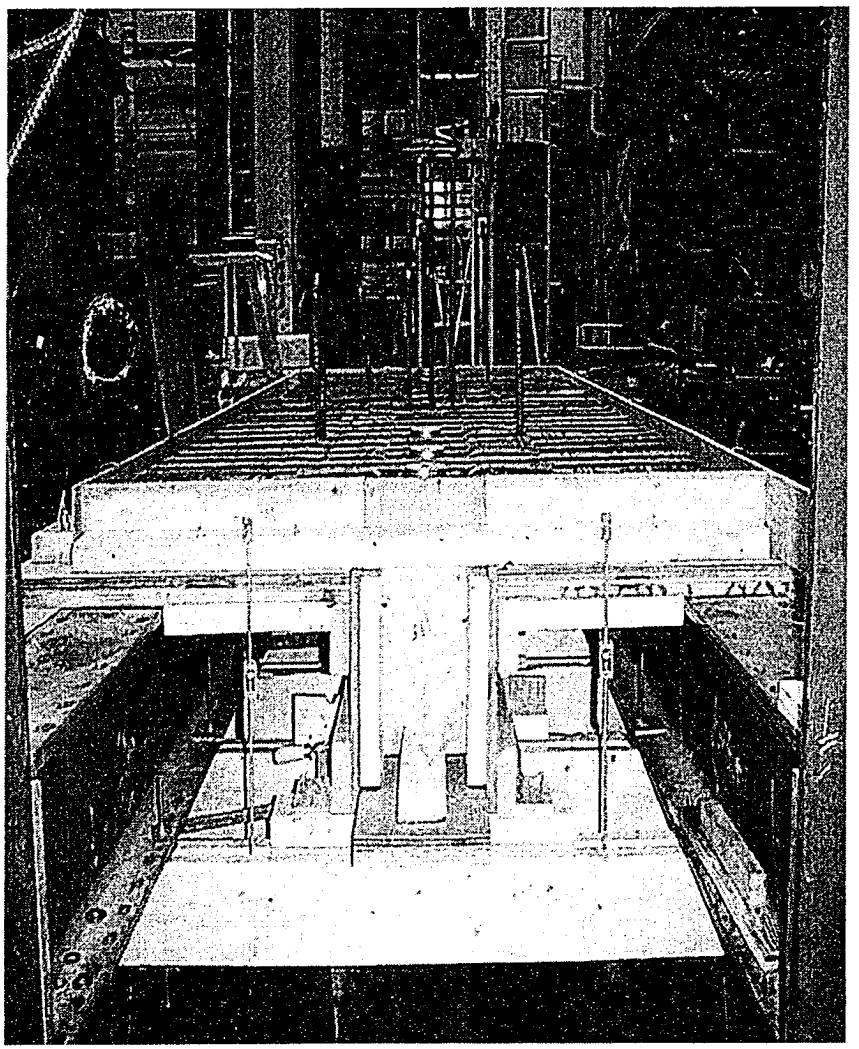

Left, Figure A.5. Specimen after Floor Forms Assembly

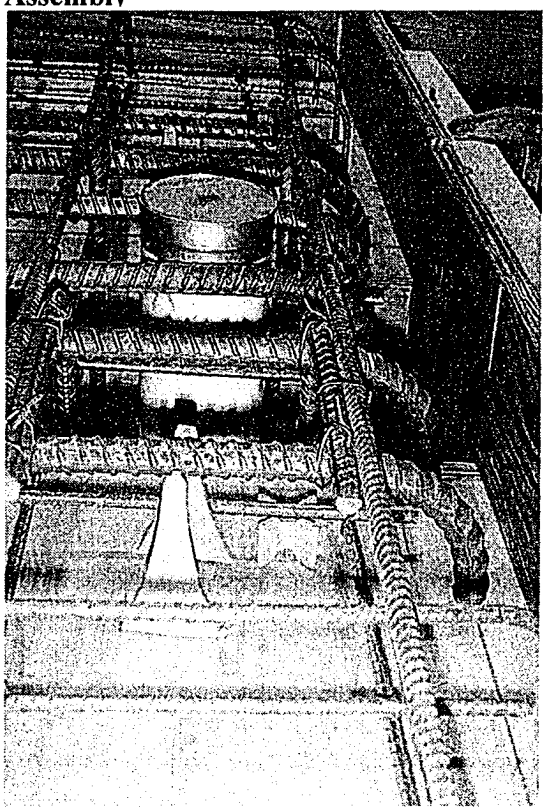

Figure A.6. Plastic Chairs for RFT and PVC Pipe for Loading Rod

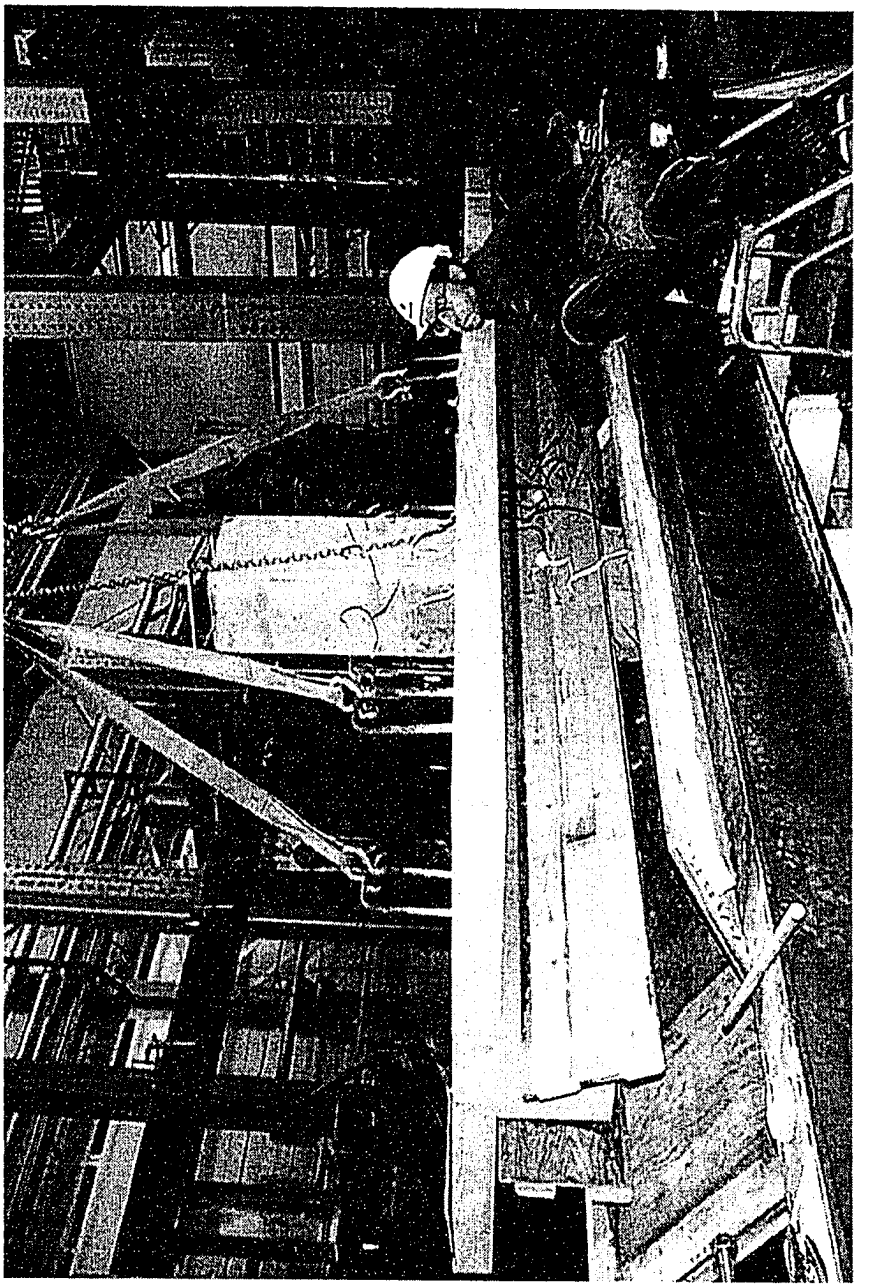

Figure A.7. Stripping of Floor Forms

APPENDIX A.2

Actual Dimensions

Table (A.1): As-Built Dimensions of Specimen 1

Specimen 1	Floor Dimensions mm											
	North						South					
	Col. Face	Col. Face	Sec. H.J.	Sec. H.J.	Main H.J.	Main H.J.	Col. Face	Col. Face	Sec. H.J.	Sec. H.J.	Main H.J.	Main H.J.
Dist. To Col. Face mm	0	0	725	725	1350	1350	0	0	725	725	1350	1350
t	101	101	101	102	101	101	102	101	101	101	101	101
d	363	362	362	363	363	362	363	362	362	362	362	363
b		250		250		250		250		250		250
L	1504	1504					1495	1495				
W		1428		1428		1428		1428		1428		1426

t: slab thickness mm

d: beam total depth mm

b: beam width mm

L: length of slab from edge to the column face mm

W: width of the slab mm

Spec. 1	Bottom Column			
	East Face	West Face	North Face	South Face
Distance from bottom	mm	mm	mm	mm
0	350	349	251	251
100	350	349	251	251
200	350	350	251	251
300	350	350	251	250
400	350	350	250	250
500	350	350	250	250
600	350	350	250	250
700	350	350	250	250
800	350	350	250	250

Spec. 1	Top Column			
	East Face	West Face	North Face	South Face
Distance from bottom	mm	mm	mm	mm
0	351	351	250	250
100	351	351	250	250
200	351	350	249	250
300	351	350	249	250
400	351	350	249	250
500	351	350	249	250
600	350	350	249	250
700	350	350	249	250
800	350	349	250	250

Misalignment:

long direction: 0 mm

short directio 2 mm

total

North (addiontal load is expected on the rebars of the North side)

Misalignment is measured as top to bottom centerline

Misalignment directions are those when specimens under MTS

Misalignment values are total actual values (+ or - 0.5 mm), no offset was done

Table (A.2): As-Built Dimensions of Specimen 2

Specimen 2	Floor Dimensions mm											
	North						South					
	Col. Face	Col. Face	Sec. H.J.	Sec. H.J.	Main H.J.	Main H.J.	Col. Face	Col. Face	Sec. H.J.	Sec. H.J.	Main H.J.	Main H.J.
Dist. To Col. Face mm	0	0	725	725	1350	1350	0	0	725	725	1350	1350
t	101	102	104	104	101	101	102	101	104	104	101	101
d	363	363	365	365	362	361	363	362	365	364	362	363
b		250		250		250		250		250		250
L	1518	1518					1485	1485				
W		1433		1432		1431		1430		1431		1432

t: slab thickness mm

d: beam total depth mm

b: beam width mm

L: length of slab from edge to the column face mm

W: width of the slab mm

Spec. 2	Bottom Column			
Distance from bottom	East Face mm	West Face mm	North Face mm	South Face mm
0	349	350	251	251
100	349	350	251	251
200	349	350	251	251
300	350	351	252	252
400	351	352	252	253
500	351	353	252	253
600	351	353	251	252
700	352	352	251	251
800	353	352	251	251

Spec. 2	Top Column			
Distance from bottom	East Face mm	West Face mm	North Face mm	South Face mm
0	351	351	250	250
100	352	351	250	250
200	352	351	250	250
300	352	351	251	250
400	352	352	251	252
500	353	352	251	252
600	353	352	251	252
700	353	352	251	252
800	353	351	251	251

Misalignment:

long direction: 0 mm

short direction 2 mm North (addiontal load is expected on the rebars of the North side)

total

Misalignment is measured as top to bottom centerline

Misalignment directions are those when specimens under MTS

Misalignment values are total actual values (+ or - 0.5 mm), no offset was done

Table (A.3): As-Built Dimensions of Specimen 3

Specimen 3	Floor Dimensions mm											
	North						South					
	Col. Face	Col. Face	Sec. H.J.	Sec. H.J.	Main H.J.	Main H.J.	Col. Face	Col. Face	Sec. H.J.	Sec. H.J.	Main H.J.	Main H.J.
Dist. To Col. Face mm	0	0	725	725	1350	1350	0	0	725	725	1350	1350
t	101	101	101	101	101	101	101	101	101	101	101	101
d	363	361	364	361	363	361	363	361	363	361	363	361
b		250		250		252		250		251		252
L	1520.5	1520.5					1466.5	1466.5				
W		1430		1432		1431		1430		1425		1423

t: slab thickness mm

d: beam total depth mm

b: beam width mm

L: length of slab from edge to the column face mm

W: width of the slab mm

Spec. 3	Bottom Column			
	East Face	West Face	North Face	South Face
Distance from bottom	mm	mm	mm	mm
0	351	352	250	250
100	351	352	251	251
200	351	352	251	250
300	351	352	251	251
400	351	352	251	251
500	351	353	250	252
600	351	352	250	252
700	350	352	250	251
800	350	351	250	251

Spec. 3	Top Column			
	East Face	West Face	North Face	South Face
Distance from bottom	mm	mm	mm	mm
0	350	350	251	252
100	350	350	251	251
200	350	351	251	251
300	352	351	251	251
400	353	352	251	251
500	354	352	251	251
600	354	352	251	251
700	350	351	251	251
800	350	350	251	251

Misalignment:

long direction: 0 mm

short direction 0 mm

Misalignment is measured as top to bottom centerline

Misalignment directions are those when specimens under MTS

Misalignment values are total actual values (+ or - 0.5 mm), no offset was done

Table (A.4): As-Built Dimensions of Specimen 4

Specimen 4	Floor Dimensions mm											
	North						South					
	Col. Face	Col. Face	Sec. H.J.	Sec. H.J.	Main H.J.	Main H.J.	Col. Face	Col. Face	Sec. H.J.	Sec. H.J.	Main H.J.	Main H.J.
Dist. To Col. Face mm	0	0	725	725	1350	1350	0	0	725	725	1350	1350
t	101	101	102	102	101	102	101	101	101	102	101	101
d	361	361	362	362	362	361	360	361	361	362	361	362
b		250		250		251		250		250		251
L	1512	1518					1495	1496				
W		1433		1433		1431		1431		1431		1431

t: slab thickness mm

d: beam total depth mm

b: beam width mm

L: length of slab from edge to the column face mm

W: width of the slab mm

Spec. 4	Bottom Column			
Distance from bottom	East Face	West Face	North Face	South Face
	mm	mm	mm	mm
0	349	349	251	251
100	350	350	251	251
200	350	350	251	251
300	351	351	251	251
400	351	352	252	251
500	351	351	251	251
600	351	351	251	251
700	350	351	251	251
800	350	351	251	251

Spec. 4	Top Column			
Distance from bottom	East Face	West Face	North Face	South Face
	mm	mm	mm	mm
0	350	350	254	251
100	350	350	253	251
200	350	350	252	251
300	350	350	252	251
400	352	351	252	252
500	353	351	252	252
600	354	352	251	251
700	354	353	251	251
800	355	352	250	251

Misalignment:

long direction: 0 mm

short direction 0 mm

Misalignment is measured as top to bottom centerline

Misalignment directions are those when specimens under MTS

Misalignment values are total actual values (+ or - 0.5 mm), no offset was done

Table (A.5): As-Built Dimensions of Specimen 5

Specimen 5	Floor Dimensions mm											
	North						South					
	Col. Face	Col. Face	Sec. H.J.	Sec. H.J.	Main H.J.	Main H.J.	Col. Face	Col. Face	Sec. H.J.	Sec. H.J.	Main H.J.	Main H.J.
Dist. To Col. Face mm	0	0	725	725	1350	1350	0	0	725	725	1350	1350
t	101	100	100	100	101	100	101	100	101	100	101	101
d	361	361	361	360	361	360	361	360	362	360	361	362
b	250		250		251		250		250		251	250
L	1510	1510					1475	1475				
W		1430		1430		1430		1430		1430		1430

t: slab thickness mm

d: beam total depth mm

b: beam width mm

L: length of slab from edge to the column face mm

W: width of the slab mm

Spec. 5	Bottom Column			
Distance from bottom	East Face	West Face	North Face	South Face
	mm	mm	mm	mm
0	350	350	251	250
100	350	350	251	250
200	350	350	251	250
300	350	350	251	250
400	350	351	250	250
500	350	351	250	250
600	350	351	250	250
700	350	351	250	250
800	350	351	250	250

Spec. 5	Top Column			
Distance from bottom	East Face	West Face	North Face	South Face
	mm	mm	mm	mm
0	349	350	250	250
100	349	350	250	250
200	349	350	250	250
300	350	350	250	250
400	350	350	250	250
500	350	350	251	251
600	350	350	251	251
700	351	350	251	251
800	351	350	252	251

Misalignment:

long direction: 0 mm

short direction 2.5 mm North (addiontal load is expected on the bottom rebars of the South side)

after offset

Misalignment is measured as top to bottom centerline

Misalignment directions are those when specimens under MTS

Misalignment values are those actual values (+ or - 0.5 mm) under MTS

(after making offset with the same amount to the opposite side)

Table (A.6): As-Built Dimensions of Specimen 6

Specimen 6	Floor Dimensions mm											
	North						South					
	Col. Face	Col. Face	Sec. H.J.	Sec. H.J.	Main H.J.	Main H.J.	Col. Face	Col. Face	Sec. H.J.	Sec. H.J.	Main H.J.	Main H.J.
Dist. To Col. Face mm	0	0	725	725	1350	1350	0	0	725	725	1350	1350
t	100	101	100	101	100	100	100	100	101	100	100	101
d	360	361	361	361	362	361	360	361	361	361	361	361
b	250		250		251		250		250		251	250
L	1535	1535					1484	1484				
W		1417		1417		1417		1415		1417		1417

t: slab thickness mm

d: beam total depth mm

b: beam width mm

L: length of slab from edge to the column face mm

W: width of the slab mm

Spec. 6	Bottom Column			
	East Face	West Face	North Face	South Face
Distance from bottom	mm	mm	mm	mm
0	348	350	250	250
100	348	350	250	250
200	348	350	250	250
300	347	348	250	250
400	347	348	251	250
500	347	348	251	250
600	347	350	251	251
700	348	350	251	251
800	348	350	251	251

Spec. 6	Top Column			
	East Face	West Face	North Face	South Face
Distance from bottom	mm	mm	mm	mm
0	348	348	250	250
100	350	349	250	250
200	350	349	250	250
300	349	350	250	250
400	348	349	250	250
500	347	348	250	250
600	348	347	251	250
700	348	348	251	250
800	348	348	251	250

Misalignment:

long direction: 0 mm

short direction 3 mm North (addiontal load is expected on the bottom reb

after offset

Misalignment is measured as top to bottom centerline

Misalignment directions are those when specimens under MTS

Misalignment values are those actual values (+ or - 0.5 mm) under MTS

(after making offset with the same amount to the opposite side)

the effect of these misaligenemt values, can be quantified by

adding/ subtracting moment-effect load equivalent values on both sides.

Table (A.7): As-Built Dimensions of Specimen 7

Specimen 7	Floor Dimensions mm											
	North						South					
	Col. Face	Col. Face	Sec. H.J.	Sec. H.J.	Main H.J.	Main H.J.	Col. Face	Col. Face	Sec. H.J.	Sec. H.J.	Main H.J.	Main H.J.
Dist. To Col. Face mm	0	0	725	725	1350	1350	0	0	725	725	1350	1350
t	100	101	100	101	100	101	101	101	102	104	103	104
d	357	359	362	362	362	361	361	361	362	363	364	364
b	250		250		250		250		250		250	
L	1520	1520					1560	1560				
W		1425		1430		1433		1425		1434		1437

t: slab thickness mm

d: beam total depth mm

b: beam width mm

L: length of slab from edge to the column face mm

W: width of the slab mm

Spec. 7	Bottom Column			
Distance from bottom	East Face	West Face	North Face	South Face
	mm	mm	mm	mm
0	347	349	250	250
100	348	347	250	250
200	348	347	250	250
300	347	348	250	250
400	347	349	250	250
500	347	350	250	250
600	347	350	250	250
700	347	349	250	250
800	346	345	250	250

Spec. 7	Top Column			
Distance from bottom	East Face	West Face	North Face	South Face
	mm	mm	mm	mm
0	350	349	250	250
100	350	350	250	250
200	353	351	250	250
300	353	351	250	250
400	353	352	250	250
500	351	353	250	250
600	350	352	250	250
700	350	351	250	250
800	349	349	250	250

Misalignment:

long direction: 3 mm East (addiontal load is expected on the bottom rebar Misalignment is measured as top to bottom centerline

short direction 3 mm South (addiontal load is expected on the bottom reb Misalignment directions are those when specimens under MTS

with offset Misalignment values are those actual values (+ or - 0.5 mm) under MTS

(after making offset with the same amount to the opposite side)

APPENDIX B

Test Observations

This appendix contains the main and important observations reported during each test. Included are when test started, when it finished, and maximum floor and column loads. The following abbreviations stand for their corresponding definitions: UTM stands for the universal testing machine 6000 used for applying the column loads; HJ is the hydraulic jack used for applying the loads on the floor. SG is the foil strain gauge mounted on the steel rebars. CG is the embedded concrete gauge placed in the core. N, S, E and W are the north, south, east and west directions of the specimen while being tested.

Test of Specimen SP1:
Test started at: 11.35 am, Monday July 28, 2003
Test finished at: 3.30 pm, Monday July 28, 2003
Maximum floor load (kN) : 342 kN
Maximum column load (kN) : 3636 kN

Applied Load (kN)		Observations	Comments
On Floor	On Column		
108 kN (31%)	1575 kN (43%)	CG38, joint part, showed a strain of –2000μ ε,	Hair cracks on slab top surface in short direction
	1770 kN (49%),	CG38 showed a strain of –2300μ ε,	
	1900 kN	CG38 showed a strain of –2570μ ε,	
	2000 kN (55%),	CG38 showed a strain of –2900μ ε,	Two cracks were found at top column/ slab edge parallel to the beam longitudinal axis
	2200 kN (61%),	SG36 showed a strain of –4230μ ε,	
	2400 kN (66%),	SG36 showed a strain of –7200μ ε, SG57 showed a strain of +1530μ ε,	
140 kN (41%)	2350 kN		Few hair cracks appeared on the top of the slab
160 kN (47%)	2450 kN (67%),	SG36 showed a strain of –7900μ ε, SG57 showed a strain of +2000μ ε,	Maximum flexural crack width, slab top surface was 0.3 mm
200 kN (58%),	2500 kN (69%),	SG36 showed a strain of –8130μ ε,	Hair cracks started to appear on the bottom surface of the slab
244 kN (71%)			Maximum flexural crack width, slab top surface was 0.5 mm
280 kN (82%)		SG37 showed a strain of –8300μ ε, SG57 showed a strain of +3600μ ε,	Maximum flexural crack width was 0.6 mm; maximum shear width crack was 0.3; beam bottom cover started pealing
	2800 kN (77%),	SG37 showed a strain of –8900μ ε, SG57 showed a strain of +4860μ ε,	Cover of the joint part started to peal off. Service column load.
324 kN (95%),		SG36 showed a strain of –9400μ ε, SG57 showed a strain of +9000μ ε,	Beam bottom cover started spalling; joint started pealing off.
342 kN (100%)			The joint cover started to spall off; beam bottom reinforcement buckled; floor collapsed.
	3043 kN (83%),	SG36 & SG33 showed a strain of –11300μ ε,	
	3600 kN (99%),	SG33 showed a strain of –20000μ ε, SG36 reading dropped to –4500 μ ε.	Joint S-face spalled off completely; Concrete in the joint area started to fall apart.
	3636 kN (100%)		Vertical rebars buckled and specimen failed.

Test of Specimen SP2:
Test started at: 8.15 am, Wednesday June 04, 2003
Test finished at: 1.00 pm, Wednesday June 04, 2003
Maximum HJ load (kN) : 80 kN
Maximum UTM load (kN) : 4607 kN

Applied Load (kN)		Observations	Comments
On Floor	On Column		
108 kN			Hair cracks on slab top surface in short direction
160 kN			More cracks were marked
	3100 kN (67%),	SG36 showed a strain of –5300μ ε,	
	3457 kN (75%),	SG36 showed a strain of –6100μ ε,	Cover started to crack on the S- face of the joint
	3800 kN (82%),	SG36 showed a strain of –7300μ ε,	Cover started to spall of the S-face
	4200 kN (91%),	SG36 showed a strain of –9700μ ε,	Cracks appeared on the bottom surface of the slab; cracks around the column widened
	4400 kN (96%),	SG37 showed a strain of –12560μ ε,	Cover completely fell off of the joint S- face;
	4590 kN (99%),	CG38 showed a strain of –18500μ ε,	First apparent peak load
	4607 kN (100%)	CG38 showed a strain of –21300μ ε	Maximum UTM load.

Test of Specimen SP3:
Test started at: 8.30 am, Monday July 07, 2003
Test finished at: 12.0 pm, Tuesday July 08, 2003
Maximum HJ load (kN) : 204 kN
Maximum UTM load (kN) : 6700 kN

Applied Load (kN)		Observations	Comments
On Floor	On Column		
160 kN (39%)		Beam top reinforcement showed a maximum strain of +1697μ ε,	Hair cracks on slab top surface in short direction
194 kN		Beam top reinforcement showed a maximum strain of +2000μ ε,	Few more cracks appeared on the slab top surface and some hair shear cracks appeared on the beam sides
	4000 kN (60%),	SG6 showed a strain of –1900μ ε,	
	4500 kN (67%),	SG6 showed a strain of –2150μ ε,	
	4750 kN (71%),	SG6 showed a strain of –2300μ ε,	
	5037 kN (75%),	SG6 showed a strain of –2660μ ε,	Some hair cracks were noticed on the bottom column
	5100 kN (76%)	SG6 showed a strain of –3150μ ε,	Service load on column
210 kN,			New cracks were merely extension of the old shear cracks
240 kN,			Cracks appeared on the slab bottom surface; shear cracks extended but not much; and previously marked cracks widened with a maximum width =0.3 mm
274 kN,		SG60 showed a strain of +2770μ ε,	
290 kN till a false load of 840 kN		Bars used for floor-loading yielded although testing sample of them showed a yield stress of 1000 MPa, enough to carry on the test.	Previously marked cracks widened with a maximum width =0.4 mm; maximum shear crack width 0.15 mm
300 kN (74%),		SG60 showed a strain of +6000 μ ε; SG6 showed a strain of -3300μ ε,	New cracks appeared and were marked; and the SW corner of the top column showed little pealing off; Maximum flexural crack width was 0.8; Maximum shear crack width was 0.4 mm;
330 kN (81%),		four out of 6 strain gages of the beam top reinforcement showed yielding;	
364 kN (89%),		SG57 showed a strain of +11000μ ε,	Maximum flexural crack width was 0.9-1.0 mm; Maximum shear crack width was 0.7 mm;
374 kN (92%),		SG57 showed a strain of +14000μ ε,	Flexural cracks condensed with maximum width of 1.3 mm; Maximum shear crack width was 1.0 mm.
408 kN			Maximum flexural crack width was 2.5 mm; Maximum shear crack width was 1.5 mm;
	6700 kN (100%)	sudden failure at the upper part of the column	Ties was snapped off at the SE corner and the rebars buckled.

Test of Specimen SP4:
Test started at: 8.30 am, Wednesday June 18, 2003
Test finished at: 12.0 pm, Wednesday June 18, 2003
Maximum HJ load (kN) : 80 kN
Maximum UTM load (kN) : 5583 kN

Applied Load (kN)		Observations	Comments
On Floor	On Column		
108 kN		beam top reinforcement showed a maximum strain value of +1080 μ ε.	Hair cracks on slab top surface in short direction
160 kN			More cracks were marked
	3200 kN (57%)	SG31 showed a strain of –1920μ ε,	
48 kN	4200 kN (75%),	SG31 showed a strain of –3500μ ε,	Minor cracks appeared on bottom of the top column
112 kN		beam top reinforcement showed a maximum strain value of +1150 μ ε.	
140 kN		beam top reinforcement showed a maximum strain value of +1370 μ ε.	
160 kN		beam top reinforcement showed a maximum strain value of +1550 μ ε.	
	5000 kN (90%)	SG31 showed a strain of –6290μ ε,	Radial cracks were marked at top of the slab;
	5180 kN (93%),	SG31 showed a strain of –6500μ ε,	Much cracking with severe ones appeared on the cover of the S- lower face
	5500 kN (98%)		Little particles were fallen off the joint
180 kN	unload		Some little shear cracks were marked on the beam
160 kN	5570 kN (99.8%)		Cover at the lower interface started to spall
	5583 kN (100%)	SG33 showed a strain of –8300μ ε	Rebars buckled on the S-side.

Test of Specimen SP5:
Test started at: 9.30 am, Thursday July 31, 2003
Test finished at: 12.30 pm, Wednesday June 18, 2003
Maximum HJ load (kN) : 94 kN
Maximum UTM load (kN) : 4558 kN

Applied Load (kN)		Observations	Comments
On Floor	On Column		
90 kN	3000 kN (66%)		Hair cracks on slab top surface in short direction
162 kN			More cracks on slab top surface in short direction; maximum flexural crack width of 0.4 mm
169 kN	3000 kN (66%),	SG57 showed a strain of +1700μ ε, SG36 showed a strain of +5500μ ε,	
	3600 kN (79%),		First vertical cracks appeared on the joint S-face
188 kN	3700 kN (81%),	one single new crack on the floor between two older cracks	Maximum flexural crack width at slab top surface was 0.5 mm while maximum shear crack width was 0.3 mm
	3690 kN	SG36 showed a strain of -7600μ ε, SG57 showed a strain of +2000μ ε,	
	3960 kN (87%),	SG36 showed a strain of -10000μ ε,	
	4000 kN (88%),		Radial cracks stemmed from the column corners
	4250kN (93%),		Cracks of the joint top portion intensified
	4300 kN (94%),		Cracks in the bottom column cover started showing up.
	4360 kN,		Joint cover started to spall off
	4400 kN (97%),	cracks at the NE corner of the top column and at the cover of the W-face appeared	Radial cracks expanded and circumferential cracks around the column widened; Maximum flexural crack width increased to 0.6 mm
	4417 kN,	SG36 showed a strain of -19000μ ε,	
	4470 kN,	SG36 showed a strain of -20000μ ε,	
	4500 kN,	SG36 showed a strain of -27000μ ε, SG57 showed a strain of +3000μ ε,	
	4528 kN (99%)	SG34 showed a strain of -2000μ ε, SG57 showed a strain of +3200μ ε,	
	4550 kN,	SG36 showed a strain of -27400μ ε, SG34 showed a strain of -26000μ ε,	Buckling of the vertical rebars
	4558 kN (100%)	SG38showed a strain of -26000μ ε,	Cracks at the top slab appeared all around the column; crack width of the W lower part of the column was 7 mm.
	4400 kN	SG60 showed a strain of -26000μ ε, SG59 showed a strain of +24000μ ε	

Test of Specimen SP6:
Test started at: 9.0 am, Thursday August 21, 2003
Test finished at: 1.0 pm, Thursday August 21, 2003
Maximum HJ load (kN) : 188 kN
Maximum UTM load (kN) : 4170 kN

Applied Load (kN)		Observations	Comments
On Floor	On Column		
92 kN			Hair cracks on slab top surface in short direction; hair cracks were noticed at the column/ beam interface and extended below the slab
	2400 kN (58%),	No cracks were observed	
161 kN (43%)			Hair shear cracks appeared on all beam sides; lots of hair flexural cracks on the slab top; Transverse cracks on bottom of the slab
	3000 kN (72%),	SG37 showed a strain of -3600μ ε, SG60 showed a strain of +1900μ ε,	Vertical hair cracks were observed on the N- face of the join
200 kN (53%)		SG60 showed a strain of +2170μ ε,	Shear cracks extended but not widened; not much extra cracks on top of the slab;
240 kN (64%),		SG60 showed a strain of +2500μ ε,	Maximum flexural crack width at slab top surface was 0.3 mm and maximum shear crack width was 0.25
282 kN (75%),		SG60 showed a strain of +2900μ ε,	Maximum flexural crack width at slab top surface was 0.5 mm and maximum shear crack width was 0.3
320 kN (85%)		SG60 showed a strain of +3600μ ε,	Maximum flexural crack width at slab top surface was 0.6 mm
360 kN (96%),		SG60 showed a strain of +6570μ ε,	Maximum flexural crack width at slab top surface was 0.9 mm and maximum shear crack width was 0.5
376 kN (100%),		SG57 showed a strain of +9600μ ε,	Floor failed, beam bottom rebars buckled
	3400 kN (81%),	SG37 showed a strain of -5800μ ε,	
	3600 kN (86%),	SG37 showed a strain of -7000μ ε, side bars yielded	Joint cover started to peal,
	3880 kN (93%),	SG35 showed a strain of -10000μ ε,	
	3930 kN,	SG31 showed a strain of -11300μ ε,	Column S-rebars buckled at the joint/column interface
	4040 kN (97%),	SG35 showed a strain of -13500μ ε,	Cover continued to spall of the joint, crack of the S- cover widened.
	4100 kN (98%),	SG35 showed a strain of -14500μ ε,	Crack of the lower S-cover widened more
	4170 kN (100%)		S-cover was almost detachable.

Test of Specimen SP7:
Test started at: 9.00 am, Wednesday August 27, 2003
Test finished at: 12.10 pm, Wednesday August 27, 2003
Maximum HJ load (kN) : 80 kN
Maximum UTM load (kN) : 2783 kN

Applied Load (kN)		Observations	Comments
On Floor	On Column		
90 kN			Hair cracks on slab top surface in short direction
	1500 kN (54%),		No change was found
48 kN			No change was found
160 kN		SG57 showed a strain of +1600μ ε,	More cracks were noticed on top of the slab with a maximum width of 0.3 mm
	1760 kN (63%),	CG20 showed a strain of -1460μ ε,	
	2000 kN (72%),	CG20 showed a strain of -1800μ ε,	
	2200 kN (79%),	CG20 showed a strain of -2300μ ε,	Vertical cracks started to appear on top column; LVDT L3-H-N was bumped down but it was put back again
	2540 kN (91%),	CG20 showed a strain of -3160μ ε, SG36 showed a strain of -2900μ ε,	More vertical cracks were seen on the top part and some vertical cracks started to appear on the lower part
	2670 kN (96%),	Maximum vertical rebar strain was as close as –4400 μ ε in all parts	Bottom column was more damaged than the top one
	2783 kN (100%)	SG6 showed a strain of -6600μ ε, SG15 showed a strain of -6990μ ε, SG36 showed a strain of -5600μ ε	Cover of top column started to spall off; NW corner rebar buckled, bottom column collapsed.

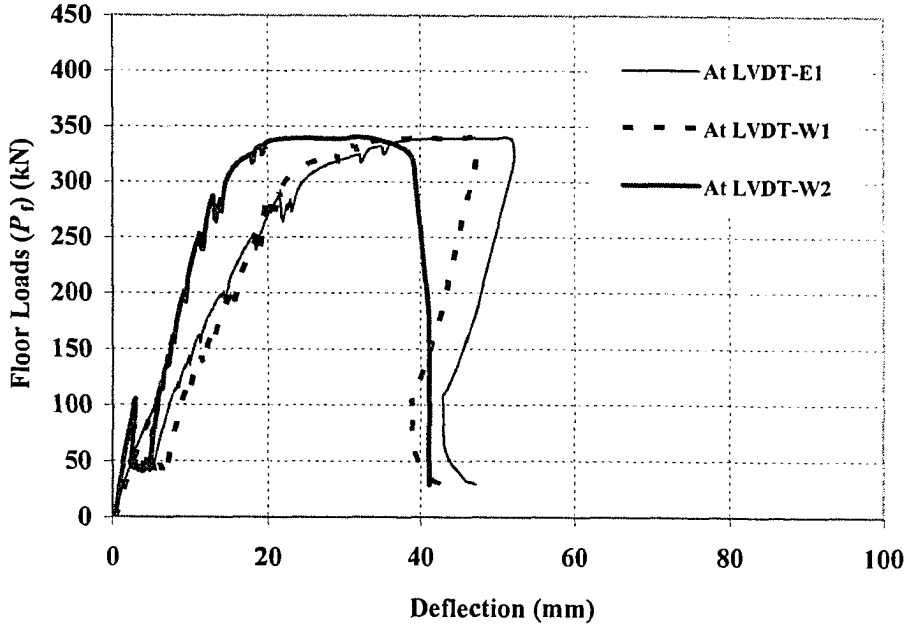

Figure B.1 Floor Loads vs. Floor Deflecetion for SP1

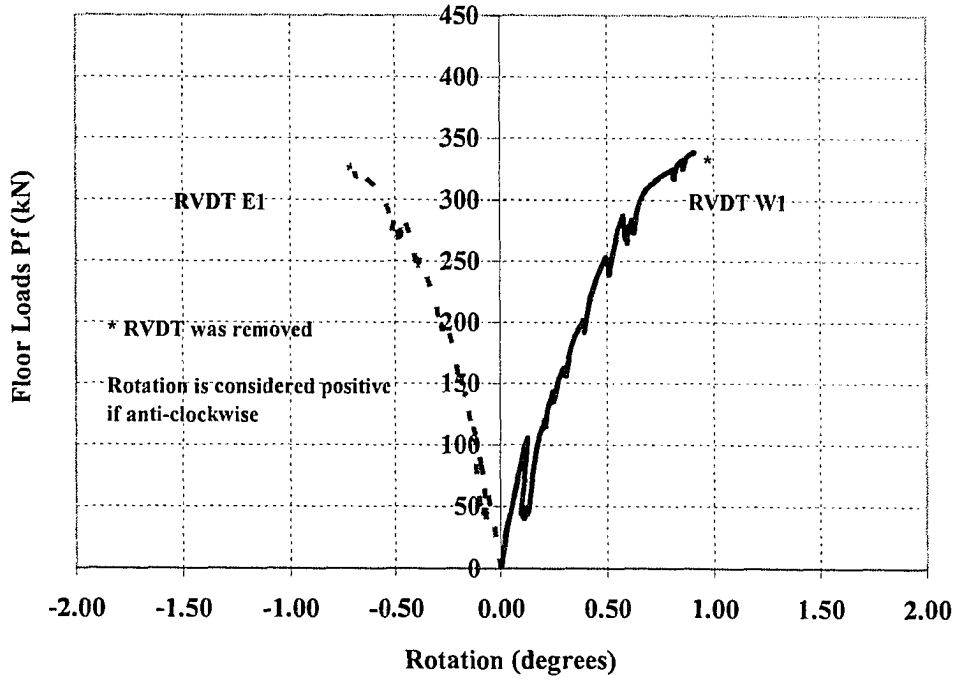

Figure B.2 Floor Loads vs. Beam Rotation for SP1

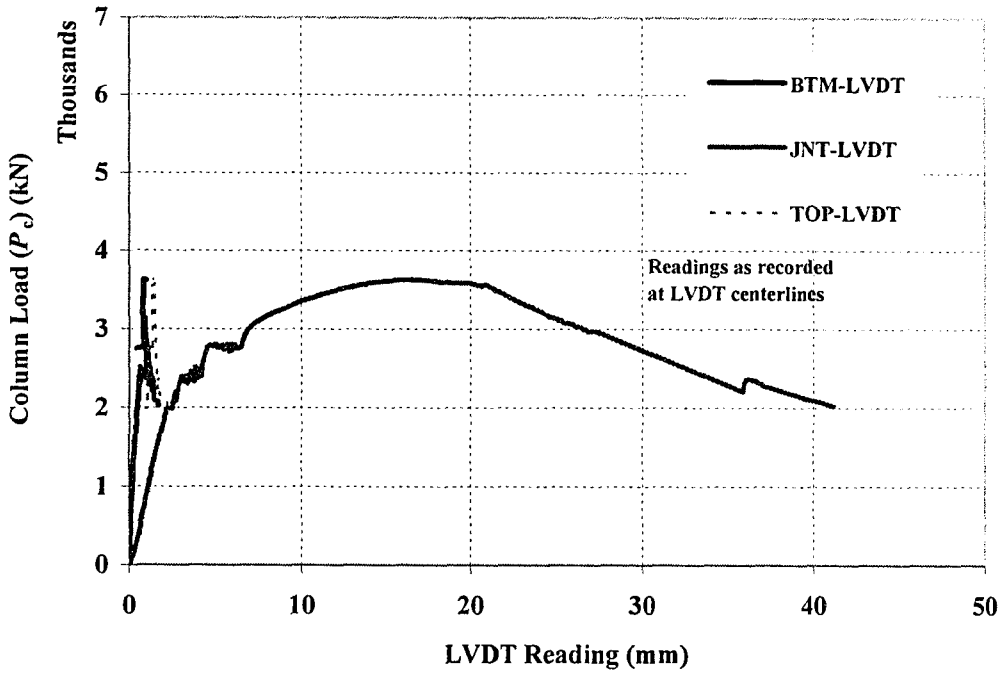

Figure B.3 Column Load vs. Vertical LVDT Readings (SP1)

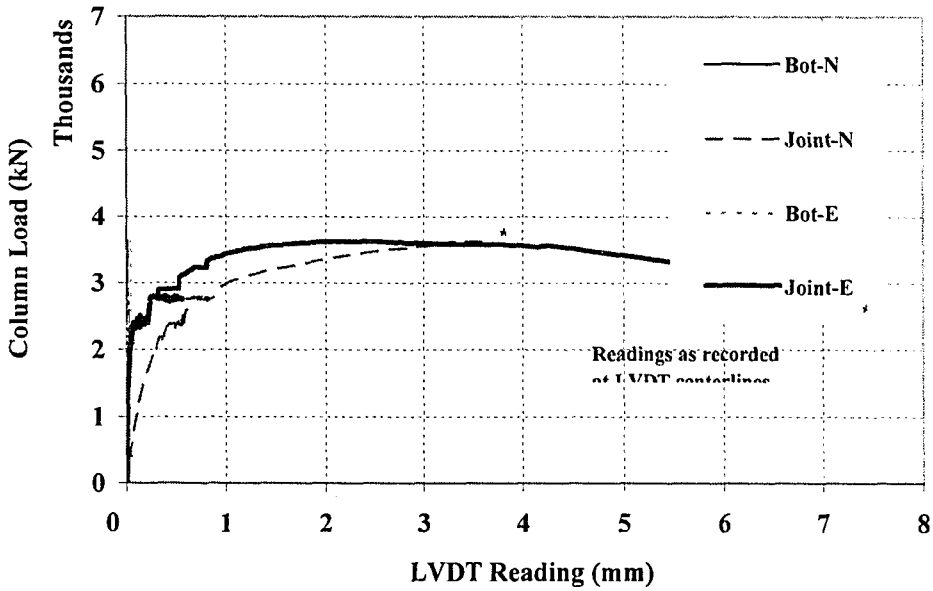

Figure B.4 Column Load vs. Horizontal LVDT Readings (SP1)

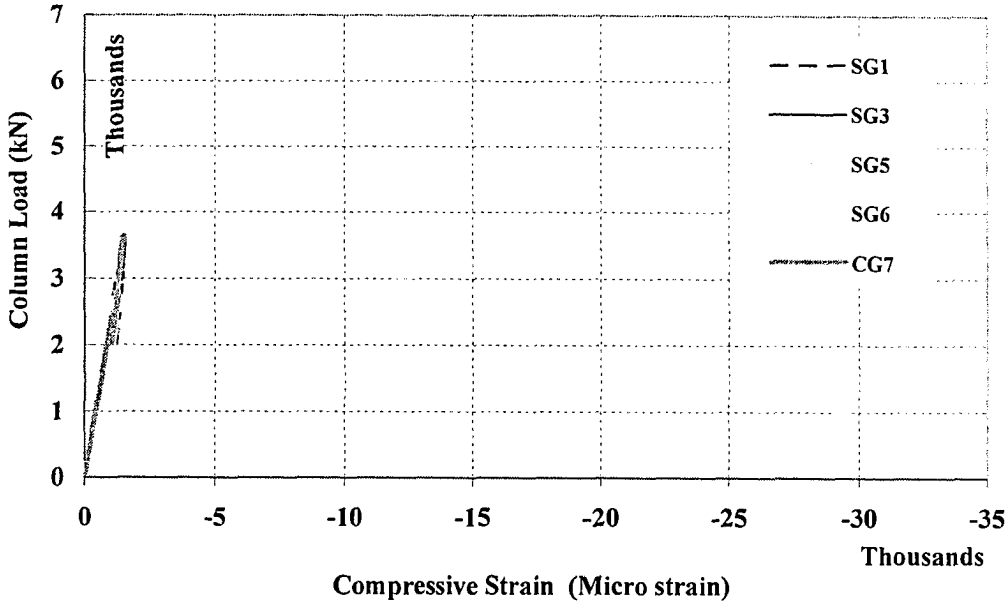

Figure B5. Vertical Load vs. Vertical Strain Values in Bottom Column of SP1

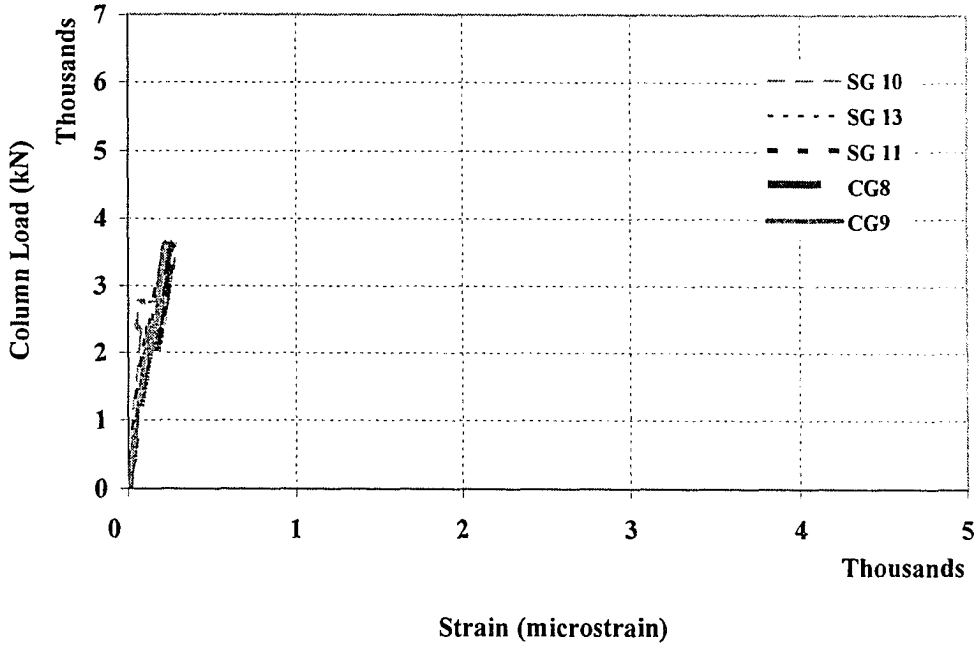

Figure B6. Vertical Load vs. Lateral Strain Values in Bottom Column of SP1

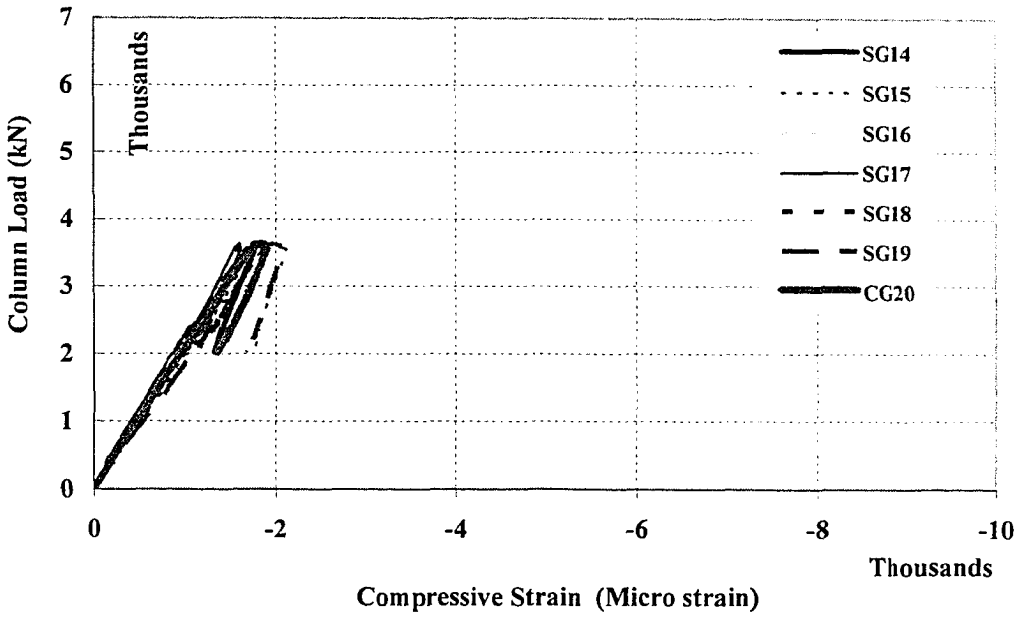

Figure B7. Vertical Load vs. Vertical Strain Values in Top Column of SP1

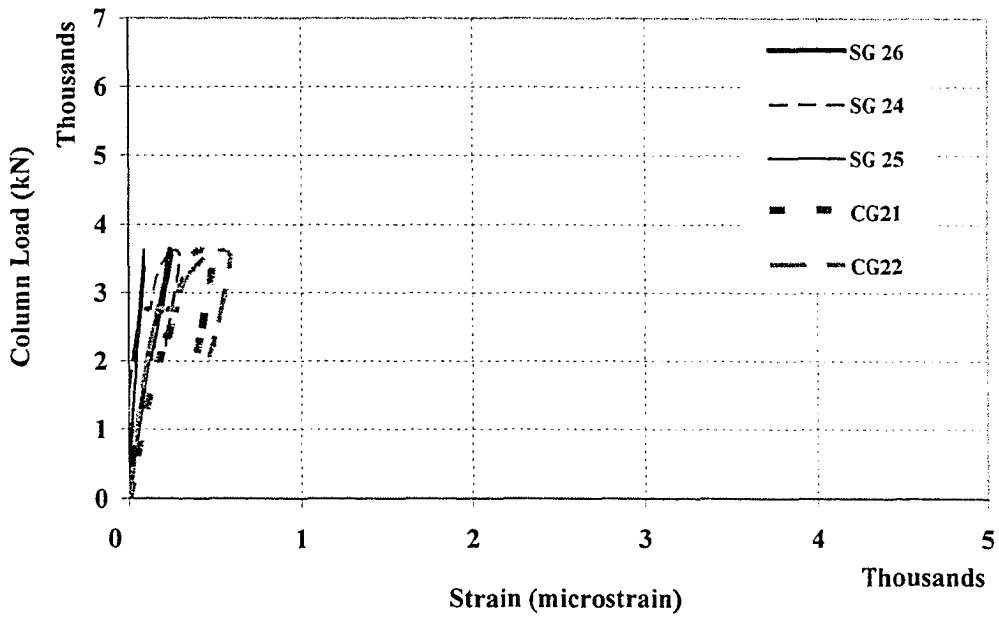

Figure B8. Vertical Load vs. Lateral Strain Values in Top Column of SP1

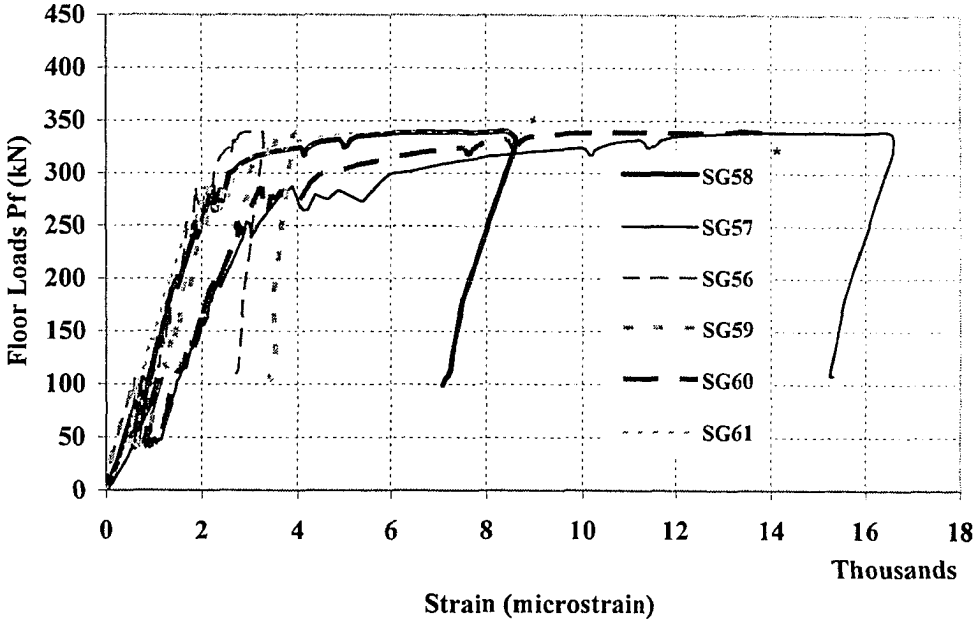

Figure B9. Floor Loads vs. Strain Values of Beam Top Rebars (SP1)

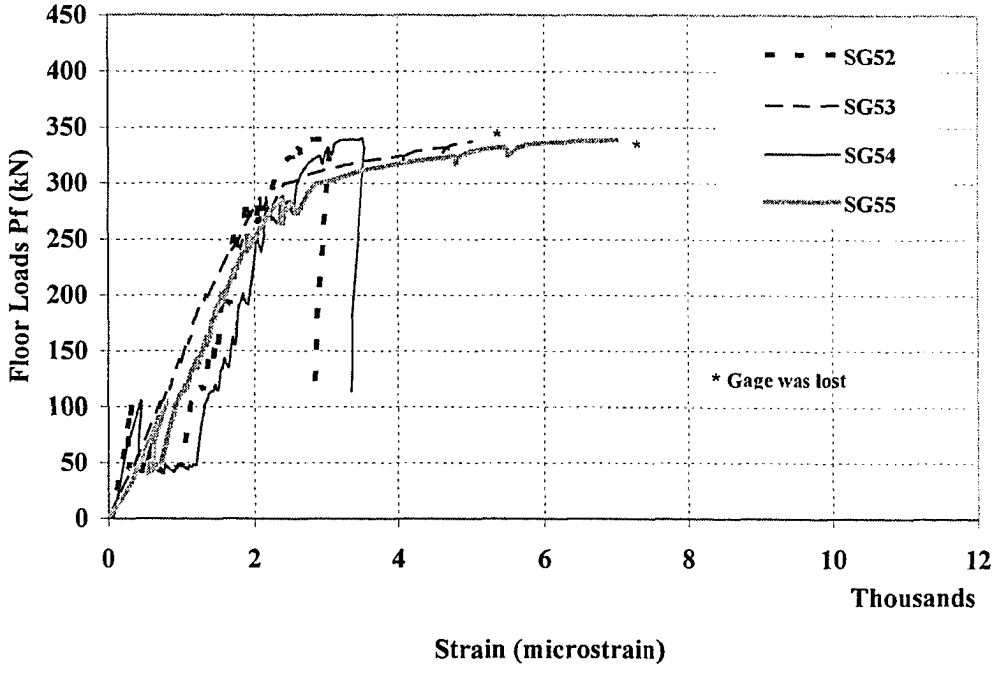

Figure B10. Floor Loads vs. Strain Values of Beam Side Rebars (SP1)

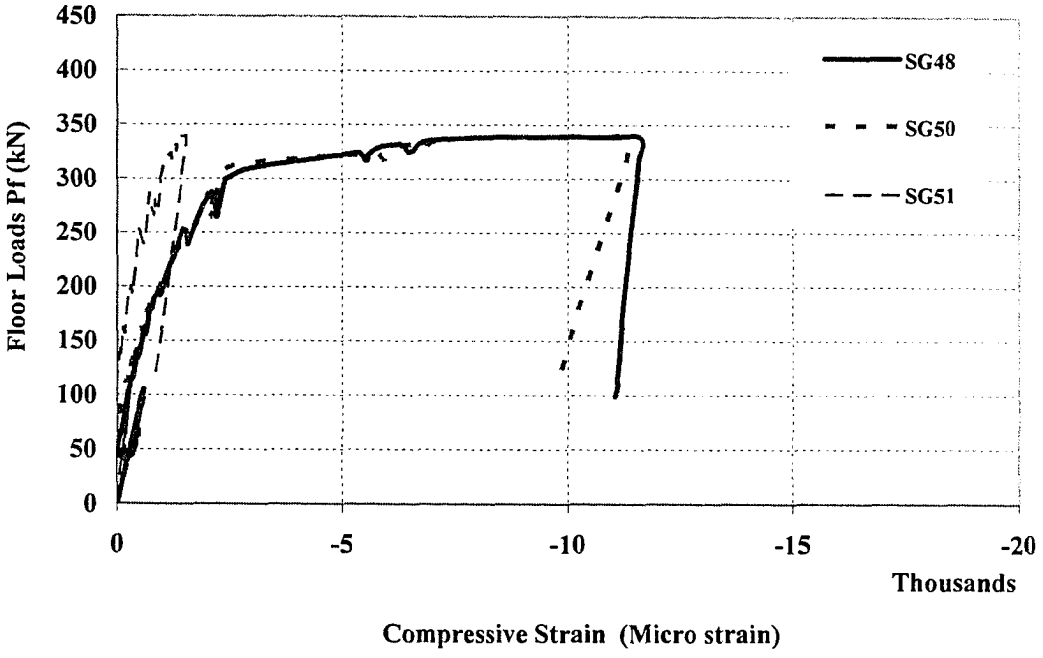

Figure B11. Floor Loads vs. Strain Values of Beam Bottom Rebars (SP1)

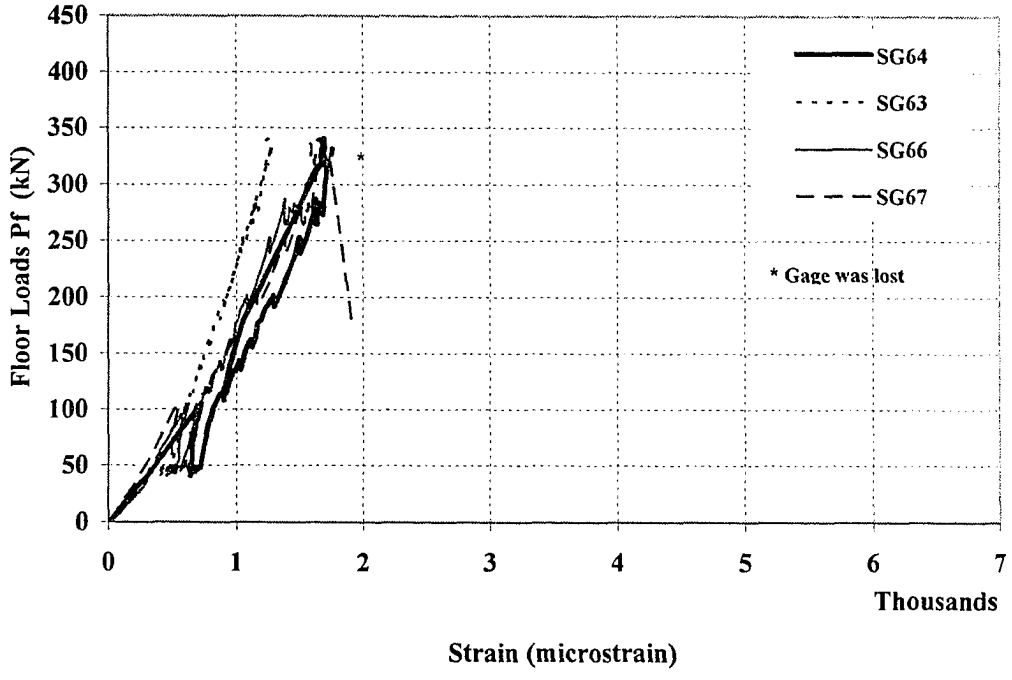

Figure B12 Floor Loads vs. Strain Values of Slab Top Rebars (SP1)

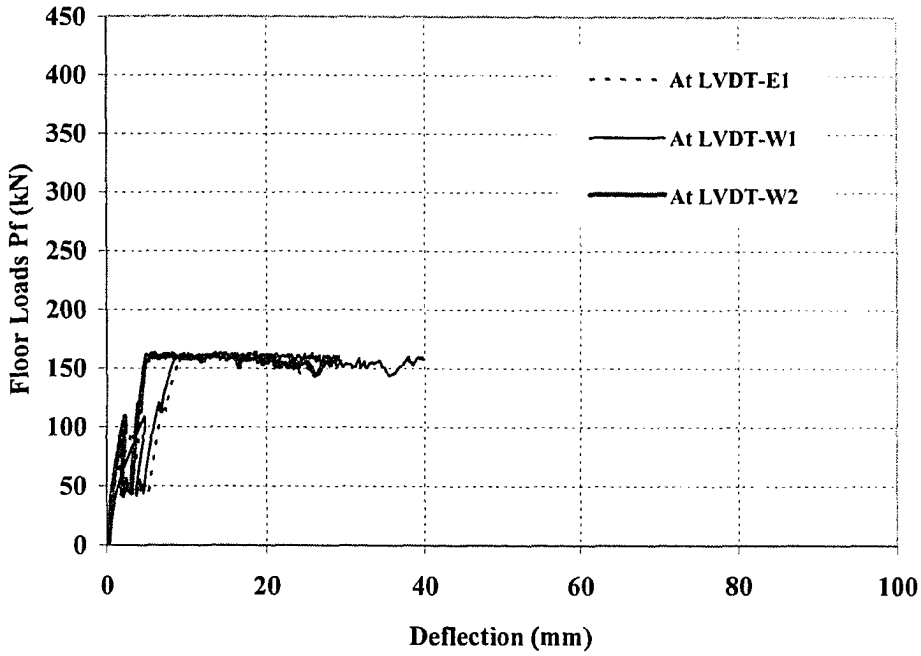

Figure B13. Floor Loads vs. Beam Deflection for SP2

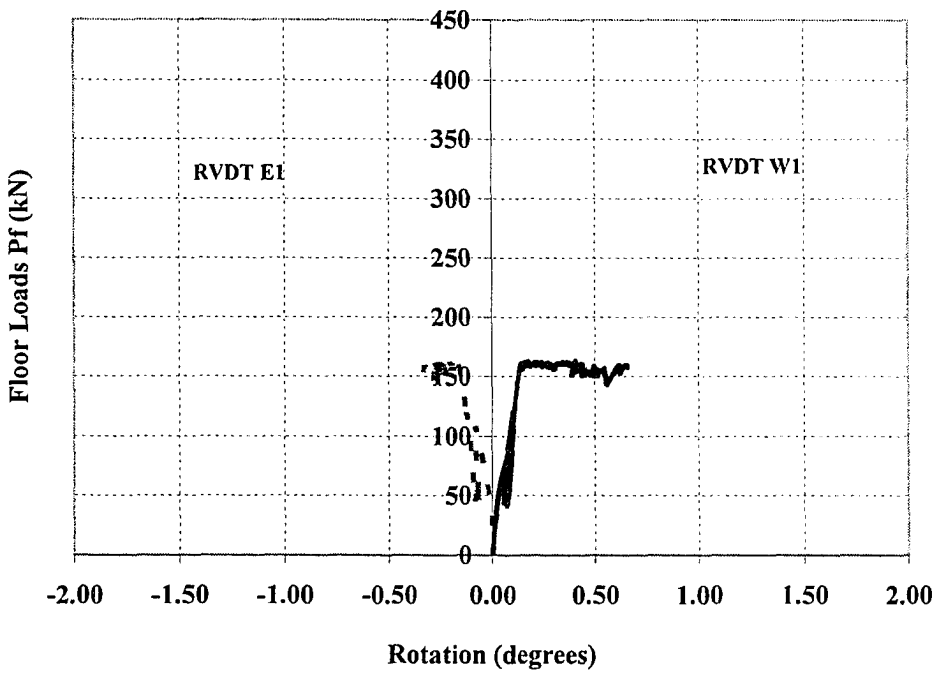

Figure B14. Floor Loads vs. Beam Rotation for SP2

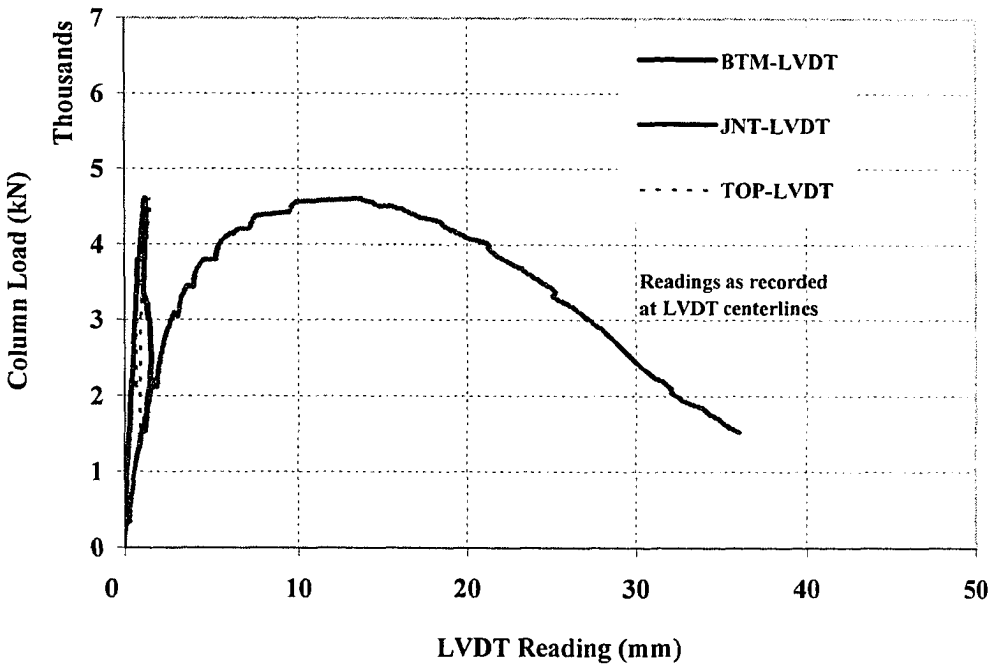

Figure B15. Column Load vs. Vertical LVDT Readings (SP2)

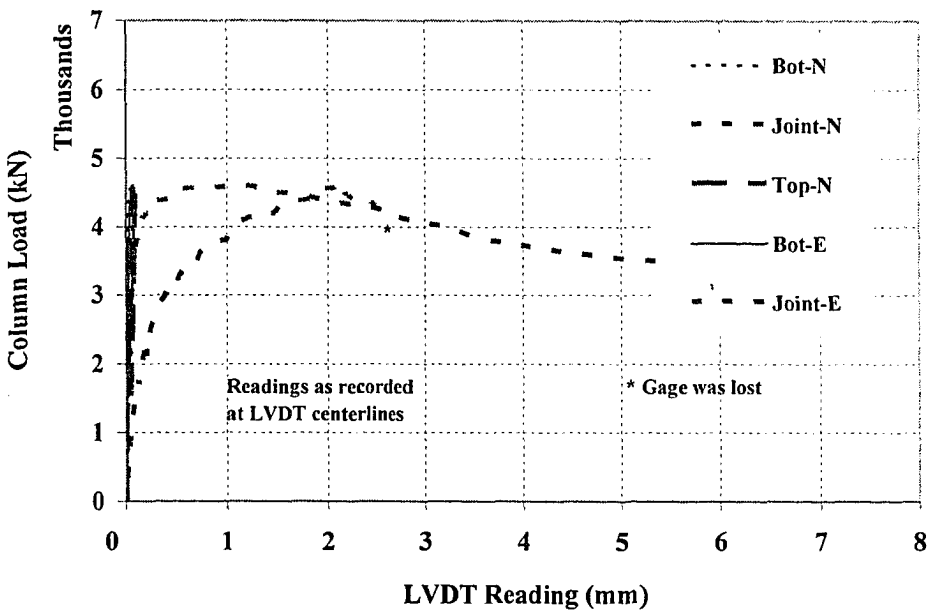

Figure B16. Column Load vs. Horizontal LVDT Readings (SP2)

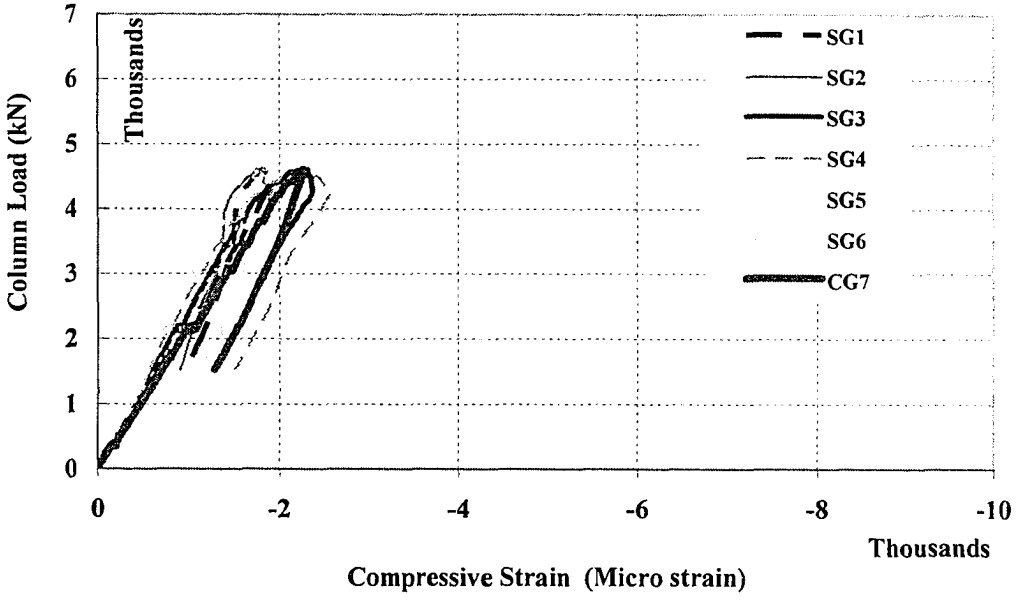

Figure B17. Vertical Load vs. Vertical Strain Values in Bottom Column of SP2

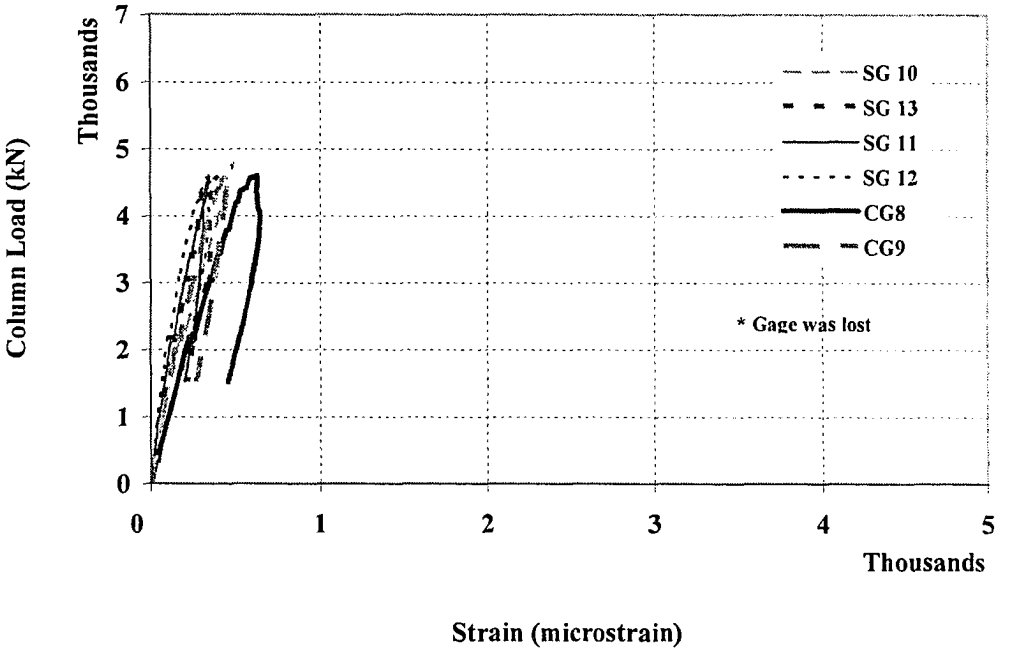

Figure B18. Vertical Load vs. Lateral Strain Values in Bottom Column of SP2

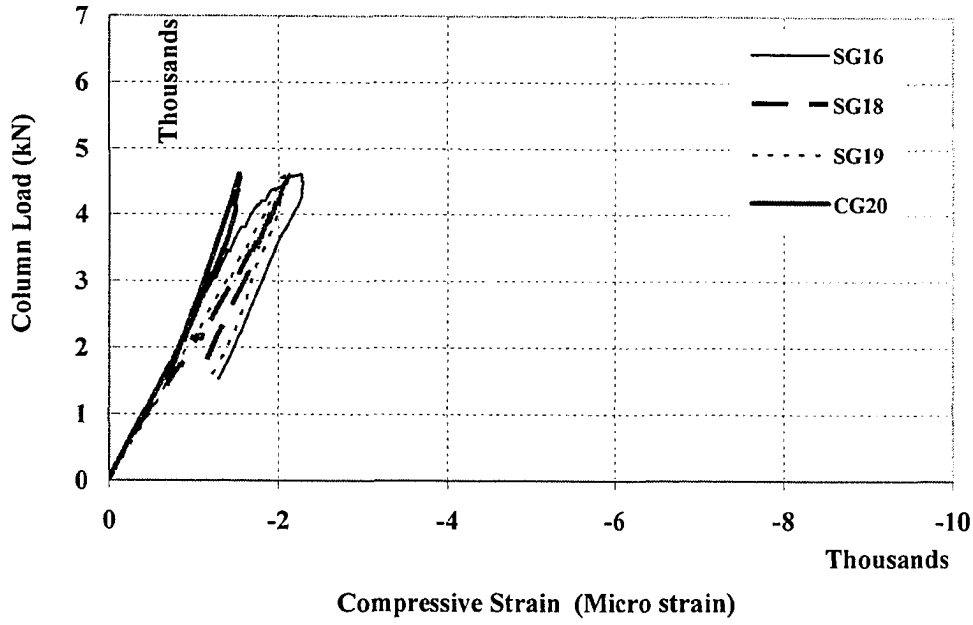

Figure B19. Vertical Load vs. Vertical Strain Values in Top Column of SP2

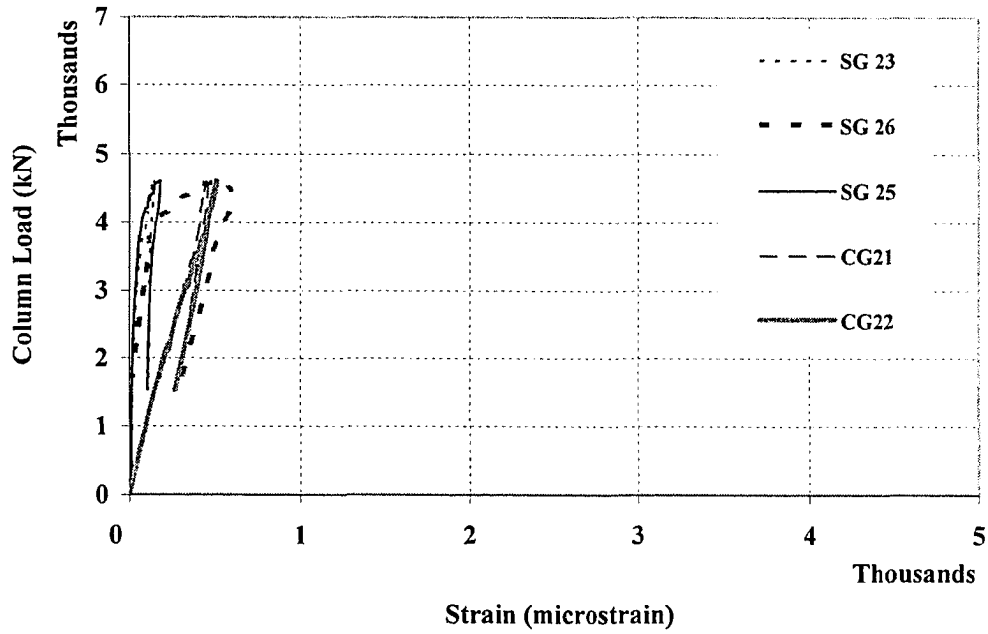

Figure B20. Vertical Load vs. Lateral Strain Values in Top Column of SP2

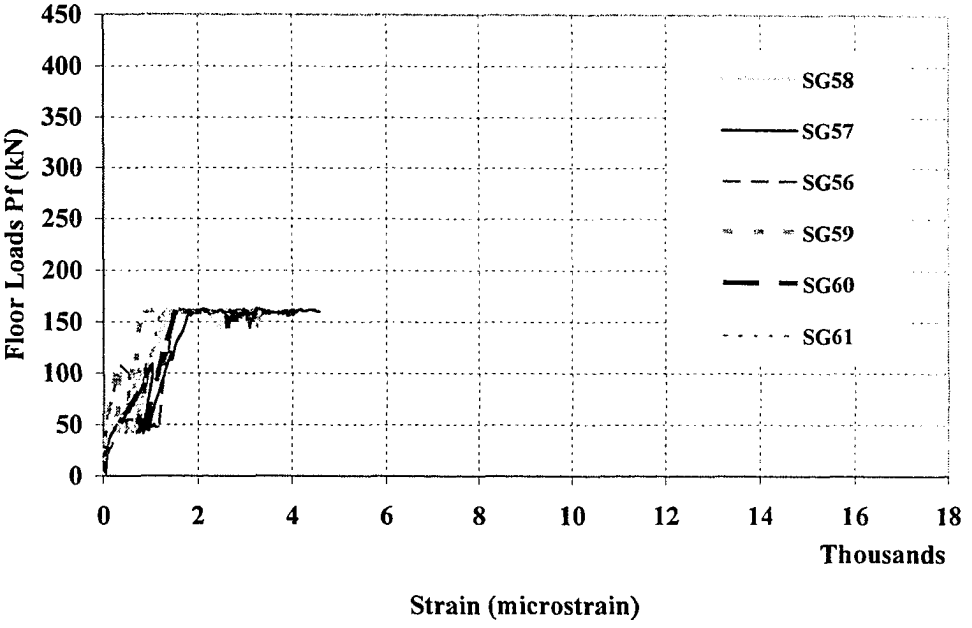

Figure B21. Floor Loads vs. Strain Values of Beam Top Rebars (SP2)

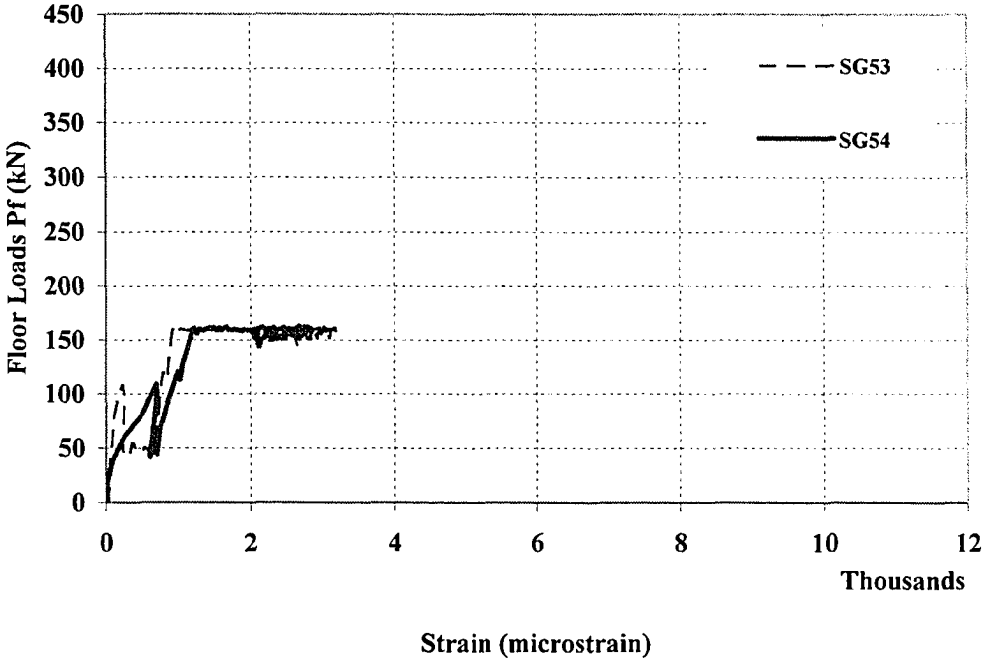

Figure B22. Floor Loads vs. Strain Values of Beam Side Rebars (SP2)

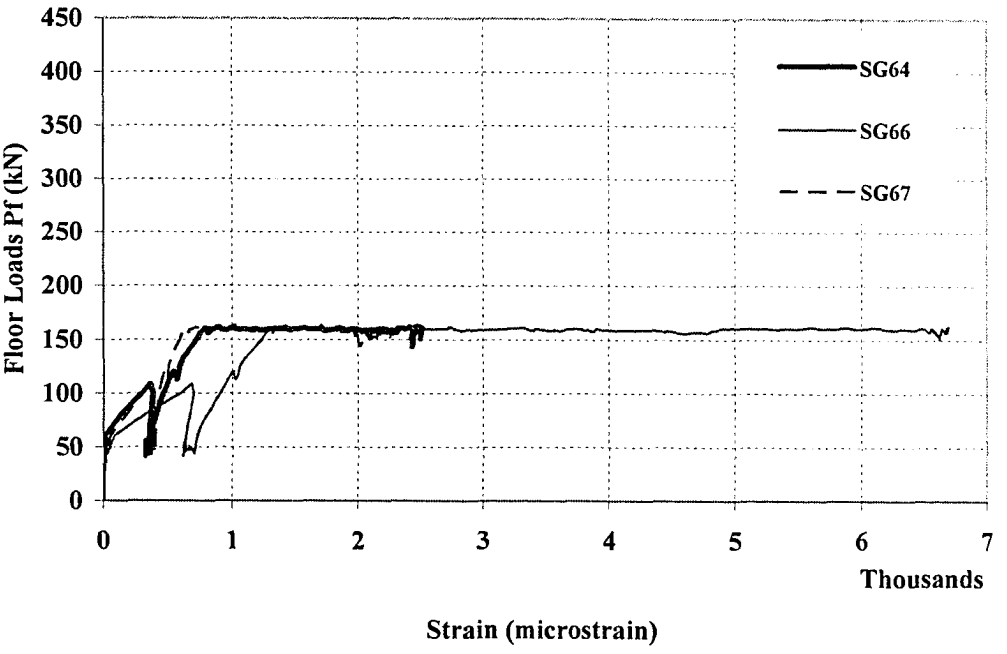

Figure B24. Floor Loads vs. Strain Values of Slab Top Rebars (SP2)

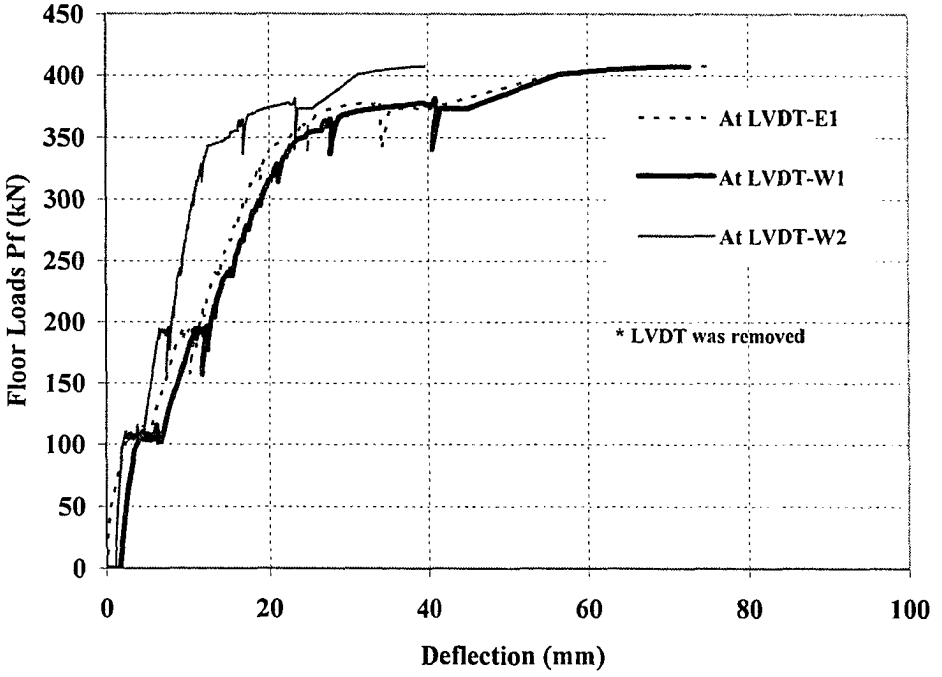

Figure B25. Floor Loads vs. Beam Deflection for SP3

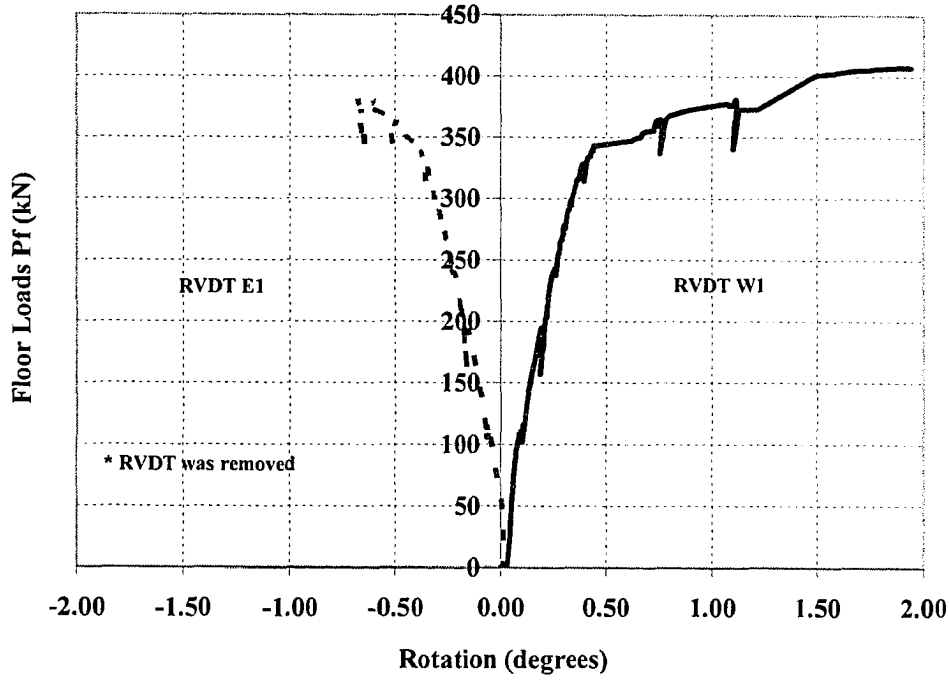

Figure B26. Floor Loads vs. Beam Rotation for SP3

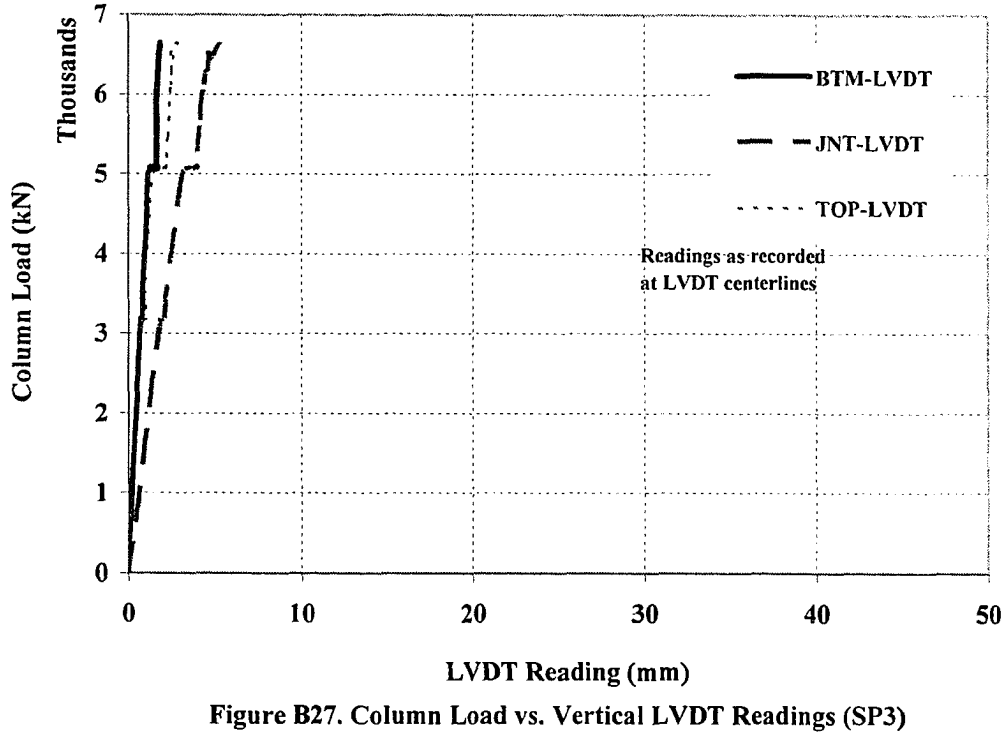

Figure B27. Column Load vs. Vertical LVDT Readings (SP3)

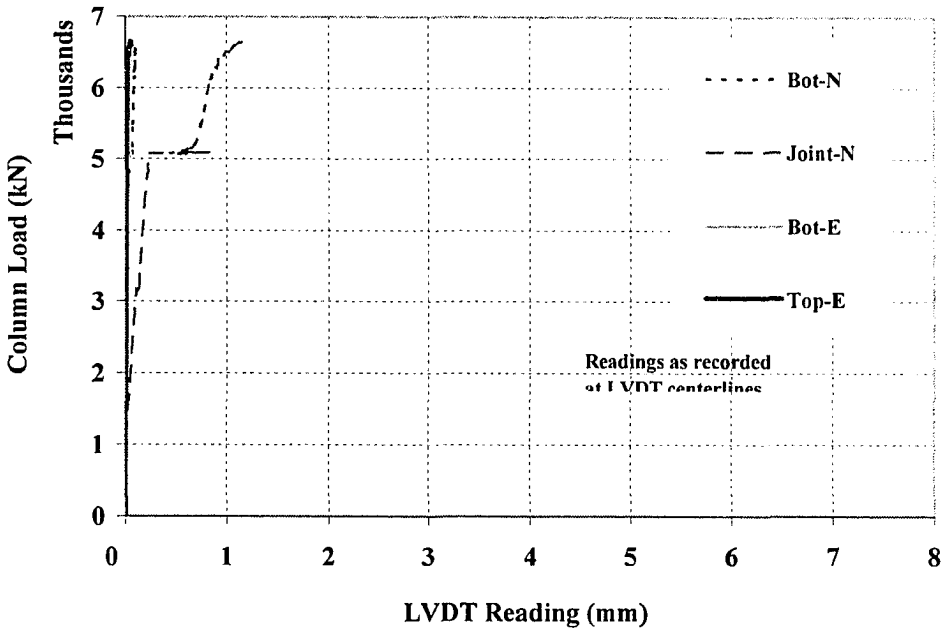

Figure B28. Column Load vs. Horizontal LVDT Readings (SP3)

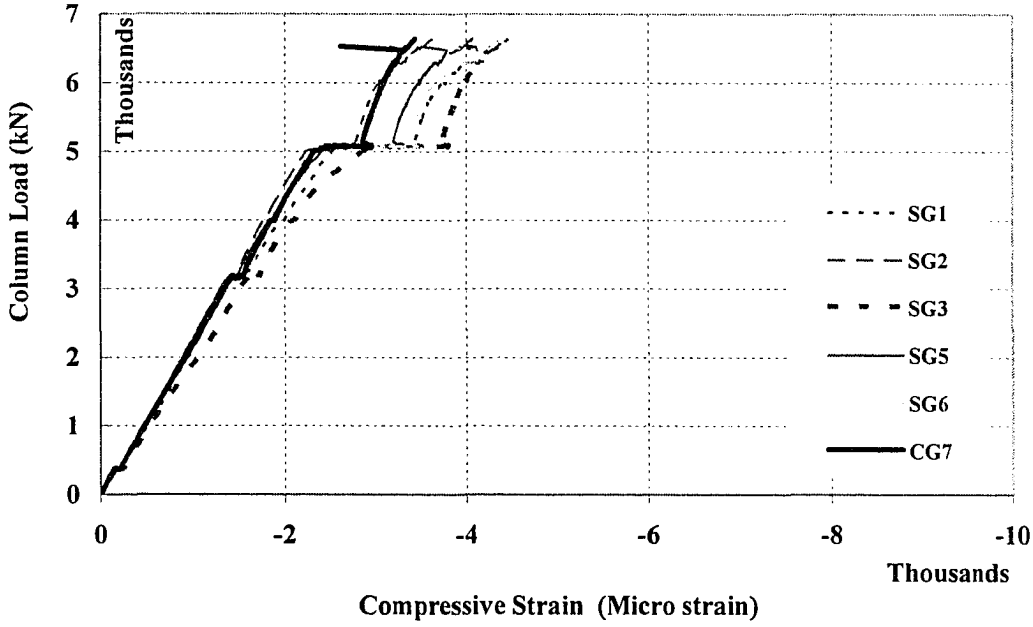

Figure B29. Vertical Load vs. Vertical Strain Values in Bottom Column of SP3

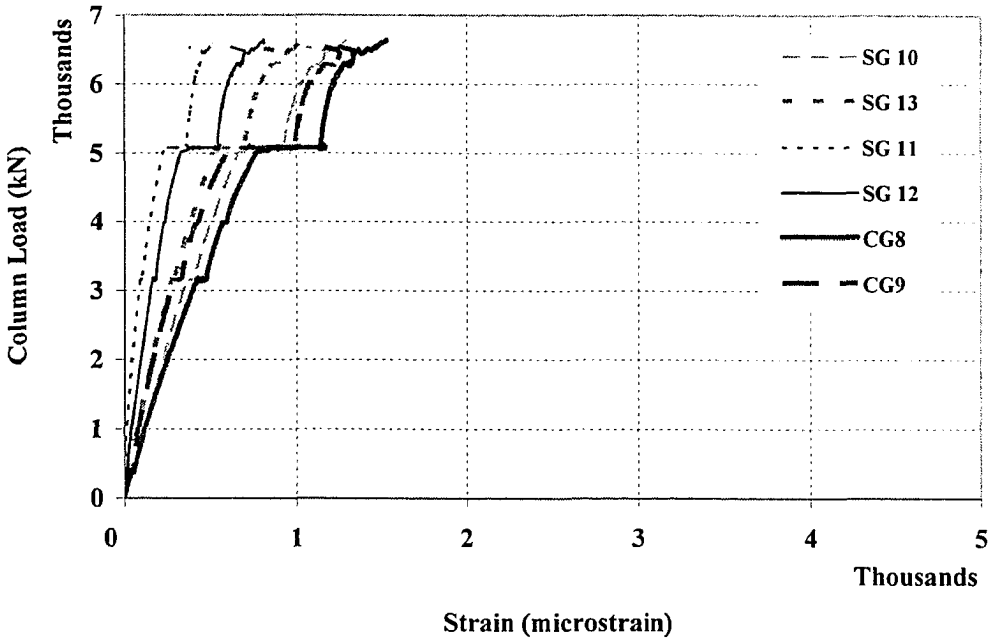

Figure B30. Vertical Load vs. Lateral Strain Values in Bottom Column of SP3

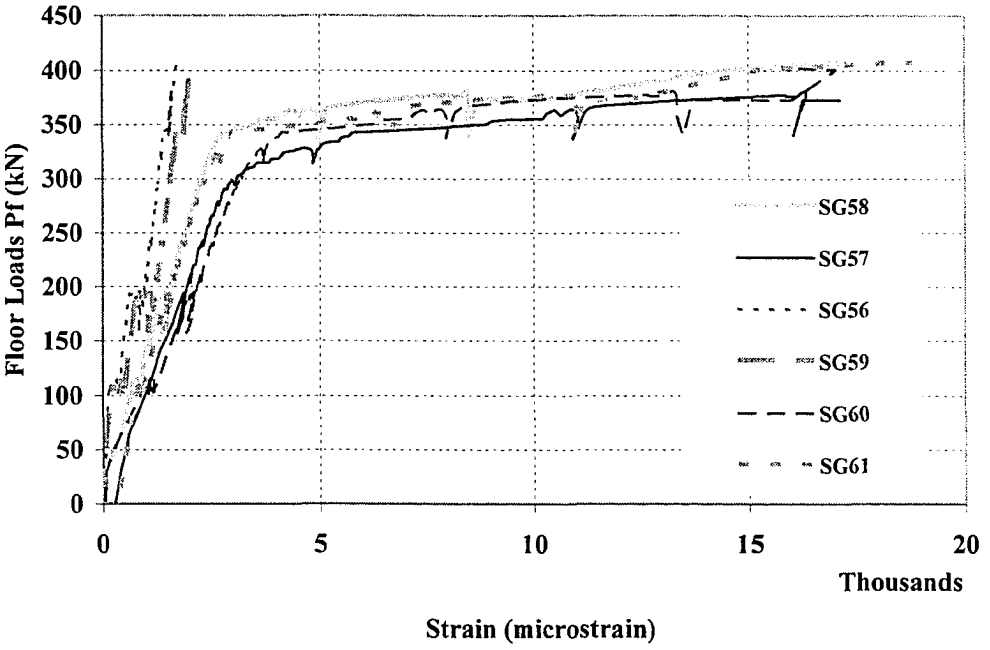

Figure B31. Floor Loads vs. Strain Values of Beam Top Rebars (SP3)

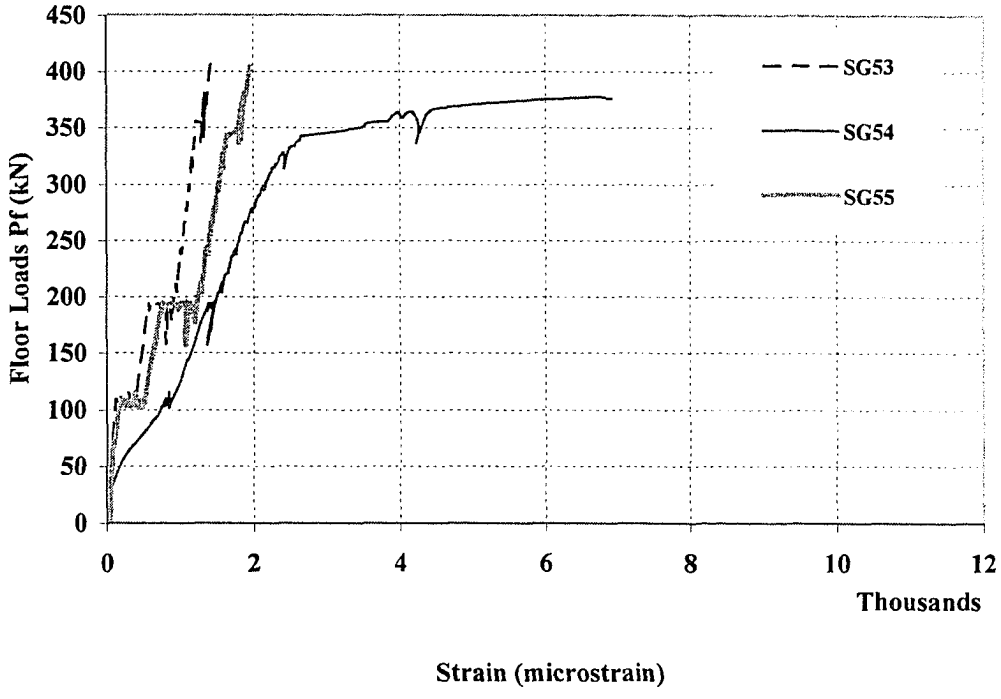

Figure B32. Floor Loads vs. Strain Values of Beam Side Rebars (SP3)

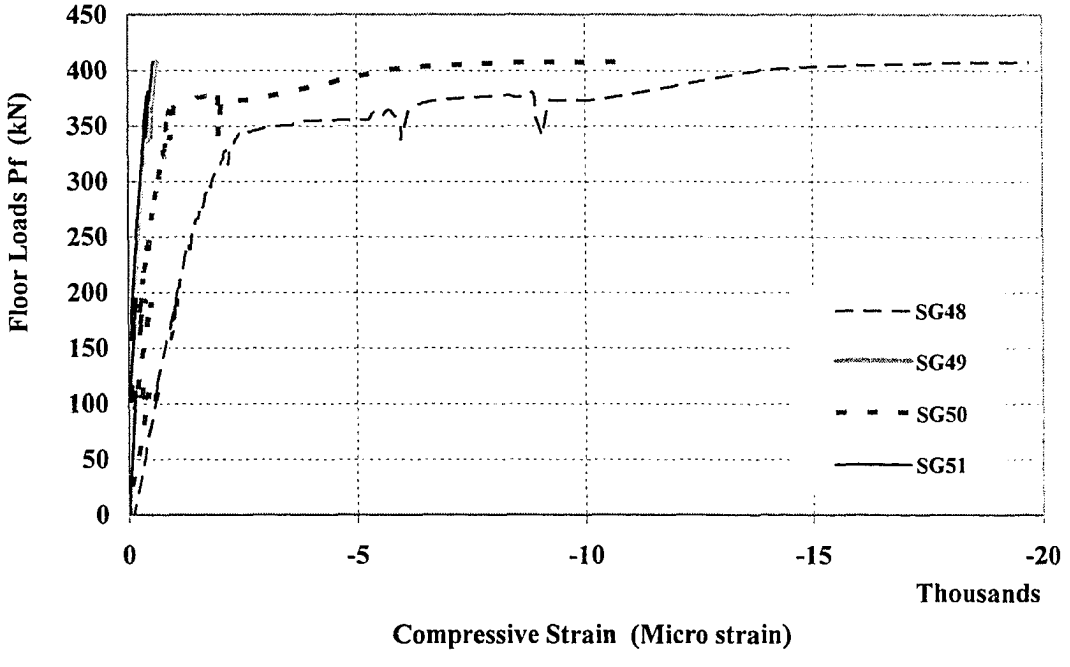

Figure B33. Floor Loads vs. Strain Values of Beam Bottom Rebars (SP3)

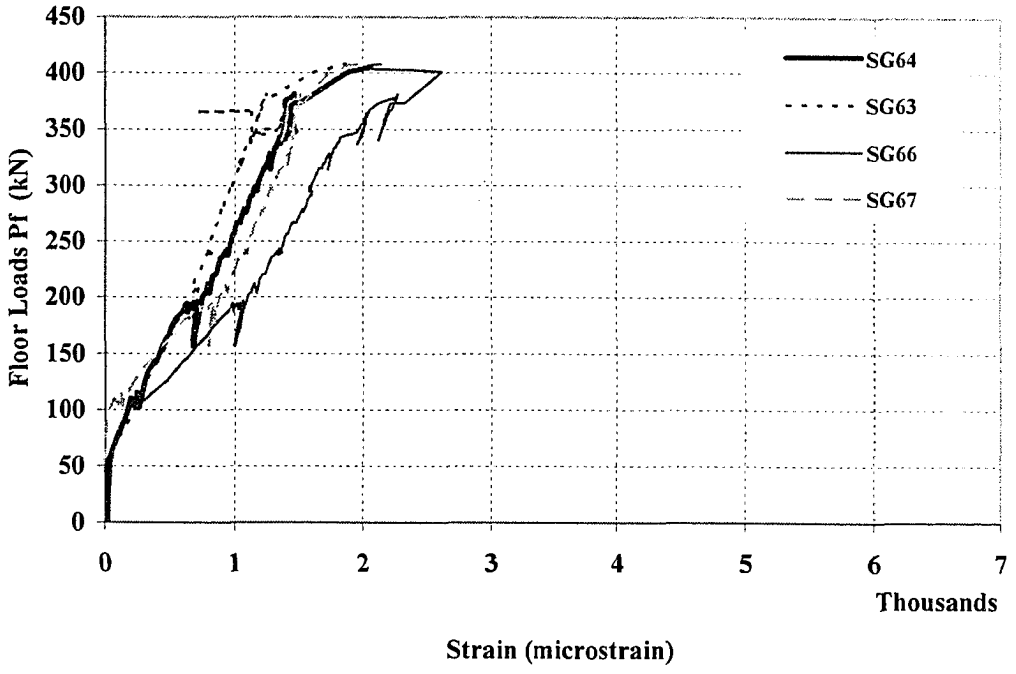

Figure B34. Floor Loads vs. Strain Values of Slab Top Rebars (SP3)

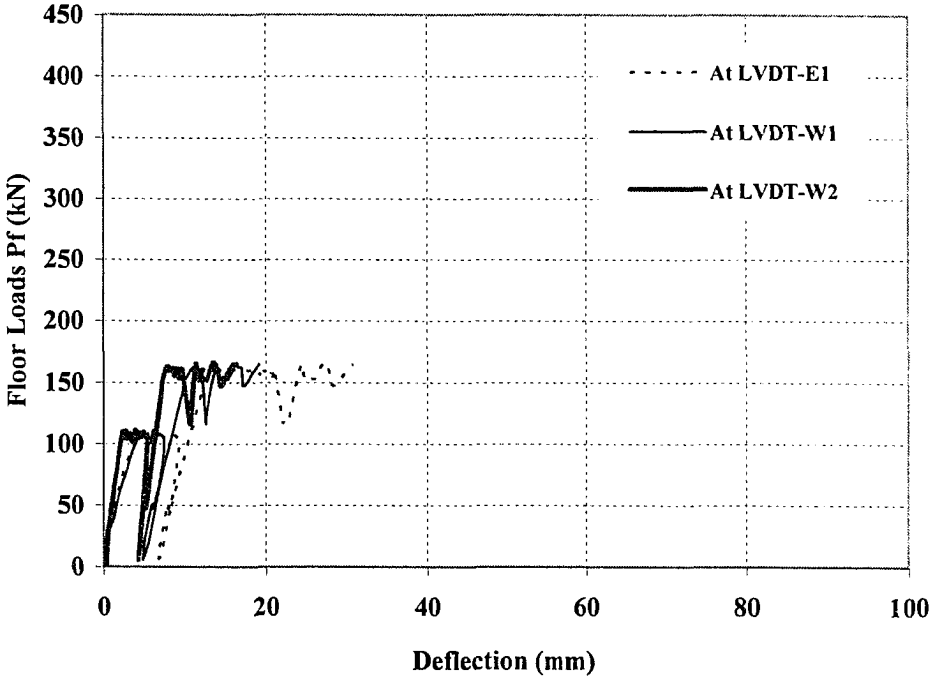

Figure B35. Floor Loads vs. Beam Deflection for SP4

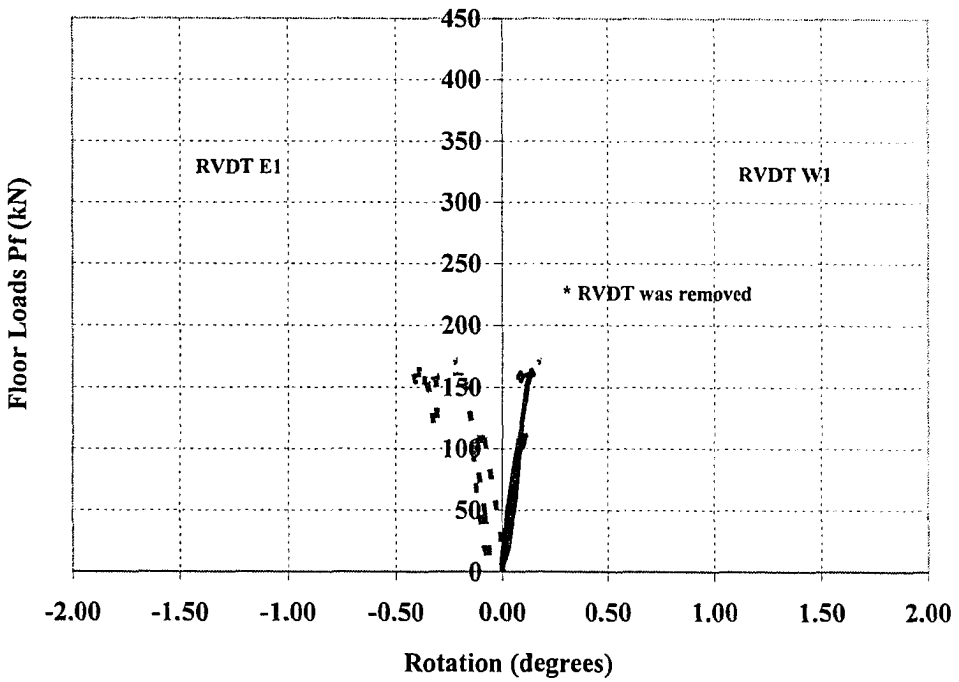

Figure B36. Floor Loads vs. Beam Rotation for SP4

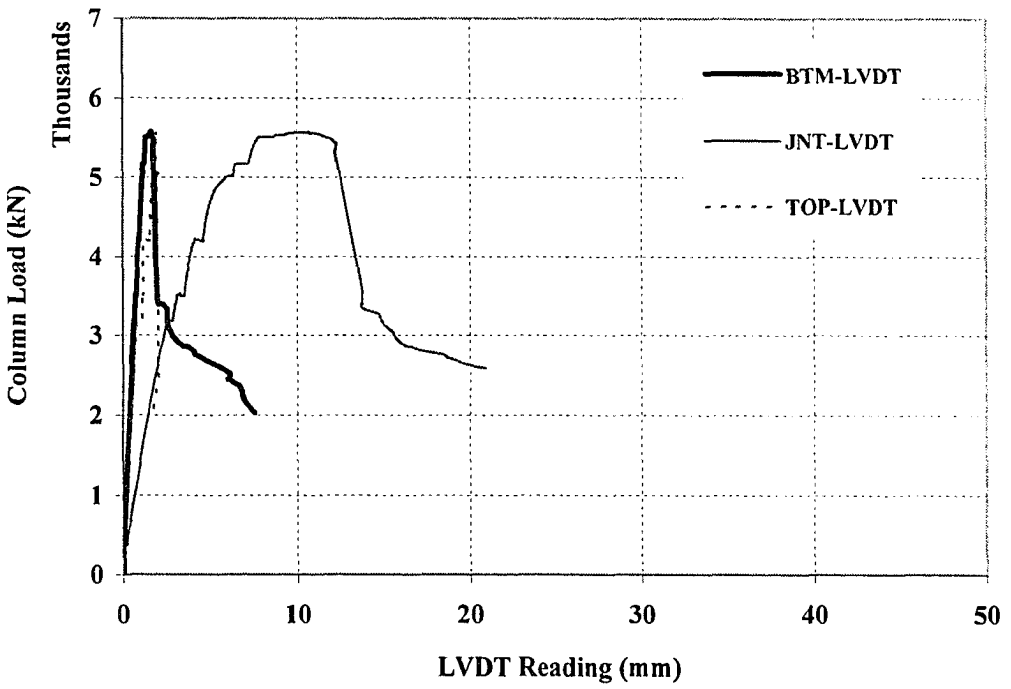

Figure B37. Column Load vs. Vertical LVDT Readings (SP4)

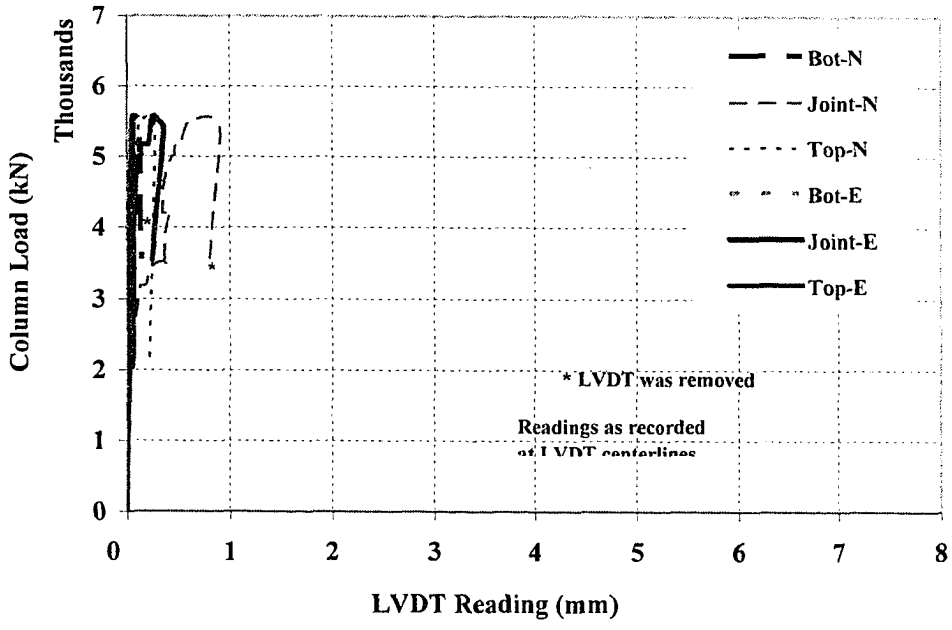

Figure B38. Column Load vs. Horizontal LVDT Readings (SP4)

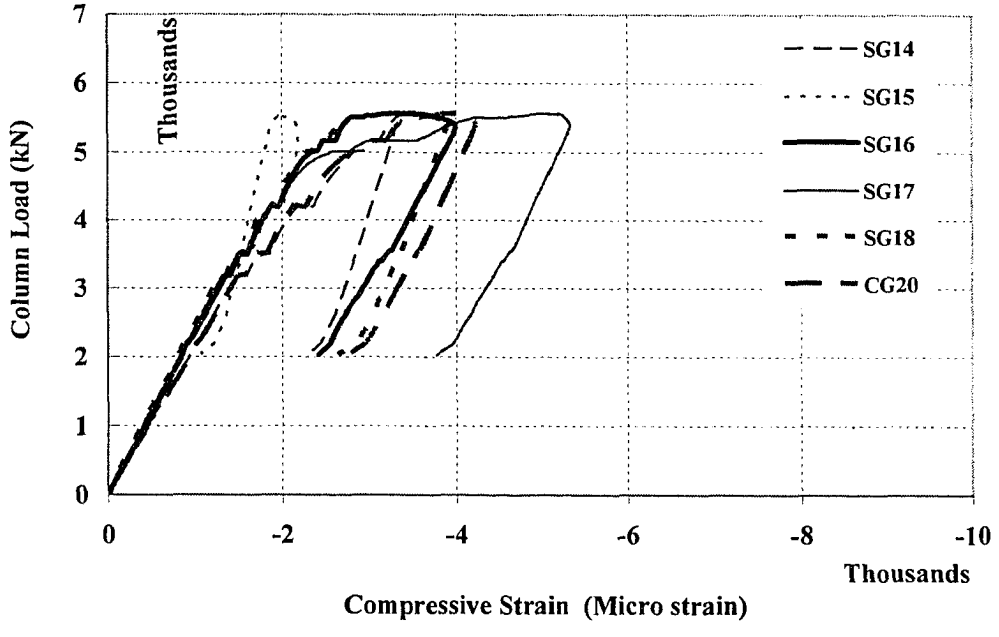

Figure B39. Vertical Load vs. Vertical Strain Values in Top Column of SP4

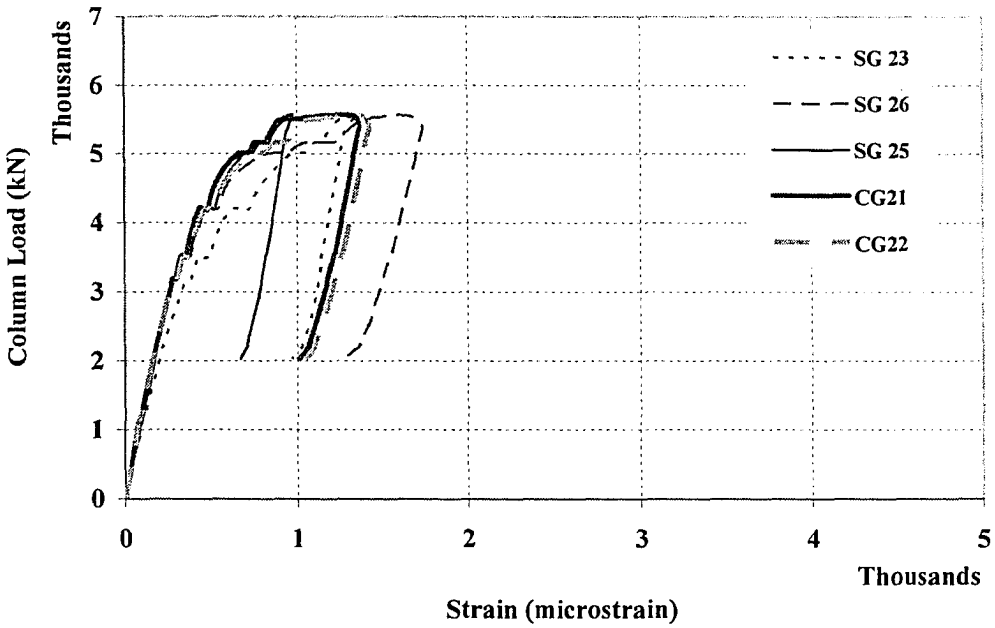

Figure B40. Vertical Load vs. Lateral Strain Values in Top Column of SP4

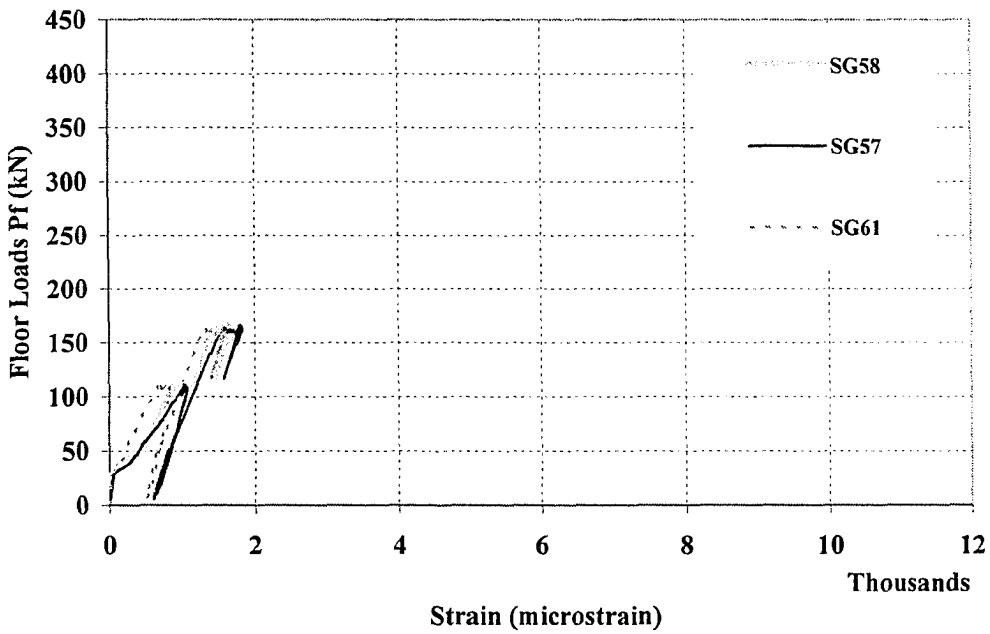

Figure B41. Floor Loads vs. Strain Values of Beam Top Rebars (SP4)

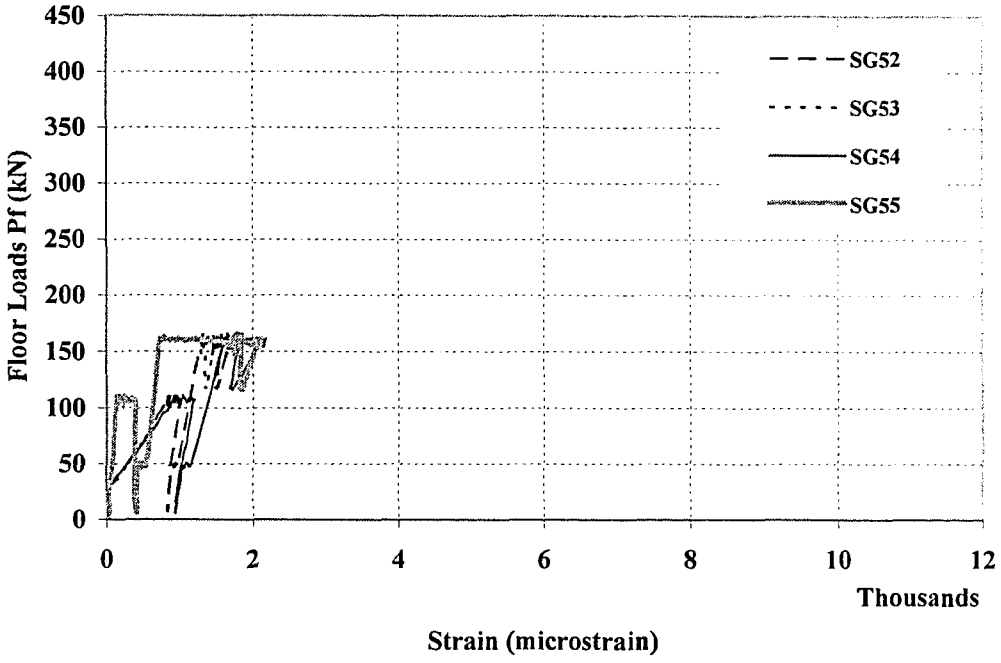

Figure B42. Floor Loads vs. Strain Values of Beam Side Rebars (SP4)

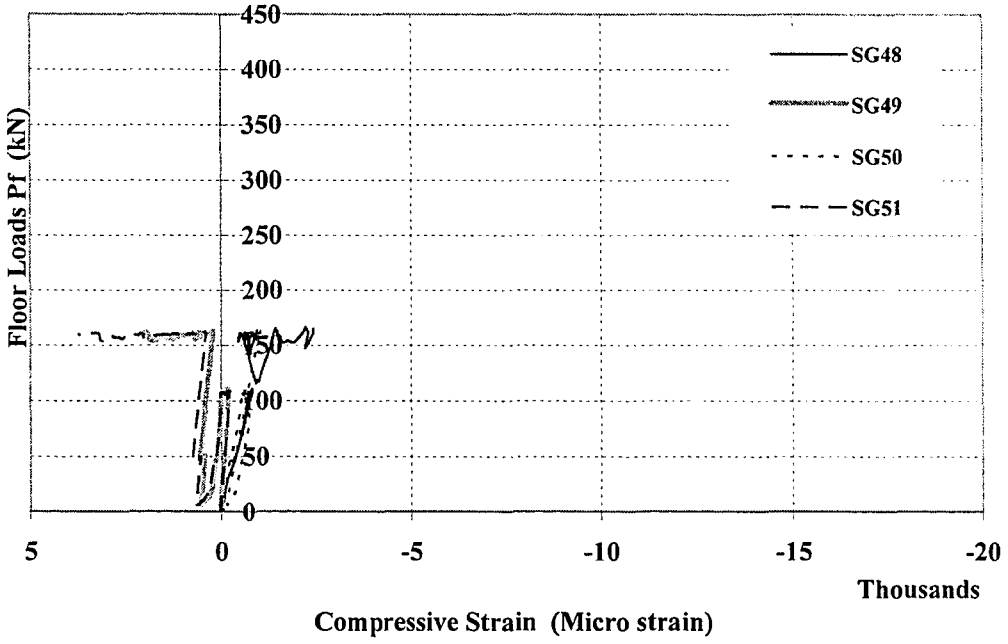

Figure B43. Floor Loads vs. Strain Values of Beam Bottom Rebars (SP4)

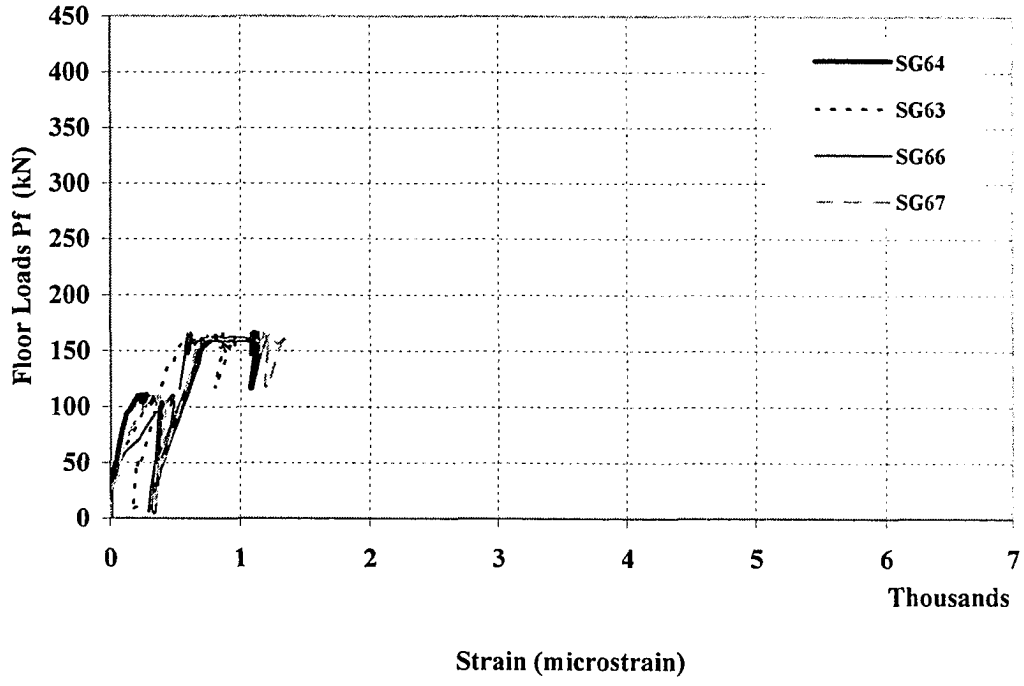

Figure B44. Floor Loads vs. Strain Values of Slab Top Rebars (SP4)

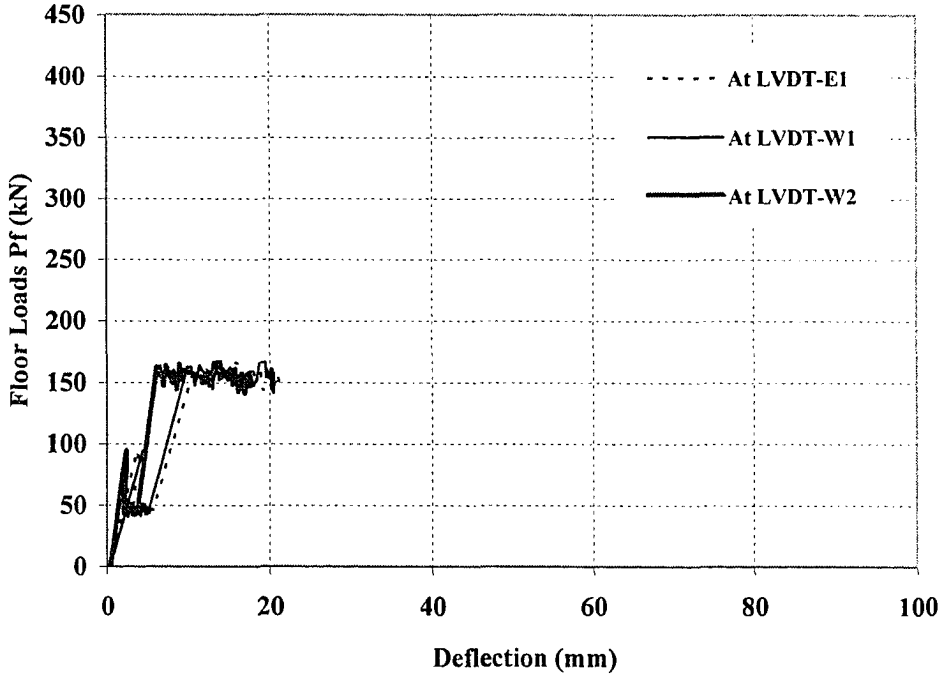

Figure B45. Floor Loads vs. Beam Deflection for SP5

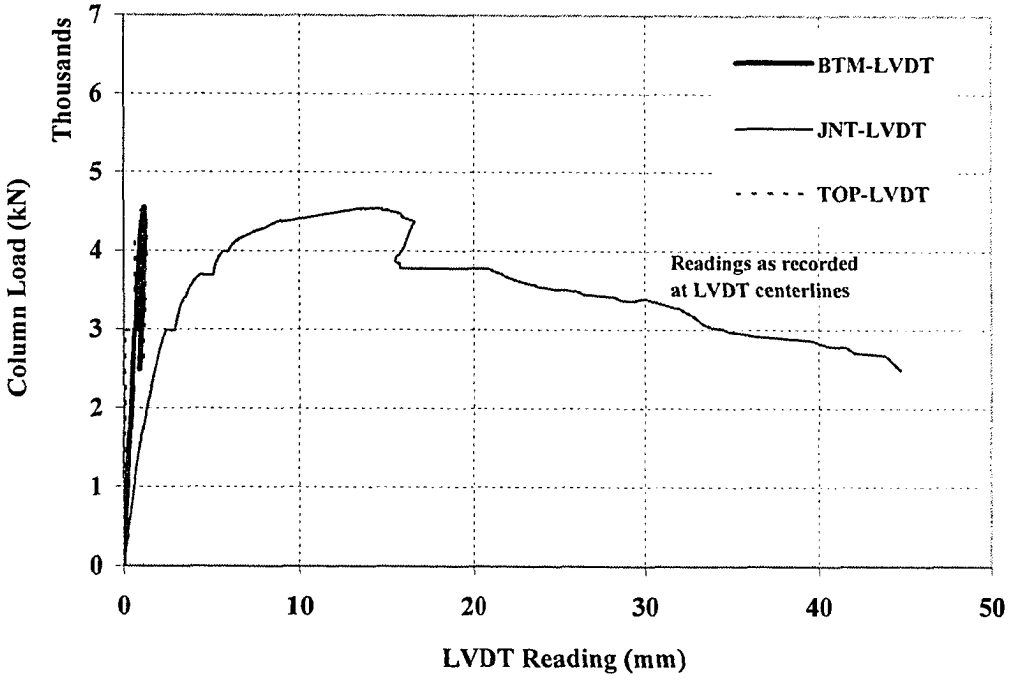

Figure B47. Column Load vs. Vertical LVDT Readings (SP5)

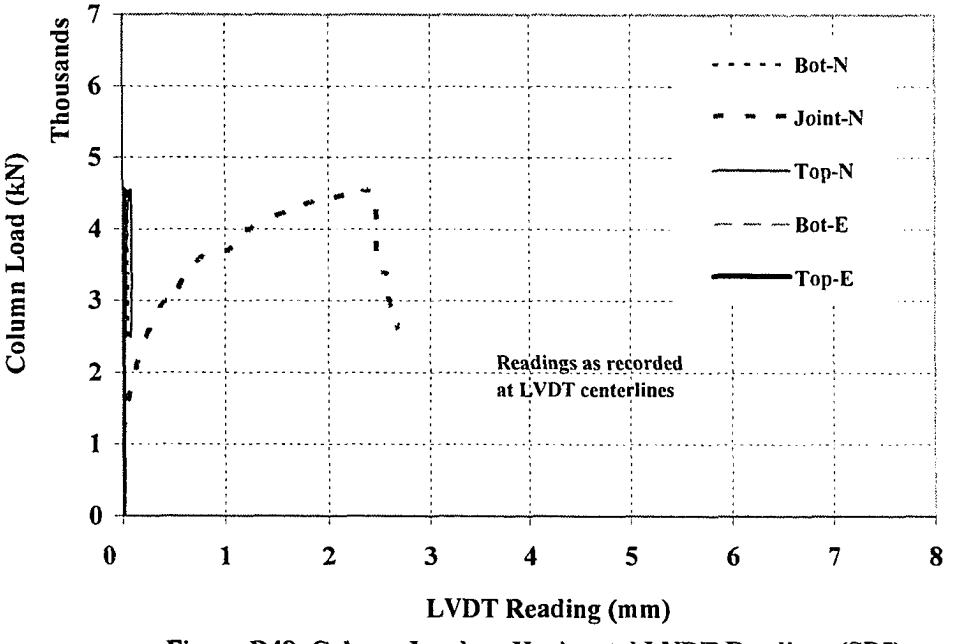

Figure B48. Column Load vs. Horizontal LVDT Readings (SP5)

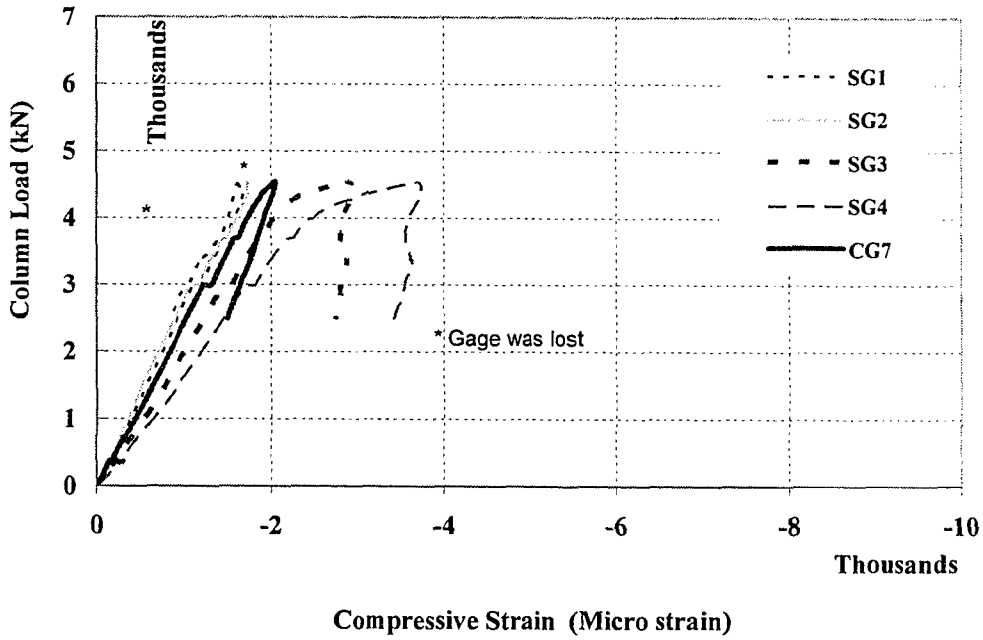

Figure B49 Vertical Load vs. Vertical Strain Values in Bottom Column of SP5

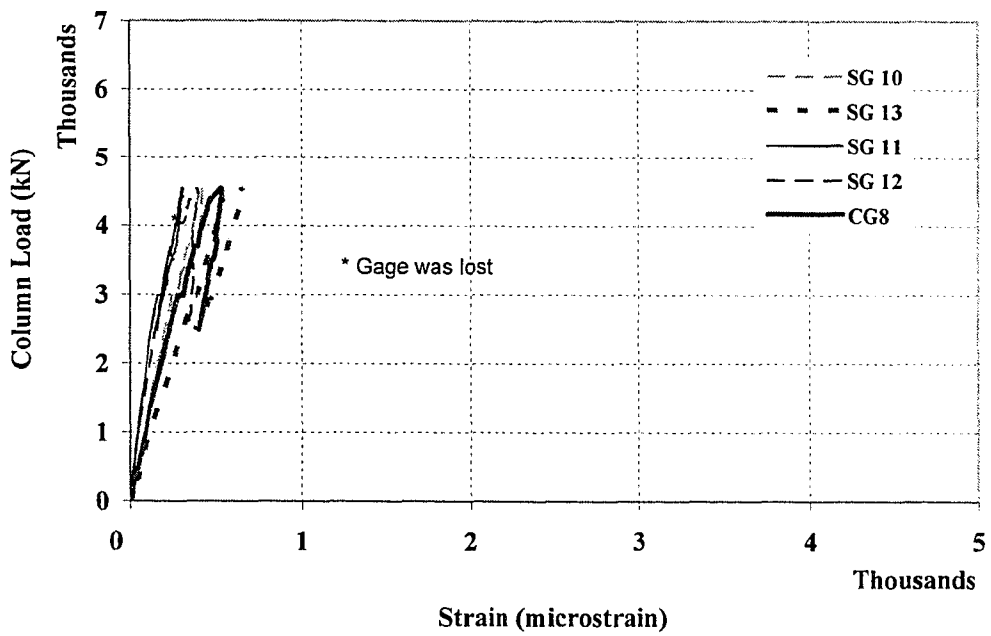

Figure B50. Vertical Load vs. Lateral Strain Values in Bottom Column of SP5

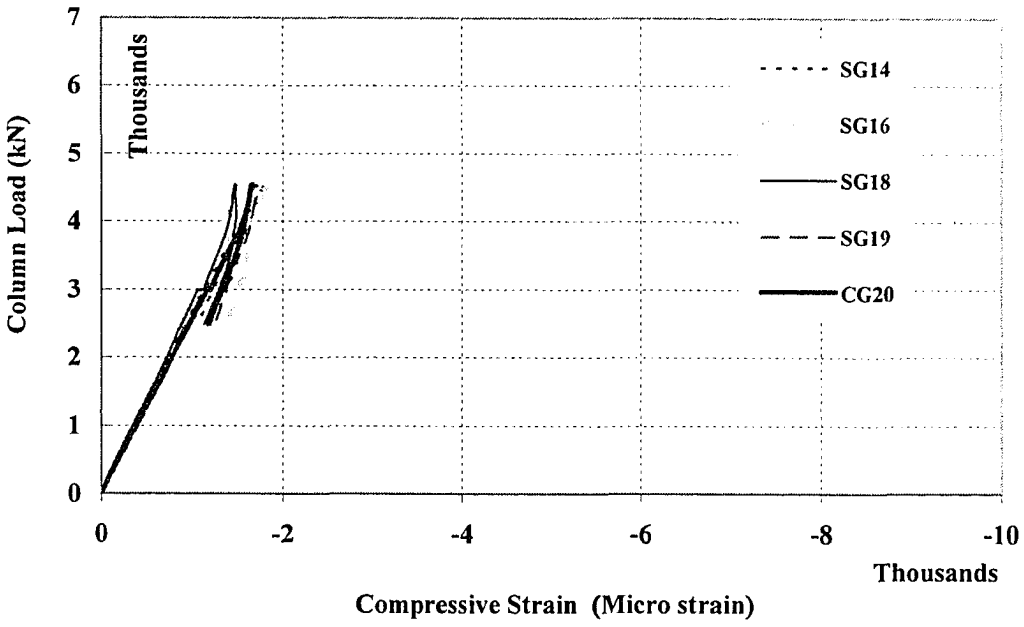

Figure B51. Vertical Load vs. Vertical Strain Values in Top Column of SP5

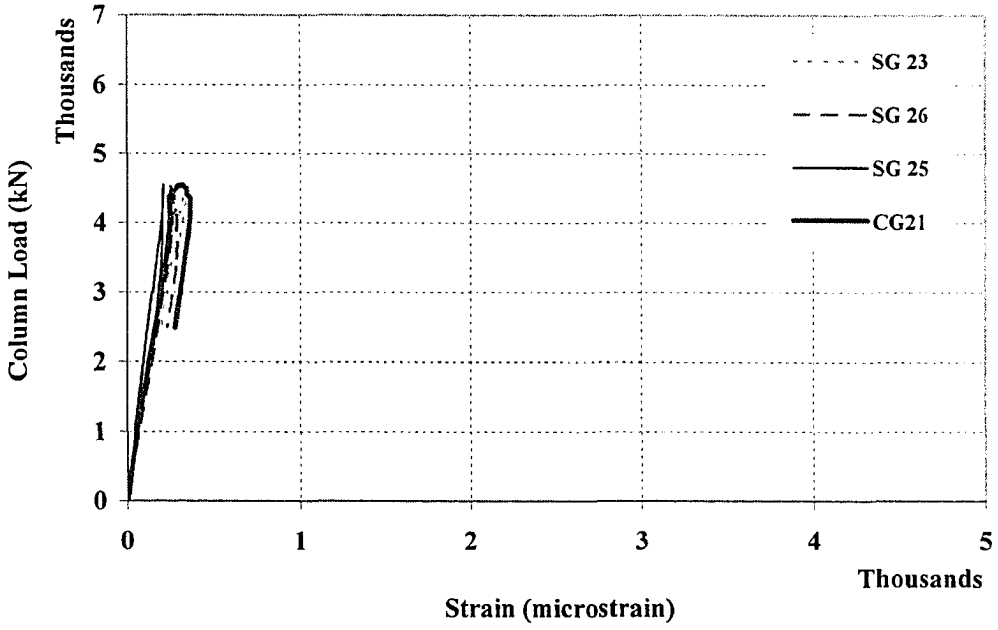

Figure B52. Vertical Load vs. Lateral Strain Values in Top Column of SP5

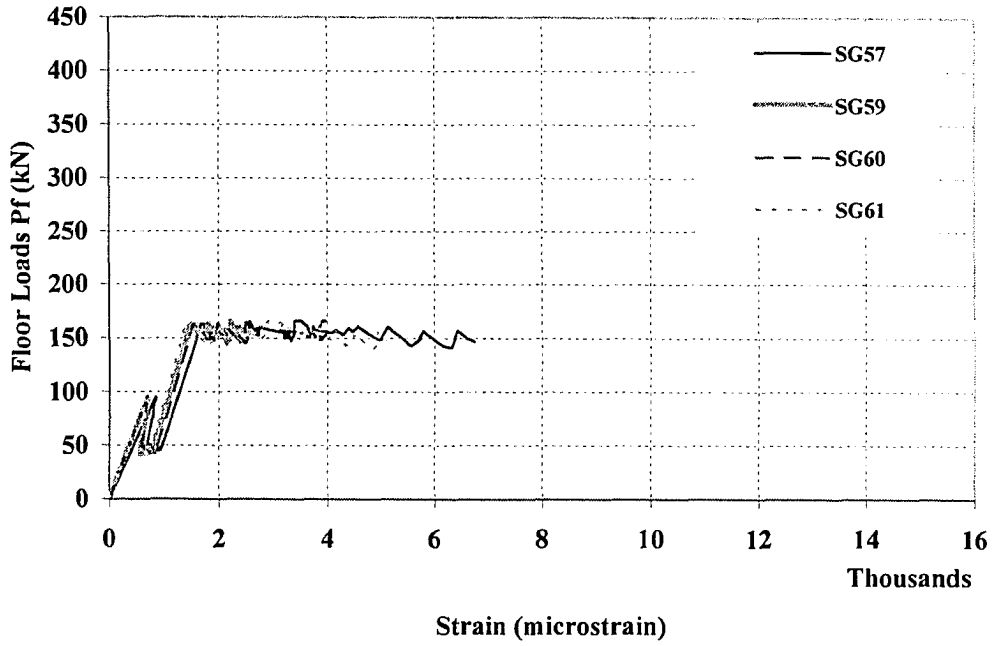

Figure B53. Floor Loads vs. Strain Values of Beam Top Rebars (SP5)

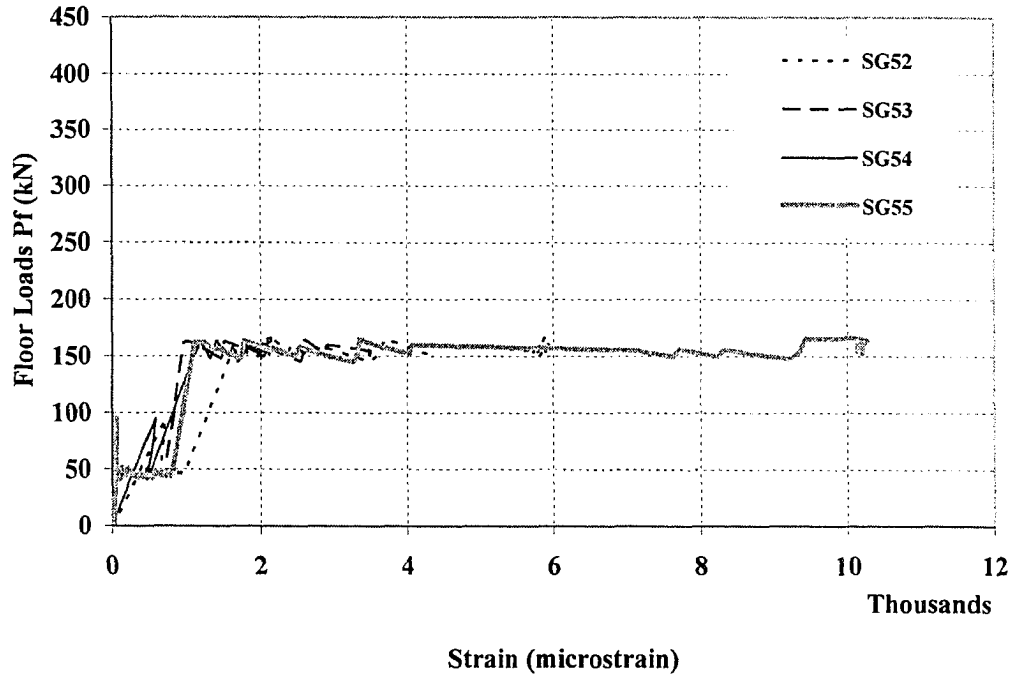

Figure B54. Floor Loads vs. Strain Values of Beam Side Rebars (SP5)

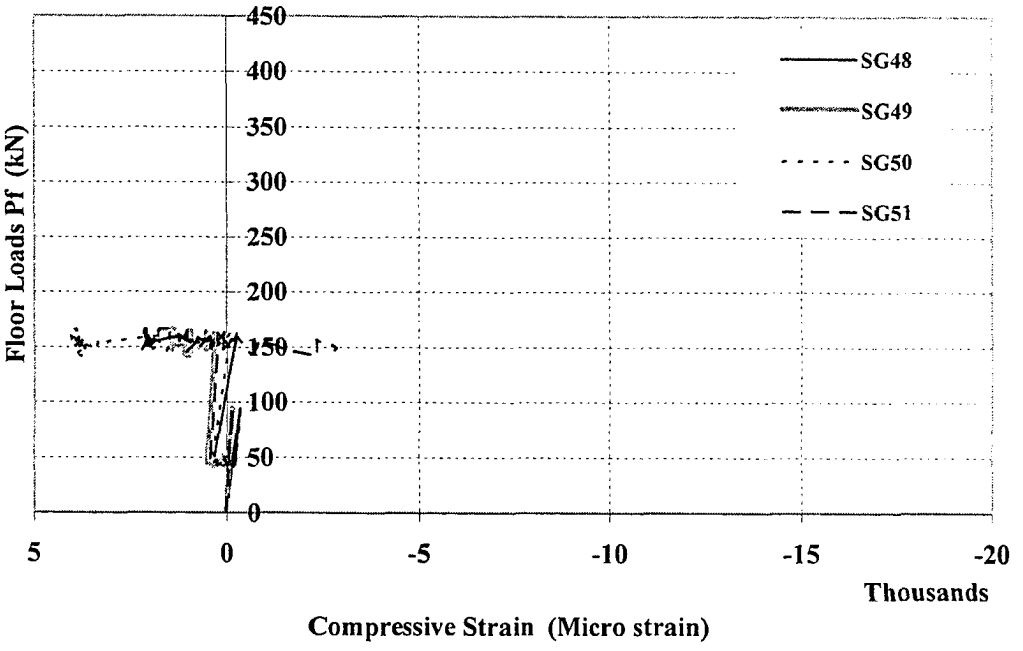

Figure B55. Floor Loads vs. Strain Values of Beam Bottom Rebars (SP5)

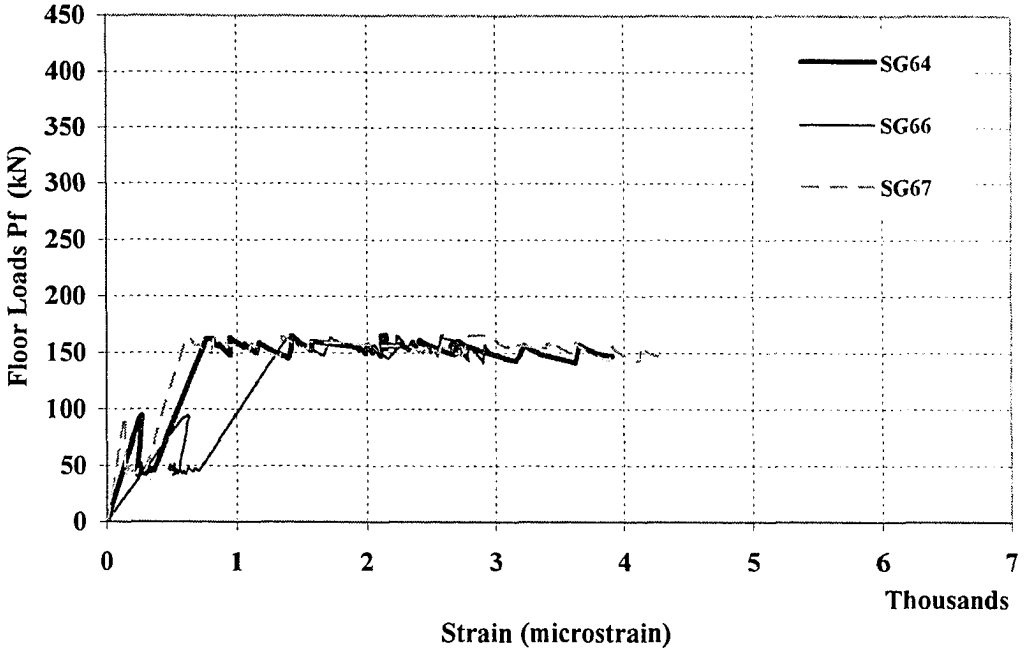

Figure B56. Floor Loads vs. Strain Values of Slab Top Rebars (SP5)

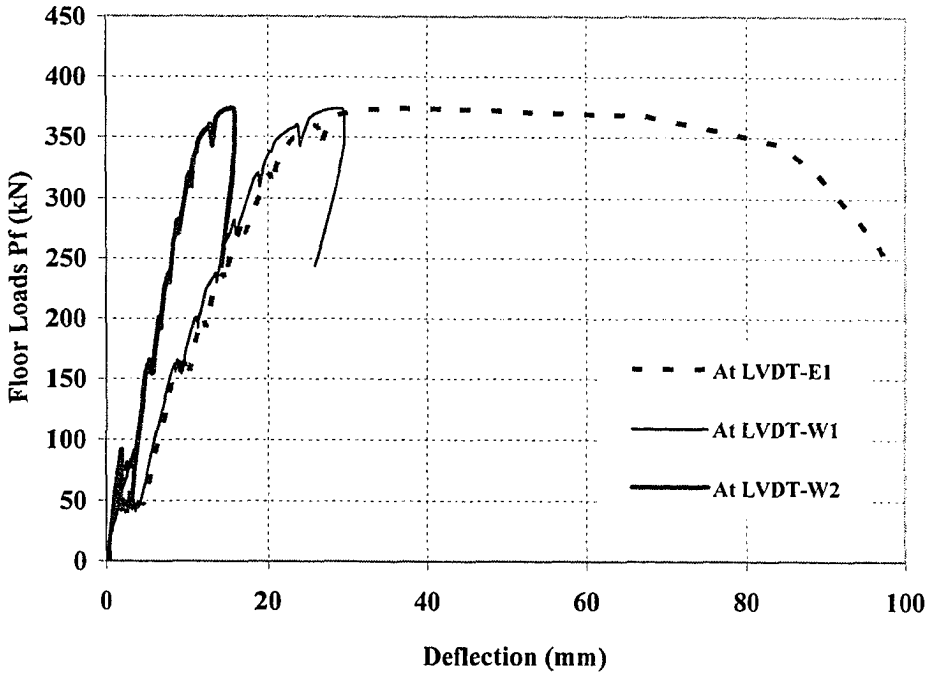

Figure B57. Floor Loads vs. Beam Deflection for SP6

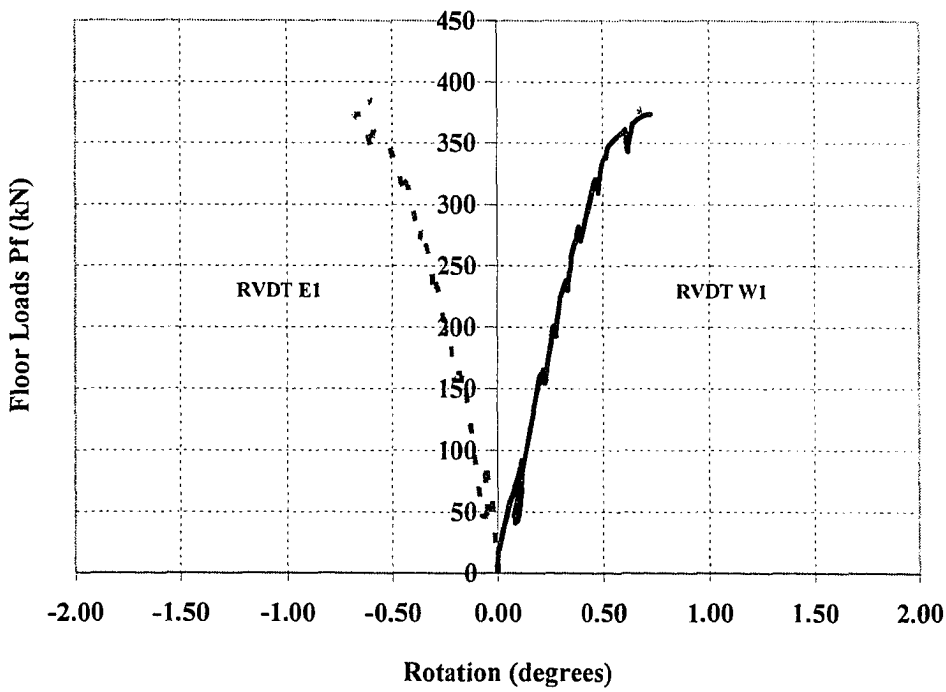

Figure B58. Floor Loads vs. Beam Rotation for SP6

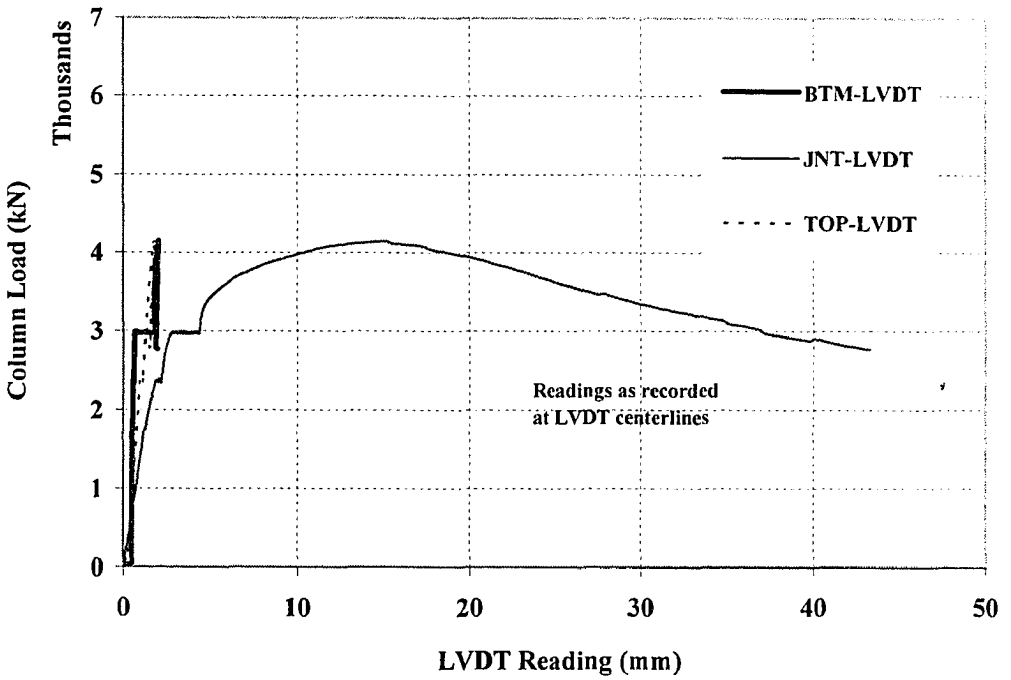

Figure B59. Column Load vs. Vertical LVDT Readings (SP6)

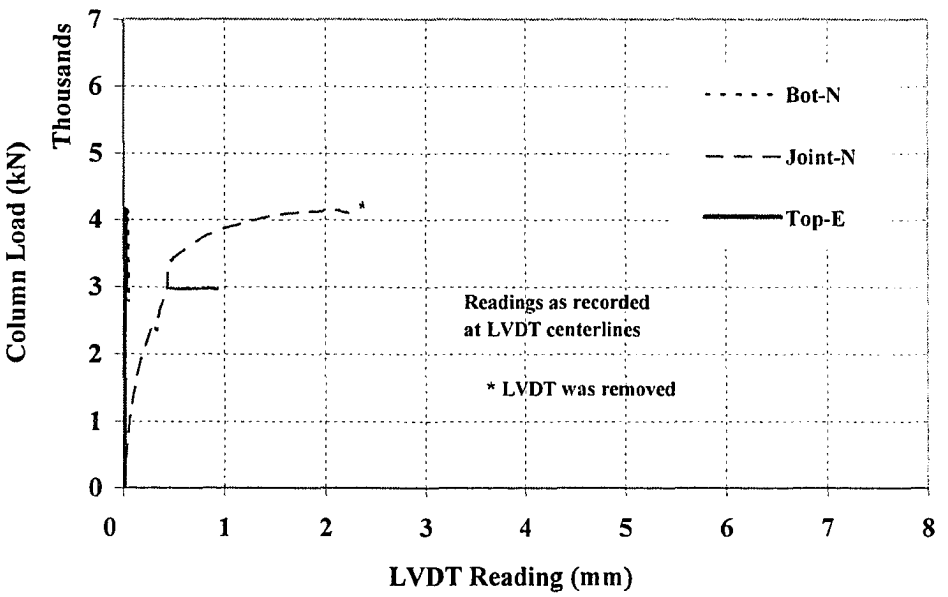

Figure B60. Column Load vs. Horizontal LVDT Readings (SP6)

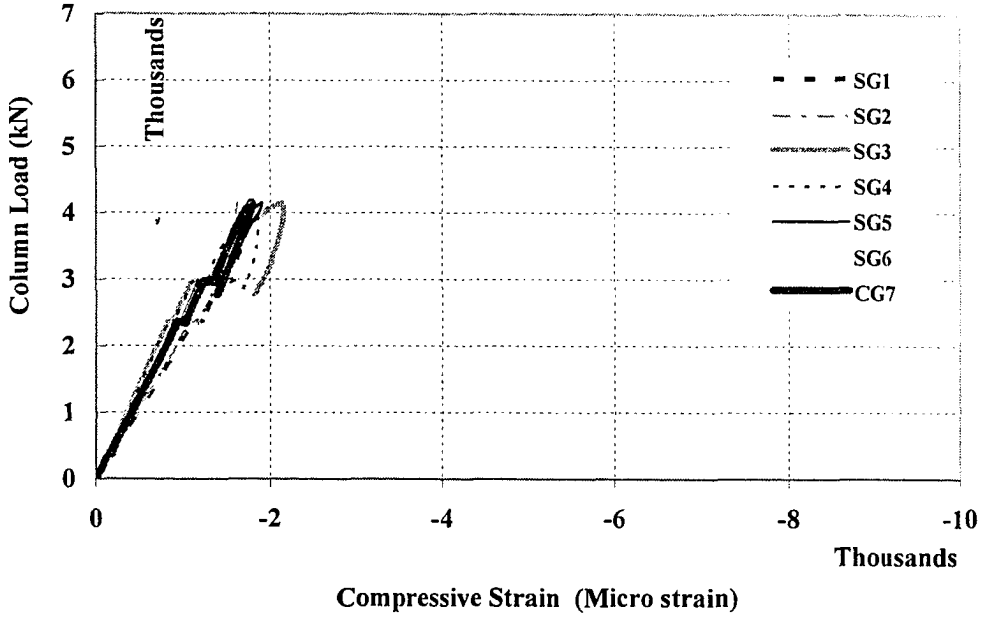

Figure B61. Vertical Load vs. Vertical Strain Values in Bottom Column of SP6

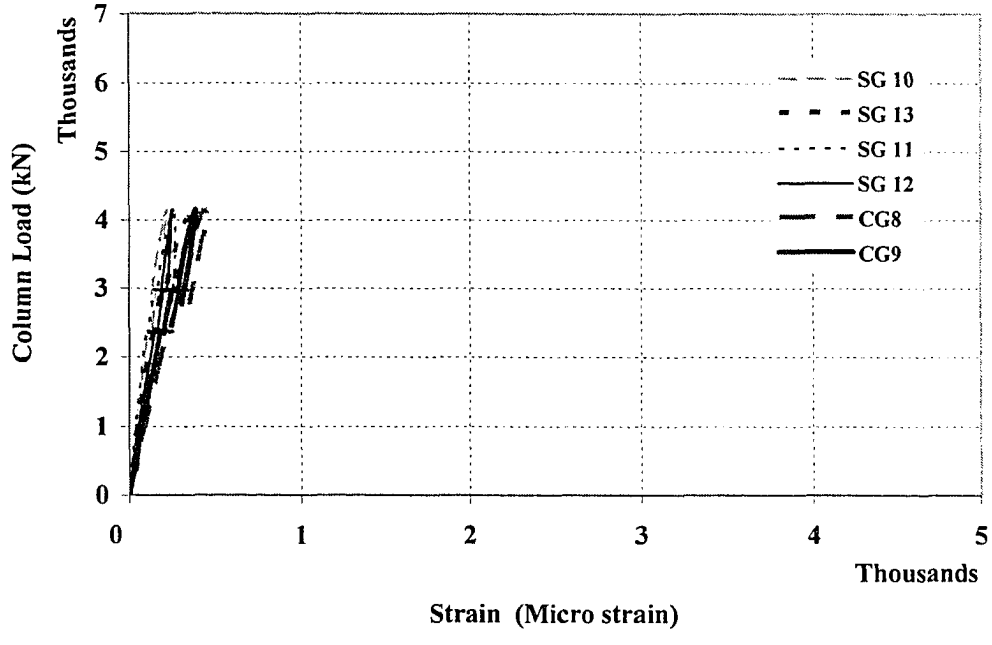

Figure B62. Vertical Load vs. Lateral Strain Values in Bottom Column of SP6

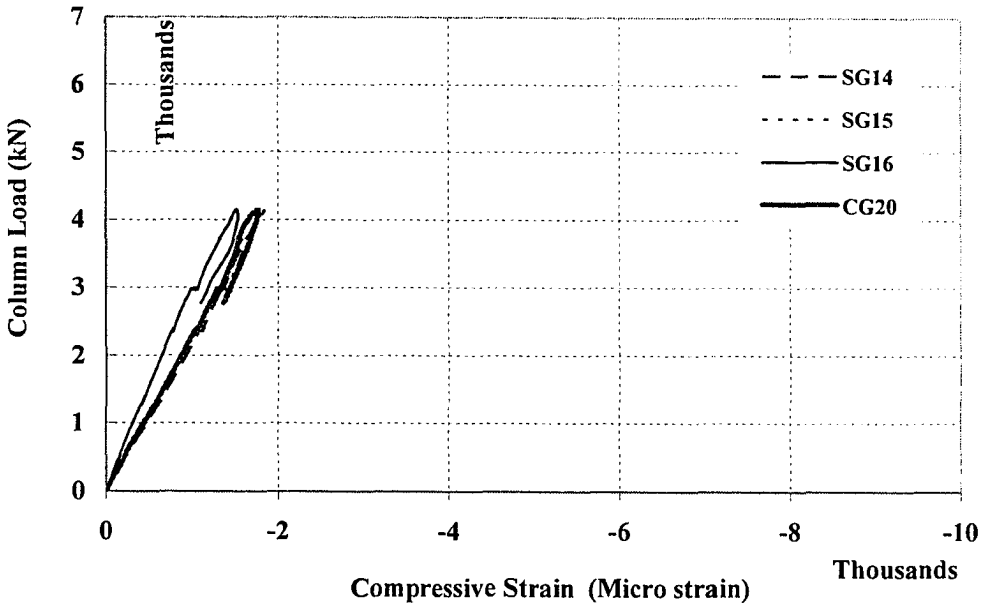

Figure B63. Vertical Load vs. Vertical Strain Values in Top Column of SP6

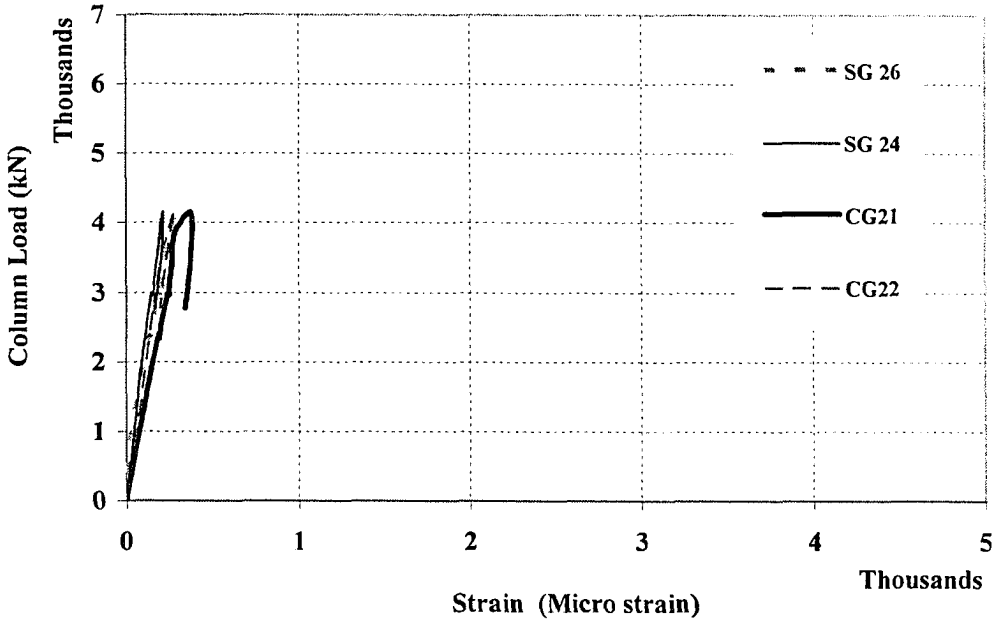

Figure B64. Vertical Load vs. Lateral Strain Values in Top Column of SP6

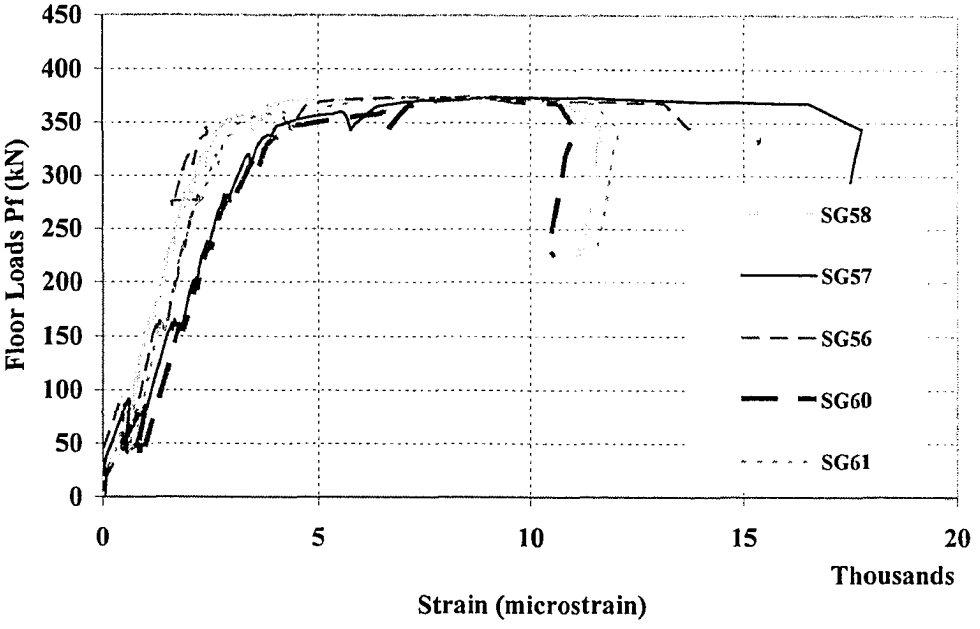

Figure B65. Floor Loads vs. Strain Values of Beam Top Rebars (SP6)

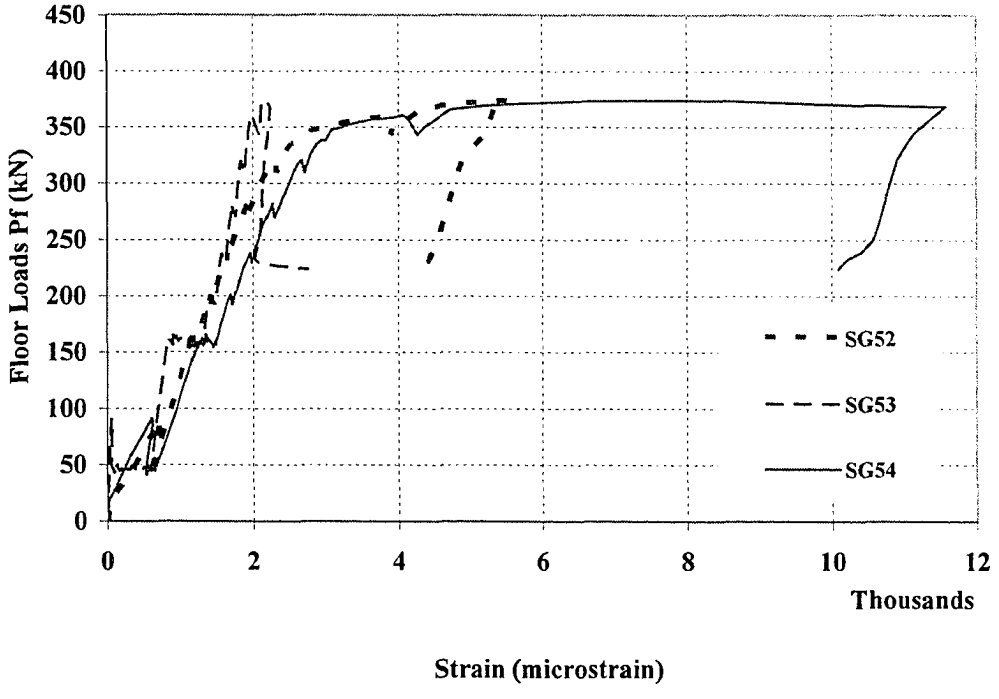

Figure B66. Floor Loads vs. Strain Values of Beam Side Rebars (SP6)

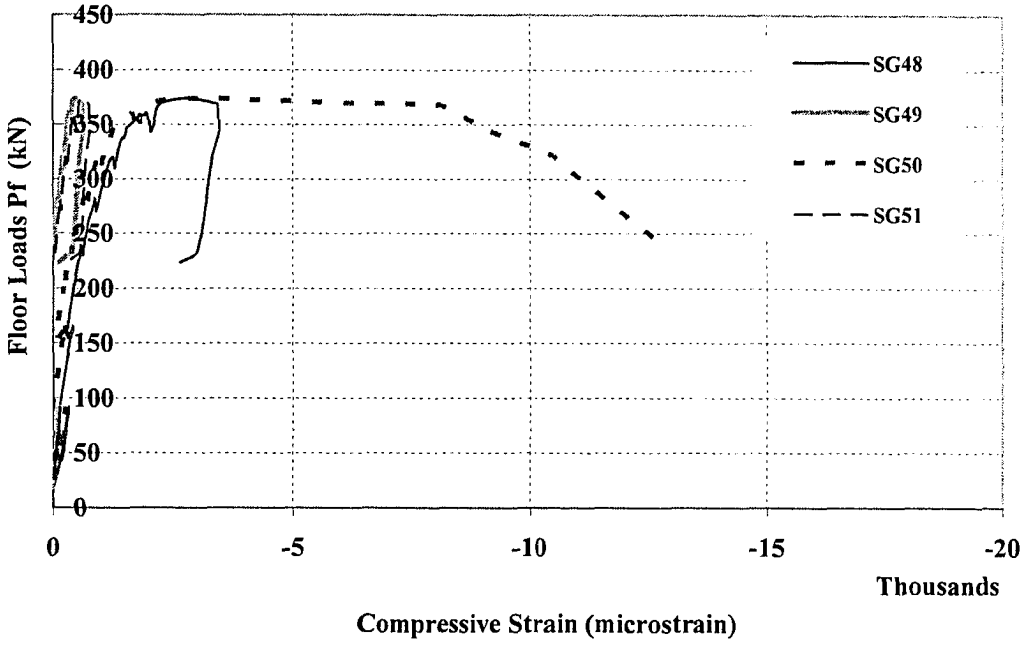

Figure B67. Floor Loads vs. Strain Values of Beam Bottom Rebars (SP6)

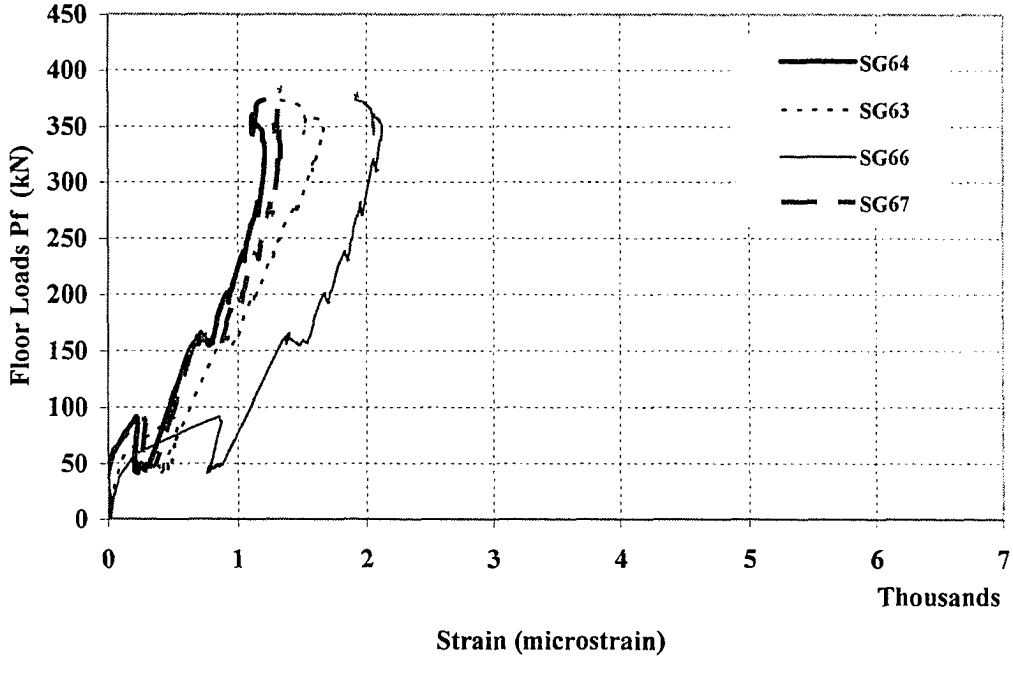

Figure B68. Floor Loads vs. Strain Values of Slab Top Rebars (SP6)

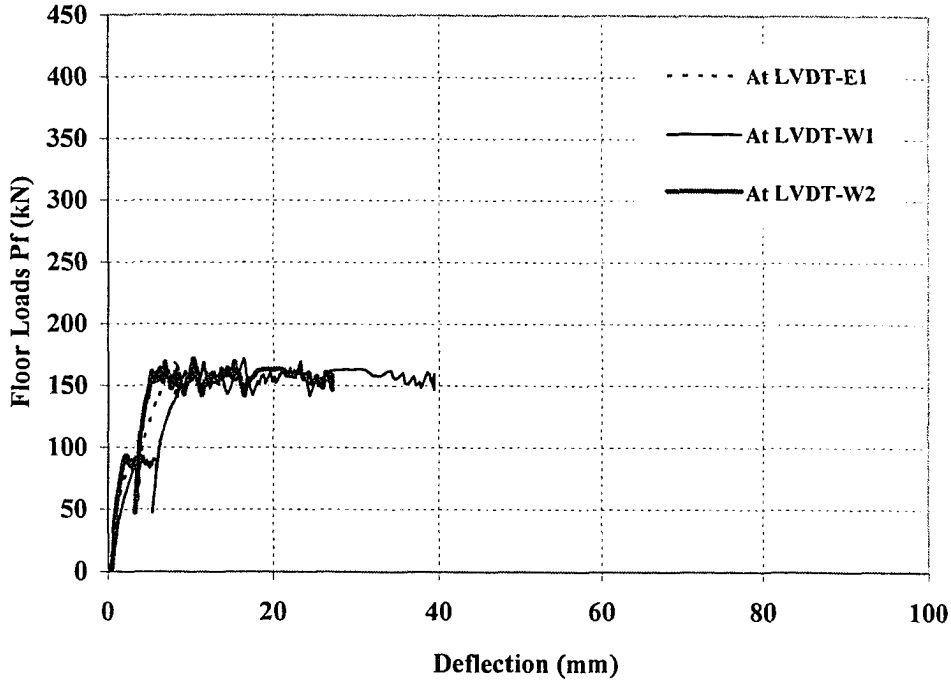

Figure B69. Floor Loads vs. Beam Deflection for SP7

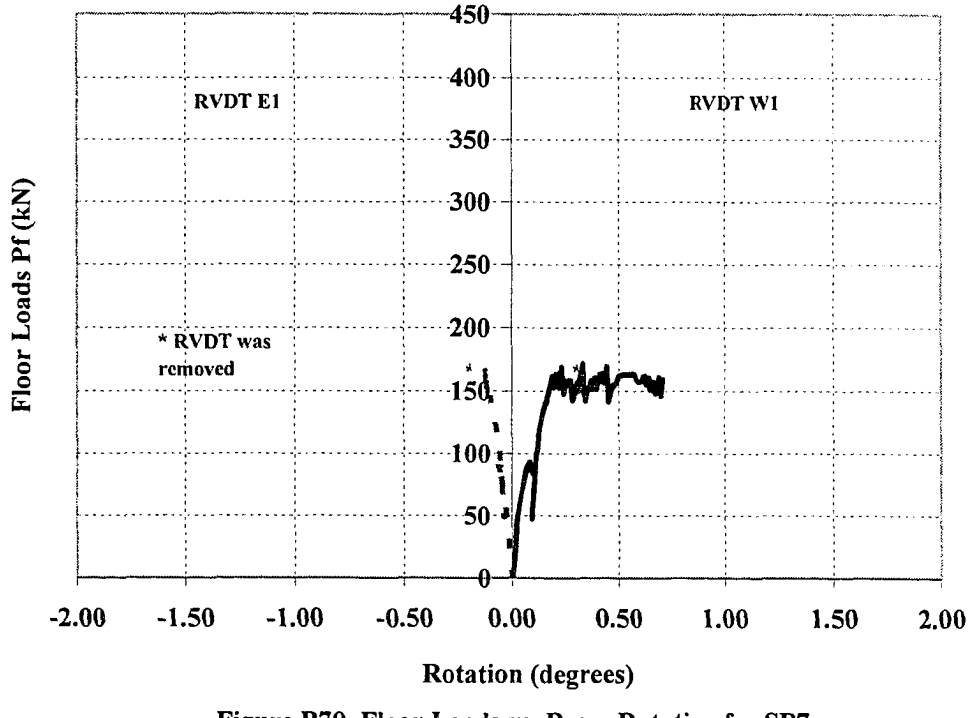

Figure B70. Floor Loads vs. Beam Rotation for SP7

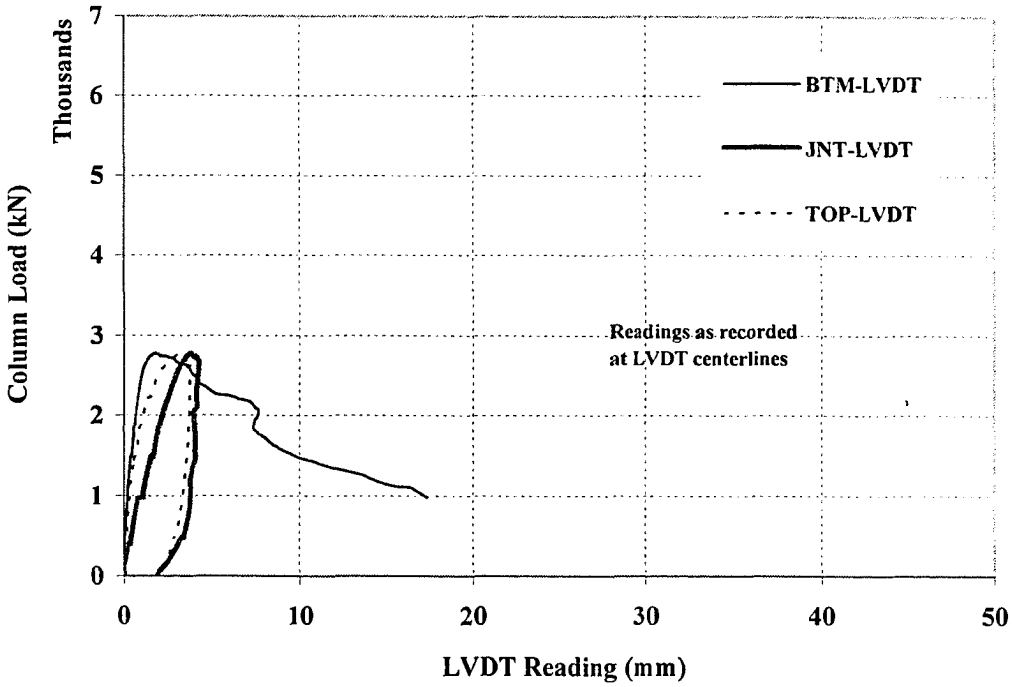

Figure B71. Column Load vs. Vertical LVDT Readings (SP7)

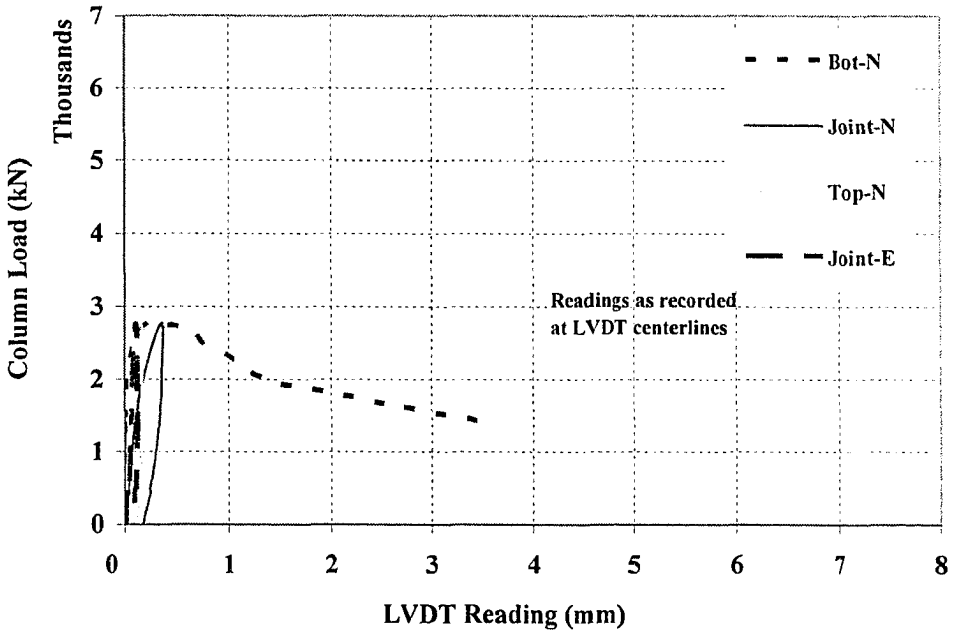

Figure B72. Column Load vs. Horizontal LVDT Readings (SP7)

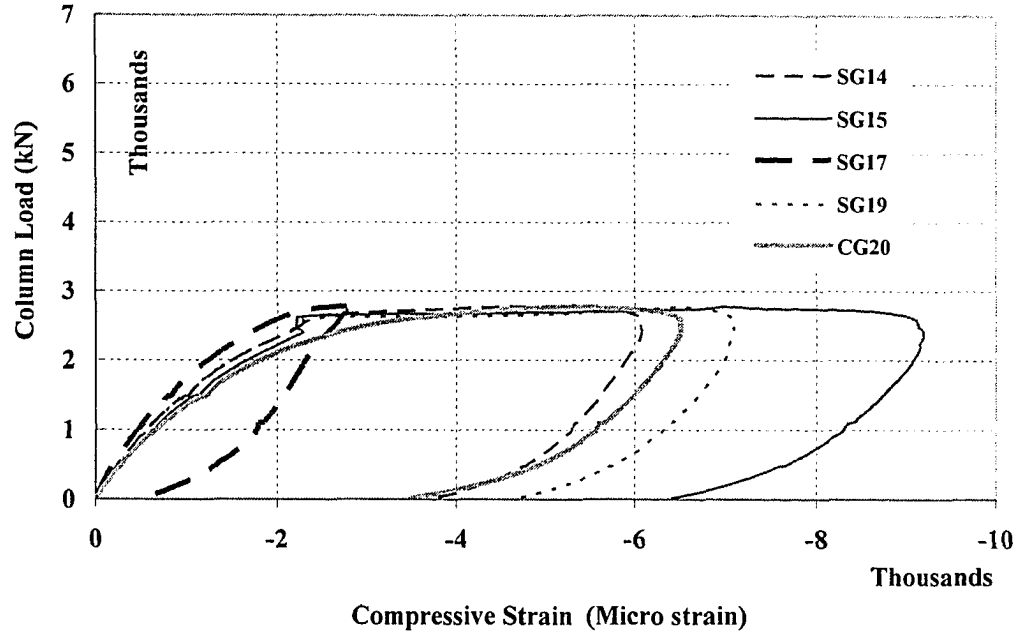

Figure B73. Vertical Load vs. Vertical Strain Values in Top Column of SP7

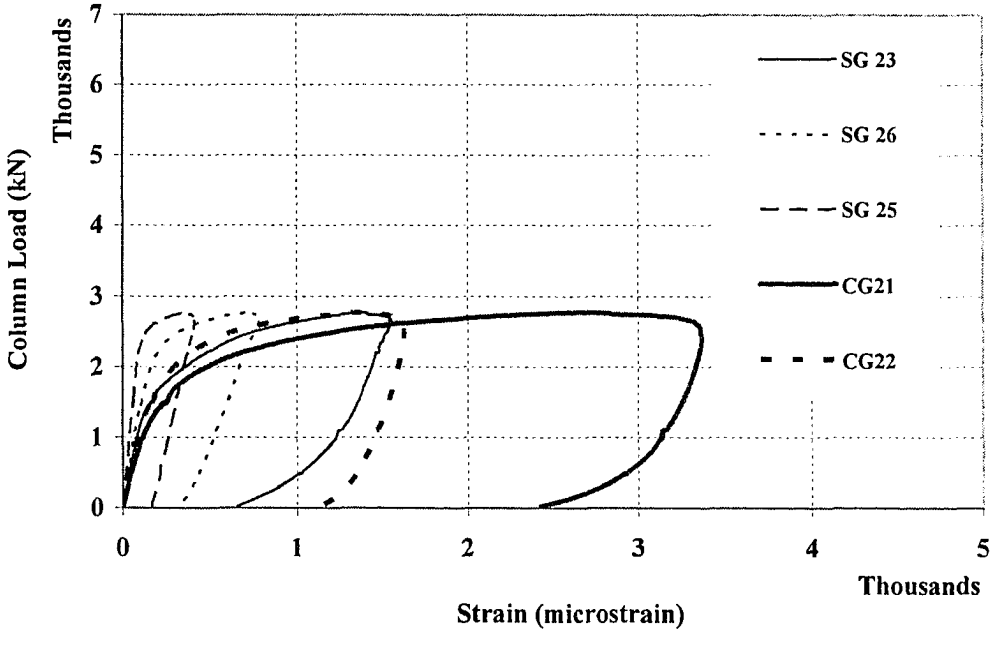

Figure B74. Vertical Load vs. Lateral Strain Values in Top Column of SP7

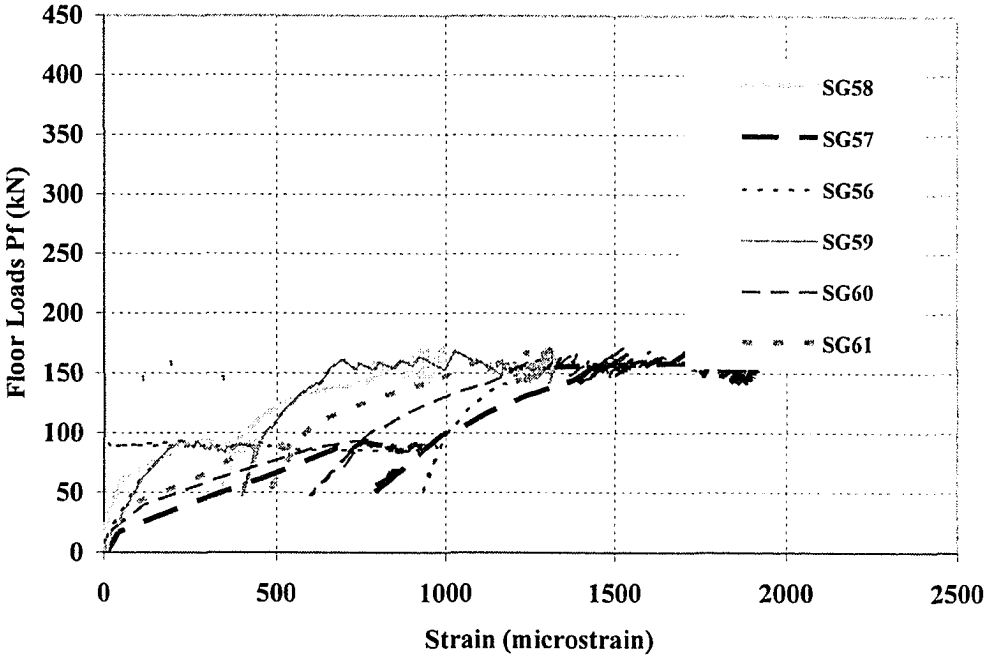

Figure B75. Floor Loads vs. Strain Values of Beam Top Rebars (SP7)

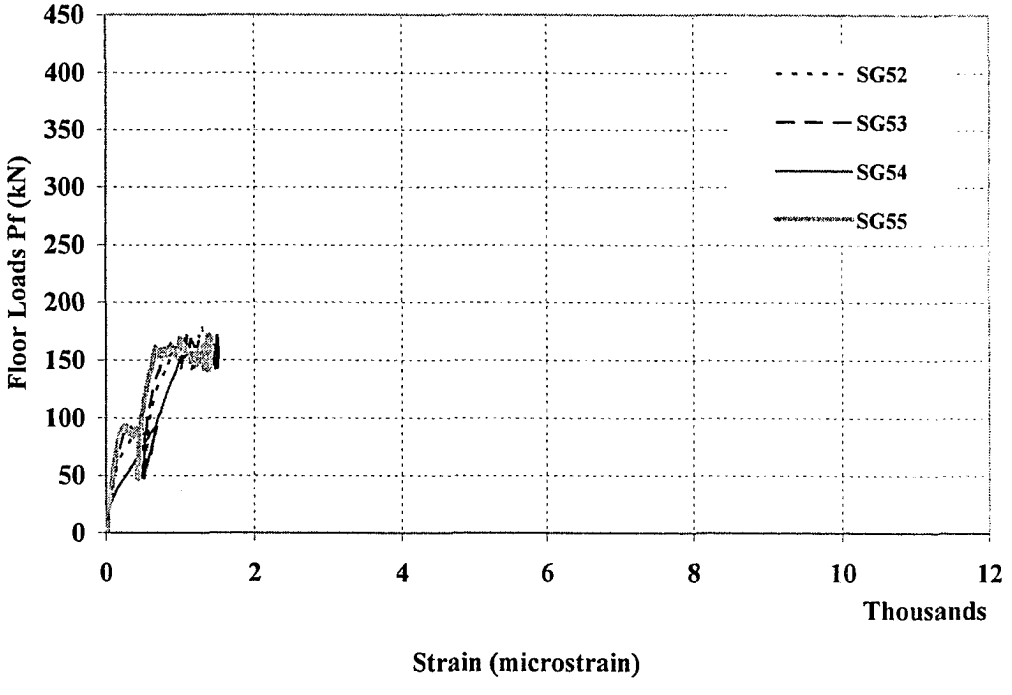

Figure B76. Floor Loads vs. Strain Values of Beam Side Rebars (SP7)

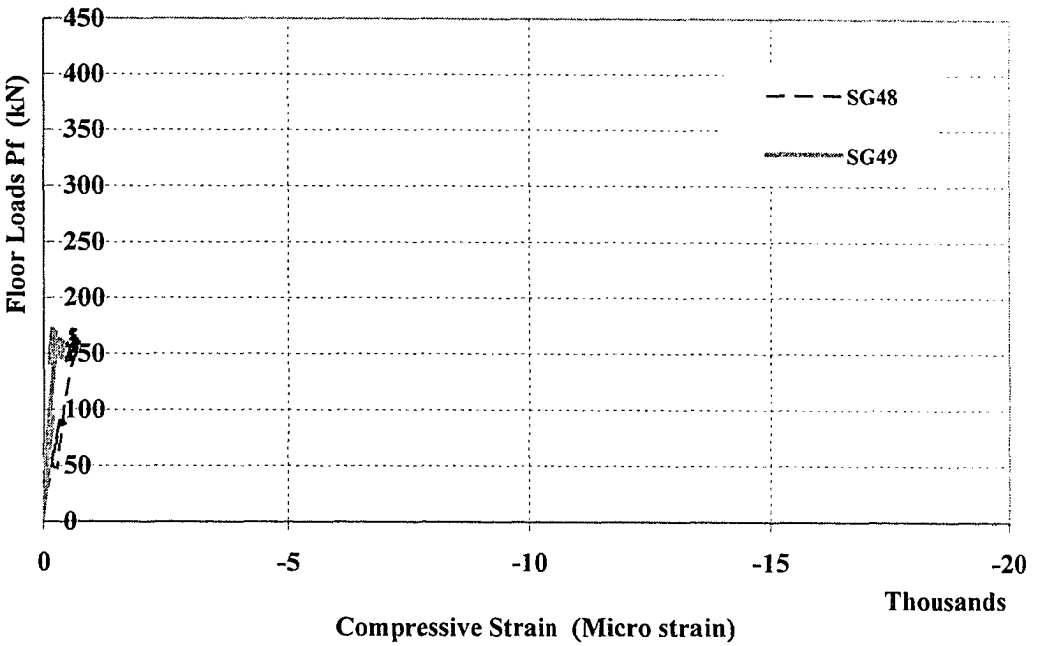

Figure B77. Floor Loads vs. Strain Values of Beam Bottom Rebars (SP7)

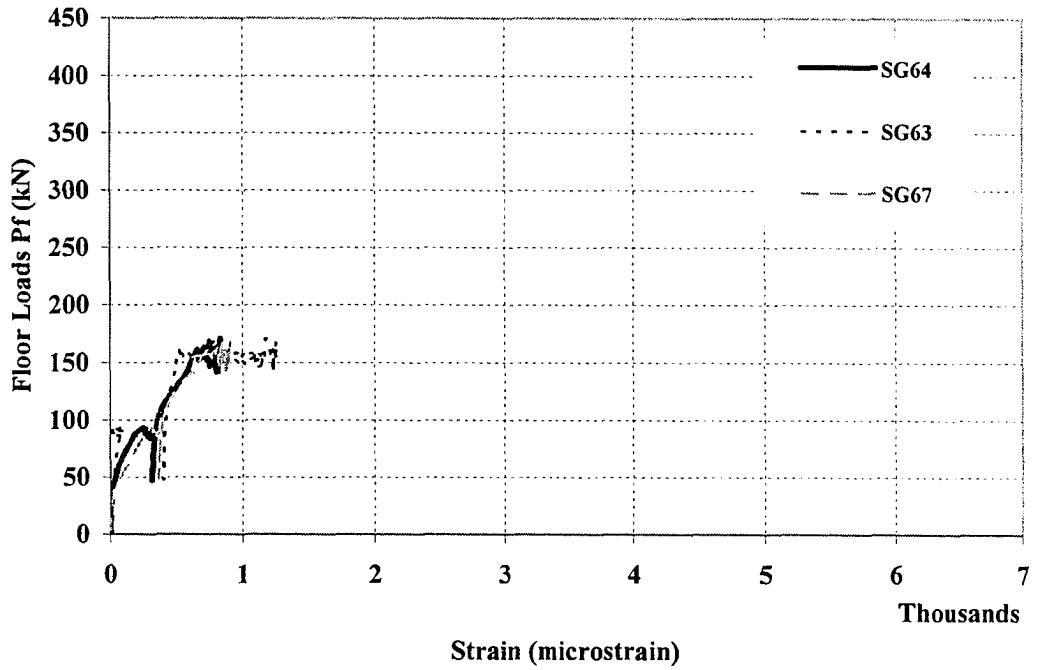

Figure B78. Floor Loads vs. Strain Values of Slab Top Rebars (SP7)

APPENDIX C

Idealized Stress-Strain Curve for Reinforcing Bars

and

Processed Test Results

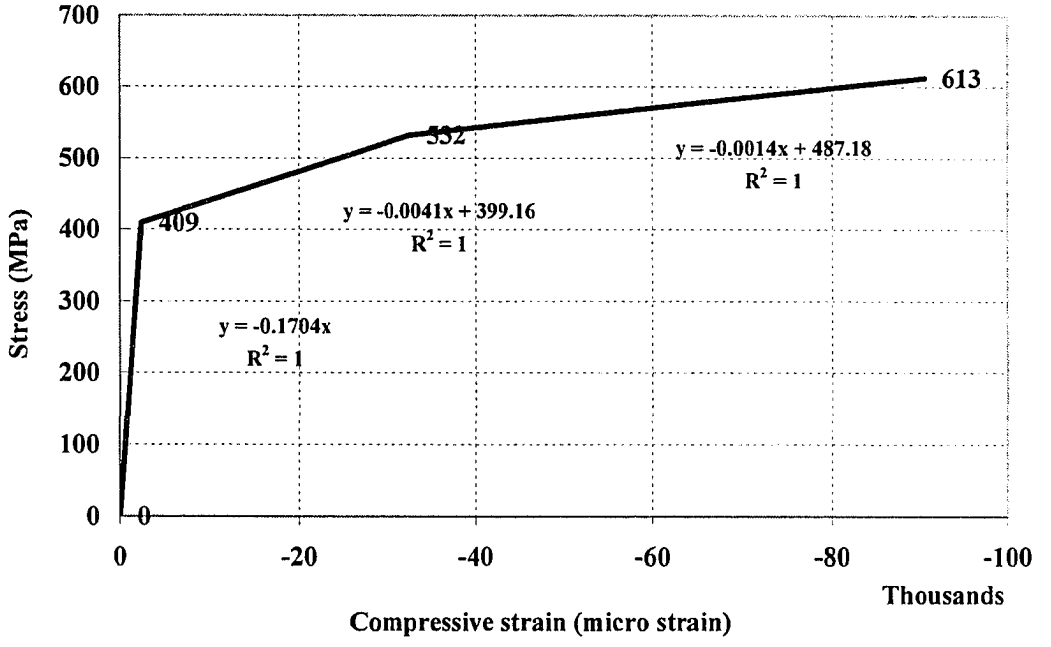

Figure C.1 Idealized Stress-Strain Curve for M15 Column Rebars for Specimens (1-6)

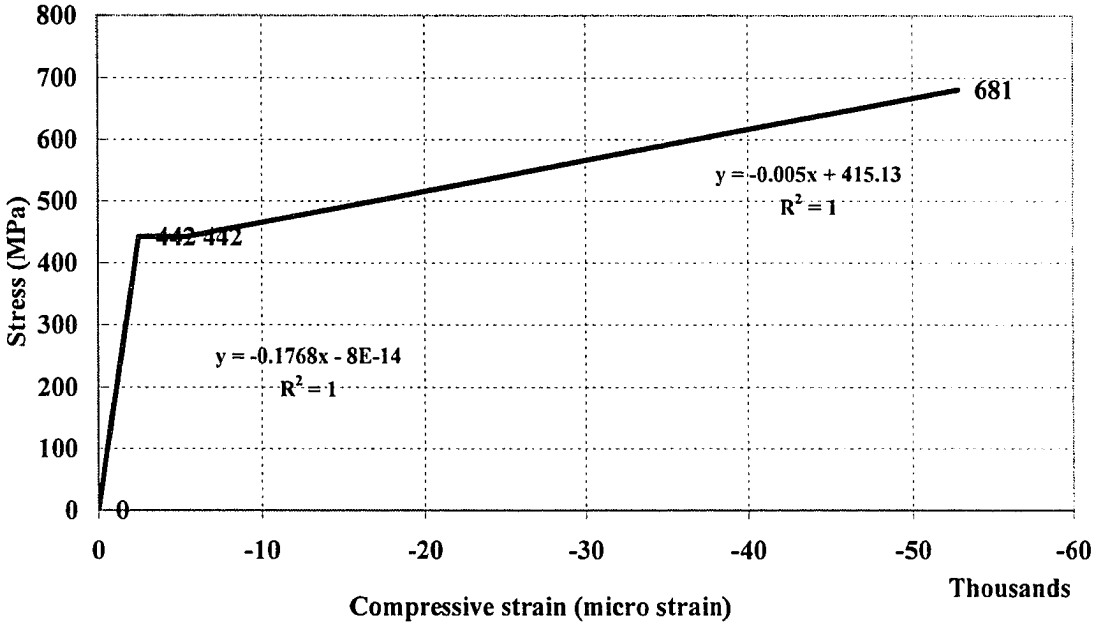

Figure C.2 Idealized Stress-Strain Curve for M15 Column Rebars for Specimen (7)

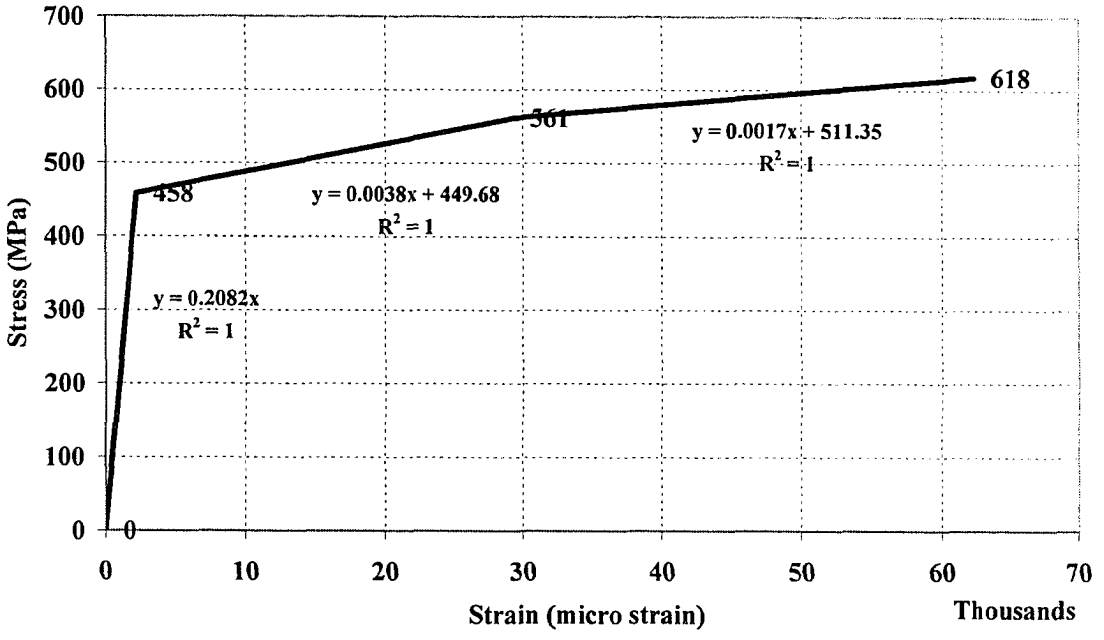

Figure C.3 Idealized Stress-Strain Curve for M10 Rebars (Ties) for Specimens (1-7)

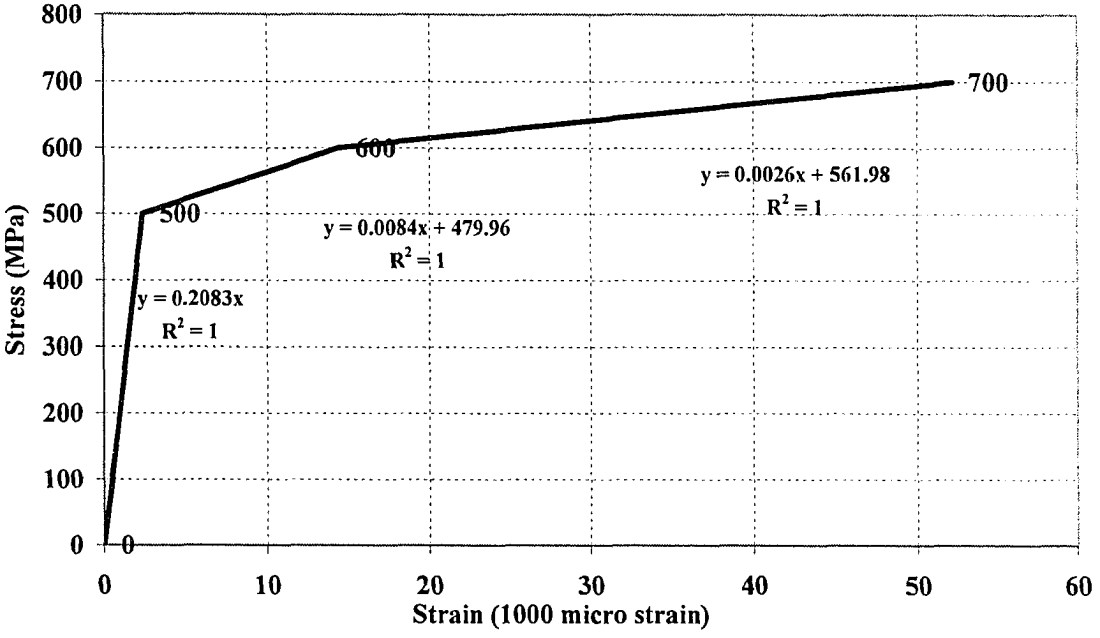

Figure C.4 Idealized Stress-Strain Curve for 9mm Imported Rebars for Specimens (1-7)

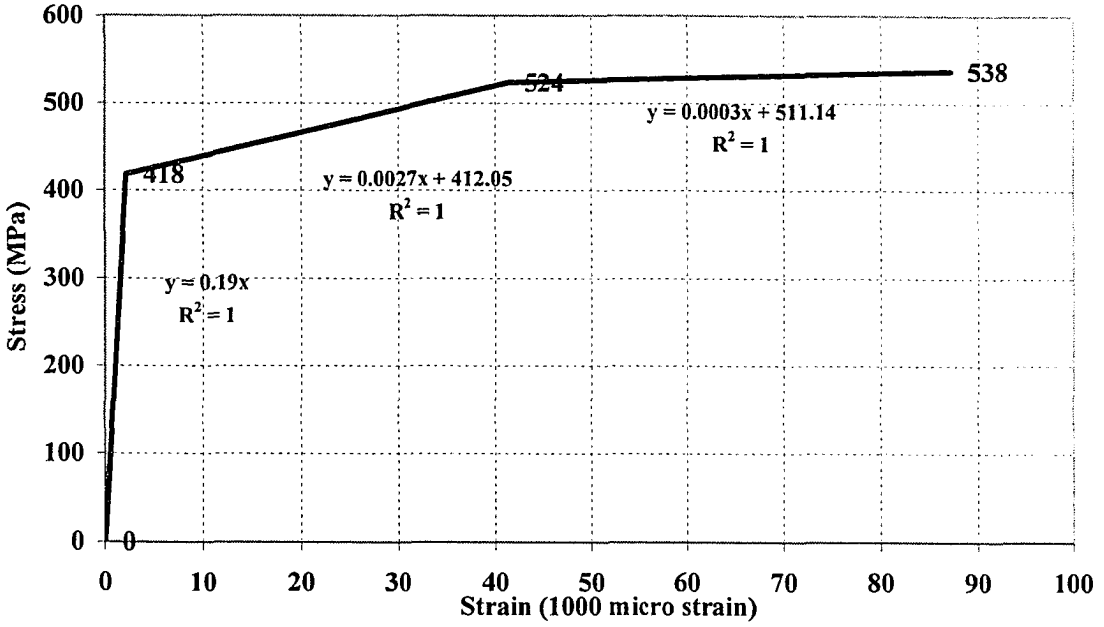

Figure C.5 Idealized Stress-Strain Curve for 6mm Imported Rebars for Specimens (1-7)

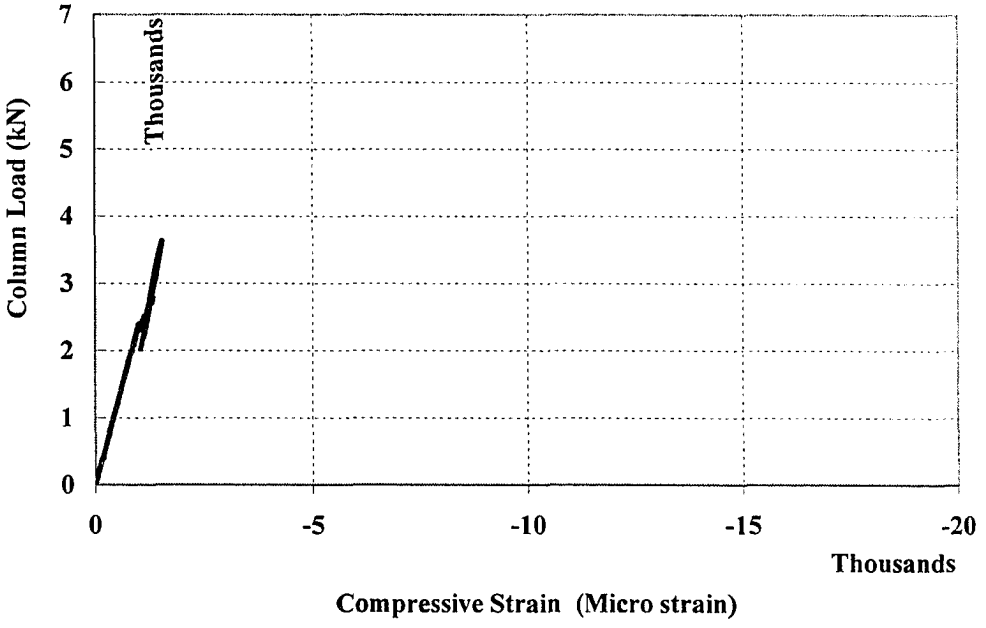

Figure C.6 Column Load vs. Average Rebar-Vertical Strain Values at SP1-Bottom Column

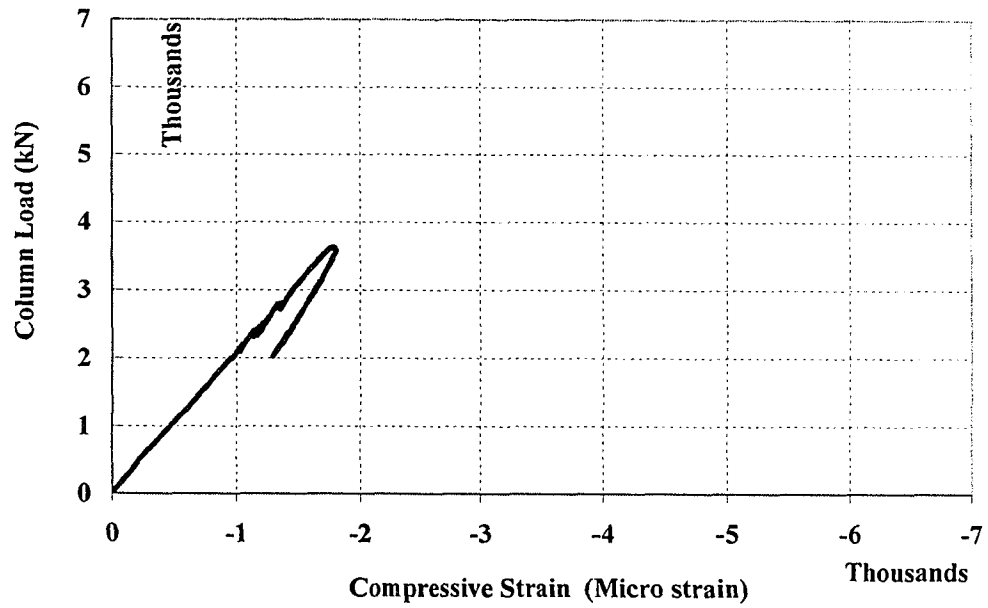

Figure C.7 Column Load vs. Average Rebar-Vertical Strain Values at SP1-Top Column

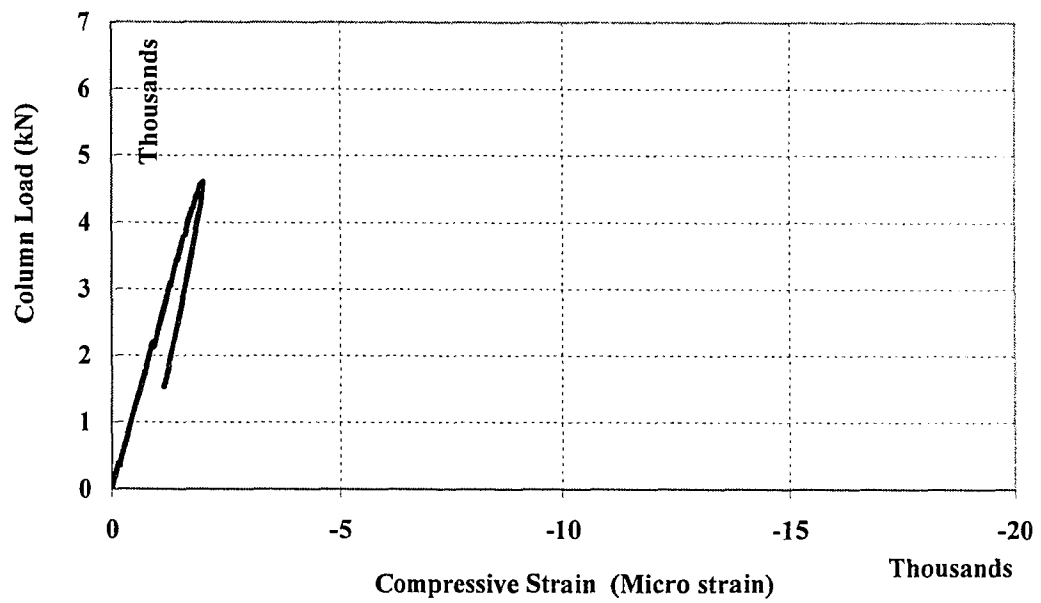

Figure C.8 Column Load vs. Average Rebar-Vertical Strain Values at SP2-Bottom Column

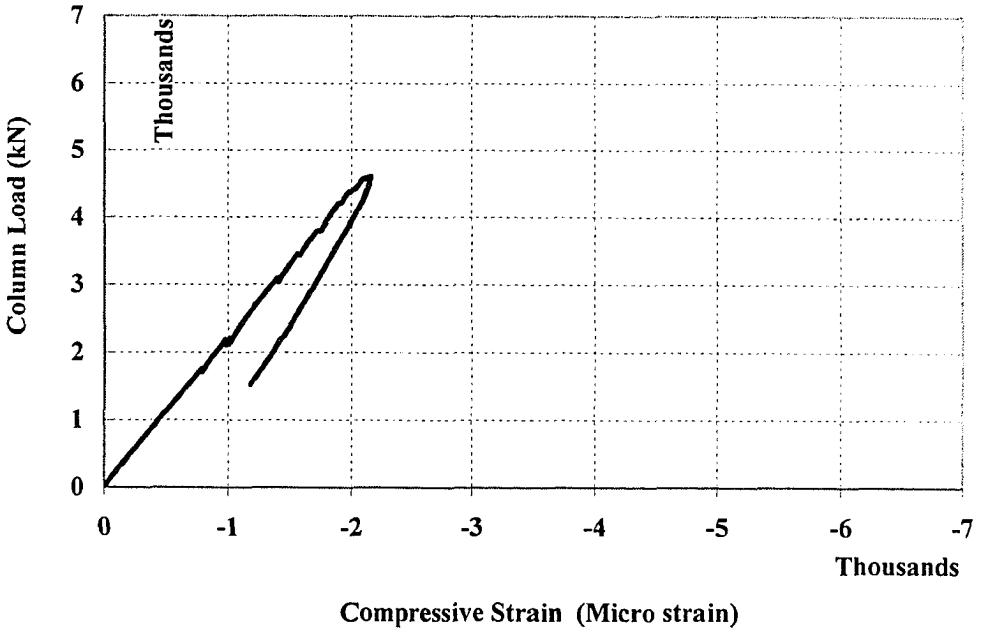

Figure C.9 Column Load vs. Average Rebar-Vertical Strain Values at SP2-Top Column

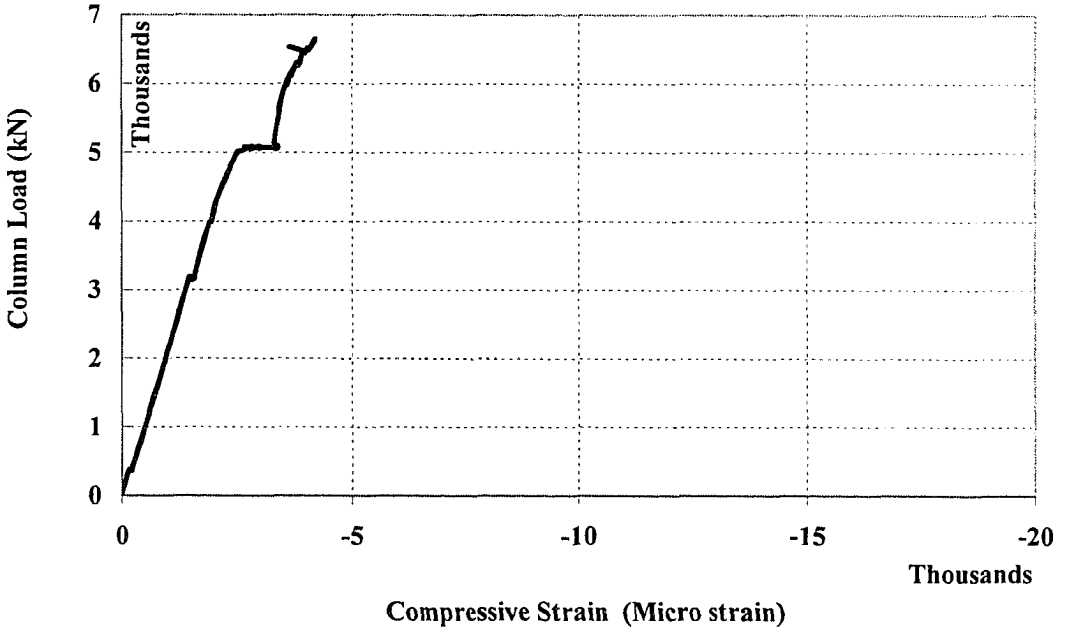

Figure C.10 Column Load vs. Average Rebar-Vertical Strain Values at SP3-Bottom Column

Figure C.11 Column Load vs. Average Rebar-Vertical Strain Values at SP3-Joint

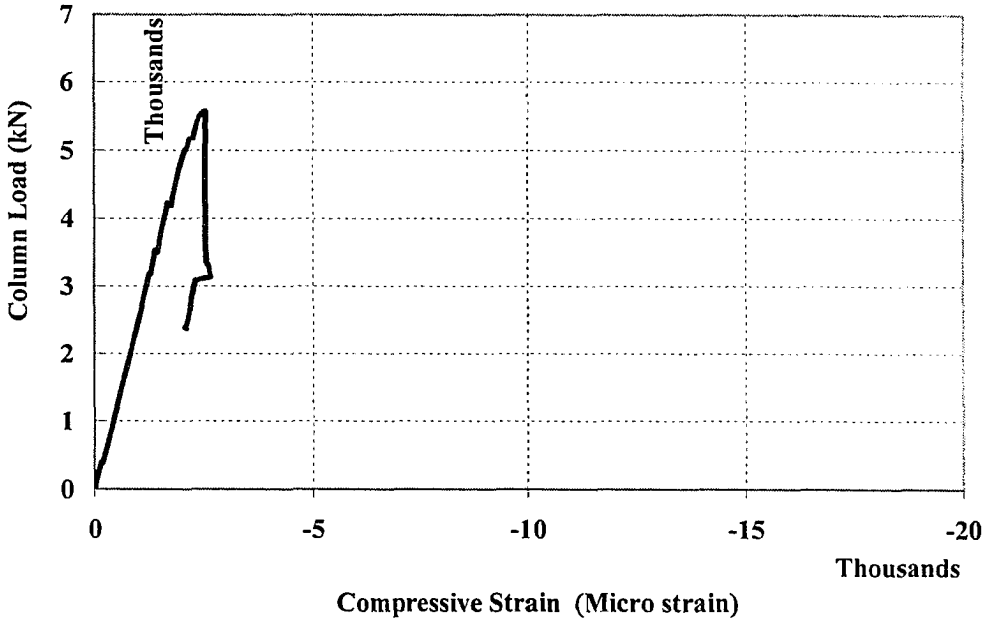

Figure C.12 Column Load vs. Average Rebar-Vertical Strain Values at SP4-Bottom Column

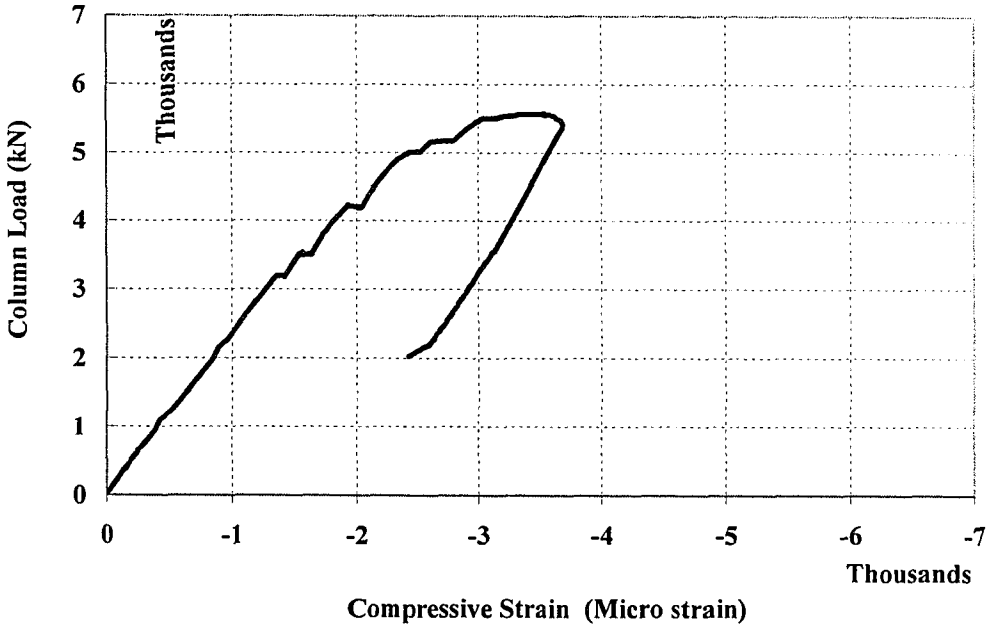

Figure C.13 Column Load vs. Average Rebar-Vertical Strain Values at SP4-Top Column

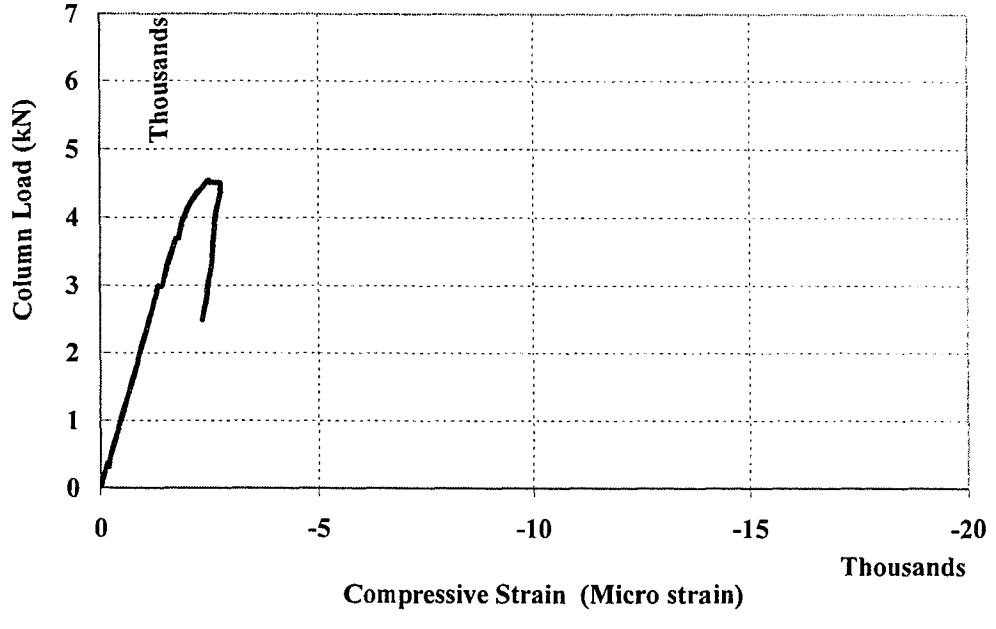

Figure C.14 Column Load vs. Average Rebar-Vertical Strain Values at SP5-Bottom Column

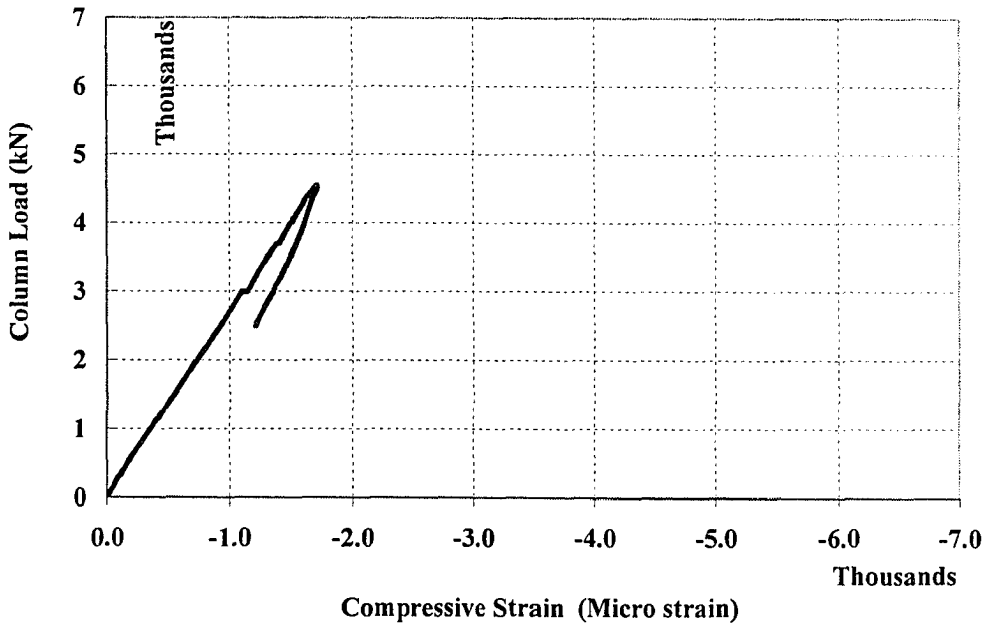

Figure C.15 Column Load vs. Average Rebar-Vertical Strain Values at SP5-Top Column

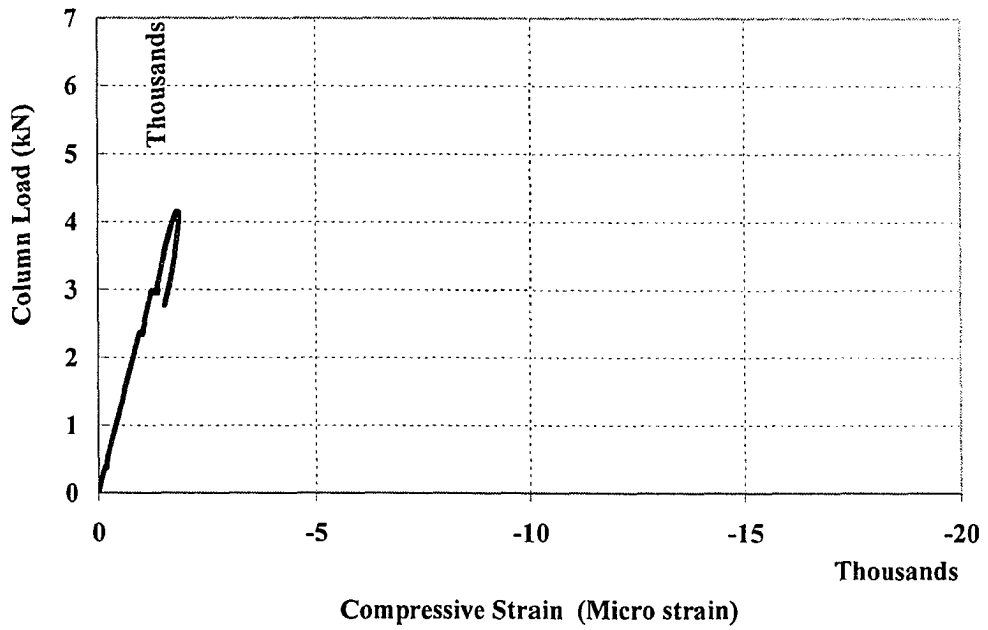

Figure C.16 Column Load vs. Average Rebar-Vertical Strain Values at SP6-Bottom Column

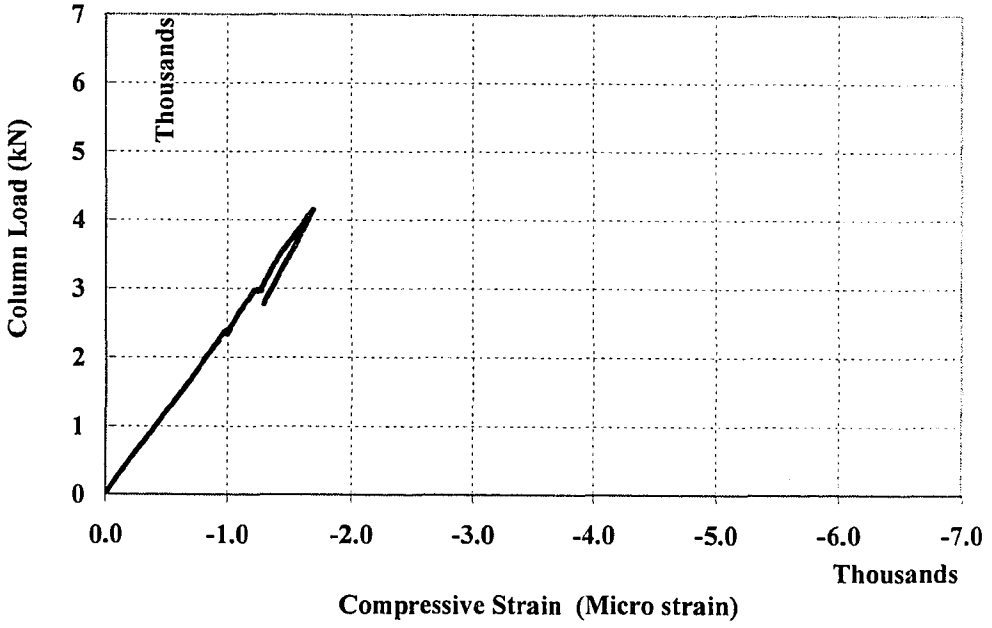

Figure C.17 Column Load vs. Average Rebar-Vertical Strain Values at SP6-Top Column

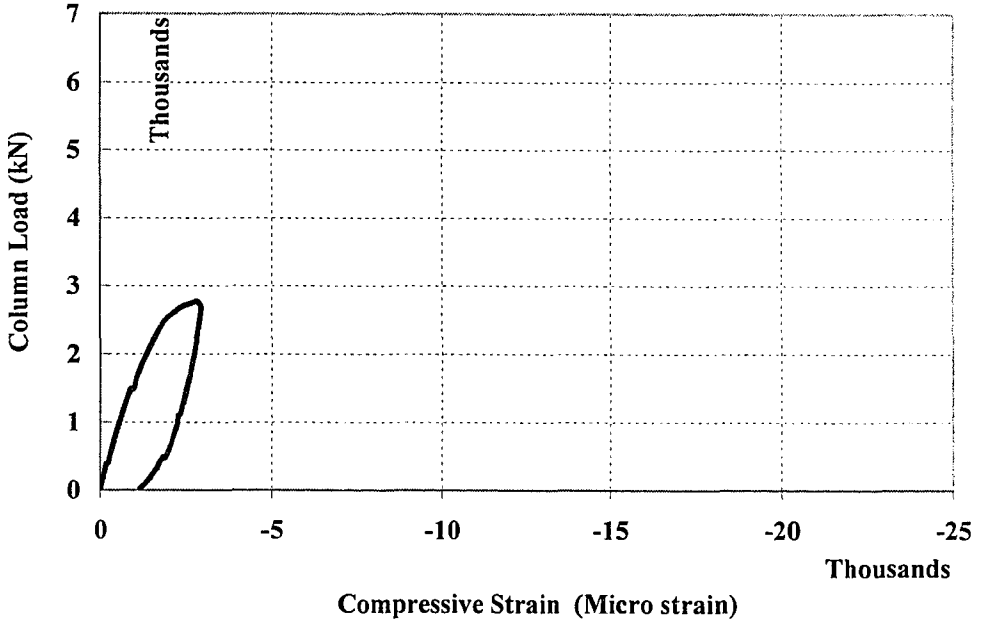

Figure C.18 Column Load vs. Average Rebar-Vertical Strain at SP7-Joint

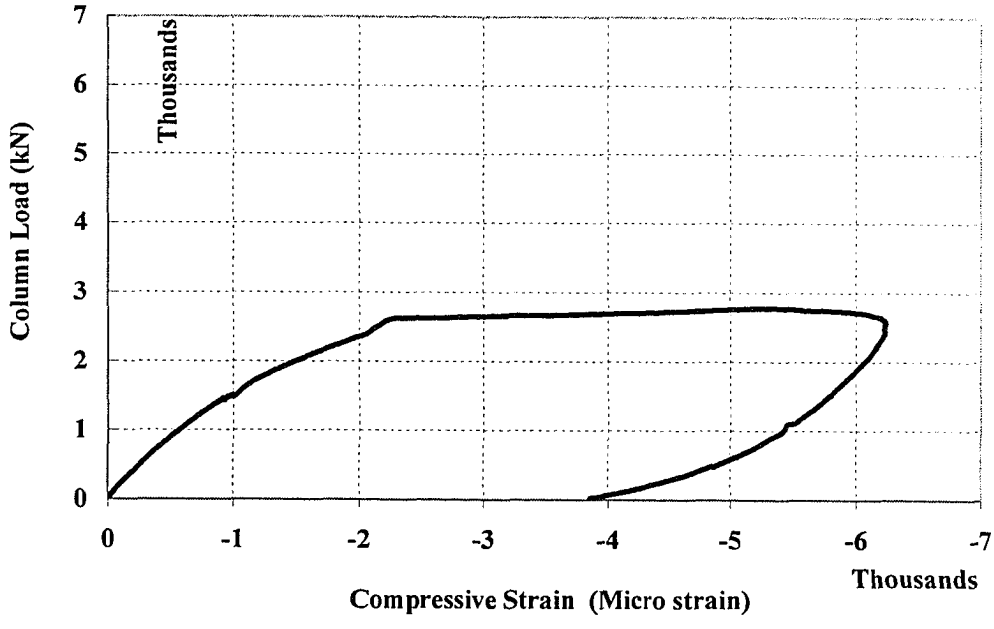

Figure C.19 Column Load vs. Average Rebar-Vertical Strain at SP7-Top Column

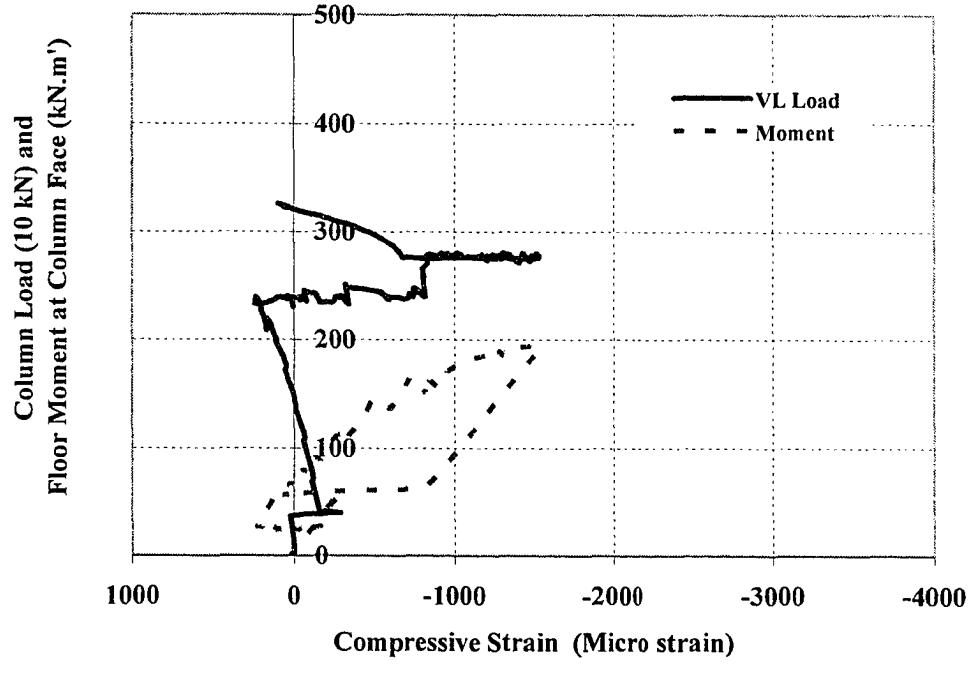

Figure C.20 Effect of Column and Floor Loads on Strain of Beam Bottom RFT at SP1-Column Core

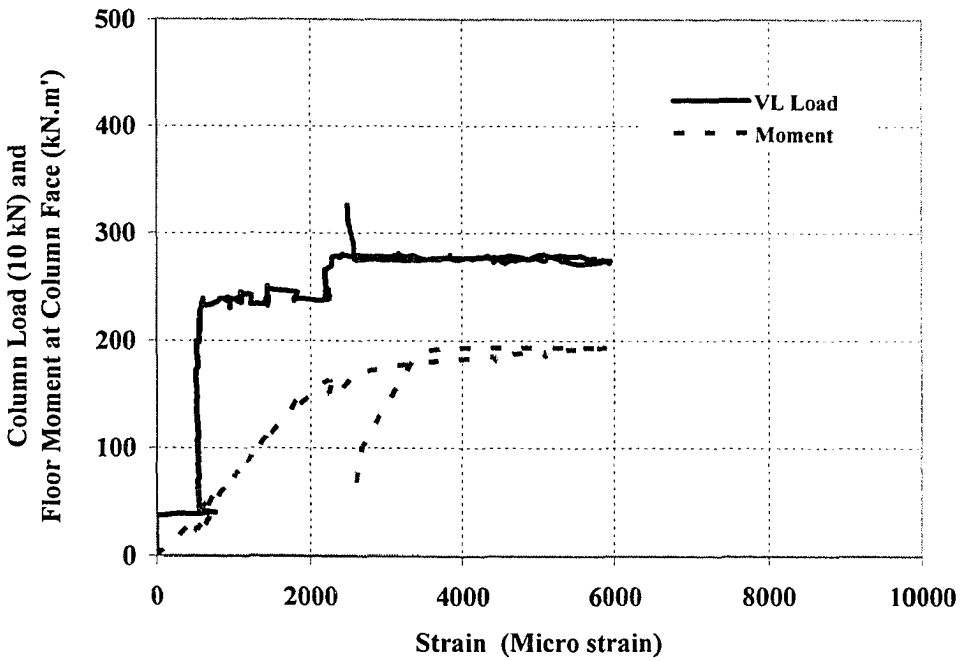

Figure C.21 Effect of Column and Floor Loads on Strain of Beam Side RFT at SP1-Column Core

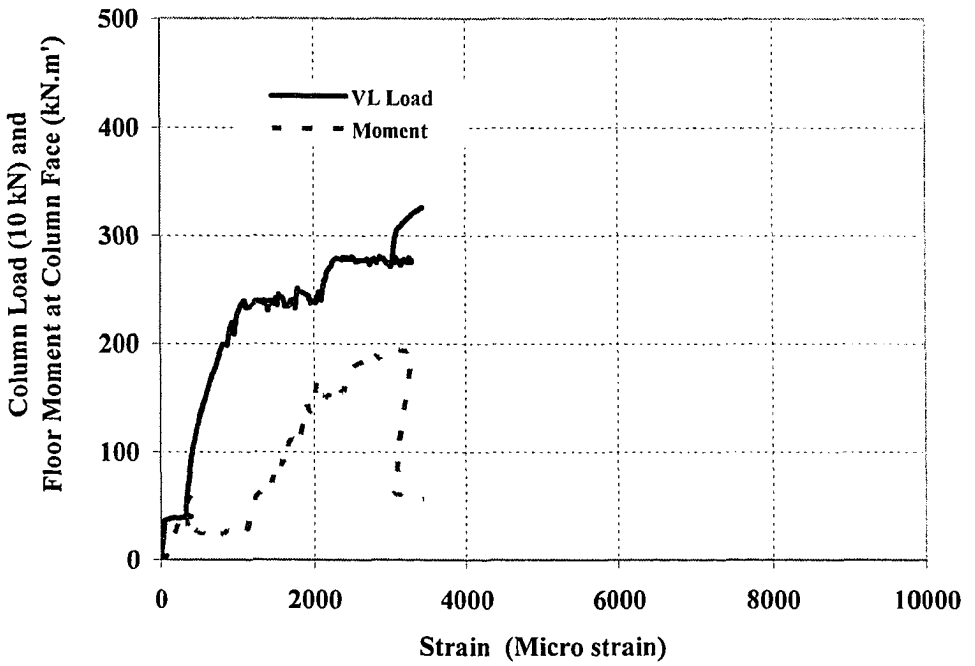

Figure C.22 Effect of Column and Floor Loads on Strain of Beam Side RFT at SP1-Column Face

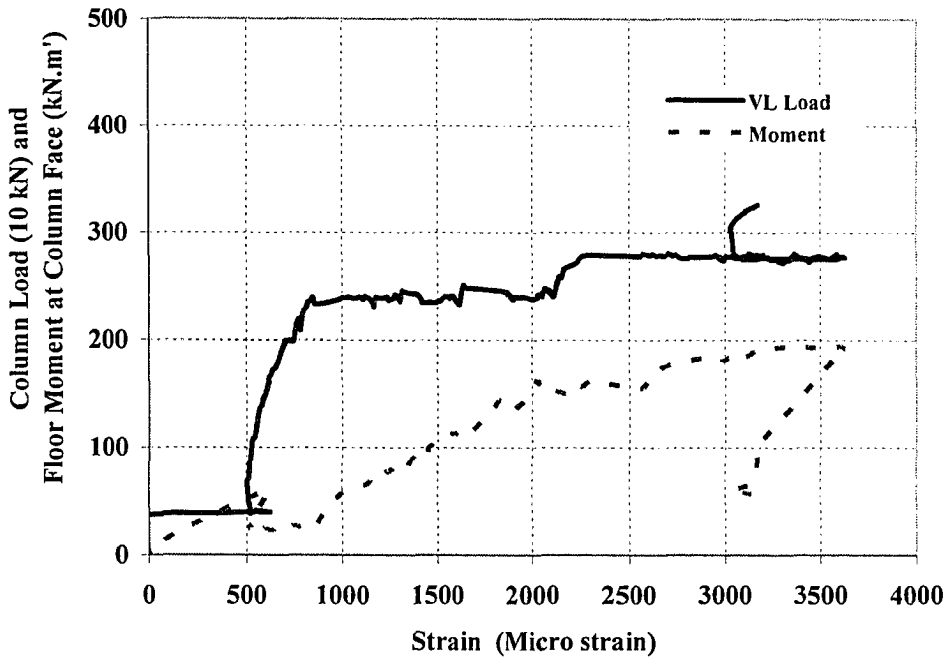

Figure C.23 Effect of Column and Floor Loads on Strain of Beam Top RFT at SP1-Column Core

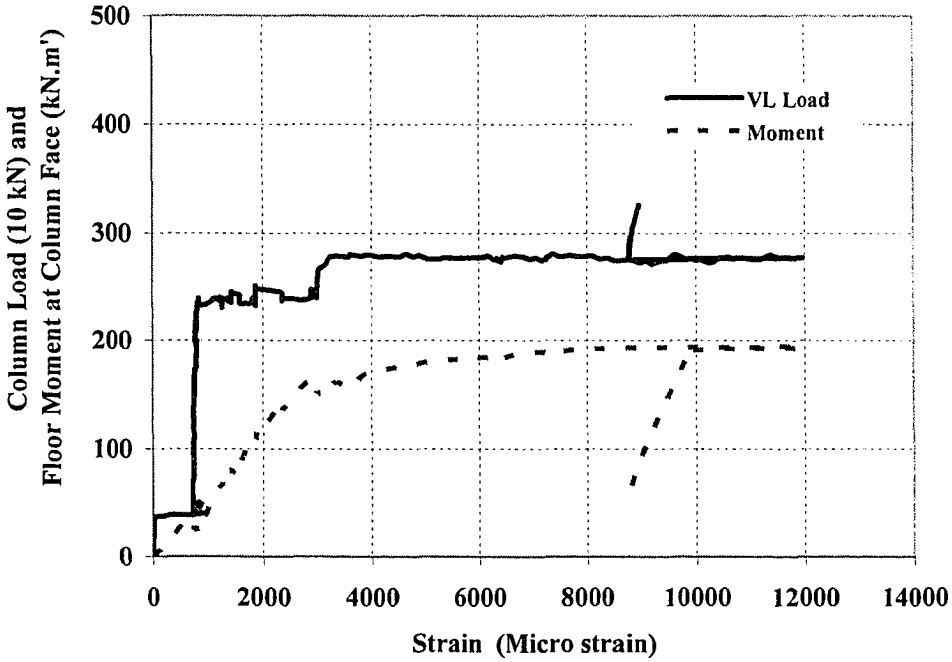

Figure C.24 Effect of Column and Floor Loads on Strain of Beam Top RFT at SP1-Column Face

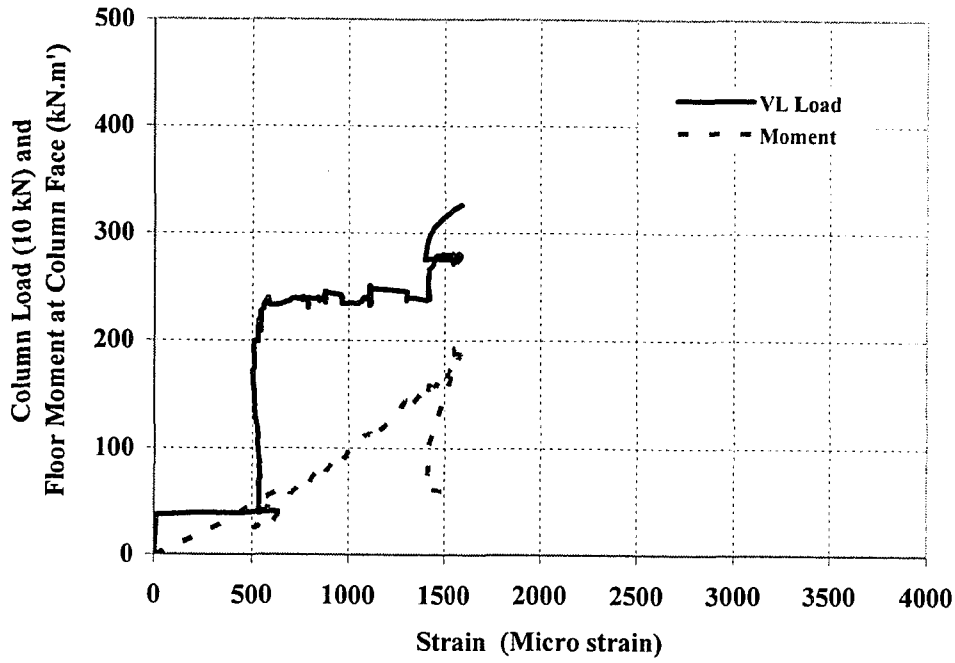

Figure C.25 Effect of Column and Floor Loads on Strain of Slab Top RFT at SP1-Column Face

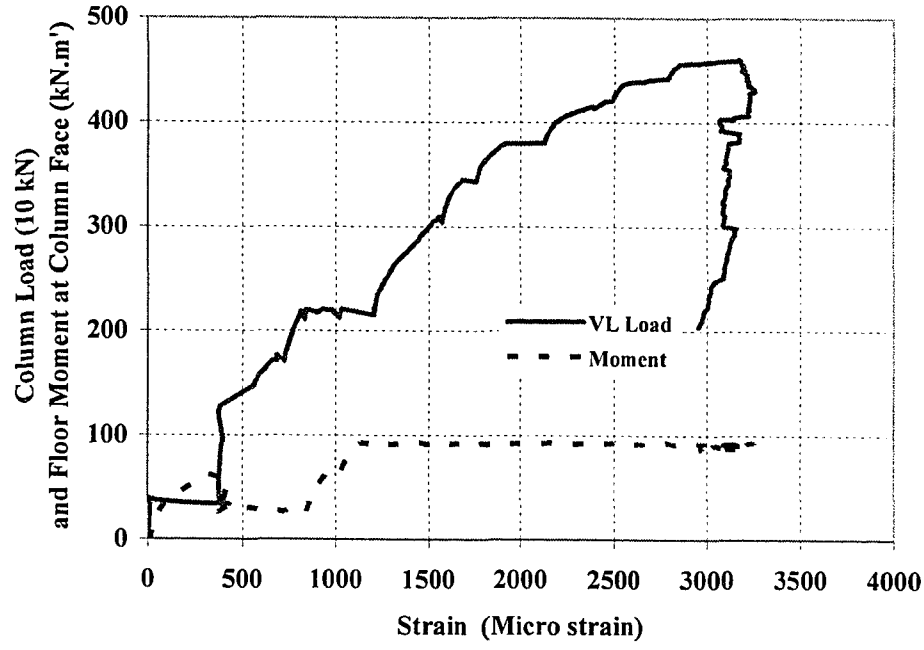

Figure C.26 Effect of Column and Floor Loads on Strain of Beam Top RFT at SP2-Joint Core

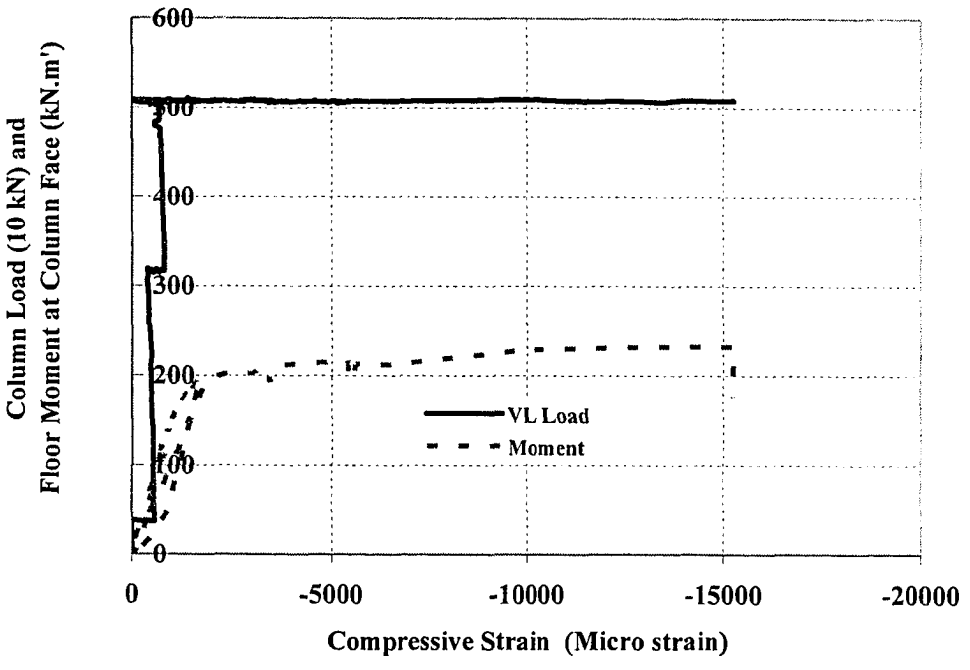

Figure C.27 Effect of Column and Floor Loads on Strain of Beam Bottom RFT at SP3-Column Face

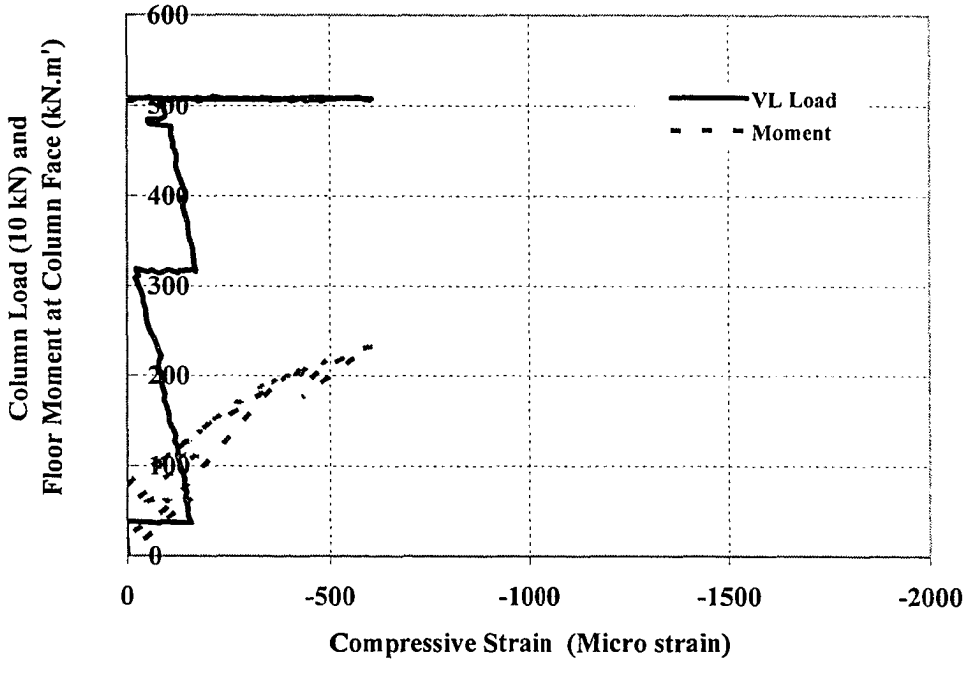

Figure C.28 Effect of Column and Floor Loads on Strain of Beam Bottom RFT at SP3-Column Face

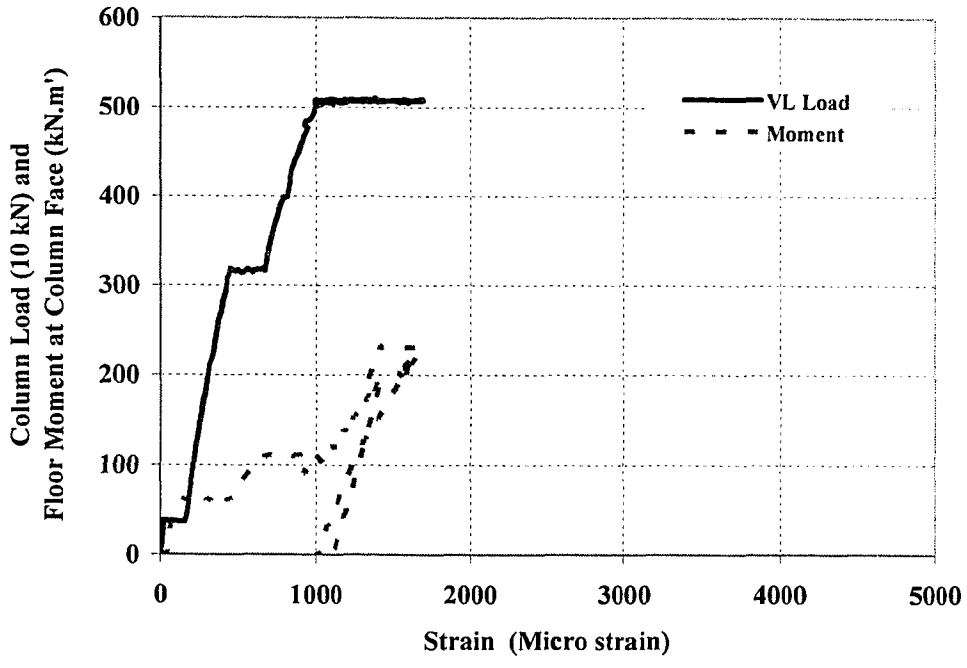

Figure C.29 Effect of Column and Floor Loads on Strain of Beam Side RFT at SP3-Column Core

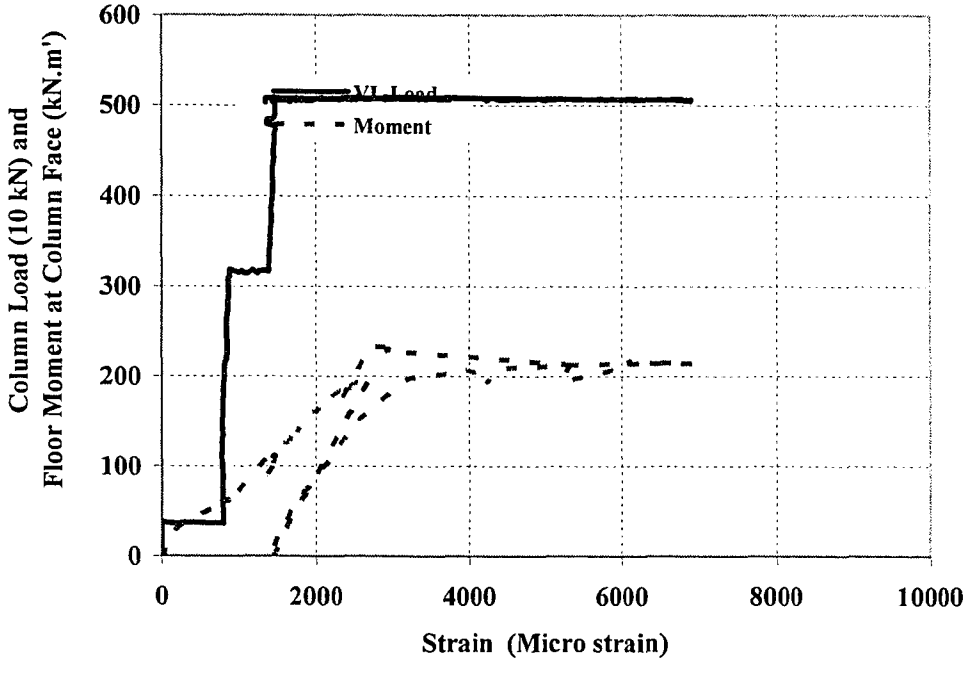

Figure C.30 Effect of Column and Floor Loads on Strain of Beam Side RFT at SP3-Column Face

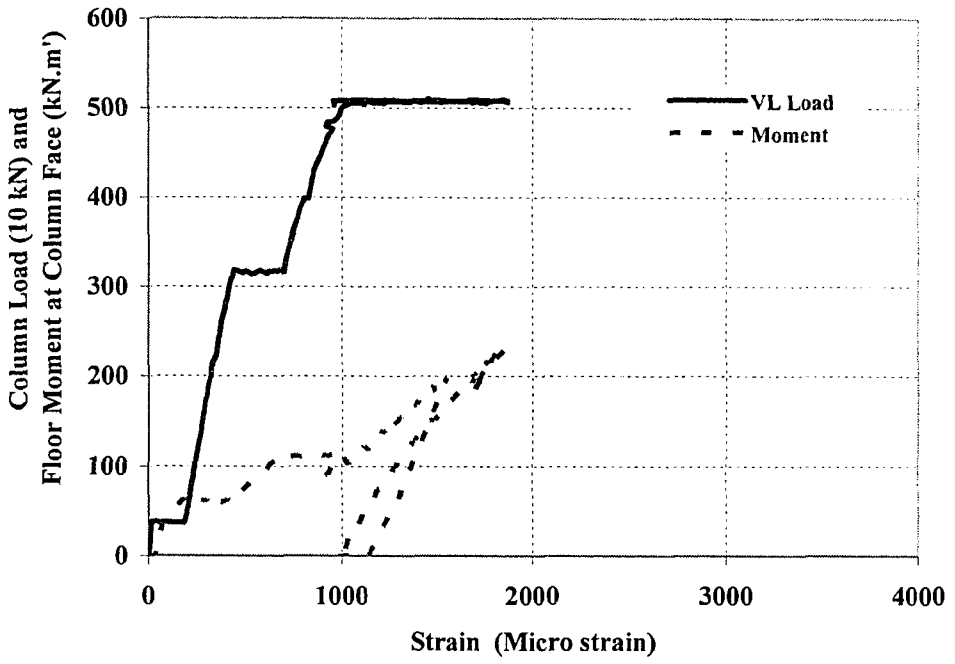

Figure C.31 Effect of Column and Floor Loads on Strain of Beam Top RFT at SP3-Column Core

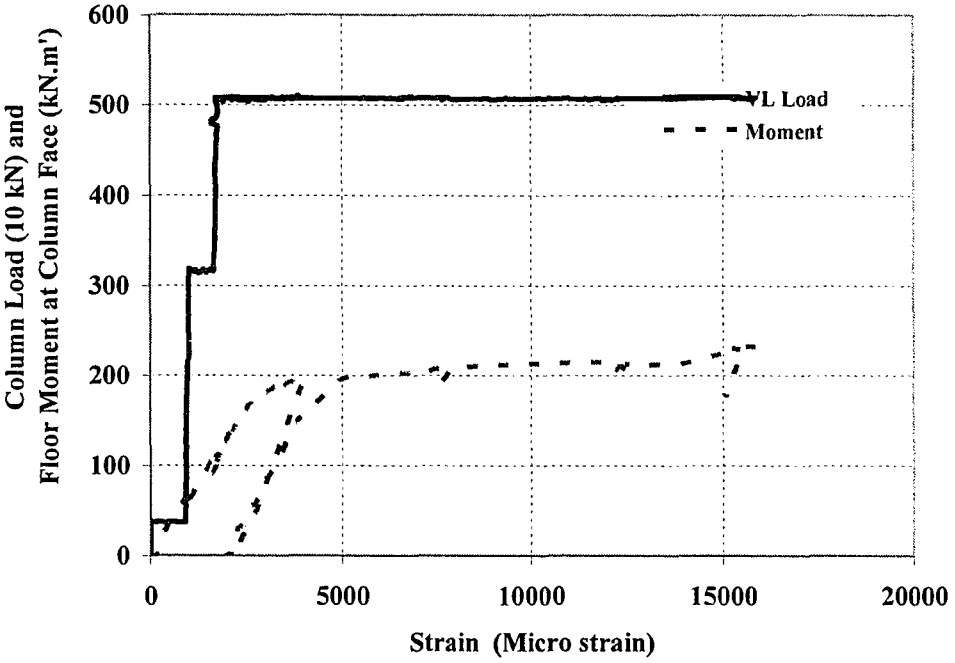

Figure C.32 Effect of Column and Floor Loads on Strain of Beam Top RFT at SP3-Column Face

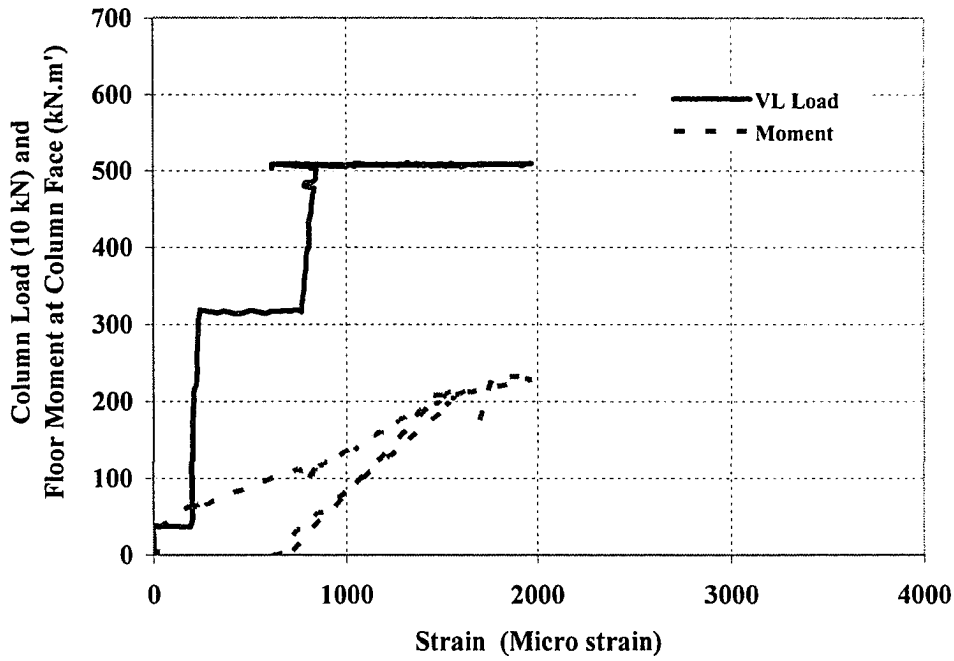

Figure C.33 Effect of Column and Floor Loads on Strain of Slab Top RFT at SP3-Column Face

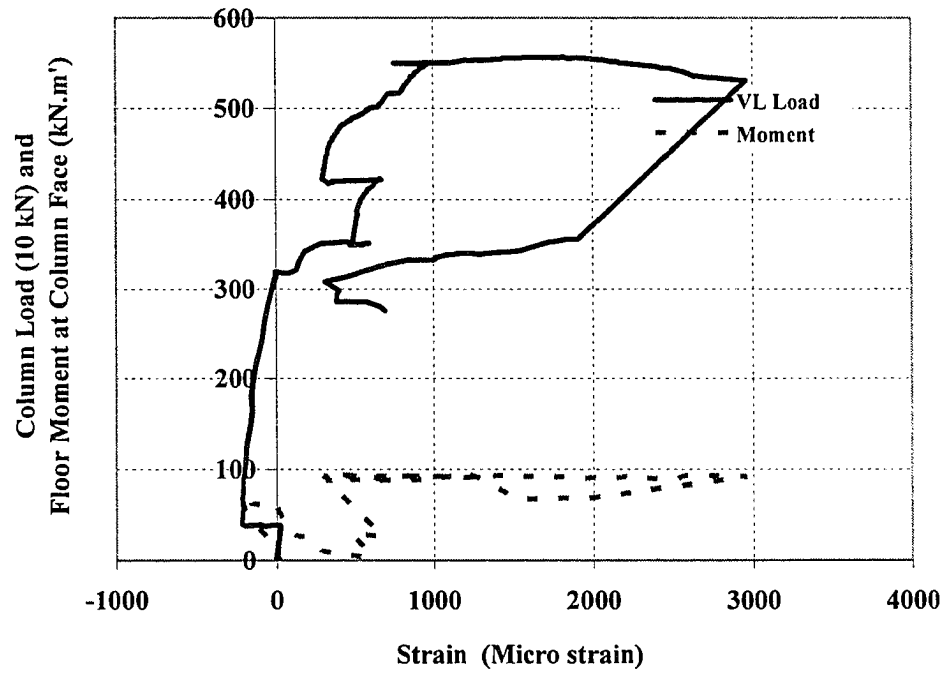

Figure C.34 Effect of Column and Floor Loads on Strain of Beam Bottom RFT at SP4-Column Face

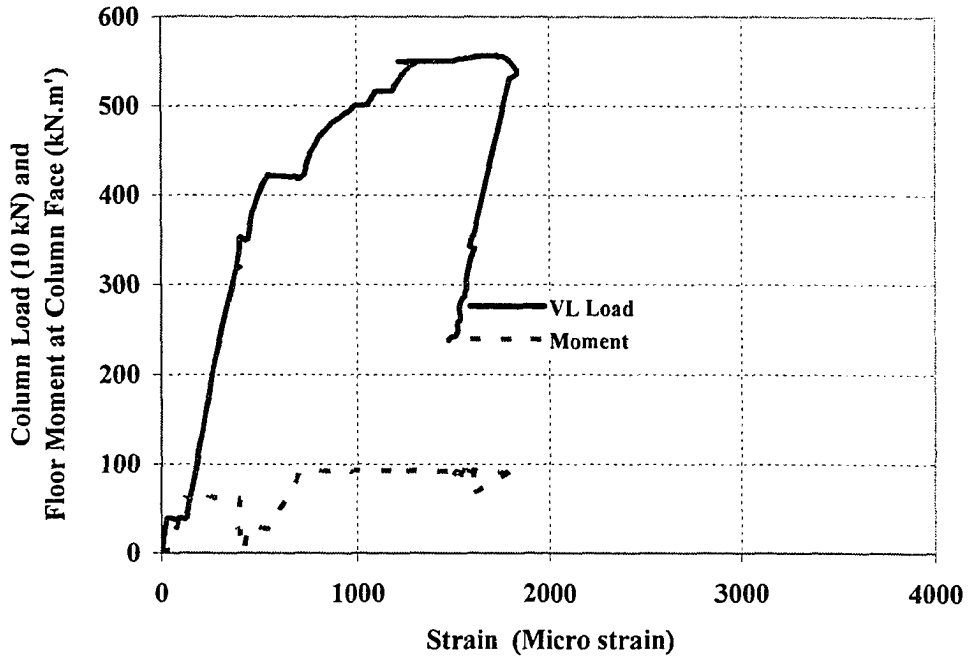

Figure C.35 Effect of Column and Floor Loads on Strain of Beam Side RFT at SP4-Column Core

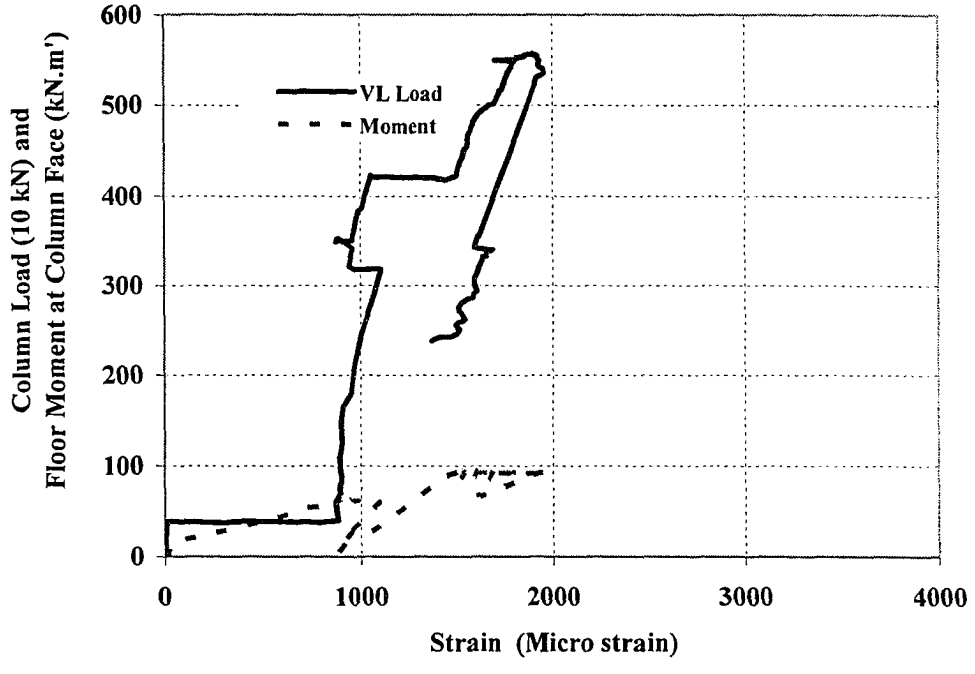

Figure C.36 Effect of Column and Floor Loads on Strain of Beam Side RFT at SP4-Column Face

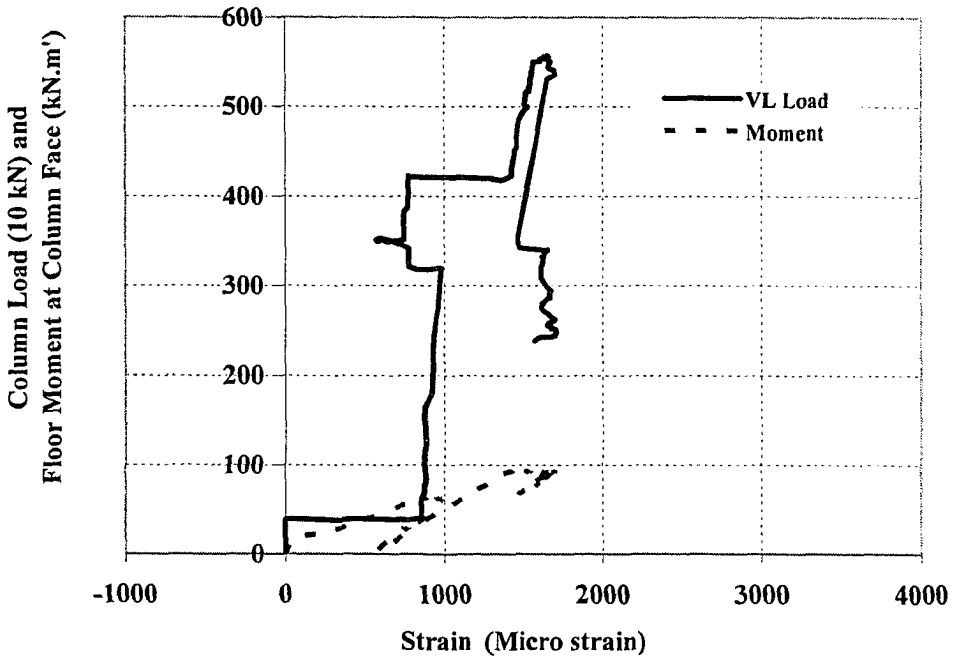

Figure C.37 Effect of Column and Floor Loads on Strain of Beam Top RFT at SP4-Column Face

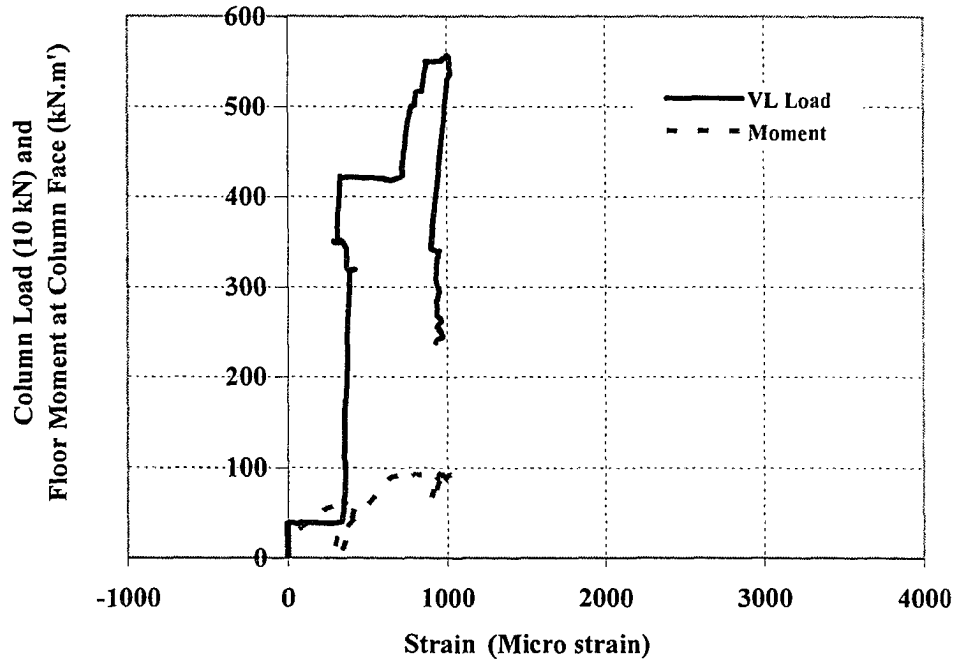

Figure C.38 Effect of Column and Floor Loads on Strain of Slab Top RFT at SP4-Column Face

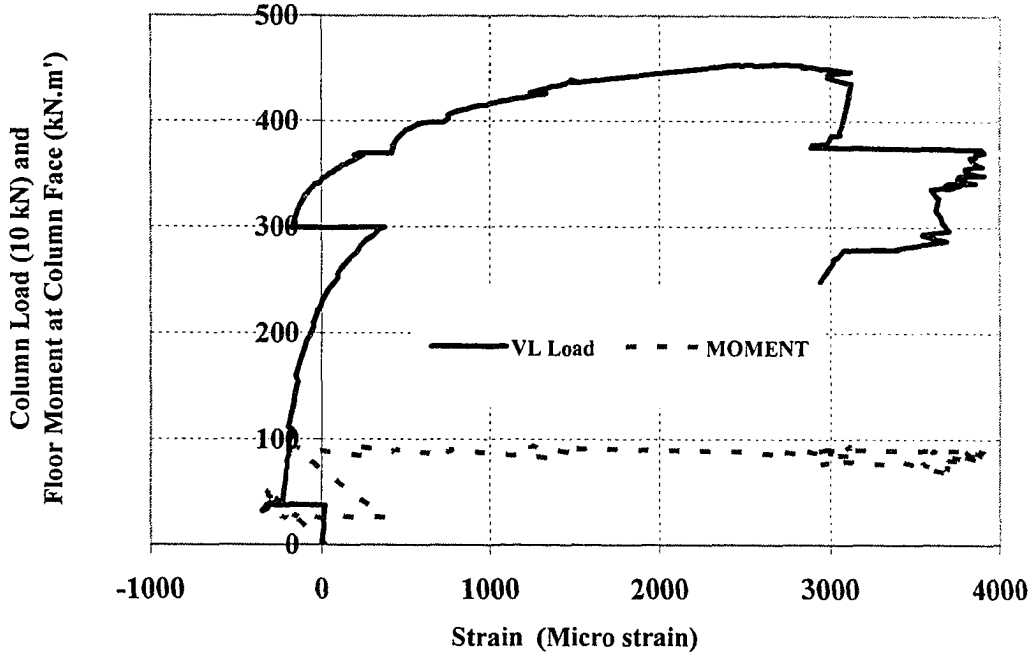

Figure C.39 Effect of Column and Floor Loads on Strain of Beam Bottom RFT at SP5-Joint Face

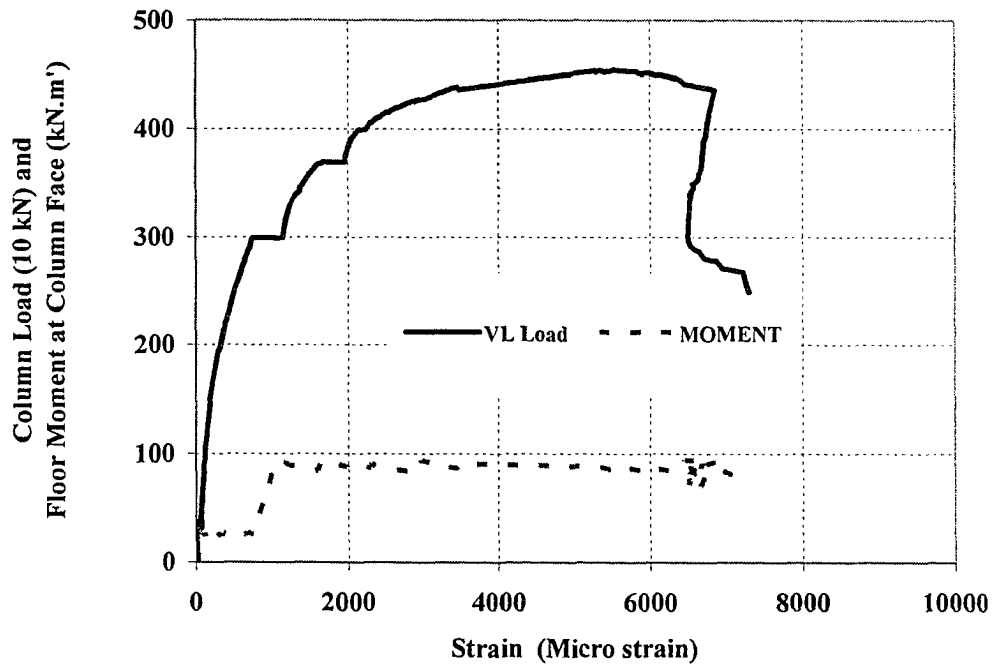

Figure C.40 Effect of Column and Floor Loads on Strain of Beam Side RFT at SP5-Joint Core

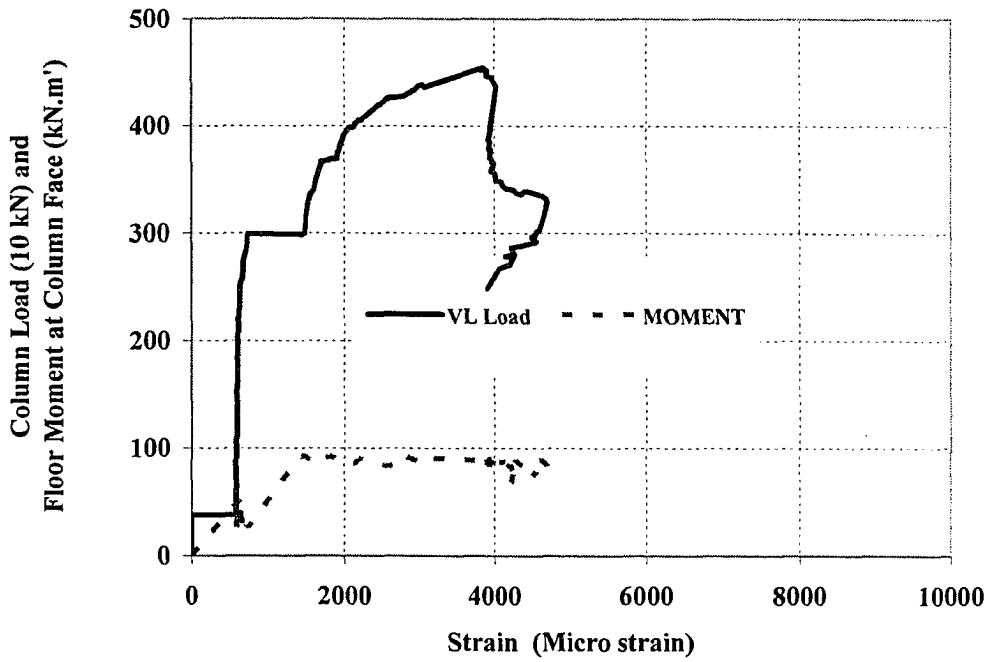

Figure C.41 Effect of Column and Floor Loads on Strain of Beam Side RFT at SP5-Joint Face

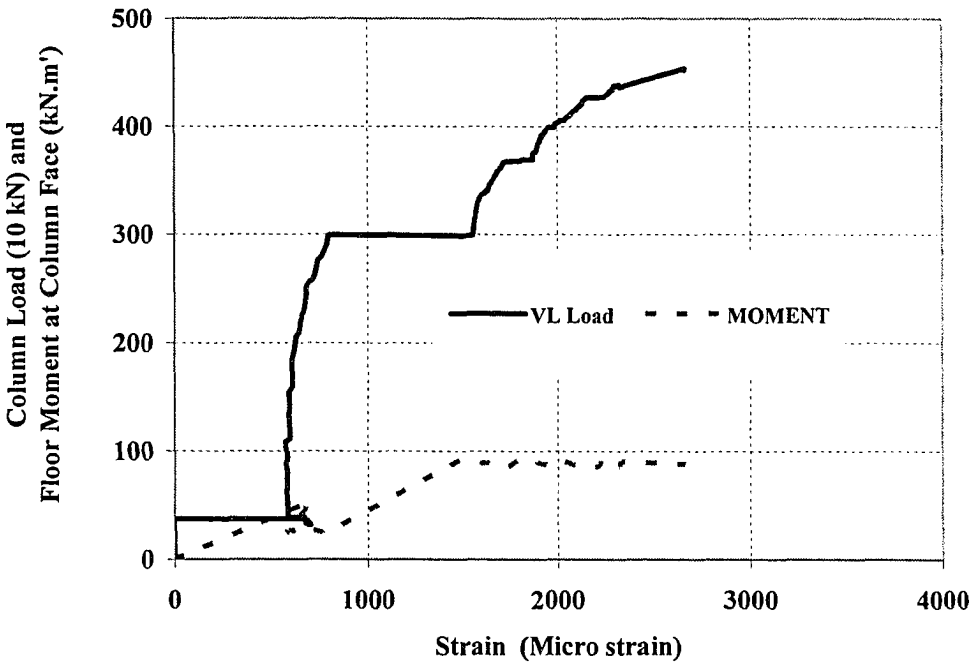

Figure C.42 Effect of Column and Floor Loads on Strain of Beam Top RFT at SP5-Joint Core

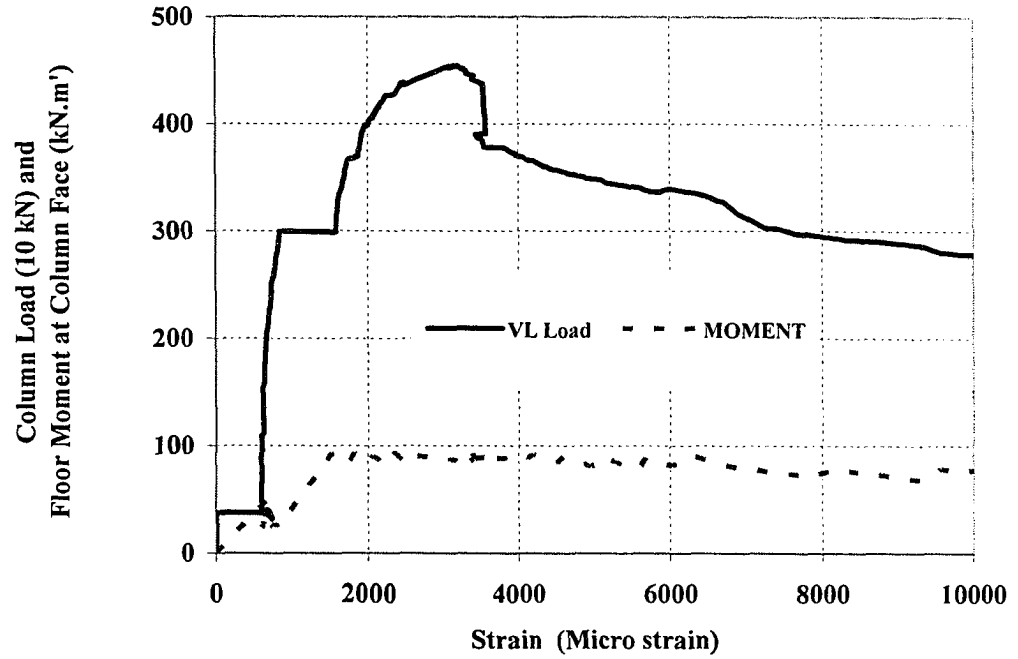

Figure C.43 Effect of Column and Floor Loads on Strain of Beam Top RFT at SP5-Joint Face

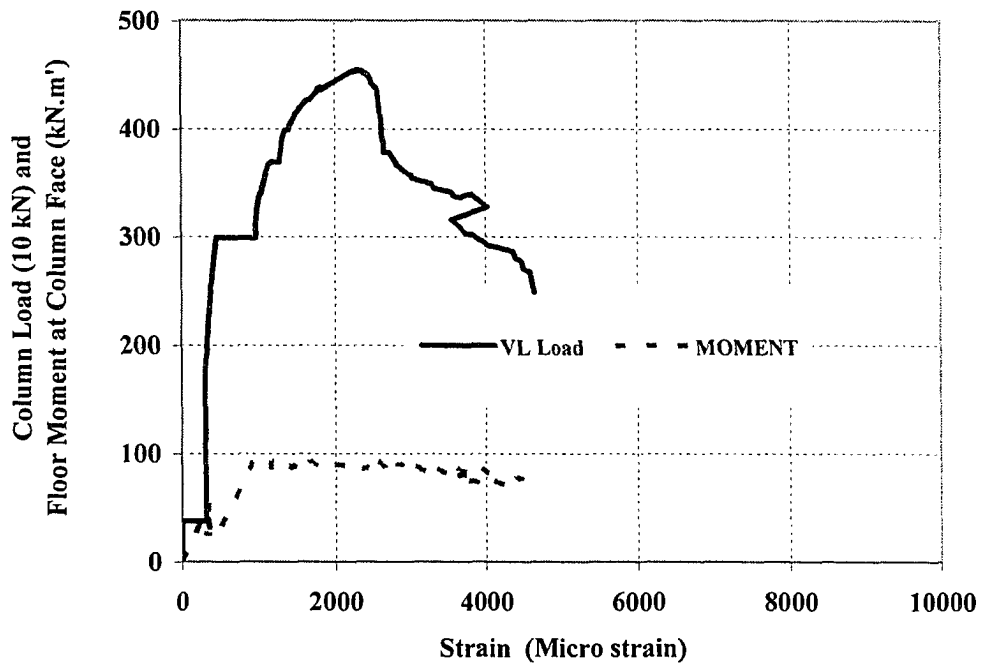

Figure C.44 Effect of Column and Floor Loads on Strain of Slab Top RFT at SP5-Column Face

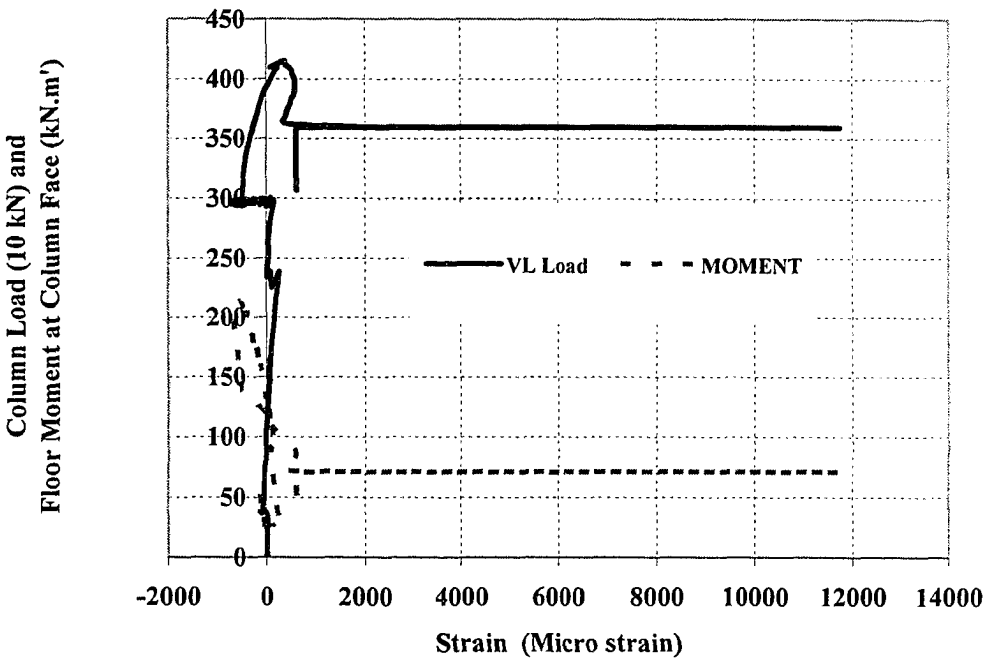

Figure C.45 Effect of Column and Floor Loads on Strain of Beam Bottom RFT at SP6-Joint Core

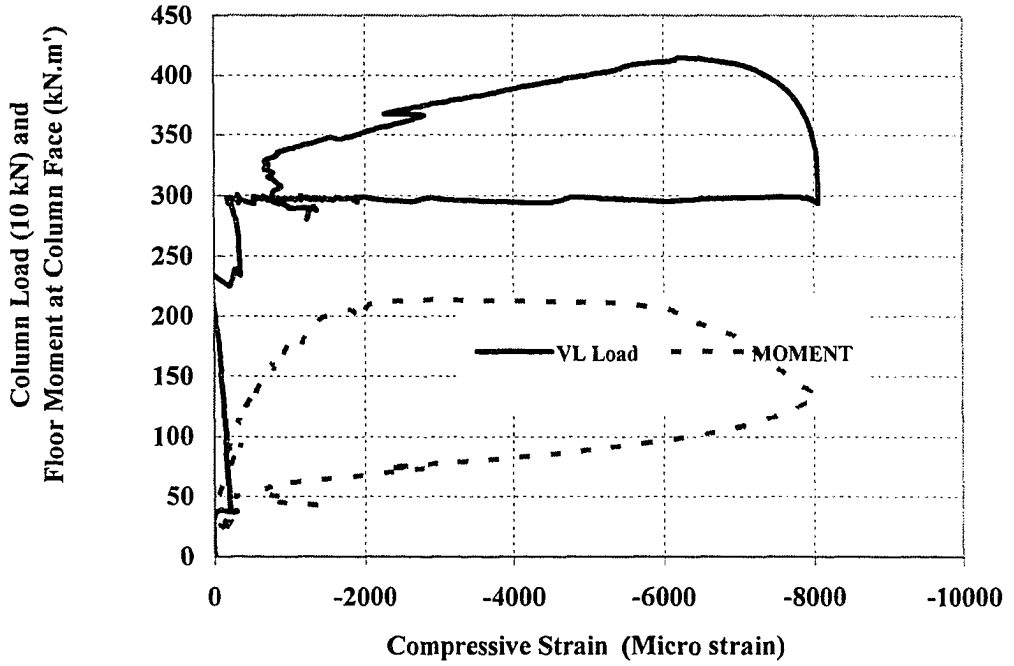

Figure C.46 Effect of Column and Floor Loads on Strain of Beam Bottom RFT at SP6-Joint Face

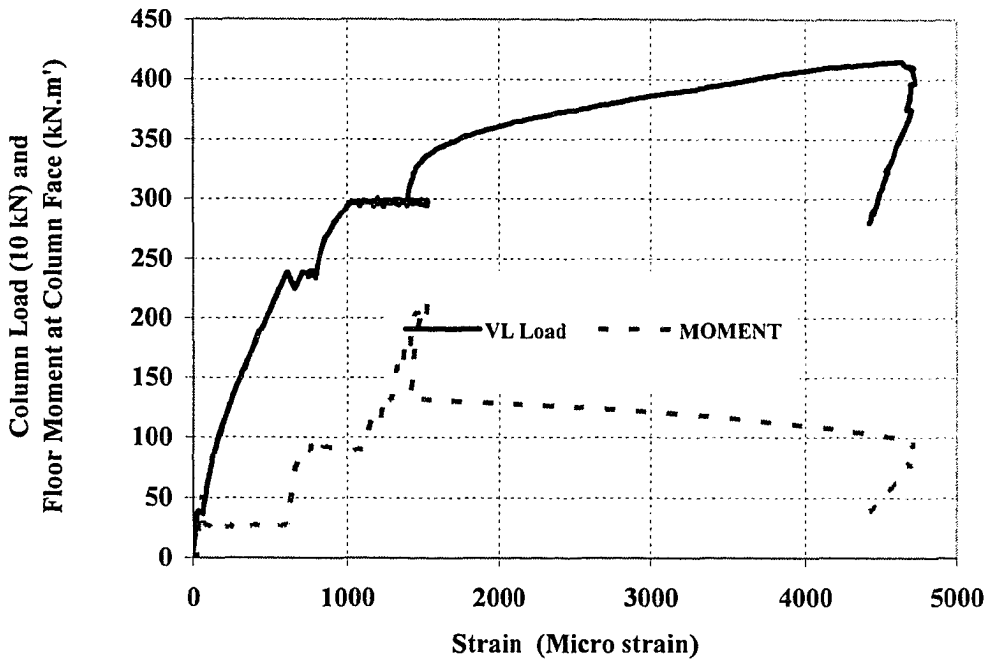

Figure C.47 Effect of Column and Floor Loads on Strain of Beam Side RFT at SP6-Joint Core

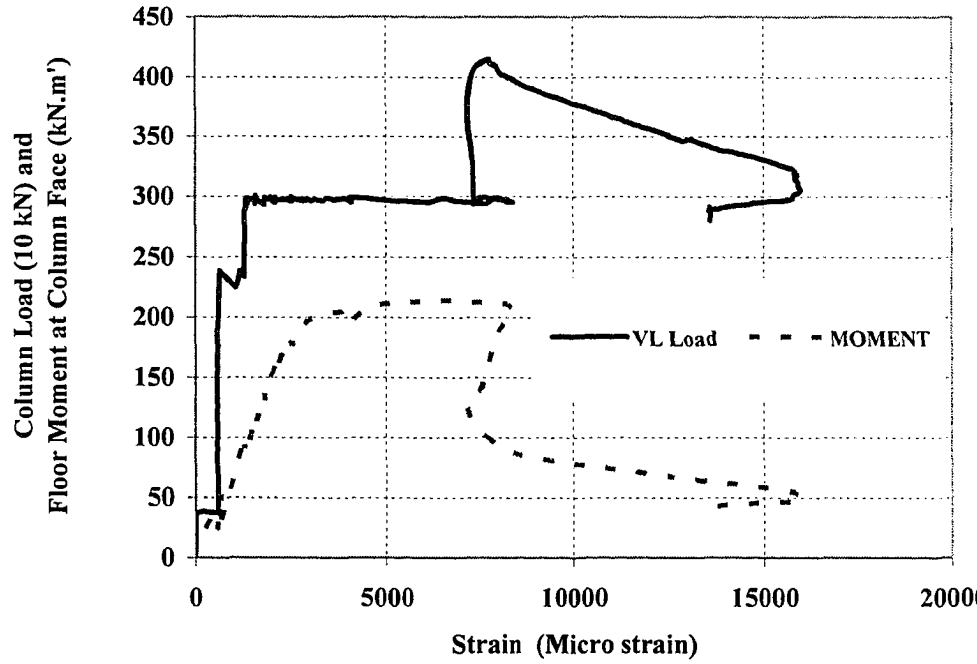

Figure C.48 Effect of Column and Floor Loads on Strain of Beam Side RFT at SP6-Joint Face

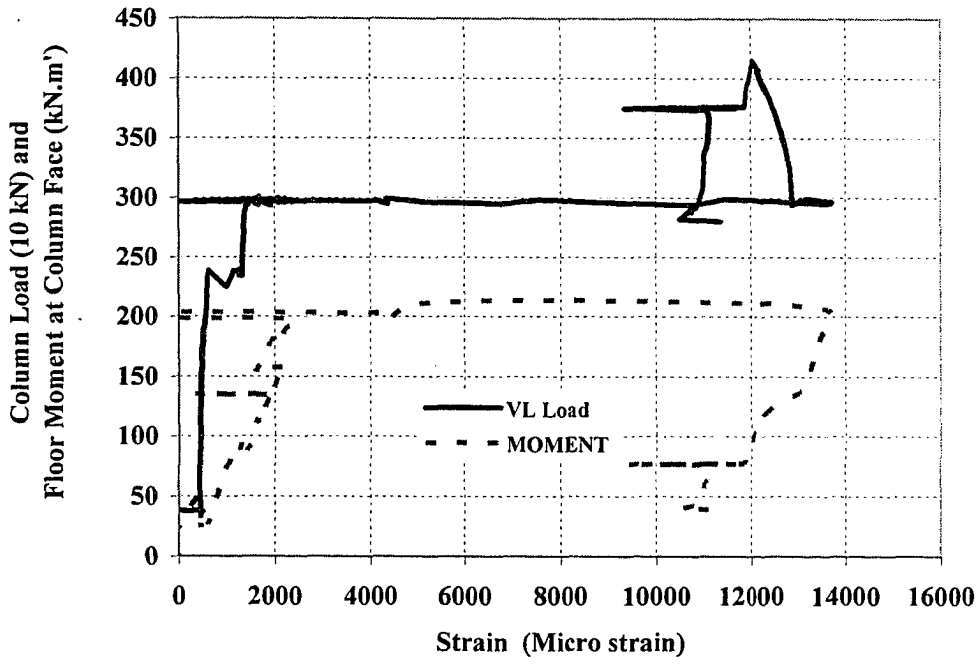

Figure C.49 Effect of Column and Floor Loads on Strain of Beam Top RFT at SP6-Joint Core

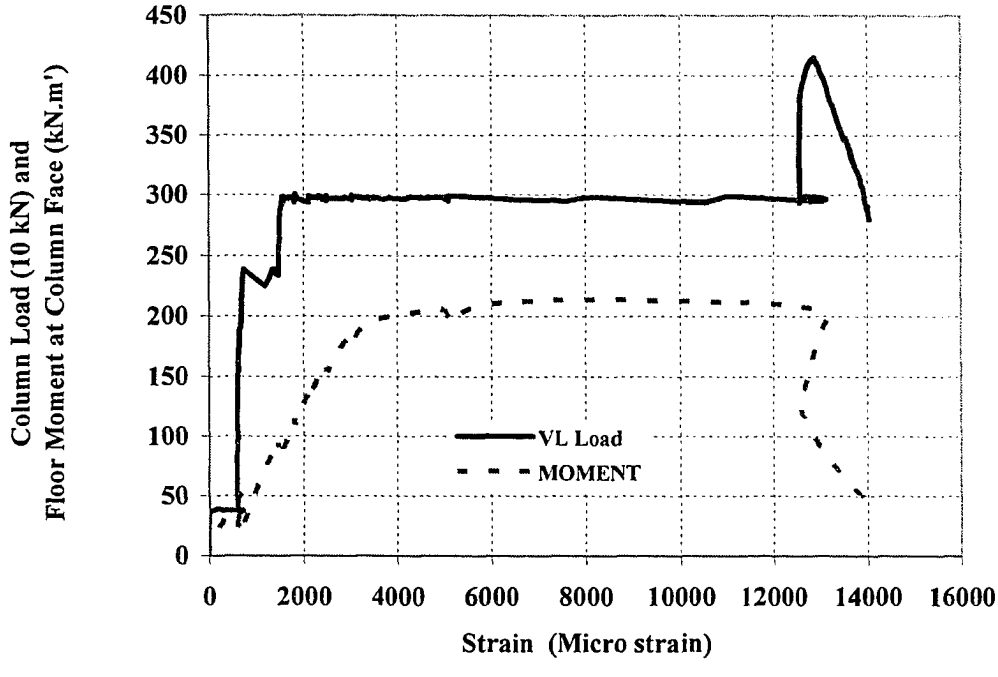

Figure C.50 Effect of Column and Floor Loads on Strain of Beam Top RFT at SP6-Joint Face

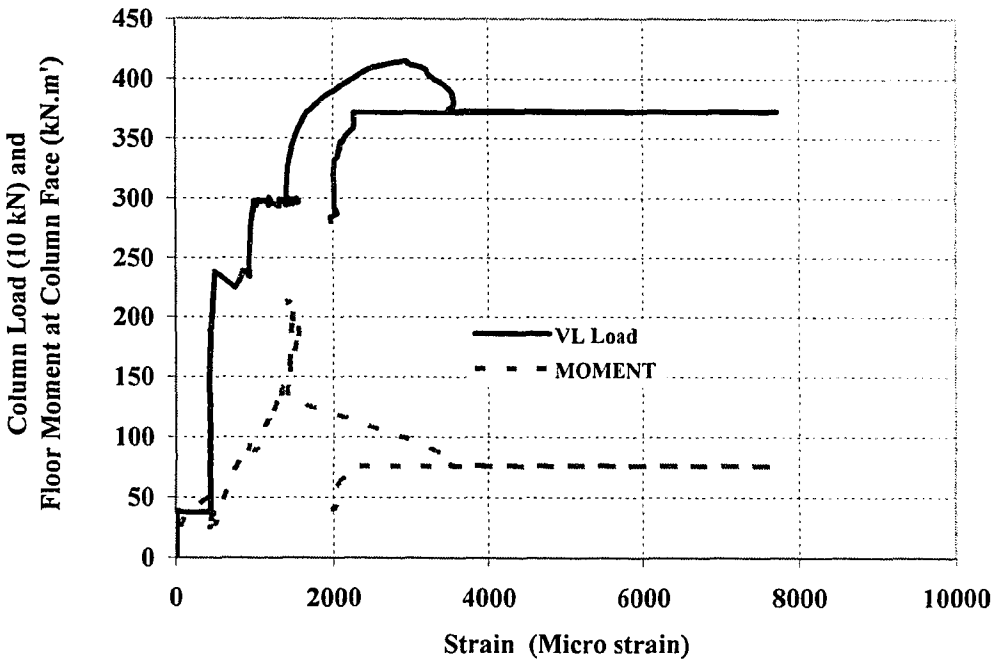

Figure C.51 Effect of Column and Floor Loads on Strain of Slab Top RFT at SP6-Column Face

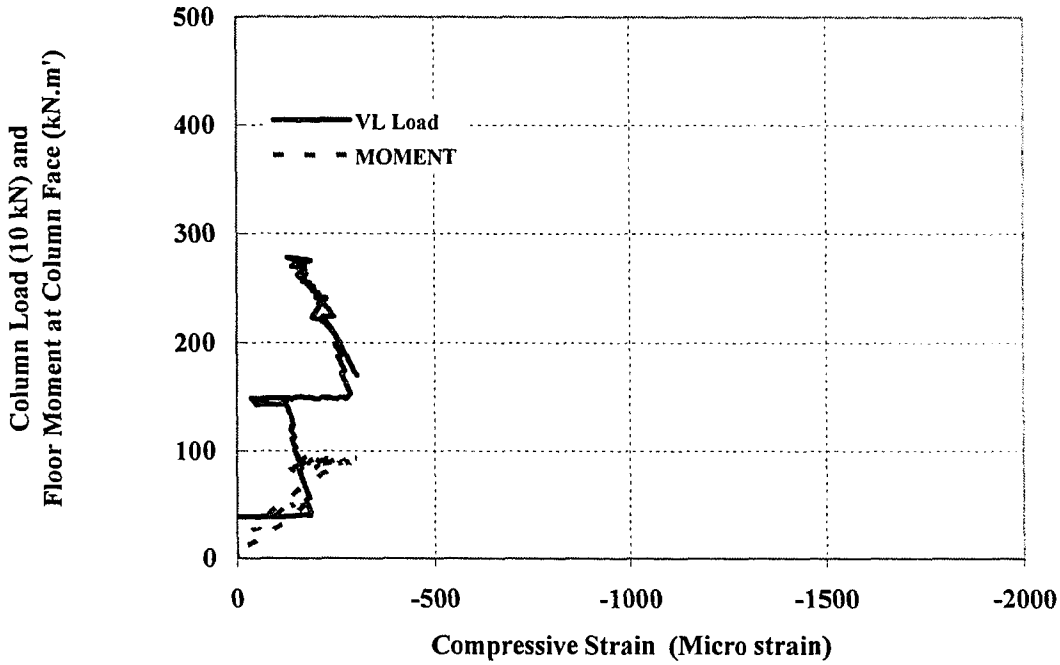

Figure C.52 Effect of Column and Floor Loads on Strain of Beam Bottom RFT at Core of SP7-Joint

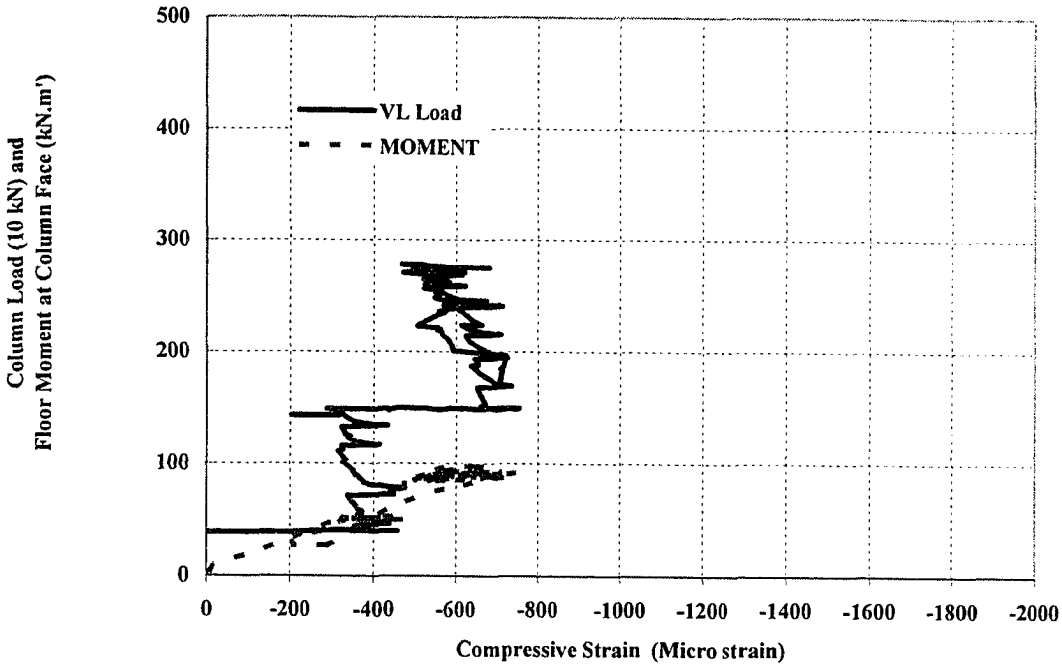

Figure C.53 Effect of Column and Floor Loads on Strain of Beam Bottom RFT at Face of SP7-Joint

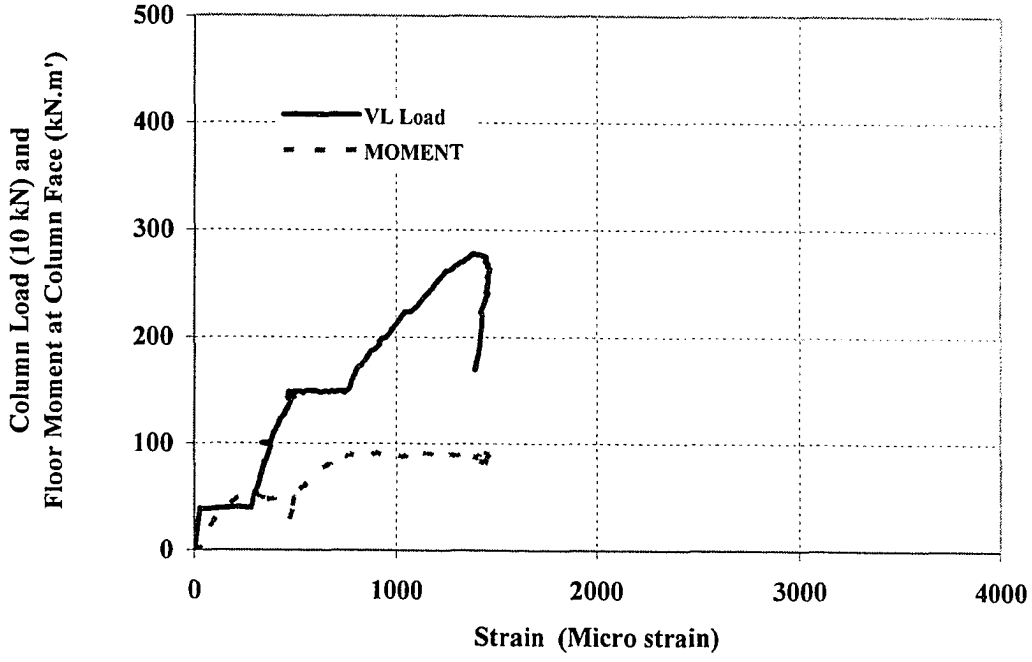

Figure C.54 Effect of Column and Floor Loads on Strain of Beam Side RFT at Core of SP7-Joint

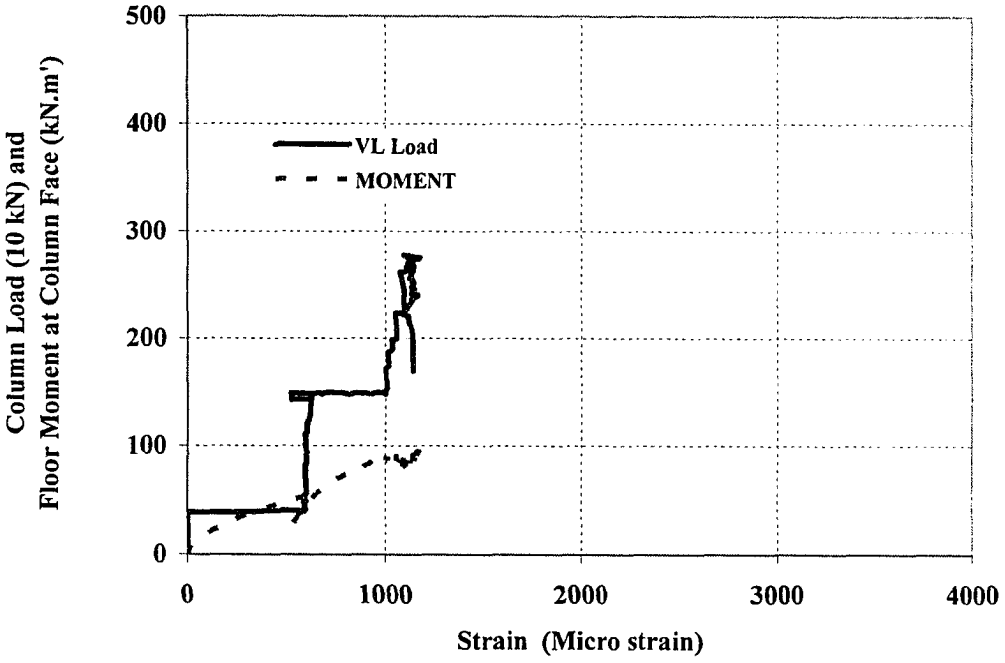

Figure C.55 Effect of Column and Floor Loads on Strain of Beam Side RFT at Face of SP7-Joint

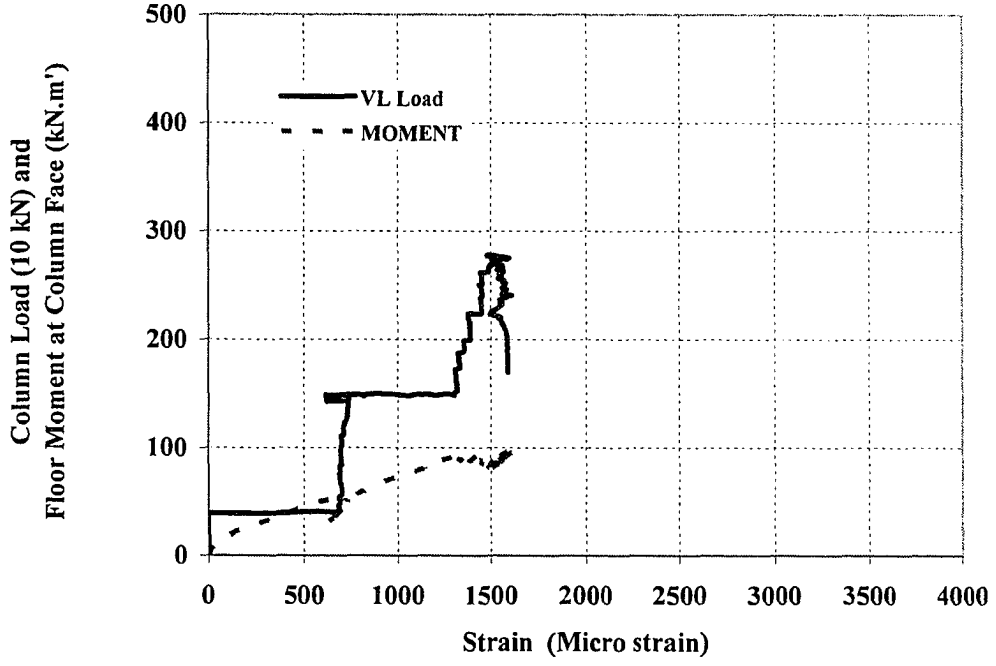

Figure C.56 Effect of Column and Floor Loads on Strain of Beam Top RFT at Face of SP7-Joint

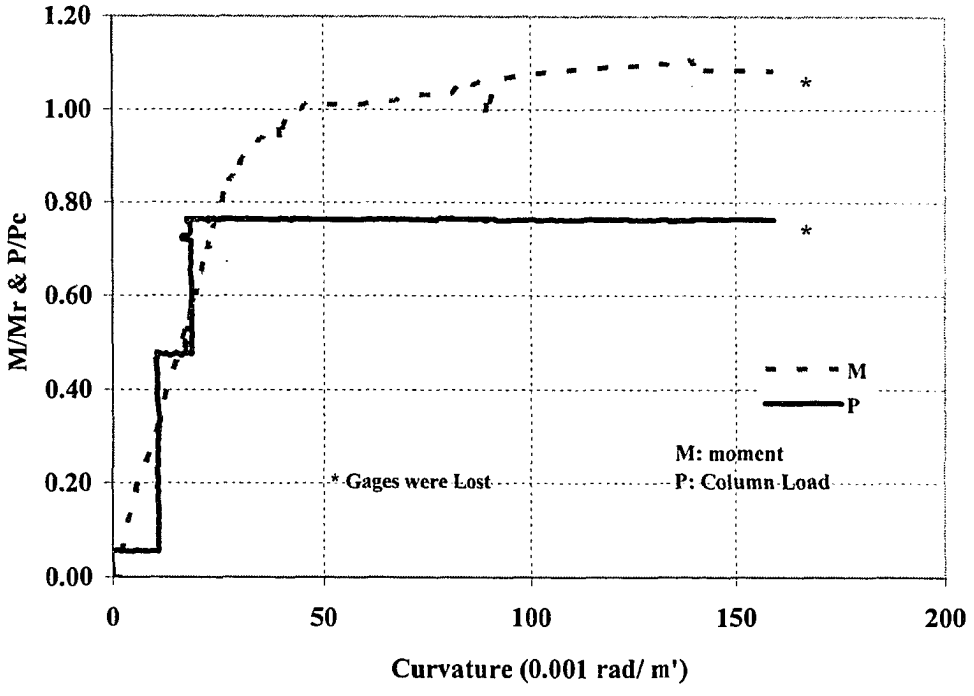

Figure C.57 Effect of Specimen Loading on Floor Curvature for SP3

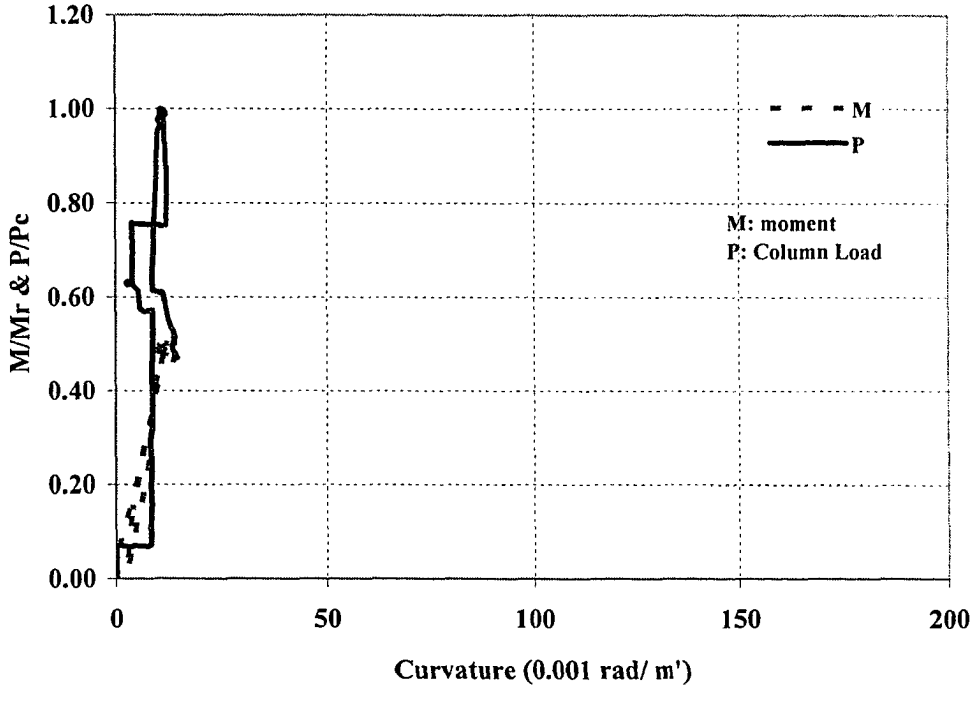

Figure C.58 Effect of Specimen Loading on Floor Curvature for SP4

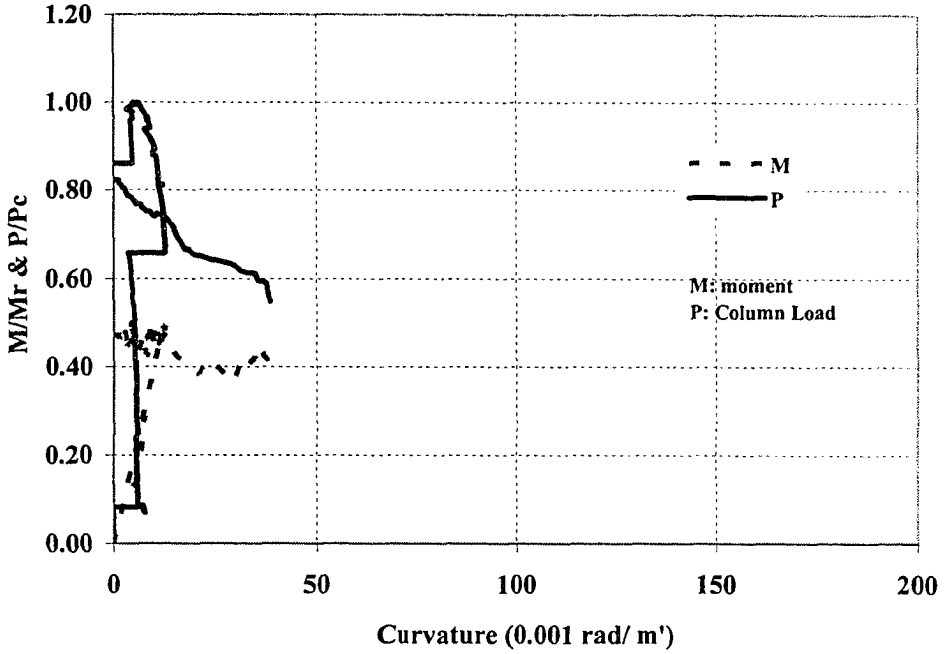

Figure C.59 Effect of Specimen Loading on Floor Curvature for SP5

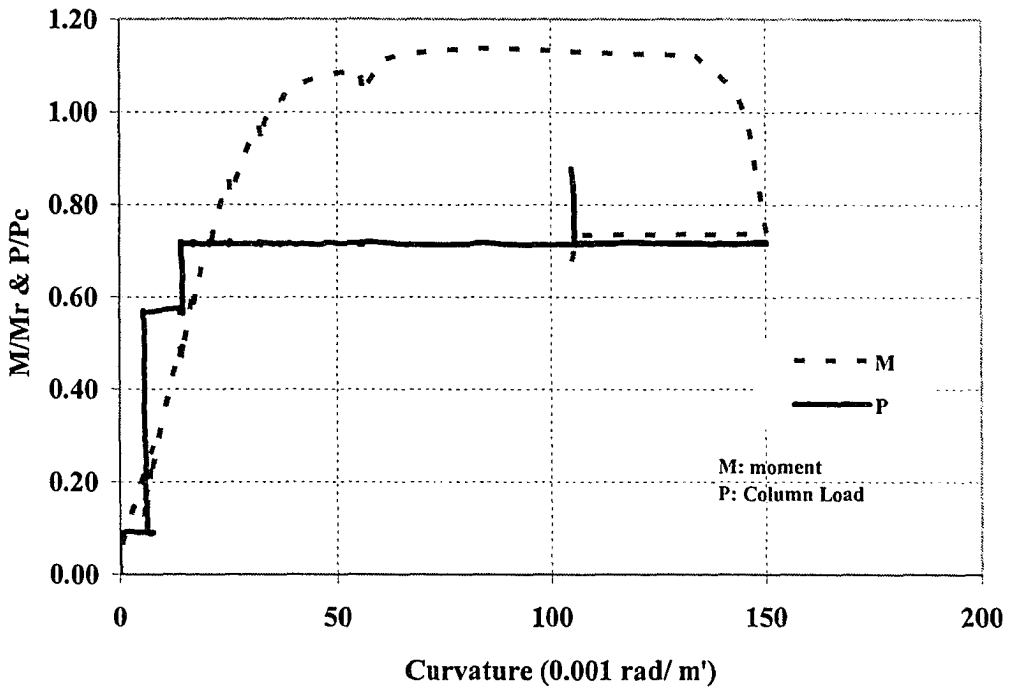

Figure C.60 Effect of Specimen Loading on Floor Curvature for SP6

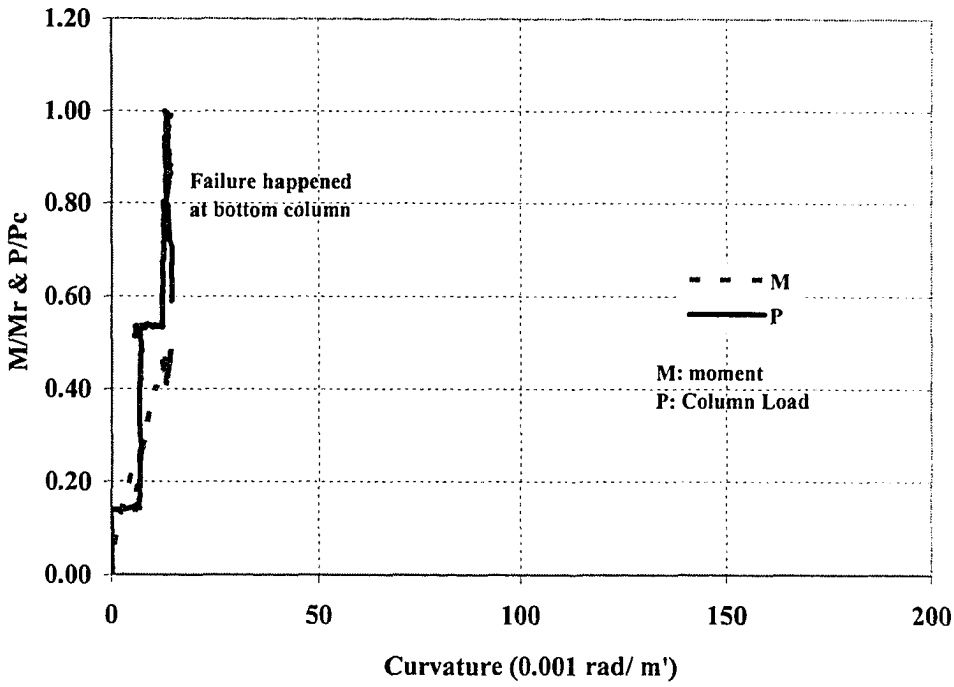

Figure C.61 Effect of Specimen Loading on Floor Curvature for SP7

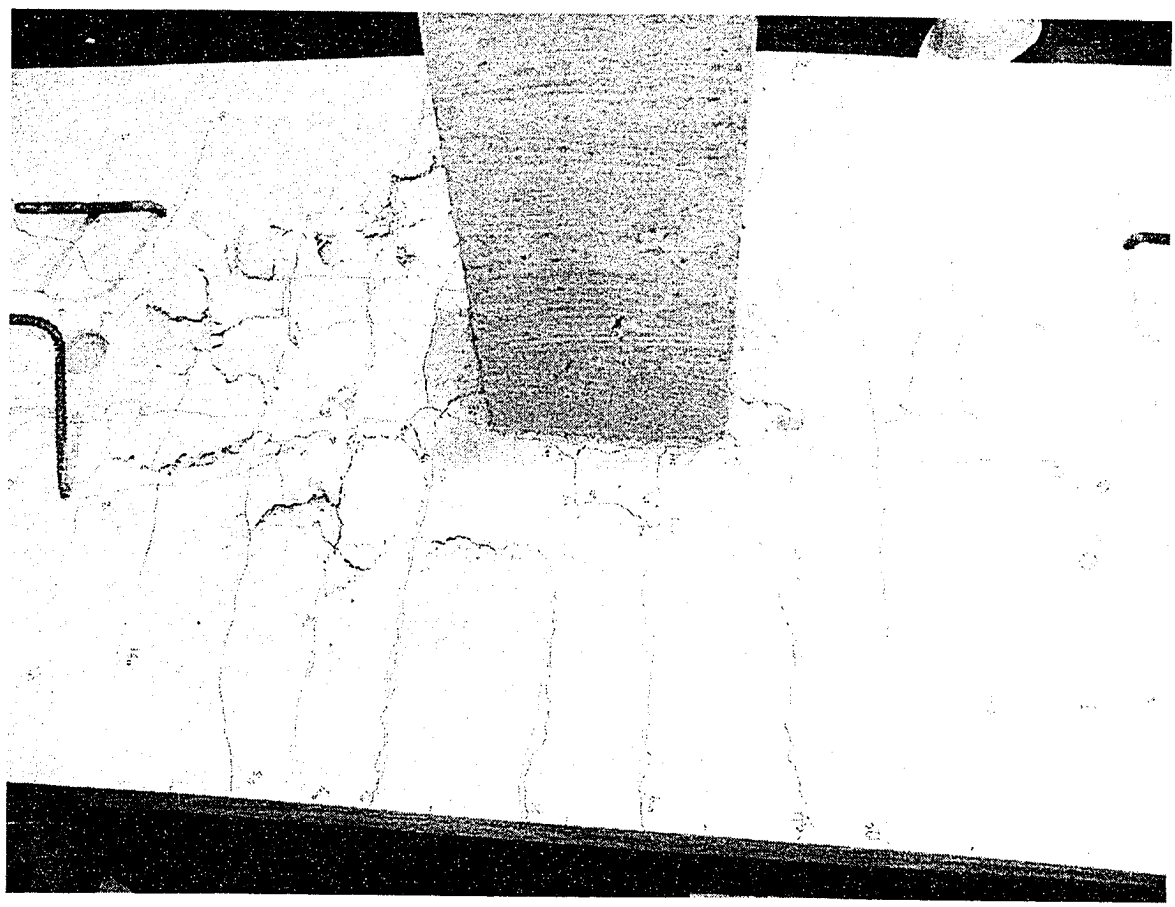

Figure C.62 SP1-Top View of the Specimen after the Test

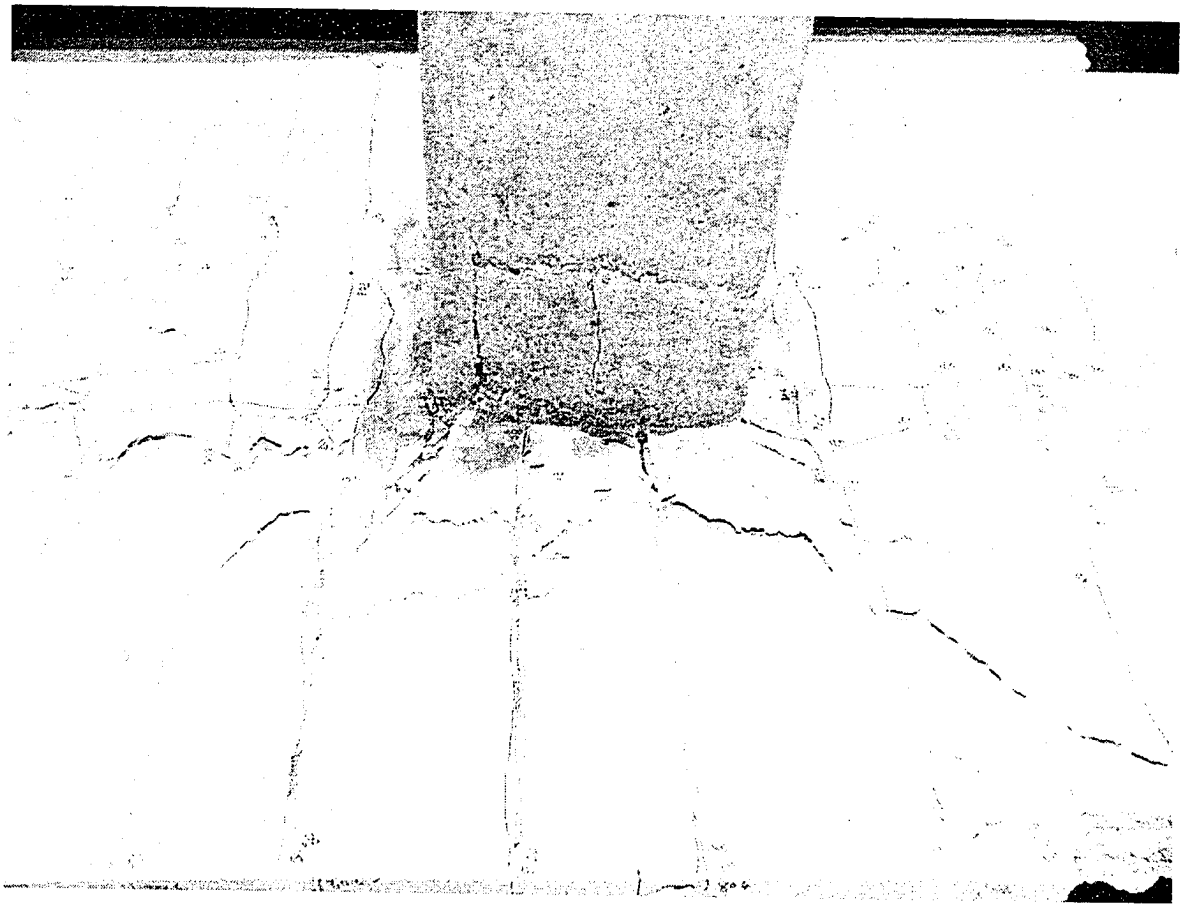

Figure C.63 SP6-Top North View after the Test

APPENDIX D

Comparison of Experimental and Analytical

Stress-Strain Curves

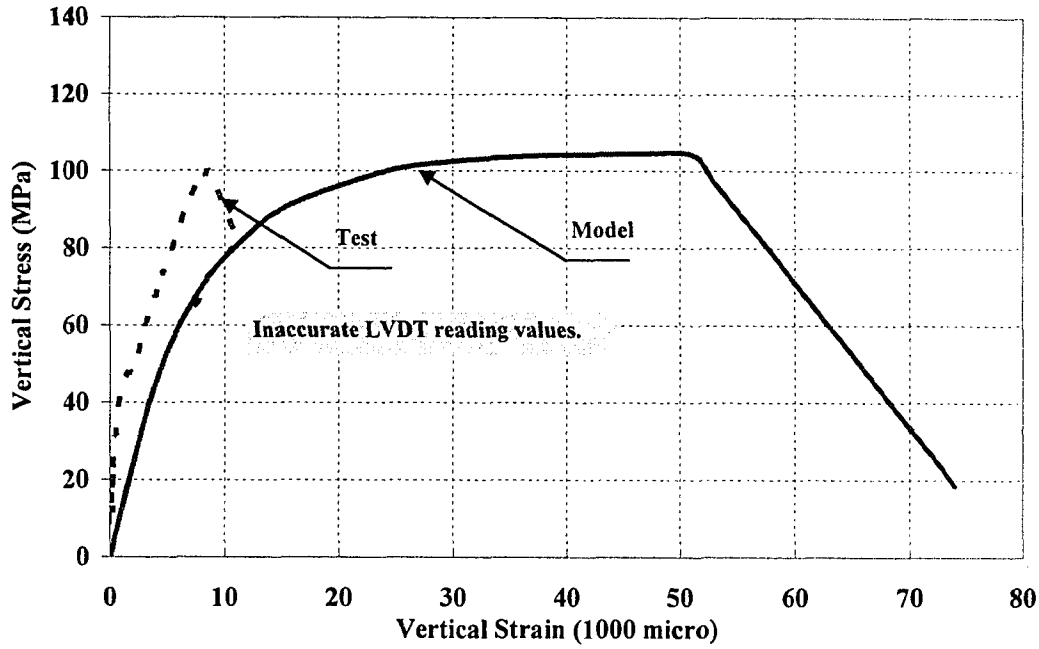

Figure D1. Comparison of Experimental and Analytical Compressive Stress-Strain Curves for A1A-Joint

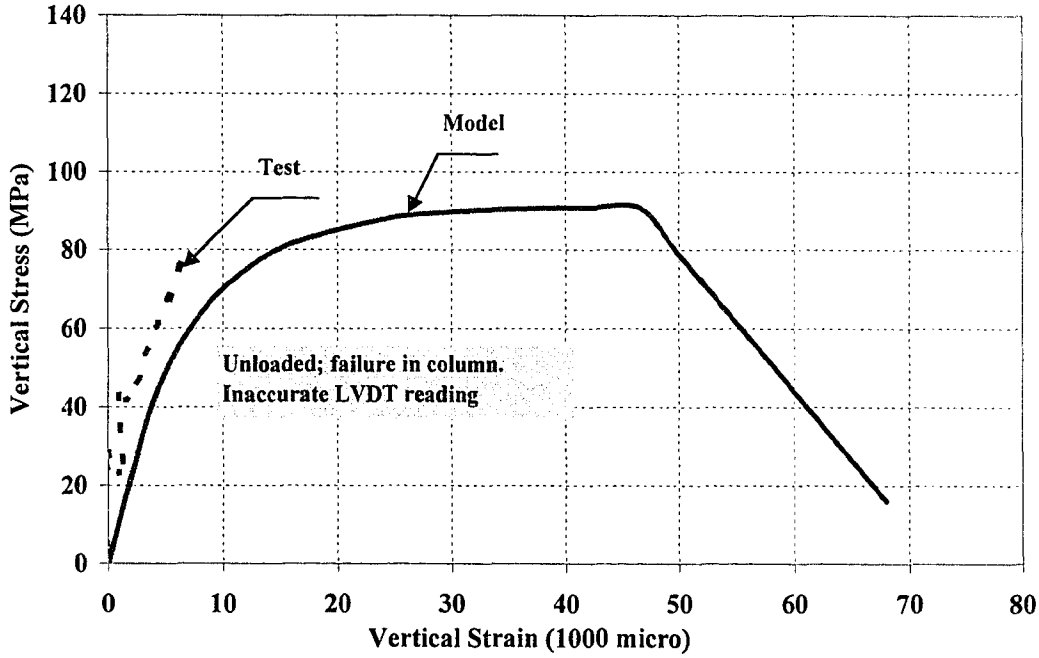

Figure D2. Comparison of Experimental and Analytical Compressive Stress-Strain Curves for A1B-Joint

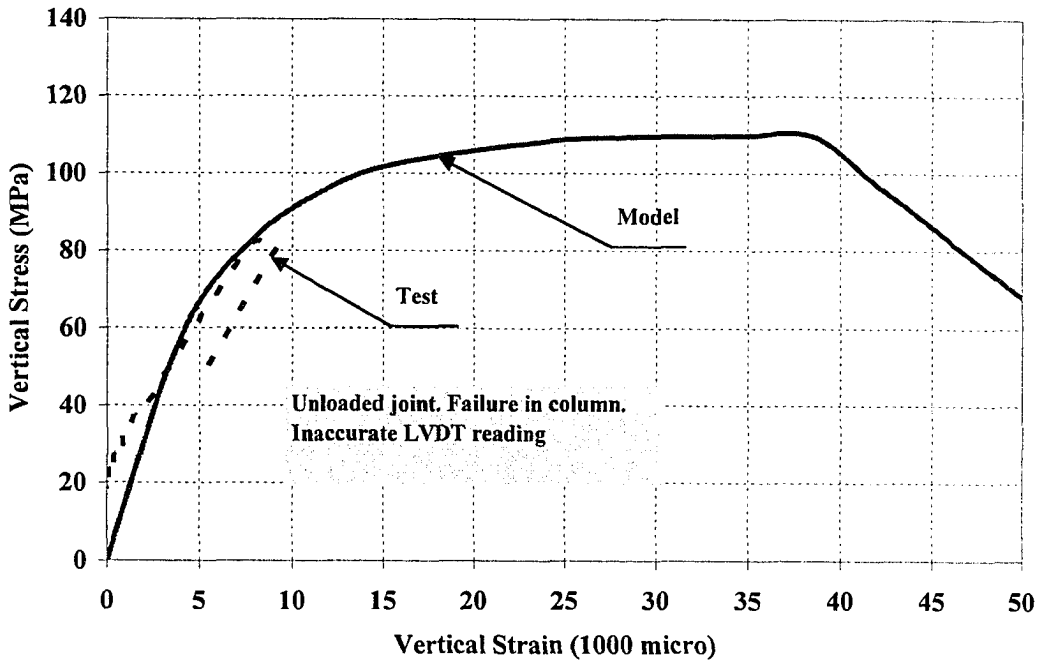

Figure D3. Comparison of Experimental and Analytical Compressive Stress-Strain Curves for A2A-Joint

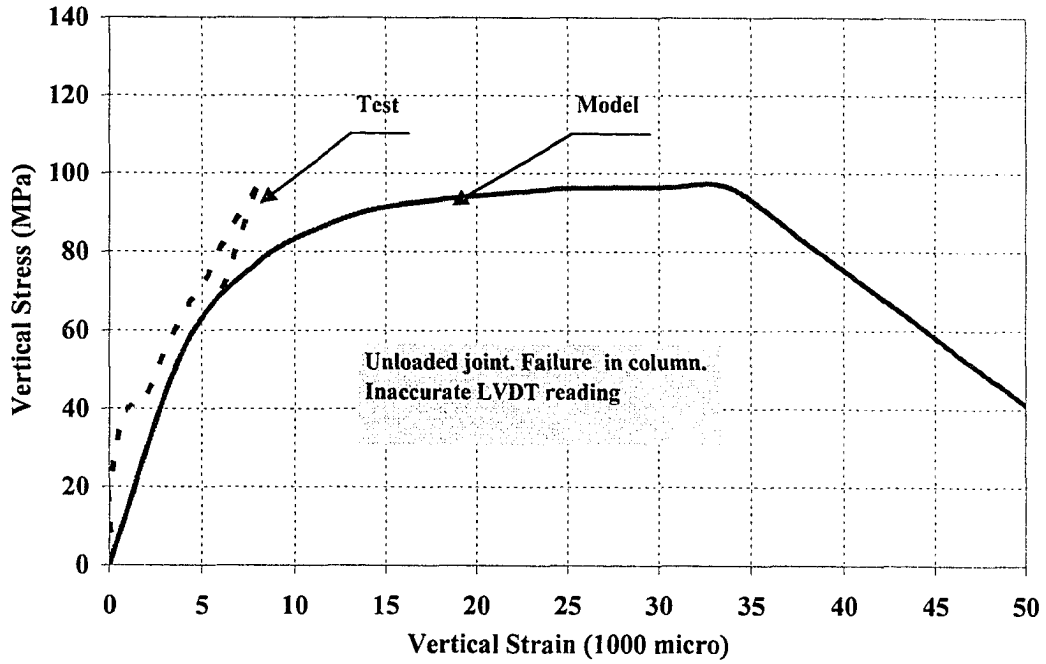

Figure D4. Comparison of Experimental and Analytical Compressive Stress-Strain Curves for A2B-Joint

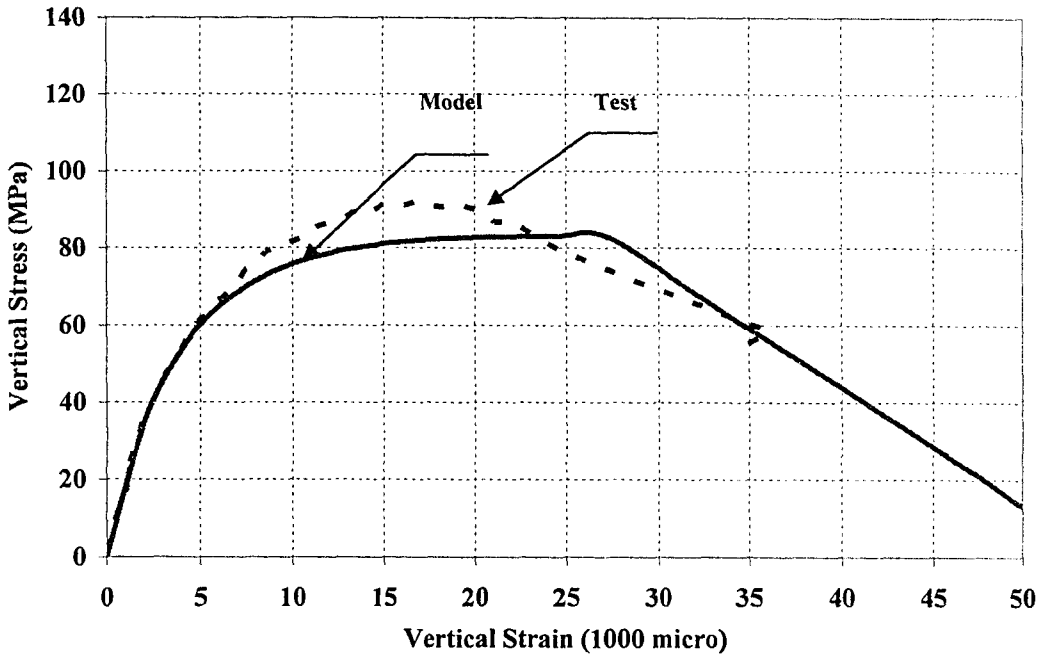

Figure D5. Comparison of Experimental and Analytical Compressive Stress-Strain Curves for A2C-Joint

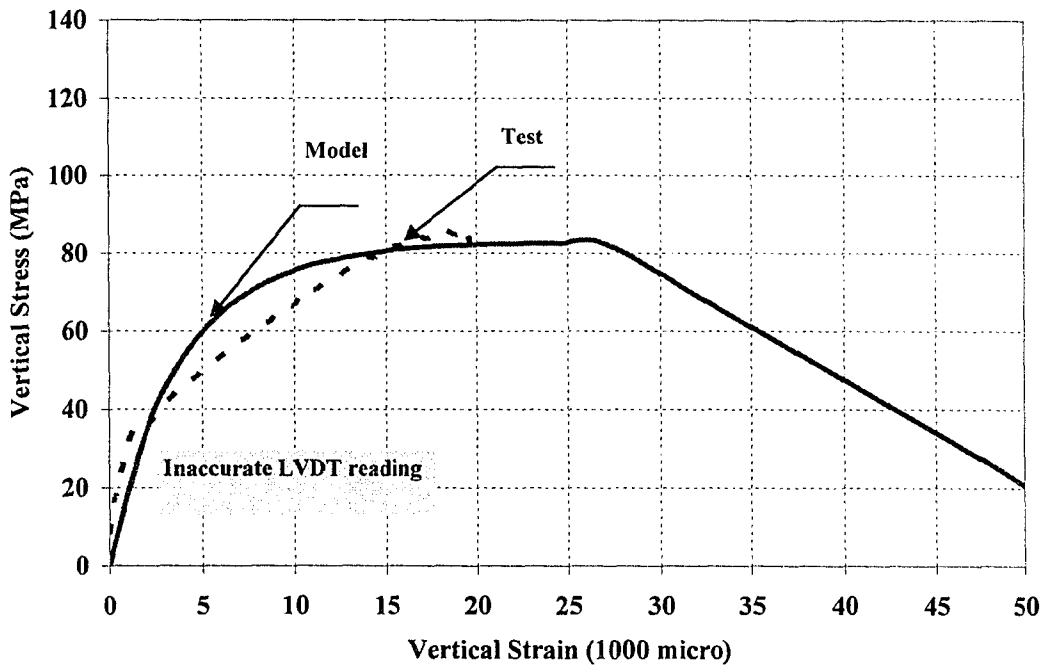

Figure D6. Comparison of Experimental and Analytical Compressive Stress-Strain Curves for A3A-Joint

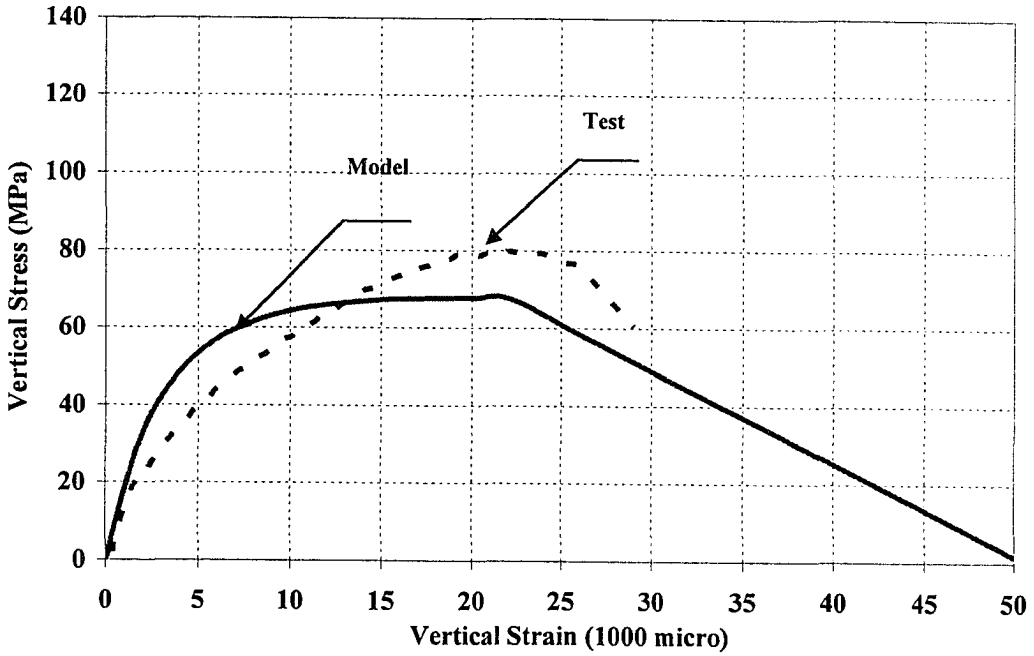

Figure D7. Comparison of Experimental and Analytical Compressive Stress-Strain Curves for A3B-Joint

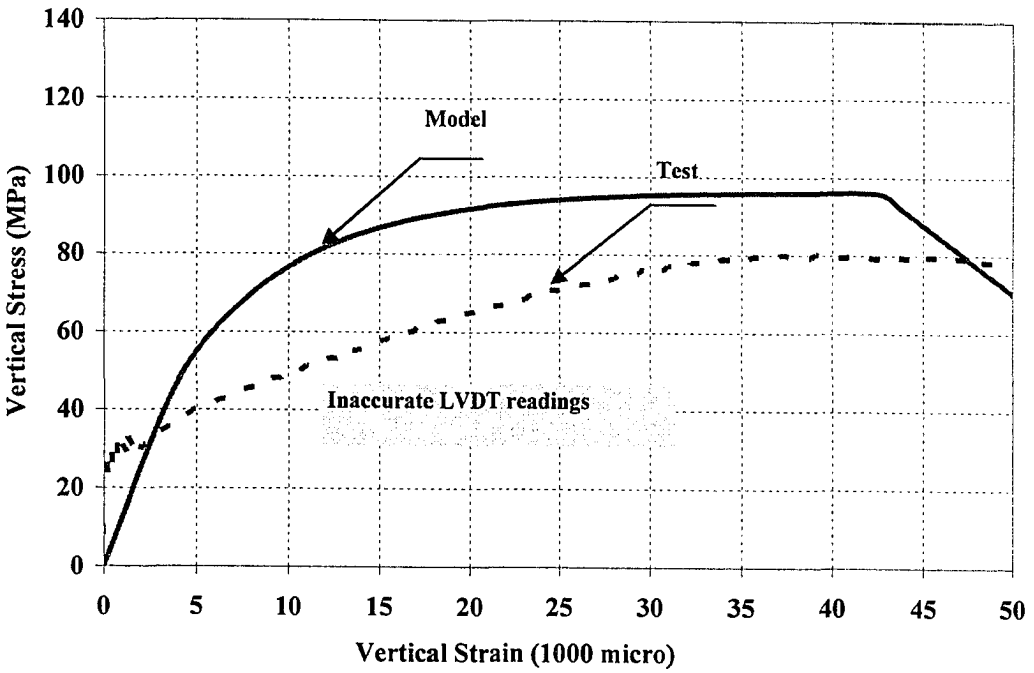

Figure D8. Comparison of Experimental and Analytical Compressive Stress-Strain Curves for A4A-Joint

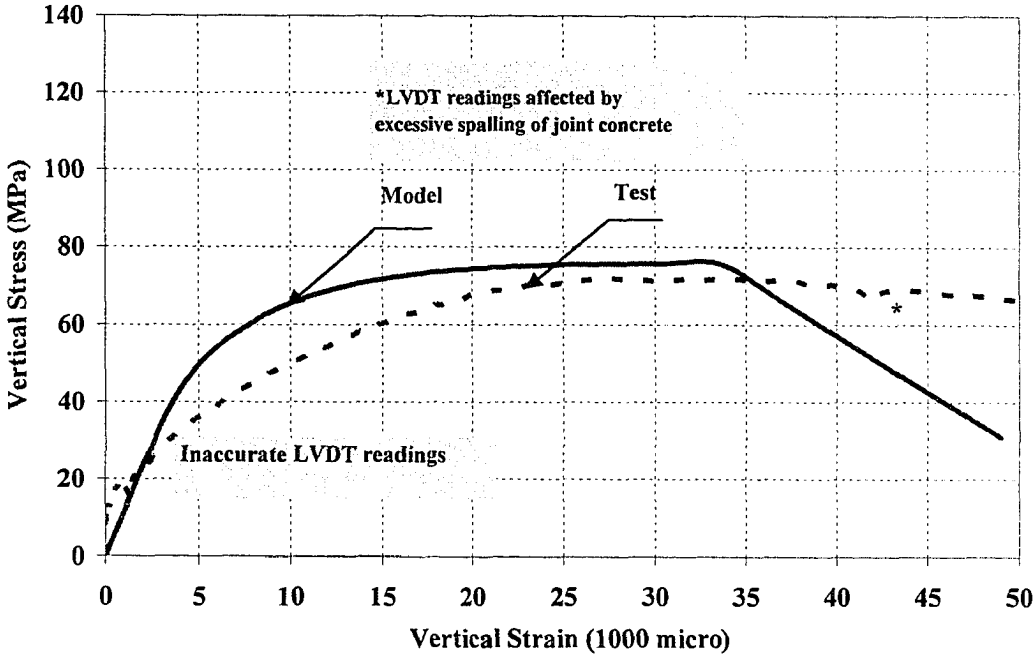

Figure D9. Comparison of Experimental and Analytical Compressive Stress-Strain Curves for A4B-Joint

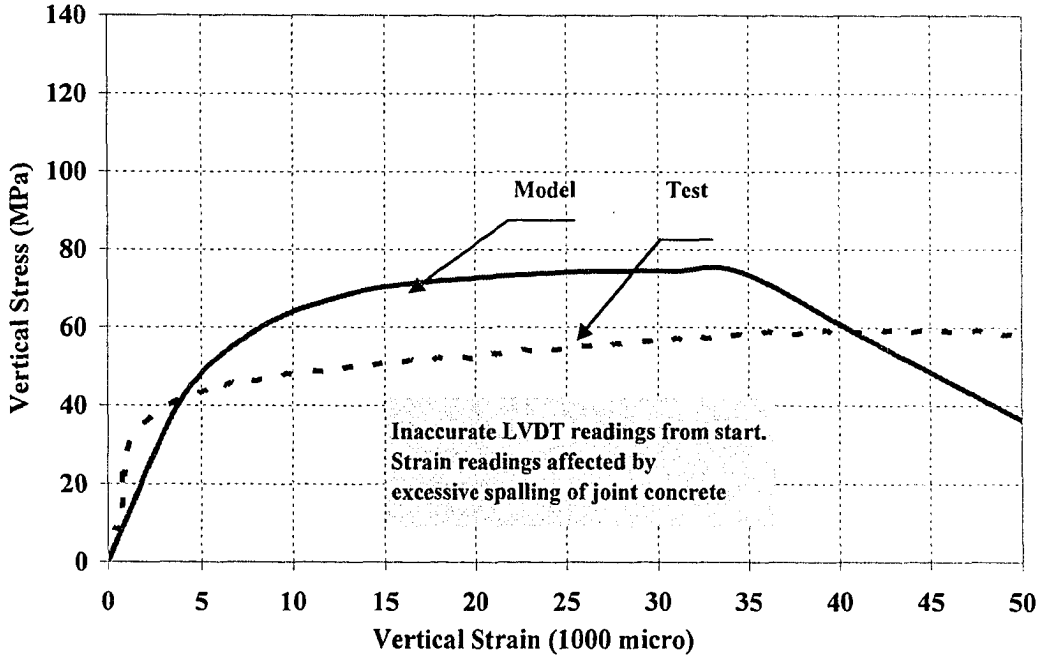

Figure D10. Comparison of Experimental and Analytical Compressive Stress-Strain Curves for C1A-Joint

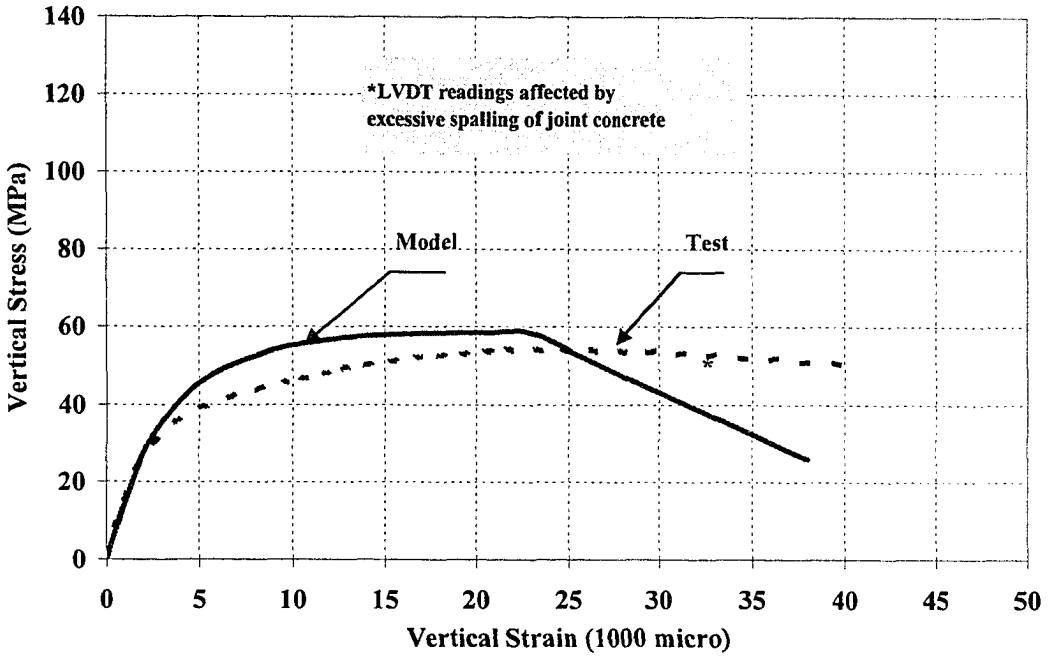

Figure D11. Comparison of Experimental and Analytical Compressive Stress-Strain Curves for C1C-Joint

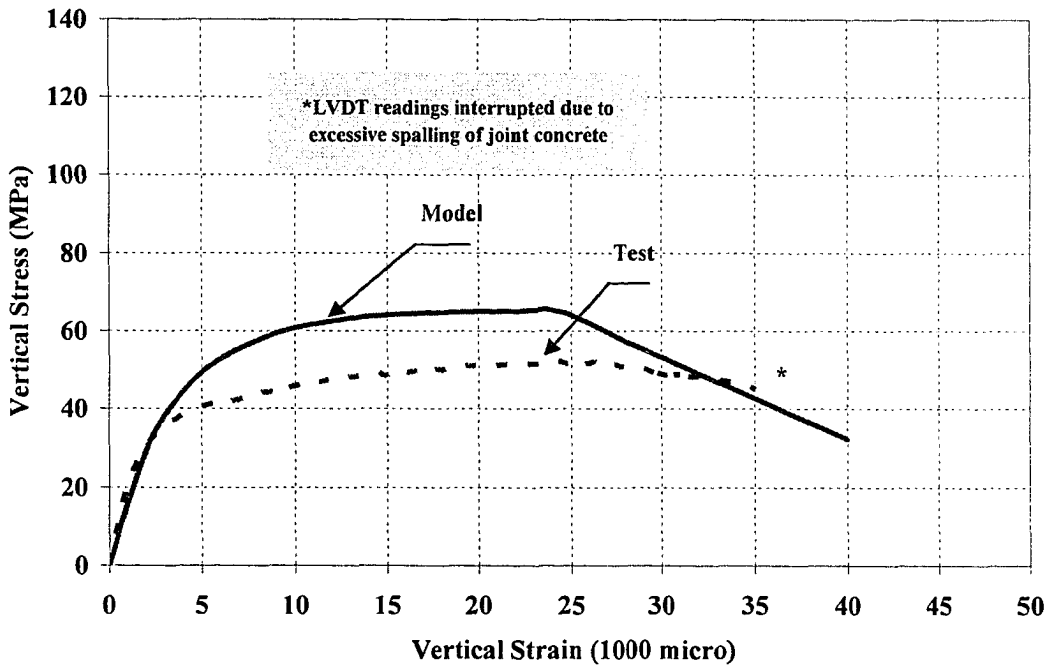

Figure D12. Comparison of Experimental and Analytical Compressive Stress-Strain Curves for C2A-Joint

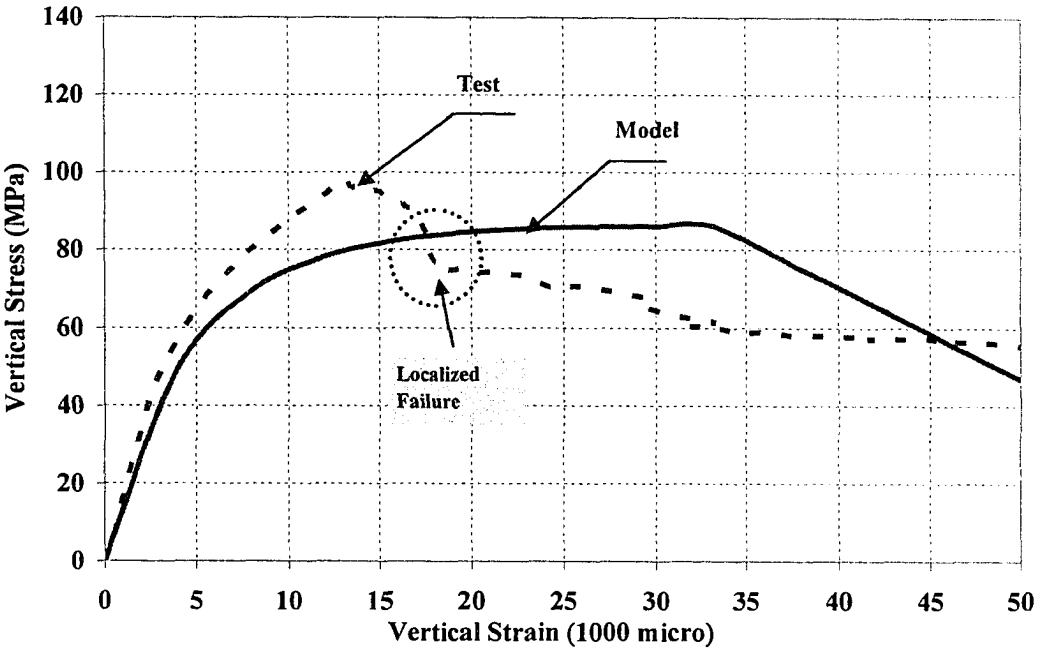

Figure D13. Comparison of Experimental and Analytical Compressive Stress-Strain Curves for B2-Joint

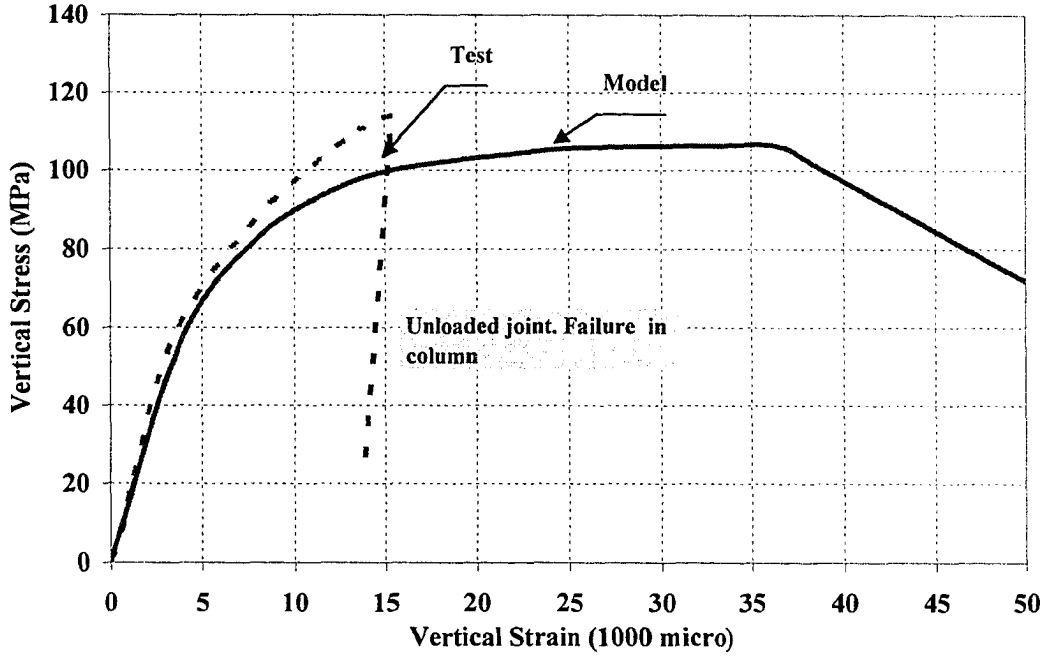

Figure D14. Comparison of Experimental and Analytical Compressive Stress-Strain Curves for B4-Joint

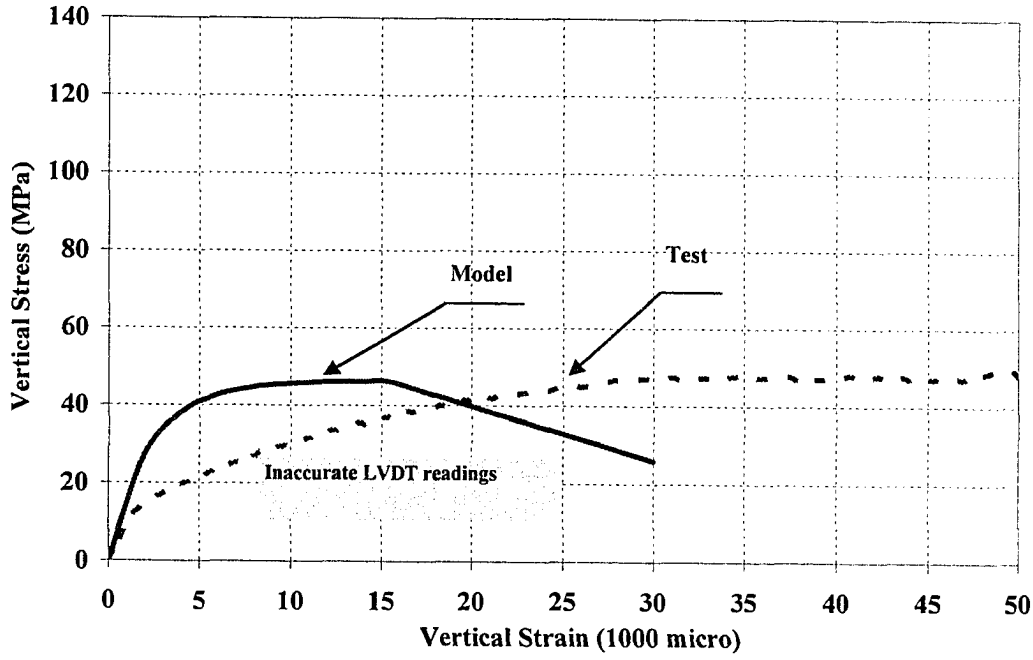

Figure D15. Comparison of Experimental and Analytical Compressive Stress-Strain Curves for B5-Joint

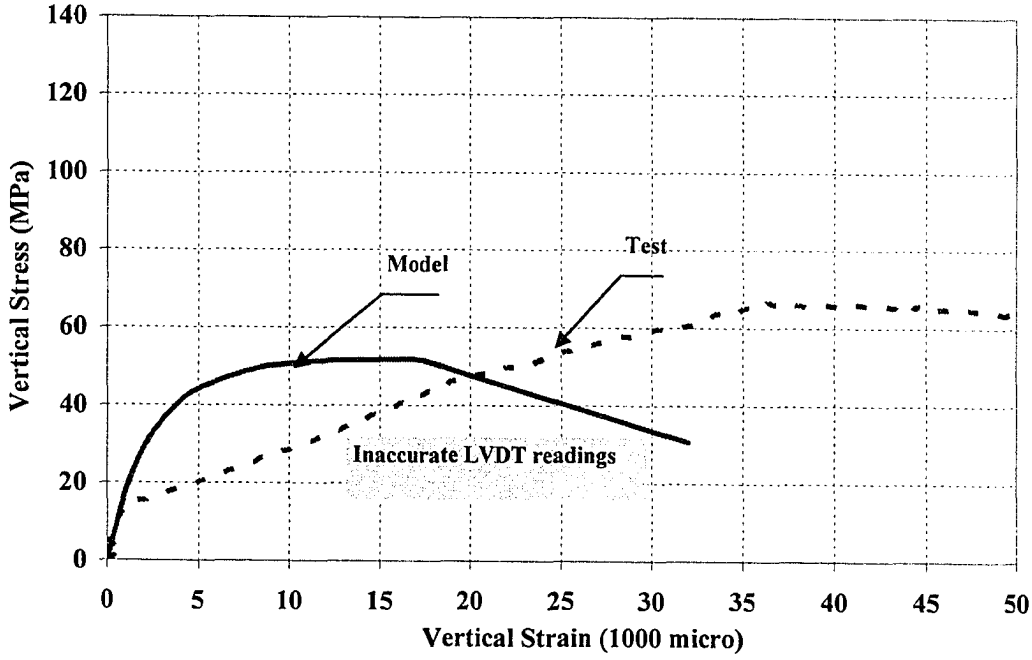

Figure D16. Comparison of Experimental and Analytical Compressive Stress-Strain Curves for B6-Joint

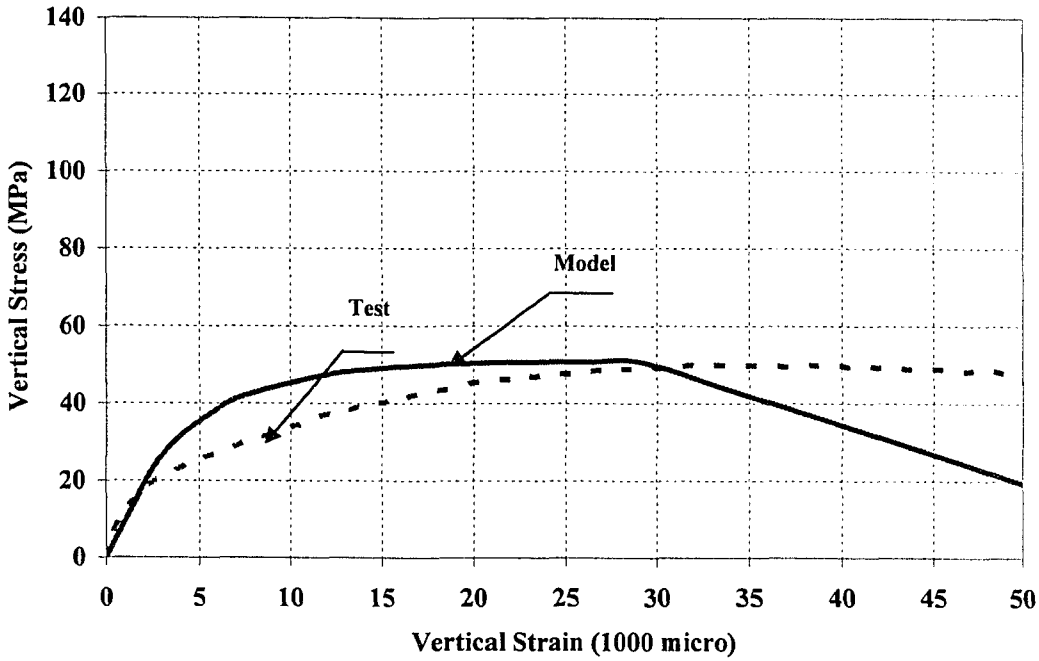

Figure D17. Comparison of Experimental and Analytical Compressive Stress-Strain Curves for B7-Joint

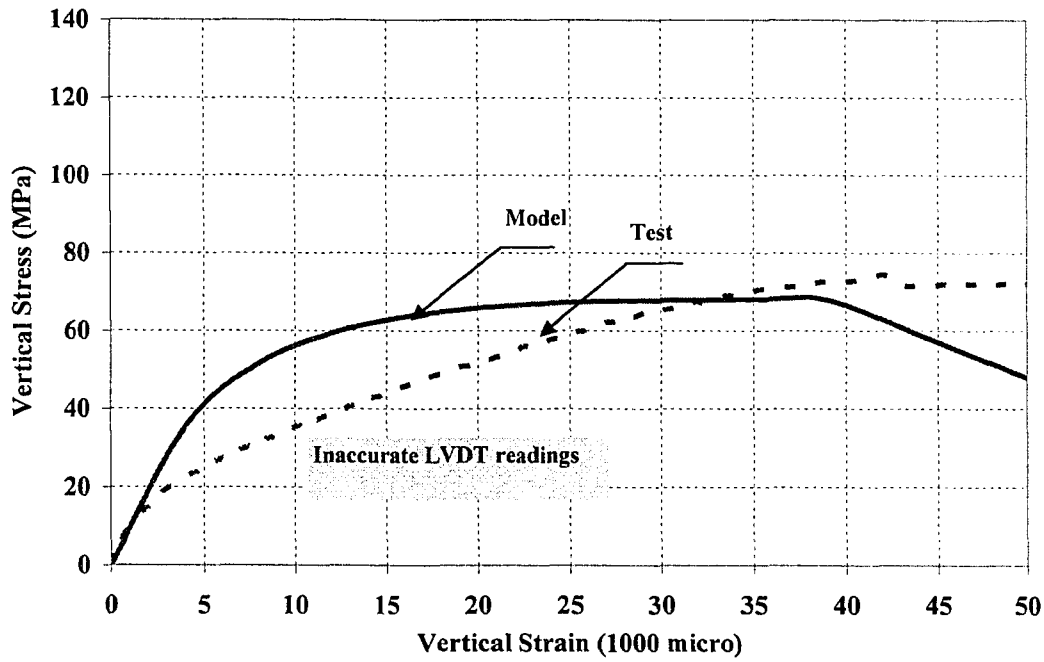

Figure D18. Comparison of Experimental and Analytical Compressive Stress-Strain Curves for B8-Joint

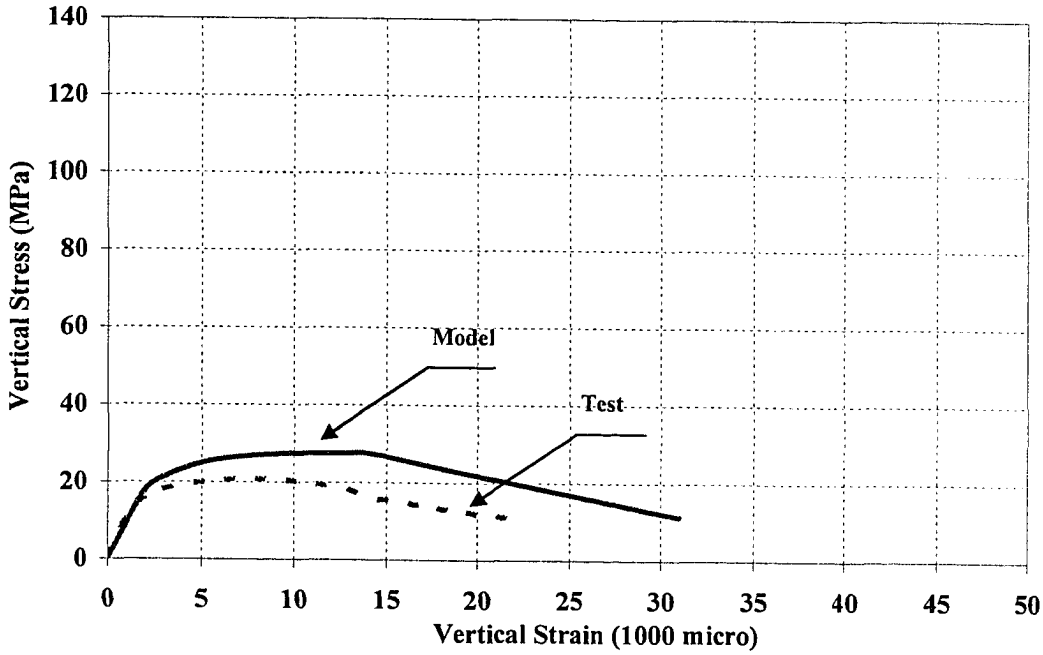

Figure D19. Comparison of Experimental and Analytical Compressive Stress-Strain Curves for SC1-Joint

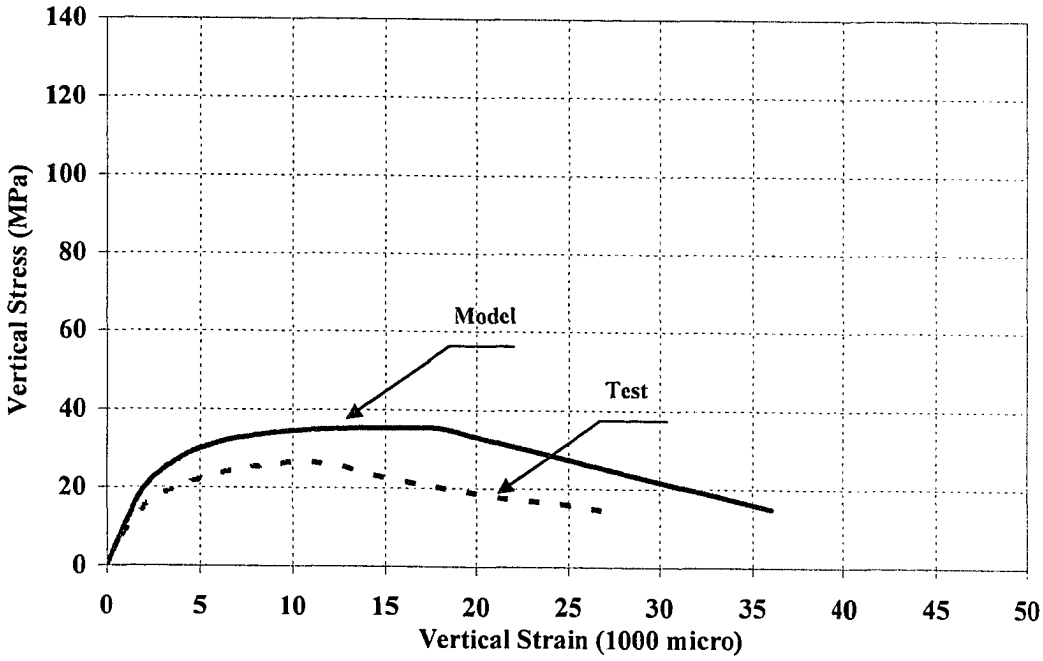

Figure D20. Comparison of Experimental and Analytical Compressive Stress-Strain Curves for SC2-Joint

APPENDIX E

Sensitivity Study for

Interior and Corner Joints

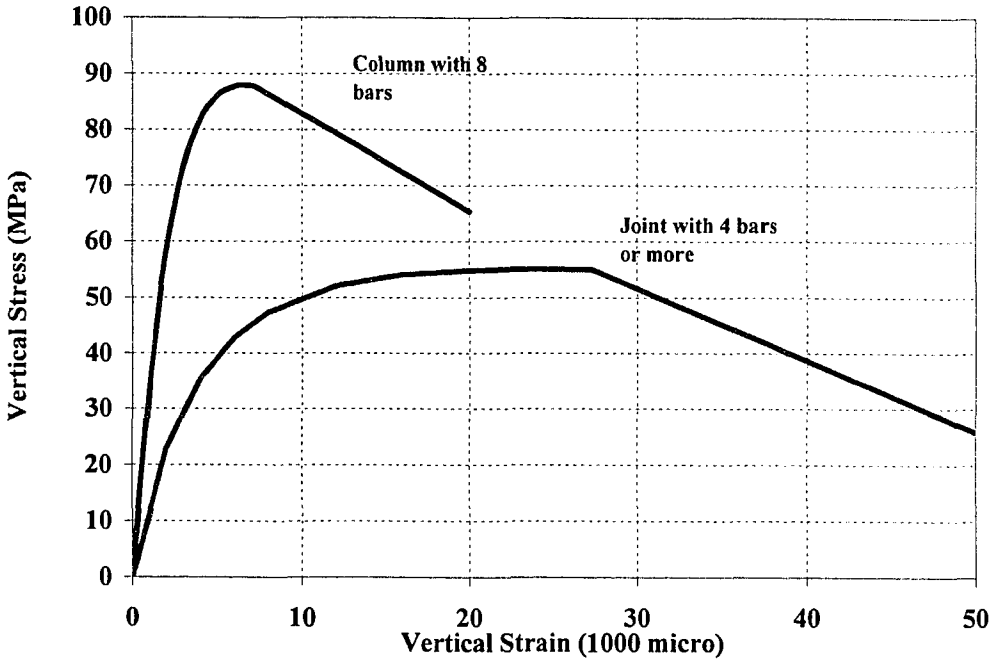

Figure E1. Effect of Rebar Arrangement on the Behavior of a Corner Joint

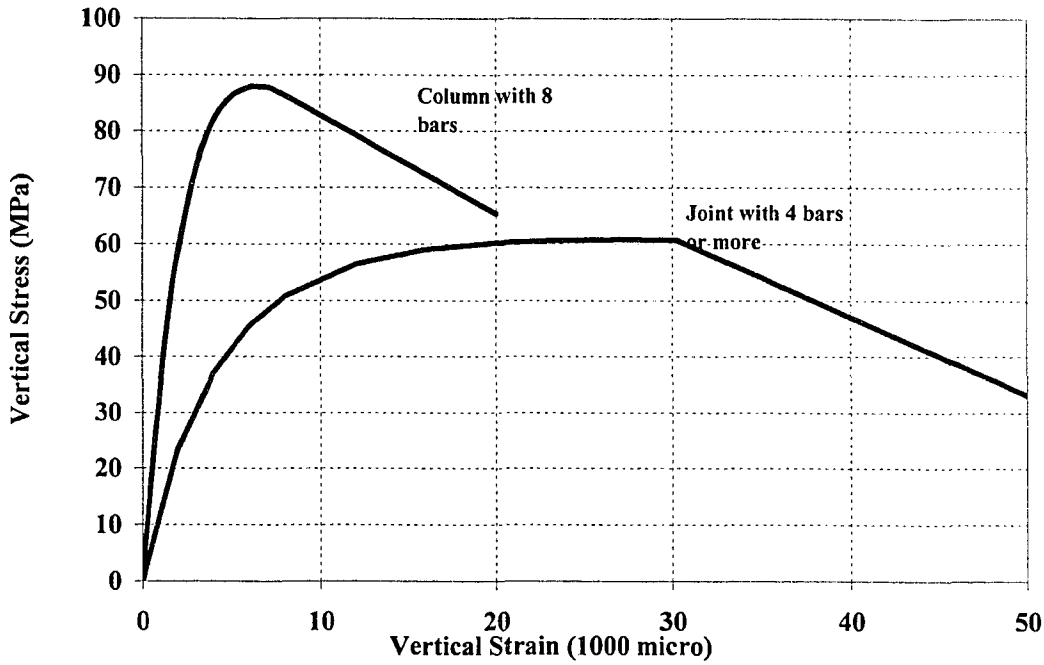

Figure E2. Effect of Rebar Arrangement on the Behavior of an Interior Joint

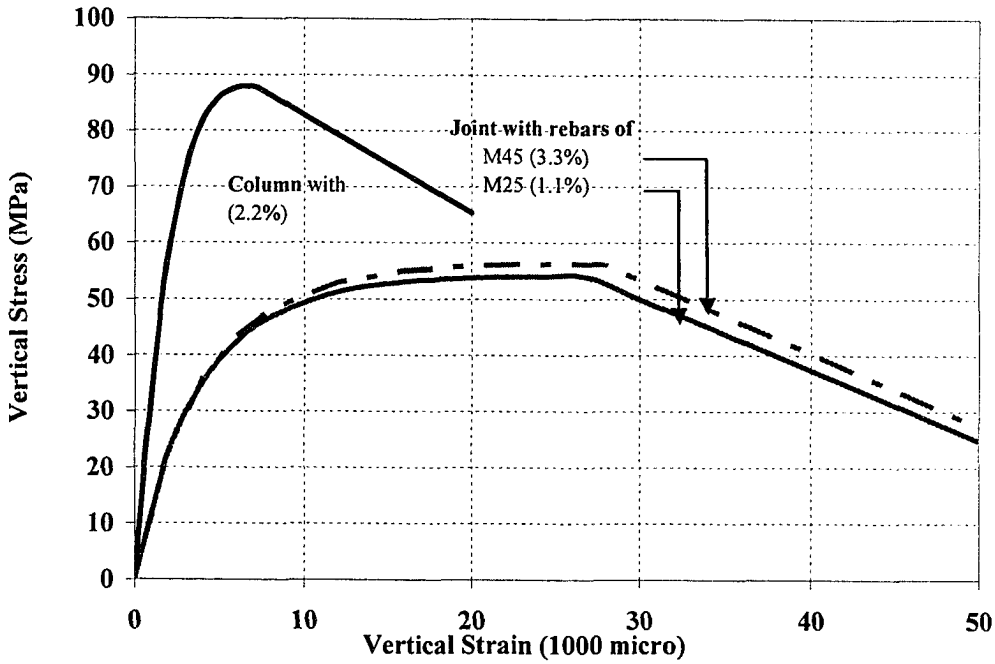

Figure E3. Effect of Rebar Diameter and Volumetric Ratio on the Behaviour of a Corner Joint

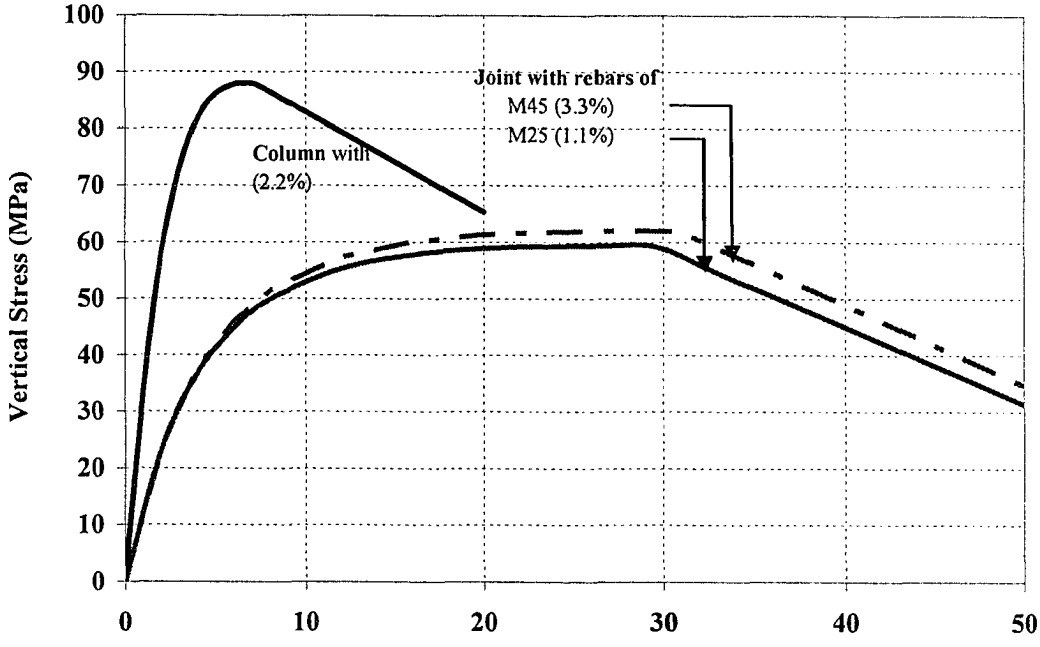

Figure E4. Effect of Rebar Diameter and Volumetric Ratio (%) on the Behavior of an Interior Joint

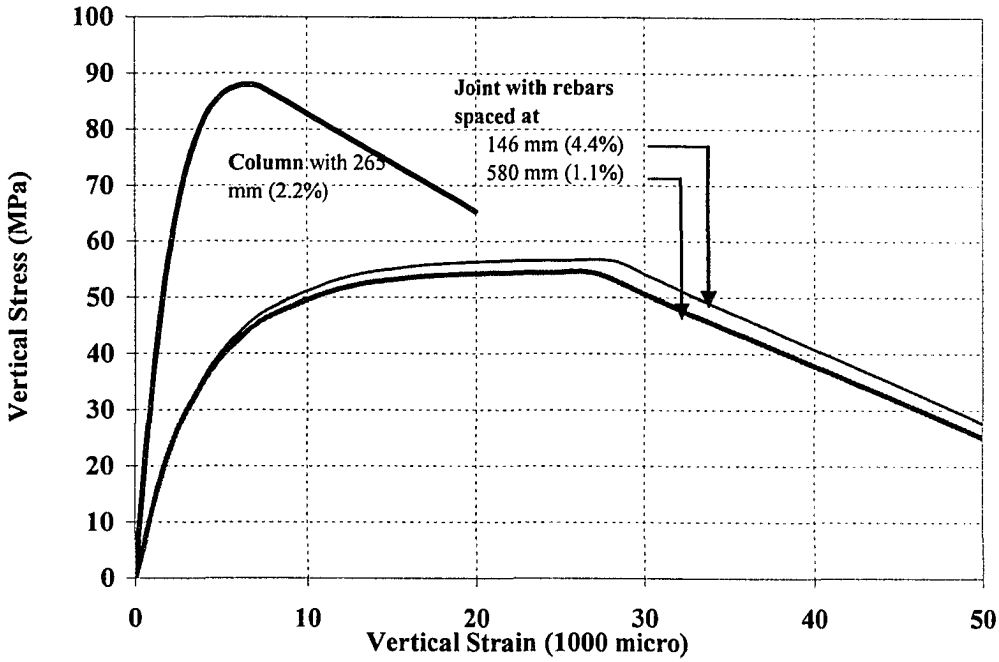

Figure E5. Effect of Rebar Spacing (mm) on the Behaviour of a Corner Joint

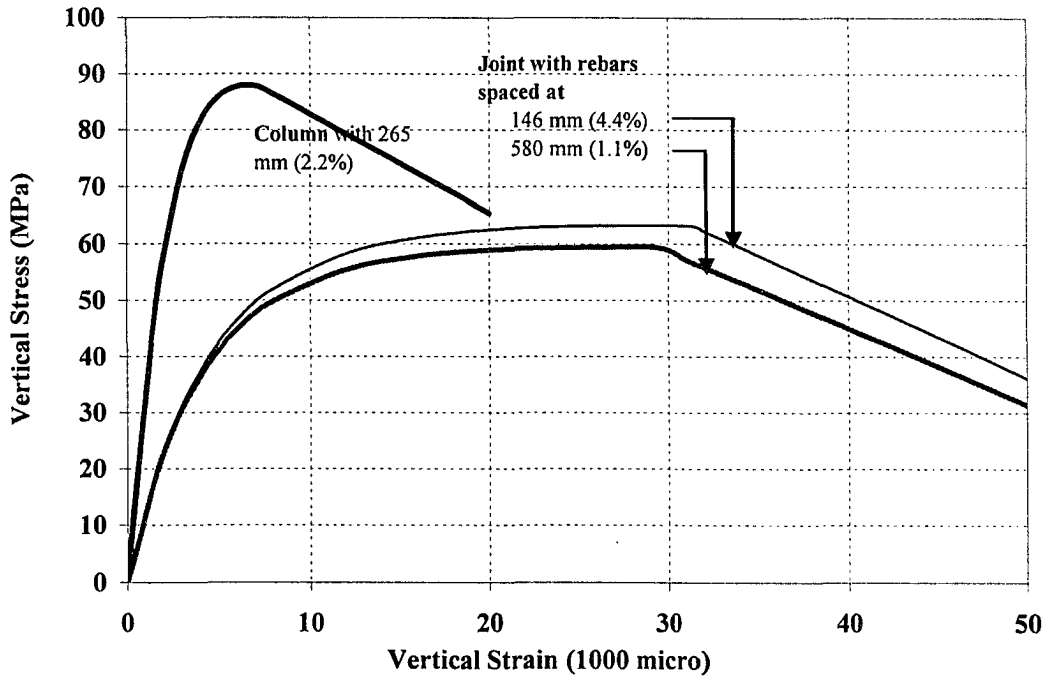

Figure E6. Effect of Rebar Volumetric Ratio (%) on the Behavior of an Interior Joint

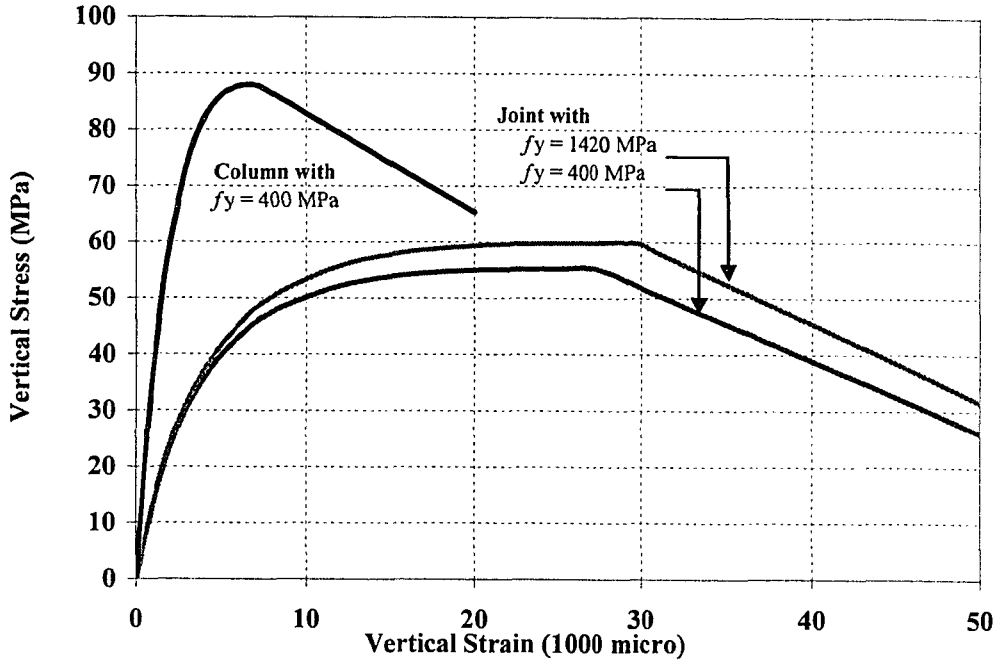

Figure E7. Effect of Rebar Yield Strength (MPa) on the Behaviour of a Corner Joint

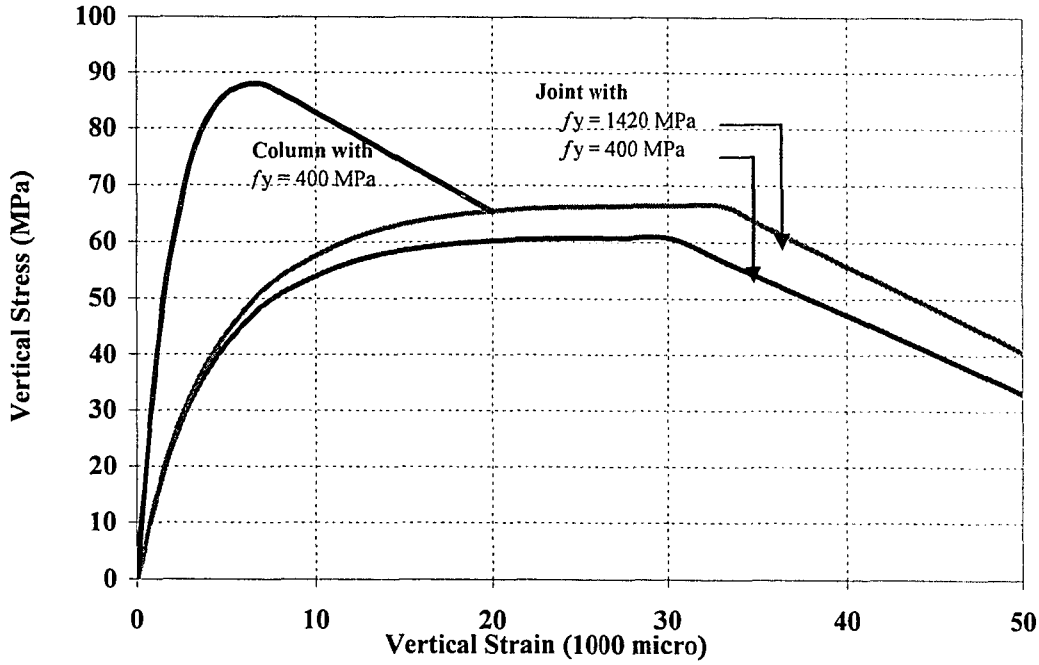

Figure E8. Effect of Rebar Yield Strength (MPa) on the Behavior of an Interior Joint

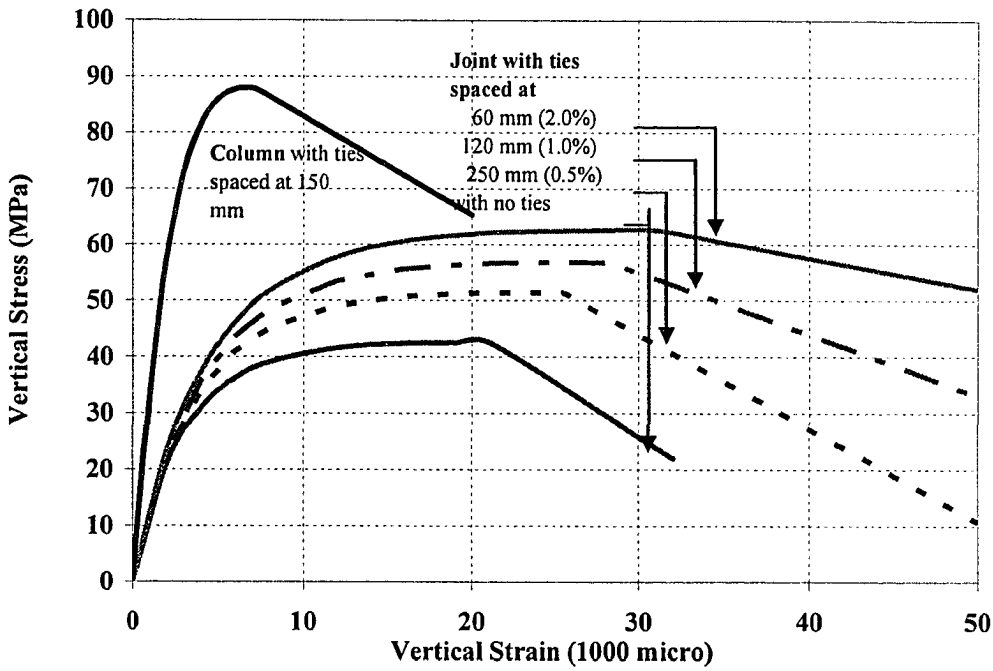

Figure E9. Effect of Tie Spacing and Volumetric Ratio on the Behaviour of a Corner Joint

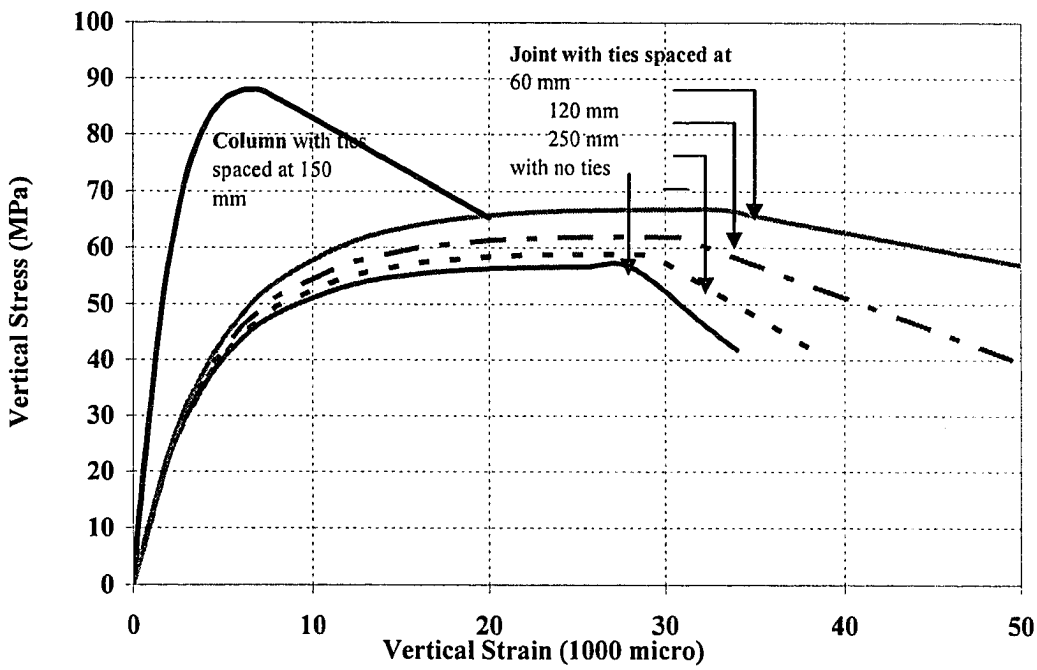

Figure E10. Effect of Tie Spacing and Volumetric Ratio on the Behavior of an Interior Joint

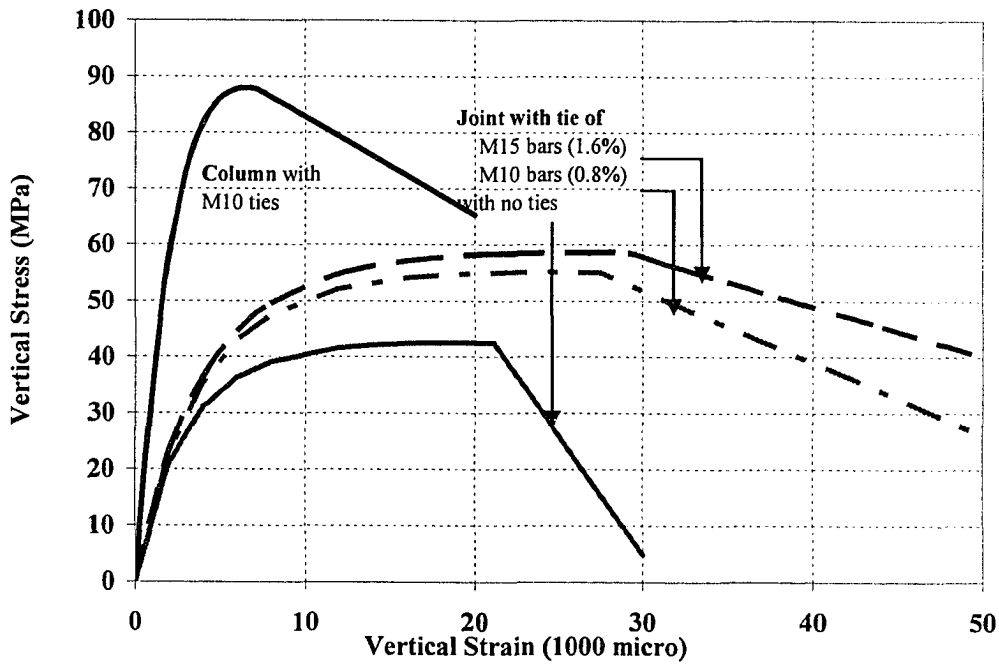

Figure E11. Effect of Tie Diameter and Volumetric Ratio (%) on the Behaviour of a Corner Joint

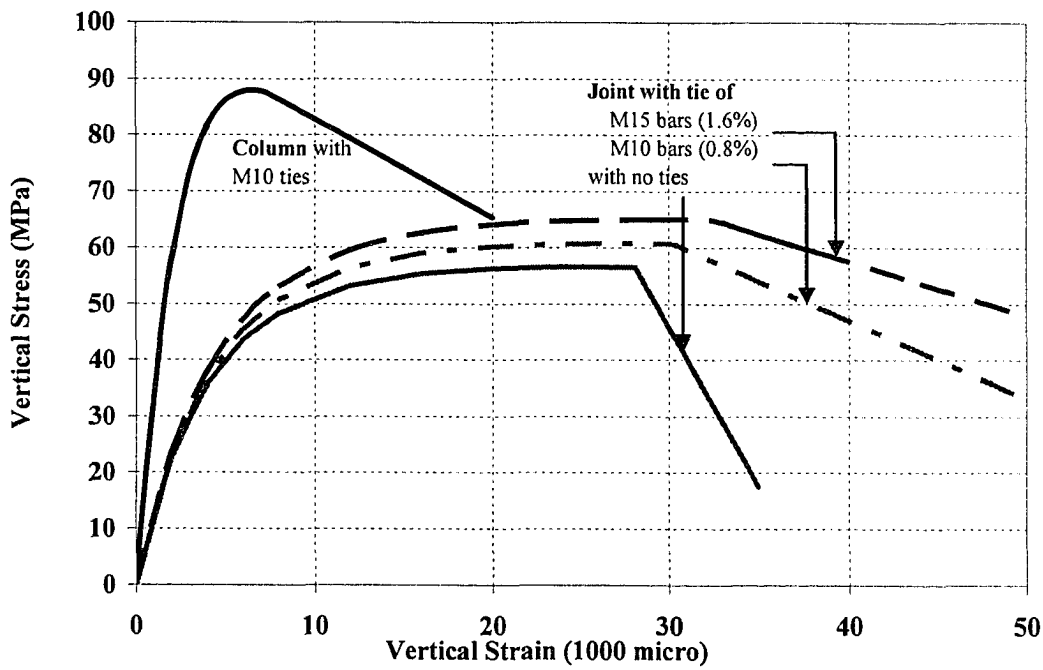

Figure E12. Effect of Tie Diameter and Volumetric Ratio (%) on the Behavior of an Interior Joint

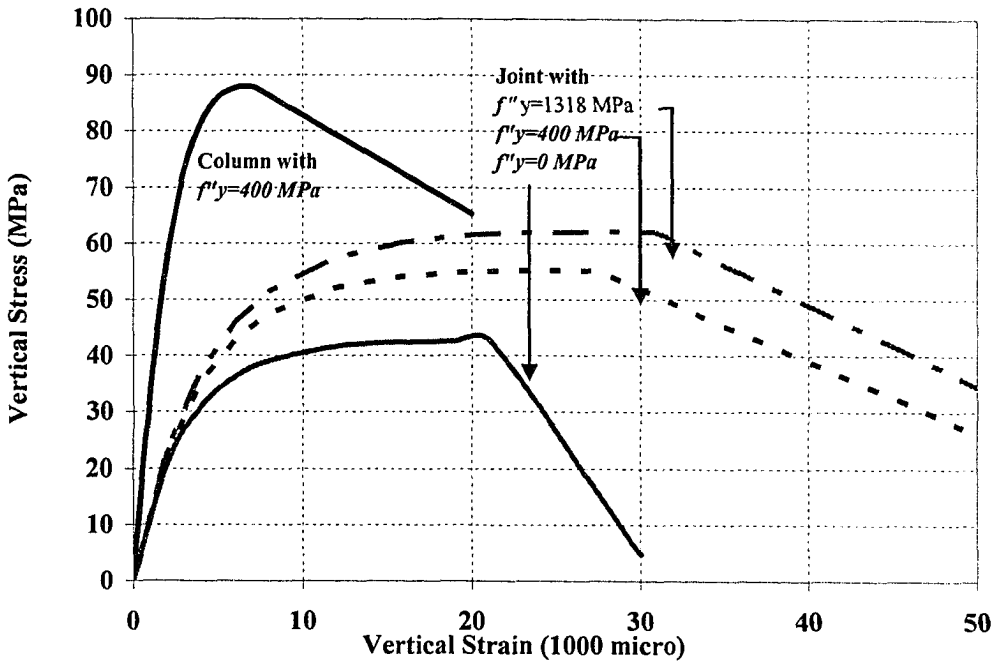

Figure E13. Effect of Tie Yield Strength (MPa) on the Behaviour of a Corner Joint

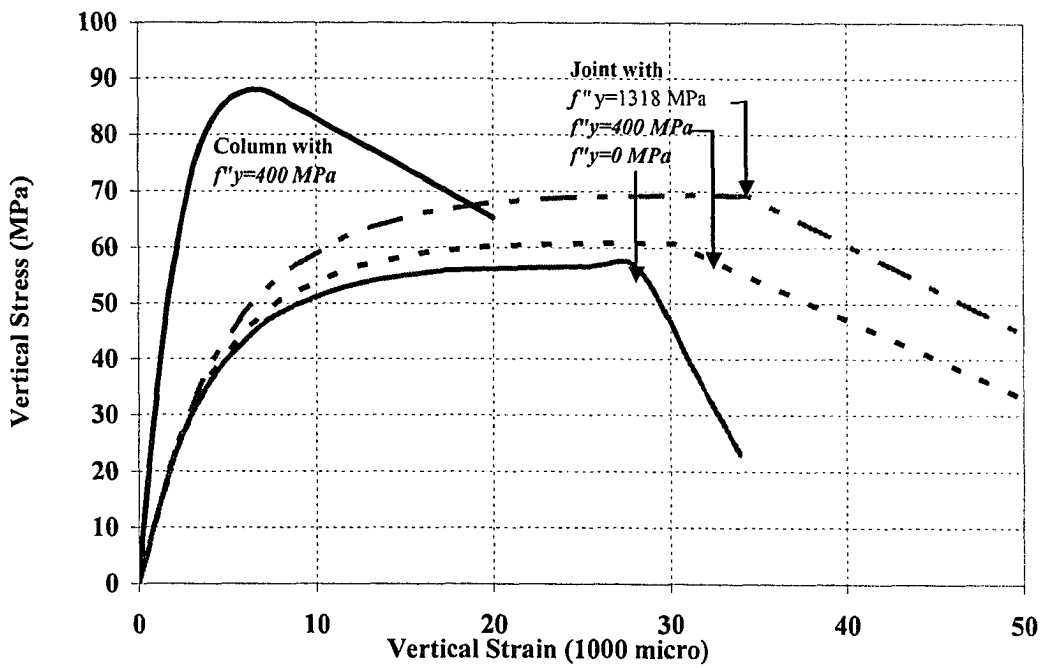

Figure E14. Effect of Tie Yield Strength (MPa) on the Behavior of an Interior Joint

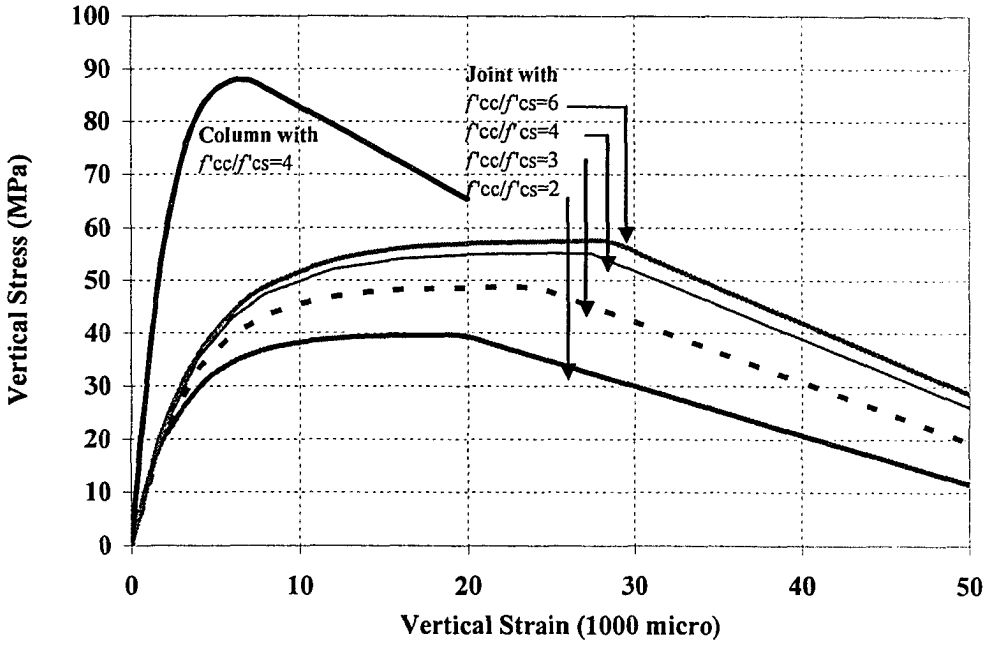

Figure E15. Effect of Column Concrete Strength (MPa) on the Behaviour of a Corner Joint

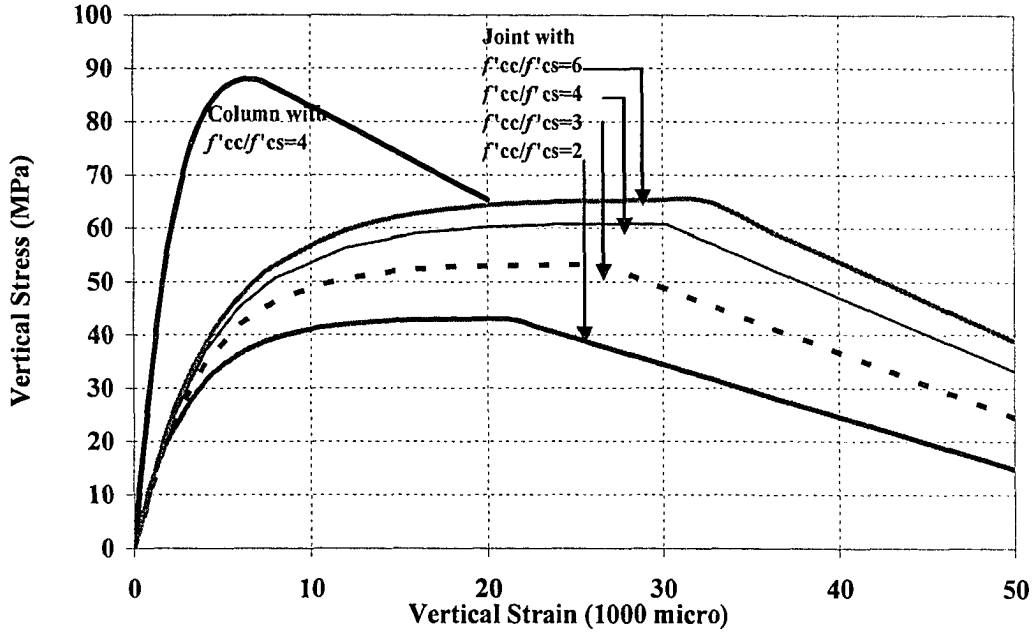

Figure E16. Effect of Column Concrete Strength (MPa) on the Behavior of an Interior Joint

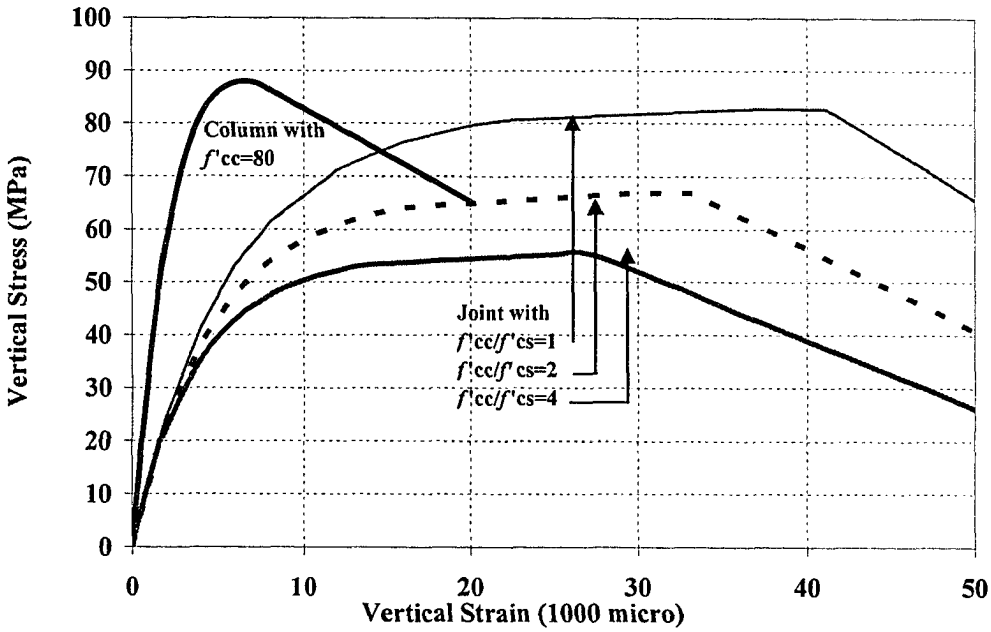

Figure E17. Effect of Floor Concrete Strength (MPa) on the Behaviour of a Corner Joint

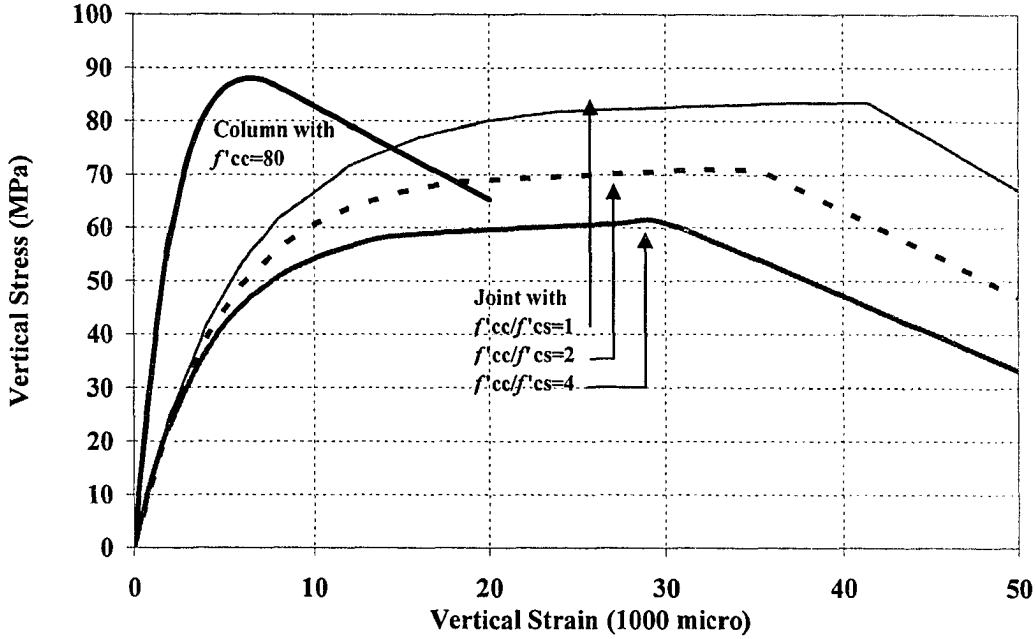

Figure E18. Effect of Floor Concrete Strength (MPa) on the Behavior of an Interior Joint

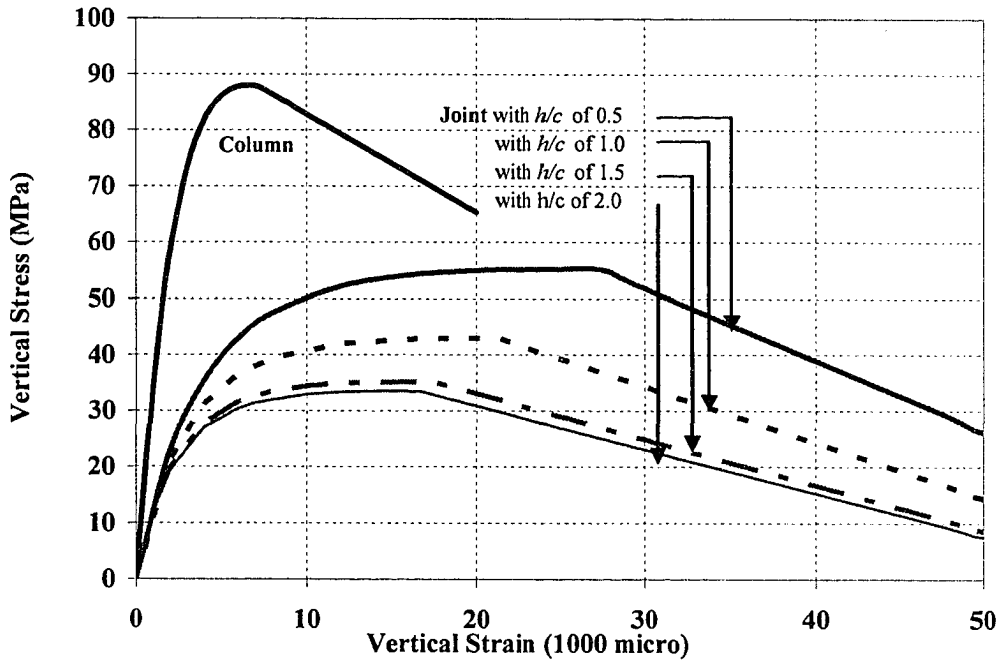

Figure E19. Effect of Joint Aspect Ratio on the Behaviour of a Corner Joint

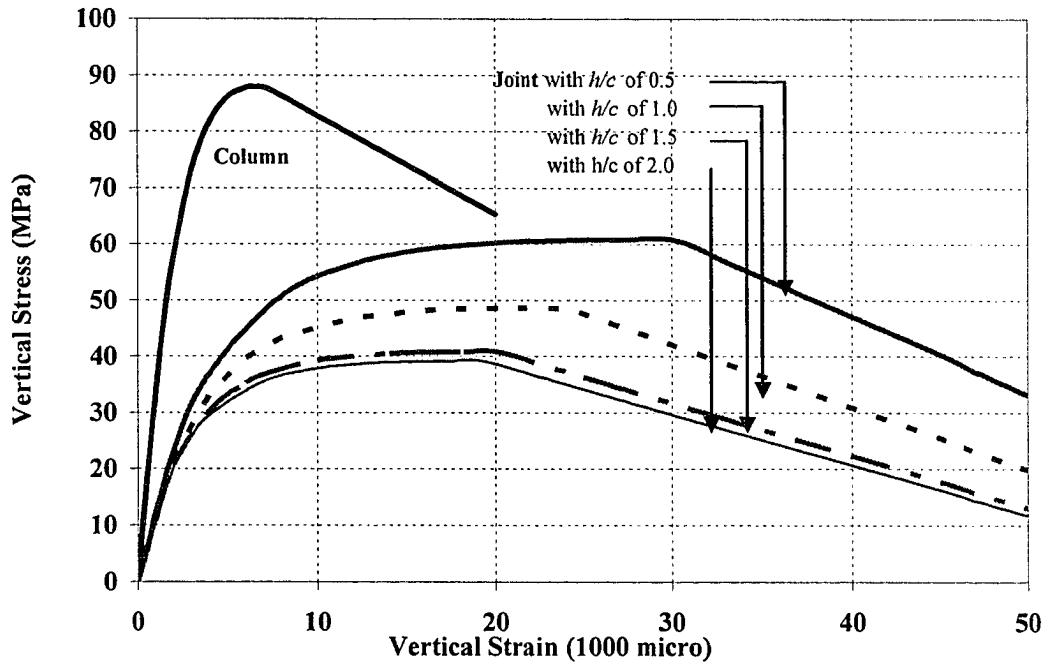

Figure E20. Effect of Joint Aspect Ratio on the Behavior of an Interior Joint

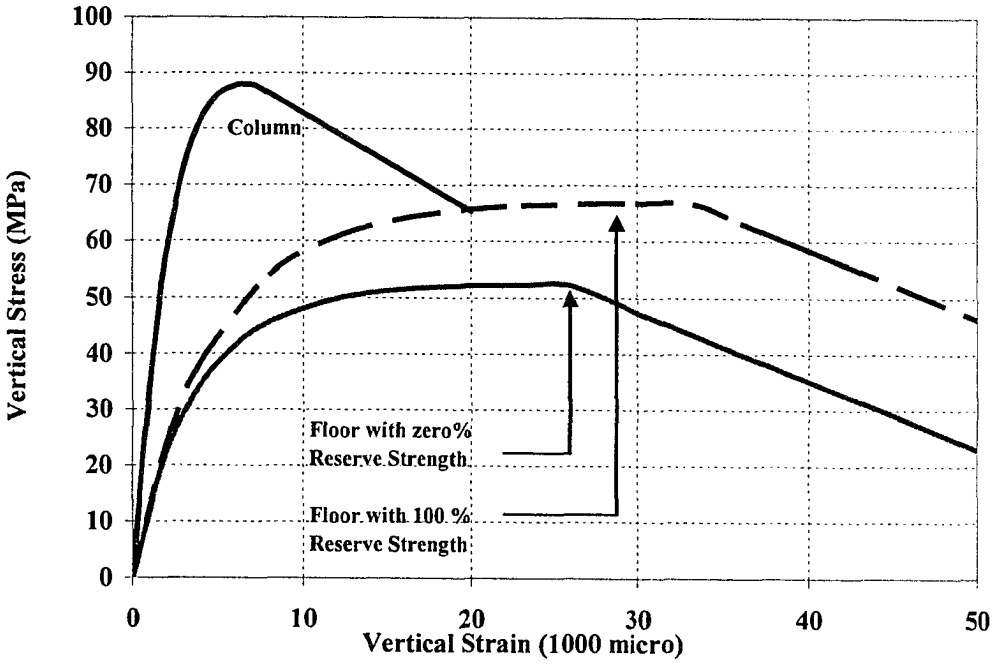

Figure E21. Effect of Floor Residual Strength on the Behaviour of a Corner Joint

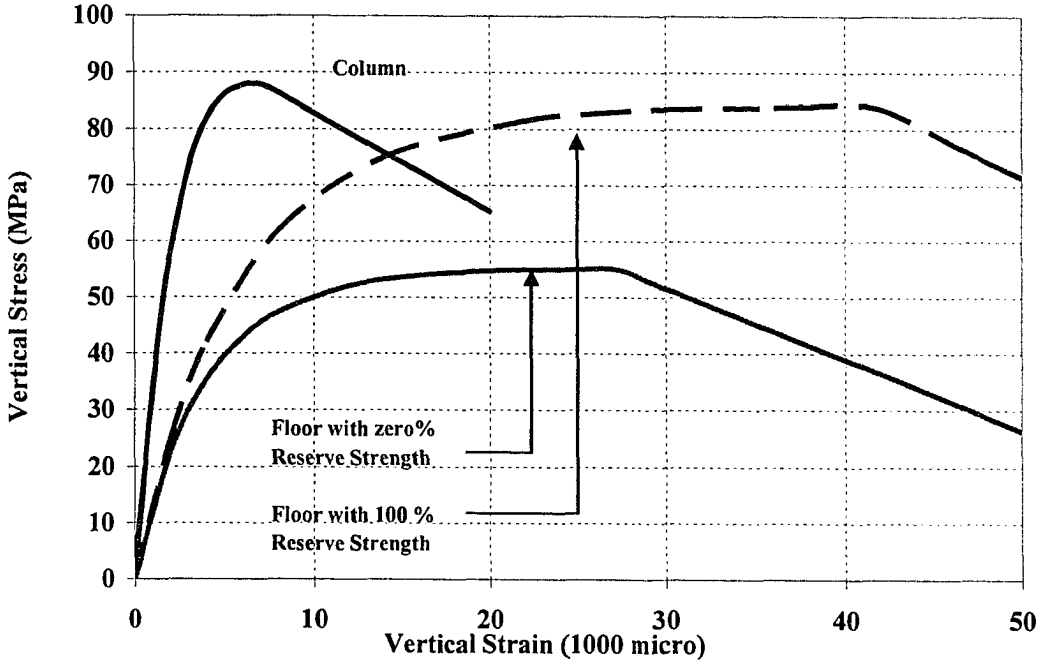

Figure E22. Effect of Floor Residual Strength on the Behavior of an Interior Joint

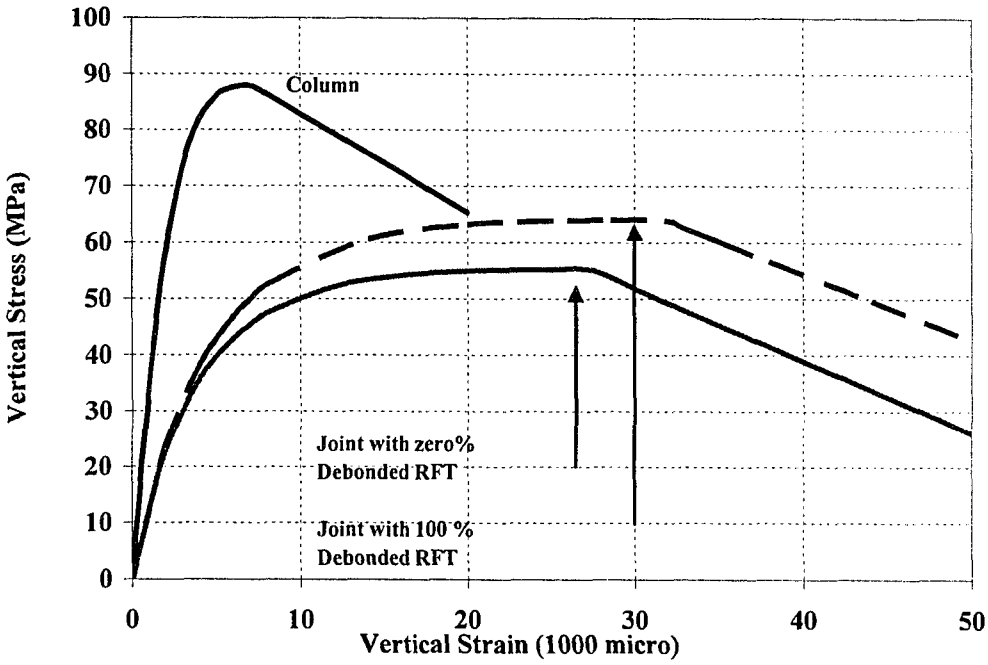

Figure E23. Effect of Debonded Floor RFT on the Behaviour of a Corner Joint

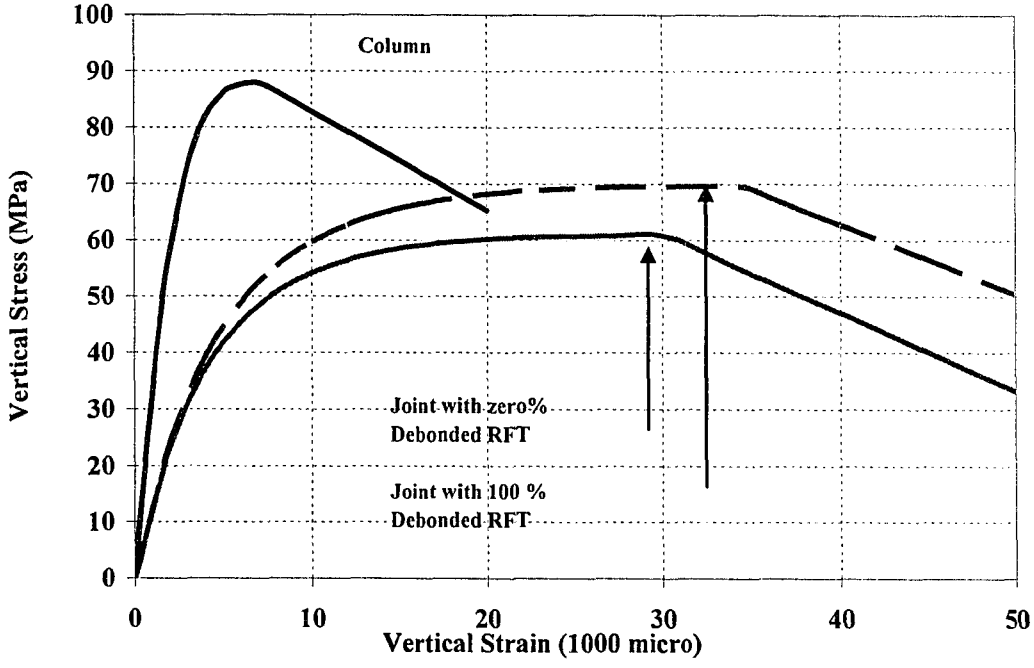

Figure E24. Effect of Debonded Floor RFT on the Behavior of an Interior Joint

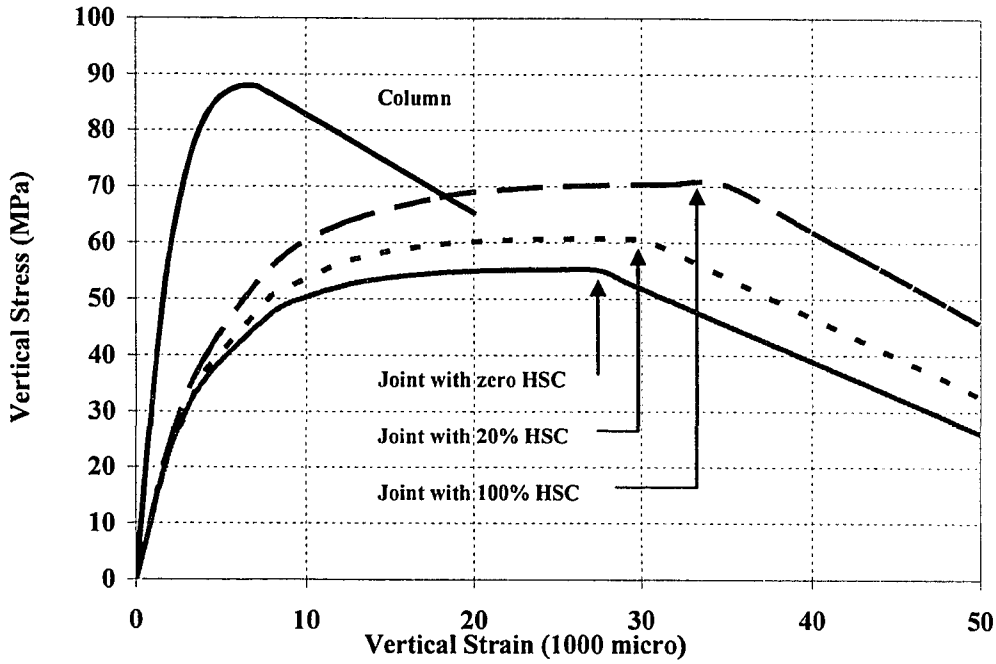

Figure E25. Effect of HSC Area Ratio inside the Joint on the Behaviour of a Corner Joint

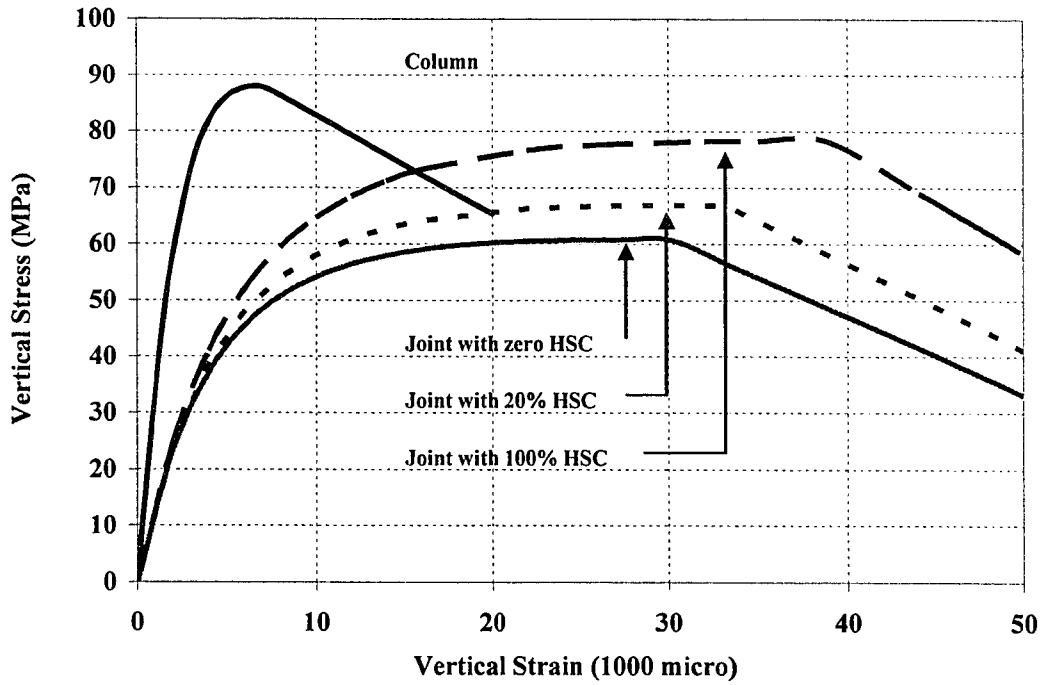

Figure E26. Effect of HSC Area Ratio inside the Joint on the Behavior of an Interior Joint